

Chapter 8 Discussion

8.1 Seasonal effects

Egli and Höpke (2020) discussed weather and seasonal influenced data for image classification purposes. They criticised that varying weather conditions change illumination patterns, which influence classification accuracies. Specifically, multi- and hyperspectral images cannot handle variable conditions, which indicated that the use of RGB images for forestry application is the better choice. Additionally, Egli and Höpke (2020) indicated that most data collections were only performed for a specific time (a day or couple of days in the summer period, usually). However, spectral characteristics influenced the reflectance of tree species and therefore their classification. Data should be collected at different times, so that the DL network can be trained on data with varying conditions, as performed in this study with image collections in all four seasons, over several weeks and months, as well as during all daytimes.

Other studies also pointed out the benefit of seasonal images to classify tree species (Lu et al., 2018; Grabska et al., 2019; Lisein et al., 2015). Leaf growth starts in spring, it is time-equal and also colour and shape of the young leaves are similar within the same species (Lisein et al., 2015). However, different species grow their leaves in different time periods, like *Albizia julibrissin* trees e.g., which start growing late in YURF (Figure 94). Colours of young leaves are often different among species, like the characteristic red leaf colour of *Aesculus turbinata*. Furthermore, some tree species grow flowers during the spring season, which increases the possibility to identify them on images; an example is *Magnolia obovata*, which grows big white blossoms in spring. Furthermore, the canopy is less dense in comparison to the summer or autumn season, which improves the identification of single trees. Images gathered in summer show the less variation regarding colour and shape of leaves, since all leaves reached their maturity level. During the summer, the forest colour is a mixture of lighter and darker greens, often merged, and therefore increased the difficulty of separating tree species from each other. In autumn the leaves of various tree species changed their colour differently. Leaf colours from yellow over orange to red increased the possibility to identify tree species. Depending on the elevation, soil and water conditions, the colour change within the same species differed from site to site and tree to tree. Hence, the timing of the colour change was a challenging factor for identifying tree species. A benefit in autumn was the timing of leaf abscission, which differed a lot for different tree species, as *Juglans ailantifolia* trees lost their leaf already in the beginning of September. Within the leave-onset season trees showed different characteristics, this can be used to identify them. The winter season was used as well in this study. Evergreen trees and deciduous trees were often mixed within the forest. Images of the winter season increased the accuracy of identifying evergreen trees, since deciduous trees do not have leaves during this season.

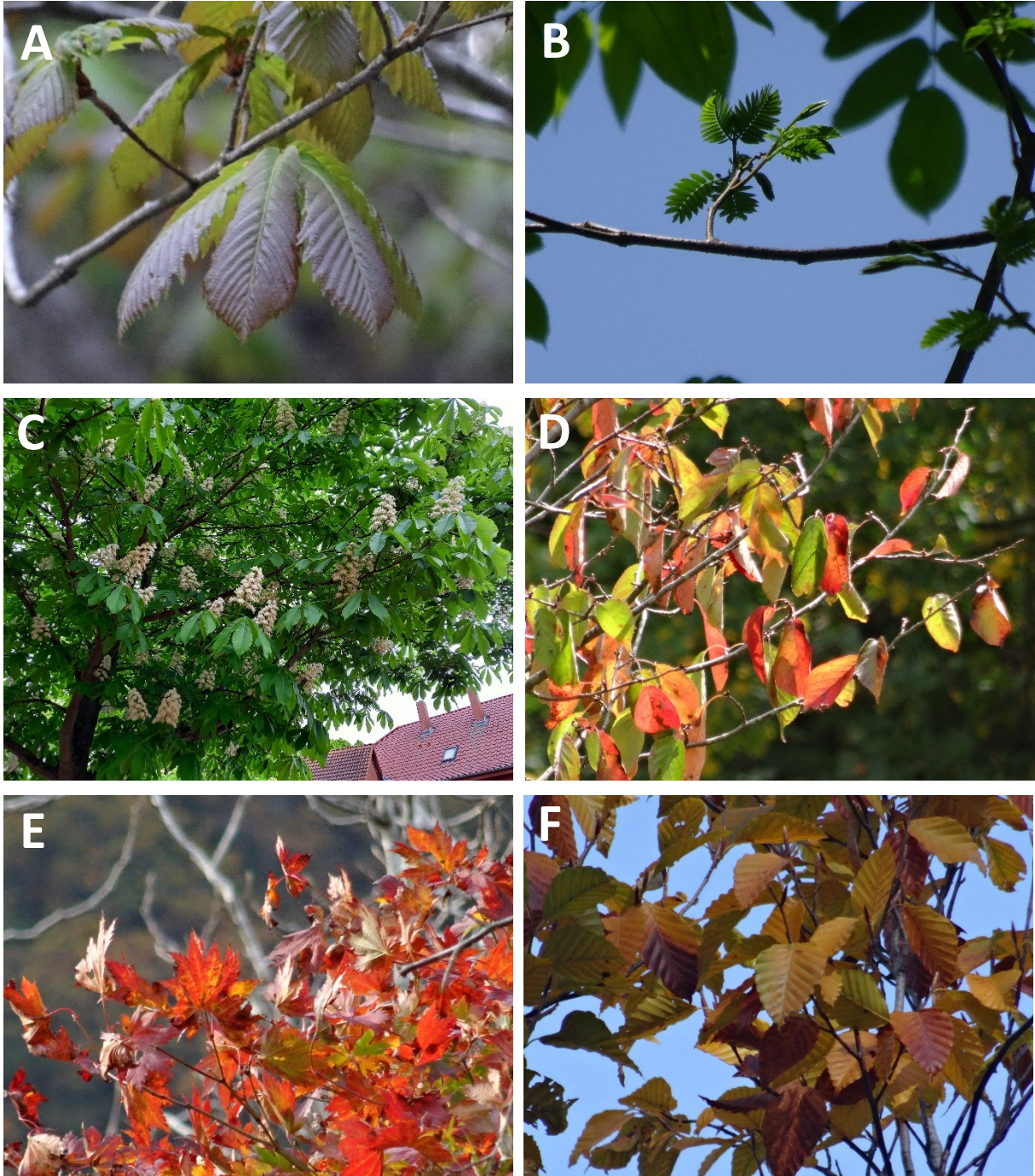


Figure 94 Six characteristic images from the forest. A) An image of an *Aesculus turbinata* tree in the spring season, B) *Albizia julibrissin* in early summer, C) *Aesculus turbinata* with their flower in early summer, D) *Prunus* species with characteristic colouring in autumn, E) *Acer* species in autumn and F) *Fagus crenata* in autumn

Furthermore, winter images of the forest showed accurately the position of the tree stems, since the branches and stems were in contrast to the white snow covering the ground. This further helped to count trees within a specific area, especially when tree stems were close together, forming a dense canopy in the summer. Since images were collected during the whole year, it was possible to use the benefits of each season to improve the localisation and identification of tree species in the forest.

Additionally, changes in the forest could be detected due to the high number of images available for the forest. It was possible to monitor forests and tree species during the year to identify the circle of life of the plants. A data collection provided with this study increases the possibility to detect forest illnesses as well as their progress and increases management possibilities.

8.2 Time consideration

Drone-imaging: Images were gathered by using pre-programmed flights. For pre-programming flight settings needed to be set, which required a few minutes per site. Those flight plans were performed for each data acquisition. The drone flew 15 to 18 min per site, only for site 1, 2 and 3 (the sites have double the size compared to the other sites) the flight time was 30 to 35 min. Since the drone flew automatically one day in the field was enough to cover all 13 sites covering an area of 61.9 ha in total. Additional working time was basically only starting and landing the drone, as well as charging the batteries. The benefit was that the mosaics, generated from these flights, had a high overlap and high resolution (less than 3 cm/pix). The required time was the minimum which could be achieved with the used equipment.

Manual drone-imaging: During manual flights the flight altitude could be changed during the whole flight, which resulted in high resolution images (less than 1.5 cm/pix). One site needed approximately one hour to be covered manually. A problem was that due to the flights closer to the canopy the top parts of high trees were not captured because the top part was often covered by only one image which resulted in a missing overlap for Metashape's image alignment. Therefore, images needed to be processed and analysed to identify holes and blurred parts in the mosaics. Several further flights needed to be done to complete the mosaics into a sufficient dataset.

Image processing: Processes in Metashape can be batched and saved, which allows running the processes automatically until the mosaic is generated. The computer needed three hours to process smaller sites and four to five hours for the larger sites. The post-processing step, to transform the DEM into a readable JPEG file, required another half-an-hour to be completed. In total the working time was less than 40 minutes, since most required time was the processing time of the computer.

Annotations: Several annotations were done during this study and all of them needed to be considered separately to evaluate the required time. The time to annotate tree tops was approximately one hour, depending on the area and the steepness of the mountain represented in the orthomosaic. The annotations of the tree canopy areas needed another 12 hours, depending on image resolution and light conditions. With resolutions lower than 2.73 cm/pix some trees species were

almost impossible to identify. High resolution images decreased the needed working time drastically. Easier annotations for winter images were performed for five classes and required approximately three to four hours to finish an orthomosaic. Annotations for all other seasons strongly depended on the number of classes which were annotated. The data needed to be accurate to submit them to the DL network; therefore, the annotations were the longest working step. As soon as a sufficient number of training data was annotated, the tree species within the database could be identified for all forest areas. Therefore, annotations need to be done only once, while fieldwork needs to be conducted for every new forest area and purpose again.

Fieldwork: In a first step, grids were considered to detect the position of trees. The grid of 50 m x 60 m in site 1 needed a man-power of ten people for around two days in the field. Additional two hours were necessary to digitalise the data. Since this grid represented only a small part of site 1, which covered in total approximately 6 ha, the estimated time and required man-power to survey the whole site exceeded the possibilities of fieldwork. The manual surveys, together with the winter images, were convenient and efficient. The fieldwork needed one day and two people to be completed for each river and mixed site, covering around three to four ha. Since the Slope sites represented a difficult working environment, a minimum of two persons and two to three days were needed. Another four hours were needed to rework the manual map and to digitalise the maps with GIMP.

8.3 Area and spatial resolution consideration

Previous studies like [Sakio \(1997\)](#), [Sakio et al. \(2002\)](#), [Fukumachi \(2020\)](#) or [Nakamura \(1997\)](#) studied Japanese forests in small plots, in order to evaluate the forest composition and structure based on site conditions. Small forest plots are useful as they provide information about the forest area, tree species composition and their structure on a small scale. Those plots are easy to conduct tree census for several years, like [Fukumachi \(2020\)](#) did. The disadvantage is that small areas might be only representative, when monocultures or forests in high altitudes are monitored, as the main limiting factors for tree species occurrences are climate conditions. However, several factors influence tree species composition in lower elevated forests, especially natural disturbances like climate conditions, water availability and plant competition. [Okitsu \(2003\)](#) pointed out that temperate forests showed a high degree of species richness because of climatic and floristic histories in Japan. Studies of [Sasaki \(1970\)](#), [Ohno \(1991\)](#), [Sakio \(2002\)](#) and [Suzuki \(2000\)](#) additionally showed the species richness in cold-temperate and riparian forests in Japan. The studied areas in YURF presented a high diverse ecosystem, changing over small distances of a couple hundred metres. Forest structures, species compositions and distributions differed not only between Riparian, Terrace and Slope sites, but also between sites of the

same class. Forest densities, tree species frequencies and abundances varied and the annotation maps further elucidated the different forest structures from above. Especially the comparison between the island part and the whole orthomosaic of site 1 demonstrated that upscaling of tree species compositions in such kind of mixed forest can easily produce wrong estimations. Image analyses can be an effective tool for classifying tree species, manually or automatically. The information about tree species composition and distribution can be gathered fast and efficient, while deeper analyses, like forest structure, can be performed afterwards. If the representativity of a forest patch is known, field investigation can be performed on a smaller scale and reasonable upscaling can be done.

The area covered during the flights ranged for this study between 3 ha and 8.1 ha. The important information is to know the tree layer, to detect and classify trees. Accurate details in the images are needed to delineate trees for applications like mapping forest density, height measurements, biomass estimations and stand growth (Miraki et al., 2021), requiring high spatial resolution of images. The best resolution was found at 10 m above the canopy, sufficient resolutions can be still achieved at 58 m (Egli and Höpke, 2020). However, higher altitudes result in drastic decreases in image resolution. Three challenges needed to be dealt with: First: most forests in Japan are in mountainous areas and the use of automatic flights can usually only be performed with a fixed height, causing varying distances between camera and tree. Second: the closer the flight to the canopy area, the higher the resolution, but the higher the flight time and therefore the needed battery. Third: the higher the resolution, the heavier the images files. The UAVs and apps used in this study had no functions to follow the terrain, which would help to maintain a constant height difference between tree and drone. Smaller areas, like in site 11, could be overflowed with a lower flight altitude. In comparison, site 2 was larger and steeper, which resulted in large differences in spatial resolutions, even though the site was split into two smaller flights. Site 3 had a less steep slope, but the large area and the relief conditions, increased the flight times to keep a constant image resolution.

The problem of large images was faced the first time when the blueberry orthomosaics were processed. The large area imaged, together with a low flight altitude, resulted in an orthomosaic file with more than 3 GB, which could neither be processed with GIMP, nor ArcGIS, as the needed memory capacity was too high. The images needed to be rescaled to keep the large area, but losing spatial information due to worse resolutions. Even though smaller areas with higher flight altitudes were chosen for the YURF sites, the high number of orthomosaics used for the classification with UNet also lead to high memory requirements.

Miraki et al. (2021) studied different spatial resolutions and species classifications, which were found to have a strong effect on overall classification performances. Depending on the used classifier and the density of sites, the overall accuracy varied strongly. Dash et al. (2017) identified 1 m resolution to be

optimal for tree health determinations, as this was slightly lower than crown radius, which were suggested to be the optimal image resolution. Schiefer et al. (2020) persist on image resolutions of 1.35 cm, so that tree species can be identified from images. Generally, too low resolutions or too high resolutions decrease the accuracy of machine learning algorithms. With too small resolutions, algorithms seem to overestimate tree areas. With too high resolutions, smaller trees can be easily incorporated into larger tree crowns. This was also seen in the Riparian YURF sites, where in summer images the canopies of *Juglans ailantifolia* and *Pterocarya rhoifolia* could not be separated from each other. The manual identification of borders between the canopies was easier with the image zoomed out, when larger structures could be identified. But at the same time, only large structures and no single leaf structures could be found. Still, as demonstrated by Miraki et al. (2021), the structure of the forest, especially the density and the relief characteristics, are often significant. Differences in height along slopes and various shapes of tree crowns can help to identify more trees. On the other side, mixed broad-leaved forests, as studied in YURF, have round and complex crowns and it was found that trees of the same species usually occur in clusters, which again increases the difficulty of detecting trees.

8.4 Benefits and difficulties during flights

Flights were mainly done automatically since pre-programmed flights offered the possibility to perform them several times with the same settings. Settings like the overlap were important for further processing, since it increased the accuracy of the orthomosaics. The drone flew with a constant speed and with insignificant changes in flight altitude which enhanced the resolution of the single images. The benefit is that the drone flies automatically the programmed route and only the start and landing of the drone need to be performed by the pilot. Furthermore, the drone will automatically adjust the flight route in case that strong wind is disturbing the flight, so that the drone will stay on the programmed line. During the flight the drone automatically shoots images in a constant time interval which can be set. Images are taken under automatic regulations of the white balance and shutter interval. Therefore, the images outcome will be similar even though the weather conditions are changing, like a change in cloud cover or sunlight intensity. A last benefit is that image collection can be performed for several sites while the only limitation are the drone batteries and the charging time.

However, automatic flights also have some negative aspects. Each flight could be programmed with only a constant flight altitude in this study, which is less suitable for mountainous environments like

YURF. Therefore, in the Slope sites different resolutions were observed for the bottom and at the top of slopes, due to the proximity of the drone to the canopy of the trees.

But also manual flights introduce several problems. The flight altitude needed to be checked and adjusted several times due to the uneven terrain and the mixture of tree species. Trees like the Japanese cedar were reaching heights up to 50 m, while the mixed forests with Japanese walnuts or wingnuts had maximum heights of 20 to 40 m. Speed and route could often not be kept stable, it was therefore difficult to maintain a constant image overlap. Since the quality of the data could not be checked in the field it was necessary to first process the gathered images, evaluate the quality and then to perform a further flight campaign to collect images where an alignment failed. In the dense forest it was often not possible to identify areas where images were missing since it was difficult to recognize those areas, since marker points were missing. Another problem was the connection between the drone and the remote control. In the case of YURF, high mountains decreased the connectivity between them, which reduced the flight distance significantly. For site 3 a manual flight could not be performed for the whole site because UAV and controller became disconnected. Further problems appeared due to the transmission between the drone and the remote control or even the app. Low transmission rates increased the danger to crash into trees. The number of images collected during manual flights was higher because more images were made in order to guarantee a sufficient overlap of the images. Overall, manual flights demanded mental concentration during the whole flight.

8.5 Tree detection and classification of tree species using image and field data

In this study, trees were detected and classified in the field, as well as on images. In this section, on the one hand, aspects of challenges and limitations of image analyses or field data were discussed. On the other hand, benefits of combining both methodologies for detecting and classification purposes were evaluated.

8.5.1 Tree detection

Field data and image data were mainly processed in ArcGIS, as the software provides useful applications for further data processing and visualisation. The collected field data were digitalised as point shapefiles, whereby winter orthomosaics were used to geolocate the tree stems. Trees belonging to the canopy and subcanopy layer could all be detected, but in some areas, where the soil was not snow covered, especially small trees were hard to identify. In monoculture patches, like the *Salix* patch

in site 4 or the *Pterocarya rhoifolia* patch in site 1, trees could be identified easily in winter images, while in summer images the canopies could not be separated. The benefit of mixed sites was that the different leaf and branch structures allowed to separate tree species from each other. The higher the mixture, the higher the number of trees, which could be identified in images and the better the annotations. However, counting of *Quercus mongolica* was challenging as the trees grew close together, so that single tree stems and branches were hard to separate.

The trees of the understory layer, like young trees, were usually not visible in the winter images of the Riparian sites. They could be placed on basis of the field data and stems of the winter images, but their stems were covered by snow. Only along the slopes or in parts where the snow was already melted, or when they exceeded a height of 2 m, stems of understory layer were detectable. In Slope sites, the snow cover was usually thinner. For some winter orthomosaics, small trees could therefore be annotated. In site 13, where the steepness of the slope did not allow intensive field work, several small trees could be detected in winter images, while a classification from summer images was not possible because of the low resolution. Those trees remained mainly unidentified. In sites 5 and 11, trees were partially close together, which hampered the annotations of tree points and might have led to miscounting.

In site 4, young trees could be all detected on summer images; several factors seemed to influence the visibility of trees in images. In comparison, the young tree area in site 4 was barely accessible, as the vegetation was dense and made counting without losing the overview difficult. A view from above made counting easy and fast. However, young trees and trees of the understory layer were rarely detectable in summer images, because of the canopy cover, but also because of image resolution, which was usually low, causing blurring effects.

There was also a high risk of miscounting *Acer* trees in summer images, as they grew in the slopes, with almost horizontal branches. This increased their canopy area, and single branches looked like single trees. *Acer* trees can be miscounted in the field as well. The trees usually grew in dense clusters of several trees and their multi-stems increased the difficulty of accurate counting. The trees in lower areas were often overseen in images, because they grew under large canopies of *Juglans ailantifolia* or *Quercus mongolica*. Trees like small-leaved *Acer*, *Cornus controversa* and *Styrax obassia* were found in the field along the rivers, but could not be detected in the images.

Summer orthomosaics, winter orthomosaics and field data together were needed to provide precise images of all studied sites. In areas, where field work was not possible, winter images could be used to count trees, while summer images helped to classify tree species. Even better was the use of high-resolution images (1.3 to 1.5 cm/pixel), as trees and sometimes even understory vegetation could be

identified better, because leaf structures were visible. Field surveys helped to identify trees, which could not be identified with summer images. Therefore, the combination of image analysis and field work allowed to study large areas with high precision.

8.5.2 Tree classification

In the field, tree species were identified by leaf and bark structures, which are characteristic for each species. Information about tree species can be found in several field guides with images and explanations about the species. However, such guides are not available for tree structures seen from above. From images, single leaf structures are usually not visible, but leaf compounds, flowers, fruits and different colours, which can be combined used to classify tree species from above.

The first step, when tree species have to be identified, is the classification in the field, except if the study area is a monoculture. Field inventories can be helpful, especially, when tree counting needs to be performed. In dense forest areas, like presented in the Slope sites, finding a tree in the field and identifying the same in the image was almost impossible. Recognising structures or patterns in tree distributions was helpful for some areas, but in others the structure below the canopy was significantly different to the canopy. In flat areas, the structures of below and above the canopy did not vary significantly (except the understory and shrub vegetation) and therefore field and image surveys could be connected. Additionally, in the field 70 tree and shrub species were identified. Some of them occurred with low numbers or even only one representative tree in the forest. Therefore, the forest composition should be evaluated first, and then a selection of trees per species, which can be detected in images, should be done. This can include trees along the pathway or river, a group of the same species or other recognisable locations. In the images, those trees can be then identified and help to find the same species in other areas of the forest. UAV images can also support the identification by flying close to the canopy, flying a straight line between markable spots in the orthomosaic or gather images of the same tree from different altitudes to analyse structure changes of the canopy due to different resolutions (Figure 95). Images close to the canopy can be enough to see leaf structures to compare them with the collected field data. From images, even with high resolutions, not all features of a leaf can be identified, for example images of different *Prunus* species have small differences, which usually cannot be imaged.

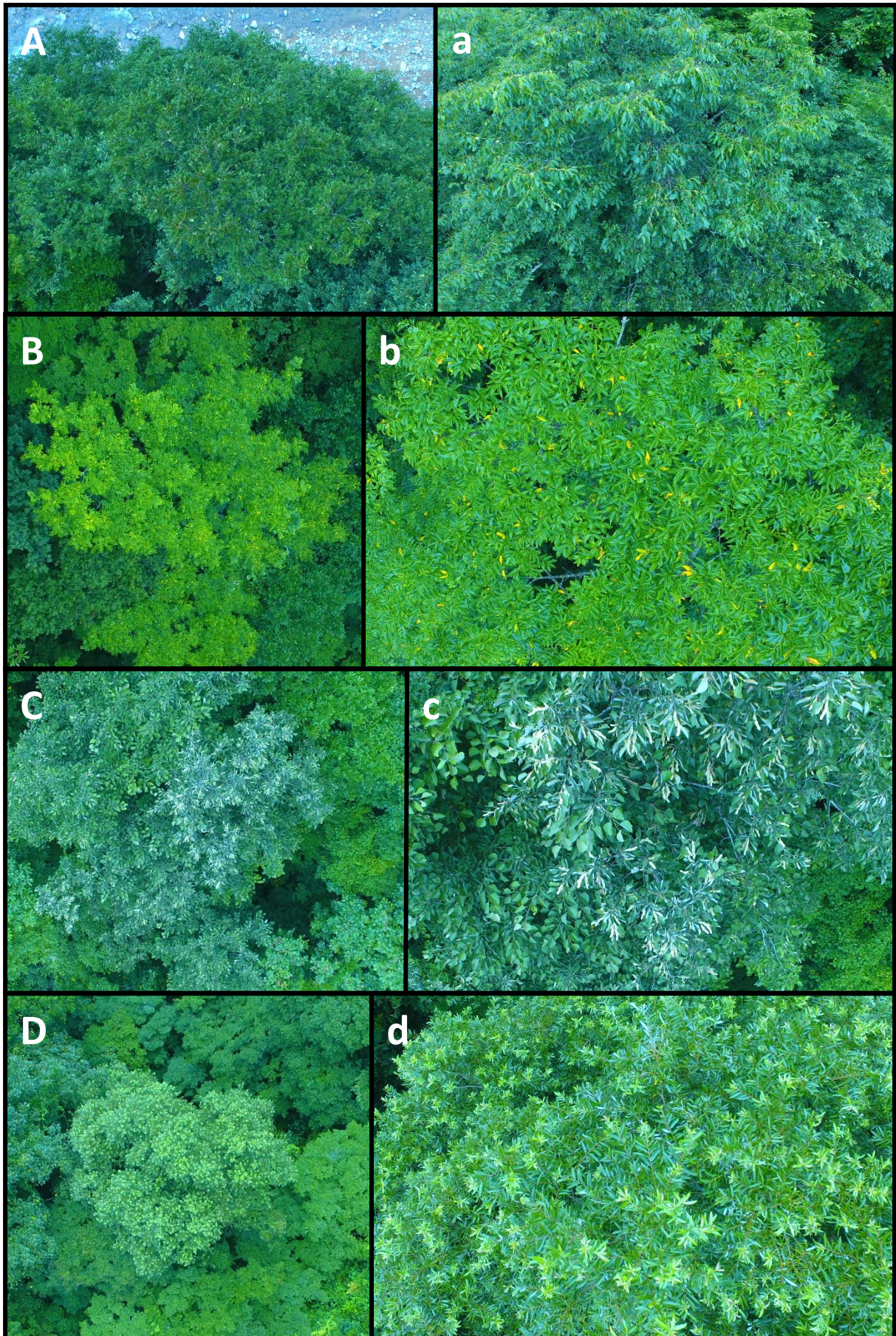


Figure 95 Example images of A) *Betula* B) *Fraxinus* C) *Tilia* D) *Salix*

As mentioned before, image resolutions are an important aspect of identifying trees from images. The closer the UAV is flying to the canopy, the easier are classification of tree species. Figure 96 shows some examples of challenges faced during the annotations, like climbing plants in the trees or dry leaves, which changed the shape and occurrence of the trees. In case of *Cornus controversa*, dry leaves resemble those of *Robinia pseudoacacia*. *Robinia pseudoacacia* is furthermore a tree, which grows in small gaps between the canopies of other trees, so that the canopy becomes a mixture of different tree species. The same seems to be the case for *Phellodendron amurense*, *Cornus controversa* and *Morus australis*. Similar were climbing plants, which mainly grew in *Juglans*, *Pterocarya* and *Cryptomeria* trees and changed their optical occurrence.

In the field, identifying *Juglans ailantifolia* and *Pterocarya rhoifolia* was sometimes challenging, as the leave number and the shape can vary, so that the leaves look similar, especially, when leaves could not be collected from the trees, because they could not be reached. In images, the differentiation between *Juglans* and *Pterocarya* was easier, as *Juglans* trees had a lighter green colour, the canopy structure was less dense and the leaf compound structure was significantly different to *Pterocarya* trees. More examples were *Aesculus turbinata* and *Magnolia obovata*, which had large leaves and looked from greater distance similar in summer and autumn. Only in spring and early summer *Magnolia obovata* trees had big white flowers, which made them recognisable. In images, *Aesculus turbinata* had a dark green colour, while *Magnolia* trees were lighter; furthermore, the structure and colour of *Aesculus* trees looked similar to *Pterocarya rhoifolia* trees, introducing confusions between *Aesculus* and *Pterocarya* in the images, but not between *Magnolia* and *Aesculus*. There were also two *Salix* species identified, which showed small differences in their leaf structure and colour, while they looked different when imaged with UAVs (Figure 97).

Difficult was also the comparison of *Fraxinus* and *Juglans* trees, which had similar shapes in the images. Generally, *Fraxinus* occurred in Slope sites, where the lower resolution of the images did not allow a differentiation of these two species. Only very high-resolution images of *Fraxinus* showed partially yellow leaf-veins. In any case, the number of *Fraxinus* trees identified in the field was significantly lower than *Juglans*, hence misclassifications were tolerated. Also, *Fagus crenata* and *Quercus mongolica* could look similar, when *Fagus* leaves had a darker colour (Figure 96). It is likely that misclassifications occurred during the manual annotations, as the difference between the trees was not obvious and no high-resolution images could be acquired, because of the steep slopes and different tree heights (also the images in Figure 95 were only single captured imaged).

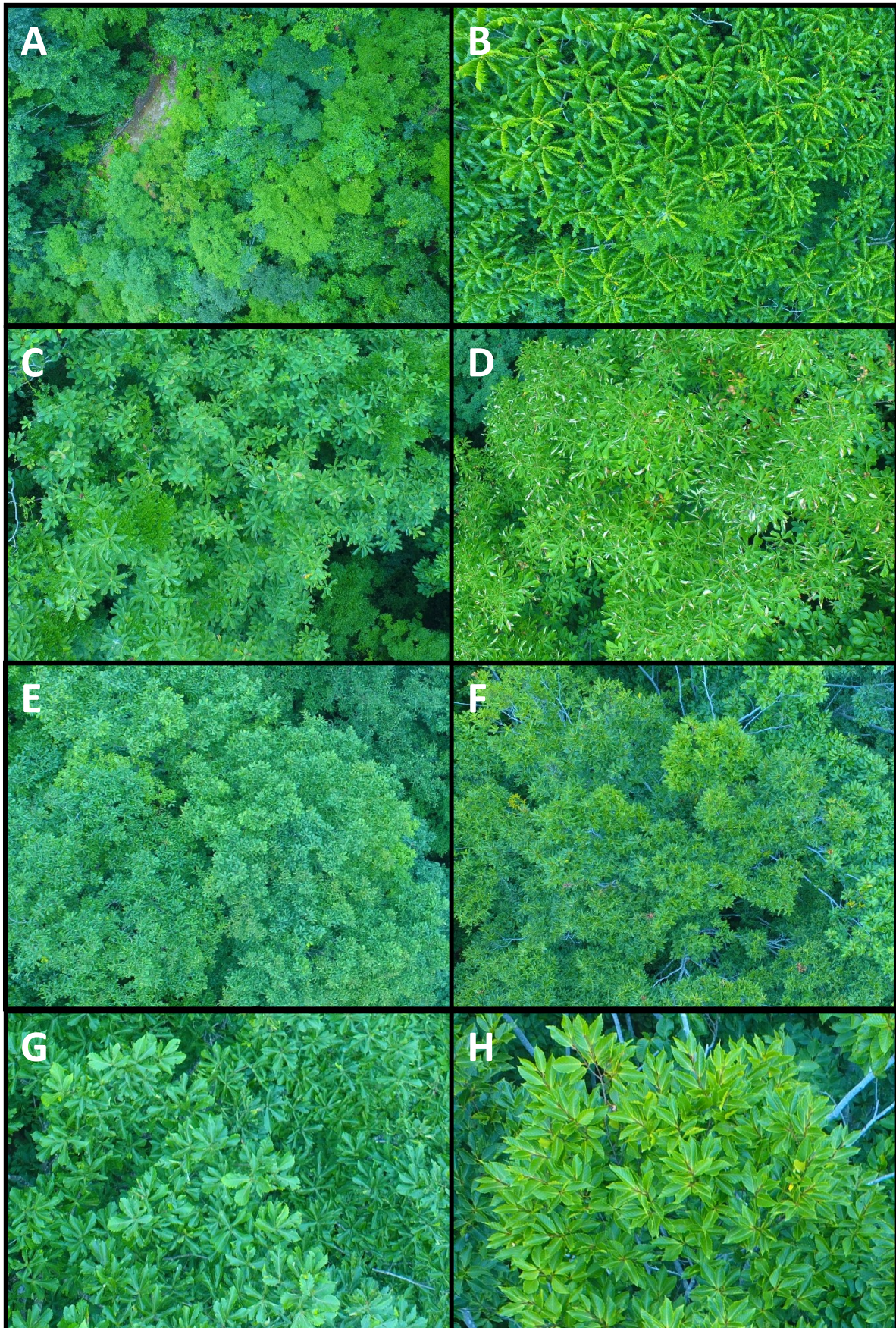


Figure 96 A) Mix of shrub and understory vegetation; B) *Juglans* with dry leaves; C) *Magnolia* with a climbing plant; D) *Magnolia* with dry leaves; E) Oak tree and G) same tree with higher resolution; F) dark leaved beech tree and H) with higher resolution

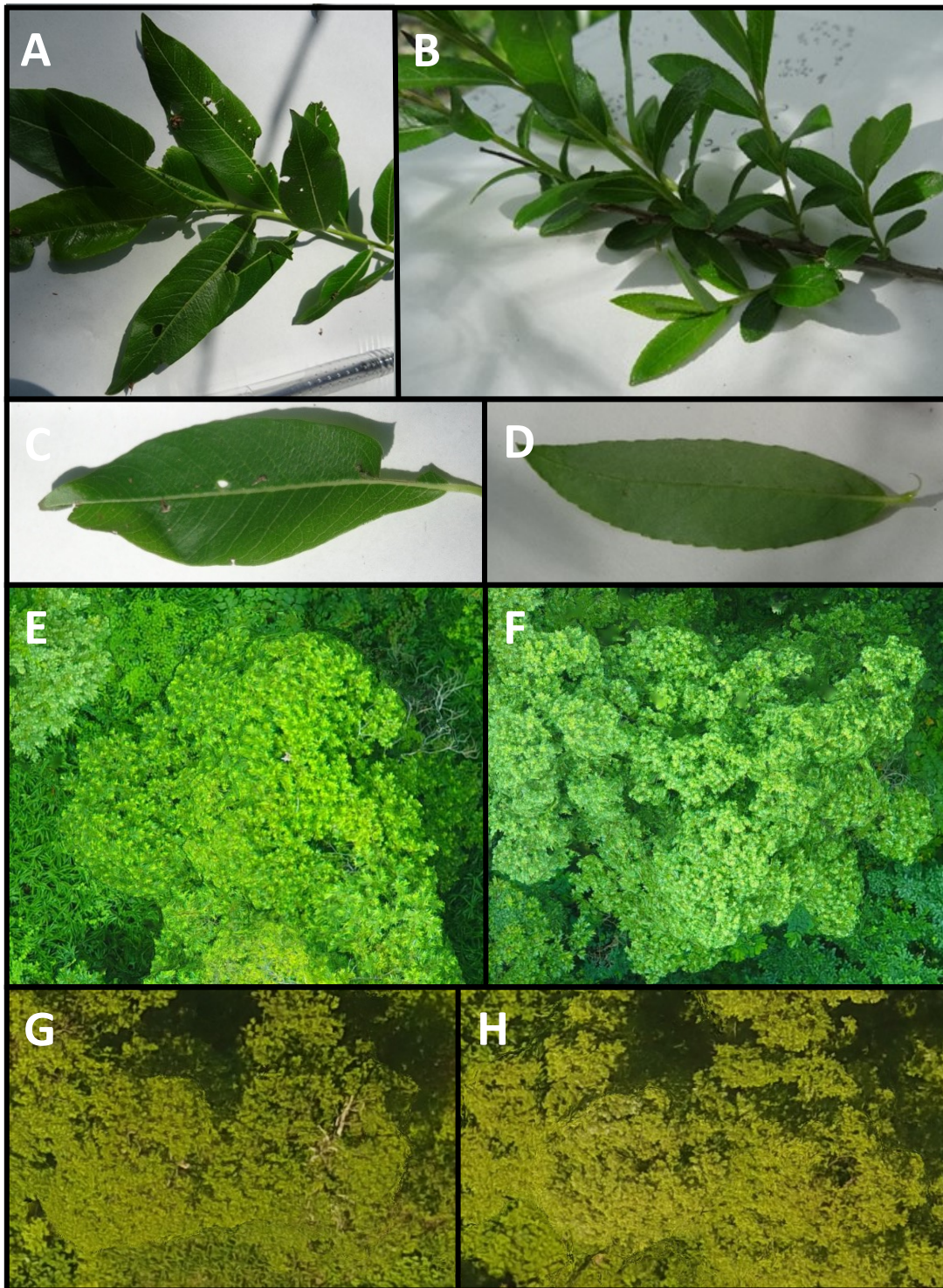


Figure 97 *Salix jessoensis* (A, C, E, G) and *Salix serissaefolia* (B, D, F, H), with leaf images in the first and second row, high resolution images (approx. 1.3 cm/pix) in the third row and normal resolution images (approx. 2,73 cm/pix)

Low image resolutions mainly occurred in Slope sites, where small-leaved and big-leaved *Acer* were imaged. The field data provided that big-leaved *Acer* were almost all *Acer mono maxim*, while there were rarely *Acer pictum*, *Acer nipponicum* and *Alangium planifolium*, which looked similar in the orthomosaics. Small-leaved *Acer* occurred everywhere and they further had no significant leaf

structures or compounds which would have helped to identify them on images. Even with higher image resolution, classifying those trees was in some cases impossible.

The discussion showed that natural mixed forests with a high density and high diversities are challenging when trees have to be classified, while the combination of field and image data can help to significantly increase the identification of trees. Further, image resolution can be an important aspect for annotations, which might also influence automatic classification approaches.

8.6 Forest structure

Forest structures were previously discussed in the context of canopy area, tree species frequencies, diversity measures and others in images and in the field. Valuable insights were already provided, which can help to understand forest structures better. In this chapter, all the factors and results together are once more considered and summarised to evaluate the structure of the forests. The main focus here is to give a comparative statement to the site structures on basis of the image analysis and the field data.

Understory vegetations, which are usually not imaged in orthomosaics, have a significant influence on soil properties, nutrient cycles and litter composition (Hedwall et al., 2018). Verheyen et al. (2012) pointed out the importance of tree species composition and canopy structures of trees in the canopy and subcanopy layer, as they significantly affect understory vegetation. The canopy and subcanopy layer are always visible on images, taken from above the forest. The composition and structure, with different tree species in these layers, significantly influence light conditions, temperatures, water and soil nutrients. Therefore, the structure of the highest forest layer must also influence understory vegetation and shrub compositions (Hedwall et al., 2018). Zhang et al. (2017) indicated that there is a positive relationship between the species richness and the understory vegetation, as different tree heights enable light to reach understory vegetations (e.g.).

8.6.1 Forest structures along rivers

A general trend of increasing canopy areas with increasing species richness was observed. This increasing trend in both, density and species richness were already discussed by Hedwall et al. (2018). The authors discussed that the mixtures of more tree species influence resource filtering. In Riparian sites, understory vegetation occurs relatively frequent, while shrubs are rare. It was discussed already, that the forest floor in Riparian sites is mainly covered by grasses and, bamboo, which might be the main reason for a low number of shrubs. In sites 4 and 7, the canopy areas were low, as well as species

richness, which should be the reason for a low density of understory vegetations, according to [Hedwall et al. \(2018\)](#). But both sites contained a higher number of understory vegetations, however it was mainly distributed along the roads and paths, where light conditions were better and competition was low. Within the sites, the number of understory vegetations was lower, most probably due to the lower species richness. [Sercu et al. \(2017\)](#) explained the effect of low densities of understory vegetations with the compact structures of the canopy and subcanopy layer, which significantly reduced light reaching the forest floor. In comparison, sites 1 and 6, with a higher mixture of tree species and higher canopy areas lead to an increase of understory vegetations, as described by [Hedwall et al. \(2018\)](#). The study of [Hedwall et al. \(2018\)](#) specified that different tree species can benefit the growth of understory vegetations and that competitions also have a significant influence, while [Hart & Chen \(2006\)](#) provided detail information on colonisation of understory vegetations by light, soil nutrients and pH values.

A comparison between the field point data with the manual image annotation allowed to evaluate not only numbers of canopy areas and species richness, but also to consider species site conditions and structures. The images showed that tree species belonging to understory layer were found, when the canopy cover was less dense. Another aspect was that these species usually occurred at higher elevation of Riparian sites, while there were no trees in depressions with higher water contents. This was observed when the annotations were compared with the DEM and slope maps. The density maps generated on basis of the tree further indicated that understory species do not occur when the densities of the canopies are too high. The provided hot spot analysis supported the previously mentioned point, as in site 1 hot spot areas occurred with the *Pterocarya rhoifolia* monocultures and no understory vegetation, like in site 4 in the *Salix* monoculture. The hot spot analyses further indicated that there were only in sites 6 and 7 trees of the shrub and understory layer in clusters of individuals.

The manual annotations, together with the ordering of tree species into the different forest layers, helped to illustrate differences between the canopy and subcanopy tree species. When tree species classifications were performed in previous studies, the forest was only observed from the ground, the high structures of the canopy and subcanopy layer were usually not analysed. With UAVs it was possible to observe canopies from above. The field data showed that there were several more trees of subcanopy tree species than were visible from above.

In comparison *Pterocarya rhoifolia* and *Juglans ailantifolia* had large canopies, which did not seem to be covered by other trees. Their canopies seemed to be only limited by their own species. The species maps showed clearly their dense structure and indicated that there were large shadows on the forest floor. The density maps (Appendix L) and the distribution/hot spot maps (Appendix N) illustrated that the tree species of the canopy layer usually grew separated from each other, in order to have enough

space. The field data indicated the same behaviour, while only subcanopy species and understory layer tree species grew close to canopy layer trees. *Pterocarya rhoifolia* trees seemed to be the only ones, which grew closer together.

8.6.2 Structures in Slope sites

The Terrace and Slope sites showed different characteristics than the Riparian sites. The Terrace site 11 had a small canopy area and less species, with a high number of understory vegetations, while sites 12 and 13 had a larger canopy area and a higher number of tree species. In site 13 the dominant species was *Juglans ailantifolia*, which built one dense canopy area without holes so that only diffuse light reached the forest floor. Along the bottom of the slopes, the numbers of understory vegetations were high, since light, water and soil conditions were better. In site 11, understory tree species and shrubs grew in several open areas along the slope, which strengthen the point that light is one of the most important aspects for understory vegetations. Most shrubs and understory vegetation tree species in site 12 were located under a dense canopy cover, where a river was located. So, it seems that in this site water availability is the most important point for the small trees and shrubs to grow.

Slope sites had higher species richness and the slope angle further benefited by light reaching the forest floor; the number of understory vegetations can reach higher numbers, as pointed out by [Hart & Chen \(2007\)](#). Furthermore, the understory species composition in slopes was a combination of shade-tolerant species. In Slope sites, the maps identified places with high numbers of understory tree species, which was most probably a result of the absence of larger trees.

The comparison between the image analyses results and the field data in Terrace and Slope sites gave interesting insights. In the Riparian sites, the borders of the orthomosaics already showed slope areas, with high numbers of tree species belonging to the shrub or understory layer. In the mixed forest part in the slope of site 1, the dominance of *Acer* species was high, and even higher at the bottom of the slope in site 13. The western and eastern slope next to site 7 and the density maps showed clearly the dominance of understory vegetations and shrubs. Even though no point data for the Slope sites were provided, the species maps already displayed open spaces in sites 5, 8, and 9, where understory vegetations would have good light conditions. In the north corner of site 9 was additionally a large area with understory vegetations, which could not be classified from the images. Especially in sites 2, 3 and 9 the main understory tree species were *Acer* trees, mainly found during the field surveys. The tree density in site 10, which was visible in the species map, corroborated the assumption that the low number of trees in the understory layer and shrub layer was the result of the high tree densities in the forest.

In general, the Slope sites looked on the maps denser than they were, which is the result of the 3D slope being processed into a 2D image, which decreased the area significantly, as example, a slope of 100 m and with 30° becomes reduced to about 85 m. Therefore, the forest looked always denser in steep slopes (sites 9 and 10 e.g.) than in less steep slopes (sites 11, 12 and 13), and further affected the visible canopy and subcanopy structure. While in the Riparian areas the canopy layer was dominant, in slope areas even the canopy or subcanopy could be dominant. *Tilia* species dominated the eastern slope of site 1 and *Acer mono maxim* dominated large patches of sites 5 and 9. Other slope areas were additionally dominated by *Hamamelis japonica* and *Styrax obassia*. Also trees, like *Cornus controversa* have been identified with larger canopy areas. The overlapping of canopies was not as significant as in the flat sites. In sites 1, 11 and 13 *Magnolia obovata* and *Juglans ailantifolia* trees were sometimes surrounded by *Cryptomeria* trees. In this case they had smaller canopy areas, it might be that there is an emergent layer in the forest, between which species need to find light sources. The image analyses supported these observations and increased the visual information regarding the distribution of the species along the slopes.

The combination of image analyses and field data allowed gaining new insights into the forest structure. Shrubs and understory vegetation can be studied from the forest floor, while subcanopy and canopy structures are challenging. Using UAVs, the situation changes, shrub and understory vegetation were only visible in open areas, however the structure of the canopy and subcanopy layer can be studied well. Still, expansions of this study are necessary to understand which factors mainly affect the forest composition. Another aspect was that in the future it should be studied if there are relationships between canopy tree species and understory tree species. Further image analyses, like density calculations, hot spot analyses and tree counting provide useful information, which can be easily split into point data, area data, species classifications and more. The study showed the effective performance of image analyses for forest structures, but also indicated that field studies are still necessary.

8.7 Tree species distribution

Tree species compositions were evaluated by assigning a number for frequency, dominance or abundance to trees, but it did not provide information about the location of the trees. Tree species distributions delivered tree name and spatial information. In this sense, forests can be evaluated, if there are clusters of trees or relationships between tree species and forests conditions. The performed analyses showed that field data and image data provided useful information about tree distributions. Image analyses, which can be performed on field data or image data, with count maps, hot spot maps

or density maps, decreased the features in the data by performing the analyses. These maps highlighted areas of high densities, distributions of single tree species and areas of significant clusters. Furthermore, adding environmental factors, like aspects of the slope, distances to rivers and elevation, allows comparing species occurrences in the different sites. These sets of information, together with species characteristics, helped to evaluate tree distributions. Based on the gathered tree distribution information about the three considered site classes, a profile was created, capturing the observed species distribution and structure of the forest focussing only on the main tree species (Figure 98).

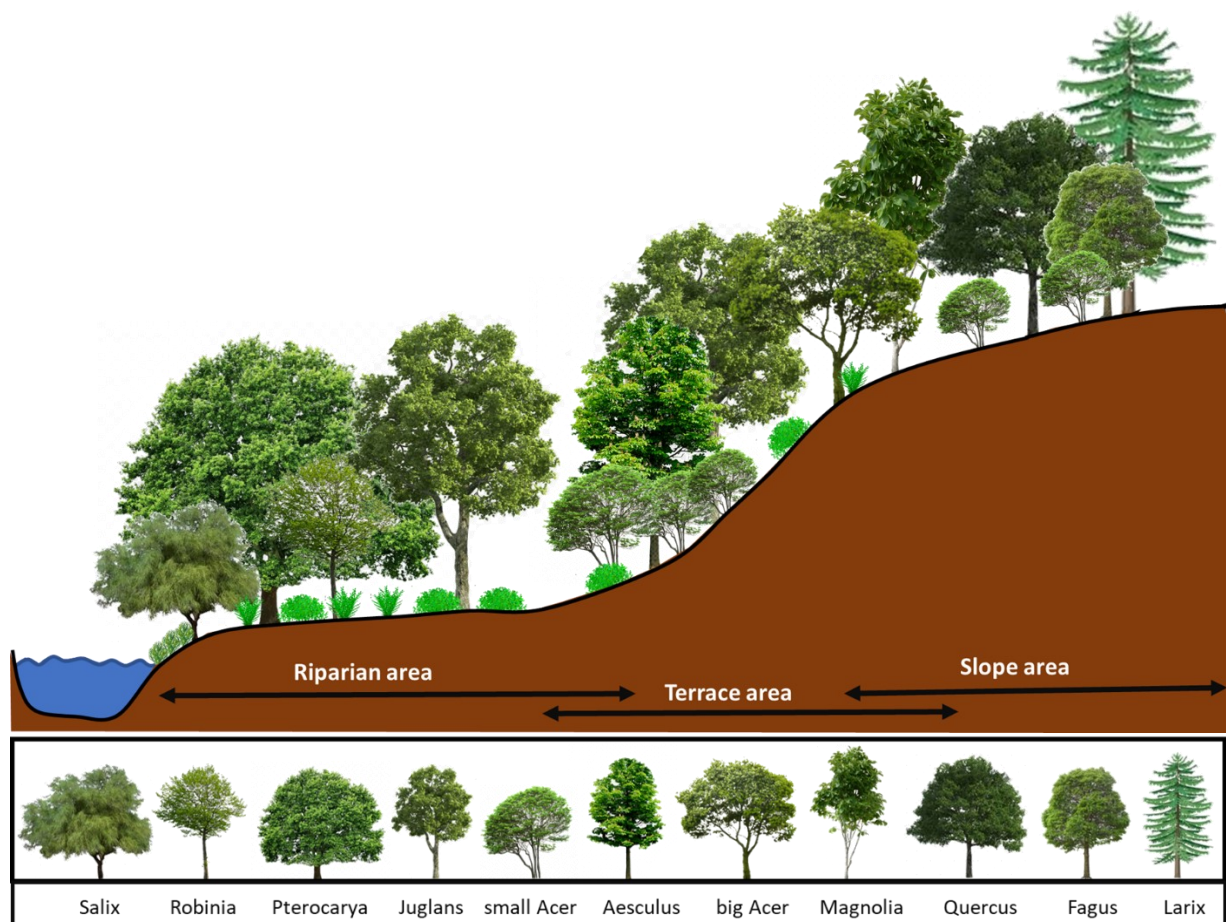


Figure 98 Forest profile with characteristic tree distribution

In riparian areas, *Juglans ailantifolia*, *Pterocarya rhoifolia* and *Salix* species were prominent. *Salix* species always occurred close to water sources, directly at the river or, like in site 6, further away but in a depression (Distribution map – Appendix I). *Pterocarya rhoifolia* trees were identified as dominant and resistant disturbances, so they grew along the river, where most disturbances in riparian areas happen (Suzuki, 2002). One minor species is added here, as *Robinia pseudoacacia* is an invasive species and therefore the occurrence in the natural forest should be observed. Additionally, the distribution of the species was also mainly along the river, but its ability to adapt to several kind of environments and stress saturations allowed the *Robinia* trees to grow well in the riparian forest. *Juglans ailantifolia*

trees dominated Riparian and Terrace sites (reasons discussed in chapter: **Field surveys**). There was an overlap between Riparian and Terrace sites, which means that species from the riparian area could distribute in the terrace area and the other way round. Furthermore, the high number of small-leaved *Acer* species at the bottom of the slopes was also found to be characteristic (Chapter: **field surveys and image analysis**). The identified species in lower slope parts were small-leaved *Acer*, *Juglans ailantifolia*, *Aesculus turbinata*, *Acer mono maxim* and *Magnolia obovata*. Their occurrence was mainly clustered, which is the result of seed spreading in low distances from their adult tree. *Aesculus turbinata* occurred in medium elevations, *Magnolia obovata* in higher elevation areas and *Acer mono maxim* had a tendency to occur in both regions, as it is shown in Figure 98. *Quercus mongolica*, *Fagus crenata* and *Larix kaempferi*, together with small-leaved *Acer* occurred mainly in higher elevations, with increasing numbers. *Larix kaempferi* was also planted in riparian areas, but this was not considered, as the focus was on natural forest compositions. Generally, the species in the slope areas were mixed containing riparian and terrace species. Furthermore, the shrub vegetation was identified to decrease from the riparian to the higher elevated forest areas, but it had to be considered that shrub and understory layer of the forests could only partially be studied from the images, as well as the challenging terrain hampered field work and therefore contain less information about these layers.

Field and image data together with the added image analyses revealed information about the occurrence, location and distribution of trees. When tree species were identified and their distribution characterised, additional information were needed. Studies of single tree species, as in [Niiyama \(1990\)](#), [Azami \(2004\)](#) or [Sakio et al. \(2002\)](#), can then help to understand the composition and distribution of species in the forest. Studying the spatial and temporal variables, especially light transmittance to the forest floor, enables forecasts about densities and stand structures and further about the composition of the understory vegetation ([Sercu et al., 2017](#)). In comparison to the study of [Nakamura et al. \(1997\)](#), who studied distances and elevation from the river and combined them with soil texture and moisture analysis to identify changes in tree species compositions, image data and GIS tools can assess and map all information faster. Therefore, a combination of both, image and field data, will help to understand the distribution of tree species in mixed forests.

8.8 Species diversities, disturbances and coexistence in Japanese forests

In this study, diversity indices were combined with field data and image data to provide measures of diversity for the studied mixed natural forest. This chapter discusses species diversities by comparing

the calculated diversities based on image and field data, then in the context of tree species compositions, and lastly distributions and disturbances in Japanese forests.

There were differences between the diversity results of the field data and the image data. Generally, the diversity values were lower for the image data. The lowest and highest values ranged between 2.14 and 2.76 for the field data and between 1.73 and 2.39 for the image data. The comparison of the evenness values showed the same trend as the diversity values. The field data provided more information regarding the understory vegetation with higher numbers of trees per species, but also more different tree species. A second calculation of diversity and evenness values was performed based on the field data, but excluding the understory vegetation, there the range of diversity values was more similar to the ones calculated with the image data. The values per site were, without the understory vegetation, slightly lower, because not all understory vegetations were imaged. On the other side, the higher diversities and evenness calculated with the field data can be explained by the understory vegetation and shrubs that are not visible in the images. In addition, the results of the Riparian sites varied significantly, as site 6 was assigned a low diversity, compared to sites 1 and 7, while it was the highest in all sites for the calculated field diversities. These differences must be the result of the influence of species richness and evenness, represented by the Shannon diversity index. The evenness in the image data was 20 % lower than in the field data, especially in site 4, which was most probably the result of the numbers of identified understory vegetation. The higher evenness significantly influenced the Shannon diversity. Also, site 6 reached higher diversity and evenness values after the exclusion of understory vegetations, except *Morus australis*, *Celtis jessoensis*, *Styrax obassia* and *Tilia maximowiczina*. The Slope sites were more similar, as in the field and in the images understory vegetation stayed unidentified, and the Terrace sites presented the most similar results, when the understory vegetation was not included. The question arose, if these differences were significant, and if image data could not be used for diversity measures. Therefore, the following paragraphs discuss other studies and the important aspects for species diversities. The relation between diversities, richness and species dominances as well as distribution was evaluated and compared with the results of this study, too.

[Azami et al. \(2004\)](#) studied flood control on riparian plant communities by conducting field surveys, identifying dominant species and plant distributions. Vegetations in the study area were examined and compared with diversity measurements. Diversities were found to be larger downstream than close to the dam. They found physical changes to be an important factor in the development of riparian forests: changes in soil moisture, frequency and intensity of disturbances and changes in the topography. A stronger influence of disturbances on species richness and diversity was further found out by [Takafumi & Hiura \(2009\)](#). Conversely it was identified for understory vegetation plants. The behaviour of

understory plants could not be studied with the results provided by the image analysis but there were sites, like sites 1, 3, 6 and 10, where disturbances were more likely because of erosion and flooding, and the species richness was high.

An increase in bamboo was correlated with a reduction of all other plant species, according to [Nagaike \(1998\)](#). In the Riparian sites, especially in sites 6 and 7, a high density of bamboo was found, which was identified to be the reason for a lower number of shrubs and understory vegetations. A significant correlation between the occurrence of bamboo and species richness and diversity and could not be identified by [Nagaike \(1998\)](#), it could also not be supported by the results in YURF. Furthermore, [Nagaike \(1998\)](#) explained that species diversity is less affected by logging or other forest managements, but the number and frequency of different species occurrences can vary in different stands. Invasive species occurred rarely, as in the YURF sites 1, 4, 6 and 7, where black locust invaded the Riparian sites. [Suzuki et al. \(2002\)](#) described riparian forests as refuge; where infrequent species can live in unstable sites and usually only contain a small number of trees, as a result of competition. Disturbance systems were identified to be the main factor, higher diversities in Riparian sites than in Terrace sites or even upland forests. In YURF, the Riparian sites, as well as the Slope sites, had high diversities. Sites 1, 7 and 12 had high diversities; however, the Slope sites 5, 8, 9 and 10 had even higher values. The reason might be that some parts of the Slope sites were in riparian areas and hence connected low and high elevations, where different water availabilities, topographic conditions, nutrients, competitions and climate conditions occurred. Furthermore, [Suzuki et al. \(2002\)](#) rose that there was a spatial correlation between higher diversities and increasing plot sizes in riparian areas. The sites were usually single islands along the river, which were not connected and all of them showed specific characteristics, along with different evenness and diversities. Also, it was more likely that Riparian sites are affected by disturbances, which was already identified by the occurrence of young trees close to rivers. [Nagaike \(1998\)](#) measured species diversities in beech forests in central Japan and the effects of logging. The authors concluded that stand structures affect diversities of forest more than logging does. Furthermore, a positive relation between the relative frequency of understory and shrub occurrences was identified, with increasing space in the forests. In YURF, sites 2 and 3 had large patches of the forest occupied by small-leaved *Acer* species. Those areas were less dominated by tall trees, as the conditions seemed to be not good enough for them or the competition might be high.

The mentioned studies show that there are many factors influencing tree species richness, mainly as a result of disturbances and competition. Further it was evaluated, that understory vegetations vary significantly in different areas and with different site characteristics. Most understory vegetations could not be identified from images, representing a large component of the forest that could not be evaluated. Therefore, field data need to be collected to complete image data. Nevertheless, the

species richness of canopy and subcanopy species can be evaluated and they also have a significant influence on the diversity and evenness of the forest. Also, stand structures significantly influence both, canopy and understory layer of the forest, and canopy structures significantly influence understory vegetations. Therefore, solid interpretations can be drawn from the images. The studied sites presented the highest differences between image and field data, when Riparian sites were observed, related to the high species richness and the varying species composition along the river, influenced by many factors mentioned above. At last, it was observed, that the numbers of tree stems and the canopy area of the species can vary significantly. Therefore, the influence of the species and their contribution to the diversity and especially evenness would be different, when canopy areas are considered. It can be assumed that diversity measurements have problems identifying those forest characteristics, as they are calculated values based on tree numbers with no further information.

The results of diversity and evenness measurements from image data can help to identify species diversities on a larger scale, when only canopy and subcanopy species are studied. For an overall view, field data must be gathered, as only those provide the detailed numbers and species compositions. Diversity and evenness values do not provide an overall view either, but they assigned simple values to different forests for better comparisons. In this sense, image data can be used with leading to similar results than field data. In the end, the purpose and the requirements decide whether image data provides enough information or intensive field surveys are necessary.

8.9 Forest classification bases on images and field surveys

In this work, two classifications of the study sites were performed: one based on the manual annotations made in images and one based on field surveys; once using the canopy area and once tree counting. Both results will be compared in this chapter, as it is necessary to point out similarities and differences to evaluate the use of both methodologies.

Site 1 was classified as a mixed forest composed of *Juglans ailantifolia* and *Pterocarya rhoifolia*. Also, sites 4 and 7 were classified as 'Japanese walnut forests', while the image analyses indicated that willows belonged to the subspecies of site 4, it was a co-dominant species when the field survey was the basis. Furthermore, site 6 had *Juglans ailantifolia* as dominant tree species, determined by both methodologies, but the field survey indicated *Pterocarya rhoifolia* as co-dominant species. The differences were based on tree counts and canopy sizes. In sites 6 and 7, tree stems numbers of *Pterocarya rhoifolia* were higher in field surveys due to the occurrence of many young trees. The high stem number of *Salix serissaefolia* made the tree co-dominant after field surveys, but the canopy area of them was small, compared to *Juglans ailantifolia* (Appendix I). The field surveys provided in general

better information regarding the *Acer* species, as *Acer palmatum*, *japonicum* and *sieboldianum* could be distinguished. Furthermore, the stem numbers of *Robinia pseudoacacia* and *Aesculus turbinata* were high in sites 4 and 6, but the canopy area of the species was that low, that the species was not counted on images.

The Terrace sites were all classified as 'Japanese walnut mixed forest', on both basis, image and field surveys. The mosaic of different tree species, when the 95 % boundary was calculated, was different between both methodologies. One main point was that there were 12, 18 and 17 different tree species identified in the images, but 29, 20 and 20 in the field for sites 11, 12 and 13. A large number of these species belong to the understory or shrub layer. Another point was that there were several small trees counted in the Terrace sites. Species like *Juglans ailantifolia* and *Pterocarya rhoifolia* had juvenile trees in the lower part of the slopes, while *Acer mono maxim*, *Aesculus turbinata* and *Quercus mongolica* had juvenile trees on the top part of the slope. Those trees were usually also not visible in summer images and are therefore not counted into the canopy area.

For the Slope sites, only sites 3, 8/9 and 10 could be compared as field surveys were conducted for them. The difference between the inventories (image/field) was that trees classified during field work were gathered along paths, while the image classification considered the whole study site. In site 3, *Acer* species, *Juglans ailantifolia* and *Quercus mongolica* were dominant in the images, as well as in the field surveys. When the image analysis of sites 8 and 9 were combined, the dominant tree species were *Acer mono maxim* and small-leaved *Acer* species, with the subspecies *Juglans ailantifolia*, *Quercus mongolica*, *Hamamelis japonica*, *Corylus sieboldiana* and *Magnolia obovata*. *Acer* trees were in both classifications the most frequent ones, but the field data counted more small-leaved *Acer* and the images more big-leaved *Acer*. The reason is that often small-leaved *Acer* were covered by large trees, also sometimes during the field work. A large patch of *Hamamelis japonica* was found in the images, which was not identified during the field surveys. In site 10, *Acer mono maxim* was identified as dominant in the images together with *Magnolia obovata*, while the field data named only *Acer mono maxim* as dominant species. An interesting aspect observed here were that *Quercus mongolica* had smaller areas in the orthomosaics but higher numbers in the field, and *Fagus crenata* was one of the dominant species in the field, while it occurred less frequent in the orthomosaic. The reason might be that *Fagus crenata* often was small-sized, as the climate conditions are not ideal for the species.

The different considered areas must have influenced the counting significantly, as already pointed out by [Bravo-Oviedo et al. \(2014\)](#). The distribution map of site 3 shows the location of small-leaved *Acer* species or *Quercus mongolica*. The black line illustrates the walk path through the forest (Figure 99). Hence, mainly these species were identified in the field. Also, in the distribution maps of sites 8 and 9

large areas of the forest are covered with *Quercus mongolica* and small-leaved *Acer*. The area, where most small-leaved *Acer* was found in site 8, was located in a small riverbed.

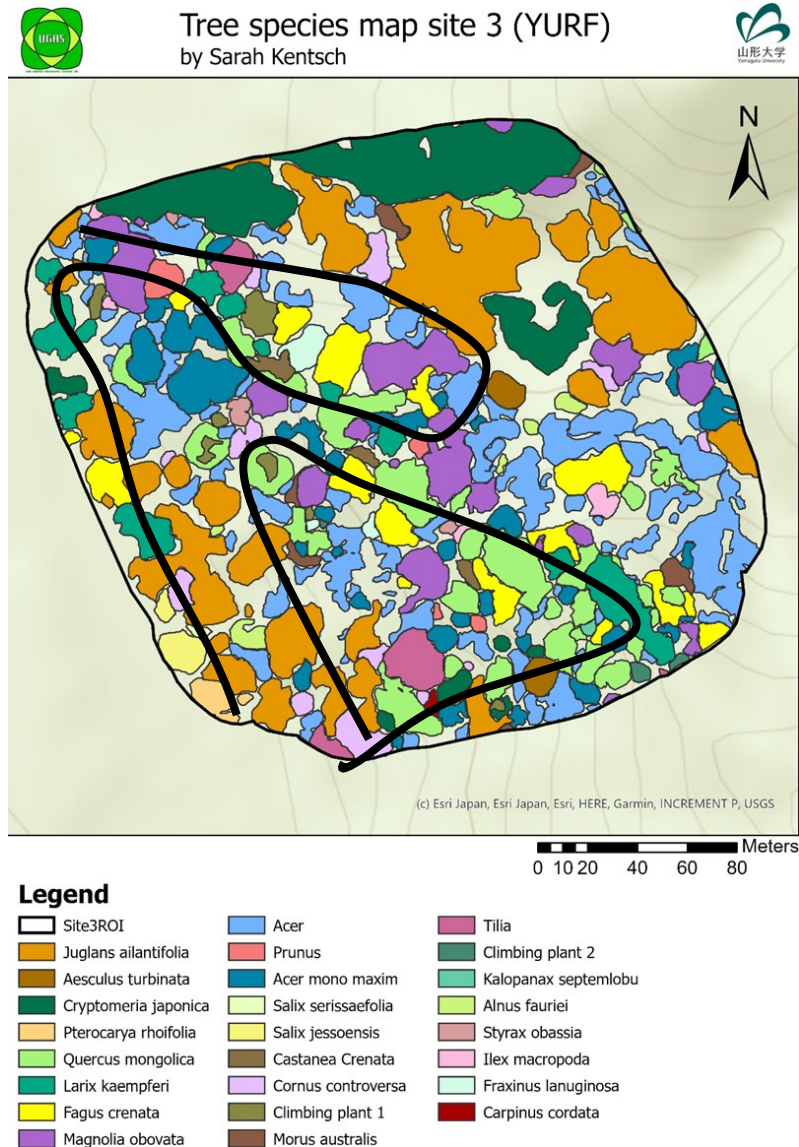


Figure 99 Walk path for the field inventory in site 3

The comparison showed that the dominant tree species could be captured in the Riparian and Terrace sites, while they differed when field and image data were compared in the Slope sites. When only canopy species and subcanopy species were used for the classification, the overlap between image and field data was better. Still, the Slope sites were difficult, because of different included areas in the field and image data.

8.10 Mixed forest classification

In the methodology chapter, different approaches of classifying forests were introduced. The most interesting study was conducted by [Bravo-Oviedo et al. \(2014\)](#). The main concerns were that there is no harmonised universal definition of mixed forests or lists of important aspects to classify them. In their study a definition was proposed, including at least two species, quantifying the proportion of the species (with stem number, basal area, volume or canopy area, e.g.) and considering proportions and patterns of mixture. All classification approaches were mentioned its benefits and difficulties. So, describing the structure of a mixed stand, horizontally and vertically spatial patterns were evaluated as important, while composition examinations do not consider all structures. Functional properties, which would increase the understanding of a mixed forest with its classification, are usually hard to measure, as several aspects can be taken into account, like shade-tolerances, rooting, crown architectures and litter. Measurements of canopy area, volumes and basal areas were identified as insufficient because measuring techniques differ. The considered survey area further influences the variability of stand mixtures.

As consequence, there is no standardised protocol to conduct field surveys or to identify tree compositions and forest structures. In general, compositions and structures are the easiest features of the forest, which can be evaluated to describe forest mixtures. The mixed forest studied in YURF showed that different characteristics identified in the Riparian or Slope forests within the same forest indicated the different developments of the sites. Especially, constantly disturbed Riparian forests make classification approaches challenging, because the composition changes fast. This further raised the need of adding a spatial scale and the need to identify patterns in the forest. The studied methodology can be used as the standardised classification protocol. The gathering of orthomosaics automatically scales to the studied area, or a scale can be set-up before image collection. In YURF, Riparian areas could be imaged using a cover area of approximately 3 ha, which also fit well for the Terrace sites. For Slope sites an area of 5 ha might be more appropriate, because of the higher variety of species. In the studied area, relief, climate and soil conditions enhanced the high number of species that can grow in all different areas. A low spatial scale seemed to be appropriate for those fast changing forests, to capture the needed information. Development stages and disturbance regimes can be characterised to understand the forest ecosystem and its changes in the future. In forests, where the degree of mixture or the stand conditions are homogeneous, a larger study scale will be appropriate.

It was further found out that counting of trees is not sufficient in natural mixed mountain forests. GIS applications or simple pixel counting codes can be used to assess the canopy area of each tree species, from which dominances can be calculated, as performed in this study. The manual annotations can be replaced by automatic classifications, which then provide the composition of tree species, in a short

amount of time. The fast and easy gathering of data, performed with this study and the indication, that automatic tree species classification can be performed, results in an efficient methodology to acquire enough data to classify forests with new scales. With knowledge about forests and tree species, a vertical component can be added, as canopy, subcanopy and understory vegetation could be identified from images. Additionally, field data gathered about the age and occurring shrubs and understory vegetation that were not visible from above can be added afterwards, but are not needed for a simple and easy classification of mixed forests.

[Bravo-Oviedo et al. \(2014\)](#) stated that the dimensions of the forest need to be assessed, which can be done with orthomosaics. The second raised point had been to assess the development stage, which is possible from images, as young trees and old-growth forest areas could be identified in the studied YURF sites. The third point was the occurrence and intensity of tree mixtures, which was analysed with GIS applications, as shown in the previous chapters. A temporal aspect can be added, as image taking can be performed once or several times, depending on the purpose. The fourth point was to identify and evaluate main drivers of the forest ecosystem. Drivers of species occurrences in forest ecosystems are species interactions, climatic and sites conditions, seedling dispersal and strategies, niche differentiation and competition, to mention only a couple of them. Using these drivers to assess the functioning of species would hamper a standardized classification strategy.

The studied methodology allows simple and fast classifications, applicable in all areas around the world. Classifying forests in development stages, horizontal and vertical or even functional structures are interesting and add an important aspect. However, different applied methodologies and characterisations make standardised classification approaches for mixed forests difficult. Therefore, using compositional features of the forest generated from manual or automatic classifications of forest images, including knowledge about forests and tree species, is an easy to apply methodology to classify mixed forests.

8.11 Automatic classification

8.11.1 Data issues

Minimizing errors for visual interpretations of images are on the one hand field data. Forest inventories provide essential information of tree species, stem locations, tree height and DBH, which can be partially used for checking manual annotations ([Schiefer et al., 2020](#)). In dense forests, the combination of field and image data is challenging and sometimes not possible. Therefore, on the other hand high resolution images can be used, which allow a better visual interpretation of the data, as performed in

this study. If parts of orthomosaics were blurred or the identification was difficult because of low spatial resolutions, these images could help to increase annotation performances. In this case, reference data for automatic classification can be produced faster and with less errors (Schiefer et al. 2020). CNNs sometimes are even able to overcome human errors in labelling reference data (Hamdi et al., 2019), as it was found for the blueberry annotations, where some smaller bushes were overseen during annotation, but the CNN was able to detect them.

Imbalances in data were identified in all studied natural environments. Tree species classification with the low overall accuracies provided the strongest influence of data imbalance, with 13 considered classes, while the reduction to six classes resulted in increased accuracy values. Grouping species into genus classes was already applied by Schiefer et al. (2020), who grouped *Acer*, *Tilia*, and *Quercus*, as they were less representative in the dataset and achieved better performances of the network. The total agreement of 90.8 % for the black locust class in the coastal forest was higher, however only two classes were considered. Highest accuracies could only be reached with low sensitivity or specificity. The imbalance in the blueberry data had a strong effect on the FPR and accuracy, where low FPR implied high accuracies. When all blueberry patches are misclassified, still the accuracy reaches 97 % with a low FPR, as only 2.53 % of the patches contained blueberry bushes. Therefore, setting values for good results is necessary to provide useful insights into the automatic classification. Good results in the blueberry application were indicated to have high TPR (> 90 %), while at the same time the FPR was low (< 2 %). Absolute numbers of FP need to be higher than TP (Cabezas et al., 2020). Presented results demonstrated that unfrozen networks perform better than frozen ones, as frozen ones seem to have a problem detecting the blueberry patches with a TPR of lower than 60 %, which makes them unsuitable for the desired application.

Egli and Höpke (2020) raised an important aspect of data collection for automatic classification. When DL applications are used spatial patterns have to be considered, like light conditions, weather and seasonal aspects influencing tree characteristics. For the classification of blueberry bushes and black locusts, only one-time images were taken, which might have had an impact on the classification accuracy. When the blueberry data were gathered, it was already late afternoon and detecting blueberry bushes became challenging, because they were covered by long shadows. For the evergreen and deciduous trees (winter images) and the tree species classification, data from one season were used, but always from several days within one season. This increases classification accuracies, according to Egli and Höpke (2020). Furthermore, the authors indicated that spatial resolutions are another important aspect when classifying tree species. Decreasing spatial resolution causes a logarithmic decrease of CNNs classification accuracy, which was also stated by Fassnacht et al. (2016) and Schiefer et al. (2020). Schiefer et al. (2020) further suggested testing CNNs to assess the influence

on spatial resolutions, forest characteristics, site conditions and stand structures for tree species classification. The imaged forest sites in YURF provided the desired characteristics, and with the future progress of the study, spatial resolutions for tree species classification can increase. The naturally different resolutions in the dataset and additionally the collected seasonal images provide interesting insights for automatic tree species classification.

8.11.2 Comparison of deep learning setting and architectures

In the study of classifying evergreen and deciduous trees in winter orthomosaics, transfer learning significantly increased classification accuracies. Also, the study of identifying black locust trees showed better performances when transfer learning was applied, while the performance did not increase significantly in the blueberry study. Although the trained networks obtained high accuracy values, they did not provide sufficiently high blueberry TPR and seemed not to work well on imbalanced datasets. Furthermore, [Shirokikh et al. \(2020\)](#) explained by only training the final layer, the network cannot properly adapt to the domain differences between the ImageNet dataset and the used network. Other studies showed the better performance of transfer learning in comparison to full-trained networks ([Sharma & Mehra, 2018](#); [Kim et al., 2018](#); [Tajbakhsh et al., 2016](#)). Approaches using ResNet-50 in combination with transfer learning have been successfully applied to different fields, like [Rezente et. al \(2017\)](#), who showed the efficiency of the technique in the field of malicious software by reaching classification accuracies of 98.62 %. ResNet-50 as base model trained with the ImageNet database can be used successfully and outperform hand-extracted features. [Ahmad et. al \(2019\)](#) showed the best performance of ResNet in comparison to AlexNet and GoogleNet by using transfer learning tasks. Long computing times, high memory resources and a high amount of data further increased the need of transfer learning, especially when dealing with small amounts of training datasets, which reduced significantly the computing time and reached high accuracies ([George et al., 2017](#)).

In the study of [Schiefer et al. \(2020\)](#), data augmentation was applied to increase size and variance in the training dataset, which was found out to reduce spatial autocorrelation of their adjacent tiles. While data augmentation was used to increase the data in the blueberry study, where the approach was to increase the infrequent species, [Schiefer et al. \(2020\)](#) mainly applied it to increase the generalisation ability of their CNN. The generalisation power of the network is important to achieve high overall accuracies ([Natesan et al. 2019](#)). Furthermore, an application of data augmentation can overcome differences between sites, like studied in the tree species classification chapter, where the considered sites had different compositions. [López-Jiménez \(2019\)](#) applied different levels of data augmentation, which was comparable with the study of [Cabezas et al. \(2020\)](#), pointing out that performances of the networks increase significantly, especially for infrequent classes. But [López-](#)

[Jiménez \(2019\)](#) raised that increasing the dataset with real world data might increase performances even more. The gathered data for the tree species classification in YURF had such data available, which was used for the experiments to discuss aspects of naturally enlarged datasets. Still, the identified imbalance in the YURF dataset with tree species, containing only a small number of trees, needs applications like data augmentation or loss function weighting.

The comparison of the architectures in the blueberry application showed that *UNFNOA* and *UNFW* networks identified 65 % of the blueberry bushes. Further, FP was detected with only 0.2 %, so that blueberry bushes could be identified correctly. Otherwise, when all blueberry bushes needed to be detected, *UNFHA* network identified 93 % of them, but added 1.77 % FP ([Cabezas et al., 2020](#)). Here, the testing of different networks, achieving different results, can be applied for different tasks. The detection of an invasive species is necessary to prevent a further spread, so all bushes needed to be identified; hence it did not matter if there was a blueberry bush or misclassified red soil. In other applications, like estimating biomass for timber prices of a specific tree species, the number of correctly classified trees has a greater importance. Here, the estimated biomass might be smaller, which might result in a higher price for timber when more trees were found in the forest afterwards. Furthermore, comparing networks allowed to evaluate performances and study training times. Larger and deeper networks usually show a higher training time, which was shown in [Cabezas et al. \(2020\)](#). The presented results showed that AlexNet needed 8 minutes, but was not successful in identifying blueberry bushes. ResNet50, a medium size network needed 25 minutes and wideResNet more than 3 hours. Best accuracies were reached with Densenet and ResNet50 networks, while best overall results were obtained by ResNeXt (TPR = 93.75, Acc = 98.11) followed by ResNet50, ResNet152, Densenet and wideResNet. This shows that, before applying DL networks, architectures need to be selected carefully with an assessment on the needed results. Comparison of networks and their performance was studied before, like in [Diez et al. \(2020\)](#), [Zhao et al. \(2018\)](#) and [Fromm et al. \(2019\)](#). In [Diez et al. \(2020\)](#) a comparison of detection algorithms was performed to evaluate tree top detection, in [Zhao et al. \(2018\)](#) a developed algorithm was compared with the state-of-the-art DL networks and [Fromm et al. \(2019\)](#) compared detection networks (Faster R-CNN, R-FCN and SSD). The comparison provided in chapter 6.1 between ResNet50 and UNet further showed that a comparison of networks is necessary to find suitable networks for the desired application.

Aspects like transfer learning, data augmentation or loss function weighting need to be considered in different applications, but the meaningfulness of an application needs to be discussed. But also, the used networks are from main importance when automatic classification want to be performed. In the end, applying DL techniques in natural environment are challenging due to the versatile characteristics of the forest but to find the DL model, which suits the application the best.

Chapter 9 Conclusion

This thesis combined the research fields of forestry, geoinformatics and computer sciences. The combination of forestry and DL has developed fast in recent years. Classifying tree species automatically is still a challenging task and studies in natural environments, especially in mixed forests, are rare. This study is one of the first ones using DL techniques in Japanese mixed forests. The study area with 13 sites is large and was imaged over different seasons to provide a complete view on the forest. With 70 identified tree species in the field and 41 species identified on orthomosaics, the study exceeds previous works focussing on usually four different tree species.

Field inventories allowed to study the forest structure and composition well, while significant insights about the distribution could not be provided well. Furthermore, the demand of man-power and time made the analyses insufficient, but at the same time necessary, when all layers of the forest need to be studied. This analysis enables to assess forest vertical structures and the composition of the forest.

Image information, based on tree top counting or area calculations, provided useful insight, by calculating diversity indices, densities, frequencies, abundances and dominances. The benefit of these studies was that forests can be characterised and compared using a simple value instead of a large amount of data. Image analyses used only species, which were visible from above, while field data contained all information of the forest and its layers. The higher amount of data of the field studies enhanced the difficulties of handling the data, while the image data focussed on the species, which dominated most of the forest area. Even though the analyses indicated significant differences between the sites, detailed analyses cannot be performed with those data. Also, the main aspect to evaluate are plant compositions with some insights into the distribution. Forest or environment structures cannot be extracted.

For evaluating forests from images, it was pointed out that canopy areas should be used, as areas of the canopy, subcanopy and some of the understory layer can be captured on images and relatively easy annotated with GIS or image manipulating software. Counting in summer images in mixed broad-leaved forests was found to be insufficient, as dense canopy areas mislead detections. Counting trees from winter images was found to be a sufficient method for Japanese mountain forests, enabling the assessment of tree numbers and densities in the forest (distribution), while the stems cannot be classified through winter images. Therefore, compositions cannot be evaluated, while the distribution and lateral structure can.

This study provided a methodology for assessing forest ecosystems with low-cost UAVs and low time demanding image analyses. The provided methodology extracted information about the forest composition, distribution and structure and even exceeded field inventory data. With the gathered

data, mixed forests were classified and the forests were named, which was not done before, whereby field and image data provided mostly the same results. The studied Riparian and Terrace sites were mainly classified as Japanese walnut forests, with varying subdominant species. While Japanese wingnuts and willows were subdominant in the Riparian sites, Terrace sites showed a higher variation with mainly maple species and horse-chestnuts. In the field Slope sites were classified as maple and oak forests with mainly beech as subspecies, while image analyses classified most sites as mix of Japanese walnuts with magnolia and maple species.

The DL part of the study should overcome time-consuming manual annotation of image data, to increase the study area. The study provided significant insights into the classification of plant species in natural environments. Even though automatic tree species classification has not been finished, the first results were promising and the provided examples of deciduous vs. evergreen and the study of invasive species indicated the practical application of the studied methodology. It was assessed that those automatic classifications can be applied reaching high accuracies, while significantly reducing the time for generating annotations. Still, the network needed a large number of training examples and several setting. The number of studies has to increase, data need to be publicly available and the methodology needs to be adapted to become a consumer application.

All in all, the study introduced a new methodology of evaluating forest and other natural ecosystems with state-of-the-art GIS and DL technologies allowing to characterise compositions, distributions and structures. The introduced methodology, using UAV and image analyses, can further be used as a standardised tool for classifying mixed forests world-wide.

VIII. Reference list

- Abd Mubin, N., Nadarajoo, E., Shafri, H., Hamedianfar, A. (2019): Young and mature oil palm tree detection and counting using convolutional neural network deep learning method. *International Journal of Remote Sensing*. 40. 10.1080/01431161.2019.1569282.
- Agisoft. Agisoft Metashape 1.5.5, Professional Edition, <http://www.agisoft.com/downloads/installer/>, Accessed: 2019-08-19.
- Ahmad, H. M., Ghuffar, S., Khurshid, K. (2019): Classification of Breast Cancer Histology Images Using Transfer Learning, 2019 16th International Bhurban Conference on Applied Sciences and Technology (IBCAST), Islamabad, Pakistan, pp. 328-332, doi: 10.1109/IBCAST.2019.8667221.
- Allendorf, F., & Lundquist, L. (2003): Introduction: Population Biology, Evolution, and Control of Invasive Species. *Conservation Biology*, 17(1), 24-30. Retrieved January 16, 2021, from <http://www.jstor.org/stable/3095269>.
- Anderegg, W., Anderegg, L., Kerr, K., Trugman, A. (2019): Widespread drought - induced tree mortality at dry range edges indicates climate stress exceeds species' compensating mechanisms. *Global Change Biology*. 25. 10.1111/gcb.14771.
- Ashqar, B., Abu-Naser, S. (2019): Identifying Images of Invasive Hydrangea Using Pre-Trained Deep Convolutional Neural Networks. *International Journal for Academic Development*. 3. 10.33832/ijca.2019.12.4.02.
- Asner G. P., Hicke J. A., Lobell D. B. (2003): Per-Pixel Analysis of Forest Structure. In: Wulder M.A., Franklin S.E. (eds) *Remote Sensing of Forest Environments*. Springer, Boston, MA. https://doi.org/10.1007/978-1-4615-0306-4_8.
- Baeten, L., Verheyen, K., Wirth, C., Bruelheide, H., Bussotti, F., Finér, L., Jaroszewicz, B., Selvi, F., Valladares, F., Allan, E., et al. (2013), A novel comparative research platform designed to determine the functional significance of tree species diversity in European forests, *Perspectives in Plant Ecology, Evolution and Systematics*, Volume 15, Issue 5, Pages 281-291, ISSN 1433-8319, <https://doi.org/10.1016/j.ppees.2013.07.002>.
- Beucher, S., Meyer, F. (1993): The Morphological Approach to Segmentation: The Watershed Transformation. 10.1201/9781482277234-12.

Boon, M., Greenfield, R., Tesfamichael, S. (2016): Wetland assessment using unmanned aerial vehicles (UAV) Photogrammetry. ISPRS - International Archives of the Photogrammetry, Remote Sensing and Spatial Information Sciences. XLI-B1. 781-788. [10.5194/isprs-archives-XLI-B1-781-2016](https://doi.org/10.5194/isprs-archives-XLI-B1-781-2016).

Boon, M., Greenfield, R., Tesfamichael, S. (2016): Unmanned Aerial Vehicle (UAV) photogrammetry produces accurate high-resolution orthophotos, point clouds and surface models for mapping wetlands. South African Journal of Geomatics. 5. 186. [10.4314/sajg.v5i2.7](https://doi.org/10.4314/sajg.v5i2.7).

Bradski, G. (2000): The OpenCV Library. Dr. Dobb's J. Softw. Tools 2000. Volume 25, pp. 120–125.

Bravo-Oviedo, A., Pretzsch, H., Ammer, C., Andenmatten, E., Barbati, A., Barreiro, S., Brang, P., Bravo, F., Coll, L., Corona, P., Ouden, J. (2014): European Mixed Forests: Definition and research perspectives. Forest Systems. 23.

Cabezas, M., Kentsch, S., Tomhave, L., Gross, J., Caceres, M.L.L., Diez, Y. (2020): Detection of Invasive Species in Wetlands: Practical DL with Heavily Imbalanced Data. Remote Sens., 12, 3431. <https://doi.org/10.3390/rs12203431>.

Caffrey, J. M., Baars, J. R., Barbour, J. H., Boets, P., Boon, P., Davenport, K., Dick, J. T. A., Early, J., Edsman, L., Gallagher, C., Gross, J., Heinimaa, P., Horrill, C., Hudin, S., Hulme, P. E., Hynes, S., MacIsaac, H. J., McLoone, P., Millane, M., Moen, T. L., Moore, N., Newman, J., O'Conchuir, R., O'Farrell, M., O'Flynn, C., Oidtmann, B., Renals, T., Ricciardi, A., Roy, H., Shaw, R., van Valkenburg, J. L. C. H., Weyl, O., Williams, F., Lucy, F. E. (2014): Tackling Invasive Alien Species in Europe: The Top 20 Issues., Management of biological invasions 5 (1): 1–20.

Caselles, V., Kimmel, R., Sapiro, G. (2005): 4.17 - Geometric Active Contours for Image Segmentation, AL BOVIK, Handbook of Image and Video Processing (Second Edition), Academic Press, Second Edition, Burlington, pages 613 - 627, Communications, Networking and Multimedia, ISBN:978-0-12-119792-6, <https://doi.org/10.1016/B978-012119792-6/50099-1>.

Chadwick, A. J., Goodbody, T. R. H., Coops, N. C., Hervieux, A., Bater, C. W., Martens, L. A., White, B., Röeser, D. (2020): Automatic Delineation and Height Measurement of Regenerating Conifer Crowns under Leaf-Off Conditions Using UAV Imagery. Remote Sens., 12, 4104. <https://doi.org/10.3390/rs12244104>.

Chao, A., Gotelli, N.J., Hsieh, T.C., Sander, E.L., Ma, K.H., Colwell, R.K. and Ellison, A.M. (2014): Rarefaction and extrapolation with Hill numbers: a framework for sampling and estimation in species diversity studies. Ecological Monographs, 84: 45-67. <https://doi.org/10.1890/13-0133.1>.

Chen, I.-C., Hill, J., Ohlemüller, R., Roy, D.B., Thomas, C. (2011): Rapid Range Shifts of Species Associated with High Levels of Climate Warming. *Science* (New York, N.Y.). 333. 1024-6. 10.1126/science.1206432.

Chen, J., Yang, L., Zhang, Y., Alber, M., Chen, D. (2016): Combining Fully Convolutional and Recurrent Neural Networks for 3D Biomedical Image Segmentation.

Coll, L., Ameztegui, A., Collet, C., Löf, M., Mason, B., Pach, M., Verheyen, K., Abrudan, I., Barbati, A., Barreiro, S., Bielak, K., Bravo-Oviedo, A., Ferrari, B., Govedar, Z., Kulhavy, J., Lazdina, D., Metslaid, M., Mohren, G.M.J., Pereira, M., Ponette, Q. (2018): Knowledge gaps about mixed forests: What do European forest managers want to know and what answers can science provide?. *Forest Ecology and Management*. 407. 106-115. 10.1016/j.foreco.2017.10.055.

Culvenor, D. (2002): TIDA: An algorithm for the delineation of tree crowns in high spatial resolution remotely sensed imagery. *Computers & Geosciences - COMPUT GEOSCI*. 28. 33-44. 10.1016/S0098-3004(00)00110-2.

Culvenor, D. S. (2003): Extracting Individual Tree Information. In: Wulder M.A., Franklin S.E. (eds) *Remote Sensing of Forest Environments*. Springer, Boston, MA. https://doi.org/10.1007/978-1-4615-0306-4_9.

Dandois, J. P., Olano, M., Ellis, E. C. (2015): "Optimal Altitude, Overlap, and Weather Conditions for Computer Vision UAV Estimates of Forest Structure" *Remote Sens*. 7, no. 10: 13895-13920. <https://doi.org/10.3390/rs71013895>.

Dash, J. P., Watt, M. S., Pearse, G. D., Heaphy, M., Dungey, H. S. (2017): Assessing very high resolution UAV imagery for monitoring forest health during a simulated disease outbreak, *ISPRS Journal of Photogrammetry and Remote Sensing*, Volume 131, Pages 1-14, ISSN 0924-2716, <https://doi.org/10.1016/j.isprsjprs.2017.07.007>.

Deilmann, H. C., Eichhorn, G., Falkenberg, H., Gü}nther, J., Hayen, H., Kuntze, H., Pollak, E., Schmatzler, E. and Steffens, P. and Tüxen J. (1990): *Moor und Torf in Niedersachsen.*, Niedersächsische Akademie der Geowissenschaften, 5.

Deng, L., Yu, R. (2015): Pest recognition system based on bio-inspired filtering and LCP features, 2015 12th International Computer Conference on Wavelet Active Media Technology and Information Processing (ICCWAMTIP), pages 202-204, doi:10.1109/ICCWAMTIP.2015.7493975.

Didham, R. K., Tylianakis, J. M., Hutchison, M. A., Ewers, R.M., Gemmell, N. J. (2005): Are invasive species the drivers of ecological change?, *Trends in Ecology & Evolution*, Volume 20, Issue 9, Pages 470-474, ISSN 0169-5347, <https://doi.org/10.1016/j.tree.2005.07.006>.

Diez, Y., Kentsch, S., Caceres, M., Nguyen, H., Serrano, D., Roure, F. (2020): Comparison of Algorithms for Tree-top Detection in Drone Image Mosaics of Japanese Mixed Forests. In *Proceedings of the 9th International Conference on Pattern Recognition Applications and Methods - Volume 1: ICPRAM*, ISBN 978-989-758-397-1, pages 75-87. DOI: 10.5220/0009165800750087.

Diez, Y., Kentsch, S., Fukuda, M., Lopez Caceres, L. M., Moritake, K., Cabezas, M. (2021): Deep Learning in Forestry using RGB data: A practical review, *Remote Sensing*. 2021; 13(14):2837. <https://doi.org/10.3390/rs13142837>

DJI Manual (2017): DJI Phantom 4 pro/pro+ Bedienungsanleitung, https://dl.djicdn.com/downloads/phantom_4_pro/20170204/Phantom+4+Pro+Pro+Plus+User+Manual+v1.2+De.pdf.

Dolezal, J., Song, J.-S., Altman, J., Janecek, S., Cerny, T., Srutek, M., Kolbek, J. (2009): Tree growth and competition in a post-logging *Quercus mongolica* forest on Mt. Sobaek, South Korea. *Ecol. Res.*, 24: 281-290. <https://doi.org/10.1007/s11284-008-0505-1>.

Dronova, I. (2015): Object-Based Image Analysis in Wetland Research: A Review. *Remote Sensing*, 7(5):6380-6413.

Dronova, I., Gong, P., Clinton, N., Wang, L., Fu, W., Qi, S., & Liu, Y. (2012): Landscape analysis of wetland plant functional types: The effects of image segmentation scale, vegetation classes and classification methods. *Remote Sensing of Environment*, 127, 357-369.

Georges, D., Masato, K., (2001): Bootstrap re-sampling for unbalanced data in supervised learning, *European Journal of Operational Research*, Volume 134, Issue 1, Pages 141-156, ISSN 0377-2217, [https://doi.org/10.1016/S0377-2217\(00\)00244-7](https://doi.org/10.1016/S0377-2217(00)00244-7).

Dvořák, P., Müllerová, J., Bartaloš, T., and Brůna, J. (2015): Unmanned aerial vehicles for alien plant species detection and monitoring. *The International Archives of the Photogrammetry, Remote Sensing and Spatial Information Sciences*. XL-1/W4. 83-90, <https://doi.org/10.5194/isprsarchives-XL-1-W4-83-2015>.

Egli, S., Höpke, M. (2020): CNN-Based Tree Species Classification Using High Resolution RGB Image Data from Automated UAV Observations. *Remote Sens.*, 12, 3892. <https://doi.org/10.3390/rs12233892>

Erikson, M. (2004): Species classification of individually segmented tree crowns in high-resolution aerial images using radiometric and morphologic image measures. *Remote Sensing of Environment*. 91. 469-477. [10.1016/j.rse.2004.04.006](https://doi.org/10.1016/j.rse.2004.04.006).

Essl, F. (2004): Erstfund eines verwilderten Vorkommens der Kultur-Heidelbeere (*Vaccinium angustifolium* x *corymbosum*) in Österreich., *Linzer biologische Beiträge*.

Esquivel - Muelbert, A., Baker, T.R., Dexter, K.G., Lewis, S. L., Brienen, R. J.W., Feldpausch, T. R., Lloyd, J., Monteagudo - Mendoza, A., Arroyo, L., Álvarez-Dávila, E., Higuchi, N., Marimon, B. S. et al. (2019): Compositional response of Amazon forests to climate change. *Glob Change Biol.*, 25: 39– 56. <https://doi.org/10.1111/gcb.14413>.

Falkowski, M. J., Smith, A. M. S., Gessler, P. E., Hudak, A. T., Vierling, L. A., Evans J. S. (2008): The influence of conifer forest canopy cover on the accuracy of two individual tree measurement algorithms using lidar data, *Canadian Journal of Remote Sensing*, 34:sup2, S338-S350, DOI: 10.5589/m08-055

Fassnacht, F.E., Latifi, H., Stereńczak, K., Modzelewska, A., Lefsky, M., Waser, L.T., et al. (2016): Review of studies on tree species classification from remotely sensed data. *Remote Sens. Environ.* 186: 64–87.

Lateef, F., Ruichek, Y. (2019): Survey on semantic segmentation using deep learning techniques, *Neuro-computing*, Volume 338, Pages 321-348, ISSN 0925-2312, <https://doi.org/10.1016/j.neucom.2019.02.003>.

Ferreira, M. P., de Almeida, D. R. A., de Almeida Papa, D., Silva Minervino, J. B., Pessoa Veras, H. F. et al. (2020): Individual tree detection and species classification of Amazonian palms using UAV images and deep learning, *Forest Ecology and Management*, Volume 475, 118397, ISSN 0378-1127, <https://doi.org/10.1016/j.foreco.2020.118397>.

Forbes, K. and Broadhead, J. (2008): The role of coastal forests in the mitigation of tsunami impacts, RAP publication 2007/1, Food and Agriculture Organization of the United Nations Regional Office for Asia and the Pacific, Bangkok, Thammada Press, ISBN 978-974-13-9321-3.

Fournier R. A., Mailly D., Walter JM. N., Soudani K. (2003): Indirect Measurement of Forest Canopy Structure from In Situ Optical Sensors. In: Wulder M.A., Franklin S.E. (eds) *Remote Sensing of Forest Environments*. Springer, Boston, MA. https://doi.org/10.1007/978-1-4615-0306-4_4.

Franklin, S.E. (2018): Pixel- and object-based multispectral classification of forest tree species from small unmanned aerial vehicles. *J. Unmanned Veh. Syst.* 6(4): 195–211.

- Franklin, S. E., Lavigne, M. B., Deuling, M. J., Wulder, M. A., Hunt Jr, E. R. (1997): Estimation of forest Leaf Area Index using remote sensing and GIS data for modelling net primary production, *International Journal of Remote Sensing*, 18:16, 3459-3471, DOI: 10.1080/014311697216973.
- Frayer, W. E., Furnival, G. M. (1999): Forest Survey Sampling Designs: A History, *Journal of Forestry*, Volume 97, Issue 12, December, Pages 4–10, <https://doi.org/10.1093/jof/97.12.4>.
- Fromm, M., Schubert, M., Castilla, G., Linke, J., McDermid, G. (2019): Automated Detection of Conifer Seedlings in Drone Imagery Using Convolutional Neural Networks. *Remote. Sens.*, 11, 2585, doi:10.3390/rs11212585.
- Fujimoto, A., Haga, C., Matsui, T., Machimura, T., Hayashi, K, Sugita, S., Takagi, H. (2019): An End to End Process Development for UAV-SfM Based Forest Monitoring: Individual Tree Detection, Species Classification and Carbon Dynamics Simulation. *Forests.*, 10(8):680. <https://doi.org/10.3390/f10080680>.
- Fujita, K., Sano, J. (2011): Structure and developmental process of a *Quercus mongolica* var. *grosseserrata* forest in the Fagetea *crenatae* region in Japan. *Canadian Journal of Forest Research*. 30. 1877-1885. 10.1139/x00-119.
- Funke, J., Tschopp, F., Grisaitis, W., Sheridan, A., Singh, C., Saalfeld, S., & Turaga, S.C. (2019): Large Scale Image Segmentation with Structured Loss Based Deep Learning for Connectome Reconstruction. *IEEE Transactions on Pattern Analysis and Machine Intelligence*, 41, 1669-1680., doi: 10.1109/TPAMI.2018.2835450.
- Fukamachi, A. S., Watanabe, N., Hoshino, Y., Yoshikawa, M., Yoshida, T. (2020): Structure and dynamics of a mountain riparian forest at an upstream valley in central Japan. *Ecological Research.*, 35: 1035–1044. <https://doi.org/10.1111/1440-1703.12150>.
- Gadow, K., Zhang, C., Wehenkel, C., Pommerening, A., Corral-Rivas, J. J., Korol, M., Myklush, S., Hui, G., Kiviste, A., Zhao, X. (2012): Forest Structure and Diversity, *Managing Forest Ecosystems*, vol 23. Springer, Dordrecht. https://doi.org/10.1007/978-94-007-2202-6_2.
- Gambella, F., Sistu, L., Piccirilli, D., Corposanto, S., Caria, M., Arcangeletti, E., Proto, A.R., Chessa, G., Pazzona, A. (2016): Forest and UAV: A bibliometric review. *Contemporary Engineering Sciences*. 9. 1359-1370. 10.12988/ces.2016.68130.
- Garcia-Garcia, A., Orts-Escolano, S., Oprea, S., Villena-Martinez, V., Martinez-Gonzalez, P., Garcia-Rodriguez, J. (2018): A survey on deep learning techniques for image and video semantic segmentation,

Applied Soft Computing, Volume 70, Pages 41-65, ISSN 1568-4946, <https://doi.org/10.1016/j.asoc.2018.05.018>.

George, D., Shen, H., Huerta, E. (2017): Deep Transfer Learning: A new deep learning glitch classification method for advanced LIGO.

Giertych, M.J., Karolewski, P., Oleksyn, J. Carbon (2015): Allocation in seedlings of deciduous tree species depends on their shade tolerance. *Acta Physiol Plant* 37, 216 (2015). <https://doi.org/10.1007/s11738-015-1965-x>.

Gini, R., Sona, G., Ronchetti, G., Passoni, D., Pinto, L. (2018): Improving tree species classification using UAS multispectral images and texture measures. *ISPRS Int. J. Geo-Inf.* 7(8): 315.

Gomes-Silva, A., Silva, I., Rodal, M., Lins e Silva, A. C. (2008): Influence of Edge and Topography on Canopy and Sub-canopy Structure of an Atlantic Forest Fragment in Igarassu, Pernambuco State, Brazil, 2., 41 -46.

Goto, S., Hayashida, M. (2008): Seed Dispersal by Rodents and Seedling Establishment of Walnut Trees (*Juglans ailanthifolia*) in a Riparian Forest., *JOURNAL OF THE JAPANESE FORESTRY SOCIETY*, 2002, Volume 84, Issue 1, Pages 1-8, Released May 16, 2008, Online ISSN 2185-8195, Print ISSN 0021-485X, https://doi.org/10.11519/jjfs1953.84.1_1.

Grabska, E., Hostert, P., Pflugmacher, D., Ostapowicz, K. (2019): Forest Stand Species Mapping Using the Sentinel-2 Time Series. *Remote Sensing*. 2019; 11(10):1197. <https://doi.org/10.3390/rs11101197>.

Grant, G. E., Swanson, F. J. (1995): Morphology and Processes of Valley Floors in Mountain Streams, Western Cascades, Oregon. In *Natural and Anthropogenic Influences in Fluvial Geomorphology* (eds J. Costa, A. Miller, K. Potter and P. Wilcock). <https://doi.org/10.1029/GM089p0083>.

Grenzdörffer, G., Teichert, B. (2008): The photogrammetric potential of low-cost UAVs in forestry and agriculture. *Int. Arch. Photogramm. Remote Sens. Spatial Inf. Sci.*. XXXVII.

Grotti, M., Chianucci, F., Puletti, N., Fardusi, M.J., Castaldi, C., Corona, P. (2019): Spatio-temporal variability in structure and diversity in a semi-natural mixed oak-hornbeam floodplain forest. *Ecological Indicators*. 104. 576-587. [10.1016/j.ecolind.2019.04.014](https://doi.org/10.1016/j.ecolind.2019.04.014).

Guimarães, N., Pádua, L., Marques, P., Silva, N., Peres, E., Sousa, J. J. (2020): Forestry Remote Sensing from Unmanned Aerial Vehicles: A Review Focusing on the Data, Processing and Potentialities. *Remote Sens.*, 12, 1046. <https://doi.org/10.3390/rs12061046>.

Guo, Y., Liu, Y., Georgiou, T., Lew, M. (2017): A review of semantic segmentation using deep neural networks. *International Journal of Multimedia Information Retrieval*, 7, 87-93.

Guo, Y., Liu, Y., Oerlemans, A., Lao, S., Wu, S., Lew, M. S. (2016): Deep learning for visual understanding: A review, *Neurocomputing*, Volume 187, Pages 27-48, ISSN 0925-2312, <https://doi.org/10.1016/j.neucom.2015.09.116>.

Guo Z., Zhang, L., Lu, L., Bagheri, M., Summers, M. R., Sonka, M., Yao, J. (2018): Deep LOGISMOS: Deep learning graph-based 3D segmentation of pancreatic tumors on CT scans, 2018 IEEE 15th International Symposium on Biomedical Imaging (ISBI 2018), Washington, DC, USA, pp. 1230-1233, doi: 10.1109/ISBI.2018.8363793.

Gurevitch, J., Padilla, D. K. (2004): Are invasive species a major cause of extinctions?, *Trends in Ecology & Evolution*, Volume 19, Issue 9, Pages 470-474, ISSN 0169-5347, <https://doi.org/10.1016/j.tree.2004.07.005>.

Hall R. J. (2003): The Roles of Aerial Photographs in Forestry Remote Sensing Image Analysis. In: Wulder M.A., Franklin S.E. (eds) *Remote Sensing of Forest Environments*. Springer, Boston, MA. https://doi.org/10.1007/978-1-4615-0306-4_3.

Haq, M. A., Rahaman, G., Baral, P., Ghosh A. (2021): Deep Learning Based Supervised Image Classification Using UAV Images for Forest Areas Classification. *J Indian Soc Remote Sens* 49, 601–606. <https://doi.org/10.1007/s12524-020-01231-3>.

Hamarneh, G., Li, X. (2009): Watershed segmentation using prior shape and appearance knowledge, *Image and Vision Computing*, Volume 27, Issues 1–2, Pages 59-68, ISSN 0262-8856, <https://doi.org/10.1016/j.imavis.2006.10.009>.

Hamdi, Z. M., Brandmeier, M., Straub, C. (2019): Forest Damage Assessment Using Deep Learning on High Resolution Remote Sensing Data. *Remote Sensing*, 11(17):1976. <https://doi.org/10.3390/rs11171976>.

Harshall, L. (2019): Understanding semantic segmentation with UNet, *Understanding Semantic Segmentation with Unet*, latest access 19. August 2019.

Hart, S. A., Chen, H. Y. H. (2006): Understory Vegetation Dynamics of North American Boreal Forests, *Critical Reviews in Plant Sciences*, 25:4, 381-397, DOI: 10.1080/07352680600819286.

He, H., Gracia, E. A. (2009): Learning from Imbalanced Data, *IEEE Transactions on Knowledge and Data Engineering*, 21, 9, pages 1263-1284).

He, K., Zhang, X., Ren, S., Sun, S. (2016): Deep Residual Learning for Image Recognition, *Proceedings of the IEEE Conference on Computer Vision and Pattern Recognition (CVPR)*, 2016, pp. 770-778.

Hedwall, P.-O., Holmström, E., Lindbladh, M., Felton, A. (2019): Concealed by darkness: How stand density can override the biodiversity benefits of mixed forests. *Ecosphere* 10(8):e02835. 10.1002/ecs2.2835.

Heipke, H., Pakzad, K. and Straub, B.M. (2000), Image Analysis for GIS Data Acquisition. *The Photogrammetric Record*, 16: 963-985. doi:10.1111/0031-868X.00160.

Hirano, Y., Todo, C., Yamase, K., Tanikawa, T., Dannoura, M., Ohashi, M., Doi, R., Wada, R., Ikeno, H. (2018): Quantification of the contrasting root systems of *Pinus thunbergii* in soils with different groundwater levels in a coastal forest in Japan. *Plant and Soil*. 426. 1-11. 10.1007/s11104-018-3630-9.

Hollenbach, M. (2014): Verstärktes Vorgehen der Naturschutzbehörde gegen die nordamerikanische Kulturheidelbeere, Niedersächsischer Landesbetrieb für Wasserwirtschaft, Küsten- und Naturschutz, https://www.nlwkn.niedersachsen.de/naturschutz/fach_und_forderprogramme/life/hannoversche_moorgeest/aktuelles_termine/verstaerktes-vorgehen-der-naturschutzbehoerde-gegen-die-nordamerikanische-kulturheidelbeere-126107.html, accessed November 11, 2020.

Hoshizaki, K., Suzuki, W. & Nakashizuka, T. (1999): Evaluation of secondary dispersal in a large-seeded tree *Aesculus turbinata*: a test of directed dispersal. *Plant Ecology* 144, 167–176, <https://doi.org/10.1023/A:1009816111057>.

Huang, Y.-H., Chen, D.-R. (2004): Watershed segmentation for breast tumor in 2-D sonography, *Ultrasound in Medicine & Biology*, Volume 30, Issue 5, Pages 625-632, ISSN 0301-5629, <https://doi.org/10.1016/j.ultrasmedbio.2003.12.001>.

Huang, G., Liu, Z., van der Maaten, L., Weinberger, K. Q. (2016): Densely Connected Convolutional Networks Proceedings of the IEEE Conference on Computer Vision and Pattern Recognition (CVPR), pp. 4700-4708.

Hokusima, T., Matsui, T., Nishio, T., Pignatti, S., Yang, L., Lu, S.-Y., Kim, M.-H., Yoshikawa, M., Honma, H., Wang, Y. (2013): In: *Phytosociology of the Beech (Fagus) Forests in East Asia*. Springer, Heidelberg, 257pp.

Iandola, F., Han, S., Moskewicz, M., Ashraf, K., Dally, W., Keutzer, K. (2016): SqueezeNet: AlexNet-level accuracy with 50x fewer parameters and <0.5MB model size.

Isagi, Y., Kanazashi, T. Suzuki, W., Tanaka, H., Abe, T. (2000): Microsatellite analysis of the regeneration process of *Magnolia obovata* Thunb. *Heredity*. 84 (Pt 2). 143-51.

Ifo, S., Moutsambote, J.-M., Koubouana, F., Yoka, J., Ndzai, S., Bouetou-Kadilamio, L., Mampouya, H., Jourdain, Charlotte & Bocko, Yannick & Mantota, Alima & Mbemba, Mackline & Mouanga-Sokath, Dul-

saint & Odende, Roland & Mondzali, Lenguiya & Wenina, Yeto & Ouissika, Brice & Joel, Loumeto. (2016). Tree Species Diversity, Richness, and Similarity in Intact and Degraded Forest in the Tropical Rainforest of the Congo Basin: Case of the Forest of Likouala in the Republic of Congo. *International Journal of Forestry Research*. 2016. 1-12. [10.1155/2016/7593681](https://doi.org/10.1155/2016/7593681).

Ito, S., Nakayama, R., Buckley, G.P. (2004): Effects of previous land-use on plant species diversity in semi-natural and plantation forests in a warm-temperate region in southeast-ern Kyushu, Japan. *Forest Ecology and Management*, Volume 196, Issues 2–3, pages 213-225, ISSN 0378-1127, <https://doi.org/10.1016/j.foreco.2004.02.050>.

Jacob, M., Leuschner, C., Thomas, F. (2010): Productivity of temperate broad-leaved forest stands differing in tree species diversity. <http://dx.doi.org/10.1051/forest/2010005>. 67. [10.1051/forest/2010005](https://doi.org/10.1051/forest/2010005).

Jiang, K., Liao, Q.-M., Dai, S.-Y. (2003): A novel white blood cell segmentation scheme using scale-space filtering and watershed clustering, *Proceedings of the 2003 International Conference on Machine Learning and Cybernetics (IEEE Cat. No.03EX693)*, Xi'an, China, pp. 2820-2825 Vol.5, doi: [10.1109/ICMLC.2003.1260033](https://doi.org/10.1109/ICMLC.2003.1260033).

Joshi, C. M., de Leeuw, J., & van Duren, I. C. (2004): Remote sensing and GIS applications for mapping and spatial modelling of invasive species. In *ISPRS 2004 : proceedings of the XXth ISPRS congress : Geo-imagery bridging continents, 12-23 July 2004, Istanbul, Turkey*. Comm. VII. pp. 669-677 (pp. 669-677). International Society for Photogrammetry and Remote Sensing (ISPRS). http://www.itc.nl/library/Papers_2004/peer_conf/joshi.pdf

Jost, L. (2006): Entropy and diversity. *Oikos*, 113: 363-375. <https://doi.org/10.1111/j.2006.0030-1299.14714.x>

Jost, L. (2007): Partitioning diversity into independent alpha and beta components. *Ecology*, 88: 2427-2439. <https://doi.org/10.1890/06-1736.1>

Jung, S.-C., Matsushita, N., Wu, B.-Y., Kondo, N., Shiraishi A. & Hogetsu, T. (2009): Reproduction of a *Robinia pseudoacacia* population in a coastal *Pinus thunbergii* windbreak along the Kujukurihama Coast, Japan. *Journal of Forest Research*, 14:2, 101-110, DOI: [10.1007/s10310-008-0109-1](https://doi.org/10.1007/s10310-008-0109-1).

Kamilaris, A., Prenafeta-Boldú, F.- X. (2018): Deep learning in agriculture: A survey, *Computers and Electronics in Agriculture*, Volume 147, Pages 70-90, ISSN 0168-1699, <https://doi.org/10.1016/j.compag.2018.02.016>.

- Kattenborn, T., Eichel, J., Fassnacht, F.E. (2019): Convolutional Neural Networks enable efficient, accurate and fine-grained segmentation of plant species and communities from high-resolution UAV imagery. *Sci Rep* 9, 17656, <https://doi.org/10.1038/s41598-019-53797-9>
- Kattenborn, T., Eichel, J., Wisser, S., Burrows, L., Fassnacht, F. E., Schmidtlein, S. (2020): Convolutional Neural Networks accurately predict cover fractions of plant species and communities in Unmanned Aerial Vehicle imagery. *Remote Sens. Ecol.*, 6: 472-486. <https://doi.org/10.1002/rse2.146>
- Kattenborn, T., Sperlich, M., Bataua, K., Koch, B. (2014): Automatic Single Palm Tree Detection in Plantations using UAV-based Photogrammetric Point Clouds. *ISPRS - International Archives of the Photogrammetry, Remote Sensing and Spatial Information Sciences*. XL-3. 10.5194/isprsarchives-XL-3-139-2014.
- Keller, R., Geist, J., Jeschke, J., Kühn, I. (2011): Invasive species in Europe: Ecology, status, and policy. *Environmental Sciences Europe*. 23. 23. 10.1186/2190-4715-23-23. K2020
- Kentsch, S., Cabezas, M., Tomhave, L., Groß, J., Burkhard, B., Lopez Caceres, M. L., Waki, K., Diez, Y. (2021): Analysis of UAV-Acquired Wetland Orthomosaics Using GIS, Computer Vision, Computational Topology and Deep Learning. *Sensors*; 21(2):471. <https://doi.org/10.3390/s21020471>.
- Kentsch, S., Lopez Caceres, M. L., Serrano, D., Roure, F., Diez, Y. (2020): Computer Vision and Deep Learning Techniques for the Analysis of Drone-Acquired Forest Images, a Transfer Learning Study. *Remote Sensing*., 12(8):1287.
- Kherchouche, D., Slimani, S., Touchan, R., Djazia, T., Malki, H., Baisan, C. (2019): Fire Human-Climate Interaction in Atlas Cedar Forests of Aurès, Northern Algeria. *Dendrochronologia*. 55. 125-134. 10.1016/j.dendro.2019.04.005.
- Kim, H., Hong, Y., Byun, H. (2018): Detecting Construction Equipment Using a Region-Based Fully Convolutional Network and Transfer Learning. *Journal of Computing in Civil Engineering*. 32. 10.1061/(ASCE)CP.1943-5487.0000731.
- Kingma, D. P., Ba., J. (2014): Adam: A Method for Stochastic Optimization, *CoRR*, 1412.6980.
- Kingsford, R. T., Basset, A., and Jackson, L. (2016): Wetlands: conservation's poor cousins. *Aquatic Conserv: Mar. Freshw. Ecosyst.*, 26: 892– 916. doi: 10.1002/aqc.2709.
- Kikuchi S. (2008): Structure and composition of riparian forests with reference to geomorphic conditions. In: Sakio H., Tamura T. (eds) *Ecology of Riparian Forests in Japan*. Springer, Tokyo. https://doi.org/10.1007/978-4-431-76737-4_9.

- Kneeshaw, D.D., Kobe, R.K., Coates, K.D., Messier, C. (2006): Sapling size influences shade tolerance ranking among southern boreal tree species. *Journal of Ecology*, 94: 471-480. <https://doi.org/10.1111/j.1365-2745.2005.01070.x>.
- Kornilov, A. S., Safonov, I. V. (2018): An Overview of Watershed Algorithm Implementations in Open Source Libraries. *J. Imaging* 2018, 4, 123. <https://doi.org/10.3390/jimaging4100123>
- Krizhevsky, A., Sutskever, I., Hinton, G. E. (2012): ImageNet Classification with Deep Convolutional Neural Networks. In *Advances in Neural Information Processing Systems 25*; Pereira, F.; Burges, C.J.C.; Bottou, L.; Weinberger, K.Q., Eds.; Curran Associates, Inc.: Dutchess County, NY, USA, 2012; pp. 1097–1105.
- Kudoh, T. (1985): Coastal Disaster Prevention Forests in Japan, *JARQ* Vol.19, No. 1.
- Lei, T., Lechowicz, M. (1990): Shade adaptation and shade tolerance in saplings of three *Acer* species from eastern North America. *Oecologia*. 84. 224-228. [10.1007/BF00318275](https://doi.org/10.1007/BF00318275).
- Lisein, J., Michez, A., Claessens, H., Lejeune, P. (2015): Discrimination of Deciduous Tree Species from Time Series of Unmanned Aerial System Imagery. *PLOS ONE* 10(11): e0141006. <https://doi.org/10.1371/journal.pone.0141006>.
- Liu, T., Abd-Elrahman, A. (2018): Deep convolutional neural network training enrichment using multi-view object-based analysis of Unmanned Aerial systems imagery for wetlands classification, *ISPRS Journal of Photogrammetry and Remote Sensing*, Volume 139, Pages 154-170, ISSN 0924-2716, <https://doi.org/10.1016/j.isprsjprs.2018.03.006>.
- Lopez C., M. L. (2014): 8th Forest Plan, Yamagata Field Research Center, Yamagata University University Forest: Watershed Preservation Section.
- López Caceres, M. L., Mizota, C., Nobori, Y., Sasaki, T., Yamanaka, T. (2014): Temporal changes in nitrogen acquisition of Japanese black pine (*Pinus thunbergii*) associated with black locust (*Robinia pseudoacacia*). *Journal of Forestry Research*. 25. [10.1007/s11676-014-0498-2](https://doi.org/10.1007/s11676-014-0498-2).
- López-Jiménez, E., Vasquez-Gomez, J. I., Sanchez-Acevedo, M. A., Herrera-Lozada, J. C., Uriarte-Arcia, A. V. (2019): Columnar cactus recognition in aerial images using a deep learning approach, *Ecological Informatics*, Volume 52, Pages 131-138, ISSN 1574-9541, <https://doi.org/10.1016/j.ecoinf.2019.05.005>.
- Lu, C., Liu, J., Jia, M., Liu, M., Man, W., Fu, W., Zhong, L., Lin, X., Su, Y., Gao, Y. (2018): Dynamic Analysis of Mangrove Forests Based on an Optimal Segmentation Scale Model and Multi-Seasonal Images in Quanzhou Bay, China. *Remote Sensing*, 10(12):2020. <https://doi.org/10.3390/rs10122020>.

- Lundbäck, M., Persson, H., Häggström, C., Nordfjell, T. (2020): Global analysis of the slope of forest land. *Forestry*. 94. 10.1093/forestry/cpaa021.
- Mafanya, M., Tsela, P., Botai, O., Manyama, P., Swart, B., Monate, T. (2017): Evaluating pixel and object based image classification techniques for mapping plant invasions from UAV derived aerial imagery: *Harrisia pomanensis* as a case study. *ISPRS Journal of Photogrammetry and Remote Sensing*. 129. 1-11. 10.1016/j.isprsjprs.2017.04.009.
- Mahdavi, S., Salehi, B., Granger, J., Amani, M., Brisco, B., Huang, W. (2018): Remote sensing for wetland classification: a comprehensive review, *GIScience & Remote Sensing*, 55:5, 623-658, DOI: 10.1080/15481603.2017.1419602
- Makimoto, K. (2019): State of Japan's Forests and Forest Management — 3rd Country Report of Japan to the Montreal Process, Forest Agency, Japan.
- Malek, S., Bazi, Y., Alajlan, N., AlHichri, H., Melgani, F. (2014): Efficient Framework for Palm Tree Detection in UAV Images, in *IEEE Journal of Selected Topics in Applied Earth Observations and Remote Sensing*, vol. 7, no. 12, pp. 4692-4703, Dec. 2014, doi: 10.1109/JSTARS.2014.2331425.
- Masaki, T., Osumi, K., Takahashi, K., Hoshizaki, K. (2005): Seedling dynamics of *Acer mono* and *Fagus crenata*: An environmental filter limiting their adult distributions. *Plant Ecology*. 177. 189-199. 10.1007/s11258-005-2177-z.
- Matsui, T., Yagihashi, T., Nakaya, T., Taoda, H., Yoshinaga, S., Daimaru, H. and Tanaka, N. (2004): Probability distributions, vulnerability and sensitivity in *Fagus crenata* forests following predicted climate changes in Japan. *Journal of Vegetation Science*, 15: 605-614. <https://doi.org/10.1111/j.1654-1103.2004.tb02302.x>
- Meera Gandhi, G. Parthiban, S., Thummalu, N., Christy, A. (2015): Ndvi: Vegetation Change Detection Using Remote Sensing and Gis – A Case Study of Vellore District, *Procedia Computer Science*, Volume 57, Pages 1199-1210, ISSN 1877-0509, <https://doi.org/10.1016/j.procs.2015.07.415>.
- Metashape manual (2018): Agisoft PhotoScan User Manual Professional Edition, Version 1.4, https://www.agisoft.com/pdf/photoscan-pro_1_4_en.pdf.
- Miraki, M., Sohrabi, H., Fatehi, P., Kneubuehler, M. (2021): Individual tree crown delineation from high-resolution UAV images in broadleaf forest. *Ecological Informatics*. 61. 101207. 10.1016/j.ecoinf.2020.101207.

Mitsch, W. J., Gosselink, J. G. (2000): The value of wetlands: importance of scale and landscape setting, *Ecological Economics*, Volume 35, Issue 1, Pages 25-33, ISSN 0921-8009, [https://doi.org/10.1016/S0921-8009\(00\)00165-8](https://doi.org/10.1016/S0921-8009(00)00165-8).

Miyawaki, S., Washitani, I. (2003): Invasive Alien Plant Species in Riparian Areas of Japan: The Contribution of Agricultural Weeds, Revegetation Species and Aquacultural Species, 8.

Masaki, T., Osumi, K., Takahashi, K., Hoshizaki, K., Matsune, K., Suzuki, W. (2007): Effects of microenvironmental heterogeneity on the seed-to-seedling process and tree coexistence in a riparian forest. *Ecological Research*. 22. 724-734. [10.1007/s11284-006-0308-1](https://doi.org/10.1007/s11284-006-0308-1).

Masaki, T., Osumi, K., Hoshizaki, K., Hoshino, D., Takahashi, K., Mastune, K. and Suzuki, W. (2008): Diversity of tree species in mountain riparian forest in relation to disturbance-mediated microtopography. In: Sakio H., Tamura T. (eds) *Ecology of Riparian Forests in Japan*. Springer, Tokyo. https://doi.org/10.1007/978-4-431-76737-4_17

Masarczyk, W., Głomb, P., Grabowski, B. Ostaszewski, M. (2020): Effective Training of Deep Convolutional Neural Networks for Hyperspectral Image Classification through Artificial Labeling. *Remote Sensing*. 12. 2653. [10.3390/rs12162653](https://doi.org/10.3390/rs12162653).

Merjulah, R., Chandra, J. (2019): Chapter 10 - Classification of Myocardial Ischemia in Delayed Contrast Enhancement Using Machine Learning, Editor(s): D. Jude Hemanth, Deepak Gupta, Valentina Emilia Balas, In *Intelligent Data-Centric Systems, Intelligent Data Analysis for Biomedical Applications*, Academic Press, Pages 209-235, ISBN 9780128155530, <https://doi.org/10.1016/B978-0-12-815553-0.00011-2>.

Mohan, M., Silva, C. A., Klauberg, C., Jat, P., Catts, G., Cardil, A., Hudak, A. T., Dia, M. (2017): Individual Tree Detection from Unmanned Aerial Vehicle (UAV) Derived Canopy Height Model in an Open Canopy Mixed Conifer Forest. *Forests*; 8(9):340. <https://doi.org/10.3390/f8090340>.

Morales, G., Kemper, G., Sevillano, G., Arteaga, D., Ortega, I., Telles, J. (2018): Automatic Segmentation of *Mauritia flexuosa* in Unmanned Aerial Vehicle (UAV) Imagery Using Deep Learning. *Forests*, 9, 736. <https://doi.org/10.3390/f9120736>

Moran, V. C., Hoffmann, J. H., Donnelly, D., Wilgen, B. W. van, Zimmermann, H. G. (2000): Biological control of alien, invasive pine trees species in South Africa. *Proceedings of the X International Symposium on Biological Control of Weeds*, Spencer, N. R., pages 941-953, Bozeman, USA.

- Möttus, M., Takala, T. (2014): A forestry GIS-based study on evaluating the potential of imaging spectroscopy in mapping forest land fertility, *International Journal of Applied Earth Observation and Geoinformation* 33, 302–311. doi:10.1016/j.jag.2014.06.010.
- Nadipally, M. (2019): Chapter 2 - Optimization of Methods for Image-Texture Segmentation Using Ant Colony Optimization, Editor(s): D. Jude Hemanth, Deepak Gupta, Valentina Emilia Balas, In *Intelligent Data-Centric Systems, Intelligent Data Analysis for Biomedical Applications*, Academic Press, Pages 21-47, ISBN 9780128155530, <https://doi.org/10.1016/B978-0-12-815553-0.00002-1>.
- Naiman, R., Fetherston, K., McKay, S., Chen, J. (1998): Riparian Forests. 10.1007/978-1-4612-1652-0_12.
- Nakamura, F., Yajima, T., Kikuchi, S. (1997): Structure and composition of riparian forests with special reference to geomorphic site conditions along the Tokachi River, northern Japan. *Plant Ecology* 133, 209–219. <https://doi.org/10.1023/A:1009787614455>.
- Nateghi R., Bricker J.D., Guikema S.D., Bessho A. (2016): Statistical Analysis of the Effectiveness of Seawalls and Coastal Forests in Mitigating Tsunami Impacts in Iwate and Miyagi Prefectures. *PLOS ONE* 11(8): e0158375, <https://doi.org/10.1371/journal.pone.0158375>.
- Natesan, S., Armenakis, C., and Vepakomma, U. (2019): Resnet-based tree species classification using UAV images, *Int. Arch. Photogramm. Remote Sens. Spatial Inf. Sci.*, XLII-2/W13, 475–481, <https://doi.org/10.5194/isprs-archives-XLII-2-W13-475-2019>, 2019.
- Natesan, S., Armenakis, C., Vepakomma, U. (2020): Individual tree species identification using Dense Convolutional Network (DenseNet) on multitemporal RGB images from UAV. *Journal of Unmanned Vehicle Systems*. 8(4): 310-333. <https://doi.org/10.1139/juvs-2020-0014>
- Nehring, S., Kowarik, I., Rabitsch, W., Essl, F., Lippe, M., Lauterbach, D., Seitz, B., Isermann, M., Etling, K. (2013): Naturschutzfachliche Invasivitätsbewertungen für in Deutschland wild lebende gebietsfremde Gefäßpflanzen. *BfN-Skripten*. 352. 1-202.
- Nentwig, W., Bacher, S., Kumschick, S., Pyšek, P., Vilà, M. (2018): Correction to: More than “100 worst” alien species in Europe. *Biological Invasions*. 20. 10.1007/s10530-018-1671-x.
- Nezami, S., Khoramshahi, E., Nevalainen, O., Pölönen, I., Honkavaara, E. (2020): Tree Species Classification of Drone Hyperspectral and RGB Imagery with Deep Learning Convolutional Neural Networks. *Remote Sensing*, 12(7):1070. <https://doi.org/10.3390/rs12071070>

- Niiyama, K. (1990): The role of seed dispersal and seedling traits in colonization and coexistence of *Salix* species in a seasonally flooded habitat. *Ecol. Res.* 5, 317–331. <https://doi.org/10.1007/BF02347007>.
- Ocer, N. E., Kaplan, G., Erdem, F., Matci D. K., Avdan, U. (2020): Tree extraction from multi-scale UAV images using Mask R-CNN with FPN, *Remote Sensing Letters*, 11:9, 847-856, DOI: 10.1080/2150704X.2020.1784491
- Ohta, T. (2013): Change of Japanese land and constuction of coastal forests, The First Asia Parks Congress, Sendai, Japan, http://www.env.go.jp/en/nature/asia-parks/pdf/wg3/APC_WG1-15_Takehiko%20Ohta.pdf (latest access 11 January 2021).
- Okitsu S. (2003): Forest Vegetation of Northern Japan and the Southern Kurils. In: Kolbek J., Šrůtek M., Box E.O. (eds) *Forest Vegetation of Northeast Asia*. Geobotany, vol 28. Springer, Dordrecht. https://doi.org/10.1007/978-94-017-0143-3_7.
- Onishi, M., & Ise, T. (2018): Automatic classification of trees using a UAV onboard camera and deep learning. ArXiv, abs/1804.10390.
- Onishi, M., Ise, T. (2021): Explainable identification and mapping of trees using UAV RGB image and deep learning. *Sci Rep* 11, 903. <https://doi.org/10.1038/s41598-020-79653-9>
- Ohno, K. (1991): A vegetation-ecological approach to the classification and evaluation of potential natural vegetation of the Fagetea crenatae region in Tohoku (northern Honshu), Japan. *Ecol. Res.* 6, p.29-49, <https://doi.org/10.1007/BF02353868>.
- Ohno K. (2008): Vegetation-geographic evaluation of the syntaxonomic system of valley-bottom forests occurring in the cooltemperate zone of the Japanese Archipelago. In: Sakio H., Tamura T. (eds) *Ecology of Riparian Forests in Japan*. Springer, Tokyo. https://doi.org/10.1007/978-4-431-76737-4_4
- Osco, L., dos Santos de Arruda, M., Gonçalves, D., Dias, A., Batistoti, J., de Souza, M., Gomes, F., Ramos, A. P., Jorge, L., Liesenberg, V., Li, J., Ma, L., Junior, J., Gonçalves, W. (2021): A CNN Approach to Simultaneously Count Plants and Detect Plantation-Rows from UAV Imagery. *ISPRS Journal of Photogrammetry and Remote Sensing*. 174. 1-17. 10.1016/j.isprsjprs.2021.01.024.
- Pan, S., Yang, Q. (2010): A Survey on Transfer Learning. *Knowledge and Data Engineering, IEEE Transactions on*. 22. 1345 - 1359. 10.1109/TKDE.2009.191.
- Patrick, A.; Li, C. (2017): High Throughput Phenotyping of Blueberry Bush Morphological Traits Using Unmanned Aerial Systems. *Remote Sens.*, 9, 1250.

Peppas, M. V., Hall, J., Goodyear, J., and Mills, J. P. (2019): Photogrammetric assessment and comparison of DJI Phantom 4 Pro and Phantom 4 RTK small unmanned aircraft systems, *Int. Arch. Photogramm. Remote Sens. Spatial Inf. Sci.*, XLII-2/W13, 503–509, <https://doi.org/10.5194/isprs-archives-XLII-2-W13-503-2019>, 2019.

Piazza, M. and Goovil, K. (2007): Brief on national forest inventory NFI Japan, forest resources development service, Forest department Food and Agriculture of the United Nations, Rome.

Pimentel, D., Zuniga, R., Morrison, D. (2005): Update on the environmental and economic costs associated with alien-invasive species in the United States, *Ecological Economics*, Volume 52, Issue 3, Pages 273-288, ISSN 0921-8009, <https://doi.org/10.1016/j.ecolecon.2004.10.002>.

Pommerening, A. (2002): Approaches to quantifying forest structures, *Forestry: An International Journal of Forest Research*, Volume 75, Issue 3, 2002, Pages 305–324, <https://doi.org/10.1093/forestry/75.3.305>.

Prentis, P. J., Wilson, J. R. U., Dormontt, E. E., Richardson, D. M., Lowe A. J. (2008): Adaptive evolution in invasive species, *Trends in Plant Science*, Volume 13, Issue 6, Pages 288-294, ISSN 1360-1385, <https://doi.org/10.1016/j.tplants.2008.03.004>.

Pyšek, P. and Richardson, D. M. (2010): Invasive Species, Environmental Change and Management, and Health. *Annual Review of Environment and Resources*. 35. 10.1146/annurev-environ-033009-095548.

Pyttel, P.L., Kunz, J., & Bauhus, J. (2013): Growth, regeneration and shade tolerance of the Wild Service Tree (*Sorbus torminalis* (L.) Crantz) in aged oak coppice forests. *Trees*, 27, 1609-1619.

Rabitsch, W. and Genovesi, P. (2012): Invasive alien species indicators in Europe, EEA Technical Report, doi 10.2800/64181.

Raparelli, E, Bajocco, S. (2019): A bibliometric analysis on the use of unmanned aerial vehicles in agricultural and forestry studies. *International Journal of Remote Sensing*. 1-14. 10.1080/01431161.2019.1569793.

Rebelo, L.-M., Finlayson, M., Nagabhatla, N. (2008): Remote Sensing and GIS for Wetland Inventory, Mapping and Change Analysis. *Journal of environmental management*. 90. 2144-53. 10.1016/j.jenvman.2007.06.027.

Rezaee, M., Mahdianpari, M., Zhang, Y., Salehi, B. (2018): Deep Convolutional Neural Network for Complex Wetland Classification Using Optical Remote Sensing Imagery. *IEEE Journal of Selected Topics in Applied Earth Observations and Remote Sensing*, 11, 3030-3039.

Rezende, E., Ruppert, G., Carvalho, T., Ramos, F., De Geus, P. (2017): Malicious Software Classification Using Transfer Learning of ResNet-50 Deep Neural Network. 10.1109/ICMLA.2017.00-19.

Richardson, D., Binggeli, P., Schroth, G. (2004): Invasive agroforestry trees – problems and solutions.

Ricklefs, R. E., He, F. (2016): Region effects on local species diversity, *Proceedings of the National Academy of Sciences* Jan 2016, 113 (3) 674-679; DOI: 10.1073/pnas.1523683113.

Ronneberger O., Fischer P., Brox T. (2015): U-Net: Convolutional Networks for Biomedical Image Segmentation. In: Navab N., Hornegger J., Wells W., Frangi A. (eds) *Medical Image Computing and Computer-Assisted Intervention – MICCAI 2015*. MICCAI 2015. Lecture Notes in Computer Science, vol 9351. Springer, Cham. https://doi.org/10.1007/978-3-319-24574-4_28

Rother, K. (2018): Can someone explain precompute = True and freeze or unfreeze? <https://forums.fast.ai/t/can-someone-explain-precompute-true-and-freeze-or-unfreeze/18169>, latest access 15. August 2019.

Sa, I., Chen, Z., Popovic, M., Khanna, R., Liebisch, F., Nieto, J., Siegart, R. (2018): weedNet: Dense Semantic Weed Classification Using Multispectral Images and MAV for Smart Farming. *IEEE Robotics and Automation Letters*, 3, 588-595.

Safonova, A., Tabik, S., Alcaraz-Segura, D., Rubtsov, A., Maglinets, Y., Herrera, F. (2019): Detection of Fir Trees (*Abies sibirica*) Damaged by the Bark Beetle in Unmanned Aerial Vehicle Images with Deep Learning. *Remote Sensing*. 11. 643. 10.3390/rs11060643.

Sakio, H., Kubo, M., Shimano, K., Ohno, K. (2002): Coexistence of three canopy tree species in a riparian forest in the Chichibu Mountains, central Japan. *Folia Geobotanica*. 37. 45-61. 10.1007/BF02803190.

Sakio H., Tamura T. (2008): *Ecology of Riparian Forests in Japan*. Springer, Tokyo. https://doi.org/10.1007/978-4-431-76737-4_4.

Sander J. (2011): Density-Based Clustering. In: Sammut C., Webb G.I. (eds) *Encyclopaedia of Machine Learning*. Springer, Boston, MA. https://doi.org/10.1007/978-0-387-30164-8_211.

Santoro, F., Tarantino, E., Figorito, B., Stefania, G., D'Onghia, A. (2013): A tree counting algorithm for precision agriculture tasks. *International Journal of Digital Earth*. 6. 94-102. 10.1080/17538947.2011.642902.

Sasaki, Y. (1970): Versuch zur systematischen und geographischen Gliederung der japanischen Buchenwaldgesellschaften, Beiträge aus dem Institut für Phyto- und Geobotanik der Hiroshima-Universität, Hiroshima, Nr. 134 und Arbeiten aus der Arbeitsstelle für Theoretische und Angewandte Pflanzensoziologie in Todenmann (46), p.215-249, <https://doi.org/10.1007/BF01965535>.

Schepker, H. and Kowarik, I. (1998): Invasive North American Blueberry Hybrids (*Vaccinium corymbosum* x *angustifolium*) in Northern Germany, *Plant Invasions: Ecological Mechanisms and Human Responses*, 253-260.

Schepker, H., Kowarik, I., Grave, E. (1997): Verwilderung nordamerikanischer Kultur - Heidelbeeren (*Vaccinium* subgen. *Cyanococcus*) in Niedersachsen und deren Einschätzung aus Naturschutzsicht., *Natur und Landschaft*, 72, 7/8, 346-351.

Schiefer, F., Kattenborn, T., Frick, A., Frey, J., Schall, P., Koch, B., Schmidtlein, S. (2020): Mapping forest tree species in high resolution UAV-based RGB-imagery by means of convolutional neural networks, *ISPRS Journal of Photogrammetry and Remote Sensing*, Volume 170, Pages 205-215, ISSN 0924-2716, <https://doi.org/10.1016/j.isprsjprs.2020.10.015>.

Schneekloth, H., Tuexen, J. (1975): Die Moore in Niedersachsen, Göttingen Kommissionsverlag Goettinger Tagesblatt, P. 1A 198, sd.

Sercu, B.K., Baeten, L., van Coillie, F., Martel, A., Lens, L. Verheyen, K. Bonte, D. (2017): How tree species identity and diversity affect light transmittance to the understory in mature temperate forests. *Ecol Evol.* 7: 10861– 10870. <https://doi.org/10.1002/ece3.3528>.

Shafri, H., Hamdan, N., Saripan, M. I. (2011): Semi-automatic detection and counting of oil palm trees from high spatial resolution airborne imagery. *International Journal of Remote Sensing.* 32. 2095-2115. 10.1080/01431161003662928.

Sharma, S., Mehra, Dr. R. (2018): Breast cancer histology images classification: Training from scratch or transfer learning?. *ICT Express.* 4. 10.1016/j.icte.2018.10.007.

Shibata, M., Kikuchi, S., Tanaka, H., Sueyoshi, M., Yoshimaru, H., Niiyama, K. (2008): Effects of population density, sex morph, and tree size on reproduction in a heterodichogamous maple, *Acer mono*, in a temperate forest of Japan. *Ecological Research.* 24. 1-9. 10.1007/s11284-008-0474-4.

Desta, H., Bewket, W., Eckert, S. (2019): Performances of machine learning algorithms for mapping fractional cover of an invasive plant species in a dryland ecosystem. *Ecology and Evolution.* 9. 10.1002/ece3.4919.

Shimada, T. (2009): State of Japan's Forests and Forest Management—2nd Country Report of Japan to the Montreal Process, Forestry Agency: Tokyo, Japan.

Shirokikh, B., Zakazov, I., Chernyavskiy, A., Feulova, I., Belyaev, M. (2020): First U-Net Layers Contain More Domain Specific Information Than The Last Ones, DART workshop at the MICCAI conference 2020.

- Siam, M., Gamal, M., Abdel-Razek, M., Yogamani, S., Jagersand, M. (2018): RTSeg: Real-Time Semantic Segmentation Comparative Study, 25th IEEE International Conference on Image Processing (ICIP), Athens, Greece, 2018, pp. 1603-1607, doi: 10.1109/ICIP.2018.8451495.
- Simonyan, K. & Zisserman, A. (2014): Very Deep Convolutional Networks for Large-Scale Image Recognition. arXiv 1409.1556.
- Smith, D. M., Larson, B. C., Kelty M. J., Ashton P. N. S. (1997): The practice of silviculture. New York, John Wiley & Sons, Inc.
- Smith, T. J., III (1992): Forest Structure. In Tropical Mangrove Ecosystems (eds A. Robertson and D. Alongi). <https://doi.org/10.1029/CE041p0101>.
- Spanner, M. A., Pierce, L. L., Peterson D. L., Running, S. W. (1990): Remote sensing of temperate coniferous forest leaf area index The influence of canopy closure, understory vegetation and background reflectance, International Journal of Remote Sensing, 11:1, 95-111, DOI: 10.1080/01431169008955002.
- Srivastava, N., Hinton, G., Krizhevsky, A., Sutskever, I. and Salakhutdinov, R. (2014): Drop-out: A Simple Way to Prevent Neural Networks from Overfitting. Journal of Machine Learning Research (JMLR), vol. 15, pp. 1929–1958.
- Starfinger, U., Kowarik, I. (2003): *Vaccinium angustifolium* x *corymbosum*, Bundesamt für Naturschutz, <https://neobiota.bfn.de/handbuch/gefaesspflanzen/vaccinium-angustifolim-x-corymbosum.html>, (ac-cessed November 11, 2020).
- Stieper, L. C. (2018): Distribution of wild growing cultivated blueberries in Krähenmoor and their impact on bog vegetation and bog development, Bachelor's Thesis, Leibniz University of Hannover, Institute of Physical Geography and Landscape Ecology.
- Straub, B.-M., Heipke, C. (2007): Automatic extraction and delineation of single trees from remote sensing data. Machine Vision and Applications. 18. 317-330. 10.1007/s00138-006-0064-9.
- Suh, M. H., Lee, D. K. (1998): Stand structure and regeneration of *Quercus mongolica* forests in Korea, Forest Ecology and Management, Volume 106, Issue 1, Pages 27-34, ISSN 0378-1127, [https://doi.org/10.1016/S0378-1127\(97\)00236-3](https://doi.org/10.1016/S0378-1127(97)00236-3).
- Sun, Y., Liu, Y., Wang, G., Zhang, H. (2017): Deep Learning for Plant Identification in Natural Environment. Computational Intelligence and Neuroscience, 2017.
- Suzuki, W., Osumi, K., Masaki, T., Takahashi, K., Daimaru, H., Hoshizaki, K. (2002): Disturbance regimes and community structures of a riparian and an adjacent terrace stand in the Kanumazawa Riparian Re-

search Forest, northern Japan, *Forest Ecology and Management*, Volume 157, Issues 1–3, Pages 285-301, ISSN 0378-1127, [https://doi.org/10.1016/S0378-1127\(00\)00667-8](https://doi.org/10.1016/S0378-1127(00)00667-8).

Svenning, J.-C., Kinner, D. A., Stallard, R. F., Engelbrecht, B. M. J., Wright, S. J. 2004: Ecological Determinism in Plant Community Structure Across a Tropical Forest Landscape. *Ecology*. 2526-2538.

Tai X. C., Hodneland E., Weickert J., Bukoreshtliev N. V., Lundervold A., Gerdes H. H. (2007): Level Set Methods for Watershed Image Segmentation. In: Sgallari F., Murli A., Paragios N. (eds) *Scale Space and Variational Methods in Computer Vision*. SSVM 2007. Lecture Notes in Computer Science, vol 4485. Springer, Berlin, Heidelberg. https://doi.org/10.1007/978-3-540-72823-8_16.

Taniguchi, T., Tamai, S., Yamanaka, N., Futai, K. (2007): Inhibition of the regeneration of Japanese black pine (*Pinus thunbergii*) by black locust (*Robinia pseudoacacia*) in coastal sand dunes. *Journal of Forest Research*, 12:5, 350-357.

Tajbakhsh N., Shin, J. Y., Gurudu, S. R., Hurst, R. T., Kendall, C. B., Gorway, M. B., Liang, J. (2016): Convolutional Neural Networks for Medical Image Analysis: Full Training or Fine Tuning?, in *IEEE Transactions on Medical Imaging*, vol. 35, no. 5, pp. 1299-1312, doi: 10.1109/TMI.2016.2535302.

Tarabalka, Y., Chanussot, J., Benediktsson, J.A. (2010): Segmentation and classification of hyperspectral images using watershed transformation, *Pattern Recognition*, Volume 43, Issue 7, Pages 2367-2379, ISSN 0031-3203, <https://doi.org/10.1016/j.patcog.2010.01.016>.

Tattoni, C., Chianucci, F., Ciolli, M., Ferrara, C., Marchino, L., Zanni, M., Zatelli P., Cutini A. (2021): A comparison of ground-based count methods for quantifying seed production in temperate broadleaved tree species. *Annals of Forest Science* 78. <https://doi.org/10.1007/s13595-020-01018-z>.

Team, T.G. (2020): GNU Image Manipulation Program. Available online: <http://gimp.org> (accessed on 19 March 2020).

Tinya, F., Márialigeti, S., Bidló, A., Ódor, P.(2019): Environmental drivers of the forest regeneration in temperate mixed forests. *Forest Ecology and Management*, Volume 433, Pages 720-728, ISSN 0378-1127, <https://doi.org/10.1016/j.foreco.2018.11.051>.

Twumasi, Y. A., Merem, E. C. (2006): GIS and remote sensing applications in the assessment of change within a coastal environment in the Niger Delta region of Nigeria. *Int J Environ Res Public Health*, Mar, 3(1):98-106. doi: 10.3390/ijerph2006030011. PMID: 16823081; PMCID: PMC3785684.

Verheyen, K., Baeten, L., De Frenne, P., Bernhardt-Römermann, M., Brunet, J., Cornelis, J., Decocq, G., Dierschke, H., Eriksson, O., Hédli, R., Heinken, T., Hermy, M., Hommel, P., Kirby, K., Naaf, T., Peterken, G., Petřík, P., Pfadenhauer, J., Van Calster, H., Walther, G.-R., Wulf, M. and Verstraeten, G. (2012): Driv-

ing factors behind the eutrophication signal in understorey plant communities of deciduous temperate forests. *Journal of Ecology*, 100: 352-365. <https://doi.org/10.1111/j.1365-2745.2011.01928.x>.

Wan, H., Wang, Q., Jiang, D., Fu, J., Yang, Y., Liu, X. (2014): Monitoring the invasion of *Spartina alterniflora* using very high resolution unmanned aerial vehicle imagery in Beihai, Guangxi (China). *Scientific World Journal*, 2014:638296. doi: 10.1155/2014/638296.

Wang, J., Yang, Y., Mao, J., Huang, Z., Huang, C., Xu, W. (2016): CNN-RNN: A Unified Framework for Multi-label Image Classification. 2285-2294. 10.1109/CVPR.2016.251.

Westhoff V., Van Der Maarel, E. (1978): The Braun-Blanquet Approach. In: Whittaker R.H. (eds) *Classification of Plant Communities*. *Classification of Plant Communities*, vol 5-1. Springer, Dordrecht. https://doi.org/10.1007/978-94-009-9183-5_9.

Whittaker, R.H. (1967): Gradient analysis of vegetation*. *Biological Reviews*, 42: 207-264. <https://doi.org/10.1111/j.1469-185X.1967.tb01419.x>.

Wierzbicki, D., Kedzierski, M., Fryskowska, A. (2015): Assessment of the influence of UAV image quality on the orthophoto production. *ISPRS - International Archives of the Photogrammetry, Remote Sensing and Spatial Information Sciences*. XL-1/W4. 1-8. 10.5194/isprsarchives-XL-1-W4-1-2015.

Wijaya, A., Kusnadi, S., Gloaguen, R., Heilmeyer, H. (2010): Improved strategy for estimating stem volume and forest biomass using moderate resolution remote sensing data and GIS. *Journal of Forestry Research* 21, 1–12. <https://doi.org/10.1007/s11676-010-0001-7>.

Wu, Q. (2018): GIS and Remote Sensing Applications in Wetland Mapping and Monitoring. In: Huang, B. (Ed.), *Comprehensive Geographic Information Systems*, Vol. 2, pp. 140–157. Oxford: Elsevier. DOI: 10.1016/B978-0-12-409548-9.10460-9.

Wulder M. A., Franklin S. E. (2003): Remote Sensing of Forest Environments, Introduction. In: Wulder M.A., Franklin S.E. (eds) *Remote Sensing of Forest Environments*. Springer, Boston, MA. https://doi.org/10.1007/978-1-4615-0306-4_1.

Xie, S., Girshick, R., Dollar, P., Tu, Z., He, K. (2017): Proceedings of the IEEE Conference on Computer Vision and Pattern Recognition (CVPR), pp. 1492-1500.

Ying, T. (2016): *GPU-based Parallel Implementation of Swarm Intelligence Algorithms*, ISBN: 0128093625, 9780128093627, Morgan Kaufmann Publishers Inc., 1st edition, San Francisco, CA, USA.

Yu, H., Yang, Z., Tan, L., Wang, Y., Sun, W., Sun, M., Tang, Y. (2018): Methods and datasets on semantic segmentation: A review, *Neurocomputing*, Volume 304, Pages 82-103, ISSN 0925-2312, <https://doi.org/10.1016/j.neucom.2018.03.037>.

Zagoruyko, S., Komodakis, N. (2016): Wide Residual Networks, CoRR, ArXiv, abs/1605.07146, <http://arxiv.org/abs/1605.07146>.

Zhang, Y., Chen, H. Y. H. and Taylor, A. R. (2017): Positive species diversity and above-ground biomass relationships are ubiquitous across forest strata despite interference from overstorey trees. *Funct Ecol*,

Zhao, Y., Ma, J., Li, X., Zhang, J. (2018): Saliency Detection and Deep Learning-Based Wildfire Identification in UAV Imagery. *Sensors*; 18(3):712. <https://doi.org/10.3390/s18030712>.

Zhao, X., Zhang, J., Tian, J., Zhuo, L., Zhang, J. (2020): Residual Dense Network Based on Channel-Spatial Attention for the Scene Classification of a High-Resolution Remote Sensing Image. *Remote Sensing*. 12. 1887. [10.3390/rs12111887](https://doi.org/10.3390/rs12111887).

Zmarz, A. (2013): UAV - A useful tool for monitoring woodlands. *Miscellanea geographica – Regional studies on development*. 18. [10.2478/mgrsd-2014-0006](https://doi.org/10.2478/mgrsd-2014-0006). 1: 419-426. <https://doi.org/10.1111/1365-2435.12699>.

IX. Internet sources

Ashish (2018): Understanding Edge Detection (Sobel Operator), <https://medium.com/datadriveninvestor/understanding-edge-detection-sobel-operator-2aada303b900>, latest access 14. February 2021.

Brett, M. (2014): An introduction to smoothing, https://matthew-brett.github.io/teaching/smoothing_intro.html, latest access 15. February 2021, October 2014.

Brownlee, J. (2017): A Gentle Introduction to Transfer Learning for Deep Learning <https://machinelearningmastery.com/transfer-learning-for-deep-learning/>, latest access 07. June 2021.

Brownlee, J. (2019a): A gentle introduction to the rectified linear unit (ReLU), <https://machinelearningmastery.com/rectified-linear-activation-function-for-deep-learning-neural-networks/>, latest access 17. February 2021.

Brownlee, J. (2019b): A Gentle Introduction to Batch Normalization for Deep Neural Networks, <https://machinelearningmastery.com/batch-normalization-for-training-of-deep-neural-networks/>, latest access 17. February 2021.

Brownlee, J. (2019c): How Do Convolutional Layers Work in Deep Learning Neural Networks?, <https://machinelearningmastery.com/convolutional-layers-for-deep-learning-neural-networks/>, latest access 17. February 2021.

Brownlee, J. (2019d): A Gentle Introduction to Pooling Layers for Convolutional Neural Networks, <https://machinelearningmastery.com/pooling-layers-for-convolutional-neural-networks/>, latest access 17. February 2021.

Brownlee, J. (2019e): How to Configure the Learning Rate When Training Deep Learning Neural Networks, <https://machinelearningmastery.com/learning-rate-for-deep-learning-neural-networks/>, latest access 23 January, 2019.

Chatterjee, S. (2020): What is Feature Extraction? Feature Extraction in Image Processing, <https://www.mygreatlearning.com/blog/feature-extraction-in-image-processing/>, latest access 17. February 2021.

DataCarpentry: Image processing with python – Thresholding (2021): <https://datacarpentry.org/image-processing/07-thresholding/>, latest access 21. March 2021.

Doxygen (2021): Morphological Transformations, https://docs.opencv.org/master/d9/d61/tutorial_py_morphological_ops.html, latest access 15. February 2021.

Dwivedi, P. (2019): Semantic Segmentation — Popular Architectures, <https://towardsdatascience.com/semantic-segmentation-popular-architectures-dff0a75f39d0>, latest access 19. August 2019.

ESRI,a: <https://desktop.arcgis.com/de/arcmap/10.3/manage-data/shapefiles/what-is-a-shapefile.htm>, latest access 09. February 2021.

ESRI,b: Optimized Hot Spot Analysis (Spatial Statistics), <https://pro.arcgis.com/en/pro-app/latest/tool-reference/spatial-statistics/optimized-hot-spot-analysis.htm>, latest access 14. March 2021.

ESRI,c: How Hot Spot Analysis (Getis-Ord G_i^*) works, <https://pro.arcgis.com/en/pro-app/latest/tool-reference/spatial-statistics/h-how-hot-spot-analysis-getis-ord-gi-spatial-stati.htm>, latest access 14 March 2021.

ESRI,d: How Filter works, <https://pro.arcgis.com/en/pro-app/latest/tool-reference/spatial-analyst/how-filter-works.htm>, latest access 03. February 2021

ESRI,e: Focal Statistics (Spatial Analyst), <https://pro.arcgis.com/en/pro-app/latest/tool-reference/spatial-analyst/focal-statistics.htm>, latest access 03. February 2021.

ESRI,f: How Slope works, <https://pro.arcgis.com/en/pro-app/latest/tool-reference/3d-analyst/how-slope-works.htm>, latest access 09. February 2021.

ESRI,g: How Aspect works, <https://desktop.arcgis.com/en/arcmap/10.3/tools/3d-analyst-toolbox/how-aspect-works.htm>, latest access 09. February 2021.

ESRI, h: Near (Analysis), <https://pro.arcgis.com/en/pro-app/latest/tool-reference/analysis/near.htm>, latest access 14.03.2021.

Fung, V. (2017): An Overview of ResNet and its Variants, <https://towardsdatascience.com/an-overview-of-resnet-and-its-variants-5281e2f56035>, latest access 18. February 2021.

Goepel, K. D. (2012a): Diversity as Business KPI – Alpha and Beta Diversity, <https://bpmsg.com/tag/hill-numbers/>, latest access 27. April 2021.

Goepel, K. D. (2012b): Diversity Index as Business Performance Indicator – The Concept of Diversity, <https://bpmsg.com/diversity-index-as-busines-performance-indicator-the-concept-of-diversity/>, latest access 27. April 2021.

Grégoire, N., Bouillot, M. (1998): Hausdorff distance between convex polygons, web project at McGill University, <http://cgm.cs.mcgill.ca/~godfried/teaching/cg-projects/98/normand/main.html>, latest access 16. February 2021.

Gupta, D. (2019): A Beginner's guide to Deep Learning based Semantic Segmentation using Keras, <https://divamgupta.com/image-segmentation/2019/06/06/deep-learning-semantic-segmentation-keras.html>, latest access 19. August 2019.

Howard, J. & Thomas, R. & Gugger, S.: Fastai. Available online: <https://github.com/fastai/fastai> (accessed on 18 April 2020).

<https://missinglink.ai/guides/neural-network-concepts/using-u-net-semantic-segmentation/>

Koplik, G. (2020): Persistent Homology: A Non-Mathy Introduction with Examples Using Topological Data Analysis (TDA) tools in Data Science, <https://towardsdatascience.com/persistent-homology-with-examples-1974d4b9c3d0>, latest access 3.11.2020.

Maklin, C. (2019): Gaussian Mixture Models Clustering Algorithm Explained, <https://towardsdatascience.com/gaussian-mixture-models-d13a5e915c8e>, latest access 15. February 2021.

MathWorks (2021): Image Processing Toolbox, <https://www.mathworks.com/help/images/morphological-dilation-and-erosion.html>, latest access 15. February 2021.

MathWorks: Types of Morphological Operations, <https://www.mathworks.com/help/images/morphological-dilation-and-erosion.html>, latest access 15. February 2021.

Missouri Botanical Garden: Magnolia obovata, <http://www.missouribotanicalgarden.org/PlantFinder/PlantFinderDetails.aspx?taxonid=282536&isprofile=0&>, latest access 9. June 2021.

Nicholson, C. (2020): A Beginner's Guide to Neural Networks and Deep Learning, <https://wiki.pathmind.com/neural-network>, latest access 17. February 2021.

OpenCV: Morphological operation, https://opencv-python-tutroals.readthedocs.io/en/latest/py_tutorials/py_imgproc/py_morphological_ops/py_morphological_ops.html, latest access 15. February 2021.

Ouaknine, A. (2019): Review of Deep Learning Algorithms for image semantic segmentation, https://medium.com/@arthur_ouaknine/review-of-deep-learning-algorithms-for-image-semantic-segmentation-509a600f7b57, latest access 19 August 2019.

Planet: Understanding the Amazon from Space. Available online: <https://www.kaggle.com/c/planet-understanding-the-amazon-from-space> (accessed on 19 August 2019).

Powel, V. (2018): Image Kernels - Explained Visually, <https://setosa.io/ev/image-kernels/>, latest access 03. February 2021.

Sagar, R. (2019): What Does Freezing A Layer Mean And How Does It Help In Fine Tuning Neural Networks, <https://analyticsindiamag.com/what-does-freezing-a-layer-mean-and-how-does-it-help-in-fine-tuning-neural-networks/>, latest access 23. March 2021.

Sharma, S. (2017): Activation Functions in Neural Networks, <https://towardsdatascience.com/activation-functions-neural-networks-1cbd9f8d91d6>, latest access 17. February 2021.

Sharma, S. (2017b): Epoch vs Batch Size vs Iterations, <https://towardsdatascience.com/epoch-vs-iterations-vs-batch-size-4dfb9c7ce9c9>, latest access 23. March 2021.

Sharma, P. (2019): The Most Comprehensive Guide to K-Means Clustering You'll Ever Need, <https://www.analyticsvidhya.com/blog/2019/08/comprehensive-guide-k-means-clustering/>, latest access 15. February 2021.

Singh, S. (2013): Confused Between DEM, DTM and DSM !, <https://www.gisresources.com/confused-dem-dtm-dsm/>, latest access 15. March 2021

Swain, A. (2018): Noise in Digital Image Processing, <https://medium.com/image-vision/noise-in-digital-image-processing-55357c9fab71>, latest access 03. February 2021.

Tsang, S.-H. (2019): Review: SqueezeNet (Image Classification), <https://towardsdatascience.com/review-squeezenet-image-classification-e7414825581a>, latest access 18. February 2021.

Wei, J. (2019a): AlexNet: The Architecture that Challenged CNNs, <https://towardsdatascience.com/alexnet-the-architecture-that-challenged-cnns-e406d5297951>, latest access 17. February 2021.

Wei, J. (2019b): VGG Neural Networks: The Next Step After AlexNet, <https://towardsdatascience.com/vgg-neural-networks-the-next-step-after-alexnet-3f91fa9ffe2c>, latest access 17. February 2021.

David Zelený (2021): Analysis of community ecology data in R - Diversity indices, <https://www.davidzeleny.net/anadat-r/doku.php/en:div-ind>, latest access 26. April 2021.

X. Appendix i – iv

Appendix i – Machine Learning

Machine learning is a technique to mimic human intelligence through algorithms. Computers follow instruction, while humans are able to learn from their experience. But computers can learn, too, not from experience but from data. Typical learning algorithms known in machine learning are linear regressions, the Naives Bayes algorithm, decision trees, logistic regressions, clustering or support vector machines. All these techniques are used to separate data giving specific features, while the computer learns to separate them by producing the smallest error possible, using the try and error approach.

In general, there are three different types of machine learning: supervised and unsupervised classifications as well as reinforcement learning. Supervised classifications use labelled and structured data as basis for the training to generate a desired output, while unsupervised classifications work with unlabelled datasets (George et al., 2017). Using an unlabelled dataset demands the computer looking for patterns in the input data and outputting those. Reinforcement learning is a dynamic environment for the computer, using rewards and punishments for its outputs.

Devices like UAVs and different kind of sensors, as well as the online connectivity between humans, enable a fast, efficient and low-cost gathering of large amounts of data. Data storage, computer memory and in general computing power enable the use of large amounts of training data, which increase the efficiency of the learning algorithms. Recently, new machine learning techniques rose, which are known as neural networks and DL.

Appendix ii – Neural network

There are several layers in neural networks (NN): the input layer, the output layer and several hidden layers (which create the depth); all are connected via channels. Every channel has a specific weight and bias for each node in the layer. The nodes hold numbers between 0 and 1, representing the Gray value of the pixel, which is called activation. The number of pixels represents the number of nodes in the input layer. Each node with its specific activation number causes an activation of a set of other nodes in the hidden layers, which again activates another set of nodes in the next layer until it finally results in the activation of the output.

As it is difficult to imagine how the machine sees images and classifies them, humans imagine the following situation. The whole image will be divided into subcomponents and ideally every node contains one of these components, which will be activated to generate the output of a labelled image. Therefore, from going to the last hidden layer to the output layer requires the computer to learn which combination of subcomponents built up the image. In the input layer pixels are analysed, the next layers of the network identify first the edges in the image, which leads for every image to an activation of specific nodes. The following layers identify then patterns, build edges, which again activate nodes and finally lead to the predicted output.

The channels, which connect the nodes, need to be adjusted to capture pixel patterns. This can be done using parameters (weights for each channel) which are multiplied with their node and summed up. For the network, the calculated value is used in a sigmoid function, so that the output value is in the range of 0 and 1. Therefore, the activation of the node in a layer is a measure of how positive the relevant weighted sum is. Furthermore, a bias is used to tell the node until when it is supposed to be inactive and only when the value is high enough the node will be activated. In the end, every channel between nodes of different layers has specific weights, which can be seen as the strength of the connection and a bias, which causes a node to be active or inactive. To sum it up, learning of a DL network means to find the right weights and biases to identify an object in an image.

The network learns first on the training data and starts doing random processes, which results in a chaotic output. Therefore, the computer needs to be told which parts were classified wrong and which correct. That is done with a cost function. The lower the output cost value, the better the network is able to classify objects. The network needs to adjust weights and biases to activate the right nodes to classify images. This will be done with the gradient decent function, which minimizes the cost function, by defining the relative importance of each weight and bias, so that the performance of the DL model increases. After training the network will get a new set of labelled data, which it has not seen before, to check its capability to identify objects.

Mathematically the NN uses the input pixel values, with mathematical functions, matrices and vectors, to output a value, which stands for an identified object. In reality the network does not see edges or patterns in the images, it sees pixels as numbers generated by weights and biases. The network finds local minima which leads them to a specific output, which is called a classification of a DL network.

Appendix iii – Addition to segmentation methods

Instance segmentation: One step further into an even more detailed segmentation is instance segmentation. The difference to semantic segmentation is the division of objects belonging to one class. Therefore, also objects, belonging to the same class, can have different labels (Dwivedi, P. 2019).

Appendix iv - Further deep learning architectures

As mentioned before, there are several architectures available and in these days the development of new architectures increased because of the higher computational power and application in several fields. Therefore, considering more than the state of art architectures is a useful approach to study the effectiveness of DL for forestry. An overview of the networks is provided in the following section.

AlexNet (Krizhevsky et al., 2012) is a widely used CNN architecture that consist of eight layers: five convolutional layers and three full connected ones. Additionally, AlexNet uses Rectified Linear Units (ReLU), which decrease training times. Furthermore, it can use multiple GPUs, which again decreases training times and increases the possibility to train a bigger model. Finally, the network uses overlapping pooling, which reduces errors by 0.5% as well as model overfitting (Wei, 2019).

The VGG (Simonyan and Zisserman, 2014) neural network followed AlexNet and was able to have an increased depth. The network uses small receptive fields together with three ReLU units, which increases the decision function. Fewer parameter and 1 x 1 convolutional layers allow the network to have a large number of layers, increasing the performance of the model (Wei, 2019b). In this work a VGG version with 19 layers including batch normalization is considered.

ResNet (here used: ResNet50, ResNet152) (He et al., 2016) was the first network, which allowed to have a high number of layers, like ResNet50 with 50 layers or ResNet152 with 152 layers. An increased deepness of the networks provides high performance results, but also has the vanishing gradient problem, which ResNet overcomes with including identity shortcut connections, skipping layers in the network. Furthermore, the network uses blocks composed of convolutions, batch normalization and ReLU (Fung, 2017).

In the Squeezenet (squeezenet1_0) ([Iandola et al., 2016](#)) architecture the usually used 3 x 3 filters are replaced with 1 x 1 filters. Also, the input channels are decreased using so-called squeeze layers, which are expanded to a combination of 1 x 1 and 3 x 3 convolutional layers. Downsampling takes place late in the network, resulting in large activation maps. The benefit of the network is the high accuracy which can be achieved using less parameters (Tsang, 2019).

DenseNet (densenet161) ([Huang et al., 2016](#)) uses dense connection, few parameters with achieving high accuracies. In the DenseNet, all layers are connected, which increases the input, while also feature maps are distributed over the connection. Since the feature maps are distributed, the network can be thinner and more compact, but can have at the same time, due to a more efficient computation and memory, more layers, like the one used in this work with 161 layers. The network is built up by a pre-activation, batch normalization, ReLU and finally the 3 x 3 convolutional layers.

Wide ResNets (wide_resnet101_2) ([Zagoruyko and Komodakis, 2016](#)) are modifications of ResNet, shallower than the ResNet, without losing accuracies. A shallow network can be reduced in the number of layers and the needed trainings time. Wide ResNets allow adding more feature maps in each layer, which enables the possibility to reduce the depth of the network. Furthermore, the order of the layers is changed from convolution – batch normalization – ReLU to batch normalization – ReLU – convolutional layer ([Zaguroyko & Komodakis, 2016](#)).

ResNeXt (resnext101_32x8d) ([Xi et al., 2016](#)) is another modification of the ResNet network. The network uses the split-transform-merge paradigm, where the outputs of paths are merged together. Introduced are hyper-parameter, the cardinality, which help to adjust the capacity of the network. The cardinality influences the outcome better than the deepness of the model and the applicability to new datasets and tasks can be better performed ([Fung, 2017](#)).

XI. Appendix A – N

Appendix A - Flights

Flight no.	Date	Site	Coverage [ha]	Flight time	Altitude [m]	Images no.
Summer 2018						
1	20.06.2018	1	1.50	14.30-15.00	40	429
2	22.06.2018	1	1.5	13.30-14.30	60	1335
3	22.06.2018	1	1.5	15.15-16.05	40	697
4	26.06.2018	2	lower part	12.30-13.30	84 -100	%
5	26.06.2018	2	higher part	15.30-16.10	120-130	%
6	03.07.2018	1	1.41	10.00-10.30	50	280
7	03.07.2018	1	1.41	12.00-12.20	50	264
8	03.07.2018	1	1.41	12.20-12.35	50	275
9	03.07.2018	2	complete	13.40-14.25	50-120	%
10	03.07.2018	1	1.41	15.05-15.20	50	265
11	03.07.2018	1	1.41	15.20-15.40	50	285
12	12.07.2018	1	6	morning	%	%
13	12.07.2018	1	6	13.00-13.15	80	216
13	12.07.2018	1	6	13.25-13.36	120	270
14	18.07.2018	1	6	8.30-8.40	120	282
14	18.07.2018	1		8.40-8.54	80	220
15	18.07.2018	1	6	13.40-13.52	80	230
15	18.07.2018	1		13.54-13.05	120	250
Autumn 2018						
16	04.10.2018	1	6	13:05-13.20	80	202
16	04.10.2018	1		13.20-13.35	120	270
17a	10.10.2018	1	6	9.45-10.15	80+120	510
17b	10.10.2018	1		13.00-13.30	80+120	495
18	16.10.2018	1	6	10.50-11.00	120	510
18	16.10.2018	1		11.01-11.16	80	/
19	16.10.2018	2	8.1	11.40-11.50	120	531
19	16.10.2018	2		12.35-12.53		/
20	16.10.2018	1	6	13.05-13.15	120	502
20	16.10.2018	1		13.16-13.30	80	/
21	22.10.2018	1	6	10.30-10.42	120	263
21	22.10.2018	1		10.45-10.59	80	201
22	22.10.2018	2	8.1	11.52-12.15	205	/
22	22.10.2018	2		12.20-12.30	150	200
23	22.10.2018	1	6	12.52-13.03	120	264
23	22.10.2018	1		13.07-13.19	80	207
24	26.10.2018	1	6	10.17-10.35	120	583
24	26.10.2018	1		10.40-10.52	80	/
25	26.10.2018	2	8.1	12.00-12.12	205	472

25	26.10.2018	2		12.14-12.29	150	/
26	26.10.2018	3	5.5	12.38-12.57	110	584
26	26.10.2018	3		13.05-13.22	145	/
27	26.10.2018	1	6	13.35-13.47	120	273
27	26.10.2018	1		13.51-14.04	80	214
28	06.11.2018	2	8.1	12.38-12.53	205	260
28	06.11.2018	2		12.54-13.02	150	220
29	06.11.2018	3	5.5	13.16-13.35	312	110
29	06.11.2018	3		13.36-13.50	254	145
30	06.11.2018	3	5.5	11.43-12.00	317	110
30	06.11.2018	3		12.02-12.17	255	145
31	06.11.2018	2	8.1	14.51-15.06	205	458
31	06.11.2018	2		15.06-15.20	150	/
32	08.11.2018	3	5.5	9.30-9.46	145	251
32	08.11.2018	3		9.51-10.13	110	320
33	08.11.2018	2	8.1	10.20-10.32	205	256
33	08.11.2018	2		10.34-10.45	150	208
34	08.11.2018	3	5.5	10.50-11.05	145	/
34	08.11.2018	3		11.08-11.20	110	322
35	08.11.2018	2	8.1	12.34-12.47	205	260
35	08.11.2018	2		12.48-13.00	150	185
Winter 2018/19						
36	27.02.2019	1	6	15.58-16.27	80+120	274
37	27.02.2019	2	8.1	15.28-15.55	150+205	472
38	28.02.2019	3	5.5	11.24-11.57	110+145	556
39	09.04.2019	1	6	11.02-11.32	80+120	503
40	09.04.2019	4	3	14:13-14:28	80	233
41	09.04.2019	6	4.1	15:11-15:26	80	279
42	16.04.2019	1	6	13:07-13:33	80+120	487
Spring 2019						
43	28.04.2019	8	4.3	14:23-14:38	100	301
44	28.04.2019	9	6.1	14:02-14:18	150	304
45	28.04.2019	2	8.1	15:47-16:17	150+205	456
46	04.05.2019	8	4.3	12:53-13:08	100	300
47	04.05.2019	9	6.1	12:33-12:49	150	325
48	04.05.2019	12	3	13:09-13:19	100	137
49	04.05.2019	13	4.8	13:21-13:35	100	264
50	04.05.2019	10	5.4	13:41-13:45	140	252
51	04.05.2019	5	3.4	14.11-14:32	130+150	385
52	04.05.2019	2	8.1	15:28-15:50	150+205	457
53	04.05.2019	3	5.5	15:52-16:26	110+145	564
54	12.05.2019	9	6.1	12:06-12:20	150	269
55	12.05.2019	8	4.3	12:24-12:39	100	293
56	12.05.2019	10	5.4	12:43-12:56	140	240

57	12.05.2019	2	8.1	13:40-14:07	150+205	458
58	12.05.2019	3	5.5	14:08-14:41	110+145	582
59	12.05.2019	1	6	14:45-15:12	80+120	486
60	12.05.2019	5	3.4	15:46-16:04	130+150	332
61	12.05.2019	6	4.1	16:15-16:30	80	294
62	20.05.2019	9	6.1	9:05-9:18	150	268
63	20.05.2019	8	4.3	9:24-9:39	100	302
64	20.05.2019	10	5.4	9:44-9:56	140	242
65	20.05.2019	7	5.1	10:01-10:13	90	244
66	20.05.2019	6	4.1	10:24-10:39	80	296
67	20.05.2019	2	8.1	11:27-11:56	150+205	459
68	20.05.2019	3	5.5	12:07-12:44	110+150	594
69	20.05.2019	1	6	12:45-13:14	80+120	497
70	20.05.2019	5	3.4	14:47-15:01	130+150	365
71	20.05.2019	4	3	15:05-15:17	80	231
Summer 2019						
72	04.06.2019	9	6.1	10:07-10:20	150	266
73	04.06.2019	2	8.1	11:52-12:21	150+205	456
74	04.06.2019	3	5.5	13:05-13:35	110+145	515
75	04.06.2019	1	6	14:03-14:36	80+120	437
76	04.06.2019	5	3.4	15:18-15:41	130+150	328
77	04.06.2019	4	3	15:45-15:58	80	234
78	04.06.2019	7	5.1	16:06-16:20	90	248
79	13.06.2019	9	6.1	16:50-17:05	150	270
80	13.06.2019	8	4.3	17:10-17:25	110	299
81	13.06.2019	10	5.4	17:29-17:42	140	233
82	13.06.2019	1	6	18:04-18:44	80+120	419
83	14.06.2019	5	3.4	9:37-10:00	130+150	324
84	14.06.2019	4	3	10:01-10:16	80	232
85	14.06.2019	6	4.1	10:25-10:38	80	218
86	14.06.2019	2	8.1	11:24-11:56	205+150	457
87	14.06.2019	7	5.1	13:25-13:38	90	240
88	14.06.2019	11	3.5	13:41-13:52	100	214
89	14.06.2019	12	3	13:55-14:08	100	236
90	14.06.2019	13	4.8	14:10-14:25	100	259
91	20.06.2019	9	6.1	9:04-9:35	150	265
92	20.06.2019	8	4.3	9:22-9:35	100	269
93	20.06.2019	10	5.4	9:35-9:51	140	241
94	20.06.2019	7	5.1	9:45-10:08	90	245
95	20.06.2019	13	4.8	10:10-10:24	100	260
96	20.06.2019	6	4.1	10:47-11:02	80	290
97	20.06.2019	2	8.1	11:57-12:24	205+150	450
98	20.06.2019	3	5.5	12:50-13:18	145+110	494
99	20.06.2019	1	6	13:26-13:54	80+120	419
100	20.06.2019	5	3.4	14:55-15:13	150+130	321
101	20.06.2019	4	3	15:16-15:29	80	230

102	20.06.2019	6	4.1	15:34-15:49	80	294
103	20.06.2019	11	3.5	16:13-16:25	100	216
104	20.06.2019	12	3	16:27-16:40	100	247
105	26.06.2019	9	6.1	9:20-9:33	150	262
106	26.06.2019	8	4.3	9:36-9:50	100	264
107	26.06.2019	6	4.1	9:57-10:11	80	290
108	26.06.2019	5	3.4	10:23-10:43	150+130	319
109	26.06.2019	Spectral 8		12:14-12:22	115	245
110	26.06.2019	6	4.1	12:25-12:50	80	291
111	26.06.2019	5	3.4	13:00-13:15	150+130	296
112	26.06.2019	Spectral 8		14:59-15:11	115	250
113	26.06.2019	6	4.1	15:20-15:34	80	292
114	26.06.2019	5	3.4	15:43-16:00	150+130	291
115	04.07.2019	9	6.1	10:30-10:41	150	263
116	04.07.2019	10	5.4	10:45-10:59	140	241
117	04.07.2019	7	5.1	11:01-11:15	90	224
118	04.07.2019	13	4.8	11:18-11:31	100	257
119	04.07.2019	12	3	11:35-11:47	100	241
120	04.07.2019	11	3.5	11:50-12:01	100	213
121	04.07.2019	2	8.1	12:45-13:12	205+150	430
122	04.07.2019	3	5.5	13:31-14:03	110+145	497
123	10.07.2019	1	6	10:20-10:46	80+120	426
124	10.07.2019	5	3.4	11:05-11:22	150+130	289
125	10.07.2019	4	3	11:26-11:35	80	242
126	10.07.2019	6	4.1	11:47-12:01	80	270
127	10.07.2019	9	6.10	12:10-12:19	150	265
128	10.07.2019	7	5.1	12:28-12:40	90	227
129	21.07.2019	Spectral 8		9:41-9:55	115	249
130	21.07.2019	7	5.1	9:55-10:11	90	236
131	21.07.2019	6	4.1	10:18-10:32	80	285
132	21.07.2019	5	3.4	10:40-10:57	150+130	296
133	21.07.2019	Spectral 8		12:05-12:18	115	245
134	21.07.2019	12	3	12:21-12:34	100	241
135	21.07.2019	6	4.1	12:42-12:57	80	291
136	21.07.2019	5	3.4	13:08-13:23	150+130	296
137	21.07.2019	3	5.5	14:05-14:34	110+145	498
138	21.07.2019	5	3.4	15:02-15:18	150+130	297
139	21.07.2019	6	4.1	15:28-15:41	80	290
140	21.07.2019	Spectral 8		15:50-16:02	115	248
141	21.07.2019	10	5.4	16:06-16:20	140	237
142	26.07.2019	13	4.8	9:17-9:30	100	256
143	26.07.2019	11	3.5	9:32-9:46	100	214
144	26.07.2019	9	6.1	9:47-10:01	150	262
145	26.07.2019	6	4.1	10:33-10:48	80	291
146	26.07.2019	10	5.4	10:59-11:12	140	240
147	26.07.2019	7	5.1	11:13-11:28	90	245
148	26.07.2019	spectral8		11:29-11:45	115	248
149	26.07.2019	12	3	11:47-11:59	100	244

150	26.07.2019	2	8.1	13:59-14:14	150+205	239
151	26.07.2019	1	6	15:27-15:50	80+120	429
152	26.07.2019	5	3.4	16:18-16:34	130+150	268
153	26.07.2019	4	3	16:38-16:46	80	224
154	26.07.2019	3	5.5	14:36-15:05	110+145	499
155	17.08.2019	13	4.8	9:29-9:42	100	255
156	17.08.2019	10	5.4	9:48-10:00	140	241
157	17.08.2019	7	5.1	10:05-10:17	90	249
158	17.08.2019	9	6.1	10:20-10:34	150	269
159	17.08.2019	11	3.5	10:42-10:53	100	202
160	17.08.2019	12	3	10:57-11:09	100	243
161	17.08.2019	6	4.1	12:29-12:44	80	290
162	17.08.2019	5	3.4	12:45-13:10	130+150	296
163	17.08.2019	4	3	13:14-13:25	80	237
164	17.08.2019	2	8.1	13:45-14:11	150+205	430
165	17.08.2019	3	5.5	14:52-15:20	110+145	498
166	17.08.2019	1	6	15:32-15:56	80+120	432
167	17.08.2019	8	4.3	16:10-16:24	100	270
168	21.08.2019	spectral 8		9:53-10:07		247
169	21.08.2019	6	4.1	10:13-10:29	80	290
170	21.08.2019	5	3.4	10:34-10:52	130+150	287
171	21.08.2019	1	6	13:42-14:04		401
172	21.08.2019	5	3.4	12:43-13:01	130+150	292
173	21.08.2019	6	4.1	12:22-12:38	80	295
174	21.08.2019	spectral 8		12:03-12:18		248
175	21.08.2019	5	3.4	15:05-15:23	130+150	290
176	21.08.2019	6	4.1	15:28-15:44	80	291
177	21.08.2019	spectral 8		15:49-16:03		242
Autumn 2019						
178	03.09.2019	1	6	9:03-9:14	80	219
179	03.09.2019	2	8.1	9:27-9:54	150+205	431
180	03.09.2019	3	5.5	9:58-10:37	110+145	497
181	03.09.2019	4	3	10:44-10:56	80	234
182	03.09.2019	5	3.4	11:00-11:15	130+150	297
183	03.09.2019	6	4.1	11:33-11:48	80	282
184	03.09.2019	7	5.1	12:12-12:24	90	245
185	03.09.2019	8	4.3	12:54-13:08	100	268
186	03.09.2019	9	6.1	13:12-13:26	150	262
187	03.09.2019	13	4.8	14:02-14:15	100	235
188	03.09.2019	12	3	14:19-14:31	100	245
189	03.09.2019	11	3.5	14:34-14:45	100	240
190	03.09.2019	10	5.4	15:08-15:20	140	242
191	18.09.2019	10	5.4	7:05-7:20	140	222
192	18.09.2019	13	4.8	7:23-7:36	100	251
193	18.09.2019	12	3	7:41-7:54	100	238
194	18.09.2019	11	3.5	8:20-8:31	100	217

195	18.09.2019	9	6.1	8:34-8:47	150	265
196	18.09.2019	8	4.3	8:51-9:04	100	268
197	18.09.2019	7	5.1	2:22-9:34	90	243
198	18.09.2019	6	4.1	9:37-9:52	80	291
199	18.09.2019	5	3.4	10:06-10:22	130+150	294
200	18.09.2019	4	3	10:25-10:37	80	235
201	18.09.2019	2	8.1	10:52-11:19	150+205	441
202	18.09.2019	3	5.5	11.34-12:03	110+145	501
203	18.09.2019	1	6	12:07-12:29	80+120	433
204	09.10.2019	13	4.8	9:24-9:39	100	280
205	09.10.2019	12	3	9:43-9:56	100	230
206	09.10.2019	11	3.5	10:02-10:13	100	215
207	09.10.2019	9	6.1	10:18-10:32	150	270
208	09.10.2019	8	4.3	10:35-10:49	100	269
209	09.10.2019	7	5.1	10:53-11:08	90	246
210	09.10.2019	5	3.4	13:39-13:56	130+150	294
211	09.10.2019	4	3	14:01-14:13	80	229
212	09.10.2019	6	4.1	14:20-14:40	80	295
213	09.10.2019	10	5.4	14:57-15:11	140	238
214	16.10.2019	10	5.4	9:05-9:21	140	248
215	16.10.2019	9	6.1	9:24-9:40	150	267
216	16.10.2019	7	5.1	9:47-10:01	90	247
217	16.10.2019	13	4.8	10:04-10:19	100	262
218	16.10.2019	6	4.1	10:30-10:47	80	294
219	16.10.2019	4	3	10:56-11:12	80	243
220	18.10.2019	1	6	8:03-8:35	80+120	446
221	18.10.2019	12	3	14:03-11:19	100	249
222	18.10.2019	11	3.5	14:21-14:34	100	216
223	29.10.2019	3	5.5	9:33-10:05	110+145	506
224	29.10.2019	5	3.4	10:29- 10:45	130+150	301
225	29.10.2019	2	8.1	10:56-11:42	150+205	447
226	29.10.2019	10	5.4	14:16-14:34	140	251
227	29.10.2019	9	6.1	14:37-14:57	150	328
228	29.10.2019	8	4.3	14:59-15:11	100	215
229	29.10.2019	13	4.8	15:13-15:28	100	265
230	29.10.2019	12	3	15:31-15:46	100	240
231	29.10.2019	11	3.5	15.49-16:02	100	219
232	08.11.2019	2	8.1	9:43-10:15	150+205	446
233	08.11.2019	3	5.5	10:33-11:03	110+145	507
234	07.11.2019	8	4.3	11:15-11:30	100	279
235	07.11.2019	9	6.1	10:56-11:12	150	266
236	07.11.2019	10	5.4	10:36-10:53	140	250
237	07.11.2019	11	3.5	10:06-12:21	100	214
238	07.11.2019	12	3	11:49-12:05	100	245
239	07.11.2019	13	4.8	11:33-11:48	100	263
Winter 2020						

240	19.02.2020	7	5.1	16:06-16:16	90	249
241	19.02.2020	8	4.3	16:38-16:53	100	277
242	19.02.2020	9	6.1	16:20-16:34	150	268
243	20.02.2020	10	5.4	11:44-12:04	140	260
244	20.02.2020	11	3.5	12:07-12:19	100	217
245	20.02.2020	12	3	12:23-12:37	100	250
246	20.02.2020	13	4.8	12:43-12:57	100	290
Summer 2020						
247	18.06.2020	Salix		16:53-17:08	50	380
248	18.06.2020	Crenata		16:23-16:38	50	296
249	02.06.2020	1	6	9:57-11:12	close	1066
250	26.06.2020	3	5.5	11:20-12:20	close	869
251	28.06.2020	7	5.1	13:46-14:30	close	576
252	28.06.2020	13	4.8	14:30-14:59	close	443
253	28.06.2020	8	4.3	12:51-13:46	close	732
254	28.06.2020	9	6.1	12:51-13:46	close	/
255	26.07.2020	4	3	13:27-14:20	close	665
256	26.07.2020	5	3.4	14:20-14:50	close	358
257	26.07.2020	6	4.1	12:24-13:19	close	751
258	26.07.2020	11	3.5	15:38-16:34	close	784
259	26.07.2020	12	3	15:38-16:34	close	/
260	02.08.2020	Black locust		12:51-12:59	50	129
261	02.08.2020	Crenata		17:17-17:29	50	296
262	02.08.2020	5	3.4	16:04-16:09	close	69
263	02.08.2020	10	5.4	16:19-16:56	close	791
264	02.08.2020	2	8.1	14:23-15:16	close	728
265	02.08.2020	4	3	15:56-16:09	close	221
266	02.08.2020	1	6	15:28-15:38	close	187
267	10.08.2020	10	5.4	15:46-15:57	close	236
268	10.08.2020	7	5.1	15:41-15:45	close	106
269	10.08.2020	2	8.1	15:15-15:31	close	258
270	10.08.2020	4	3	14:31-14:35	close	138
271	10.08.2020	1	6	14:56-15:04	close	175
272	16.08.2020	1	6	12:45-12:59	close	182
273	16.08.2020	5	3.4	13:22-13:24	close	54
274	16.08.2020	6	4.1	12:22-12:32	close	245
275	16.08.2020	10	5.4	10:27-10:34	close	119
276	16.08.2020	12	3	11:16-11:40	close	487
277	16.08.2020	8	4.3	11:41-12:10	close	539
278	16.08.2020	9	6.1	11:41-12:10	close	/
Autumn 2020						
279	08.10.2020	7	5.1	9:47-9:59	90	361
280	08.10.2020	13	4.8	10:07-10:20	100	382

281	08.10.2020					
282	08.10.2020	12	3	14:21-14:34	100	355
283	08.10.2020	11	3.5	14:36-14:49	100	365
284	08.10.2020	9	6.1	14:52-15:03	150	337
285	08.10.2020	10	5.4	15:07-15:18	140	320
286	08.10.2020	8	4.3	15:21-15:35	100	396
287	08.10.2020	4	3	11:18-11:32	80	412
288	08.10.2020	6	4.1	10:53-11:09	80	454
Winter 2021						
289	08.03.2021	5	3.4	11:37-11:51	130+150	358
290	08.03.2021	8	4.3	12:29-12:43	100	397
291	08.03.2021	9	6.1	12:10-12:24	150	403
292	08.03.2021	10	5.4	12:47-12:57	140	322
293	08.03.2021	11	3.5	13:03-13:16	100	365
294	08.03.2021	13	4.8	13:19-13:24	100	382
295	08.03.2021	7	5.1	13:36-13:49	90	361

Appendix B – Programmed setting for flights

Site	Waypoints	Flight length	Cover area	Shooting angle	Capture mode	Shutter interval	Speed	Altitude	Flight time	Photo	Front + Side overlap
1.1	52	2258	2.47	Parallel to main path	at equal time interval	3 sec	3.5	80	13 min 3 sec	227	90 + 90
1.2	10	1702	1.83	Parallel to main path	at equal time interval	2 sec	3.7	120	9 min 11 sec	221	95 + 95
2.1	26	1665	1.45	Parallel to main path	at equal time interval	3 sec	2.6	150	12 min 38 sec	203	96 + 96
2.2	22	2219	2.19	Parallel to main path	at equal time interval	3 sec	2.8	205	15 min 40 sec	245	97 + 97
3.1	20	1980	1.9	Parallel to main path	at equal time interval	3 sec	2.5	110	15 min 33 sec	254	95 + 95
3.2	20	2064	1.96	Parallel to main path	at equal time interval	3 sec	2.6	145	15 min 52 sec	254	96 + 96
4	27	2007	1.94	Parallel to main path	at equal time interval	3 sec	2.8	80	14 min 29 sec	241	92 + 92
5.1	8	1201	1.18	Parallel to main path	at equal time interval	3 sec	2.8	130	8 min 29 sec	131	95 + 95
5.2	12	1447	1.25	Parallel to main path	at equal time interval	3 sec	2.6	150	11 min 8 sec	172	96 + 96
6	20	2466	2.45	Parallel to main path	at equal time interval	3 sec	2.8	80	17 min 48 sec	296	92 + 92
7	16	2094	2.05	Parallel to main path	at equal time interval	3 sec	2.7	90	15 min 14 sec	250	93 + 93
8	18	2175	1.79	Parallel to main path	at equal time interval	3 sec	2.6	100	16 min 44 sec	276	94 + 95
9	20	2658	2.34	Parallel to main path	at equal time interval	3 sec	3.2	150	16 min 22 sec	269	95 + 96
10	30	2284	2.18	Parallel to main path	at equal time interval	3 sec	3	140	15 min 4 sec	249	95 + 96
11	24	1748	1.56	Parallel to main path	at equal time interval	3 sec	2.6	100	13 min 23 sec	220	94 + 94
12	26	1961	1.49	Parallel to main path	at equal time interval	3 sec	2.6	100	15 min 1 sec	251	94 + 95
13	16	2091	1.62	Parallel to main path	at equal time interval	3 sec	2.6	100	16 min 4 sec	264	94 + 95
spectral 8	22	2320	2.03	Parallel to main path	at equal time interval	3 sec	3	115	15 min 32 sec	253	94 + 95

Appendix C – Density measures per site

Site 1

Tree species	Abbreviation	Number	relative Density	Density per ha and species
<i>Juglans ailantifolia</i>	S01	107	13.67	24.95
<i>Aesculus turbinata</i>	S02	24	3.07	5.60
<i>Cryptomeria japonica</i>	S03	201	25.67	46.87
<i>Pterocarya rhoifolia</i>	S04	125	15.96	29.15
<i>Quercus mongolica</i> subsp. <i>crispula</i>	S05	9	1.15	2.10
<i>Larix kaempferi</i>	S06	19	2.43	4.43
<i>Fagus crenata</i>	S07		0.00	0.00
<i>Magnolia obovata</i>	S08	19	2.43	4.43
<i>Acer japonicum</i> , <i>sieblodium</i> , <i>palmatum</i>	S09	145	18.52	33.81
<i>Prunus salicina</i> Lindley, <i>Prunus serrulata/grayana</i> , <i>Prunus speciosa</i>	S10	13	1.66	3.03
<i>Acer mono maxim</i> , <i>Acer pictum</i> subsp. <i>mono</i>	S11	15	1.92	3.50
<i>Salix serissaefolia</i>	S12		0.00	0.00
<i>Salix jessoensis</i>	S13	8	1.02	1.87
<i>Castanea Crenata</i>	S14	4	0.51	0.93
<i>Robinia pseudoaccacia</i>	S15	14	1.79	3.26
<i>Cornus controversa</i>	S16	23	2.94	5.36
<i>Phelledendron amurense</i>	S17	9	1.15	2.10
<i>Betula corylifolia</i>	S18		0.00	0.00
<i>Alnus inokumae</i> , <i>Alnus hirsuta</i>	S19		0.00	0.00
<i>Picea abies</i>	S20		0.00	0.00
<i>Cercidiphyllum japonicum</i> var. <i>Magnificum</i>	S21		0.00	0.00
<i>Albizia julibrissin</i>	S22		0.00	0.00
Japanese <i>Hydrangea</i> , <i>Schizophragma hydrangeoides</i> and <i>Smilax</i>	S23	13	1.66	3.03
<i>Morus australis</i>	S24		0.00	0.00
<i>Clethra barvinervis</i> Sieb. et Zucc.	S25		0.00	0.00
<i>Tilia japonica</i> , <i>Tilia maximowicziana</i>	S26	28	3.58	6.53
Japanese honeysuckle, <i>Lonicera japonica</i>	S27		0.00	0.00
<i>Kalopanax septemlobu</i>	S28		0.00	0.00
<i>Acer nipponicum</i>	S29		0.00	0.00
<i>Celtis jessoensis</i>	S30		0.00	0.00
<i>Alnus fauriei</i>	S31	0	0.00	0.00
<i>Betula corylifolia</i>	S32		0.00	0.00
<i>Aralia elata</i>	S33		0.00	0.00
<i>Zanthoxylum piperitum</i> ,	S34		0.00	0.00
<i>Fraxinus lanugiosa</i>	S35		0.00	0.00
<i>Fraxinus mandshurica</i> var. <i>japonica</i>	S36		0.00	0.00
<i>Ginko biloba</i>	S38		0.00	0.00
<i>Styrax obassia</i> ,	S39	0	0.00	0.00

Hamamelis japonica	S40	0	0.00	0.00
Acer japonica	S41		0.00	0.00
Corylus sieboldiana	S42	5	0.64	1.17
Carpinus Cordata	S43	2	0.26	0.47
	mix		0.00	0.00
	Sum	783		

Site 2

Tree species	Abbreviation	Number	relative Density	Density per ha and species
Juglans ailantifolia	S01	23	2.77	5.73
Aesculus turbinata	S02	35	4.21	8.73
Cryptomeria japonica	S03	195	23.47	48.62
Pterocarya rhoifolia	S04	3	0.36	0.75
Quercus mongolica subsp. crispula	S05	45	5.42	11.22
Larix kaempferi	S06		0.00	0.00
Fagus crenata	S07		0.00	0.00
Magnolia obovata	S08	63	7.58	15.71
Acer japonicum, sieblodium, palmatum	S09	351	42.24	87.51
Prunus salicina Lindley, Prunus serrulata/grayana, Prunus speciosa	S10		0.00	0.00
Acer mono maxim, Acer pictum subsp. Mono	S11	63	7.58	15.71
Salix serissaefolia	S12		0.00	0.00
Salix jessoensis	S13		0.00	0.00
Castanea Crenata	S14		0.00	0.00
Robinia pseudoaccacia	S15		0.00	0.00
Cornus controversa	S16	7	0.84	1.75
Phelledendron amurense	S17		0.00	0.00
Betula corylifolia	S18	2	0.24	0.50
Alnus inokumae, Alnus hirsuta	S19		0.00	0.00
Picea abies	S20		0.00	0.00
Cercidiphyllum japonicum var. Magnificum	S21		0.00	0.00
Albizia julibrissin	S22		0.00	0.00
Japanese Hydrangea, Schizophragma hydrangeoides and Smilax	S23	2	0.24	0.50
Morus australis	S24	6	0.72	1.50
Clethra barvinervis Sieb. et Zucc.	S25		0.00	0.00
Tilia japonica, Tilia maximowicziana	S26	4	0.48	1.00
Japanese honeysuckle, Lonicera japonica	S27		0.00	0.00
Kalopanax septemlobu	S28		0.00	0.00
Acer nipponicum	S29		0.00	0.00
Celtic jessoensis	S30		0.00	0.00
Alnus fauriei	S31		0.00	0.00
Betula corylifolia	S32		0.00	0.00
Aralia elata	S33		0.00	0.00

Zanthoxylum piperitum,	S34		0.00	0.00
Fraxinus lanugiosa	S35		0.00	0.00
Fraxinus mandshurica var. japonica	S36		0.00	0.00
Ginko biloba	S38		0.00	0.00
Styrax obassia,	S39	6	0.72	1.50
Hamamelis japonica	S40	10	1.20	2.49
Acer japonica	S41		0.00	0.00
Corylus sieboldiana	S42		0.00	0.00
Carpinus Cordata	S43	14	1.68	3.49
	mix	2	0.24	0.50
	Sum	831	100	

Site 3

Tree species	Abbreviation	Number	relative Density	Density per ha and species
Juglans ailantifolia	S01	53	4.83	15.18
Aesculus turbinata	S02	3	0.27	0.86
Cryptomeria japonica	S03	122	11.11	34.95
Pterocarya rhoifolia	S04	3	0.27	0.86
Quercus mongolica subsp. crispula	S05	66	6.01	18.91
Larix kaempferi	S06	27	2.46	7.73
Fagus crenata	S07	27	2.46	7.73
Magnolia obovata	S08	32	2.91	9.17
Acer japonicum, sieblodium, palmatum	S09	605	55.10	173.31
Prunus salicina Lindley, Prunus serrulata/grayana, Prunus speciosa	S10	3	0.27	0.86
Acer mono maxim, Acer pictum subsp. Mono	S11	75	6.83	21.48
Salix serissaefolia	S12	1	0.09	0.29
Salix jessoensis	S13	2	0.18	0.57
Castanea Crenata	S14	4	0.36	1.15
Robinia pseudoaccaccia	S15		0.00	0.00
Cornus controversa	S16	17	1.55	4.87
Phelledendron amurense	S17		0.00	0.00
Betula corylifolia	S18		0.00	0.00
Alnus inokumae, Alnus hirsuta	S19		0.00	0.00
Picea abies	S20		0.00	0.00
Cercidiphyllum japonicum var. Magnificum	S21		0.00	0.00
Albizia julibrissin	S22		0.00	0.00
Japanese Hydrangea, Schizophragma hydrangeoides and Smilax	S23	14	1.28	4.01
Morus australis	S24	7	0.64	2.01
Clethra barvinervis Sieb. et Zucc.	S25		0.00	0.00
Tilia japonica, Tilia maximowicziana	S26	7	0.64	2.01
Japanese honeysuckle, Lonicera japonica	S27	2	0.18	0.57
Kalopanax septemlobu	S28	1	0.09	0.29

Acer nipponicum	S29		0.00	0.00
Celtis jessoensis	S30		0.00	0.00
Alnus fauriei	S31	19	1.73	5.44
Betula corylifolia	S32		0.00	0.00
Aralia elata	S33		0.00	0.00
Zanthoxylum piperitum,	S34		0.00	0.00
Fraxinus lanugiosa	S35	3	0.27	0.86
Fraxinus mandshurica var. japonica	S36		0.00	0.00
Ginkgo biloba	S38		0.00	0.00
Styrax obassia,	S39	4	0.36	1.15
Hamamelis japonica	S40		0.00	0.00
Acer japonica	S41	1	0.09	0.29
Corylus sieboldiana	S42		0.00	0.00
Carpinus Cordata	S43		0.00	0.00
	mix		0.00	0.00
	Sum	1098	100.00	314.53

Site 4

Tree species	Abbreviation	Number	relative Density	Density per ha and species
Juglans ailantifolia	S01	58	17.79	32.87
Aesculus turbinata	S02		0.00	0.00
Cryptomeria japonica	S03	129	39.57	73.12
Pterocarya rhoifolia	S04	9	2.76	5.10
Quercus mongolica subsp. crispula	S05	7	2.15	3.97
Larix kaempferi	S06	7	2.15	3.97
Fagus crenata	S07		0.00	0.00
Magnolia obovata	S08	6	1.84	3.40
Acer japonicum, sieboldium, palmatum	S09	12	3.68	6.80
Prunus salicina Lindley, Prunus serrulata/grayana, Prunus speciosa	S10	0	0.00	0.00
Acer mono maxim, Acer pictum subsp. Mono	S11	1	0.31	0.57
Salix serissaefolia	S12	78	23.93	44.21
Salix jessoensis	S13	1	0.31	0.57
Castanea Crenata	S14		0.00	0.00
Robinia pseudoaccacia	S15		0.00	0.00
Cornus controversa	S16	2	0.61	1.13
Phelledendron amurense	S17		0.00	0.00
Betula corylifolia	S18		0.00	0.00
Alnus inokumae, Alnus hirsuta	S19		0.00	0.00
Picea abies	S20		0.00	0.00
Cercidiphyllum japonicum var. Magnificum	S21	2	0.61	1.13
Albizia julibrissin	S22		0.00	0.00
Japanese Hydrangea, Schizophragma hydrangeoides and Smilax	S23	12	3.68	6.80

Morus australis	S24	1	0.31	0.57
Clethra barvinervis Sieb. et Zucc.	S25		0.00	0.00
Tilia japonica, Tilia maximowicziana	S26		0.00	0.00
Japanese honeysuckle, Lonicera japonica	S27		0.00	0.00
Kalopanax septemlobu	S28		0.00	0.00
Acer nipponicum	S29		0.00	0.00
Celtis jessoensis	S30		0.00	0.00
Alnus fauriei	S31	0	0.00	0.00
Betula corylifolia	S32	1	0.31	0.57
Aralia elata	S33		0.00	0.00
Zanthoxylum piperitum,	S34		0.00	0.00
Fraxinus lanugiosa	S35		0.00	0.00
Fraxinus mandshurica var. japonica	S36		0.00	0.00
Ginko biloba	S38		0.00	0.00
Styrax obassia,	S39		0.00	0.00
Hamamelis japonica	S40		0.00	0.00
Acer japonica	S41		0.00	0.00
Corylus sieboldiana	S42		0.00	0.00
Carpinus Cordata	S43		0.00	0.00
	mix		0.00	0.00
	Sum	326		

Site 5

Tree species	Abbreviation	Number	relative Density	Density per ha and species
Juglans ailantifolia	S01	47	9.13	23.52
Aesculus turbinata	S02	18	3.50	9.01
Cryptomeria japonica	S03	51	9.90	25.53
Pterocarya rhoifolia	S04	14	2.72	7.01
Quercus mongolica subsp. crispula	S05	53	10.29	26.53
Larix kaempferi	S06	0	0.00	0.00
Fagus crenata	S07	4	0.78	2.00
Magnolia obovata	S08	42	8.16	21.02
Acer japonicum, sieblodium, palmatum	S09	176	34.17	88.09
Prunus salicina Lindley, Prunus serrulata/grayana, Prunus speciosa	S10	0	0.00	0.00
Acer mono maxim, Acer pictum subsp. Mono	S11	52	10.10	26.03
Salix serissaefolia	S12		0.00	0.00
Salix jessoensis	S13	3	0.58	1.50
Castanea Crenata	S14	1	0.19	0.50
Robinia pseudoaccacia	S15		0.00	0.00
Cornus controversa	S16	13	2.52	6.51
Phelledendron amurense	S17		0.00	0.00
Betula corylifolia	S18		0.00	0.00
Alnus inokumae, Alnus hirsuta	S19		0.00	0.00

<i>Picea abies</i>	S20		0.00	0.00
<i>Cercidiphyllum japonicum</i> var. <i>Magnificum</i>	S21		0.00	0.00
<i>Albizia julibrissin</i>	S22		0.00	0.00
Japanese Hydrangea, <i>Schizophragma hydrangeoides</i> and <i>Smilax</i>	S23	17	3.30	8.51
<i>Morus australis</i>	S24		0.00	0.00
<i>Clethra barvinervis</i> Sieb. et Zucc.	S25		0.00	0.00
<i>Tilia japonica</i> , <i>Tilia maximowicziana</i>	S26		0.00	0.00
Japanese honeysuckle, <i>Lonicera japonica</i>	S27	12	2.33	6.01
<i>Kalopanax septemlobu</i>	S28	4	0.78	2.00
<i>Acer nipponicum</i>	S29		0.00	0.00
<i>Celtis jessoensis</i>	S30		0.00	0.00
<i>Alnus fauriei</i>	S31		0.00	0.00
<i>Betula corylifolia</i>	S32		0.00	0.00
<i>Aralia elata</i>	S33		0.00	0.00
<i>Zanthoxylum piperitum</i> ,	S34		0.00	0.00
<i>Fraxinus lanugiosa</i>	S35		0.00	0.00
<i>Fraxinus mandshurica</i> var. <i>japonica</i>	S36		0.00	0.00
<i>Ginkgo biloba</i>	S38		0.00	0.00
<i>Styrax obassia</i> ,	S39		0.00	0.00
<i>Hamamelis japonica</i>	S40	4	0.78	2.00
<i>Acer japonica</i>	S41	0	0.00	0.00
<i>Corylus sieboldiana</i>	S42	6	1.17	3.00
<i>Carpinus Cordata</i>	S43		0.00	0.00
	mix		0.00	0.00
	Sum	515		

Site 6

Tree species	Abbreviation	Number	relative Density	Density per ha and species
<i>Juglans ailantifolia</i>	S01	47	14.33	21.78
<i>Aesculus turbinata</i>	S02	4	1.22	1.85
<i>Cryptomeria japonica</i>	S03	156	47.56	72.30
<i>Pterocarya rhoifolia</i>	S04	25	7.62	11.59
<i>Quercus mongolica</i> subsp. <i>crispula</i>	S05	3	0.91	1.39
<i>Larix kaempferi</i>	S06		0.00	0.00
<i>Fagus crenata</i>	S07		0.00	0.00
<i>Magnolia obovata</i>	S08	5	1.52	2.32
<i>Acer japonicum</i> , <i>sieboldium</i> , <i>palmatum</i>	S09	10	3.05	4.63
<i>Prunus salicina</i> Lindley, <i>Prunus serrulata/grayana</i> , <i>Prunus speciosa</i>	S10		0.00	0.00
<i>Acer mono maxim</i> , <i>Acer pictum</i> subsp. <i>Mono</i>	S11	5	1.52	2.32
<i>Salix serissaefolia</i>	S12	8	2.44	3.71
<i>Salix jessoensis</i>	S13	16	4.88	7.42
<i>Castanea Crenata</i>	S14	10	3.05	4.63

Robinia pseudoaccacia	S15	7	2.13	3.24
Cornus controversa	S16	5	1.52	2.32
Phelledendron amurense	S17		0.00	0.00
Betula corylifolia	S18	6	1.83	2.78
Alnus inokumae, Alnus hirsuta	S19	1	0.30	0.46
Picea abies	S20	4	1.22	1.85
Cercidiphyllum japonicum var. Magnificum	S21		0.00	0.00
Albizia julibrissin	S22		0.00	0.00
Japanese Hydrangea, Schizophragma hydrangeoides and Smilax	S23	9	2.74	4.17
Morus australis	S24		0.00	0.00
Clethra barvinervis Sieb. et Zucc.	S25		0.00	0.00
Tilia japonica, Tilia maximowicziana	S26		0.00	0.00
Japanese honeysuckle, Lonicera japonica	S27		0.00	0.00
Kalopanax septemlobu	S28		0.00	0.00
Acer nipponicum	S29		0.00	0.00
Celtis jessoensis	S30		0.00	0.00
Alnus fauriei	S31		0.00	0.00
Betula corylifolia	S32		0.00	0.00
Aralia elata	S33		0.00	0.00
Zanthoxylum piperitum,	S34	5	1.52	2.32
Fraxinus lanugiosa	S35		0.00	0.00
Fraxinus mandshurica var. japonica	S36		0.00	0.00
Ginkgo biloba	S38		0.00	0.00
Styrax obassia,	S39		0.00	0.00
Hamamelis japonica	S40		0.00	0.00
Acer japonica	S41		0.00	0.00
Corylus sieboldiana	S42		0.00	0.00
Carpinus Cordata	S43		0.00	0.00
	mix		0.00	0.00
	Sum	328		

Site 7

Tree species	Abbreviation	Number	relative Density	Density per ha and species
Juglans ailantifolia	S01	72	23.84	32.69
Aesculus turbinata	S02	3	0.99	1.36
Cryptomeria japonica	S03	55	18.21	24.97
Pterocarya rhoifolia	S04	22	7.28	9.99
Quercus mongolica subsp. crispula	S05	13	4.30	5.90
Larix kaempferi	S06		0.00	0.00
Fagus crenata	S07		0.00	0.00
Magnolia obovata	S08	1	0.33	0.45
Acer japonicum, sieblodium, palmatum	S09	67	22.19	30.42

<i>Prunus salicina</i> Lindley, <i>Prunus serrulata</i> /grayana, <i>Prunus speciosa</i>	S10		0.00	0.00
<i>Acer mono maxim</i> , <i>Acer pictum</i> subsp. Mono	S11	16	5.30	7.27
<i>Salix serissaefolia</i>	S12		0.00	0.00
<i>Salix jessoensis</i>	S13	14	4.64	6.36
<i>Castanea Crenata</i>	S14		0.00	0.00
<i>Robinia pseudoaccacia</i>	S15	14	4.64	6.36
<i>Cornus controversa</i>	S16		0.00	0.00
<i>Phelledendron amurense</i>	S17		0.00	0.00
<i>Betula corylifolia</i>	S18		0.00	0.00
<i>Alnus inokumae</i> , <i>Alnus hirsuta</i>	S19		0.00	0.00
<i>Picea abies</i>	S20		0.00	0.00
<i>Cercidiphyllum japonicum</i> var. <i>Magnificum</i>	S21		0.00	0.00
<i>Albizia julibrissin</i>	S22	2	0.66	0.91
Japanese <i>Hydrangea</i> , <i>Schizophragma hydrangeoides</i> and <i>Smilax</i>	S23	1	0.33	0.45
<i>Morus australis</i>	S24		0.00	0.00
<i>Clethra barvinervis</i> Sieb. et Zucc.	S25	1	0.33	0.45
<i>Tilia japonica</i> , <i>Tilia maximowicziana</i>	S26		0.00	0.00
Japanese honeysuckle, <i>Lonicera japonica</i>	S27		0.00	0.00
<i>Kalopanax septemlobu</i>	S28		0.00	0.00
<i>Acer nipponicum</i>	S29		0.00	0.00
<i>Celtis jessoensis</i>	S30		0.00	0.00
<i>Alnus fauriei</i>	S31	20	6.62	9.08
<i>Betula corylifolia</i>	S32		0.00	0.00
<i>Aralia elata</i>	S33		0.00	0.00
<i>Zanthoxylum piperitum</i> ,	S34		0.00	0.00
<i>Fraxinus lanugiosa</i>	S35		0.00	0.00
<i>Fraxinus mandshurica</i> var. <i>japonica</i>	S36	1	0.33	0.45
<i>Ginko biloba</i>	S38		0.00	0.00
<i>Styrax obassia</i> ,	S39		0.00	0.00
<i>Hamamelis japonica</i>	S40		0.00	0.00
<i>Acer japonica</i>	S41		0.00	0.00
<i>Corylus sieboldiana</i>	S42		0.00	0.00
<i>Carpinus Cordata</i>	S43		0.00	0.00
	mix		0.00	0.00
	Sum	302		

Site 8

Tree species	Abbreviation	Number	relative Density	Density per ha and species
<i>Juglans ailantifolia</i>	S01	32	6.30	19.45
<i>Aesculus turbinata</i>	S02	8	1.57	4.86
<i>Cryptomeria japonica</i>	S03	7	1.38	4.25
<i>Pterocarya rhoifolia</i>	S04	1	0.20	0.61

Quercus mongolica subsp. crispula	S05	42	8.27	25.52
Larix kaempferi	S06		0.00	0.00
Fagus crenata	S07	1	0.20	0.61
Magnolia obovata	S08	7	1.38	4.25
Acer japonicum, sieblodium, palmatum	S09	241	47.44	146.45
Prunus salicina Lindley, Prunus serrulata/grayana, Prunus speciosa	S10		0.00	0.00
Acer mono maxim, Acer pictum subsp. Mono	S11	38	7.48	23.09
Salix serissaefolia	S12		0.00	0.00
Salix jessoensis	S13	1	0.20	0.61
Castanea Crenata	S14	2	0.39	1.22
Robinia pseudoaccacia	S15		0.00	0.00
Cornus controversa	S16	14	2.76	8.51
Phelledendron amurense	S17		0.00	0.00
Betula corylifolia	S18	13	2.56	7.90
Alnus inokumae, Alnus hirsuta	S19		0.00	0.00
Picea abies	S20		0.00	0.00
Cercidiphyllum japonicum var. Magnificum	S21		0.00	0.00
Albizia julibrissin	S22		0.00	0.00
Japanese Hydrangea, Schizophragma hydrangeoides and Smilax	S23	15	2.95	9.12
Morus australis	S24	14	2.76	8.51
Clethra barvinervis Sieb. et Zucc.	S25		0.00	0.00
Tilia japonica, Tilia maximowicziana	S26	3	0.59	1.82
Japanese honeysuckle, Lonicera japonica	S27	2	0.39	1.22
Kalopanax septemlobu	S28		0.00	0.00
Acer nipponicum	S29		0.00	0.00
Celtis jessoensis	S30		0.00	0.00
Alnus fauriei	S31		0.00	0.00
Betula corylifolia	S32		0.00	0.00
Aralia elata	S33		0.00	0.00
Zanthoxylum piperitum,	S34		0.00	0.00
Fraxinus lanugiosa	S35		0.00	0.00
Fraxinus mandshurica var. japonica	S36		0.00	0.00
Ginko biloba	S38		0.00	0.00
Styrax obassia,	S39		0.00	0.00
Hamamelis japonica	S40	33	6.50	20.05
Acer japonica	S41		0.00	0.00
Corylus sieboldiana	S42	18	3.54	10.94
Carpinus Cordata	S43	16	3.15	9.72
	mix		0.00	0.00
	Sum	508		

Tree species	Abbreviation	Number	relative Density	Density per ha and species
<i>Juglans ailantifolia</i>	S01	7	0.98	3.99
<i>Aesculus turbinata</i>	S02	30	4.18	17.10
<i>Cryptomeria japonica</i>	S03	53	7.39	30.20
<i>Pterocarya rhoifolia</i>	S04		0.00	0.00
<i>Quercus mongolica</i> subsp. <i>crispula</i>	S05	51	7.11	29.06
<i>Larix kaempferi</i>	S06		0.00	0.00
<i>Fagus crenata</i>	S07	53	7.39	30.20
<i>Magnolia obovata</i>	S08	22	3.07	12.54
<i>Acer japonicum</i> , <i>sieboldium</i> , <i>palmatum</i>	S09	140	19.53	79.78
<i>Prunus salicina</i> Lindley, <i>Prunus serrulata/grayana</i> , <i>Prunus speciosa</i>	S10		0.00	0.00
<i>Acer mono maxim</i> , <i>Acer pictum</i> subsp. Mono	S11	169	23.57	96.31
<i>Salix serissaefolia</i>	S12		0.00	0.00
<i>Salix jessoensis</i>	S13		0.00	0.00
<i>Castanea Crenata</i>	S14		0.00	0.00
<i>Robinia pseudoaccacia</i>	S15		0.00	0.00
<i>Cornus controversa</i>	S16	24	3.35	13.68
<i>Phelledendron amurense</i>	S17		0.00	0.00
<i>Betula corylifolia</i>	S18	45	6.28	25.64
<i>Alnus inokumae</i> , <i>Alnus hirsuta</i>	S19		0.00	0.00
<i>Picea abies</i>	S20		0.00	0.00
<i>Cercidiphyllum japonicum</i> var. Magnificum	S21		0.00	0.00
<i>Albizia julibrissin</i>	S22		0.00	0.00
Japanese <i>Hydrangea</i> , <i>Schizophragma hydrangeoides</i> and <i>Smilax</i>	S23	8	1.12	4.56
<i>Morus australis</i>	S24	6	0.84	3.42
<i>Clethra barvinervis</i> Sieb. et Zucc.	S25		0.00	0.00
<i>Tilia japonica</i> , <i>Tilia maximowicziana</i>	S26	7	0.98	3.99
Japanese honeysuckle, <i>Lonicera japonica</i>	S27	4	0.56	2.28
<i>Kalopanax septemlobu</i>	S28		0.00	0.00
<i>Acer nipponicum</i>	S29		0.00	0.00
<i>Celtis jessoensis</i>	S30		0.00	0.00
<i>Alnus fauriei</i>	S31		0.00	0.00
<i>Betula corylifolia</i>	S32		0.00	0.00
<i>Aralia elata</i>	S33		0.00	0.00
<i>Zanthoxylum piperitum</i> ,	S34		0.00	0.00
<i>Fraxinus lanugiosa</i>	S35		0.00	0.00
<i>Fraxinus mandshurica</i> var. <i>japonica</i>	S36		0.00	0.00
<i>Ginkgo biloba</i>	S38		0.00	0.00
<i>Styrax obassia</i> ,	S39		0.00	0.00
<i>Hamamelis japonica</i>	S40	30	4.18	17.10
<i>Acer japonica</i>	S41		0.00	0.00
<i>Corylus sieboldiana</i>	S42	1	0.14	0.57
<i>Carpinus Cordata</i>	S43	14	1.95	7.98

	mix	53	7.39	30.20
	Sum	717	100	

Site 10

Tree species	Abbreviation	Number	relative Density	Density per ha and species
<i>Juglans ailantifolia</i>	S01	14	2.35	6.41
<i>Aesculus turbinata</i>	S02	29	4.87	13.28
<i>Cryptomeria japonica</i>	S03	74	12.42	33.88
<i>Pterocarya rhoifolia</i>	S04		0.00	0.00
<i>Quercus mongolica</i> subsp. <i>crispula</i>	S05	51	8.56	23.35
<i>Larix kaempferi</i>	S06		0.00	0.00
<i>Fagus crenata</i>	S07	10	1.68	4.58
<i>Magnolia obovata</i>	S08	35	5.87	16.02
<i>Acer japonicum</i> , <i>sieblodium</i> , <i>palmatum</i>	S09	167	28.02	76.45
<i>Prunus salicina</i> Lindley, <i>Prunus serrulata/grayana</i> , <i>Prunus speciosa</i>	S10	4	0.67	1.83
<i>Acer mono maxim</i> , <i>Acer pictum</i> subsp. Mono	S11	88	14.77	40.29
<i>Salix serissaefolia</i>	S12		0.00	0.00
<i>Salix jessoensis</i>	S13		0.00	0.00
<i>Castanea Crenata</i>	S14	1	0.17	0.46
<i>Robinia pseudoaccacia</i>	S15		0.00	0.00
<i>Cornus controversa</i>	S16	16	2.68	7.32
<i>Phelledendron amurense</i>	S17		0.00	0.00
<i>Betula corylifolia</i>	S18	13	2.18	5.95
<i>Alnus inokumae</i> , <i>Alnus hirsuta</i>	S19		0.00	0.00
<i>Picea abies</i>	S20		0.00	0.00
<i>Cercidiphyllum japonicum</i> var. Magnificum	S21		0.00	0.00
<i>Albizia julibrissin</i>	S22		0.00	0.00
Japanese <i>Hydrangea</i> , <i>Schizophragma hydrangeoides</i> and <i>Smilax</i>	S23	5	0.84	2.29
<i>Morus australis</i>	S24	8	1.34	3.66
<i>Clethra barvinervis</i> Sieb. et Zucc.	S25		0.00	0.00
<i>Tilia japonica</i> , <i>Tilia maximowicziana</i>	S26	19	3.19	8.70
Japanese honeysuckle, <i>Lonicera japonica</i>	S27	1	0.17	0.46
<i>Kalopanax septemlobu</i>	S28	13	2.18	5.95
<i>Acer nipponicum</i>	S29		0.00	0.00
<i>Celtis jessoensis</i>	S30		0.00	0.00
<i>Alnus fauriei</i>	S31		0.00	0.00
<i>Betula corylifolia</i>	S32		0.00	0.00
<i>Aralia elata</i>	S33		0.00	0.00
<i>Zanthoxylum piperitum</i> ,	S34		0.00	0.00
<i>Fraxinus lanugiosa</i>	S35		0.00	0.00
<i>Fraxinus mandshurica</i> var. <i>japonica</i>	S36		0.00	0.00
<i>Ginkgo biloba</i>	S38		0.00	0.00

Styrax obassia,	S39	3	0.50	1.37
Hamamelis japonica	S40	30	5.03	13.73
Acer japonica	S41	11	1.85	5.04
Corylus sieboldiana	S42	4	0.67	1.83
Carpinus Cordata	S43		0.00	0.00
	mix		0.00	0.00
	Sum	596		

Site 11

Tree species	Abbreviation	Number	relative Density	Density per ha and species
Juglans ailantifolia	S01	54	17.20	29.53
Aesculus turbinata	S02	26	8.28	14.22
Cryptomeria japonica	S03	125	39.81	68.35
Pterocarya rhoifolia	S04	31	9.87	16.95
Quercus mongolica subsp. crispula	S05		0.00	0.00
Larix kaempferi	S06	1	0.32	0.55
Fagus crenata	S07		0.00	0.00
Magnolia obovata	S08	6	1.91	3.28
Acer japonicum, sieblodium, palmatum	S09	36	11.46	19.68
Prunus salicina Lindley, Prunus serrulata/grayana, Prunus speciosa	S10		0.00	0.00
Acer mono maxim, Acer pictum subsp. Mono	S11	16	5.10	8.75
Salix serissaefolia	S12		0.00	0.00
Salix jessoensis	S13		0.00	0.00
Castanea Crenata	S14		0.00	0.00
Robinia pseudoaccaccia	S15		0.00	0.00
Cornus controversa	S16	9	2.87	4.92
Phelledendron amurense	S17		0.00	0.00
Betula corylifolia	S18		0.00	0.00
Alnus inokumae, Alnus hirsuta	S19		0.00	0.00
Picea abies	S20		0.00	0.00
Cercidiphyllum japonicum var. Magnificum	S21		0.00	0.00
Albizia julibrissin	S22		0.00	0.00
Japanese Hydrangea, Schizophragma hydrangeoides and Smilax	S23	5	1.59	2.73
Morus australis	S24		0.00	0.00
Clethra barvinervis Sieb. et Zucc.	S25		0.00	0.00
Tilia japonica, Tilia maximowicziana	S26	2	0.64	1.09
Japanese honeysuckle, Lonicera japonica	S27		0.00	0.00
Kalopanax septemlobu	S28		0.00	0.00
Acer nipponicum	S29		0.00	0.00
Celtic jessoensis	S30		0.00	0.00
Alnus fauriei	S31		0.00	0.00
Betula corylifolia	S32		0.00	0.00

Aralia elata	S33		0.00	0.00
Zanthoxylum piperitum,	S34		0.00	0.00
Fraxinus lanugiosa	S35		0.00	0.00
Fraxinus mandshurica var. japonica	S36		0.00	0.00
Ginko biloba	S38		0.00	0.00
Styrax obassia,	S39		0.00	0.00
Hamamelis japonica	S40		0.00	0.00
Acer japonica	S41		0.00	0.00
Corylus sieboldiana	S42		0.00	0.00
Carpinus Cordata	S43		0.00	0.00
	mix		0.00	0.00
	Sum	314		

Site 12

Tree species	Abbreviation	Number	relative Density	Density per ha and species
Juglans ailantifolia	S01	91	18.06	47.14
Aesculus turbinata	S02	31	6.15	16.06
Cryptomeria japonica	S03	73	14.48	37.82
Pterocarya rhoifolia	S04	29	5.75	15.02
Quercus mongolica subsp. crispula	S05	12	2.38	6.22
Larix kaempferi	S06	1	0.20	0.52
Fagus crenata	S07		0.00	0.00
Magnolia obovata	S08	7	1.39	3.63
Acer japonicum, sieblodium, palmatum	S09	144	28.57	74.60
Prunus salicina Lindley, Prunus serrulata/grayana, Prunus speciosa	S10		0.00	0.00
Acer mono maxim, Acer pictum subsp. Mono	S11	38	7.54	19.69
Salix serissaefolia	S12		0.00	0.00
Salix jessoensis	S13		0.00	0.00
Castanea Crenata	S14		0.00	0.00
Robinia pseudoaccaccia	S15		0.00	0.00
Cornus controversa	S16	21	4.17	10.88
Phelledendron amurense	S17		0.00	0.00
Betula corylifolia	S18		0.00	0.00
Alnus inokumae, Alnus hirsuta	S19		0.00	0.00
Picea abies	S20		0.00	0.00
Cercidiphyllum japonicum var. Magnificum	S21		0.00	0.00
Albizia julibrissin	S22		0.00	0.00
Japanese Hydrangea, Schizophragma hydrangeoides and Smilax	S23	17	3.37	8.81
Morus australis	S24	14	2.78	7.25
Clethra barvinervis Sieb. et Zucc.	S25		0.00	0.00
Tilia japonica, Tilia maximowicziana	S26	9	1.79	4.66
Japanese honeysuckle, Lonicera japonica	S27	4	0.79	2.07

Kalopanax septemlobu	S28	3	0.60	1.55
Acer nipponicum	S29		0.00	0.00
Celtis jessoensis	S30	5	0.99	2.59
Alnus fauriei	S31	4	0.79	2.07
Betula corylifolia	S32		0.00	0.00
Aralia elata	S33		0.00	0.00
Zanthoxylum piperitum,	S34		0.00	0.00
Fraxinus lanugiosa	S35		0.00	0.00
Fraxinus mandshurica var. japonica	S36		0.00	0.00
Ginkgo biloba	S38		0.00	0.00
Styrax obassia,	S39	1	0.20	0.52
Hamamelis japonica	S40		0.00	0.00
Acer japonica	S41		0.00	0.00
Corylus sieboldiana	S42		0.00	0.00
Carpinus Cordata	S43		0.00	0.00
	mix		0.00	0.00
	Sum	504		

Site 13

Tree species	Abbreviation	Number	relative Density	Density per ha and species
Juglans ailantifolia	S01	106	20.08	47.60
Aesculus turbinata	S02	10	1.89	4.49
Cryptomeria japonica	S03	229	43.37	102.83
Pterocarya rhoifolia	S04	2	0.38	0.90
Quercus mongolica subsp. crispula	S05	2	0.38	0.90
Larix kaempferi	S06		0.00	0.00
Fagus crenata	S07		0.00	0.00
Magnolia obovata	S08	17	3.22	7.63
Acer japonicum, sieblodium, palmatum	S09	60	11.36	26.94
Prunus salicina Lindley, Prunus serrulata/grayana, Prunus speciosa	S10		0.00	0.00
Acer mono maxim, Acer pictum subsp. Mono	S11	21	3.98	9.43
Salix serissaefolia	S12		0.00	0.00
Salix jessoensis	S13		0.00	0.00
Castanea Crenata	S14		0.00	0.00
Robinia pseudoaccaccia	S15		0.00	0.00
Cornus controversa	S16	22	4.17	9.88
Phelledendron amurense	S17		0.00	0.00
Betula corylifolia	S18		0.00	0.00
Alnus inokumae, Alnus hirsuta	S19		0.00	0.00
Picea abies	S20		0.00	0.00
Cercidiphyllum japonicum var. Magnificum	S21		0.00	0.00
Albizia julibrissin	S22		0.00	0.00

Japanese Hydrangea, Schizophragma hydrangeoides and Smilax	S23	26	4.92	11.68
Morus australis	S24	2	0.38	0.90
Clethra barvinervis Sieb. et Zucc.	S25		0.00	0.00
Tilia japonica, Tilia maximowicziana	S26	1	0.19	0.45
Japanese honeysuckle, Lonicera japonica	S27	15	2.84	6.74
Kalopanax septemlobu	S28	3	0.57	1.35
Acer nipponicum	S29		0.00	0.00
Celtis jessoensis	S30		0.00	0.00
Alnus fauriei	S31	8	1.52	3.59
Betula corylifolia	S32		0.00	0.00
Aralia elata	S33		0.00	0.00
Zanthoxylum piperitum,	S34		0.00	0.00
Fraxinus lanugiosa	S35		0.00	0.00
Fraxinus mandshurica var. japonica	S36		0.00	0.00
Ginko biloba	S38		0.00	0.00
Styrax obassia,	S39	1	0.19	0.45
Hamamelis japonica	S40	3	0.57	1.35
Acer japonica	S41		0.00	0.00
Corylus sieboldiana	S42		0.00	0.00
Carpinus Cordata	S43		0.00	0.00
	mix		0.00	0.00
	Sum	528		

Appendix D – Density calculations for the three forest types

Riparian sites

Tree species	Abbreviation	Tree count	relative Density	Density per ha and species
Juglans ailantifolia	S01	284	16.33	1.57
Aesculus turbinata	S02	31	1.78	0.17
Cryptomeria japonica	S03	541	31.11	2.99
Pterocarya rhoifolia	S04	181	10.41	1.00
Quercus mongolica subsp. crispula	S05	32	1.84	0.18
Larix kaempferi	S06	26	1.50	0.14
Fagus crenata	S07	0	0.00	0.00
Magnolia obovata	S08	31	1.78	0.17
Acer japonicum, sieblodium, palmatum	S09	234	13.46	1.29
Prunus salicina Lindley, Prunus serrulata/grayana, Prunus speciosa	S10	13	0.75	0.07
Acer mono maxim, Acer pictum subsp. Mono	S11	37	2.13	0.20
Salix serissaefolia	S12	86	4.95	0.47
Salix jessoensis	S13	39	2.24	0.22
Castanea Crenata	S14	14	0.81	0.08
Robinia pseudoaccacia	S15	35	2.01	0.19
Cornus controversa	S16	30	1.73	0.17

Phelledendron amurense	S17	9	0.52	0.05
Betula corylifolia	S18	6	0.35	0.03
Alnus inokumae, Alnus hirsuta	S19	1	0.06	0.01
Picea abies	S20	4	0.23	0.02
Cercidiphyllum japonicum var. Magnificum	S21	2	0.12	0.01
Albizia julibrissin	S22	2	0.12	0.01
Japanese Hydrangea, Schizophragma hydrangeoides and Smilax	S23	35	2.01	0.19
Morus australis	S24	1	0.06	0.01
Clethra barvinervis Sieb. et Zucc.	S25	1	0.06	0.01
Tilia japonica, Tilia maximowicziana	S26	28	1.61	0.15
Japanese honeysuckle, Lonicera japonica	S27	0	0.00	0.00
Kalopanax septemlobu	S28	0	0.00	0.00
Acer nipponicum	S29	0	0.00	0.00
Celtis jessoensis	S30	0	0.00	0.00
Alnus fauriei	S31	20	1.15	0.11
Betula corylifolia	S32	1	0.06	0.01
Aralia elata	S33	0	0.00	0.00
Zanthoxylum piperitum,	S34	5	0.29	0.03
Fraxinus lanugiosa	S35	0	0.00	0.00
Fraxinus mandshurica var. japonica	S36	1	0.06	0.01
Ginkgo biloba	S38	0	0.00	0.00
Styrax obassia,	S39	0	0.00	0.00
Hamamelis japonica	S40	0	0.00	0.00
Acer japonica	S41	0	0.00	0.00
Corylus sieboldiana	S42	5	0.29	0.03
Carpinus Cordata	S43	2	0.12	0.01
	mix	0	0.00	0.00
	Sum	1739	100	

Terrace sites

Tree species	Abbreviation	Tree count	relative Density	Density per ha and species
Juglans ailantifolia	S01	251	19.76	3.30
Aesculus turbinata	S02	67	5.28	0.88
Cryptomeria japonica	S03	427	33.62	5.62
Pterocarya rhoifolia	S04	62	4.88	0.82
Quercus mongolica subsp. crispula	S05	14	1.10	0.18
Larix kaempferi	S06	2	0.16	0.03
Fagus crenata	S07	0	0.00	0.00
Magnolia obovata	S08	30	2.36	0.39
Acer japonicum, sieblodium, palmatum	S09	240	18.90	3.16
Prunus salicina Lindley, Prunus serrulata/grayana, Prunus speciosa	S10	0	0.00	0.00
Acer mono maxim, Acer pictum subsp. Mono	S11	75	5.91	0.99

Salix serissaefolia	S12	0	0.00	0.00
Salix jessoensis	S13	0	0.00	0.00
Castanea Crenata	S14	0	0.00	0.00
Robinia pseudoaccacia	S15	0	0.00	0.00
Cornus controversa	S16	52	4.09	0.68
Phelledendron amurense	S17	0	0.00	0.00
Betula corylifolia	S18	0	0.00	0.00
Alnus inokumae, Alnus hirsuta	S19	0	0.00	0.00
Picea abies	S20	0	0.00	0.00
Cercidiphyllum japonicum var. Magnificum	S21	0	0.00	0.00
Albizia julibrissin	S22	0	0.00	0.00
Japanese Hydrangea, Schizophragma hydrangeoides and Smilax	S23	48	3.78	0.63
Morus australis	S24	16	1.26	0.21
Clethra barvinervis Sieb. et Zucc.	S25	0	0.00	0.00
Tilia japonica, Tilia maximowicziana	S26	12	0.94	0.16
Japanese honeysuckle, Lonicera japonica	S27	19	1.50	0.25
Kalopanax septemlobu	S28	6	0.47	0.08
Acer nipponicum	S29	0	0.00	0.00
Celtis jessoensis	S30	5	0.39	0.07
Alnus fauriei	S31	12	0.94	0.16
Betula corylifolia	S32	0	0.00	0.00
Aralia elata	S33	0	0.00	0.00
Zanthoxylum piperitum,	S34	0	0.00	0.00
Fraxinus lanugiosa	S35	0	0.00	0.00
Fraxinus mandshurica var. japonica	S36	0	0.00	0.00
Ginkgo biloba	S38	0	0.00	0.00
Styrax obassia,	S39	2	0.16	0.03
Hamamelis japonica	S40	3	0.24	0.04
Acer japonica	S41	0	0.00	0.00
Corylus sieboldiana	S42	0	0.00	0.00
Carpinus Cordata	S43	0	0.00	0.00
	mix	0	0.00	0.00
	Sum	1270		

Slope sites

Tree species	Abbreviation	Tree count	relative Density	Density per ha and species
Juglans ailantifolia	S01	169	4.76	0.31
Aesculus turbinata	S02	93	2.62	0.17
Cryptomeria japonica	S03	449	12.66	0.82
Pterocarya rhoifolia	S04	21	0.59	0.04
Quercus mongolica subsp. crispula	S05	257	7.24	0.47
Larix kaempferi	S06	27	0.76	0.05
Fagus crenata	S07	42	1.18	0.08

Magnolia obovata	S08	179	5.05	0.33
Acer japonicum, sieblodium, palmatum	S09	1540	43.40	2.82
Prunus salicina Lindley, Prunus serrulata/grayana, Prunus speciosa	S10	7	0.20	0.01
Acer mono maxim, Acer pictum subsp. Mono	S11	316	8.91	0.58
Salix serissaefolia	S12	1	0.03	0.00
Salix jessoensis	S13	6	0.17	0.01
Castanea Crenata	S14	8	0.23	0.01
Robinia pseudoaccaccia	S15	0	0.00	0.00
Cornus controversa	S16	67	1.89	0.12
Phelledendron amurense	S17	0	0.00	0.00
Betula corylifolia	S18	28	0.79	0.05
Alnus inokumae, Alnus hirsuta	S19	0	0.00	0.00
Picea abies	S20	0	0.00	0.00
Cercidiphyllum japonicum var. Magnificum	S21	0	0.00	0.00
Albizia julibrissin	S22	0	0.00	0.00
Japanese Hydrangea, Schizophragma hydrangeoides and Smilax	S23	53	1.49	0.10
Morus australis	S24	35	0.99	0.06
Clethra barvinervis Sieb. et Zucc.	S25	0	0.00	0.00
Tilia japonica, Tilia maximowicziana	S26	33	0.93	0.06
Japanese honeysuckle, Lonicera japonica	S27	17	0.48	0.03
Kalopanax septemlobu	S28	18	0.51	0.03
Acer nipponicum	S29	0	0.00	0.00
Celtic jessoensis	S30	0	0.00	0.00
Alnus fauriei	S31	19	0.54	0.03
Betula corylifolia	S32	0	0.00	0.00
Aralia elata	S33	0	0.00	0.00
Zanthoxylum piperitum,	S34	0	0.00	0.00
Fraxinus lanugiosa	S35	3	0.08	0.01
Fraxinus mandshurica var. japonica	S36	0	0.00	0.00
Ginko biloba	S38	0	0.00	0.00
Styrax obassia,	S39	13	0.37	0.02
Hamamelis japonica	S40	77	2.17	0.14
Acer japonica	S41	12	0.34	0.02
Corylus sieboldiana	S42	28	0.79	0.05
Carpinus Cordata	S43	30	0.85	0.05
	mix	2	0.06	0.00
	Sum	3548		

Appendix E – Tree counts

Tree counts results analysed by the Census code, which counted tree top annotation for all sites.

Part 1

SPECIES LABEL	SITE1	SITE4	SITE6	SITE7	SITE11	SITE12	SITE13	SITE2	SITE3	SITE5	SITE8	SITE9	SITE10
S01	107	58	47	72	54	91	106	23	53	47	32	7	14
S02	24		4	3	26	31	10	35	3	18	8	30	29
S03	201	129	156	55	125	73	229	195	122	51	7	53	74
S04	125	9	25	22	31	29	2	3	3	14	1		
S05	9	7	3	13		12	2	45	66	53	42	51	51
S06	19	7			1	1			27	0			
S07									27	4	1	53	10
S08	19	6	5	1	6	7	17	63	32	42	7	22	35
S09	145	12	10	67	36	144	60	351	605	176	241	140	167
S10	13	0							3	0			4
S11	15	1	5	16	16	38	21	63	75	52	38	169	88
S12		78	8						1				
S13	8	1	16	14					2	3	1		
S14	4		10						4	1	2		1
S15	14		7	14									
S16	23	2	5		9	21	22	7	17	13	14	24	16
S17	9												
S18			6					2			13	45	13
S19			1										
S20			4										
S21		2											
S22				2									
S23	13	12	9	1	5	17	26	2	14	17	15	8	5
S24		1				14	2	6	7		14	6	8

Part 2

	SITE1	SITE4	SITE6	SITE7	SITE11	SITE12	SITE13	SITE2	SITE3	SITE5	SITE8	SITE9	SITE10
S25				1									
S26	28				2	9	1	4	7		3	7	19
S27						4	15		2	12	2	4	1
S28						3	3		1	4			13
S29													
S30						5							
S31	0	0		20		4	8		19				
S32		1											
S33													
S34			5										
S35									3				
S36				1									
S37			2		3								
S38													
S39	0					1	1	6	4				3
S40	0						3	10		4	33	30	30
S41													11
S42	5									6	18	1	4
S43	2							14			16	14	
MIX								2				53	
SUM	783	326	328	302	314	504	528	831	1098	515	508	717	596

Appendix F – Pixel counting

Area calculations performed on basis of counted black pixels, which were previously annotated in GIMP. The black pixels together with the set image resolution allowed the calculation of the area in m².

Part 1

	SITE 1	SITE 4	SITE 6	SITE 7	SITE 11	SITE 12	SITE 13	SITE 2	SITE 3	SITE 5	SITE 8	SITE 9	SITE 10
SPECIES LABEL	Area in m²	Area in m²	Area in m²	Area in m²	Area in m²	Area in m²	Area in m²	Area in m²	Area in m²	Area in m²	Area in m²	Area in m²	Area in m²
S01	9864.20	4629.35	2655.65	5463.61	3608.91	5546.10	8920.32	1246.46	5899.66	3397.58	2410.54	240.25	1326.07
S02	1235.52	0.00	68.33	84.53	978.47	1035.81	534.25	1637.10	217.83	594.62	339.75	763.86	1708.42
S03	5838.15	2151.46	4207.55	1094.08	2370.87	1037.72	4565.50	5926.63	3155.72	563.15	242.78	1348.74	2236.27
S04	7250.37	471.91	1338.17	1257.24	1875.15	1520.57	41.28	211.27	144.43	661.84	118.41	0.00	0.00
S05	442.84	135.66	101.00	293.28	0.00	234.29	71.68	1649.56	2953.23	1096.13	1126.18	1193.48	1790.17
S06	580.36	220.75	0.00	0.00	33.25	0.65	0.00	0.00	1253.27	0.00	0.00	0.00	0.00
S07	0.00	0.00	0.00	0.00	0.00	0.00	0.00	0.00	1423.92	230.61	69.42	1062.12	502.52
S08	915.87	199.97	290.72	30.67	365.01	286.80	551.13	4951.32	2044.01	3222.04	443.02	1163.13	2247.97
S09	949.24	95.23	52.09	352.73	459.91	818.98	658.71	5241.54	4724.15	773.31	1935.43	1084.42	1388.53
S10	572.30	0.00	0.00	0.00	0.00	0.00	0.00	0.00	148.63	0.00	0.00	0.00	162.15
S11	438.59	9.39	147.17	238.91	462.16	682.14	576.79	2451.67	1860.74	1707.42	921.75	3991.45	2842.49
S12	0.00	778.19	260.01	0.00	0.00	0.00	0.00	0.00	21.05	0.00	0.00	0.00	0.00
S13	371.63	85.48	632.19	618.05	0.00	0.00	0.00	0.00	191.60	230.39	63.53	0.00	0.00
S14	110.08	0.00	395.07	0.00	0.00	0.00	0.00	0.00	152.13	57.55	16.47	0.00	51.62
S15	326.76	0.00	124.94	230.42	0.00	0.00	0.00	0.00	0.00	0.00	0.00	0.00	0.00
S16	616.13	16.72	81.62	0.00	239.45	301.93	539.54	337.76	647.66	349.88	383.62	367.17	482.77
S17	512.97	0.00	0.00	0.00	0.00	0.00	0.00	0.00	0.00	0.00	0.00	0.00	0.00
S18	0.00	0.00	370.35	0.00	0.00	0.00	0.00	52.80	0.00	0.00	185.34	779.80	787.20
S19	0.00	0.00	88.16	0.00	0.00	0.00	0.00	0.00	0.00	0.00	0.00	0.00	0.00
S20	0.00	0.00	294.20	0.00	0.00	0.00	0.00	0.00	0.00	0.00	0.00	0.00	0.00
S21	0.00	112.77	0.00	0.00	0.00	0.00	0.00	0.00	0.00	0.00	0.00	0.00	0.00

Part 2

	SITE 1	SITE 4	SITE 6	SITE 7	SITE 11	SITE 12	SITE 13	SITE 2	SITE 3	SITE 5	SITE 8	SITE 9	SITE 10
SPECIES LABEL	Area in m ²	Area in m ²	Area in m ²	Area in m ²	Area in m ²	Area in m ²	Area in m ²	Area in m ²	Area in m ²	Area in m ²	Area in m ²	Area in m ²	Area in m ²
S22	0.00	0.00	0.00	44.04	0.00	0.00	0.00	0.00	0.00	0.00	0.00	0.00	0.00
S23	274.79	151.27	262.27	10.11	89.78	221.80	474.56	94.47	378.12	324.42	429.79	110.03	153.09
S24	0.00	23.45	0.00	0.00	0.00	265.49	118.11	232.15	228.07	0.00	338.38	69.48	265.87
S25	0.00	0.00	0.00	43.57	0.00	0.00	0.00	0.00	0.00	0.00	0.00	0.00	0.00
S26	1091.48	0.00	0.00	0.00	36.00	253.38	23.89	131.96	478.42	0.00	129.90	283.58	721.37
S27	0.00	0.00	0.00	0.00	0.00	107.29	232.21	0.00	0.00	266.48	83.84	55.99	76.08
S28	0.00	0.00	0.00	0.00	0.00	55.71	47.51	0.00	17.07	107.12	0.00	0.00	179.63
S29	0.00	0.00	0.00	0.00	0.00	0.00	0.00	0.00	0.00	0.00	0.00	0.00	0.00
S30	0.00	0.00	0.00	0.00	0.00	74.50	0.00	0.00	0.00	0.00	0.00	0.00	0.00
S31	68.57	0.00	0.00	98.75	0.00	85.83	93.35	0.00	164.28	0.00	0.00	0.00	0.00
S32	0.00	85.24	0.00	0.00	0.00	0.00	0.00	0.00	0.00	0.00	0.00	0.00	0.00
S33	0.00	0.00	0.00	0.00	0.00	0.00	0.00	0.00	0.00	0.00	0.00	0.00	0.00
S34	0.00	0.00	43.42	0.00	0.00	0.00	0.00	0.00	0.00	0.00	0.00	0.00	0.00
S35	0.00	0.00	0.00	0.00	0.00	0.00	0.00	0.00	168.80	0.00	0.00	0.00	0.00
S36	0.00	0.00	0.00	82.38	0.00	0.00	0.00	0.00	0.00	0.00	0.00	0.00	0.00
S37	0.00	0.00	57.50	0.00	86.98	0.00	0.00	0.00	0.00	0.00	0.00	0.00	0.00
S38	0.00	0.00	0.00	0.00	0.00	0.00	0.00	0.00	0.00	0.00	0.00	0.00	0.00
S39	41.04	0.00	0.00	0.00	0.00	27.77	20.77	110.39	80.70	0.00	77.34	8.70	138.96
S40	0.00	0.00	0.00	0.00	0.00	0.00	50.51	376.19	0.00	65.98	855.53	778.96	825.09
S41	0.00	0.00	0.00	0.00	0.00	0.00	0.00	0.00	0.00	5.13	0.00	0.00	86.97
S42	157.85	0.00	0.00	0.00	0.00	0.00	0.00	0.00	0.00	247.56	397.31	57.79	103.09
S43	27.97	0.00	0.00	0.00	0.00	0.00	0.00	605.12	7.83	0.00	364.07	266.57	0.00
MIX		0.00	0.00	0.00	0.00	0.00	0.00	56.36	0.00	0.00	0.00	435.41	0.00
SUM	31686.7	9166.82	11100.1	9942.39	10605.9	12556.8	17520.1	25256.4	26361.3	13901.2	10932.4	14060.9	18076.3

Part 3:

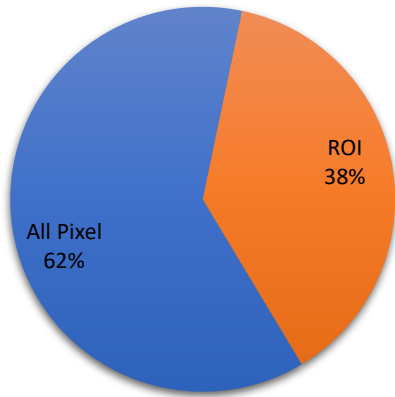
Calculation of area per tree based on the basal area and tree top counting.

	SITE1	SITE4	SITE6	SITE7	SITE11	SITE12	SITE13	SITE2	SITE3	SITE5	SITE8	SITE9	SITE10
S01	92.19	79.82	56.5	75.88	66.83	60.95	84.15	54.19	111.31	72.29	75.33	34.32	94.72
S02	51.48		17.08	28.18	37.63	33.41	53.42	46.77	72.61	33.03	42.47	25.46	58.91
S03	29.05	16.68	26.97	19.89	18.97	14.22	19.94	30.39	25.87	11.04	34.68	25.45	30.22
S04	58	52.43	53.53	57.15	60.49	52.43	20.64	70.42	48.14	47.27	118.41		
S05	49.2	19.38	33.67	22.56		19.52	35.84	36.66	44.75	20.68	26.81	23.4	35.1
S06	30.55	31.54			33.25	0.65			46.42				
S07									52.74	57.65	69.42	20.04	50.25
S08	48.2	33.33	58.14	30.67	60.84	40.97	32.42	78.59	63.88	76.72	63.29	52.87	64.23
S09	6.55	7.94	5.21	5.26	12.78	5.69	10.98	14.93	7.81	4.39	8.03	7.75	8.31
S10	44.02								49.54				40.54
S11	29.24	9.39	29.43	14.93	28.89	17.95	27.47	38.92	24.81	32.84	24.26	23.62	32.3
S12		9.98	32.5						21.05				
S13	46.45	85.48	39.51	44.15					95.8	76.8	63.53		
S14	27.52		39.51						38.03	57.55	8.23		51.62
S15	23.34		17.85	16.46									
S16	26.79	8.36	16.32		26.61	14.38	24.52	48.25	38.1	26.91	27.4	15.3	30.17
S17	57												
S18			61.72					26.4			14.26	17.33	60.55
S19			88.16										
S20			73.55										
S21		56.38											
S22				22.02									
S23	21.14	12.61	29.14	10.11	17.96	13.05	18.25	47.23	27.01	19.08	28.65	13.75	30.62
S24		23.45					18.96	59.06	38.69	32.58	24.17	11.58	33.23
S25				43.57									
S26	38.98				18	28.15	23.89	32.99	68.35		43.3	40.51	37.97
S27						26.82	15.48		0	22.21	41.92	14	76.08

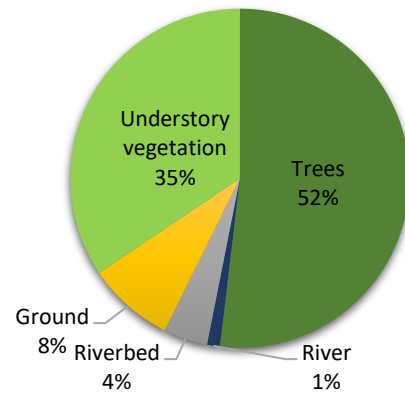
S28			18.57	15.84		17.07	26.78		13.82
S29									
S30			14.9						
S31		4.94	21.46	11.67		8.65			
S32	85.24								
S33									
S34		8.68							
S35						56.27			
S36		82.38							
S37		28.75	28.99						
S38									
S39			27.77	20.77	18.4	20.18			46.32
S40				16.84	37.62		16.5	25.93	25.97
S41									7.91
S42	31.57						41.26	22.07	57.79
S43	13.98				43.22			22.75	19.04
MIX					28.18				8.22

Appendix G – Area distribution based on pixel counting

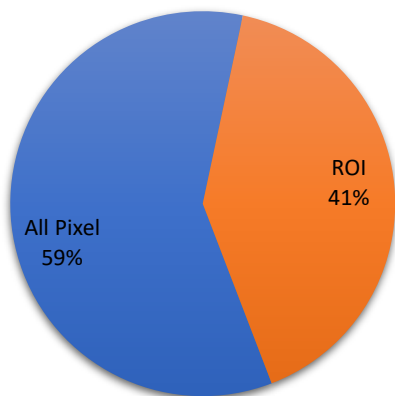
Area distribution Site 4



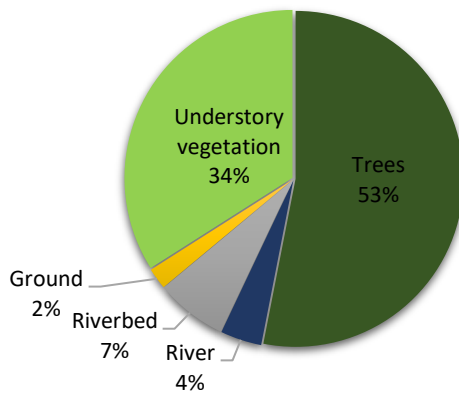
Area distribution in Site 4 ROI



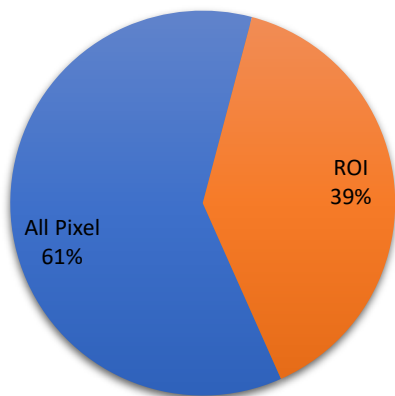
Area distribution Site 6



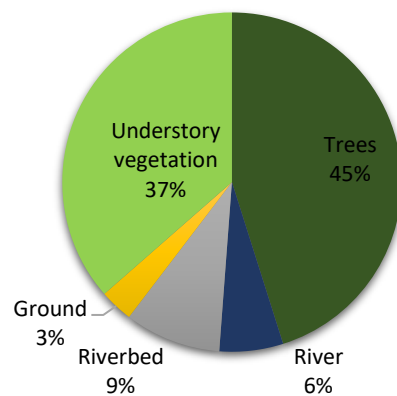
Area distribution in Site 6 ROI



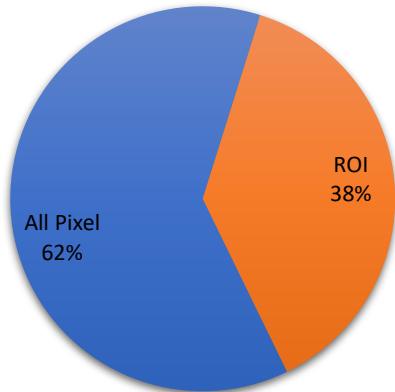
Area distribution Site 7



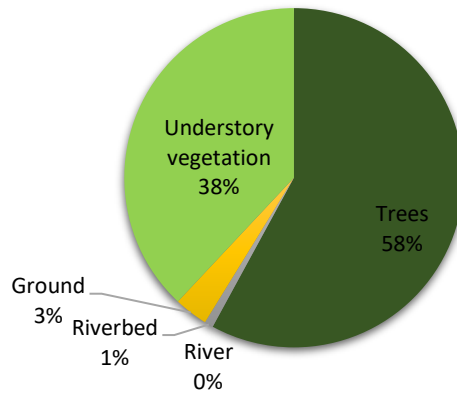
Area distribution in Site 7 ROI



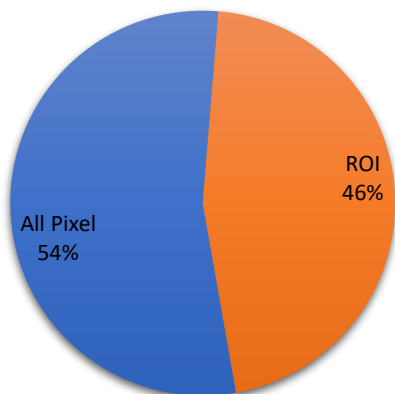
Area distribution Site 11



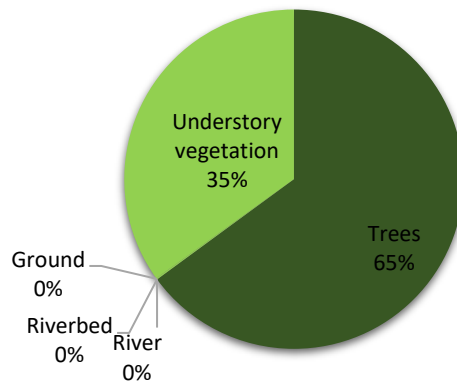
Area distribution in Site 11 ROI



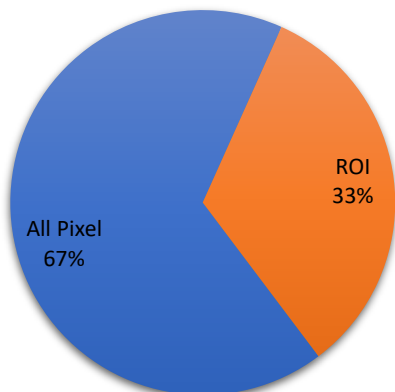
Area distribution Site 12



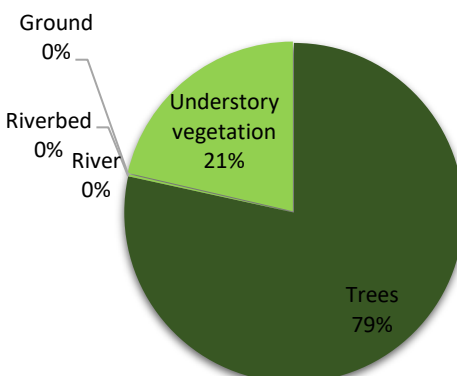
Area distribution in Site 12 ROI



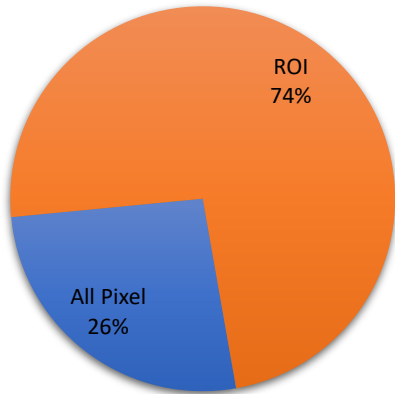
Area distribution Site 13



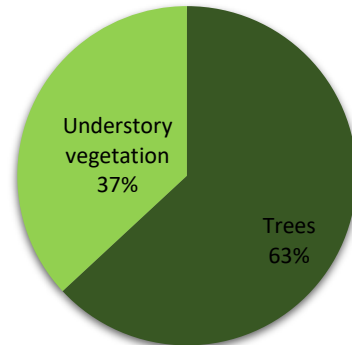
Area distribution in Site 13 ROI



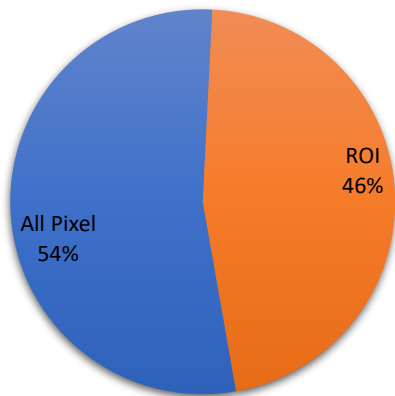
Area distribution Site 2



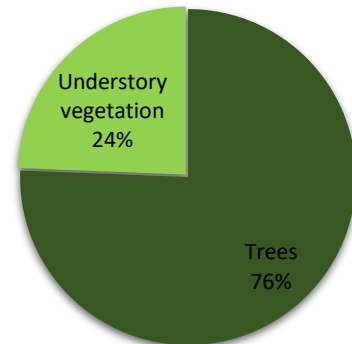
Area distribution in Site 2 ROI



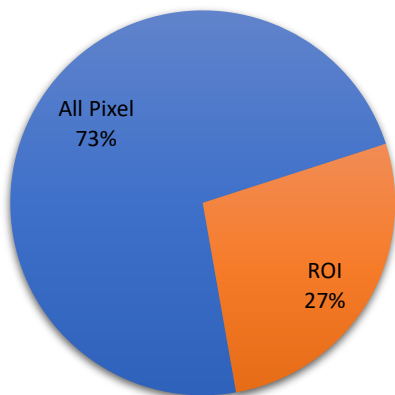
Area distribution Site 3



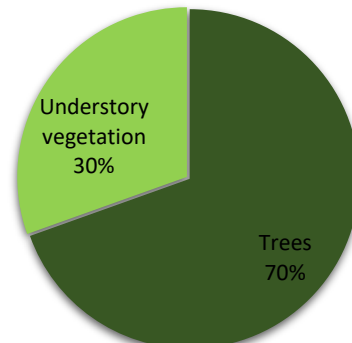
Area distribution in Site 3 ROI



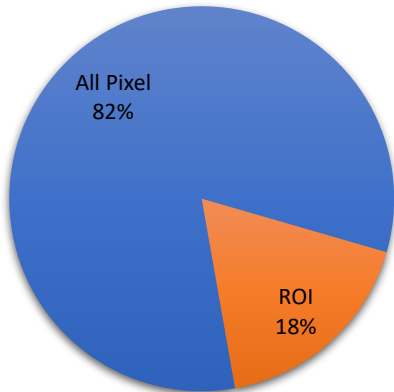
Area distribution Site 5



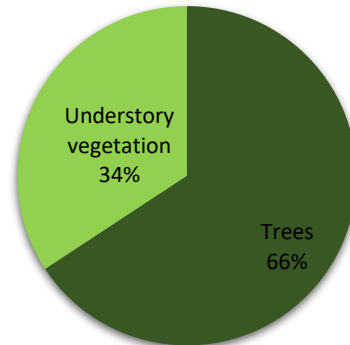
Area distribution in Site 5 ROI



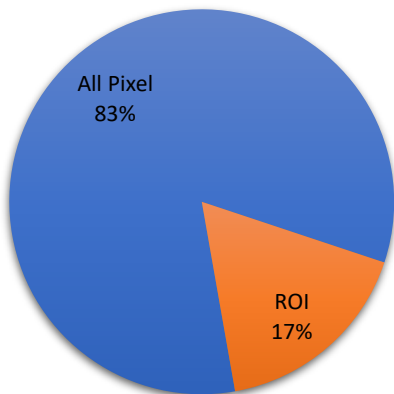
Area distribution Site 8



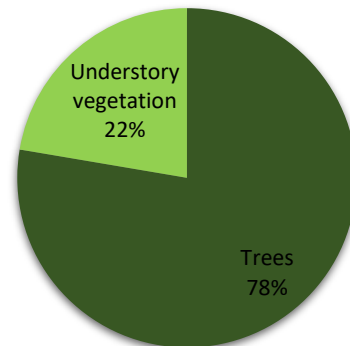
Area distribution in Site 8 ROI



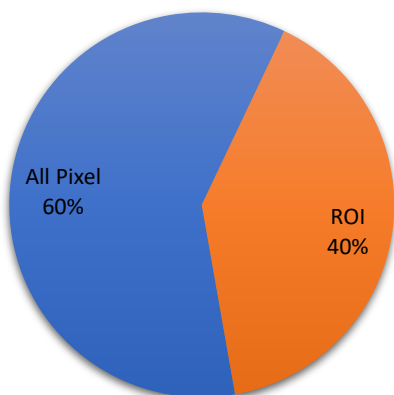
Area distribution Site 9



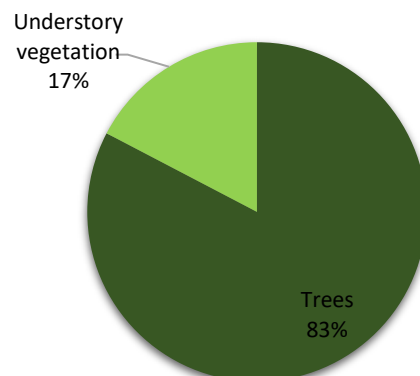
Area distribution in Site 9 ROI



Area distribution Site 10



Area distribution in Site 10 ROI



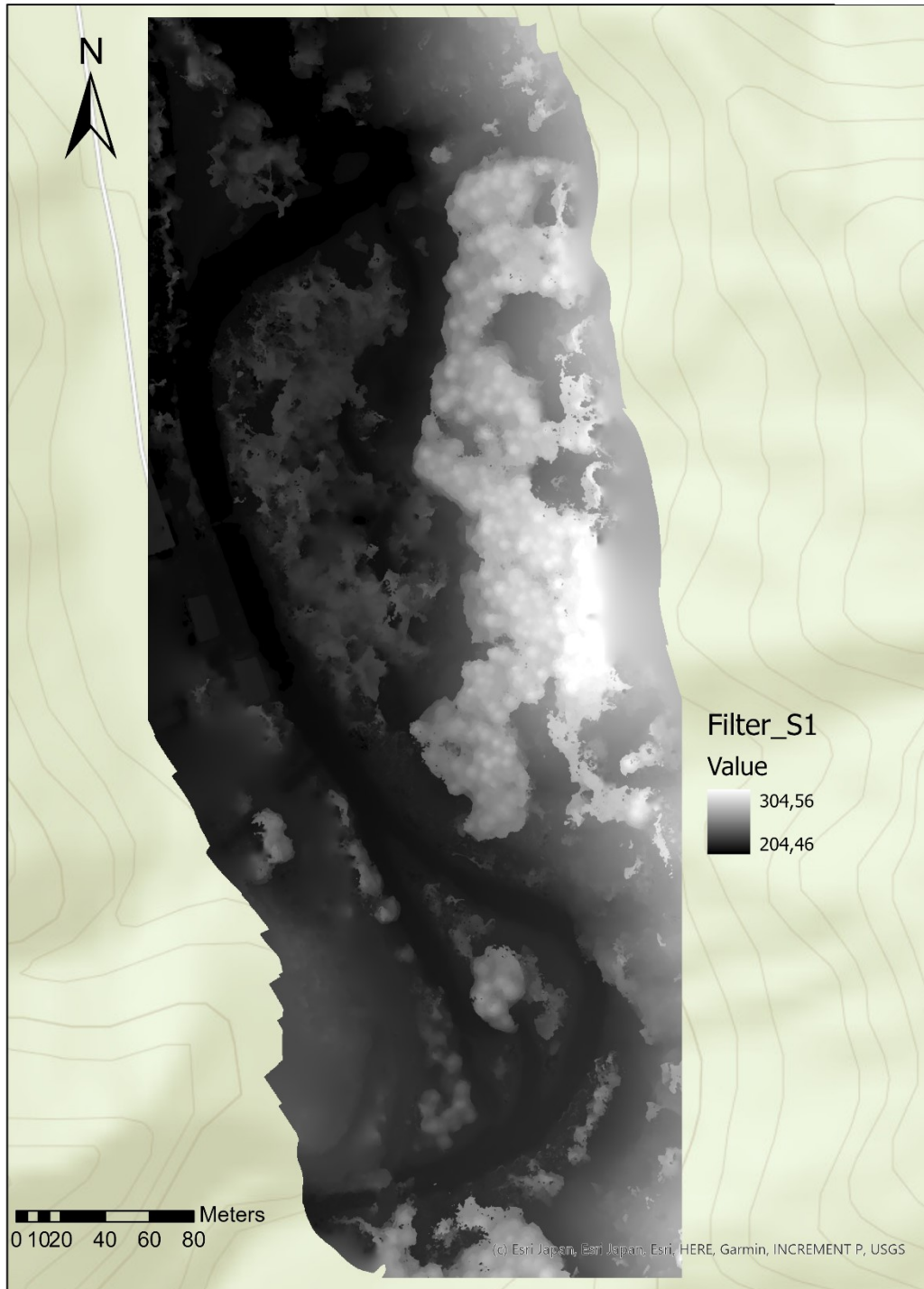
Appendix H: DEMs, Aspect and Slopes

The appendix is divided into three parts: DEM, Aspect and Slope.

Part 1: DEM - The following pages contain the DEMs of all sites, processed in ArcGIS. The applied processing is that the DEM was filtered before it was used to generate a map for each site.



DEM site 1
by Sarah Kentsch





DEM site 2
by Sarah Kentsch



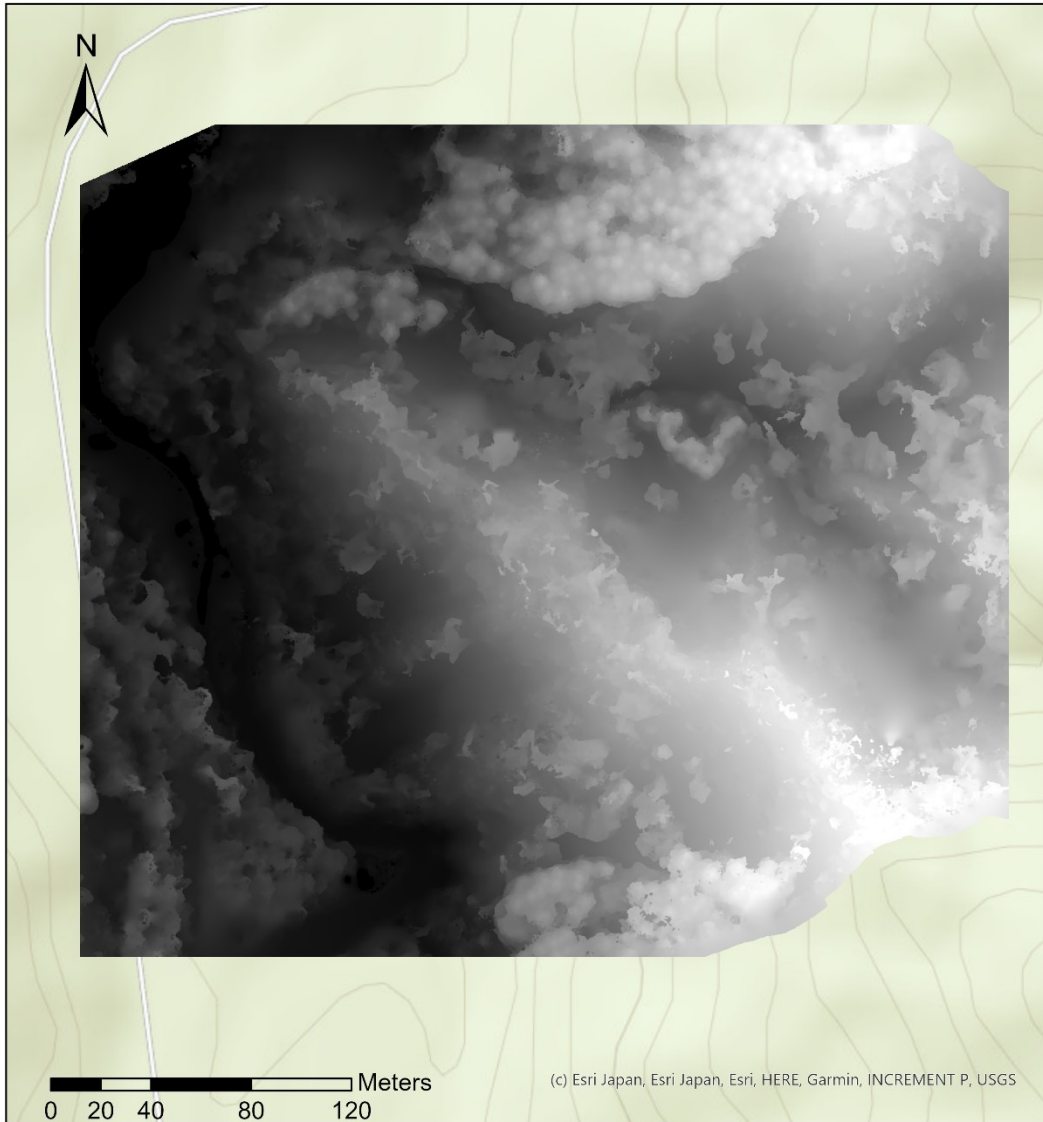
Filter_S2

Value





DEM site 3
by Sarah Kentsch



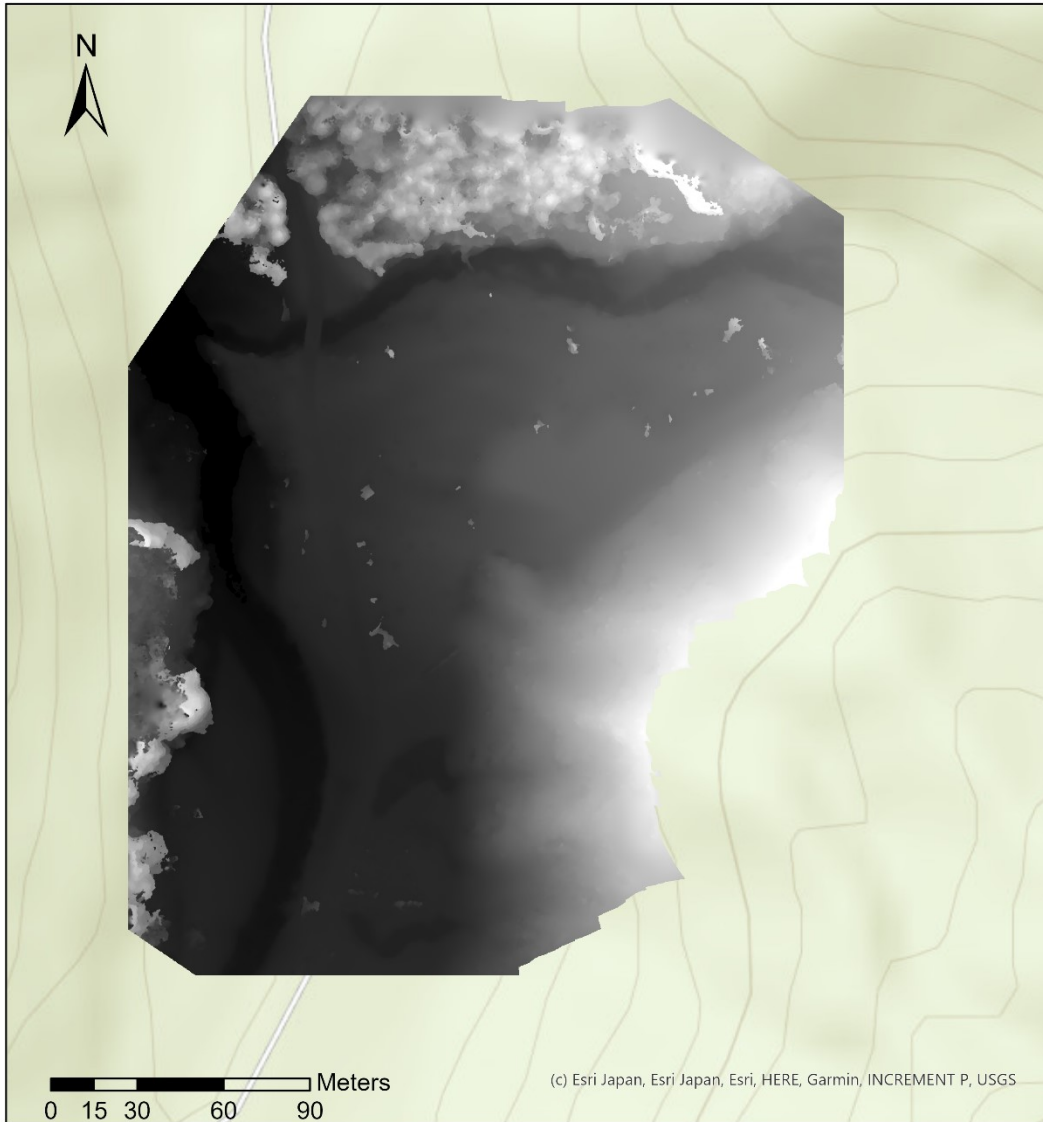
Filter_3

Value





DEM site 4 by Sarah Kentsch



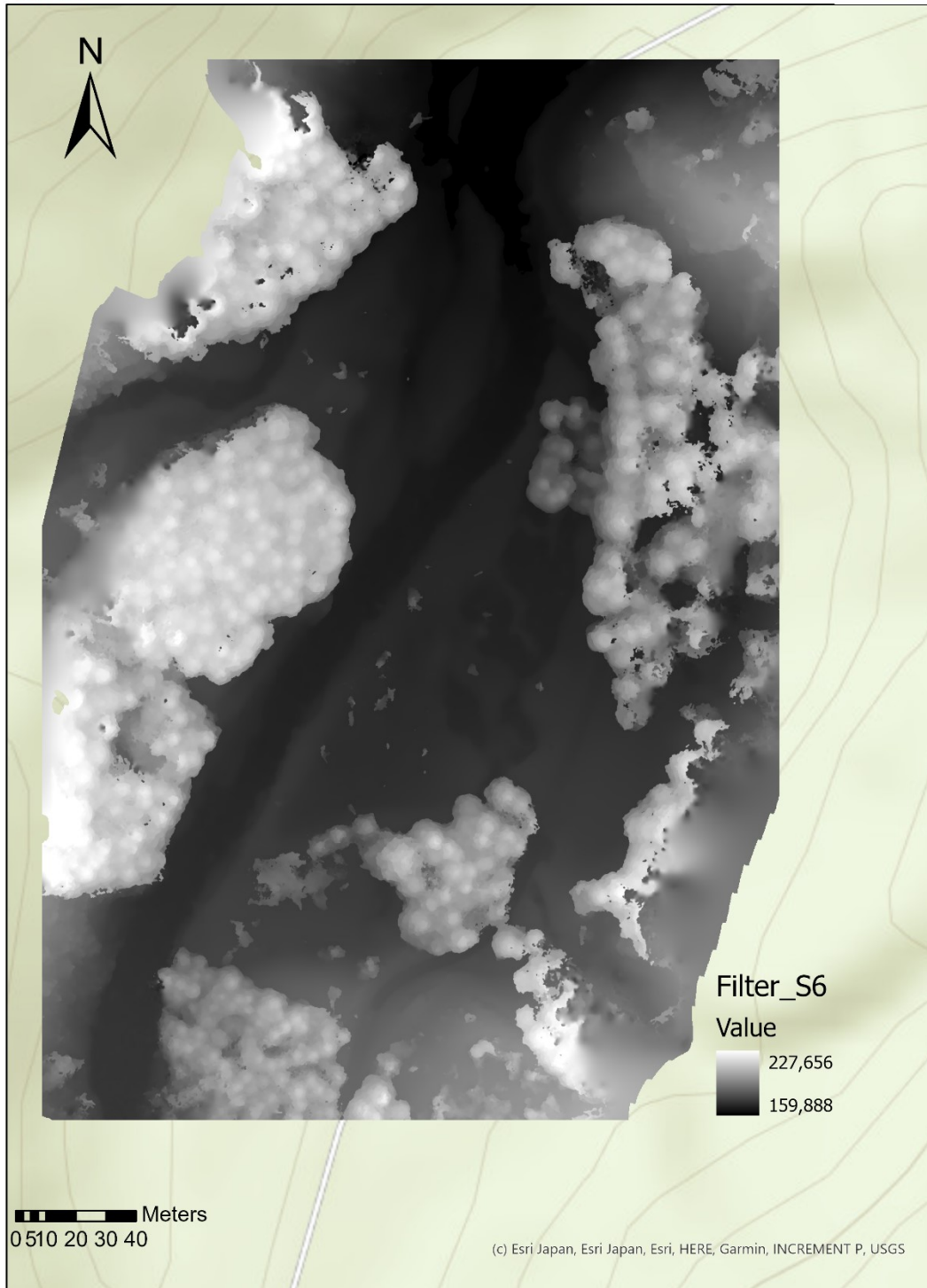
Filter_S4

Value



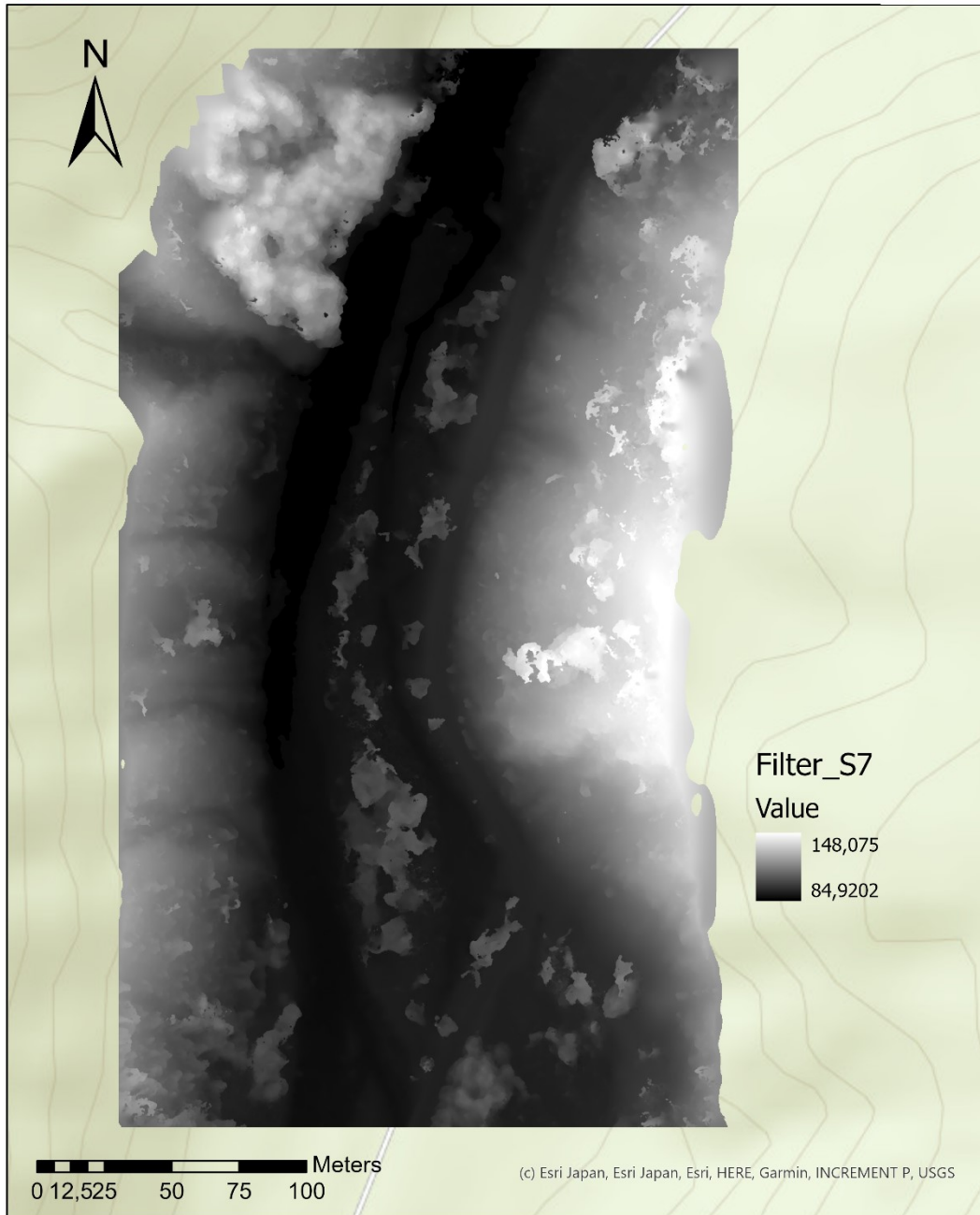


DEM site 6
by Sarah Kentsch



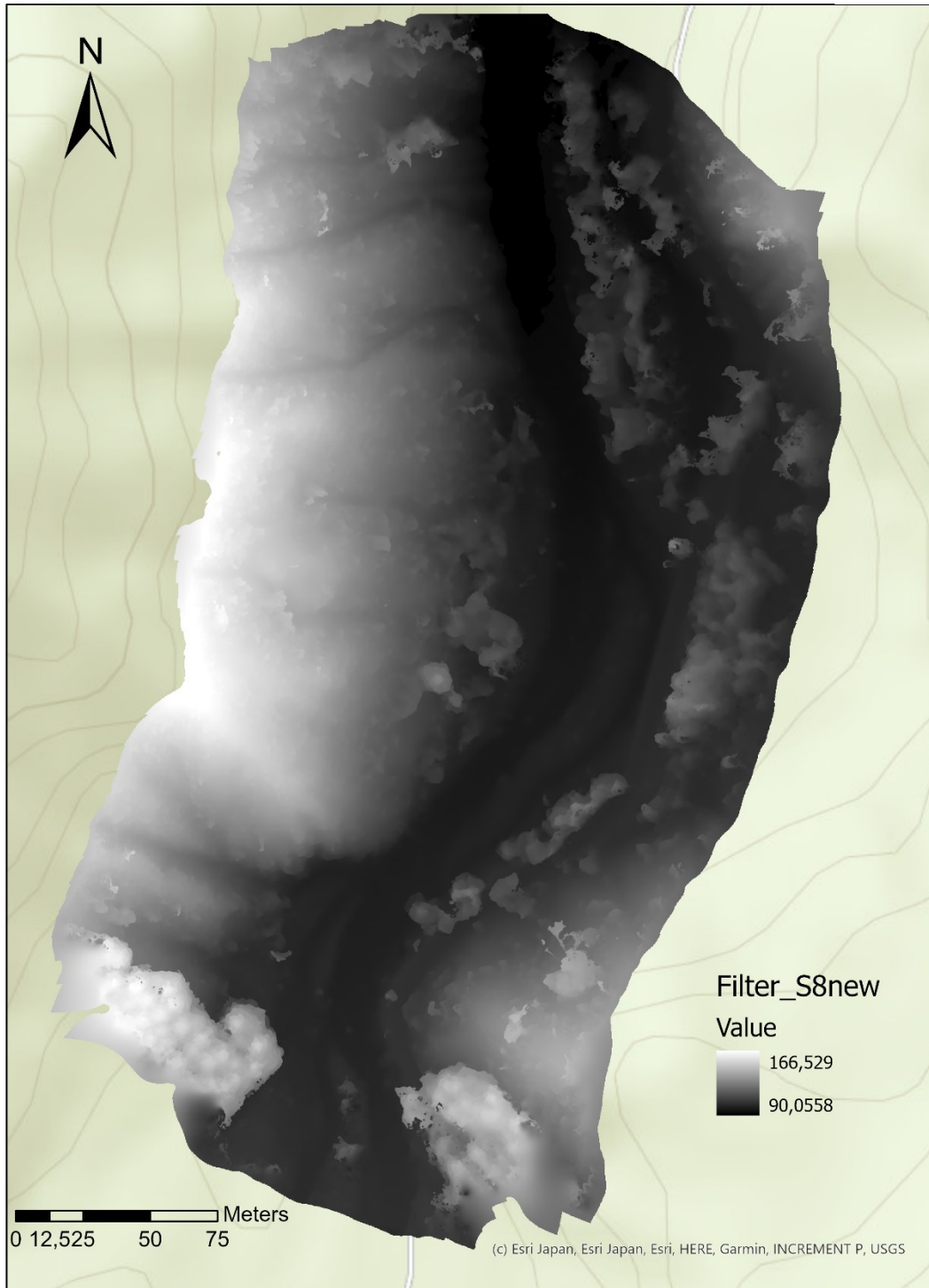


DEM site 7
by Sarah Kentsch



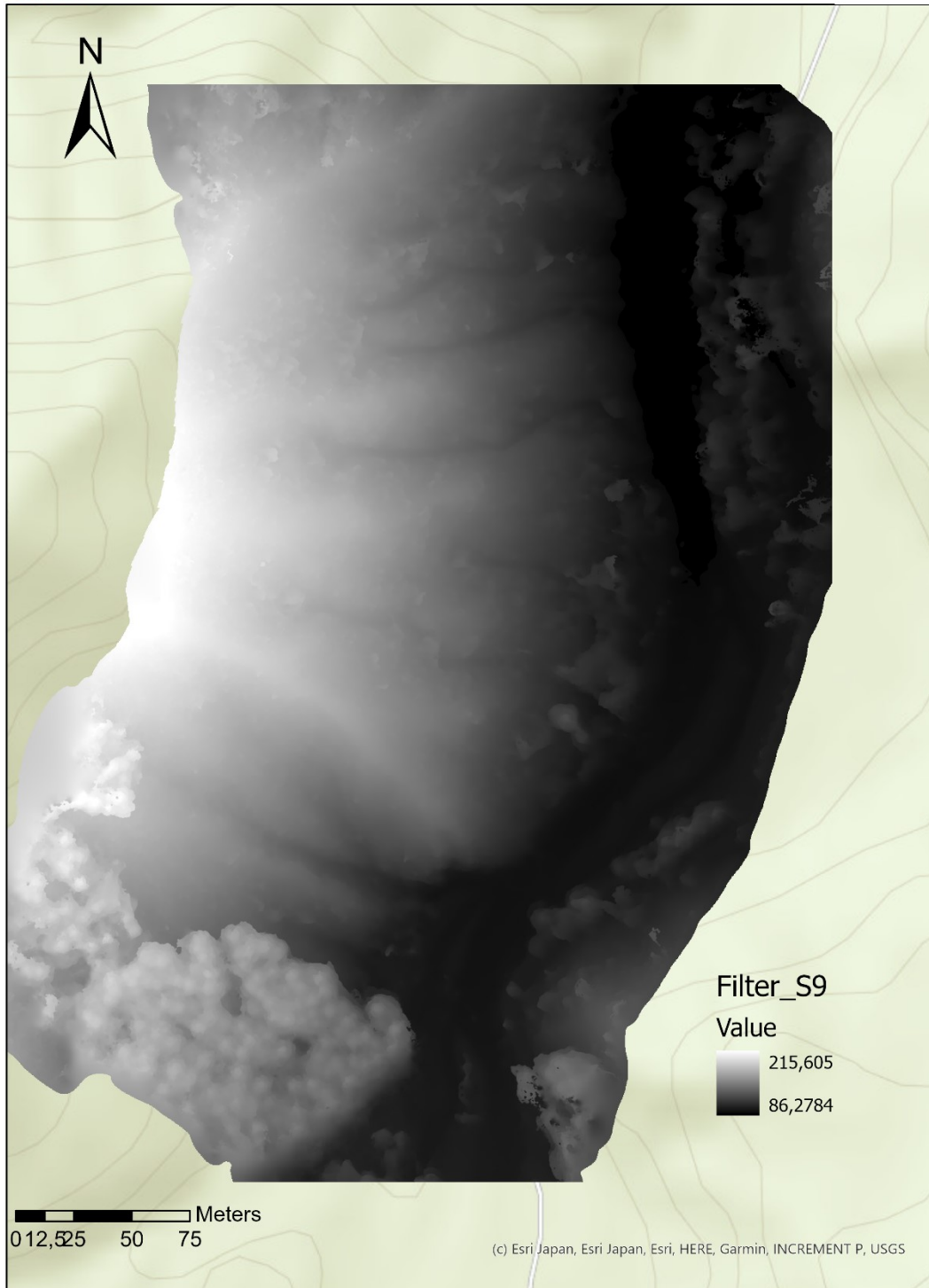


DEM site 8 by Sarah Kentsch





DEM site 9
by Sarah Kentsch





DEM site 10
by Sarah Kentsch



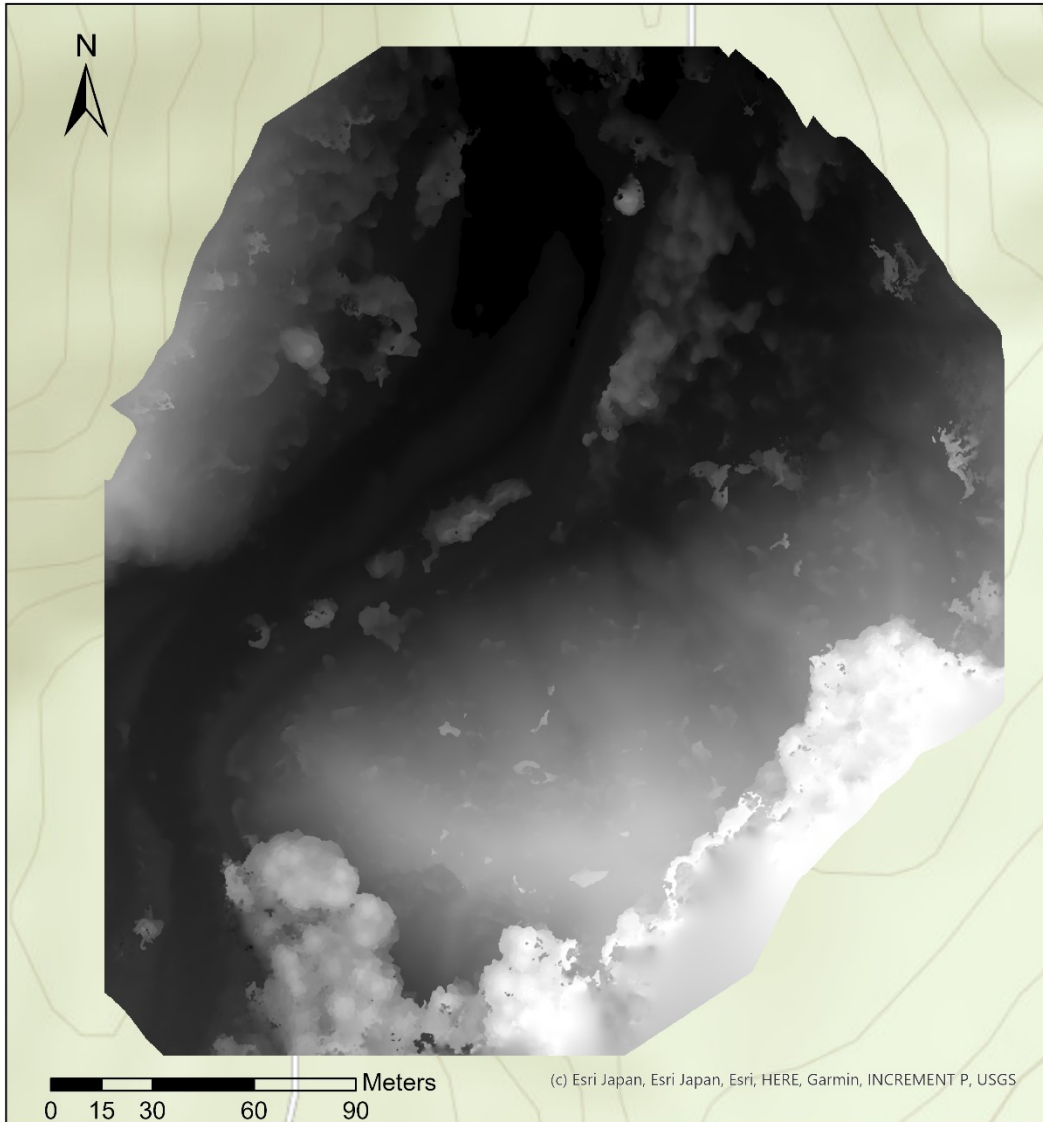
Filter_S10

Value





DEM site 11
by Sarah Kentsch



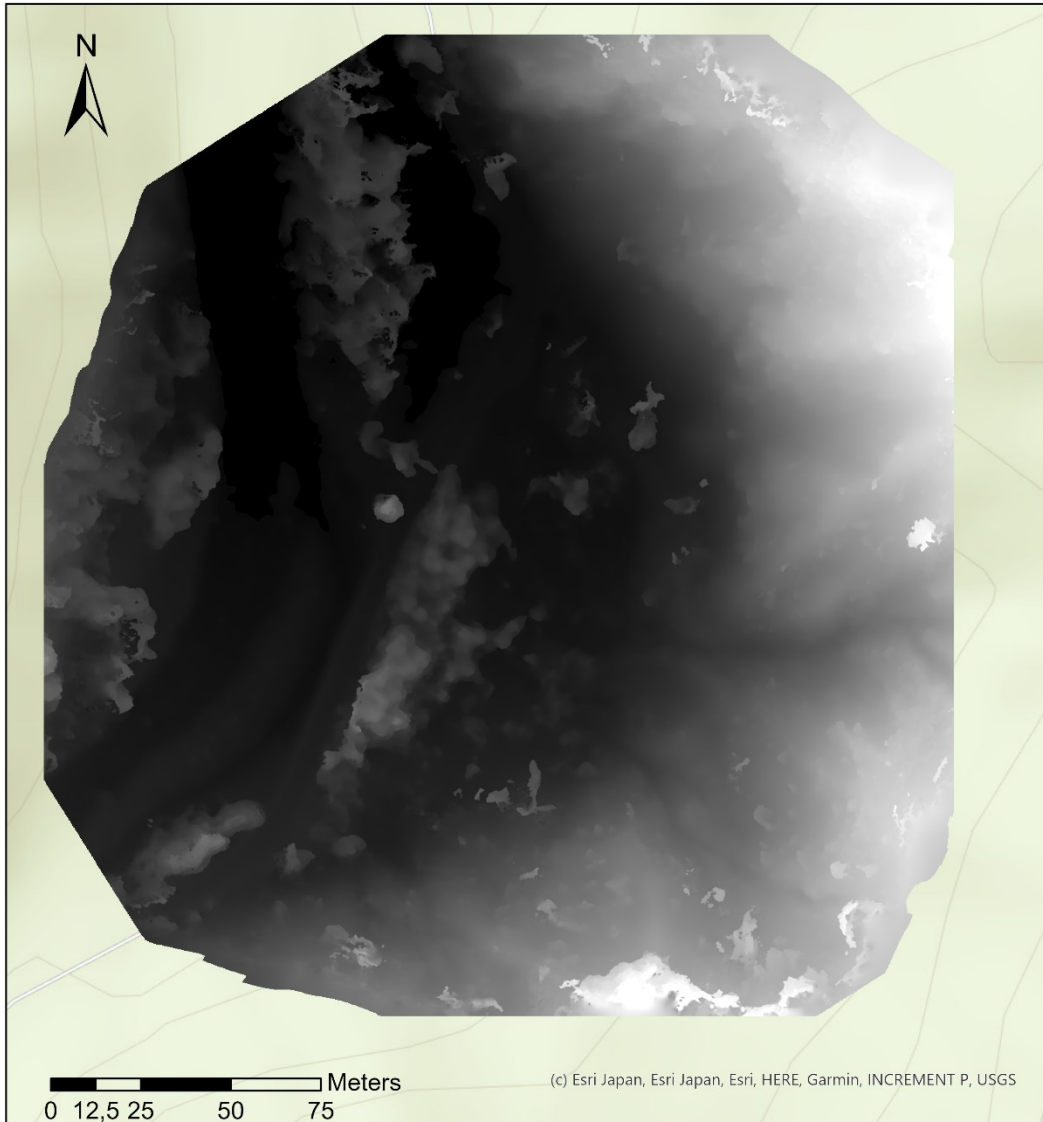
Filter_S11

Value





DEM site 12
by Sarah Kentsch



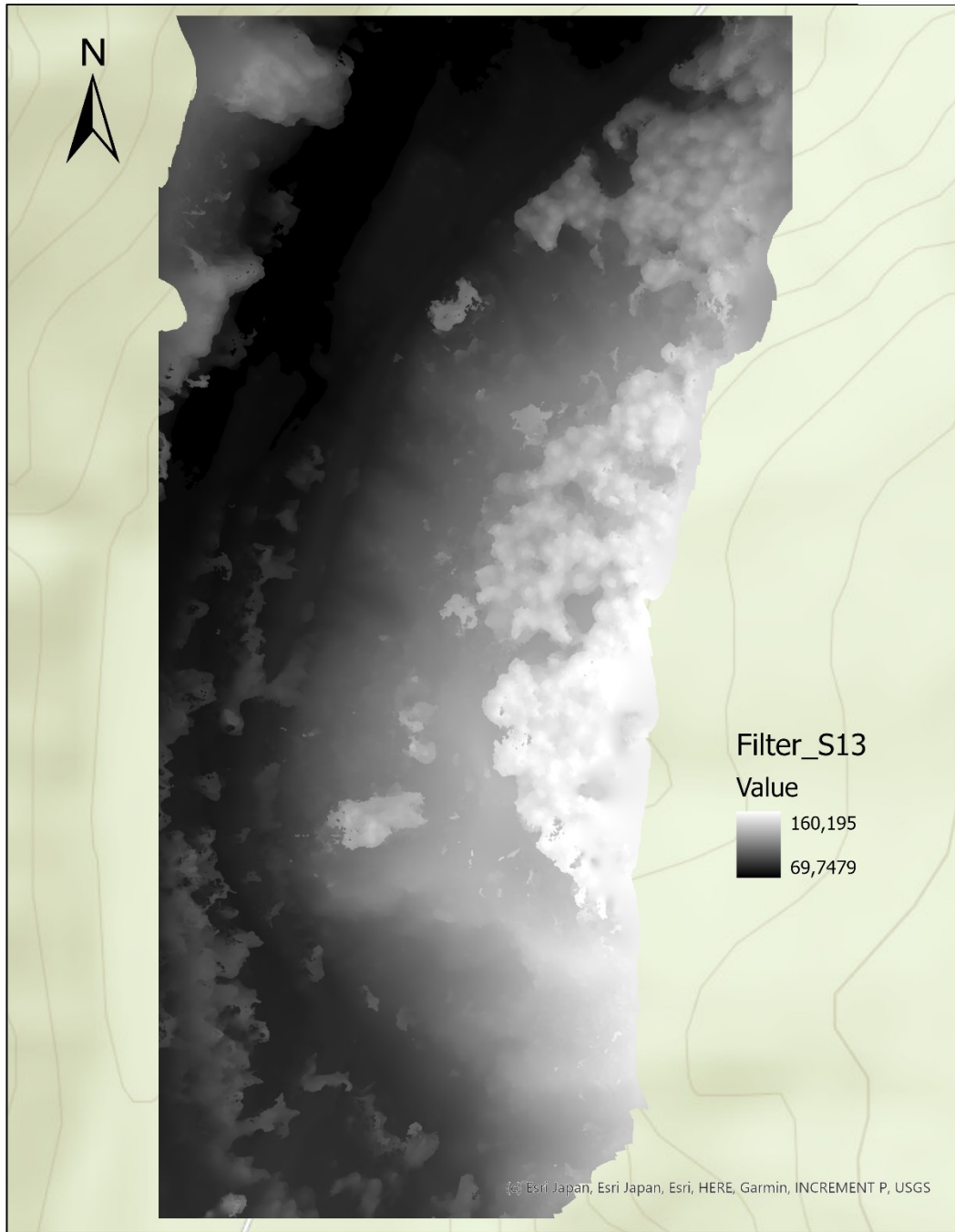
Filter_S12

Value





DEM site 13
by Sarah Kentsch

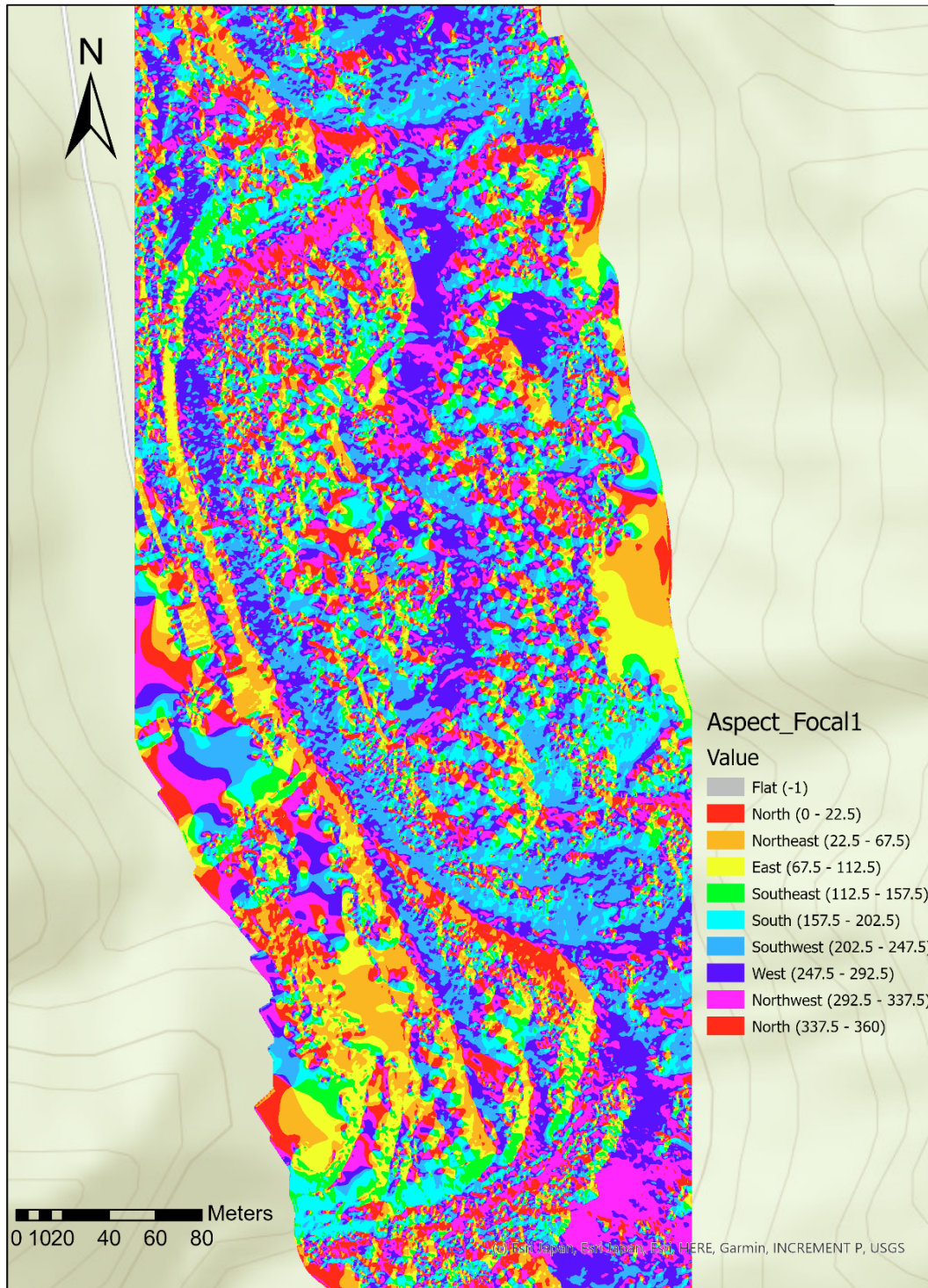


Part 2: Aspect

The following pages contain the Aspect maps for each site, generated with ArcGIS under the use of the tool *Aspect*. As basis of the analysis the DEM was used, which were first filtered and then the tool *Focal Statistics* was used to smooth the DEM, before the tool *Aspect* was used.

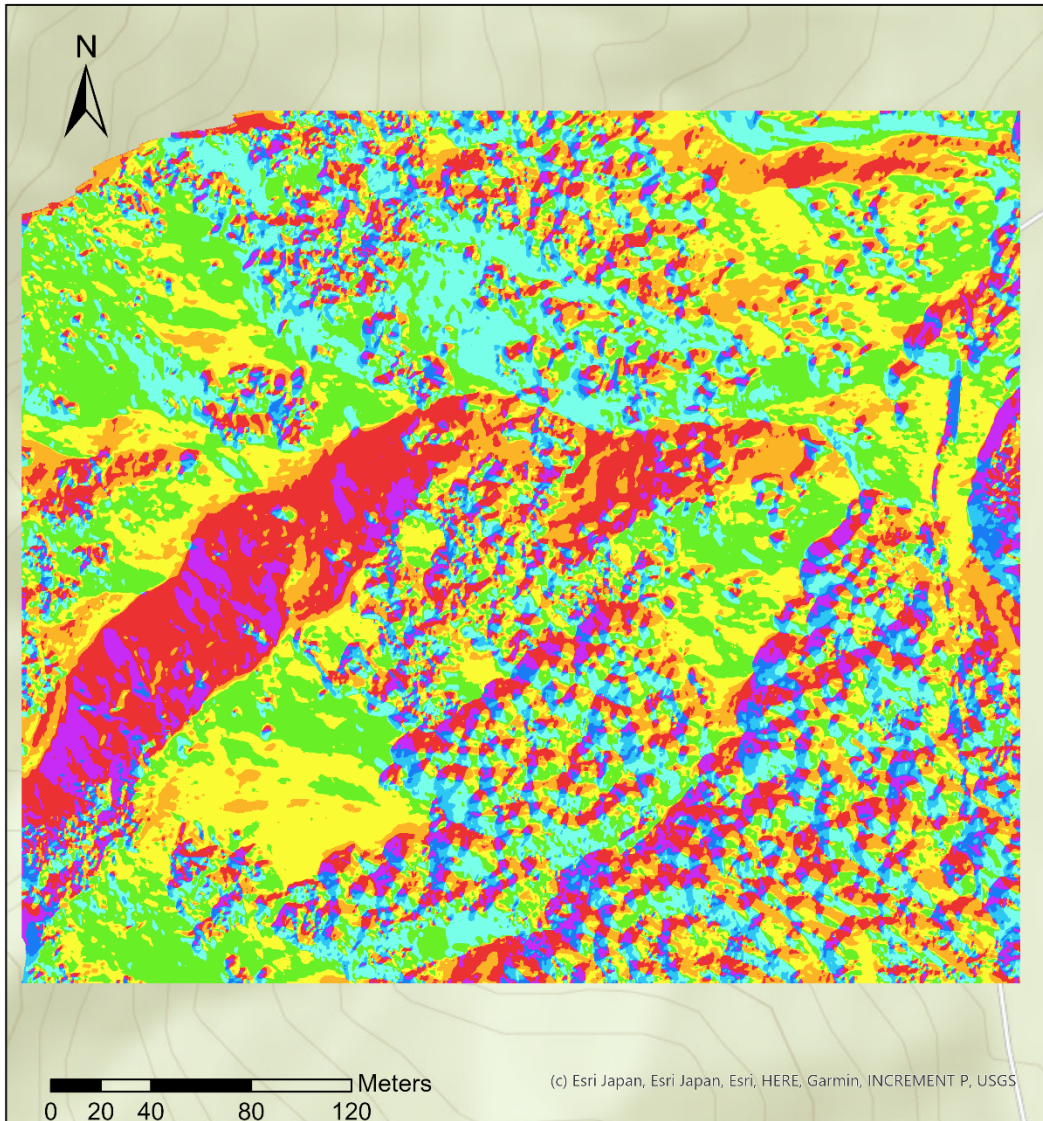


Aspect site 1 by Sarah Kentsch





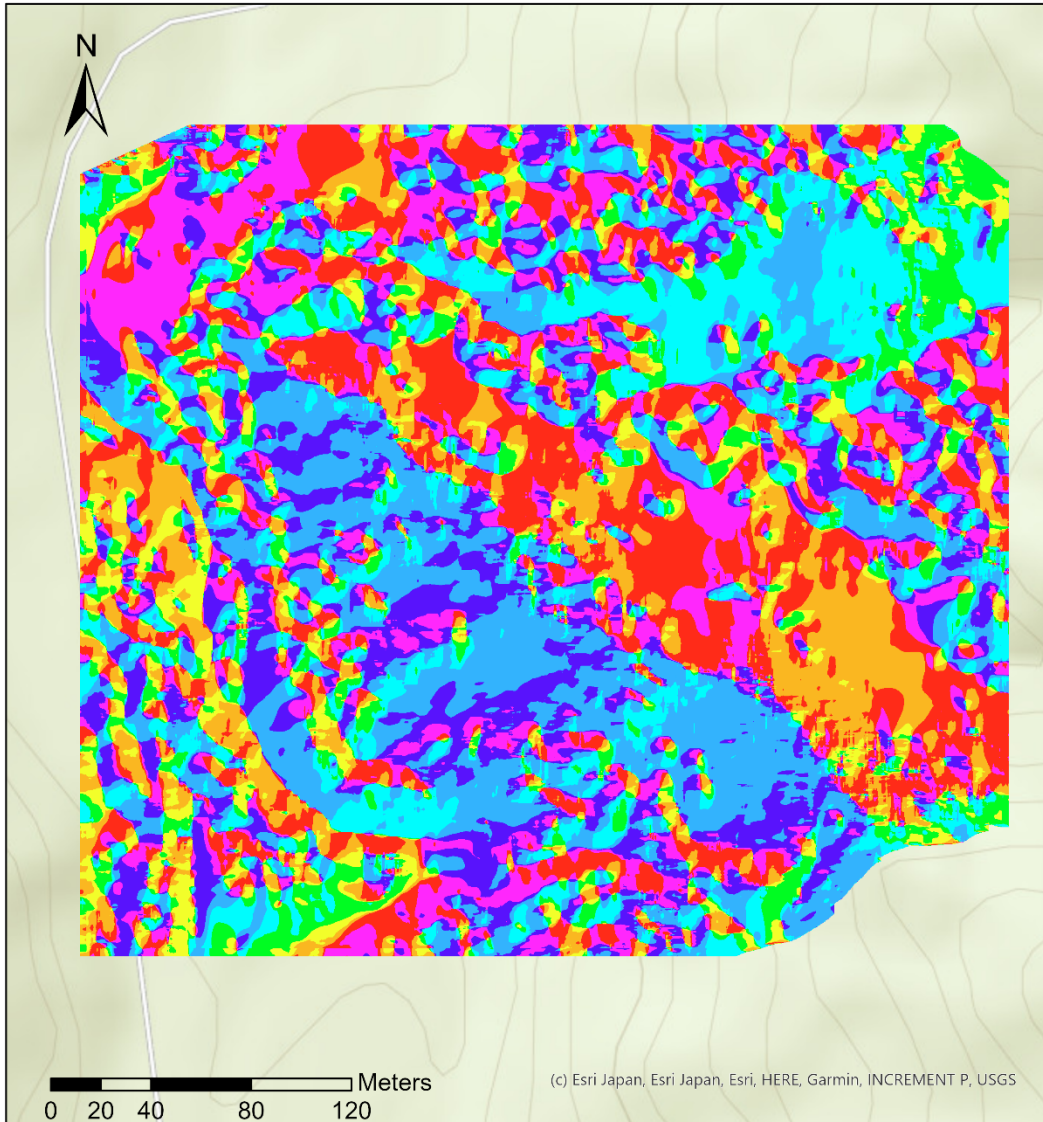
Aspect site 2 by Sarah Kentsch



Aspect_S2 Value	Color	Direction (Value Range)
Flat (-1)	Grey	-
North (0-22.5)	Red	North (0-22.5)
Northeast (22.5-67.5)	Orange	Northeast (22.5-67.5)
East (67.5-112.5)	Yellow	East (67.5-112.5)
Southeast (112.5-157.5)	Light Green	Southeast (112.5-157.5)
South (157.5-202.5)	Cyan	South (157.5-202.5)
Southwest (202.5-247.5)	Light Blue	Southwest (202.5-247.5)
West (247.5-292.5)	Blue	West (247.5-292.5)
Northwest (292.5-337.5)	Purple	Northwest (292.5-337.5)
North (337.5-360)	Dark Red	North (337.5-360)



Aspect site 3 by Sarah Kentsch



Aspect_3

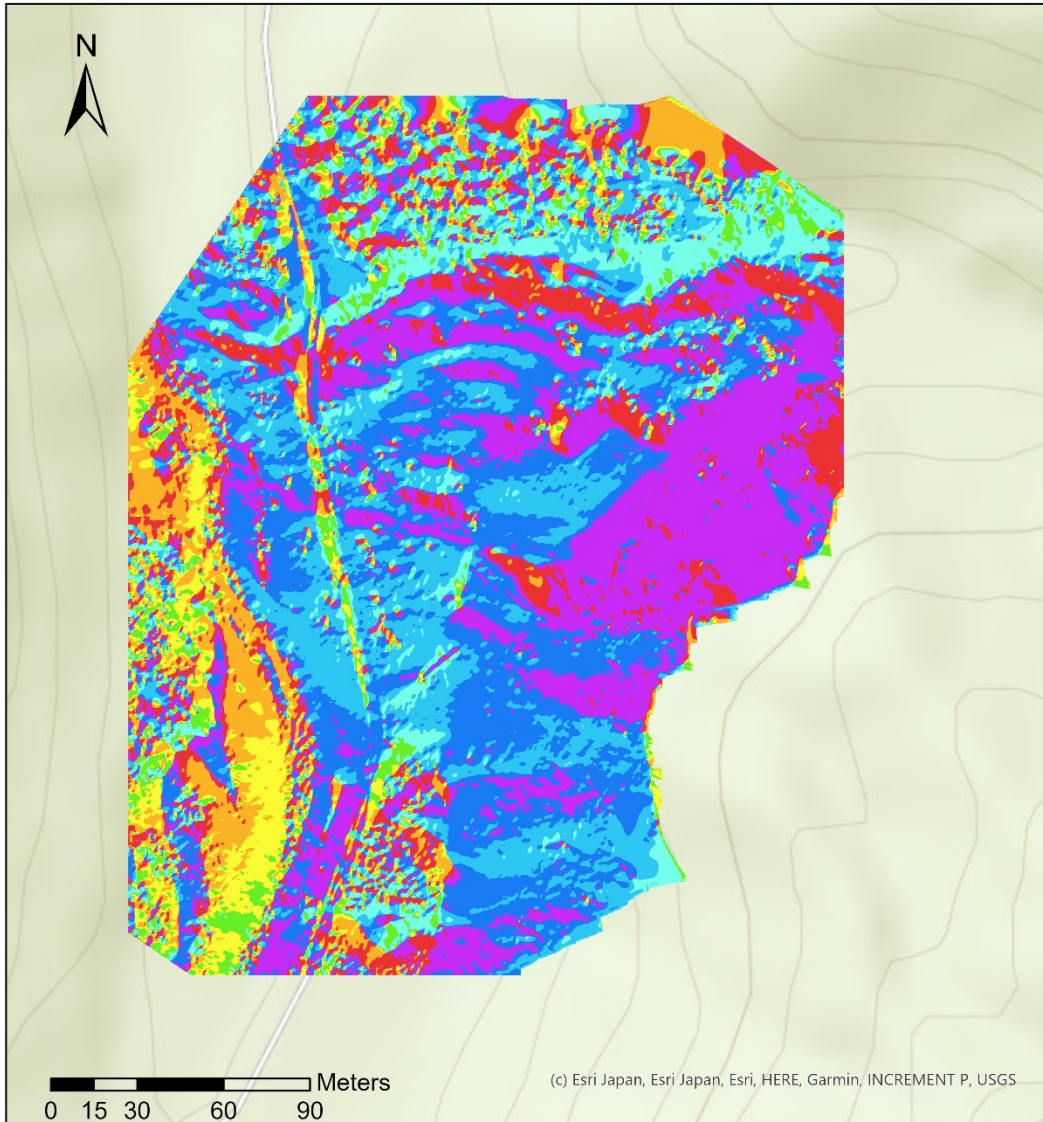
Value

- Flat (-1)
- North (0 - 22.5)

- | | |
|---------------------------|---------------------------|
| Northeast (22.5 - 67.5) | Southwest (202.5 - 247.5) |
| East (67.5 - 112.5) | West (247.5 - 292.5) |
| Southeast (112.5 - 157.5) | Northwest (292.5 - 337.5) |
| South (157.5 - 202.5) | North (337.5 - 360) |



Aspect site 4 by Sarah Kentsch



Aspect_S4

Value

Flat (-1)

North (0-22.5)

Northeast (22.5-67.5)

East (67.5-112.5)

Southeast (112.5-157.5)

South (157.5-202.5)

Southwest (202.5-247.5)

West (247.5-292.5)

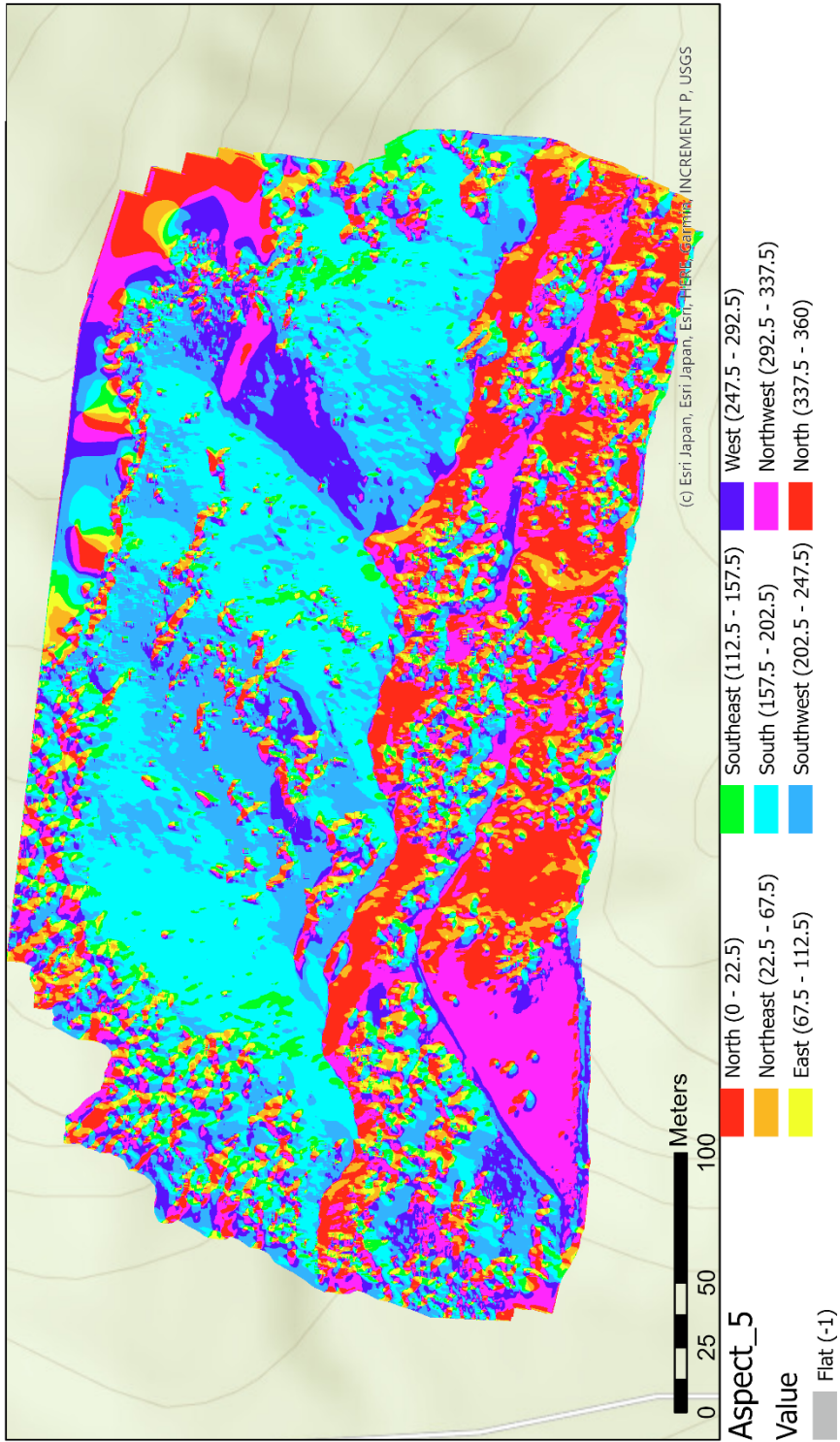
Northwest (292.5-337.5)

North (337.5-360)

(c) Esri Japan, Esri Japan, Esri, HERE, Garmin, INCREMENT P, USGS

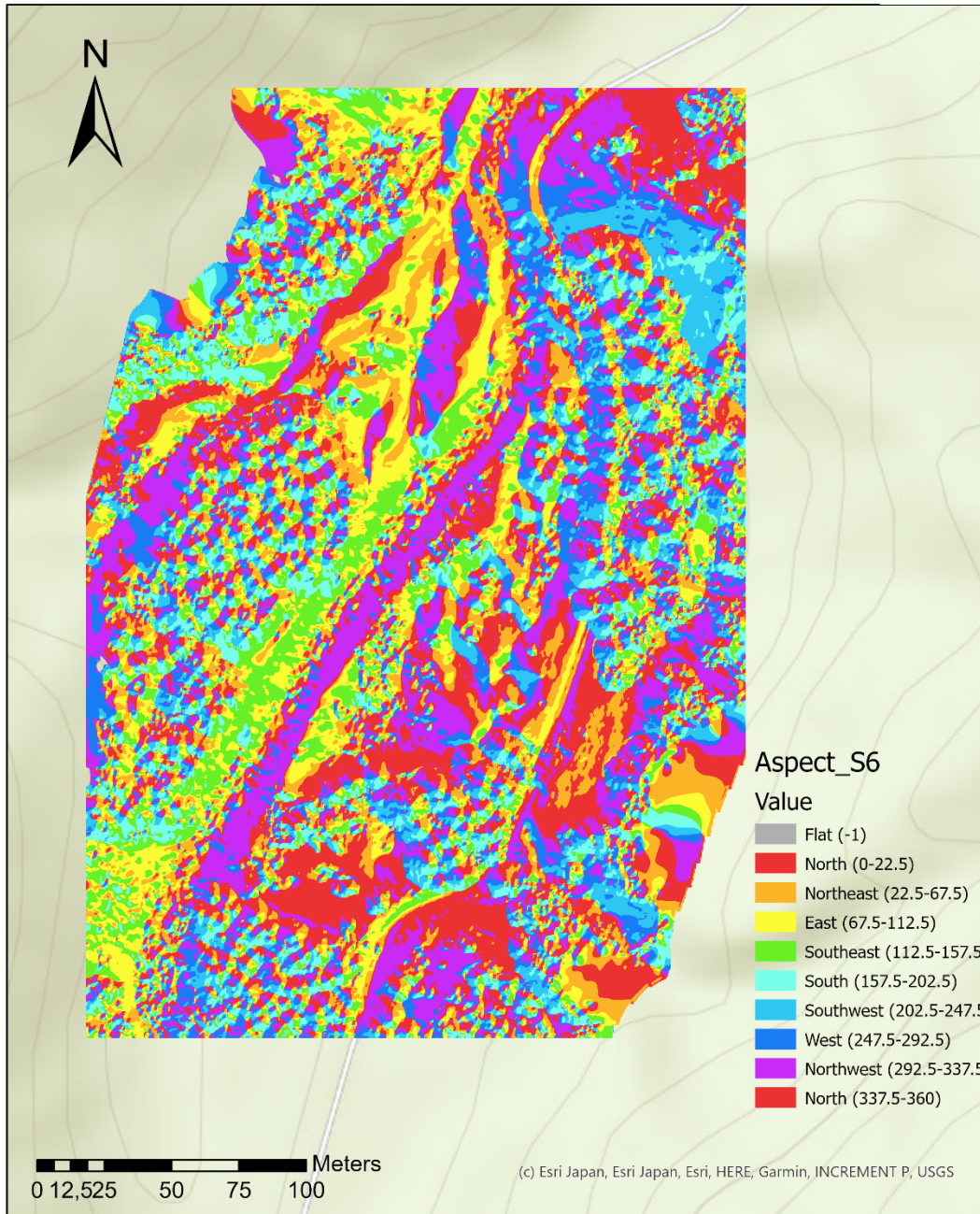


Aspect site 5
by Sarah Kentsch



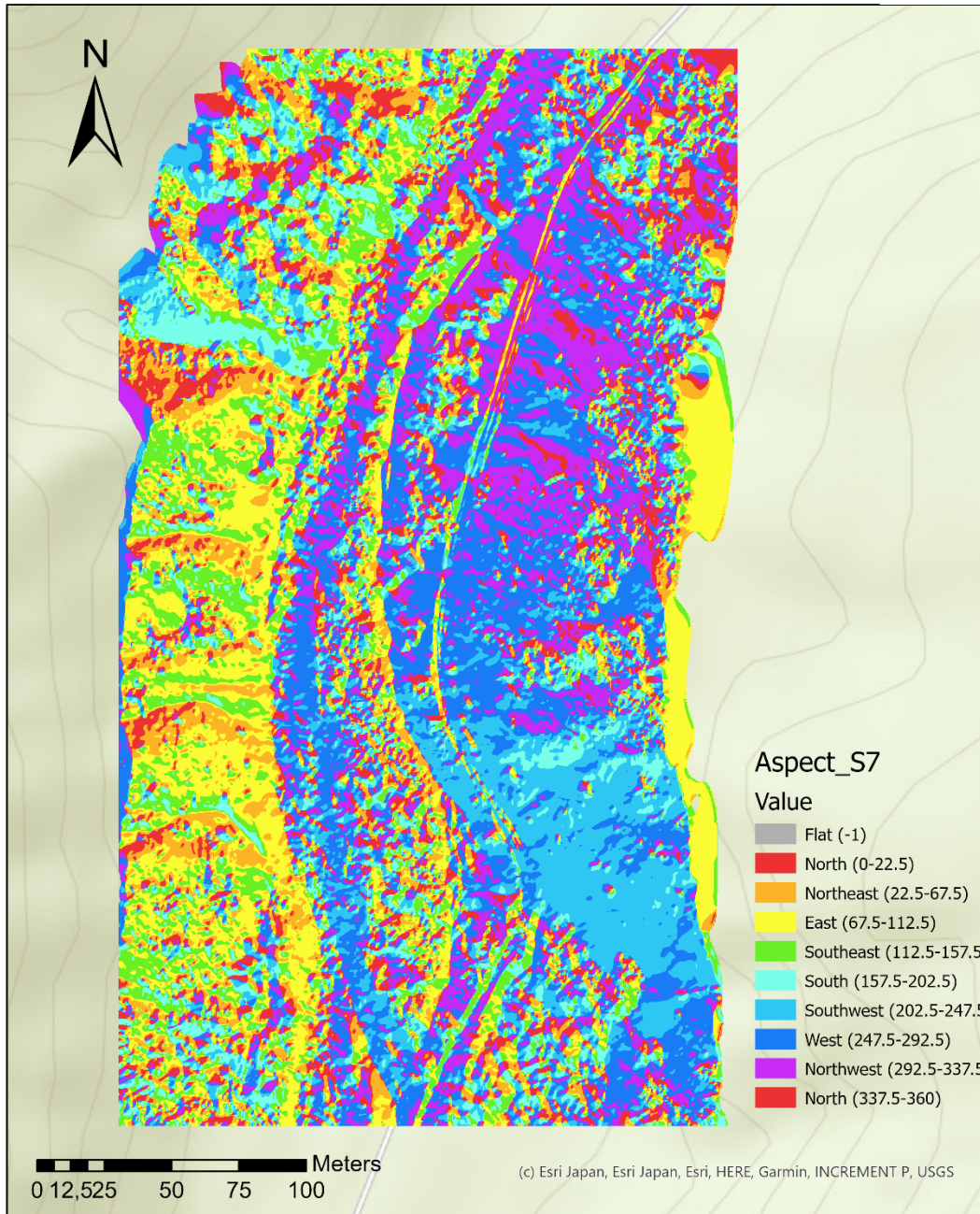


Aspect site 6 by Sarah Kentsch



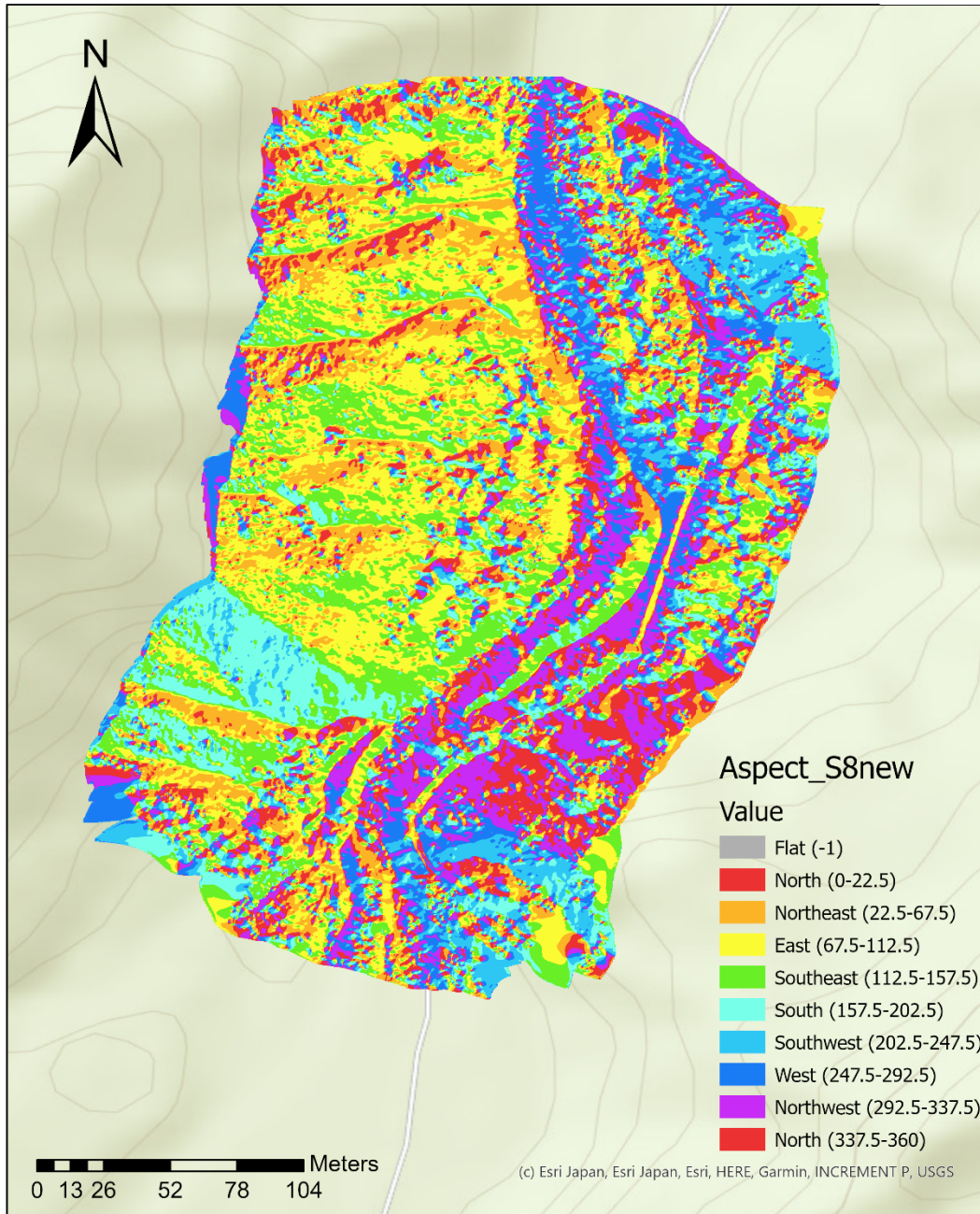


Aspect site 7 by Sarah Kentsch



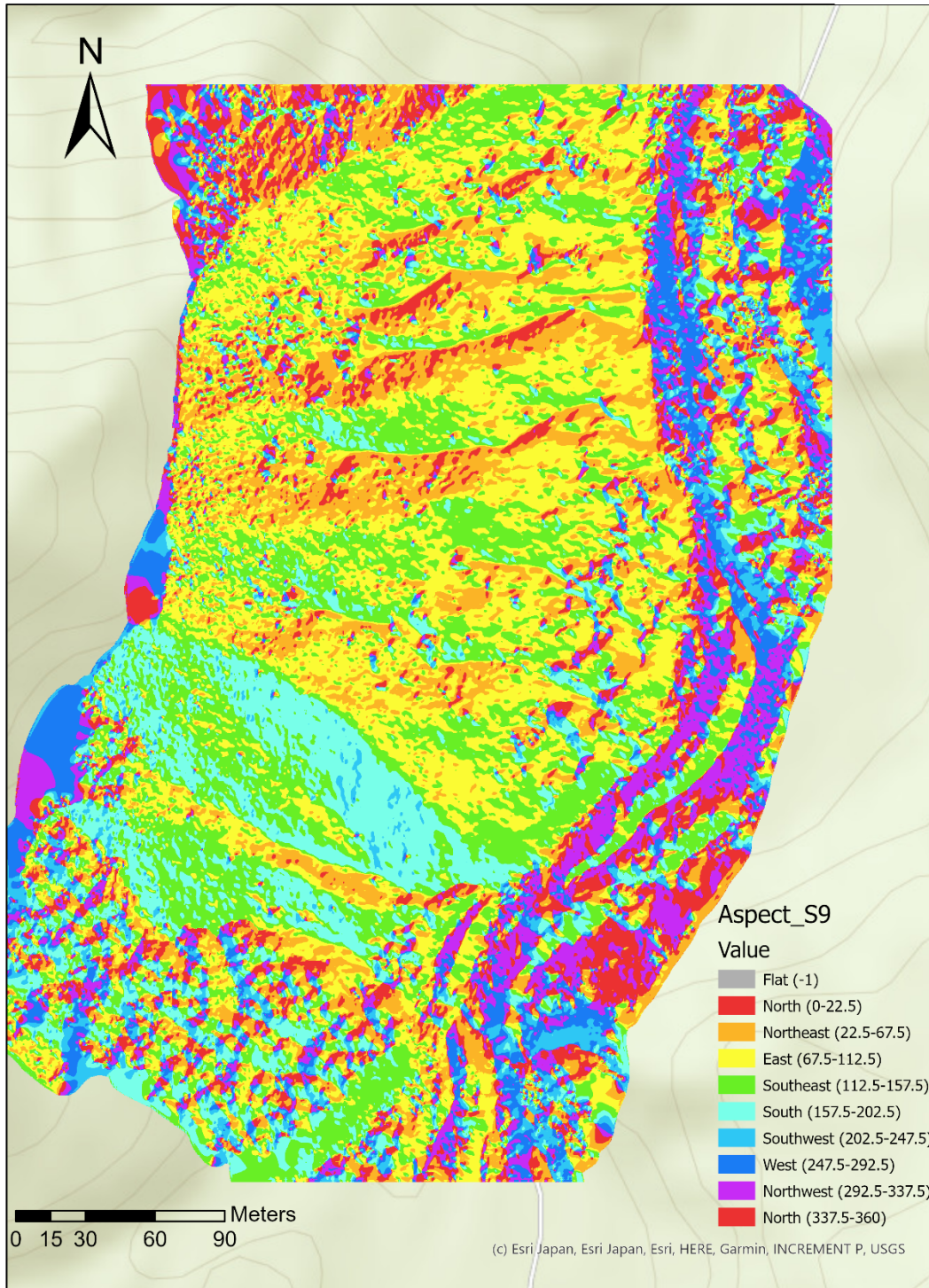


Aspect site 8 by Sarah Kentsch





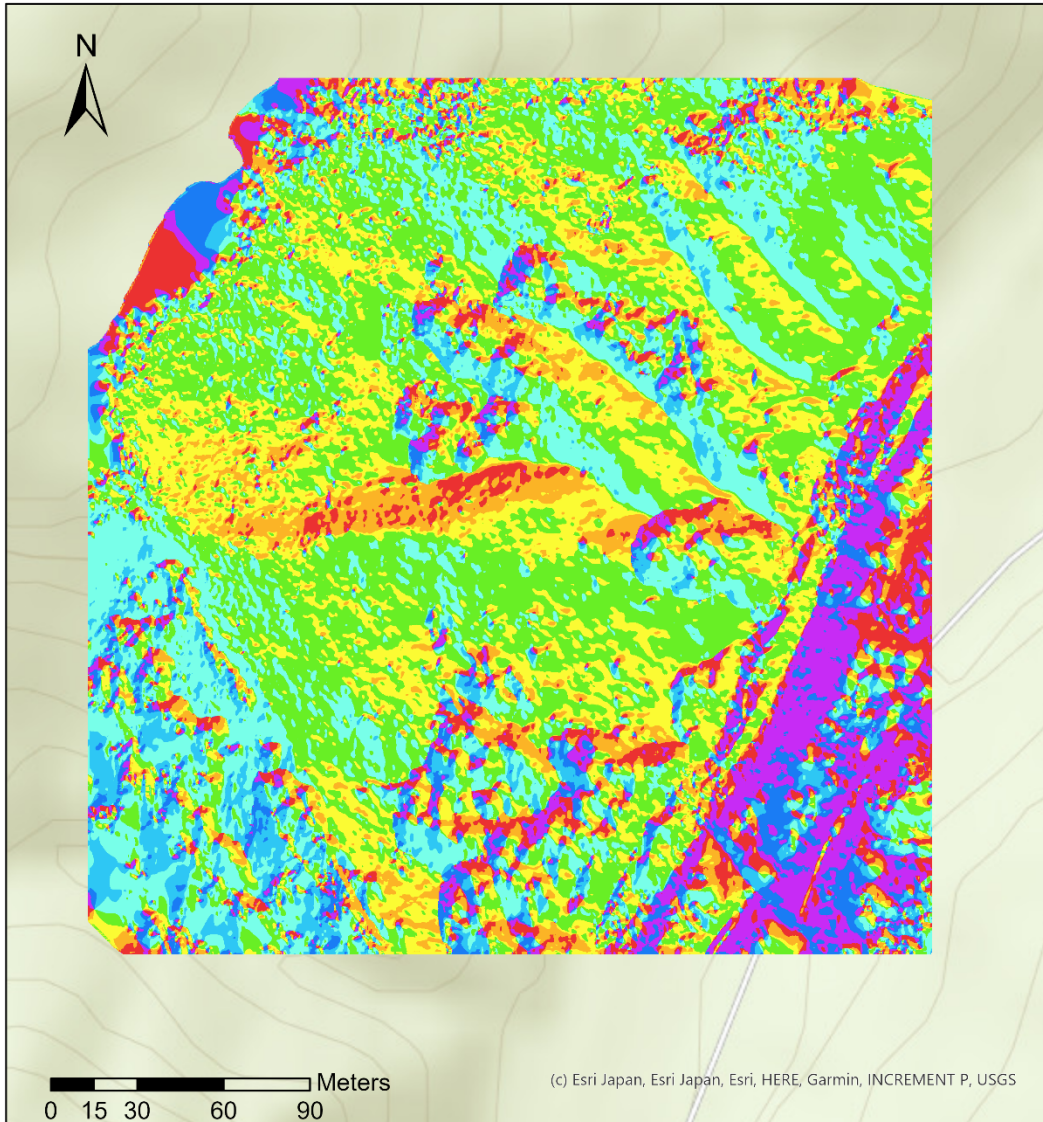
Aspect site 9 by Sarah Kentsch





Aspect site 10

by Sarah Kentsch



Aspect_S10

Value

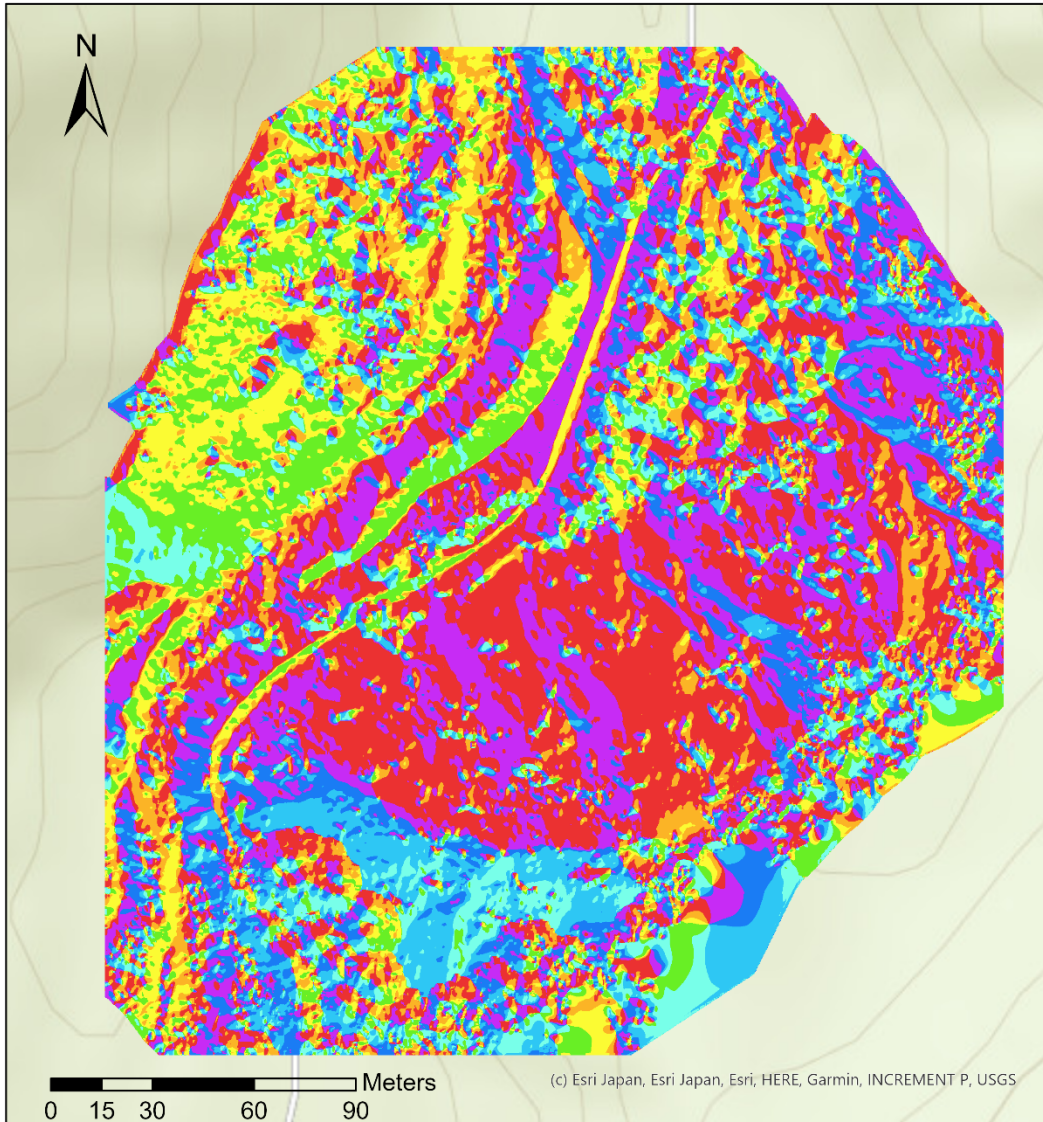
- Flat (-1)
- North (0-22.5)

- Northeast (22.5-67.5)
- East (67.5-112.5)
- Southeast (112.5-157.5)
- South (157.5-202.5)
- Southwest (202.5-247.5)
- West (247.5-292.5)
- Northwest (292.5-337.5)
- North (337.5-360)



Aspect site 11

by Sarah Kentsch

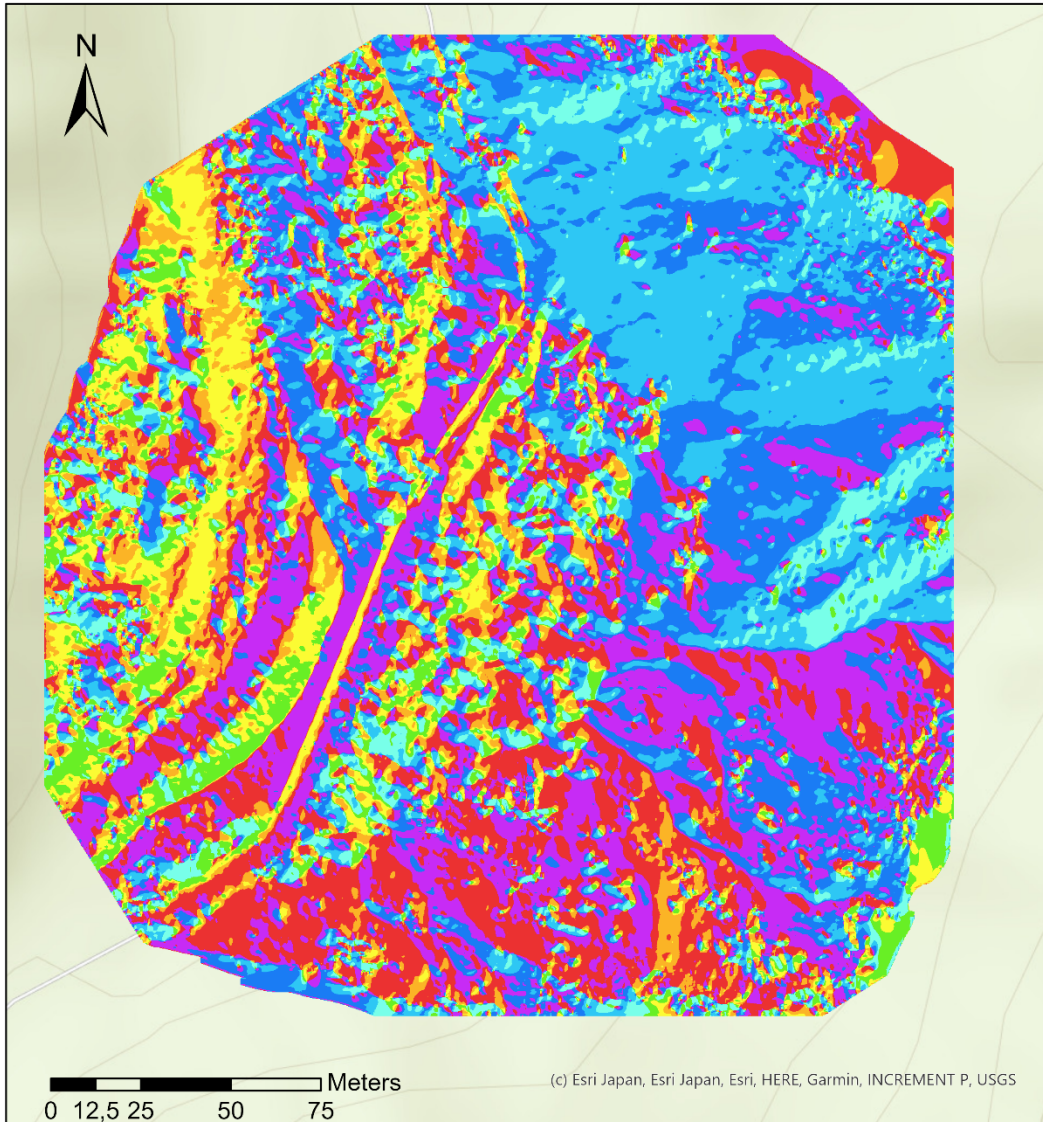


Aspect_S11 Value	Color	Direction (Value Range)
Flat (-1)	Grey	-
North (0-22.5)	Red	North (0-22.5)
Northeast (22.5-67.5)	Orange	Northeast (22.5-67.5)
East (67.5-112.5)	Yellow	East (67.5-112.5)
Southeast (112.5-157.5)	Light Green	Southeast (112.5-157.5)
South (157.5-202.5)	Cyan	South (157.5-202.5)
Southwest (202.5-247.5)	Light Blue	Southwest (202.5-247.5)
West (247.5-292.5)	Blue	West (247.5-292.5)
Northwest (292.5-337.5)	Purple	Northwest (292.5-337.5)
North (337.5-360)	Dark Red	North (337.5-360)



Aspect site 12

by Sarah Kentsch



Aspect_S12

Value

Flat (-1)

North (0-22.5)

Northeast (22.5-67.5)

East (67.5-112.5)

Southeast (112.5-157.5)

South (157.5-202.5)

Southwest (202.5-247.5)

West (247.5-292.5)

Northwest (292.5-337.5)

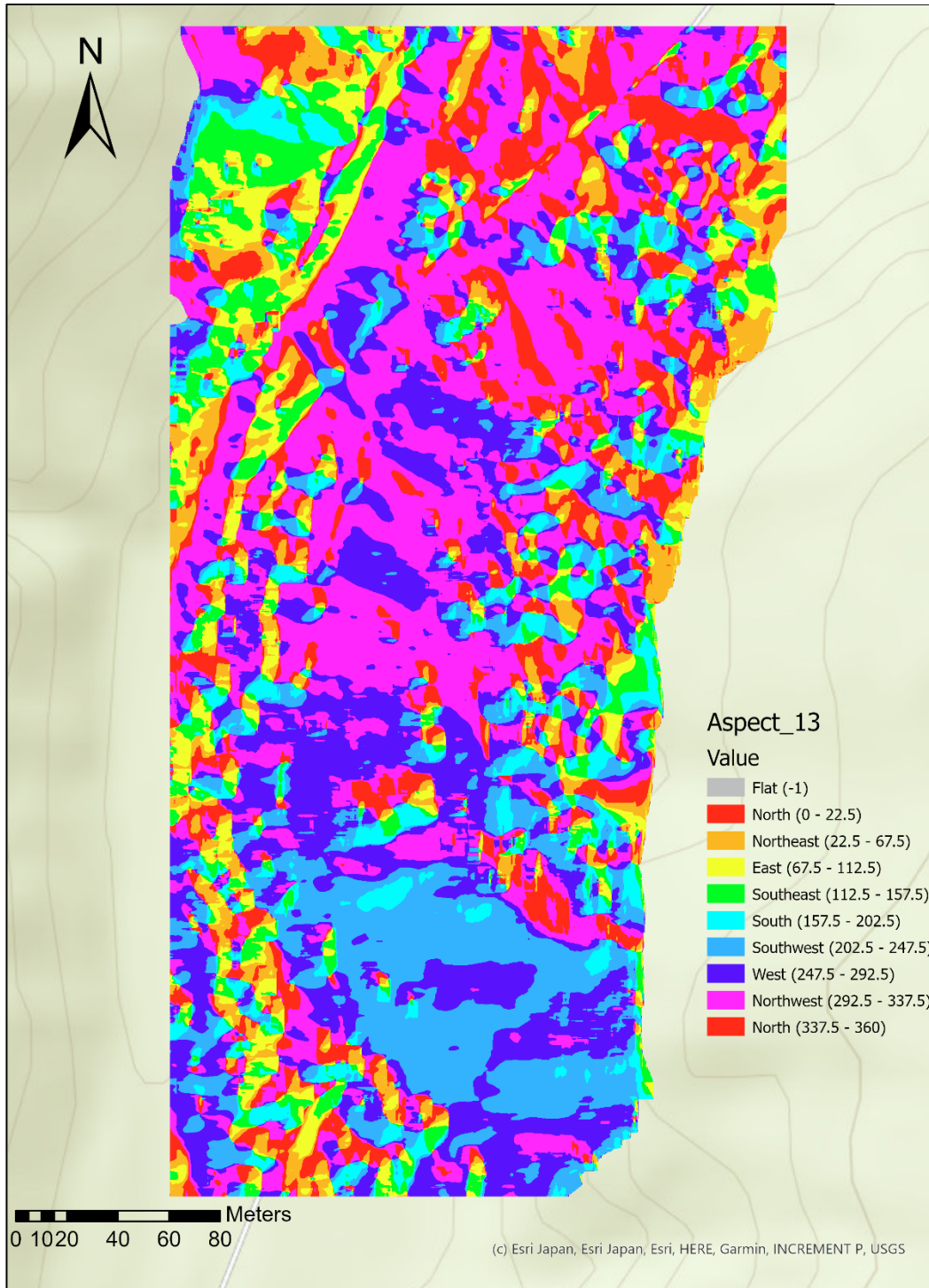
North (337.5-360)

(c) Esri Japan, Esri Japan, Esri, HERE, Garmin, INCREMENT P, USGS



Aspect site 13

by Sarah Kentsch

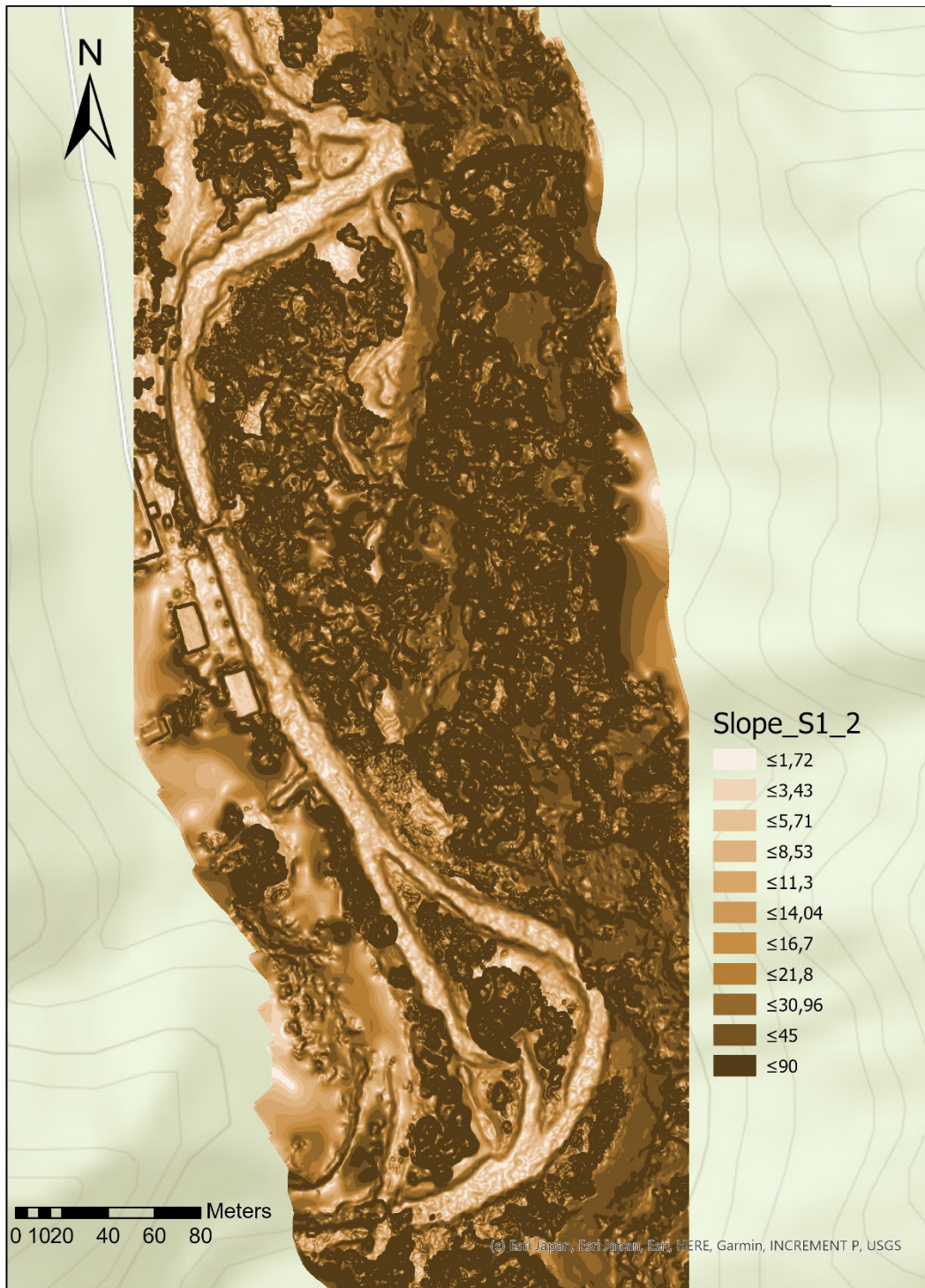


Part 3: Slope

The following pages contain the slope maps generated with ArcGIS using the tool *Slope* after the DEM of each site was filtered and smoothed.

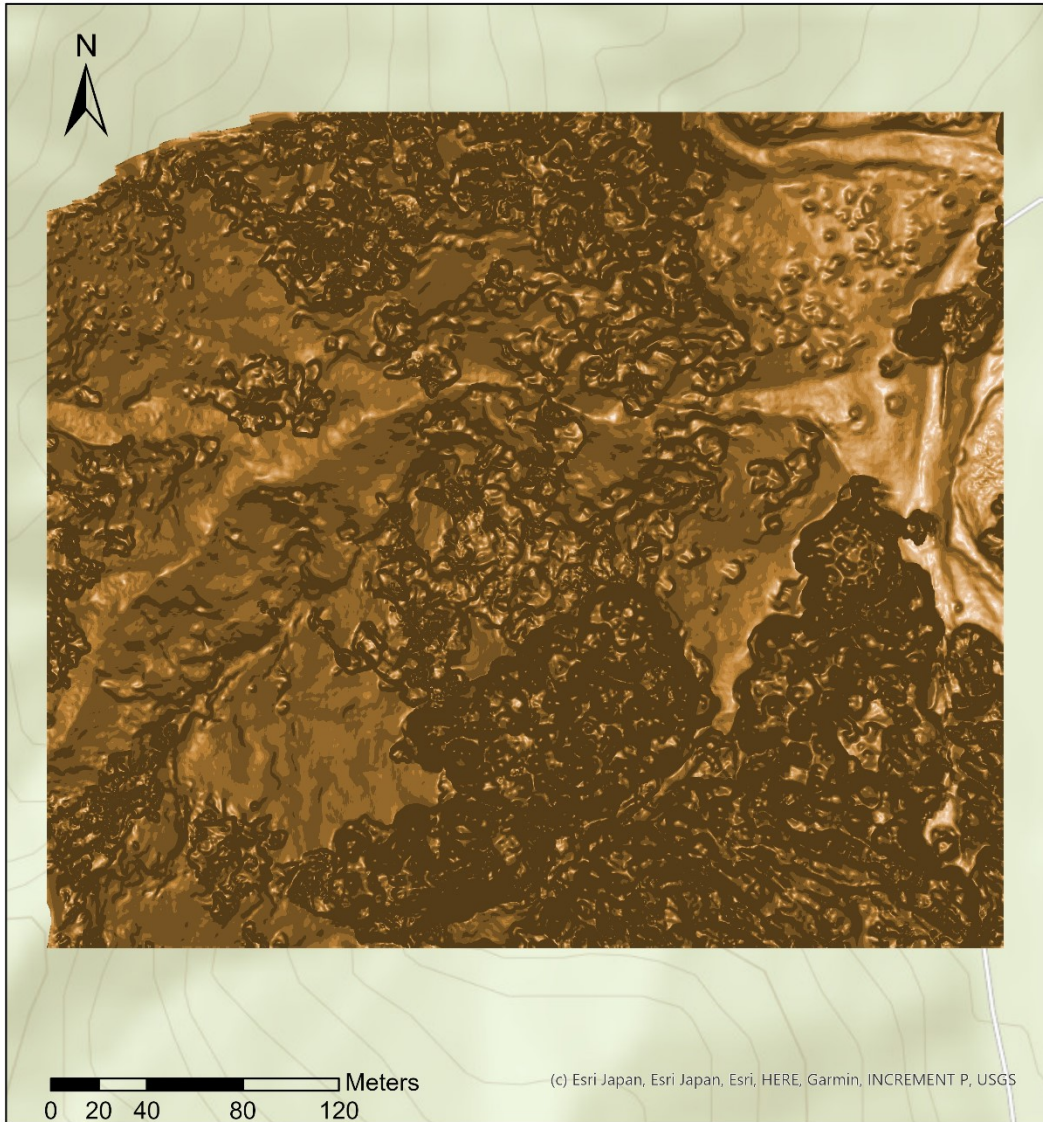


Slope site 1
by Sarah Kentsch





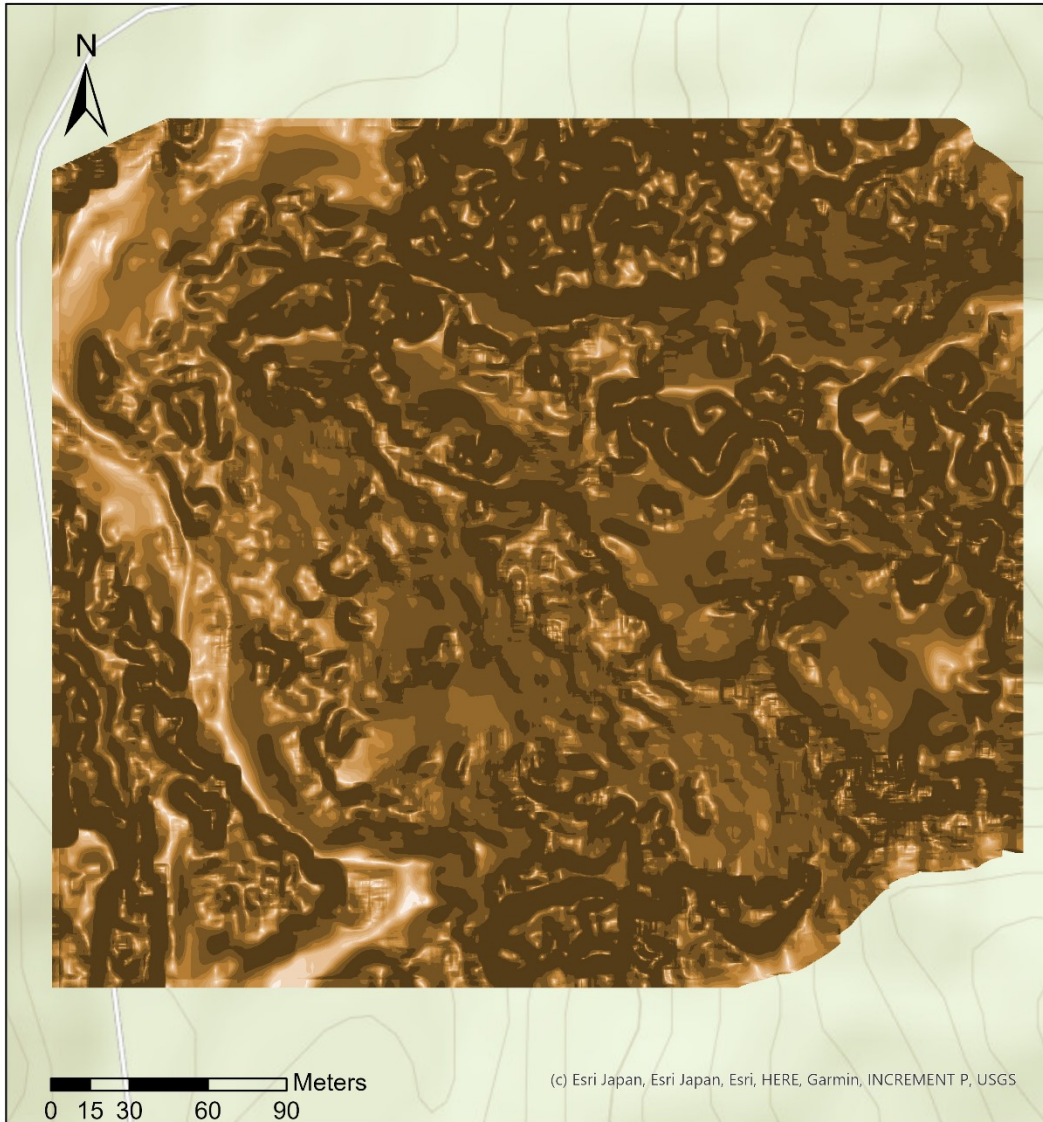
Slope site 2 by Sarah Kentsch



Slope_S2	≤5,71	≤14,04	≤30,96
	≤1,72	≤8,53	≤16,7
	≤3,43	≤11,3	≤21,8
			≤45
			≤90



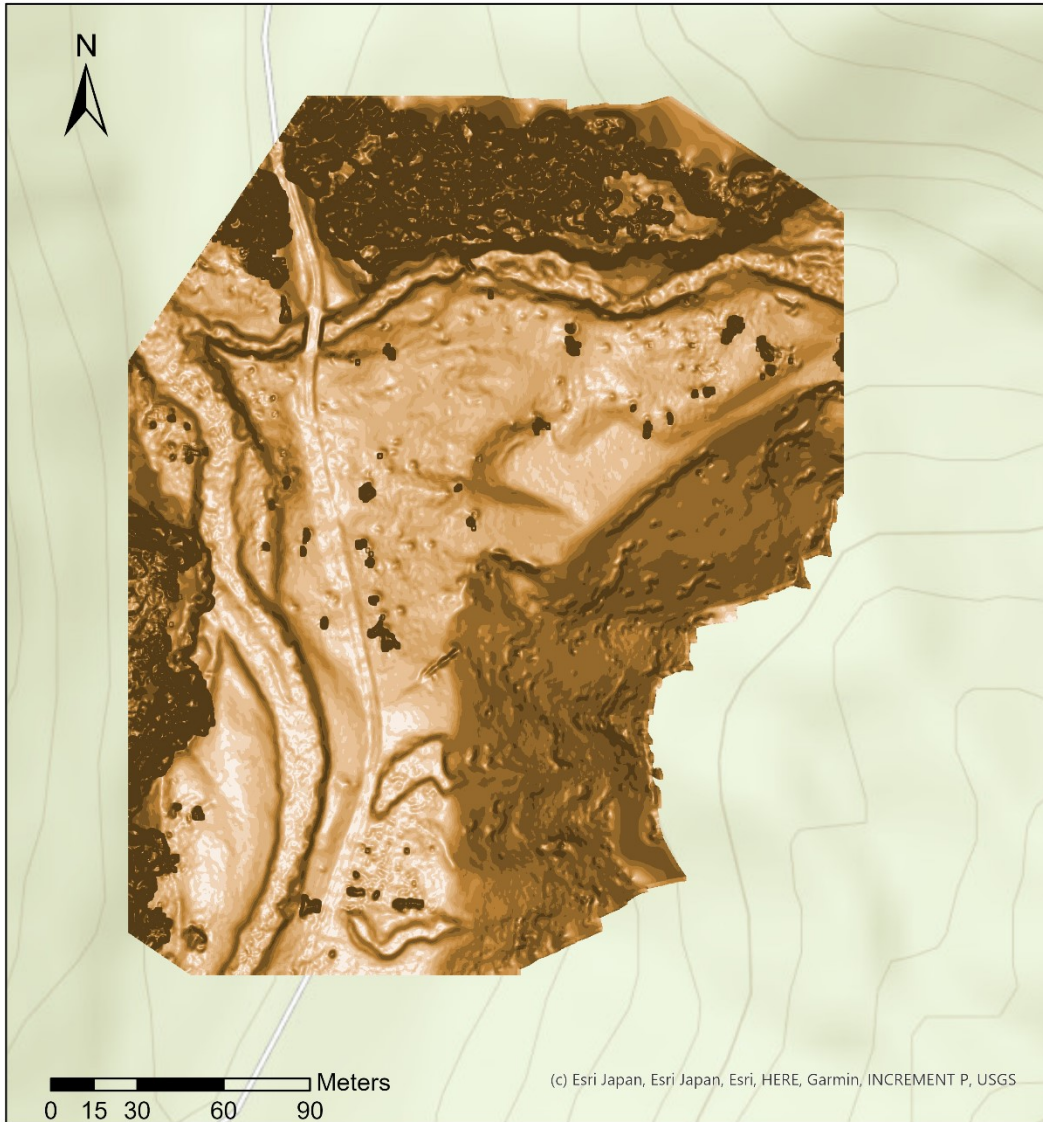
Slope site 3 by Sarah Kentsch



Slope3	≤3.43	≤11.3	≤21.8	≤90
	≤5.71	≤14.04	≤30.96	
Value	≤8.53	≤16.7	≤45	
	≤1.72			



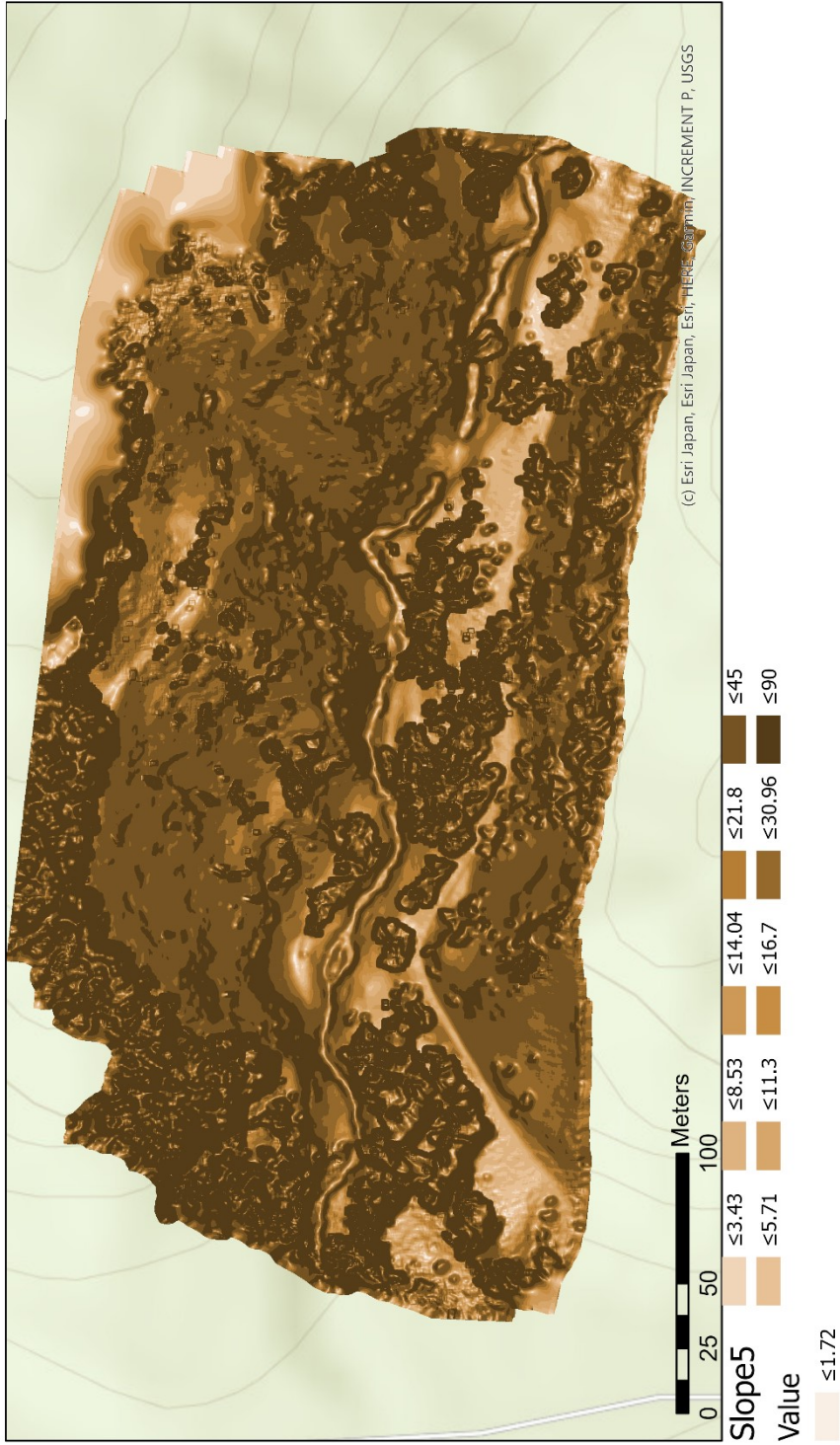
Slope site 4 by Sarah Kentsch



Slope_S4	≤5,71	≤14,04	≤30,96
≤1,72	≤8,53	≤16,7	≤45
≤3,43	≤11,3	≤21,8	≤90

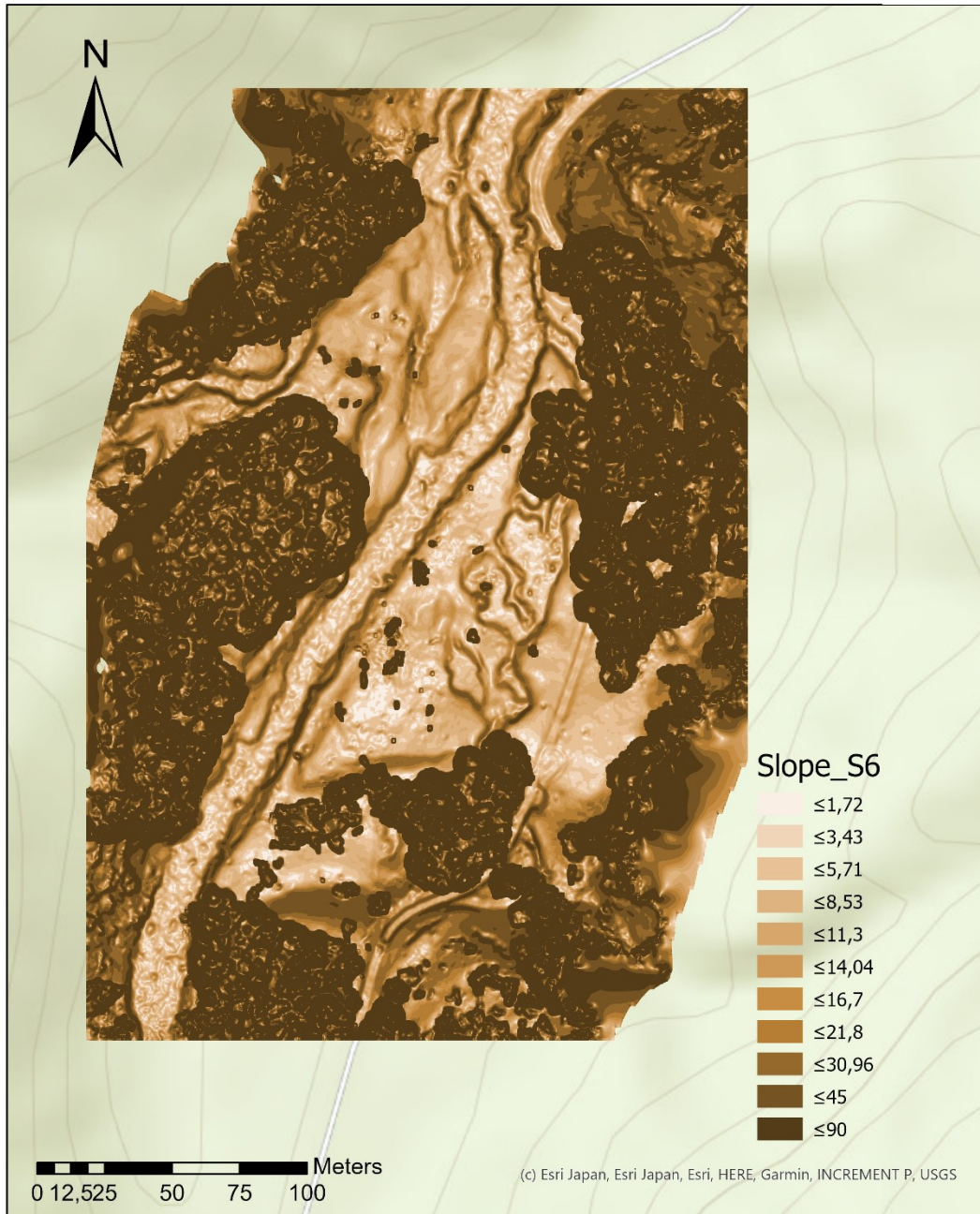


Slope site 5 by Sarah Kentsch



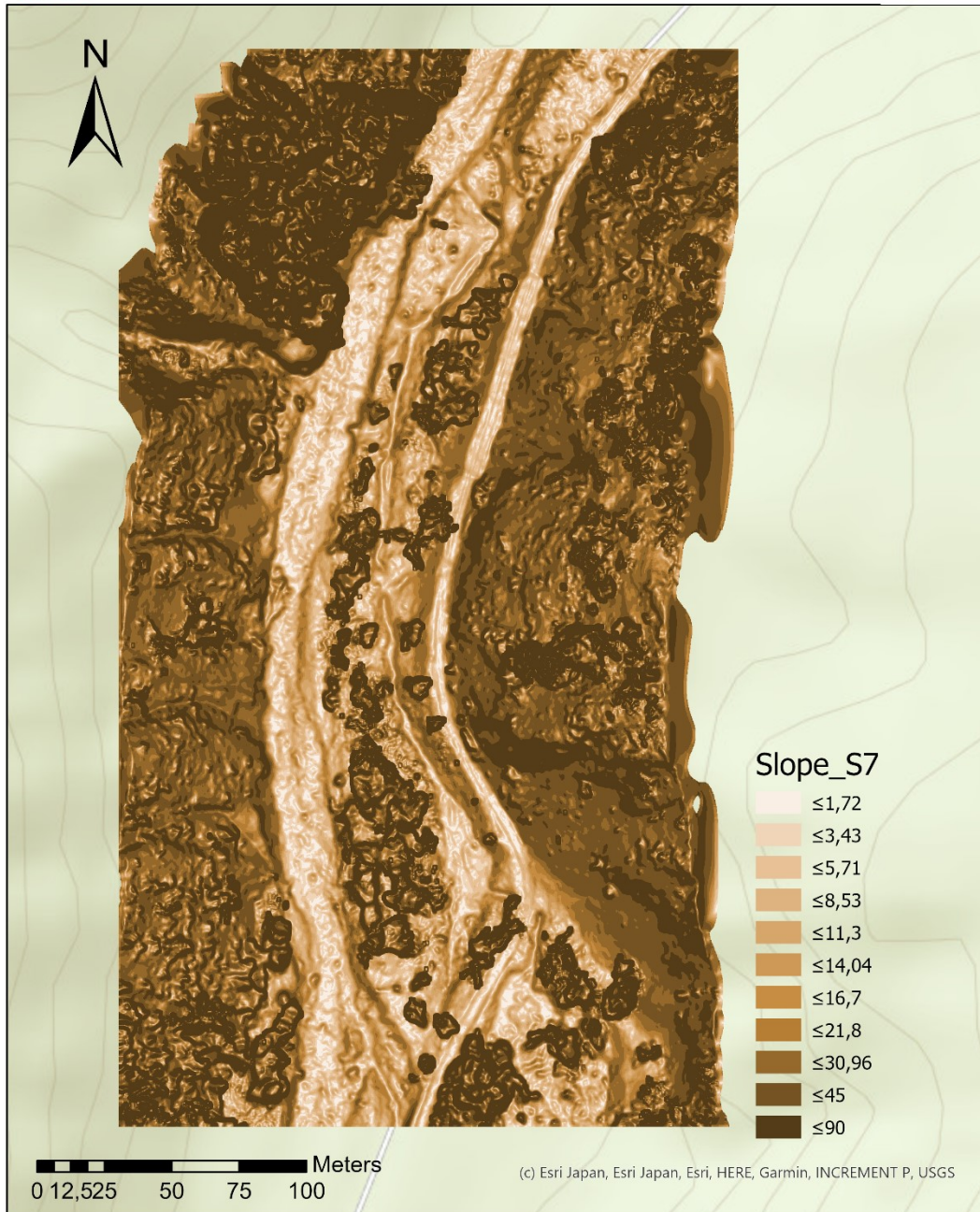


Slope site 6 by Sarah Kentsch





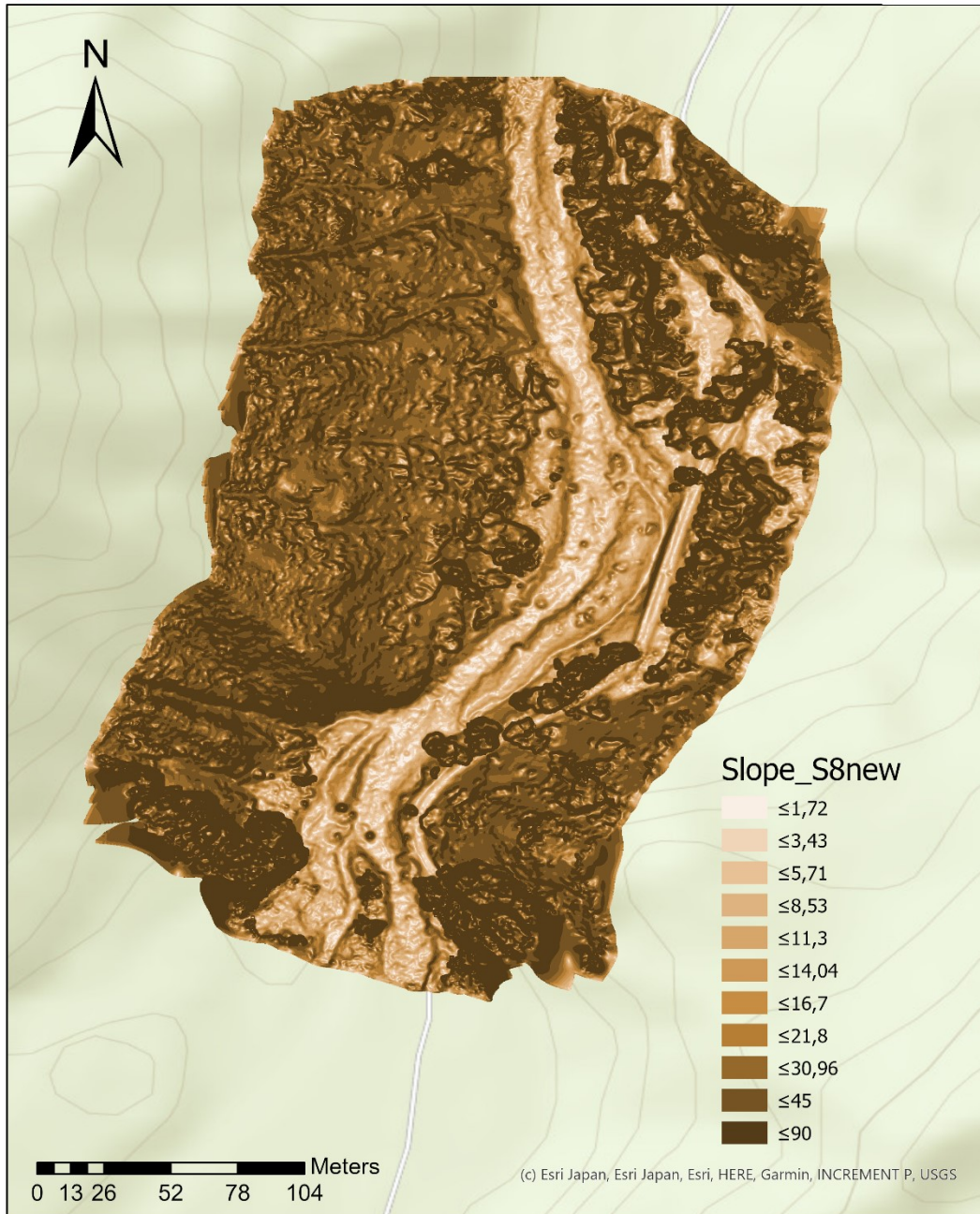
Slope site 7 by Sarah Kentsch





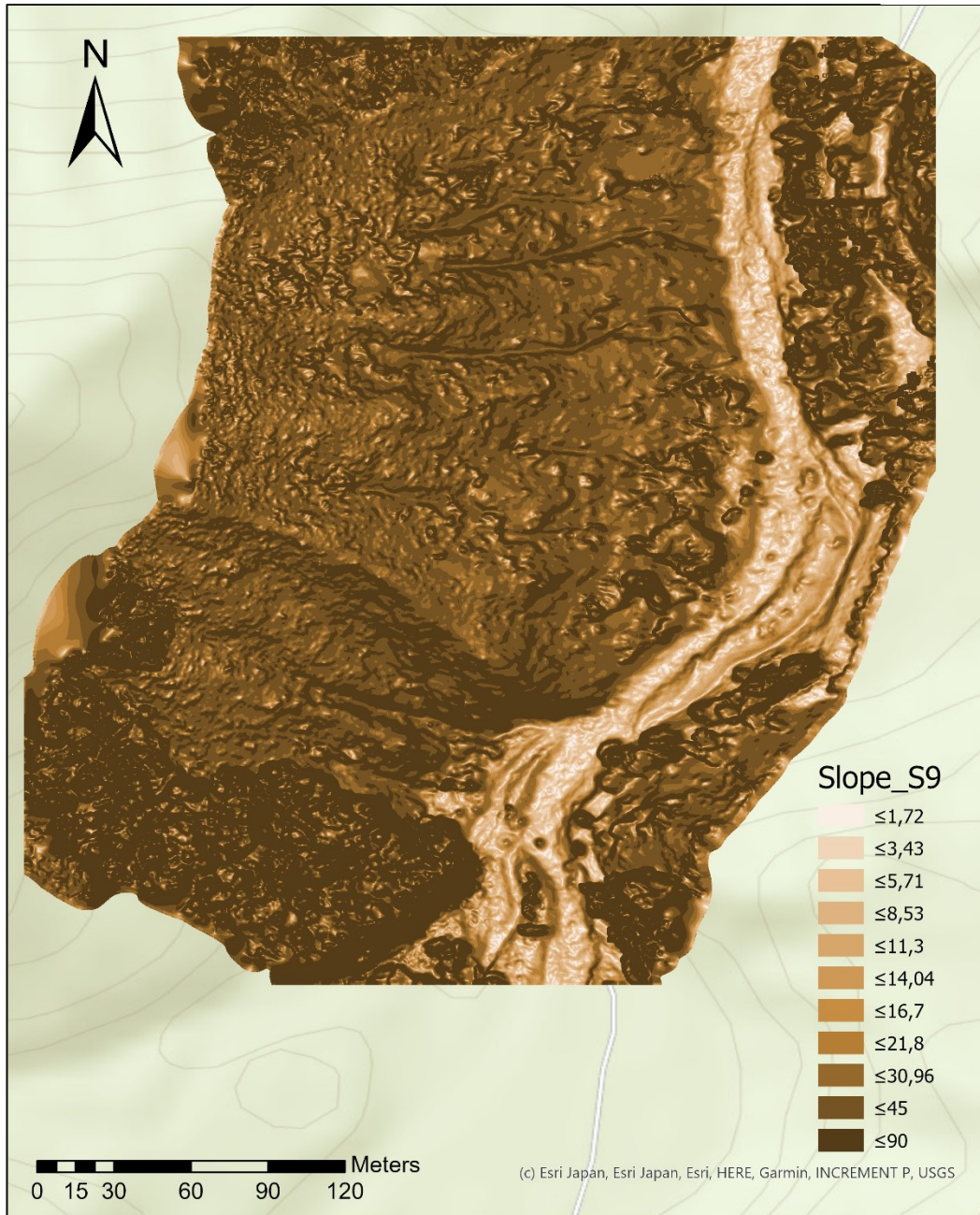
Slope site 8

by Sarah Kentsch





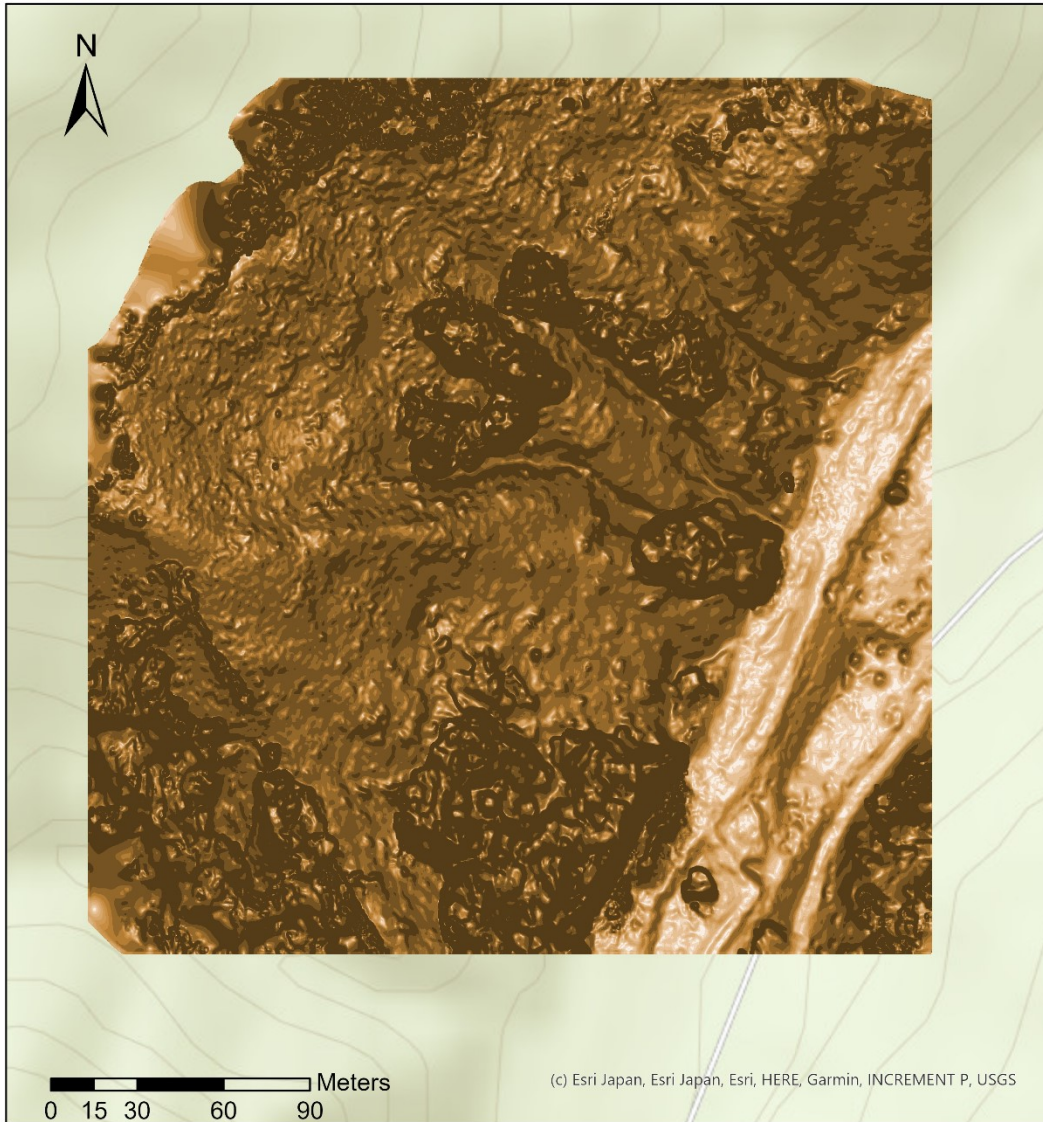
Slope site 9 by Sarah Kentsch





Slope site 10

by Sarah Kentsch



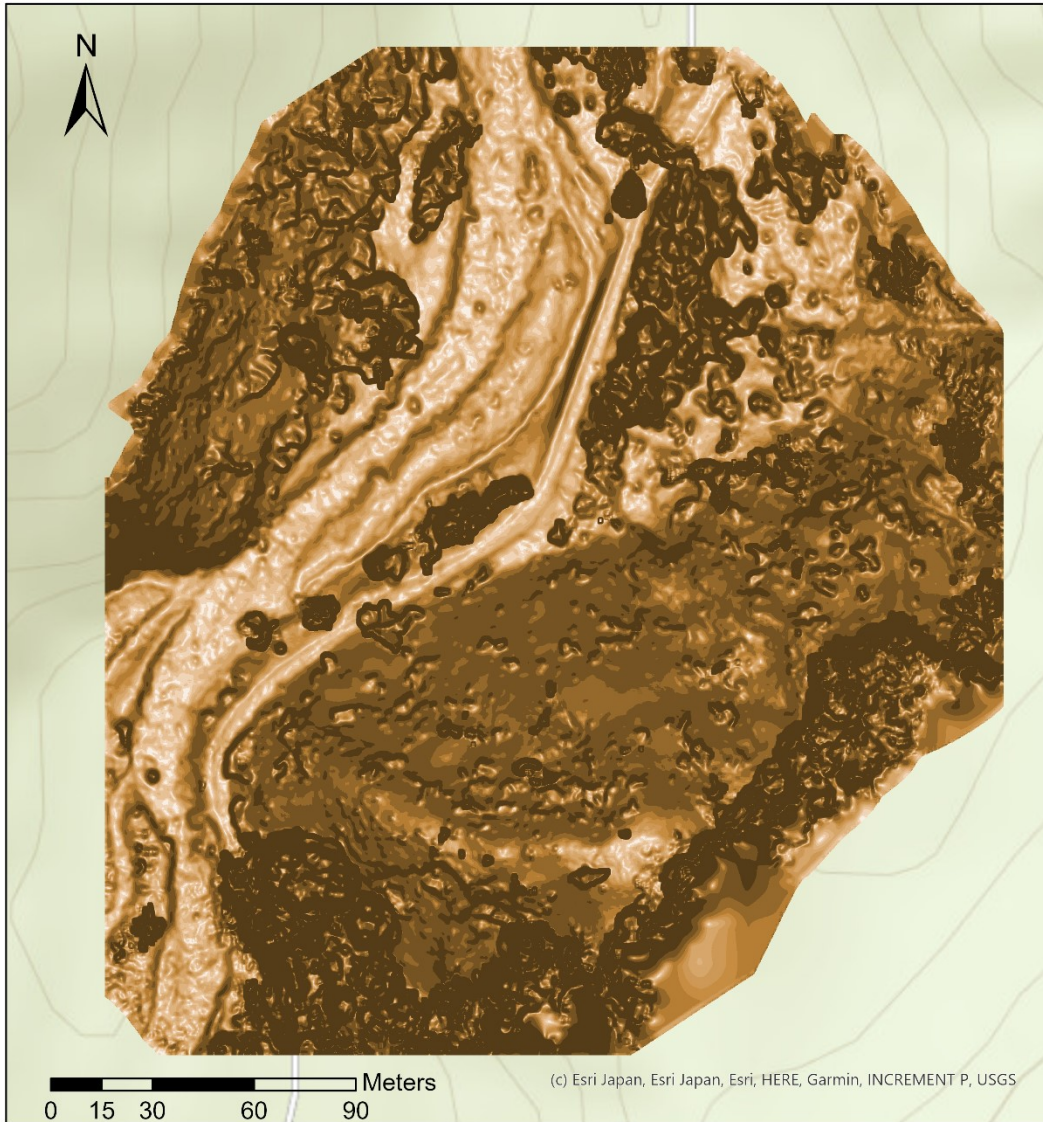
(c) Esri Japan, Esri Japan, Esri, HERE, Garmin, INCREMENT P, USGS

Slope_S10		
≤5,71	≤14,04	≤30,96
≤1,72	≤8,53	≤45
≤3,43	≤11,3	≤21,8



Slope site 11

by Sarah Kentsch

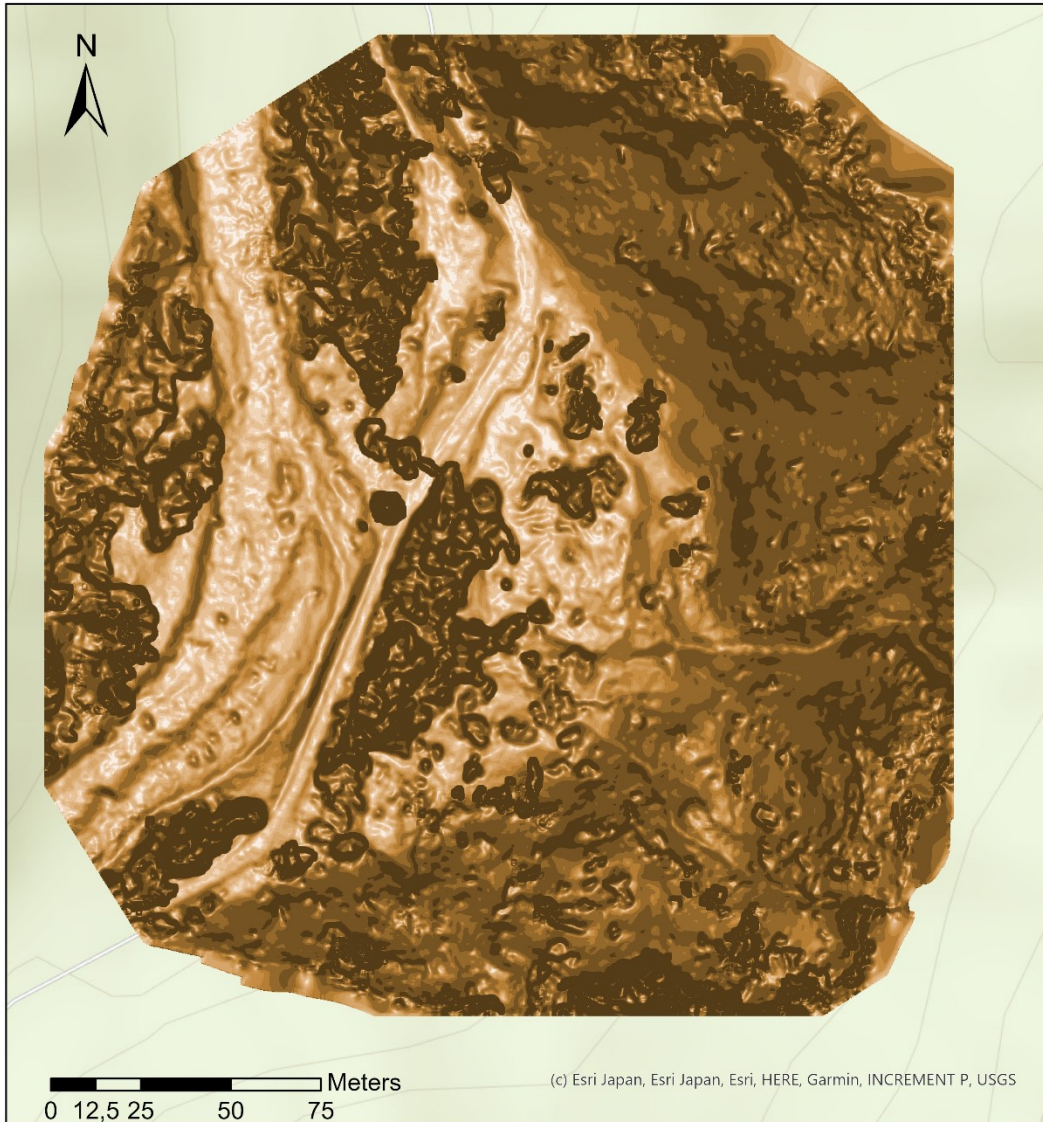


Slope_S11					
	$\leq 5,71$		$\leq 14,04$		$\leq 30,96$
	$\leq 1,72$		$\leq 8,53$		≤ 45
	$\leq 3,43$		$\leq 11,3$		≤ 90
			$\leq 16,7$		
			$\leq 21,8$		



Slope site 12

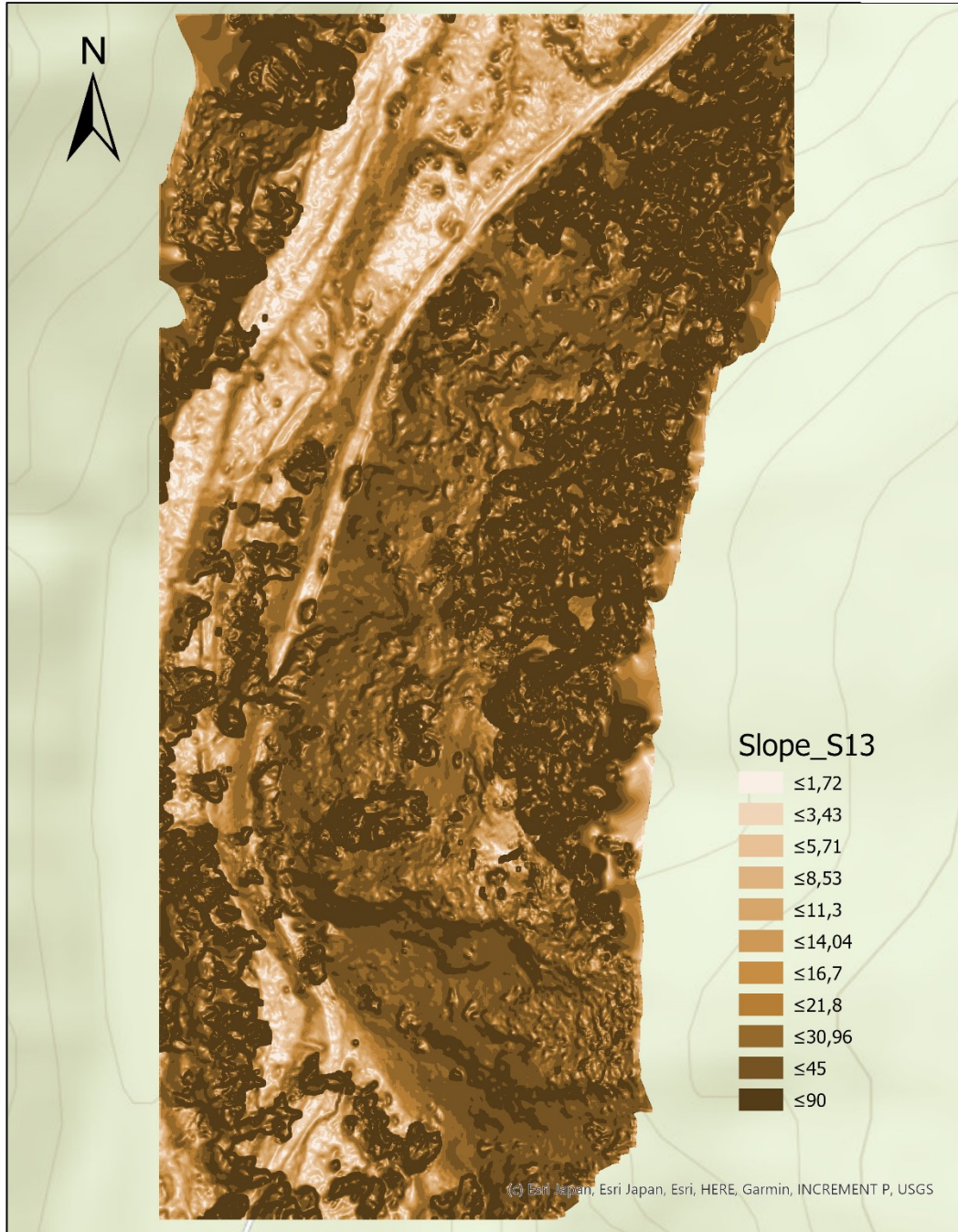
by Sarah Kentsch



Slope_S12			
≤5,71	≤8,53	≤11,3	≤14,04
≤1,72	≤3,43	≤16,7	≤21,8
≤30,96	≤45	≤90	



Slope site 13 by Sarah Kentsch



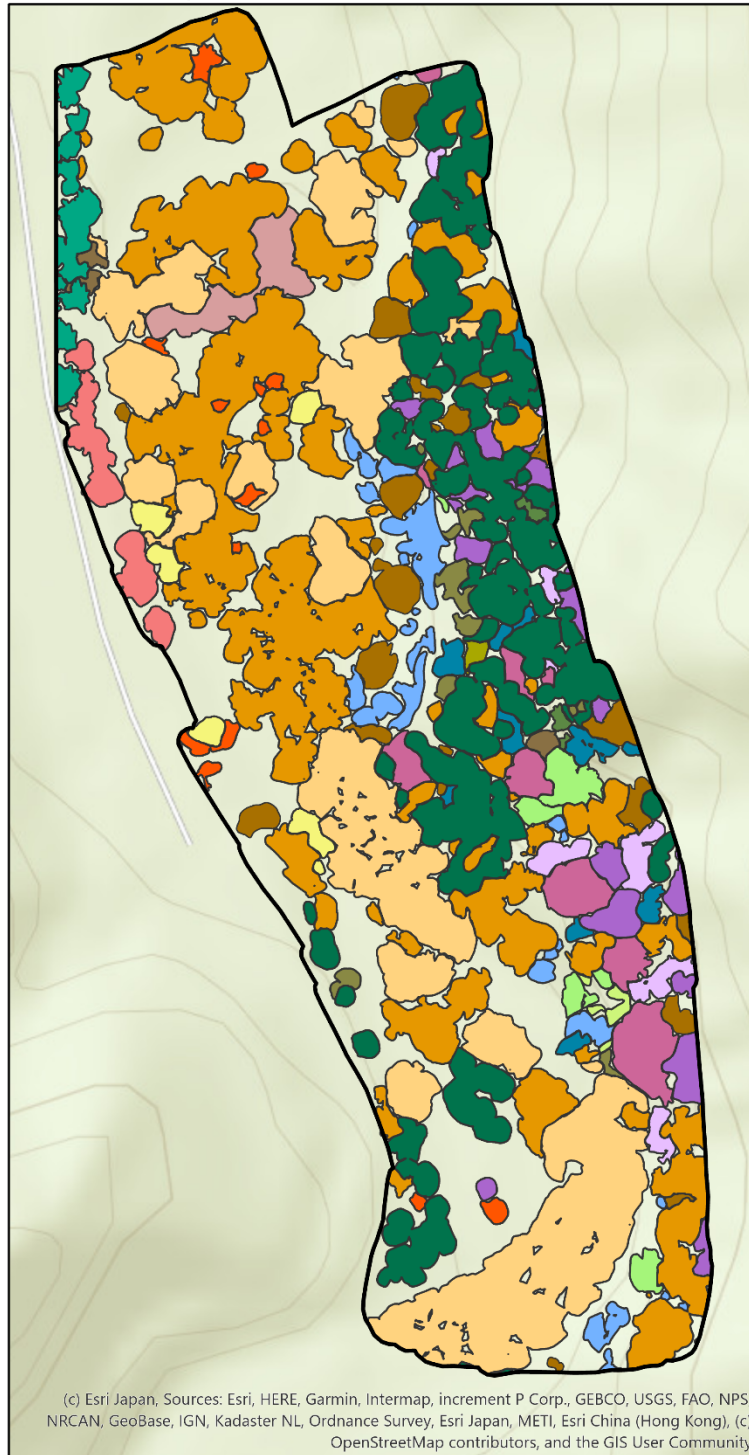
0 12,525 50 75 100 Meters

Appendix I – Species maps

Species maps generated on basis of manual annotations for all 13 study sites.

Species map site 1 (YURF)

by Sarah Kentsch



Legend

Species labels

-  ROI
-  *Juglans ailantifolia*
-  *Aesculus turbinata*
-  *Cryptomeria japonica*
-  *Pterocarya rhoifolia*
-  *Quercus mongolica*
-  *Larix kaempferi*
-  *Magnolia obovata*
-  *Acer*
-  *Prunus*
-  *Acer mono maxim*
-  *Salix jessoensis*
-  *Castanea crenata*
-  *Robinia pseudoaccacia*
-  *Cornus controversa*
-  Climbing plant 1
-  *Tilia*
-  *Alnus fauriei*
-  *Phelledendron amurense*
-  *Corylus sieboldiana*
-  *Carpinus cordata*



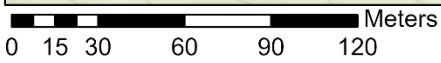


Tree species map site 2

by Sarah Kentsch



(c) Esri Japan, Esri Japan, Esri, HERE, Garmin, INCREMENT P, USGS



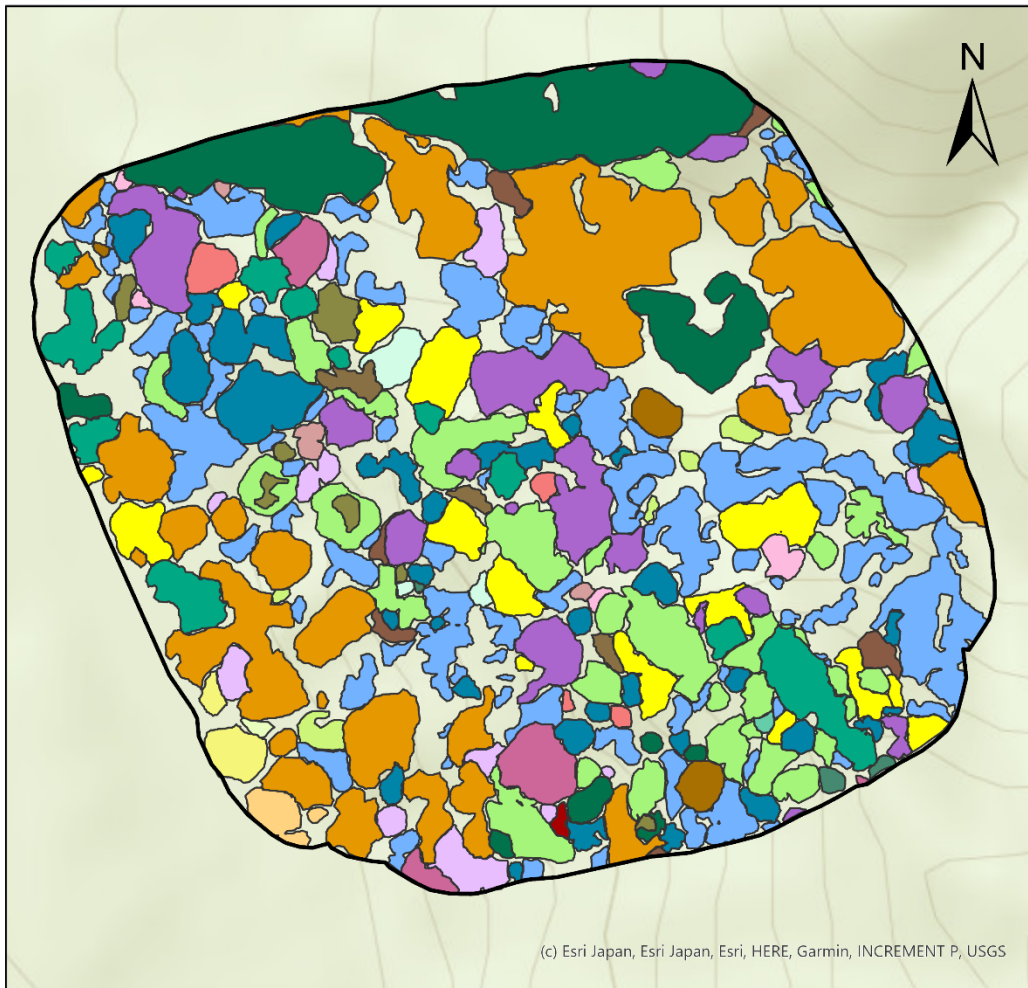
Legend

- | | | |
|----------------------|--------------------|------------------------------------|
| S2ROI | Magnolia obovata | Tilia |
| Juglans ailantifolia | Acer | Styrax obassia/Corylus sieboldiana |
| Aesculus turbinata | Acer mono maxim | Carpinus cordata |
| Cryptomeria japonica | Cornus controversa | Betula corylifolia |
| Pterocarya rhoifolia | Climbing plant 1 | Hamamelis japonica |
| Quercus mongolica | Morus australis | mixed tree canopies |

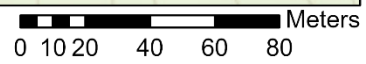


Tree species map site 3 (YURF)

by Sarah Kentsch



(c) Esri Japan, Esri Japan, Esri, HERE, Garmin, INCREMENT P, USGS



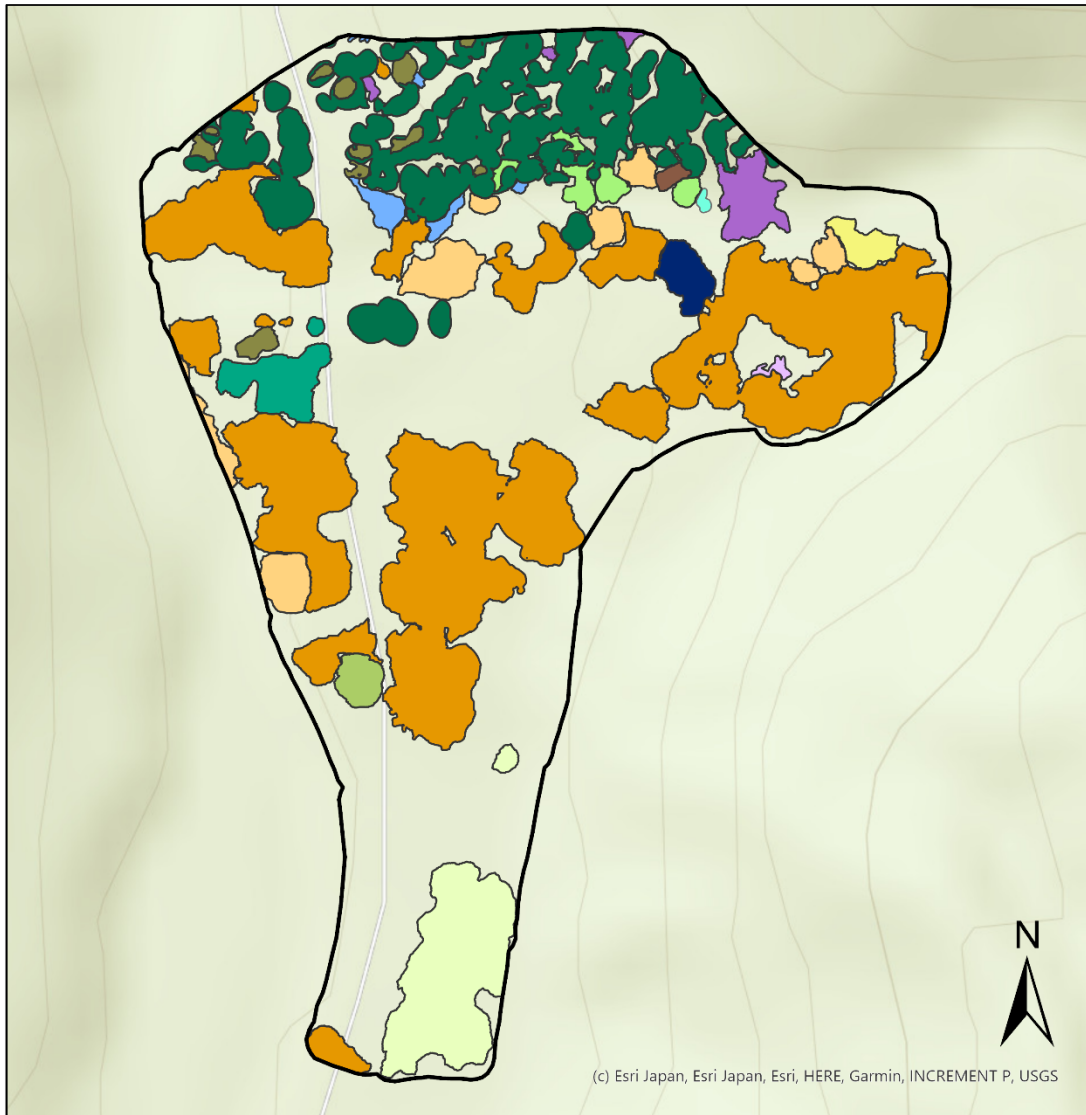
Legend

Site3ROI	Acer	Tilia
Juglans ailantifolia	Prunus	Climbing plant 2
Aesculus turbinata	Acer mono maxim	Kalopanax septemlobu
Cryptomeria japonica	Salix serissaefolia	Alnus fauriei
Pterocarya rhoifolia	Salix jessoensis	Styrax obassia
Quercus mongolica	Castanea Crenata	Ilex macropoda
Larix kaempferi	Cornus controversa	Fraxinus lanuginosa
Fagus crenata	Climbing plant 1	Carpinus cordata
Magnolia obovata	Morus australis	

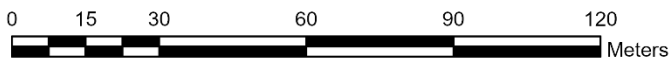


Species map Site 4 (YURF)

by Sarah Kentsch



(c) Esri Japan, Esri Japan, Esri, HERE, Garmin, INCREMENT P, USGS

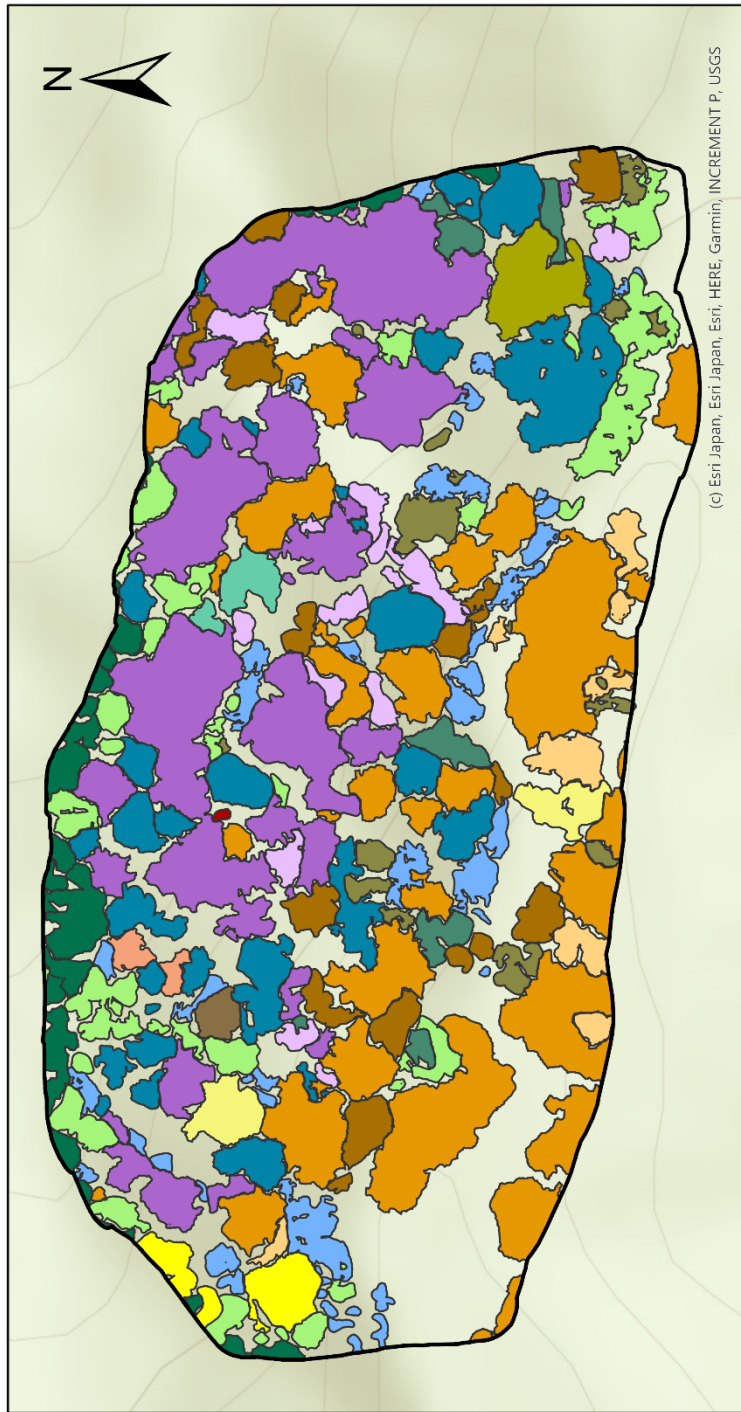


Legend

- | | | |
|----------------------|--------------------------|------------------|
| Site4ROI | Magnolia obovata | Climbing plant 1 |
| Juglans ailantifolia | Acer | Morus australis |
| Cryptomeria japonica | Salix serissaefolia | Betula coryfolia |
| Pterocarya rhoifolia | Salix jessoensis | Acer distylum |
| Quercus mongolica | Cornus controversa | |
| Larix kaempfer | Cercidiphyllum japonicum | |

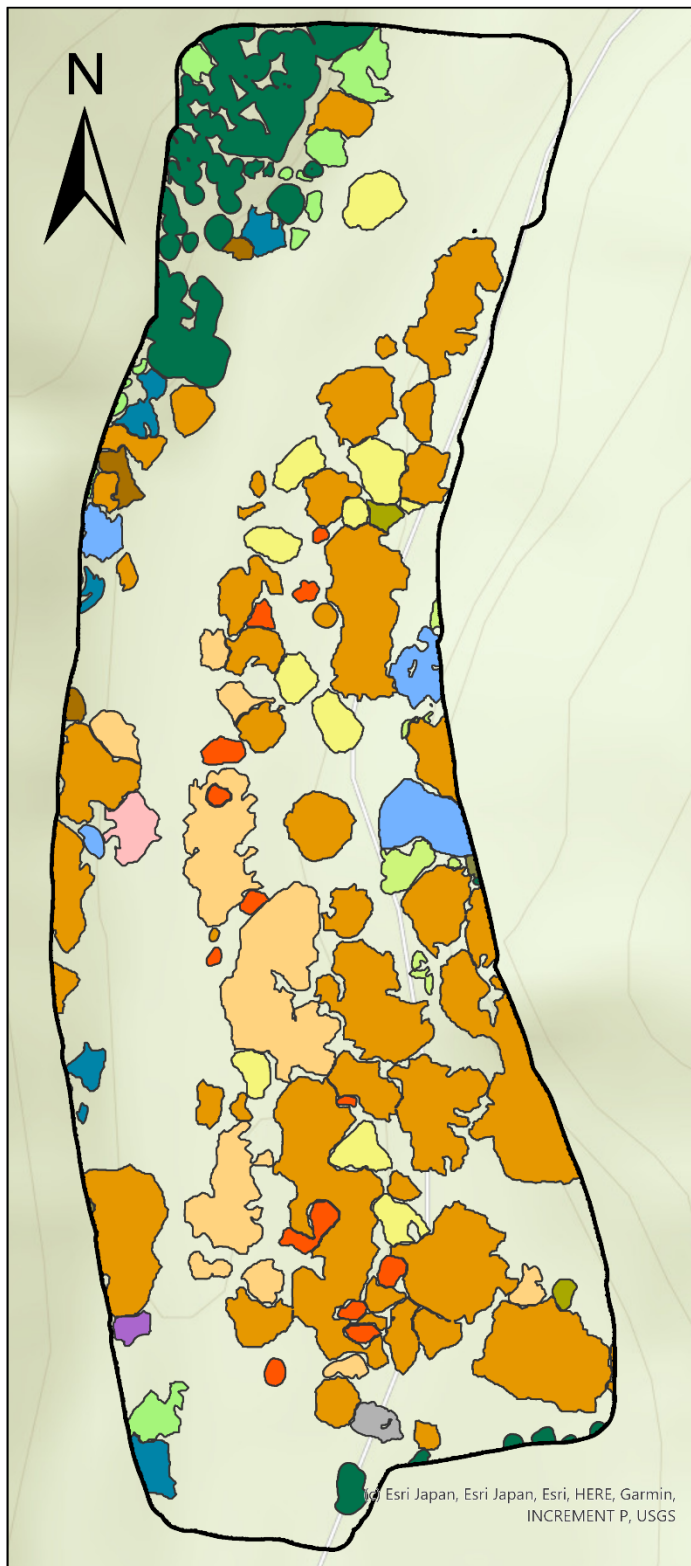
Tree species map site 5 (YURF)

by Sarah Kentsch



(c) Esri, Japan, Esri, HERE, Garmin, INCREMENT P, USGS

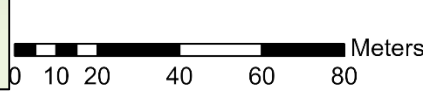




Species map Site 7 by Sarah Kentsch

Legend

- ROI
- Juglans ailantifolia*
- Aesculus turbinata*
- Cryptomeria japonica*
- Pterocarya rhoifolia*
- Quercus mongolica*
- Magnolia obovata*
- Acer*
- Acer mono maxim*
- Salix jessoensis*
- Robinia pseudoaccacia*
- Climbing plant 1
- Clethra barbinervis*
- Alnus fauriei*
- Albizia julibrissin*
- Fraxinus mandshurica*



Tree species map site 8

by Sarah Kentsch



Legend

- S8ROI
- Juglans ailantifolia
- Aesculus turbinata
- Cryptomeria japonica
- Pterocarya rhoifolia
- Quercus mongolica
- Fagus crenata
- Magnolia obovata
- Acer
- Prunus
- Acer mono maxim
- Salix jessoensis
- Castanea Crenata
- Cornus controversa
- Betula corylifolia
- Climbing plant 1
- Morus australis
- Tilia
- Climbing plant 2
- Carpinus Cordata
- Hamamelis japonica
- Corylus Sieboldiana

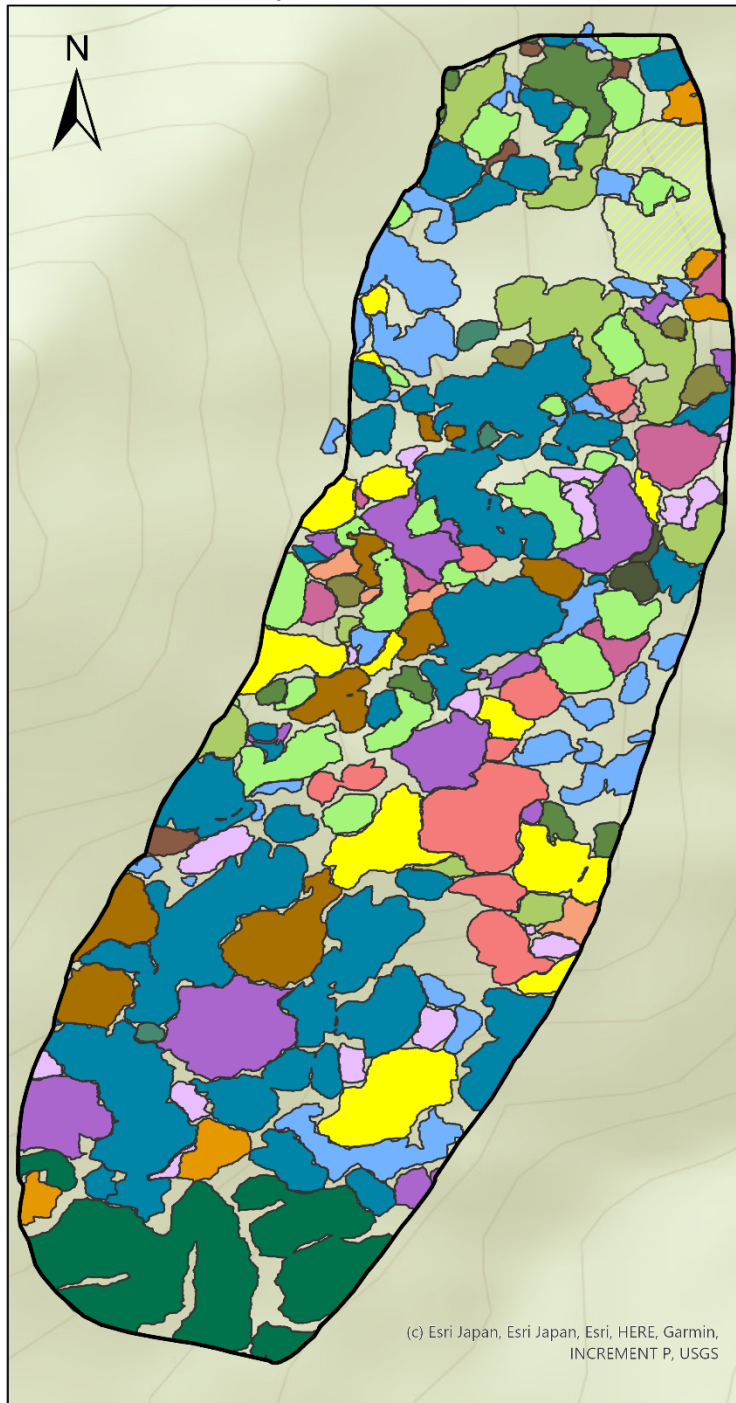


(c) Esri Japan, Esri Japan, Esri, HERE, Garmin, INCREMENT P, USGS

0 5 10 20 30 40 Meters

Species map Site 9

by Sarah Kentsch



Legend

- S9ROI
- Juglans ailantifolia*
- Aesculus turbinata*
- Cryptomeria japonica*
- Quercus mongolica*
- Fagus crenata*
- Magnolia obovata*
- Acer*
- Prunus*
- Acer mono maxim*
- Cornus controversa*
- Betula corylifolia*
- Climbing plant 1
- Morus australis*
- Tilia*
- Climbing plant 2
- Styrax obassia*
- Carpinus cordata*
- Corylus sieboldiana*
- Hamamelis japonica*
- Understory vegetation



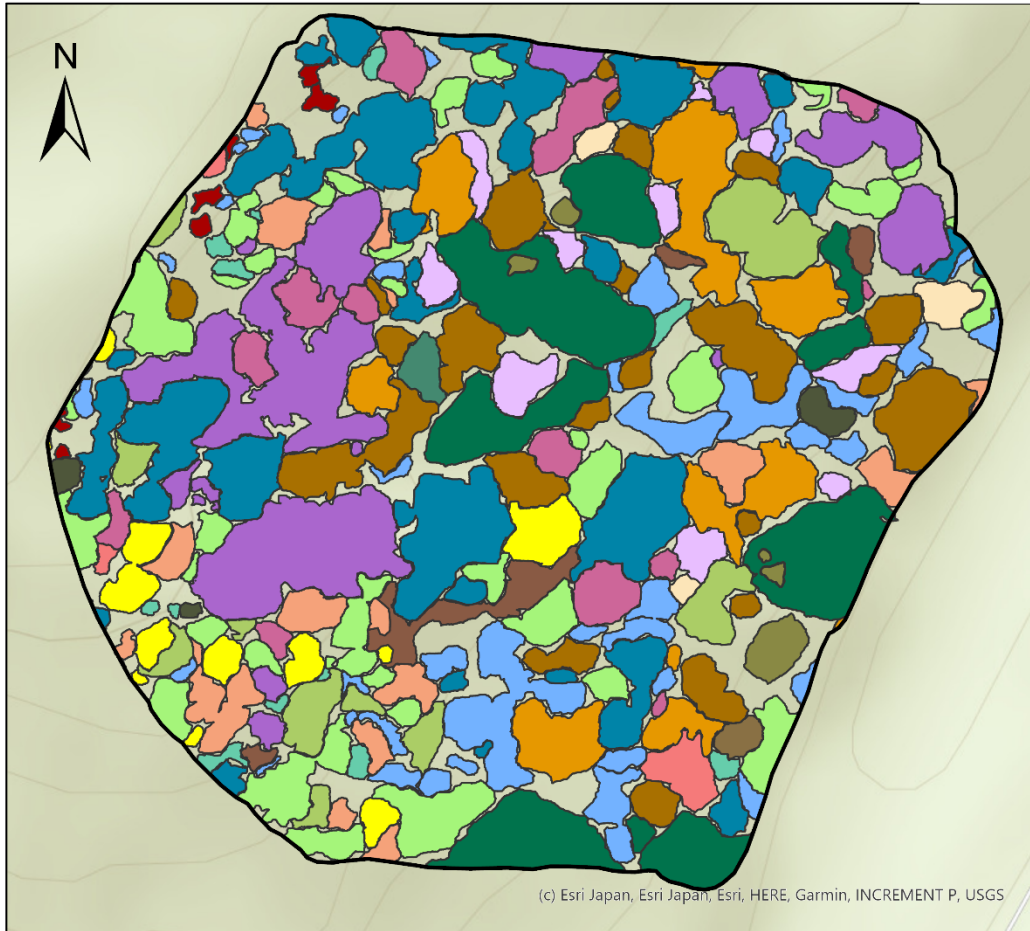
(c) Esri Japan, Esri Japan, Esri, HERE, Garmin, INCREMENT P, USGS

0 10 20 40 60 80 Meters



Tree species map site 10 (YURF)

by Sarah Kentsch



0 10 20 40 60 80 Meters

Legend

Site10ROI	Prunus	Kalopanax septemlobu
Juglans ailantifolia	Acer mono maxim	Acer palmatum
Aesculus turbinata	Castanea Crenata	Corylus sieboldiana
Cryptomeria japonica	Cornus controversa	Styrax obassia
Quercus mongolica	Betula corylifolia	Hamamelis japonica
Fagus crenata	Climbing plant 1	Climbing plant 2
Magnolia obovata	Morus australis	
Acer	Tilia	



Species map site 11 (YURF)

by Sarah Kentsch



0 10 20 40 60 80 Meters

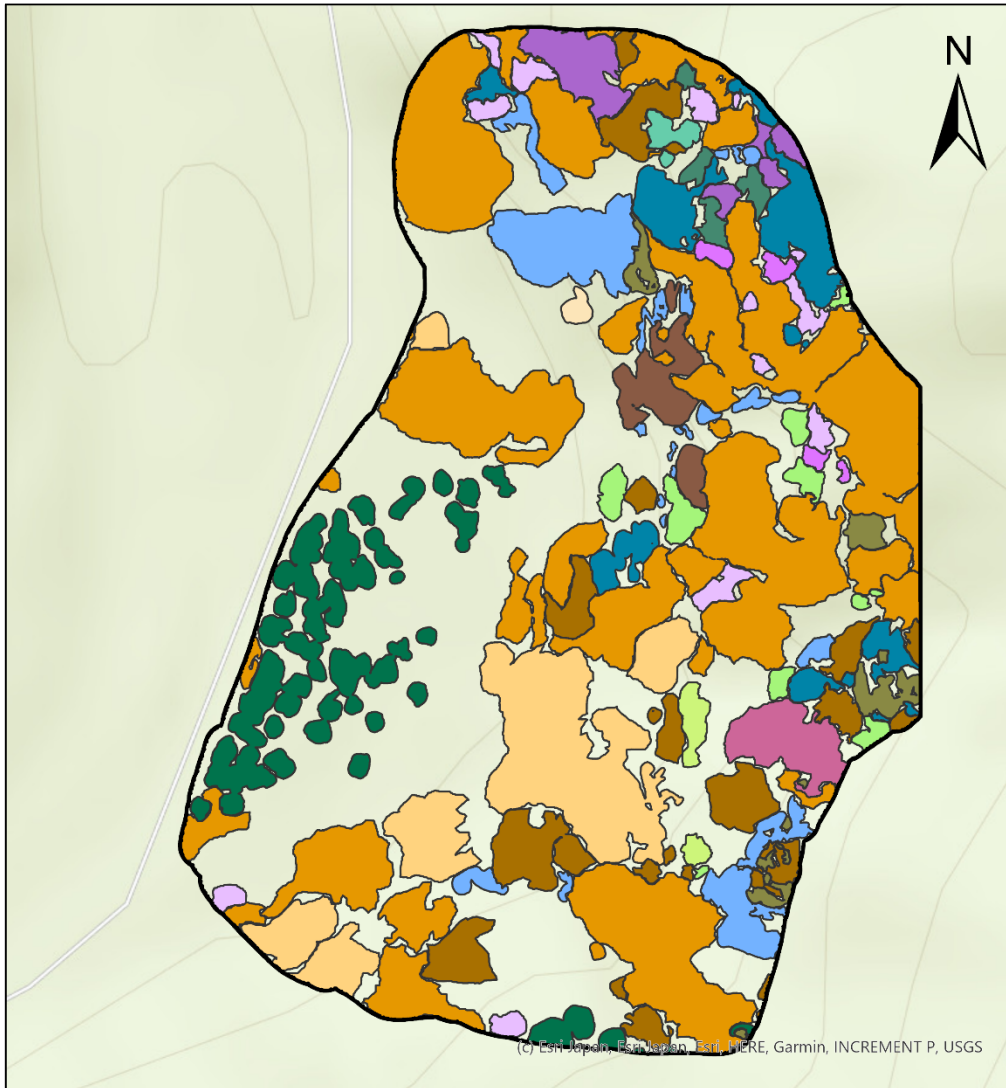
Legend

- | | | |
|-----------------------------|---------------------------|--------------------------|
| ROI | <i>Larix kaempferi</i> | Climbing plant 1 |
| <i>Juglans ailantifolia</i> | <i>Magnolia obovata</i> | <i>Tilia</i> |
| <i>Aesculus turbinata</i> | <i>Acer</i> | <i>Celtis jessoensis</i> |
| <i>Cryptomeria japonica</i> | <i>Acer mono maxim</i> | |
| <i>Pterocarya rhoifolia</i> | <i>Cornus controversa</i> | |



Species map site 12 (YURF)

by Sarah Kentsch



(C) Esri Japan, Esri Japan, Esri, HERE, Garmin, INCREMENT P, USGS

0 10 20 40 60 80 Meters

Legend

ROI	Magnolia obovata	Climbing plant 2
Juglans ailantifolia	Acer	Kalopanax septemlobu
Aesculus turbinata	Acer mono maxim	Celtic jessoensis
Cryptomeria japonica	Cornus controversa	Alnus fauriei
Pterocarya rhoifolia	Climbing plant 1	Styrax obassia
Quercus mongolica	Morus australis	
Larix kaempferi	Tilia	

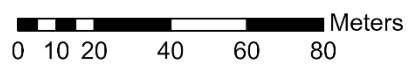
Species map site 13 (YURF)

by Sarah Kentsch



Legend

- S13ROI
- Juglans ailantifolia*
- Aesculus turbinata*
- Cryptomeria japonica*
- Pterocarya rhoifolia*
- Quercus mongolica*
- Acer*
- Acer mono maxim*
- Cornus controversa*
- Climbing plant 1
- Morus australis*
- Tilia*
- Kalopanax septemlobu*
- Hamamelis japonica*
- Alnus fauriei*
- Climbing plant 2
- Styrax obassia*



Appendix I (a) – Species maps with orthomosaics

Species map site 1 (YURF)

by Sarah Kentsch



Legend

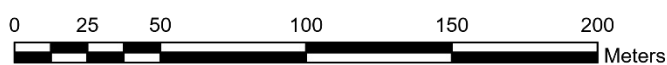
Species labels

- ROI
- Juglans ailantifolia
- Aesculus turbinata
- Cryptomeria japonica
- Pterocarya rhoifolia
- Quercus mongolica
- Larix kaempferi
- Magnolia obovata
- Acer
- Prunus
- Acer mono maxim
- Salix jessoensis
- Castanea crenata
- Robinia pseudoaccacia
- Cornus controversa
- Climbing plant 1
- Tilia
- Alnus fauriei
- Phelledendron amurense
- Corylus sieboldiana
- Carpinus cordata

S1.jpg

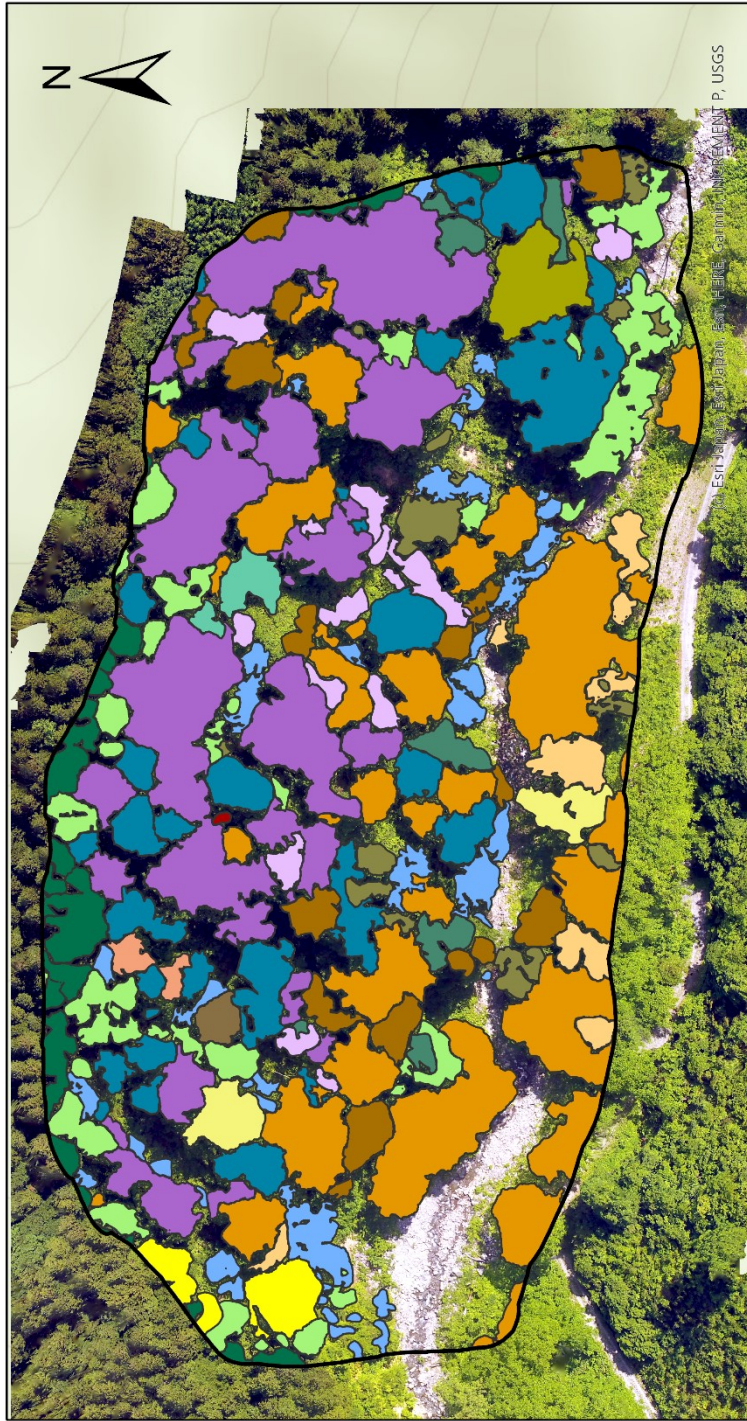
RGB

- Red: Band_1
- Green: Band_2
- Blue: Band_3



Tree species map site 5 (YURF)

by Sarah Kentsch



Juglans ailantifolia	Acer	Kalopanax septemlobu
Aesculus turbinata	Acer mono maxim	Acer palmatum
Cryptomeria japonica	Salix jessoensis	Hamamelis japonica
Pterocarya rhoifolia	Castanea Crenata	Corylus sieboldiana
Quercus mongolica	Cornus controversa	ROI
Fagus crenata	Climbing plant 1	
Magnolia obovata	Climbing plant 2	

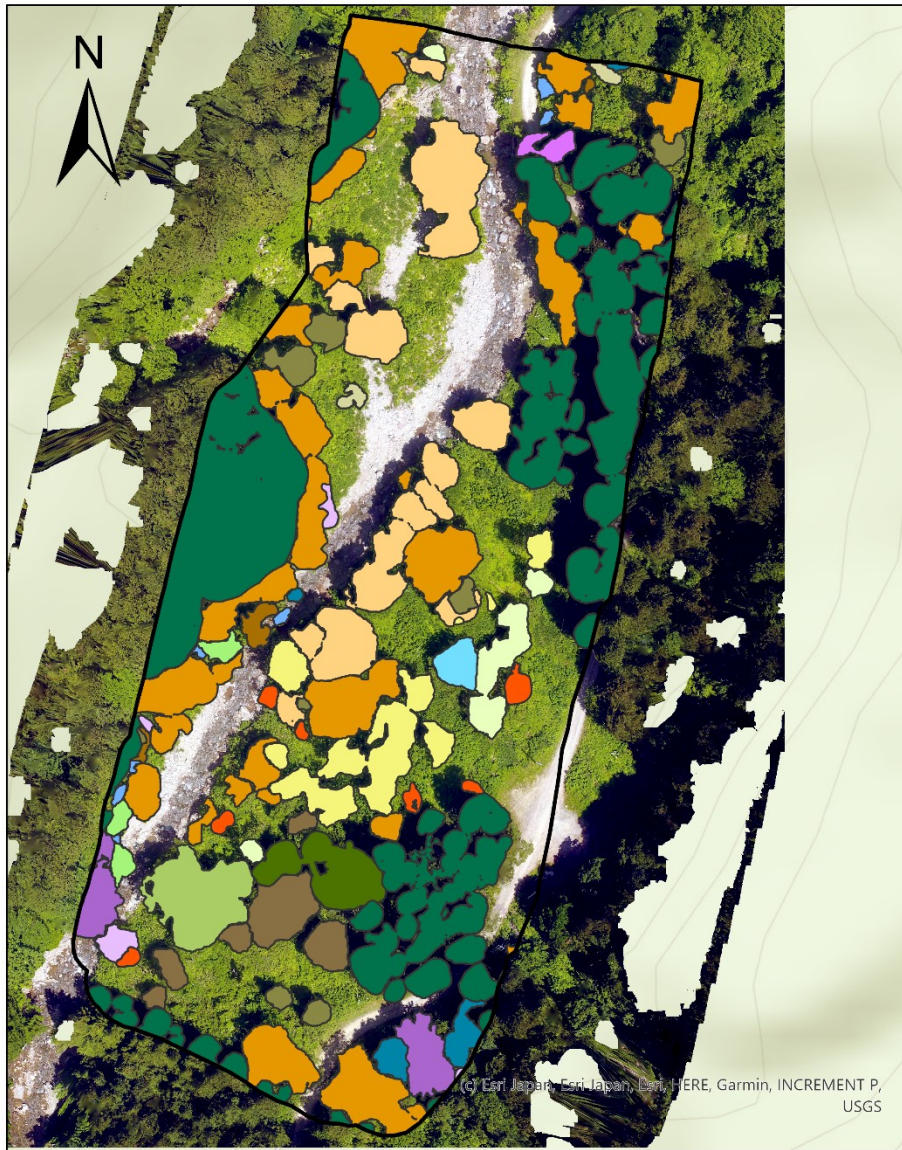
Site5.tif	Red: Band_1
RGB	Green: Band_2
	Blue: Band_3
	ROI

0 10 20 40 60 80 Meters



Tree species map site 6

by Sarah Kentsch



© Esri, Japan, Esri Japan, Esri, HERE, Garmin, INCREMENT P, USGS

0 10 20 40 60 80 Meters

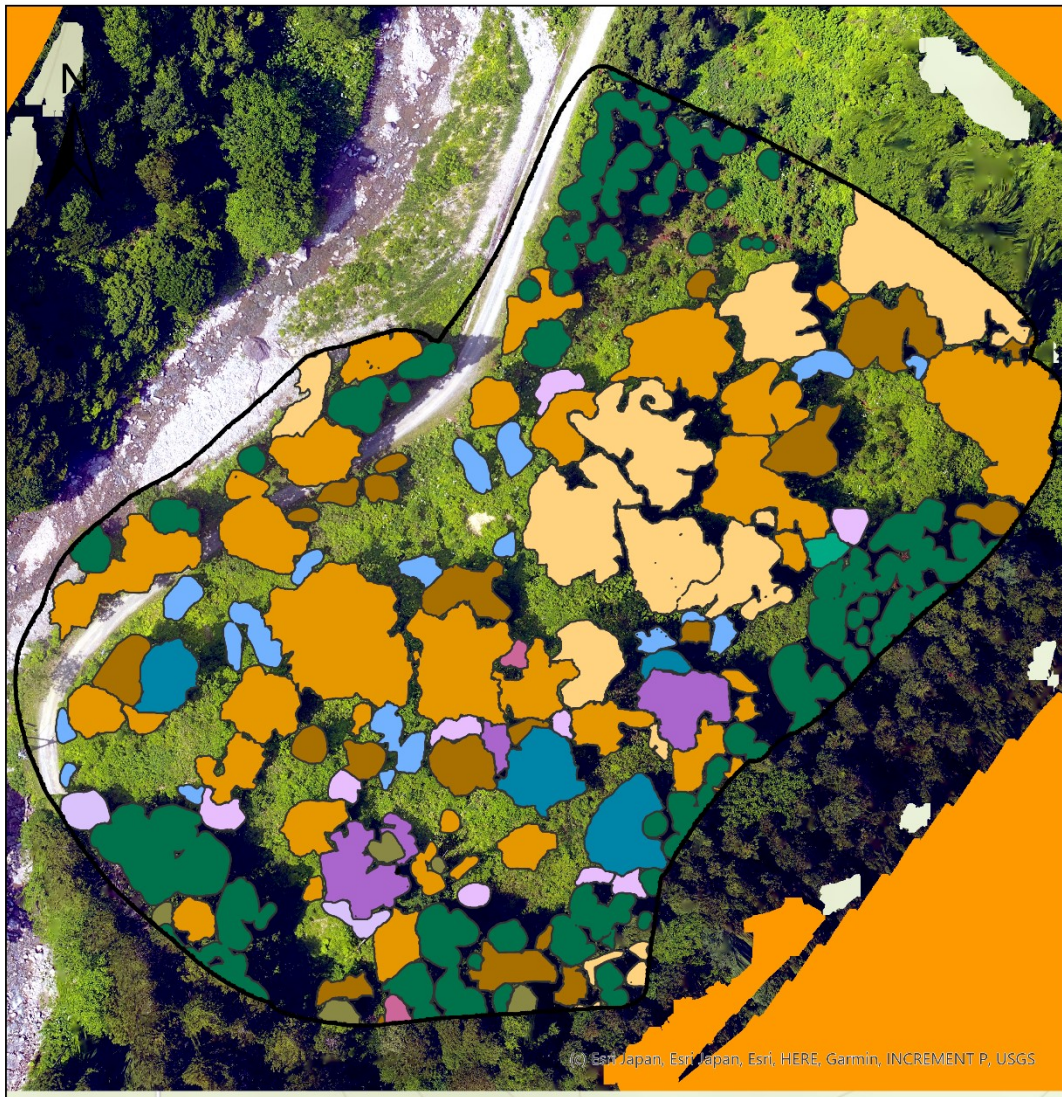
Legend

ROI	Acer	Betula corylifolia	Site6.tif RGB Red: Band_1 Green: Band_2 Blue: Band_3
Juglans ailantifolia	Acer mono maxim	Alnus inokumae	
Aesculus turbinata	Salix serissaefolia	Picea abies	
Cryptomeria japonica	Salix jessoensis	Climbing plant 1	
Pterocarya rhoifolia	Castanea crenata	Zanthoxylum piperitum	
Quercus mongolica	Robinia pseudoaccacia	Celtic jessoensis	
Magnolia obovata	Cornus controversa		

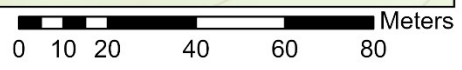


Species map site 11 (YURF)

by Sarah Kentsch



© Esri, DeLorme, Esri, HERE, Garmin, INCREMENT P, USGS



Legend

- | | |
|-----------------------------|---------------------------|
| ROI | Acer |
| <i>Juglans ailantifolia</i> | <i>Acer mono maxim</i> |
| <i>Aesculus turbinata</i> | <i>Cornus controversa</i> |
| <i>Cryptomeria japonica</i> | Climbing plant 1 |
| <i>Pterocarya rhoifolia</i> | <i>Tilia</i> |
| <i>Larix kaempferi</i> | <i>Celtis jessoensis</i> |
| <i>Magnolia obovata</i> | |

S11mosaic.png

RGB

- | |
|---------------|
| Red: Band_1 |
| Green: Band_2 |
| Blue: Band_3 |

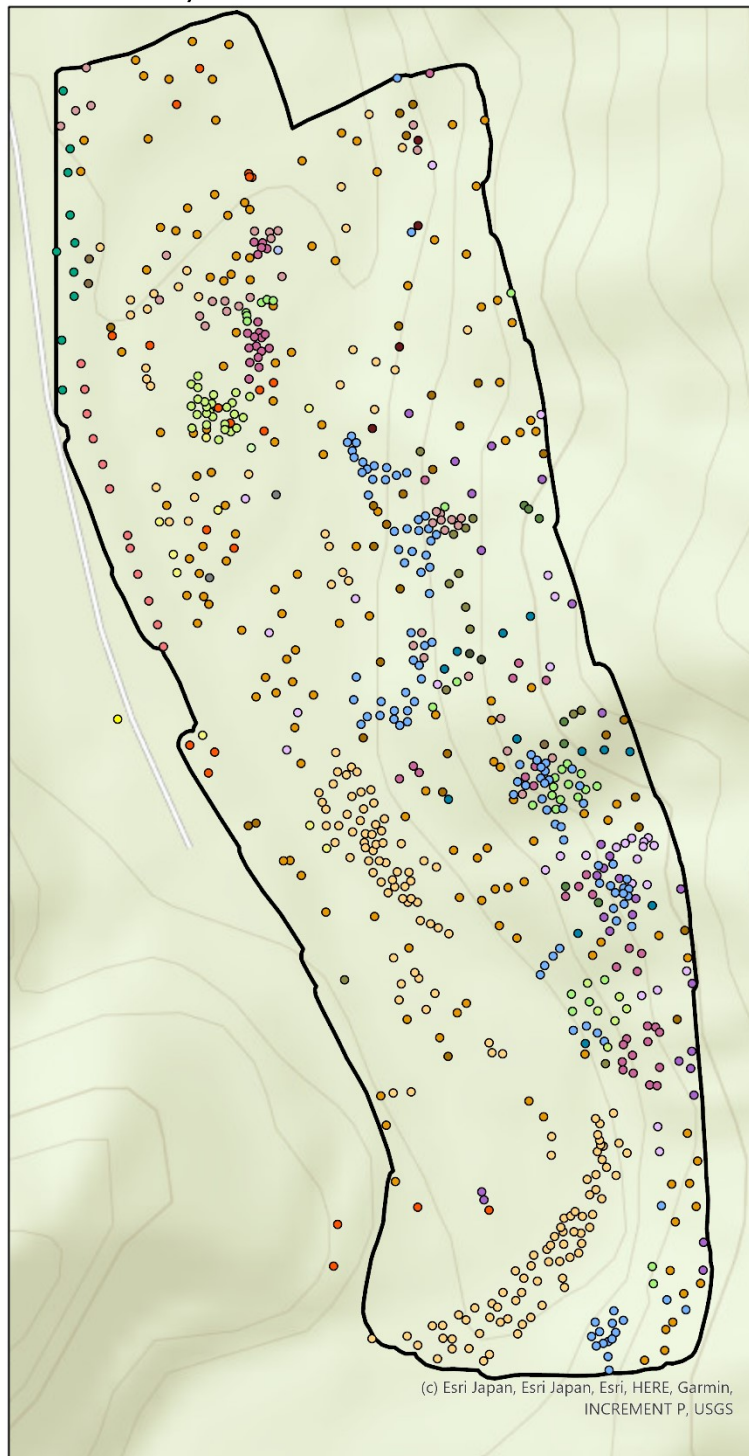
Appendix J – Field and image surveys

This appendix is divided into two parts: part 1 field survey information, part 2 winter counting

Part 1: Count maps based on field surveys.

Field survey site 1 (YURF)

by Sarah Kentsch



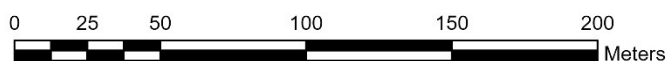
Legend

Species labels

Species_lat_name

- Acer
- Acer mono maxim
- Aesculus turbinata
- Alnus fauriei
- Aralia elata
- Carpinus cordata
- Castanea crenata
- Climbing plant 1
- Cornus controversa
- Corylus sieboldiana
- Ginko biloba
- Juglans ailantifolia
- Larix kaemferi
- Linderia umbellata
- Magnolia obovata
- Phellodendron amurense
- Prunus
- Pterocarya rhoifolia
- Quercus mongolica
- Robinia pseudoaccaccia
- Salix jessoensis
- Styrax obassia
- Tilia
- dead
- unknown
- <all other values>

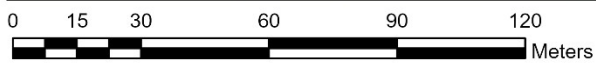
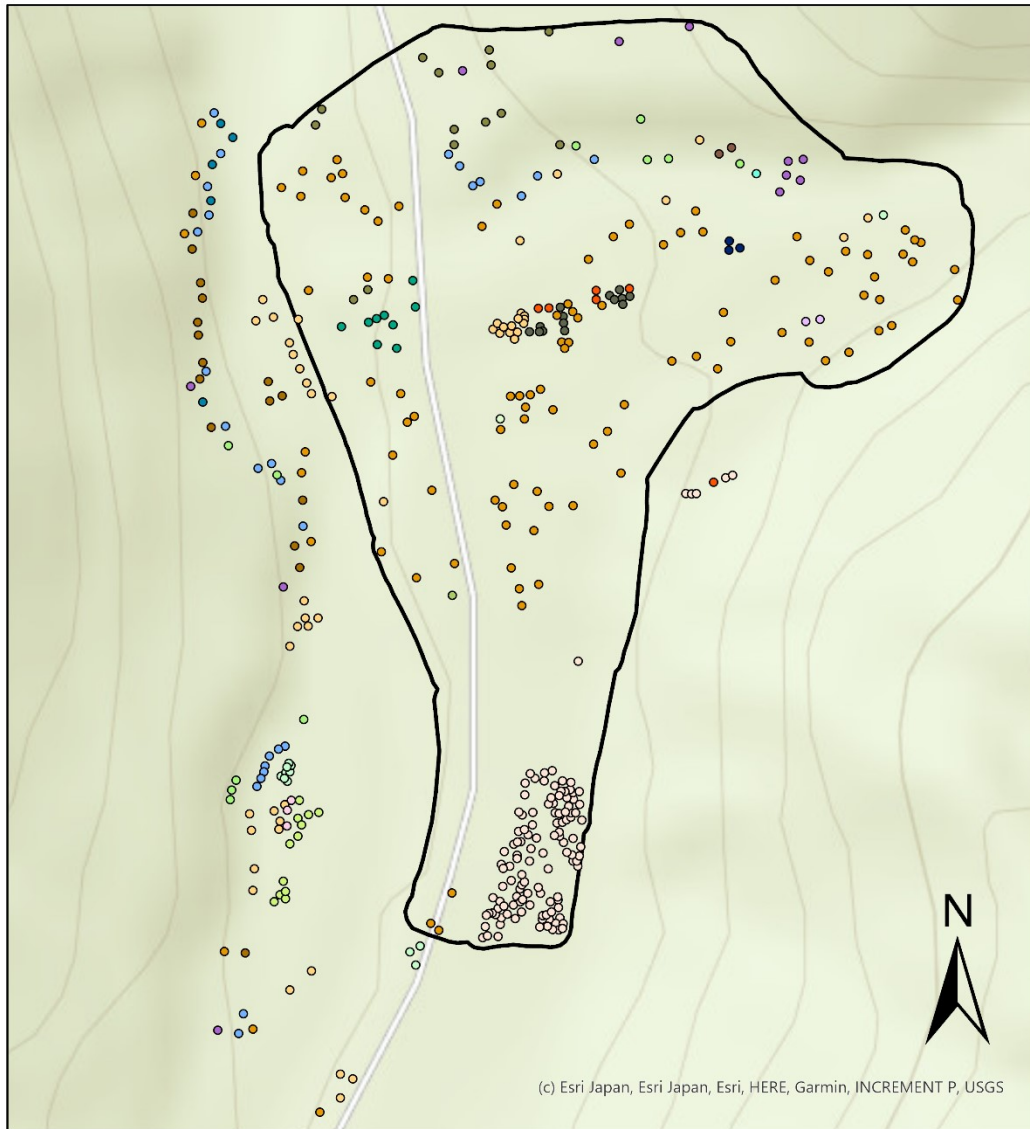
□ ROI





Field survey site 4 (YURF)

by Sarah Kentsch



Legend

FieldData

Species_lat_name

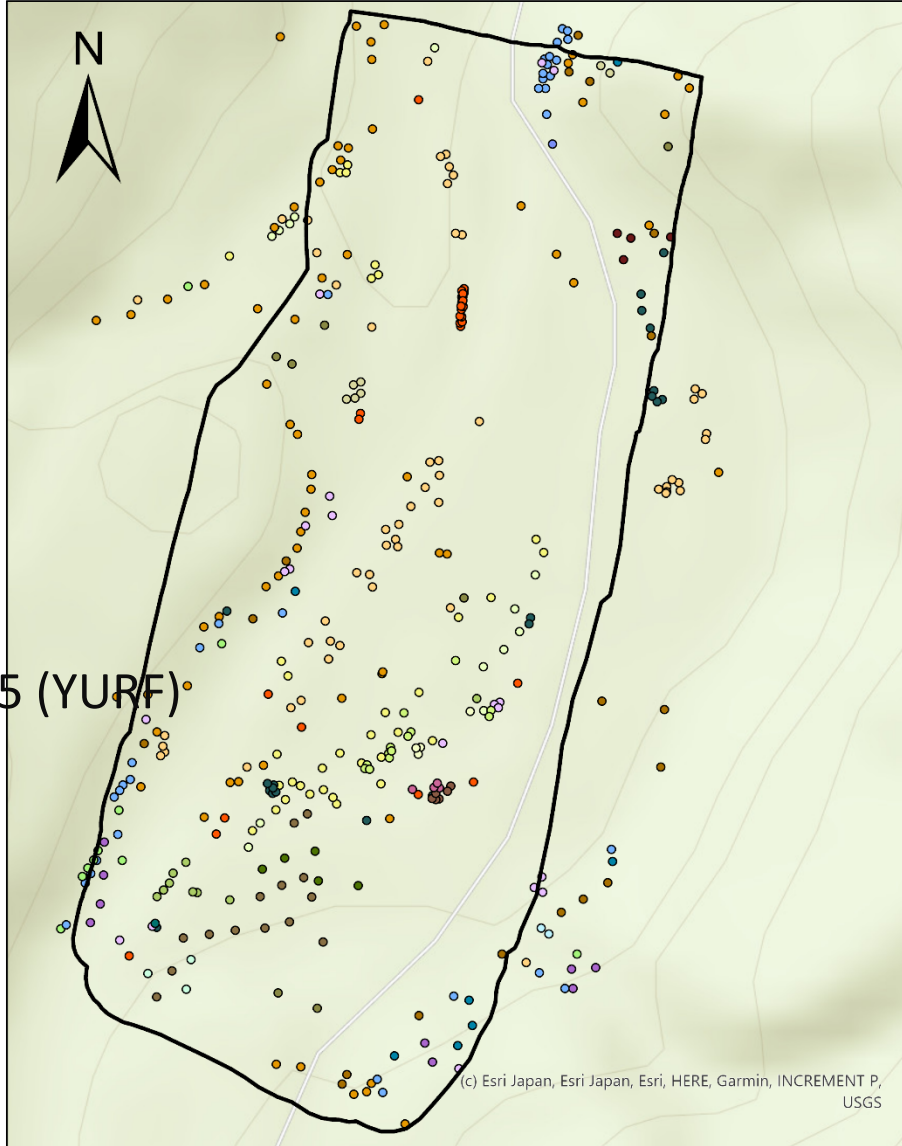
- Acer
- Acer distylum
- Acer mono maxim
- Aesculus turbinata
- Alnus fauriei
- Betula coryfolia

- Cercidiphyllum japonicum var. Magnificum
- Climbing plant 1
- Cornus controversa
- Juglans ailantifolia
- Larix kaempferi
- Magolia obovata
- Morus australis
- Pterocarya rhoifolia
- Quercus mongolica
- Robinia pseudoaccacia
- Salix jessonsis
- Salix serissaefolia
- Sorbus alnifolia
- Fraxinus species
- unknown
- <all other values>
- ▭ Site4ROI



Field survey site 6 (YURF)

by Sarah Kentsch



field survey site 5 (YURF)

Legend



FieldData

Species_lat_name

- Acer
- Acer mono maxim
- Acer nipponicum
- Aesculus turbinata

- Alnus fauriei
- Betula corylifolia
- Castanea crenata
- Celtis jessoensis
- Climbing plant 1
- Cornus controversa
- Juglans ailantifolia
- Lindera umbellata

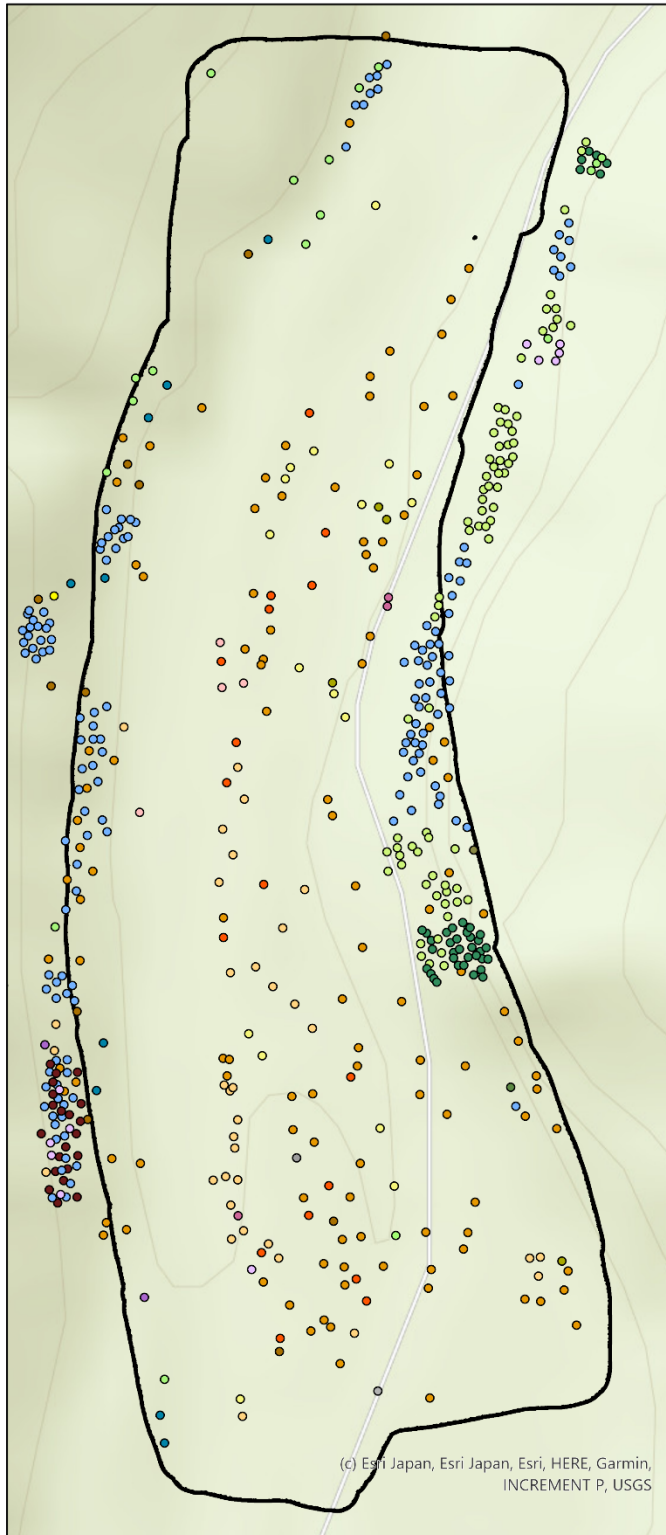
- Magnolia obovata
- Morus australis
- Picea abies
- Pterocarya rhoifolia
- Quercus mongolica
- Robinia pseudoaccacia
- Salix jessoensis
- Salix serissaefolia

- Sorbus alnifolia
- Styrax obassia
- Hydrangea species
- Tilia
- Zanthoxylum piperitum
- dead
- <all other values>

0 10 20 40 60 80 Meters

Field survey site 7 (YURF)

by Sarah Kentsch

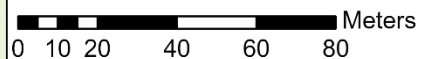


FieldData

Species_lat_name

- Acer
- Acer mono maxim
- Aesculus turbinata
- Albizia julibrissin
- Alnus fauriei
- Alnus wirsata
- Carpinus cordata
- Clethra barvinervis
- Climbing plant 1
- Cornus controversa
- Fagus crenata
- Fraxinus mandshurica
- Juglans ailantifolia
- Lindera umbellata
- Magnolia obovata
- Pterocarya rhoifolia
- Quercus mongolica
- Robinia pseudoaccacia
- Salix jessoensis
- Tilia
- Weigela japonica
- dead
- <all other values>

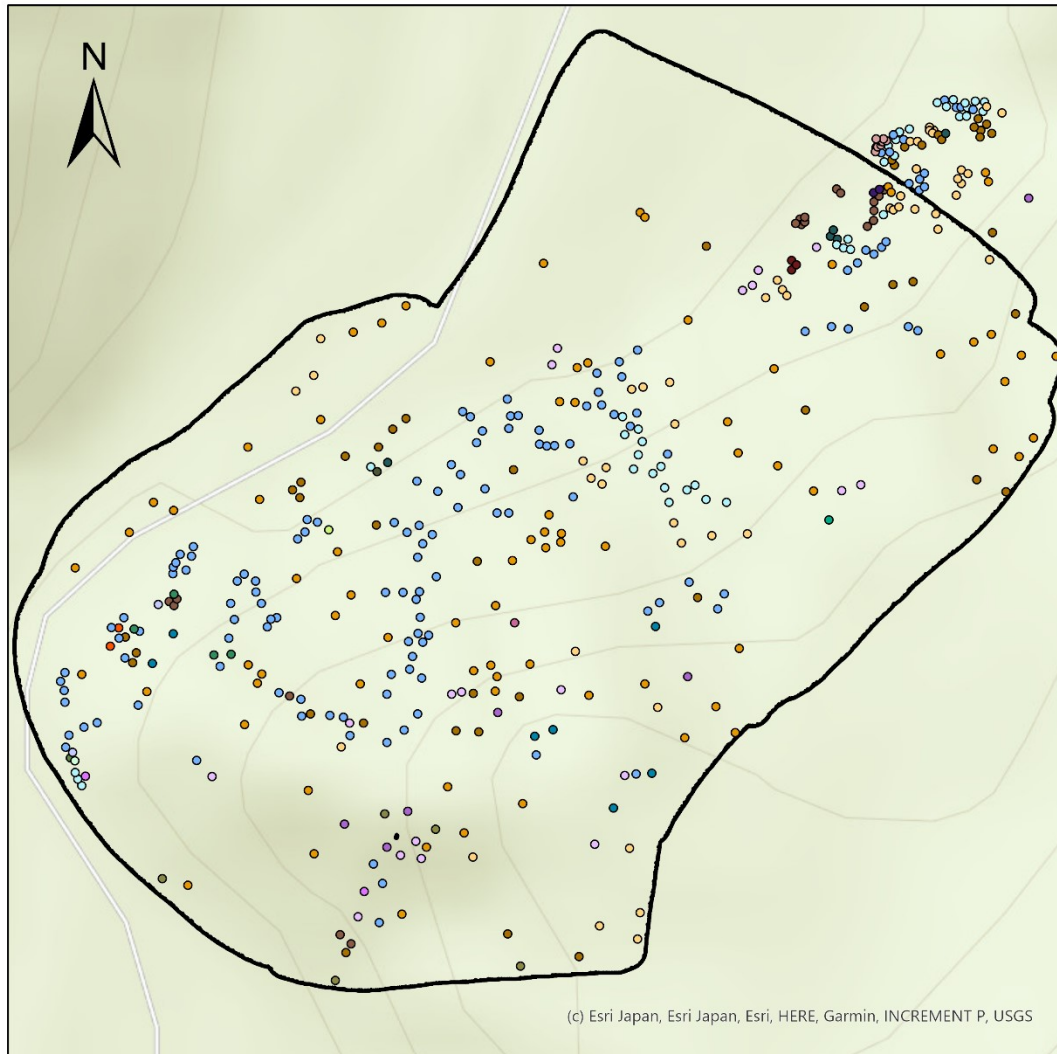
ROI





Field survey site 11 (YURF)

by Sarah Kentsch



(c) Esri Japan, Esri Japan, Esri, HERE, Garmin, INCREMENT P, USGS

0 10 20 40 60 80 Meters

Legend

FieldData

Species_lat_name

- Acer
- Acer mono maxim
- Aesculus turbinata
- Alnus fauriei
- Camellia japonica

- Carpinus cordata
- Celtic jessoensis
- Climbing plant 1
- Cornus controversa
- Corylus sieboldiana
- Juglans ailantifolia
- Larix kaempferi

- Lindera umbellata
- Magnolia obovata
- Morus australis
- Pterocarya rhoifolia
- Robinia pseudoaccacia
- Sorbus alnifolia
- SpeciesD

- Styrax obassia
- Synpolcas chinesis
- Tilia
- Vaccinium oldhamii
- Weigela hortensia
- <all other values>
- ROI



Field survey site 12 (YURF)

by Sarah Kentsch



0 10 20 40 60 80 Meters

Legend

ROI

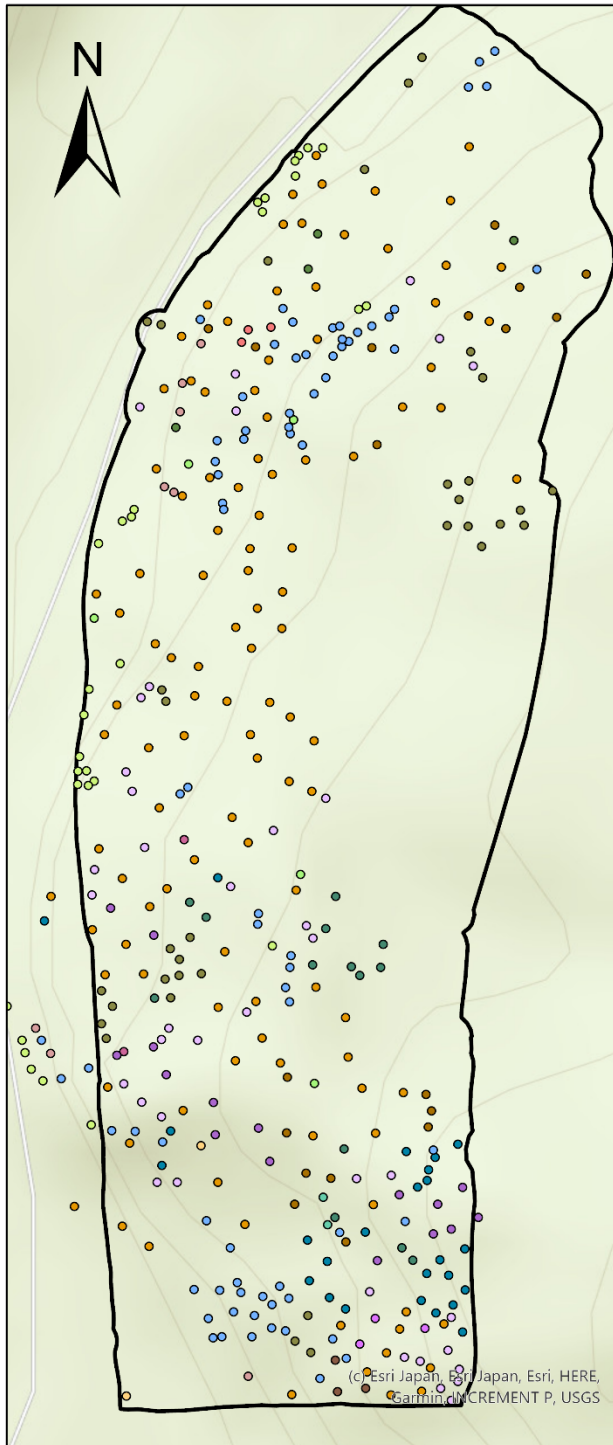
FieldData_Site12

Species_lat_name

- | | |
|------------------------|-------------------------|
| ● Climbing plant 1 | ○ Pterocarya rhoifolia |
| ● Climbing plant 2 | ○ Quercus monglica |
| ● Cornus controversa | ● Robinia pseudoaccacia |
| ○ Corylus sieboldiana | ○ Salix jessoensis |
| ● Juglans ailantifolia | ● Sorbus alnifolia |
| ● Kalopanax septemlobu | ○ Styrax obassia |
| ● Larix kaempferi | ● Synpolcas chinensis |
| ● Lindera umbellata | ○ Tilia |
| ● Magnolia obovata | ● Weigela hortensia |
| ● Morus australis | ● <all other values> |

Field survey site 13 (YURF)

by Sarah Kentsch



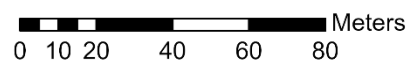
Legend

FieldData

Species_lat_name

- Acer
- Acer mono maxim
- Aesculus turbinata
- Alnus fauriei
- Carpinus Cordata
- Celtic jessoensis
- Climbing plant 1
- Climbing plant 2
- Cornus controversa
- Juglans ailantifolia
- Kalopanax septemlobu
- Magnolia obovata
- Morus australis
- Prunus maximowiczii
- Pterocarya rhoifolia
- Quercus mongolica
- Styrax obassia
- Tilia
- <all other values>

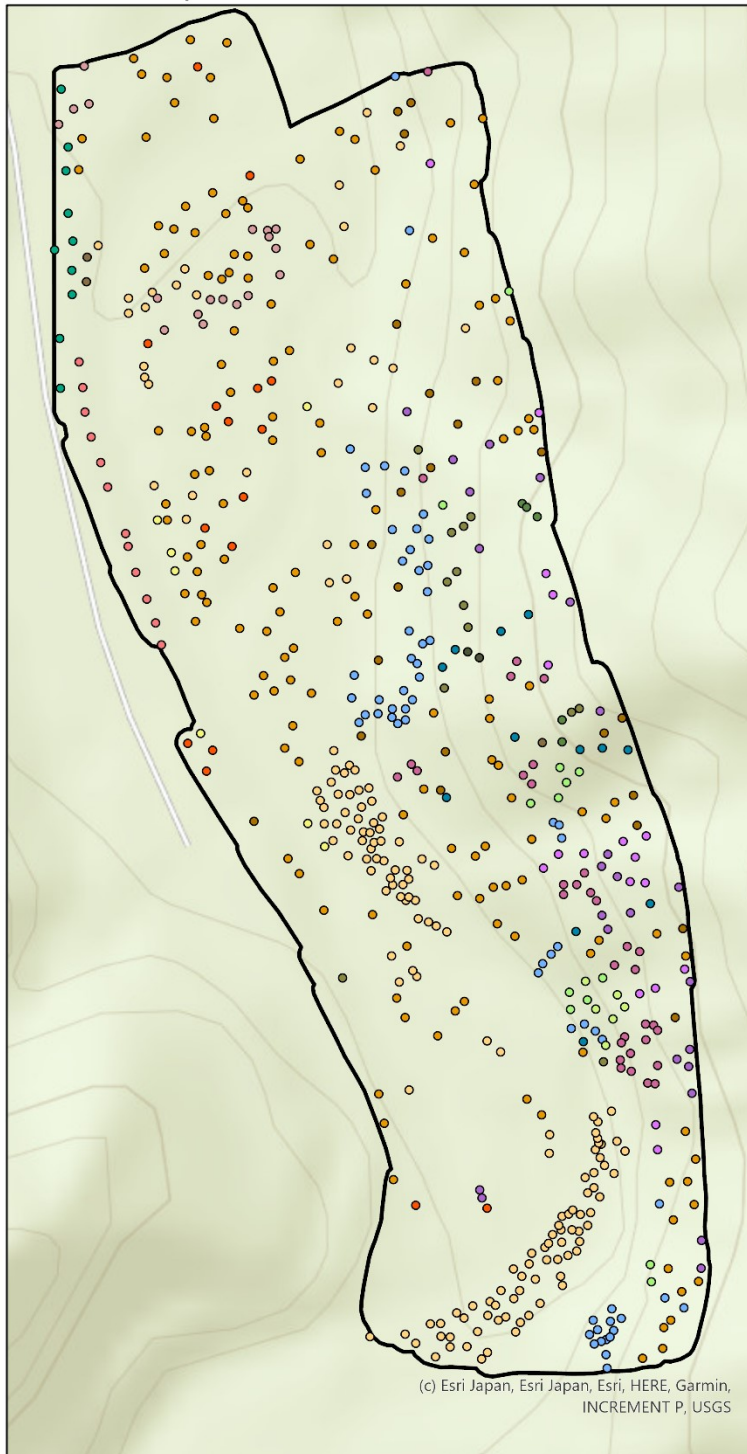
▭ S13ROI



Part 2: Winter orthomosaic surveys based on manual annotation of winter images.

Image survey site 1 (YURF)

by Sarah Kentsch



Legend

Species labels

ROI

Species_lat_name

- Acer
- Acer mono maxim
- Aesculus turbinata
- Alnus fauriei
- Carpinus cordata
- Castanea crenata
- Climbing plant 1
- Cornus controversa
- Corylus sieboldiana
- Juglans ailantifolia
- Larix kaemferi
- Magnolia obvata
- Phelledendron amurense
- Prunus
- Pterocarya rhoifolia
- Quercus mongolica
- Robinia pseudoaccaccia
- Salix jessoensis
- Styrax obassia
- Tilia
- <all other values>

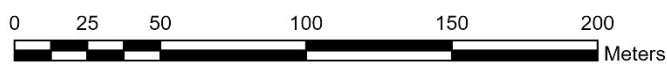
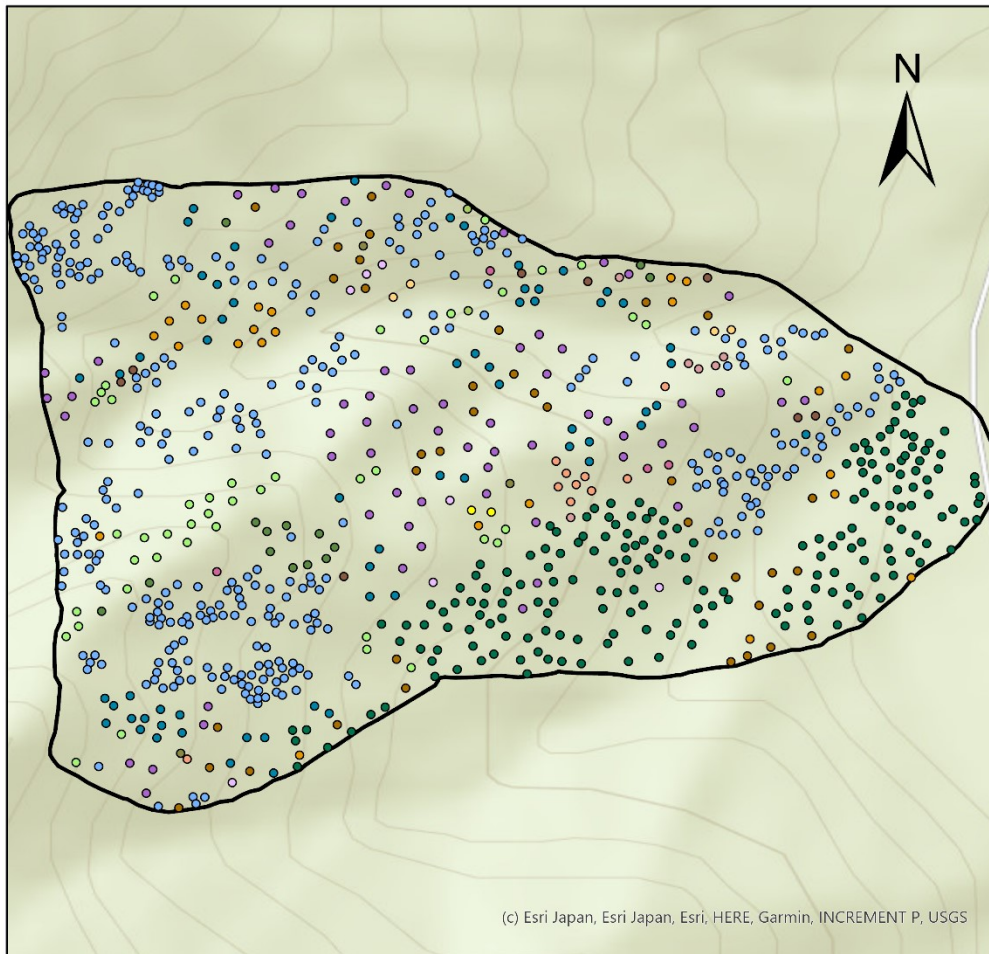




Image survey site 2 (YURF)

by Sarah Kentsch



(c) Esri Japan, Esri Japan, Esri, HERE, Garmin, INCREMENT P, USGS

0 15 30 60 90 120 Meters

Legend

S2treetops

Species_lat_name

- Acer
- Acer mono maxim
- Aesculus turbinata
- Carpinus cordata
- Climbing plant 1

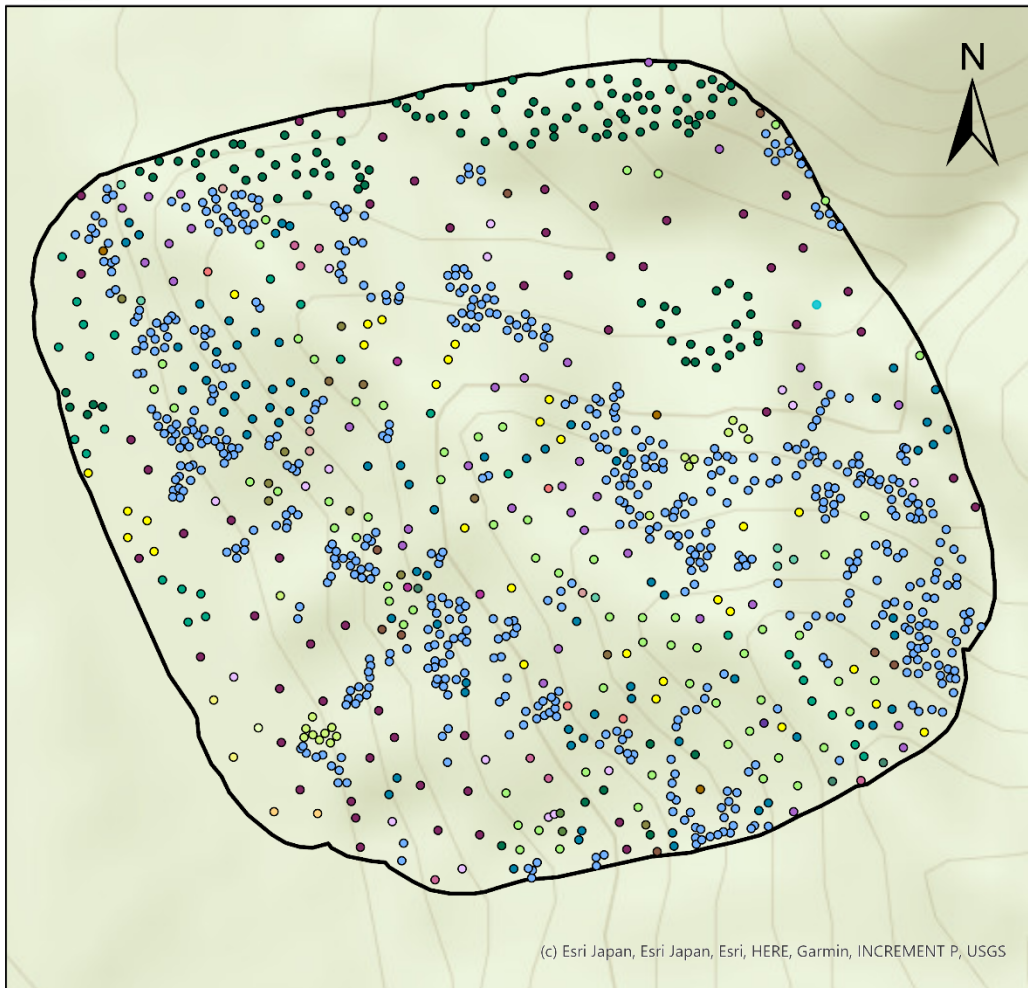
- Cornus controversa
- Cryptomeria japonica
- Juglans ailantifolia
- Magnolia obovata
- Morus australis
- Prunus
- Pterocarya rhoifolia
- Quercus mongolica
- Styxax obassia
- Tilia
- unknown
- <all other values>

□ S2ROI

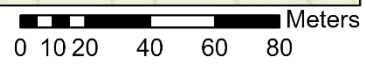


Image survey site 3 (YURF)

by Sarah Kentsch



(c) Esri Japan, Esri Japan, Esri, HERE, Garmin, INCREMENT P, USGS



Legend

Site3treetops

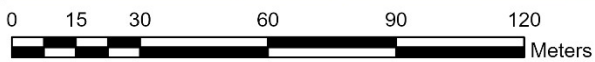
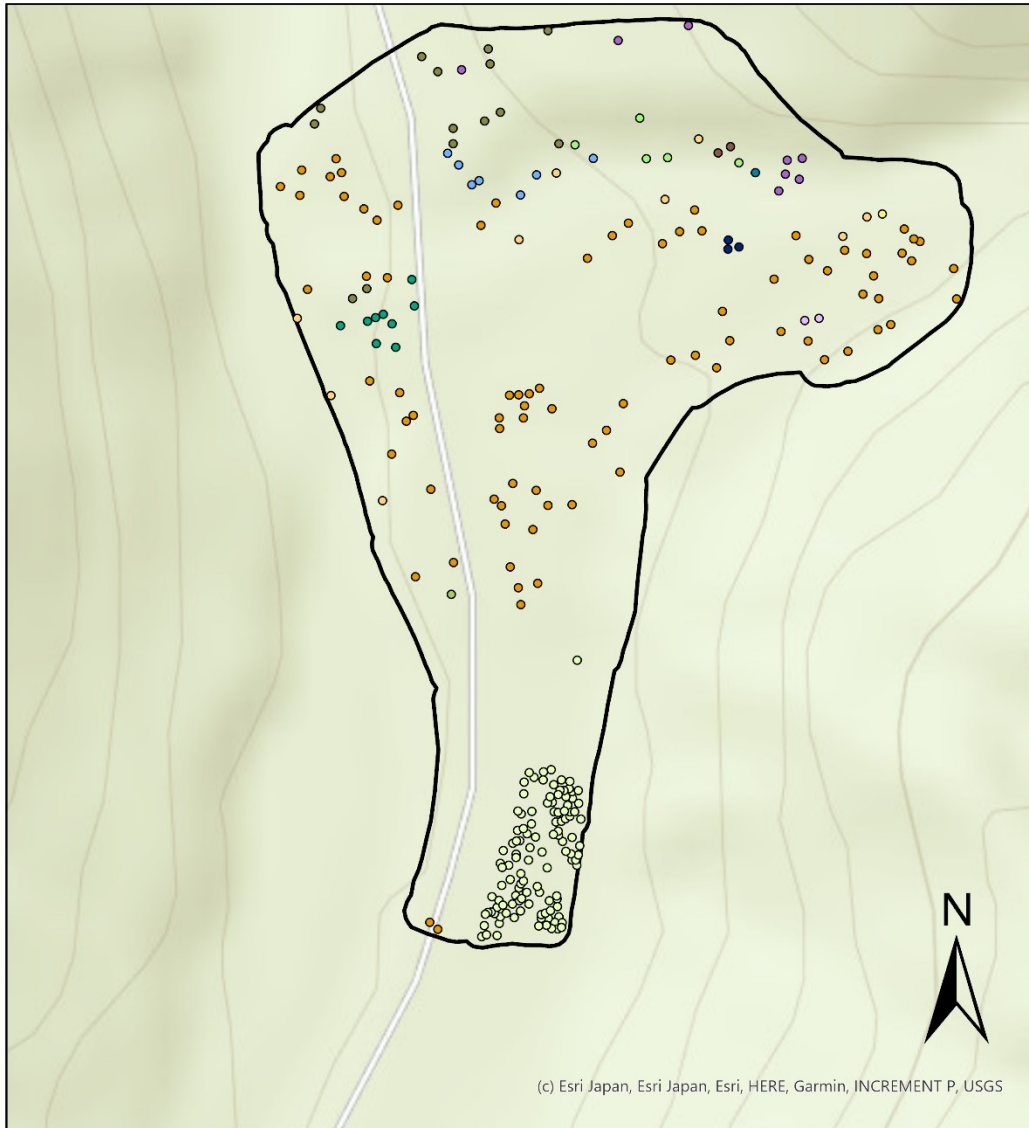
Species_lat_name

- | | | |
|----------------------|------------------------|------------------------|
| ● Acer | ● Climbing plant 2 | ● Morus australis |
| ● Acer mono maxim | ○ Cornus controversa | ● Prunus |
| ● Aesculus turbinata | ● Cryptomeria japonica | ● Pterocarya rhoifolia |
| ● Alnus fauriei | ● Fagus crenata | ● Quercus mongolica |
| ● Carpinus cordata | ● Fraxinus lanugiosa | ● Salix jessoensis |
| ● Castanea crenata | ● Ilex macropoda | ○ Salix serissaefolia |
| ● Climbing plant 1 | ● Juglans ailantifolia | ● Styrax obassia |
| | ● Kalopanax septemlobu | ● Tilia |
| | ● Larix kaempferi | ● <all other values> |
| | ● Magnolia obovata | ▭ Site3ROI |



Image survey site 4 (YURF)

by Sarah Kentsch



Legend

Wintertrees

Species_lat_name

- Acer
- Acer distylum
- Betula coryfolia
- Cercidiphyllum japonicum var. Magnificum

- Climbing plant 1
- Cornus controversa
- Juglans ailantifolia
- Larix kaempferi
- Magolia obovata
- Morus australis
- Pterocarya rhoifolia
- Quercus mongolica
- Salix jessonsis
- Salix serissaefolia
- <all other values>
- ▭ Site4ROI

Large survey site 5 (YURF)

by Sarah Kentsch

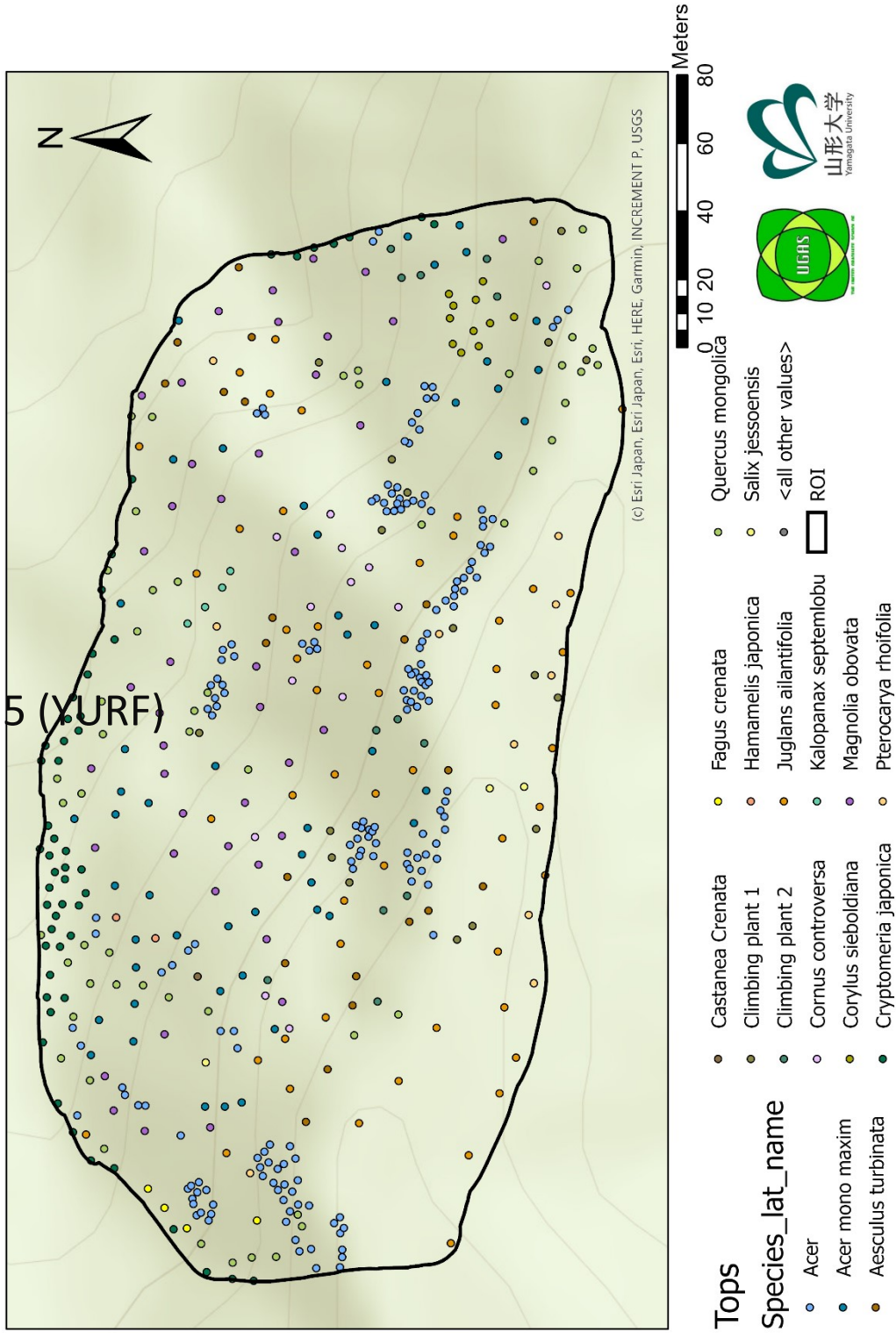




Image survey site 6 (YURF)

by Sarah Kentsch



0 10 20 40 60 80 Meters

Legend



WinterTrees

Species_lat_name

- Acer
- Acer mono maxim
- Aesculus turbinata

- Alnus inokumae
- Betula corylifolia
- Castanea crenata
- Celtic jessoensis
- Climbing plant 1
- Cornus controversa
- Cryptomeria japonica

- Juglans ailantifolia
- Magnolia obovata
- Picea abies
- Pterocarya rhoifolia
- Quercus mongolica
- Robinia pseudoaccacia
- Salix jessoensis

- Salix serissaefolia
- Zanthoxylum piperitum
- dead
- <all other values>

Image survey site 8 (YURF)

by Sarah Kentsch

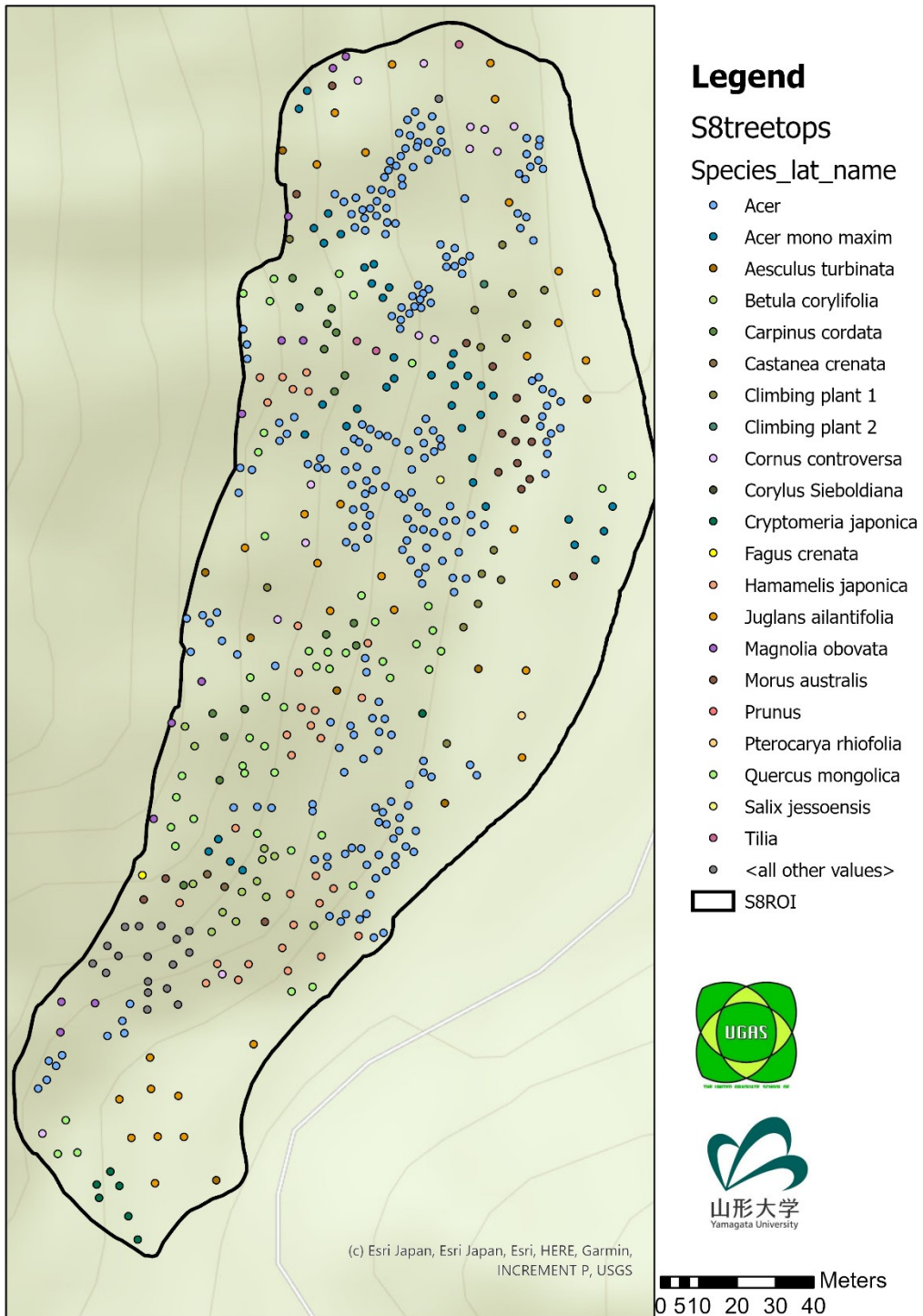
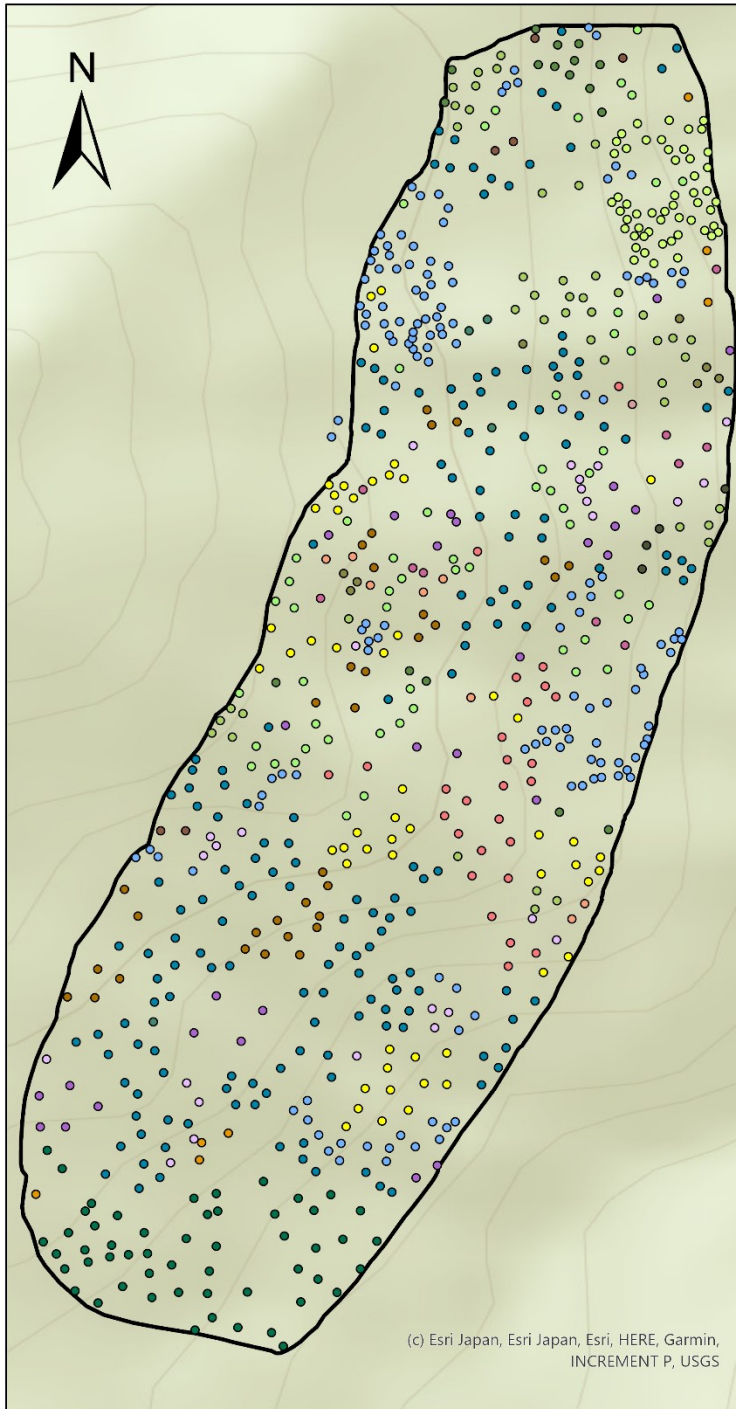


Image survey site 9 (YURF)

by Sarah Kentsch



Legend

S9treetops

Species_lat_name

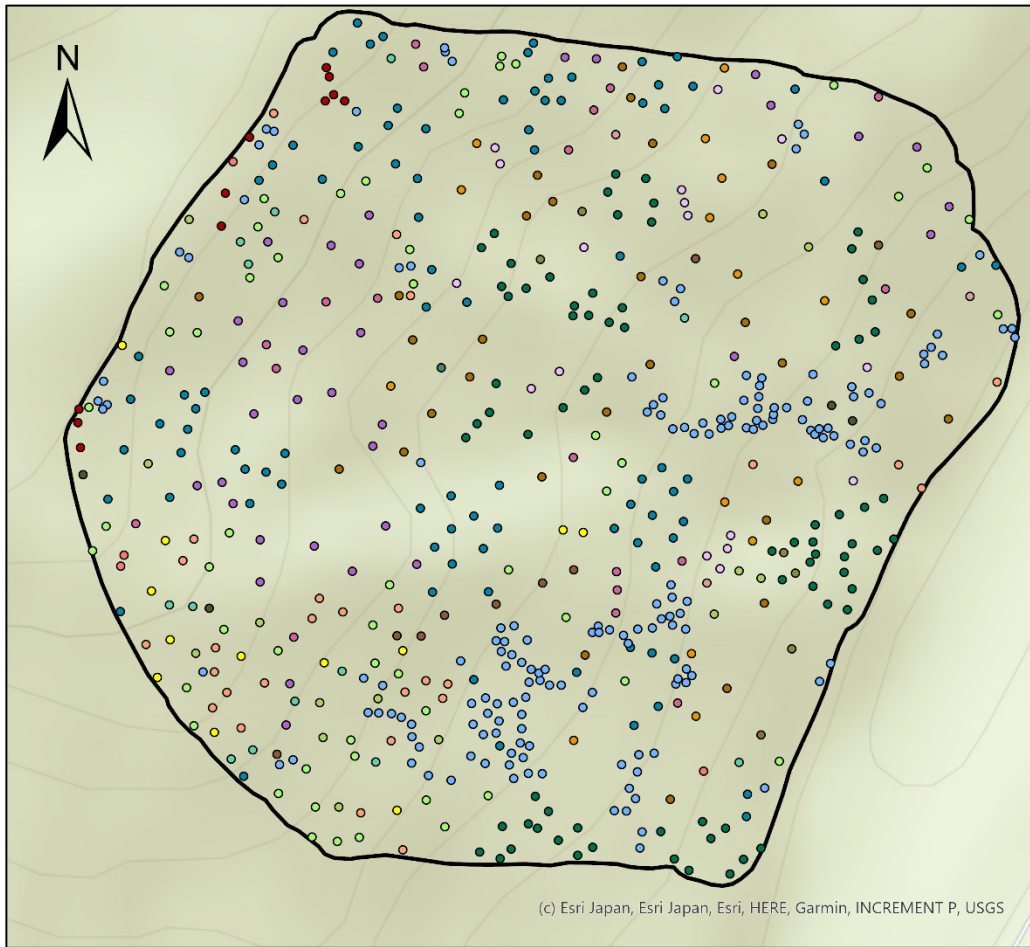
- Acer
- Acer mono maxim
- Aesculus turbinata
- Betula corylifolia
- Carpinus cordata
- Climbing plant 1
- Climbing plant 2
- Cornus controversa
- Corylus sieboldiana
- Cryptomeria japonica
- Fagus crenata
- Hamamelis japonica
- Juglans ailantifolia
- Magnolia obovata
- Morus australis
- Prunus
- Quercus mongolica
- Styrax obassia
- Tilia
- Understory vegetation
- <all other values>
- S9ROI





Image survey site 10 (YURF)

by Sarah Kentsch



0 10 20 40 60 80 Meters

Legend

Site10_treetops

Species_lat_name

- Acer
- Acer mono maxim
- Acer palmatum
- Aesculus turbinata
- Betula corylifolia
- Castanea Crenata

- Climbing plant 1
- Climbing plant 2
- Cornus controversa
- Corylus sieboldiana
- Cryptomeria japonica
- Fagus crenata
- Hamamelis japonica
- Juglans ailantifolia
- Kalopanax septemlobu

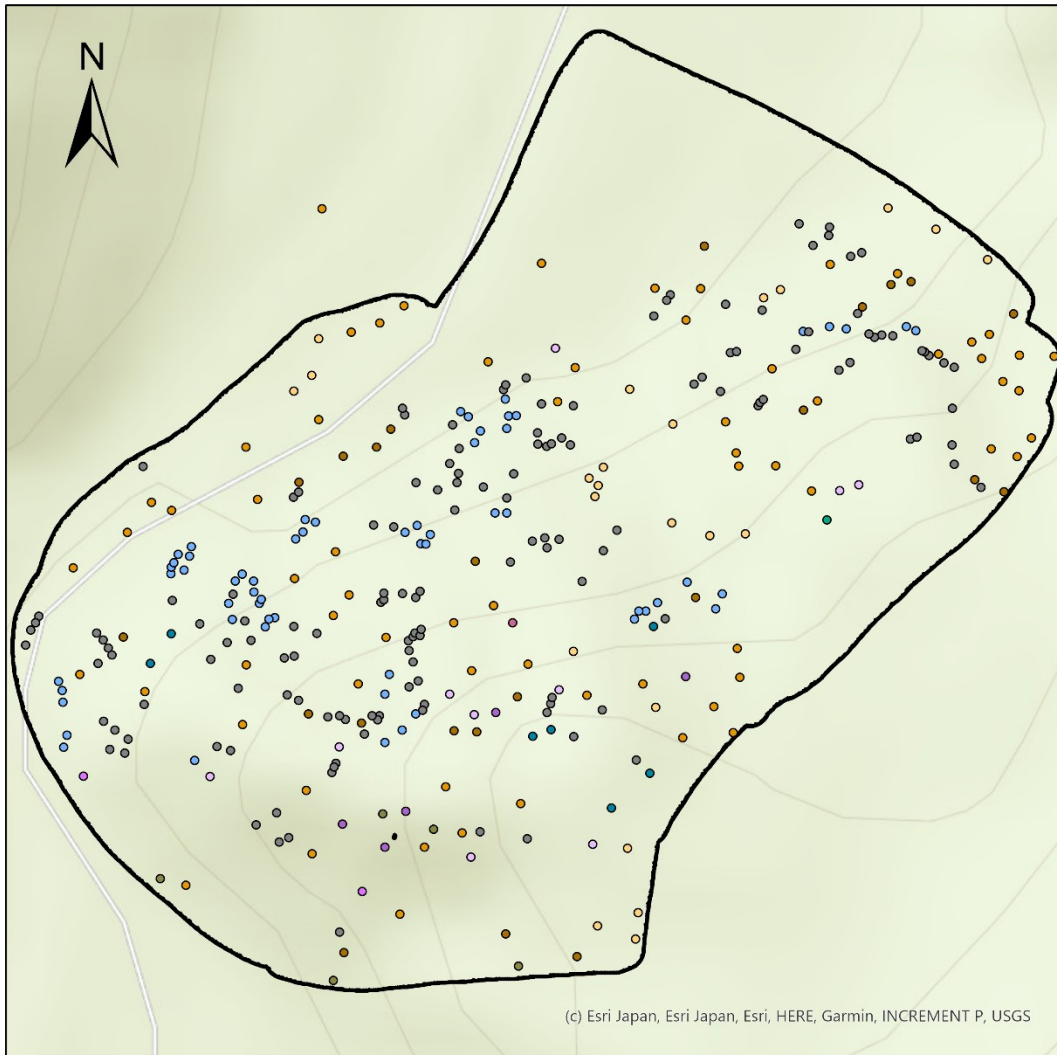
- Magnolia obovata
- Morus australis
- Prunus
- Quercus mongolica
- Styrax obassia
- Tilia
- <all other values>

▭ Site10ROI



Image survey site 11 (YURF)

by Sarah Kentsch



0 10 20 40 60 80 Meters

Legend

WinterTrees

Species_lat_name

- Acer
- Acer mono maxim
- Aesculus turbinata

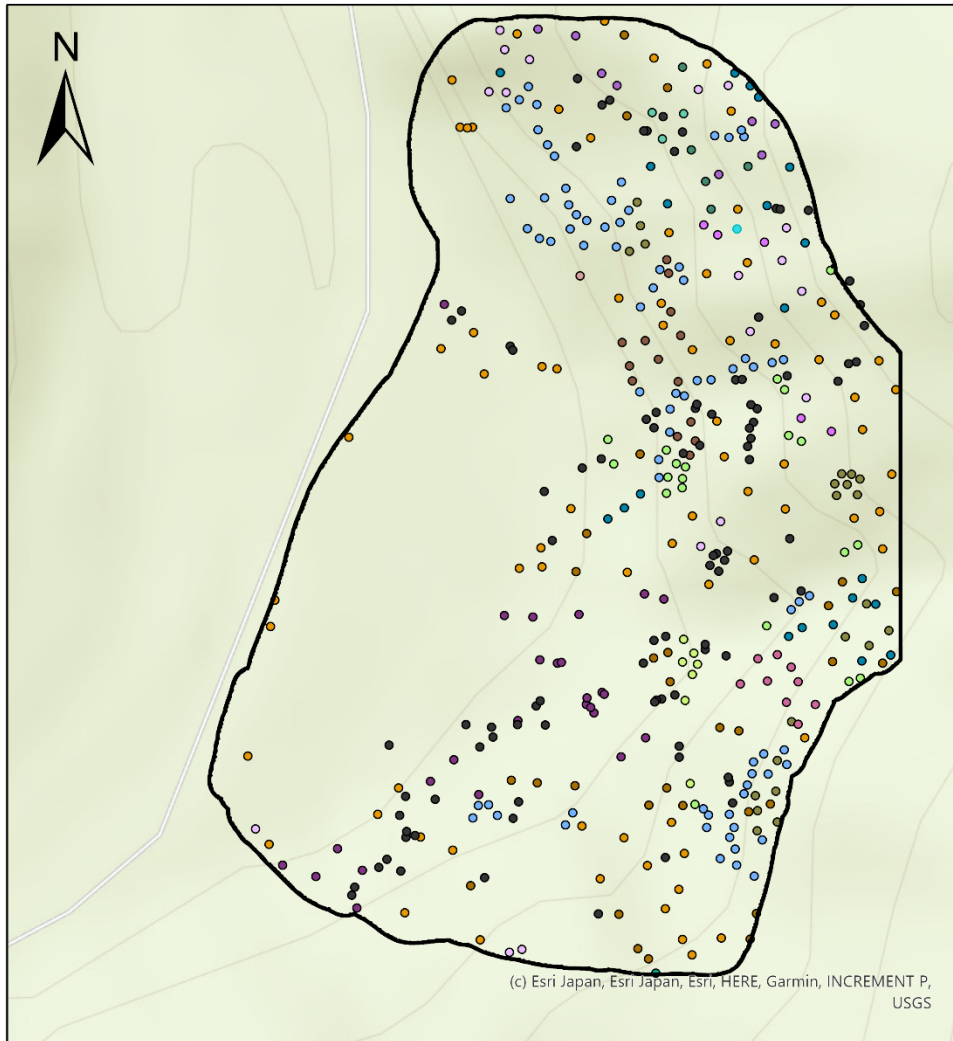
- Celtic jessoensis
- Climbing plant 1
- Cornus controversa
- Juglans ailantifolia
- Larix kaempferi
- Magnolia obovata
- Pterocarya rhoifolia
- Tilia
- <all other values>

ROI



Image survey site 12 (YURF)

by Sarah Kentsch



0 10 20 40 60 80 Meters

Legend

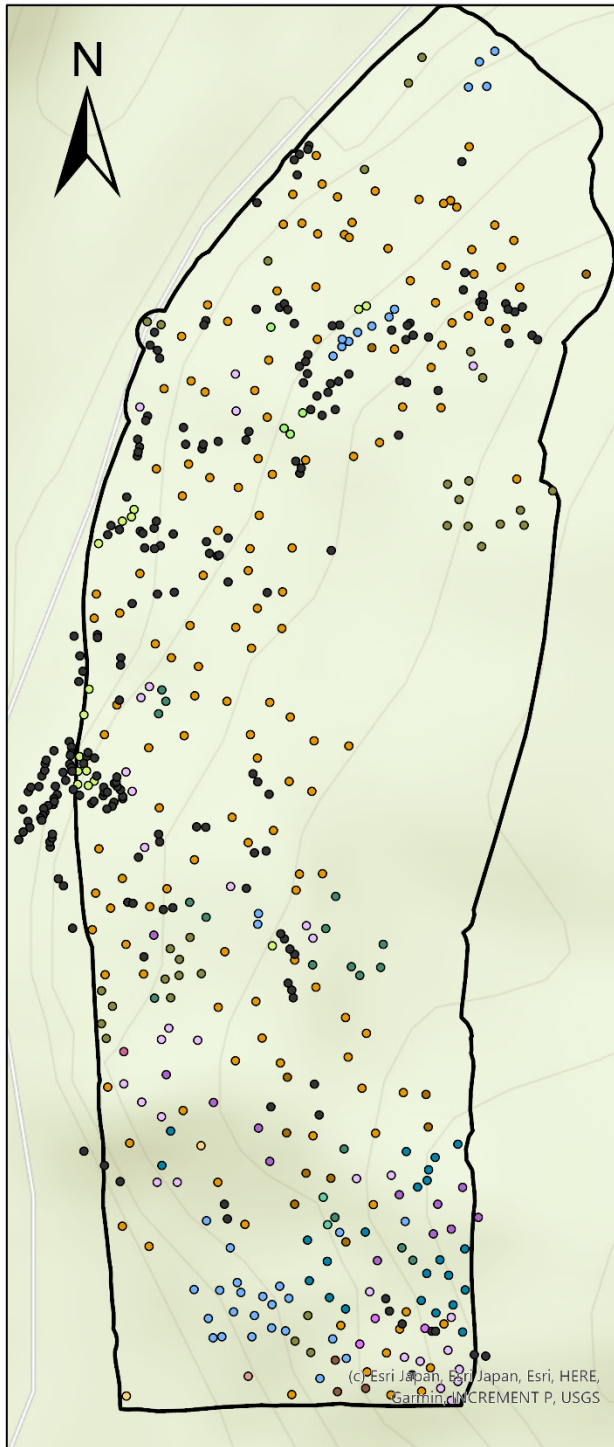
ROI

Species_lat_name

- | | | |
|----------------------|------------------------|----------------------------------|
| ● Acer | ● Climbing plant 1 | ● Morus australis |
| ● Acer mono maxim | ● Climbing plant 2 | ● Pterocarya rhoifolia |
| ● Aesculus turbinata | ● Cornus controversa | ● Quercus mongolica |
| ● Alnus fauriei | ● Juglans ailantifolia | ● Styrax obassia |
| ● Celtic jessoensis | ● Kalopanax septemlobu | ● Tilia |
| | ● Larix kaempferi | ● detected but unidentified tree |
| | ● Magnolia obovata | ● <all other values> |

Image survey site 13 (YURF)

by Sarah Kentsch



Legend

WinterTrees

Species_lat_name

- Acer
- Acer mono maxim
- Aesculus turbinata
- Alnus fauriei
- Celtic jessoensis
- Climbing plant 1
- Climbing plant 2
- Cornus controversa
- Juglans ailantifolia
- Kalopanax septemlobu
- Magnolia obovata
- Morus australis
- Pterocarya rhoifolia
- Quercus mongolica
- Styrax obassia
- Tilia
- detected but unidentified tree
- <all other values>

□ S13ROI



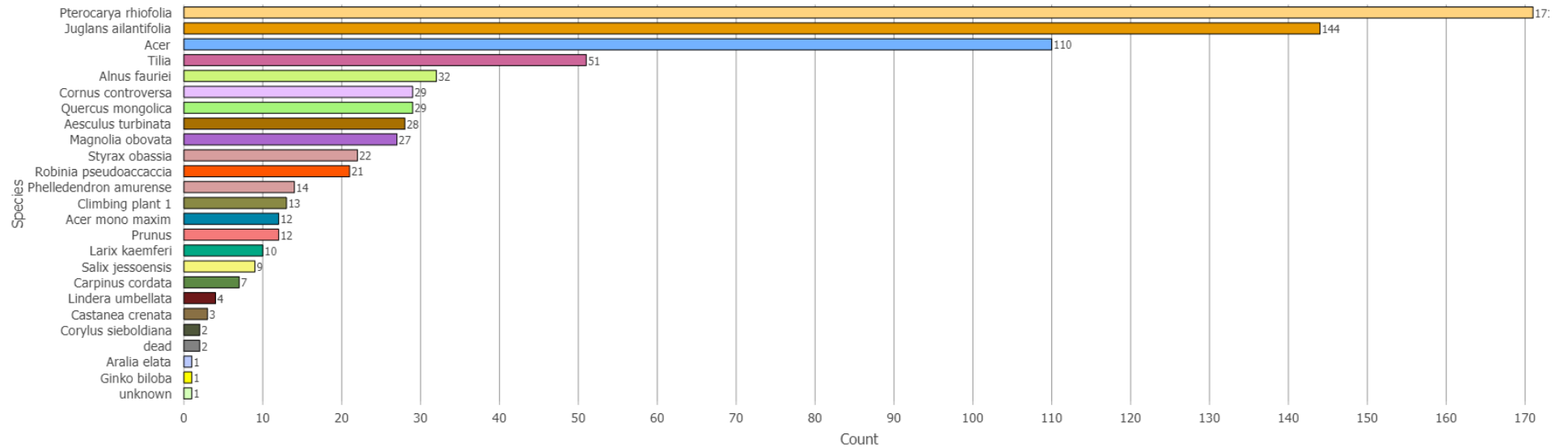
0 10 20 40 60 80 Meters

Appendix K – Counting data

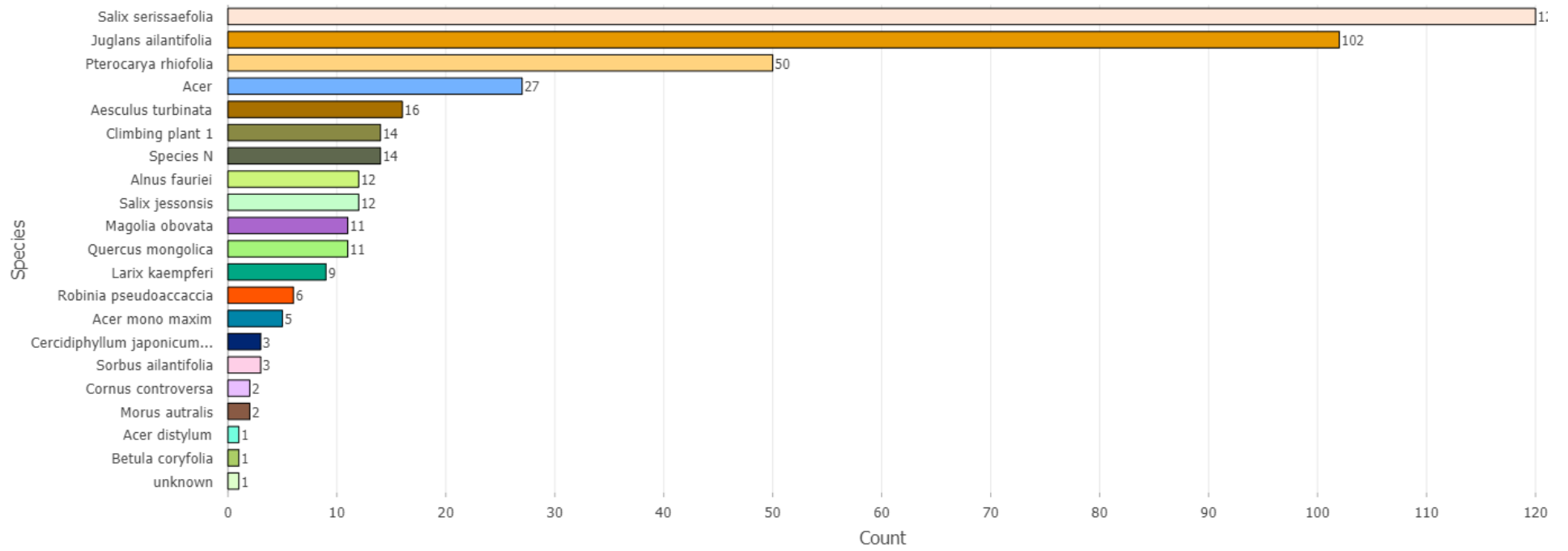
Tree species counting divided into three parts: part 1 field surveys, part 2 image counting, part 3 winter image counting

Part 1: Contains the counts performed in the field for each site.

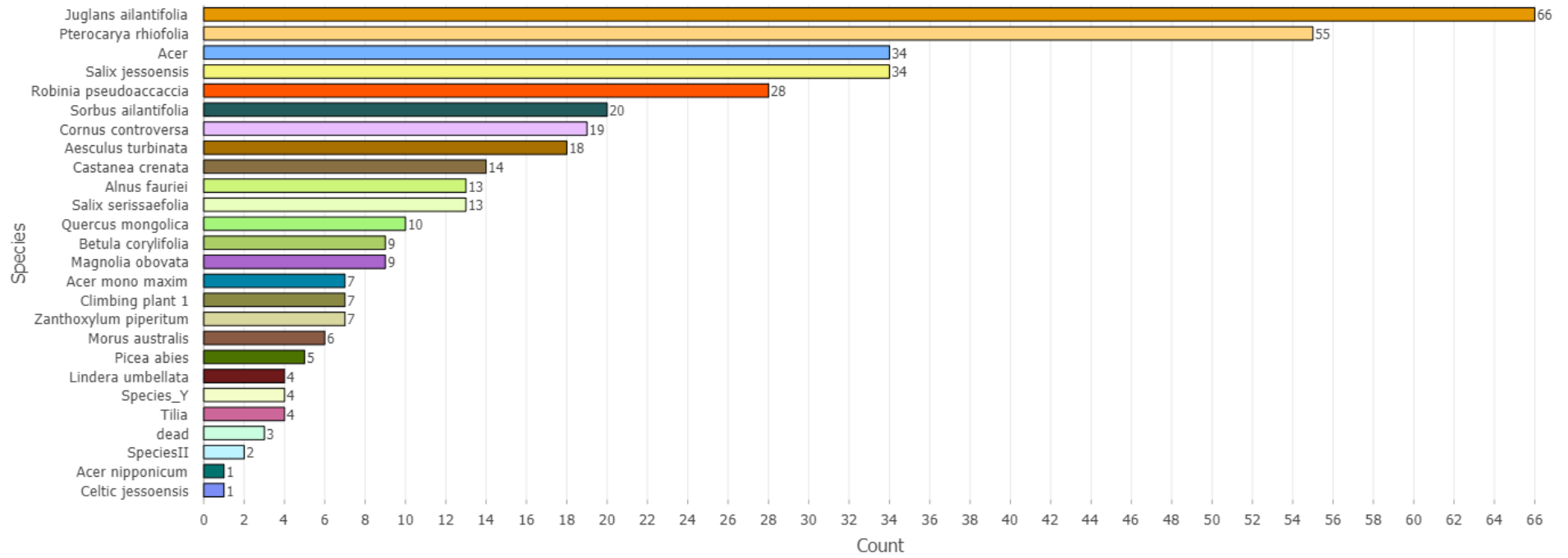
Field survey data site 1



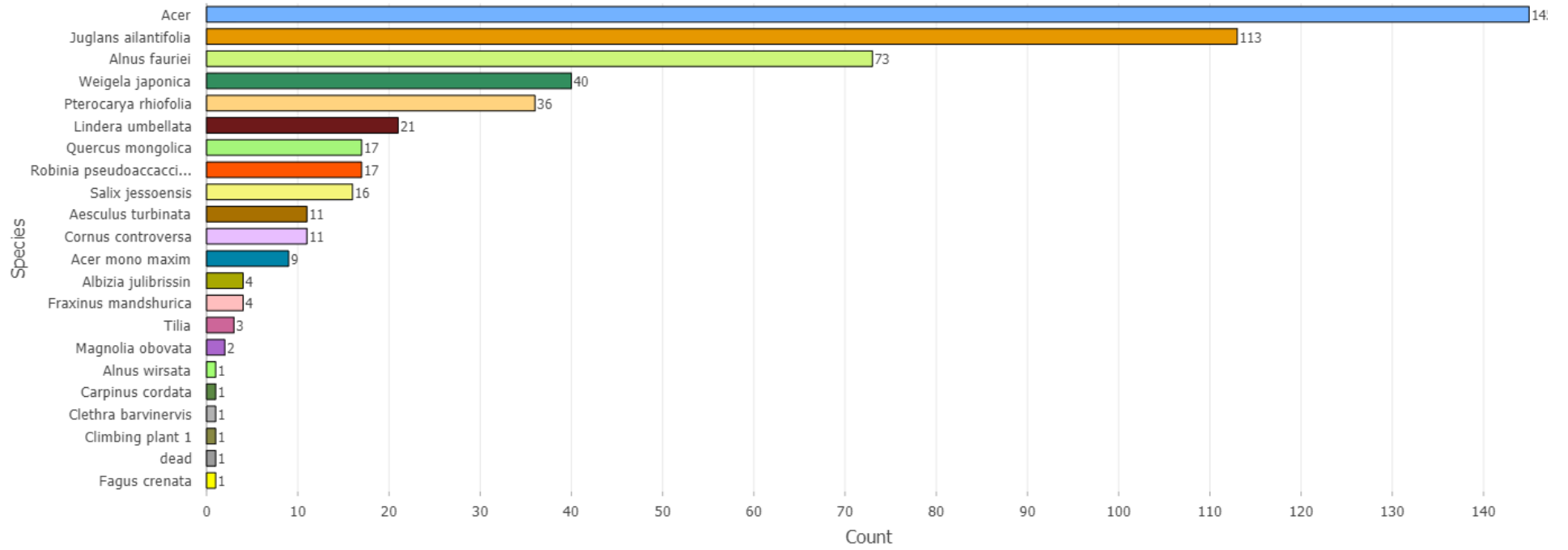
Field survey data site 4



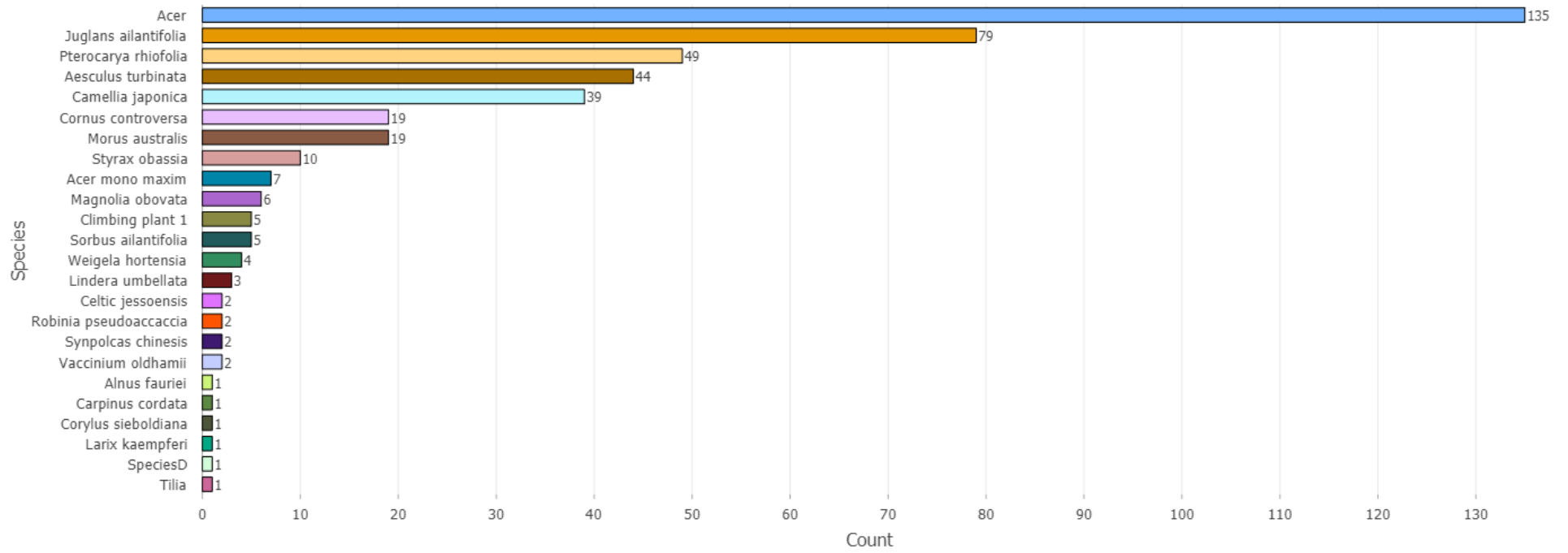
Field survey data site 6



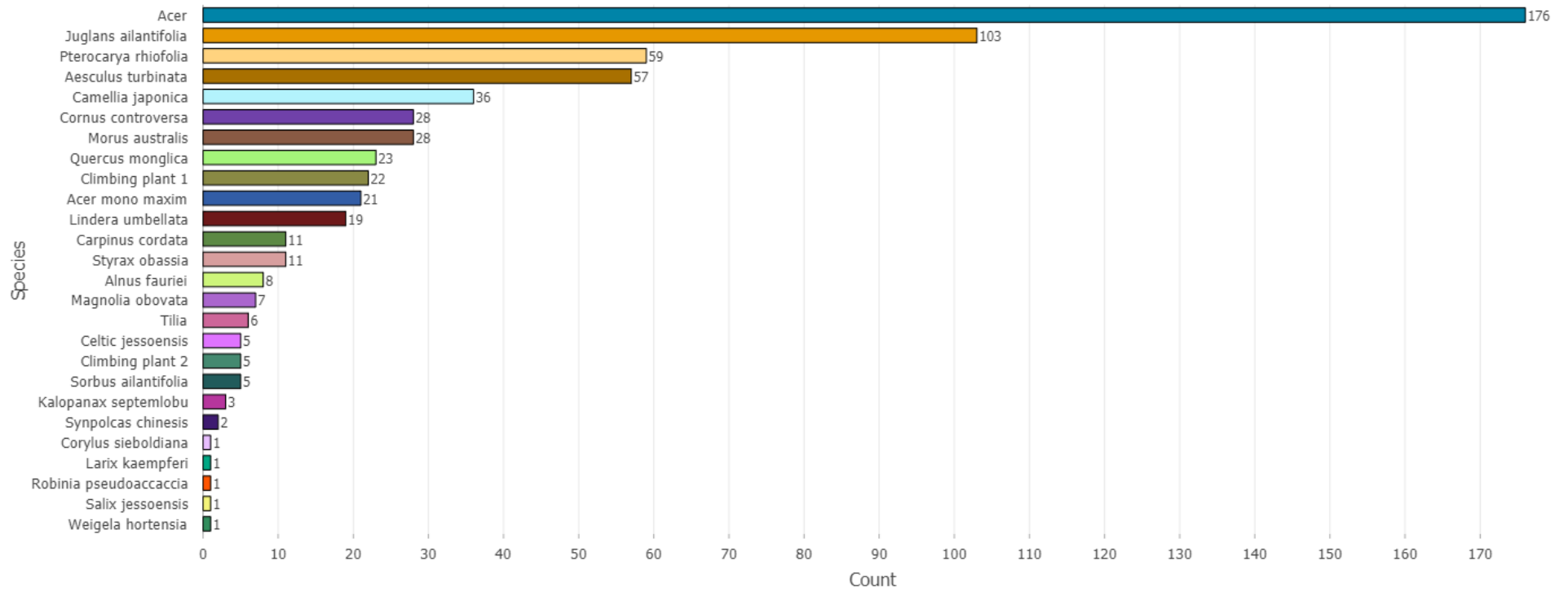
Field survey data site 7



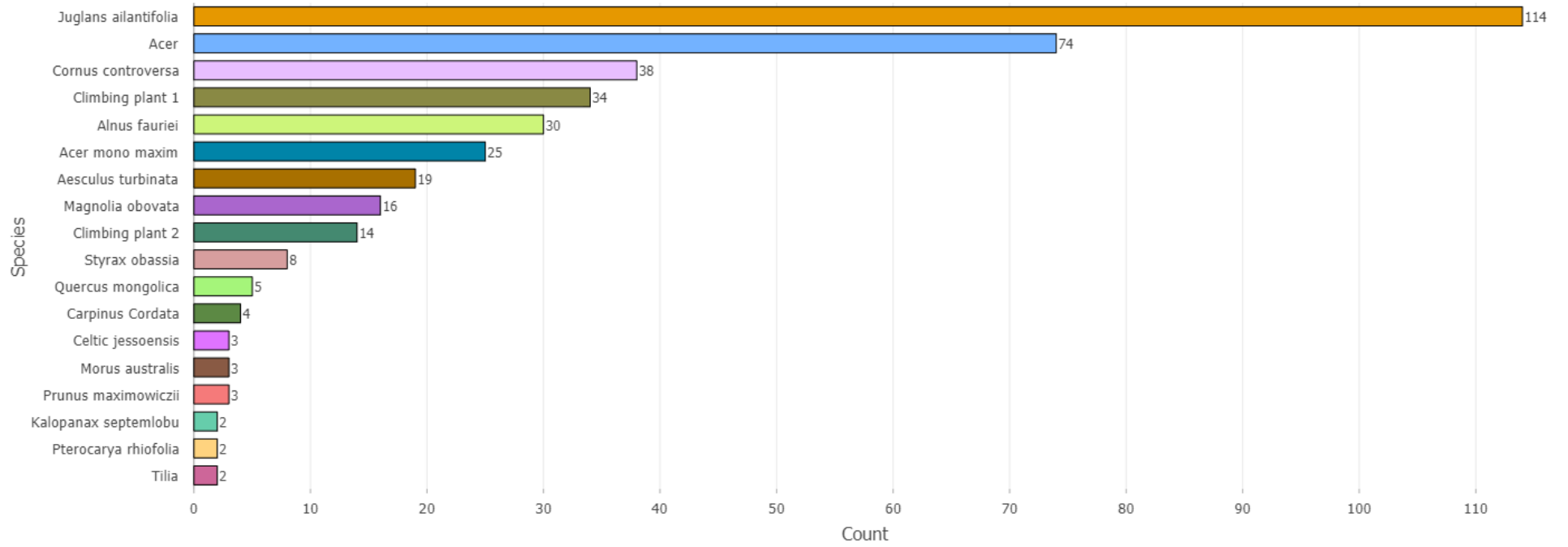
Field survey data site 11



Field survey data site 12

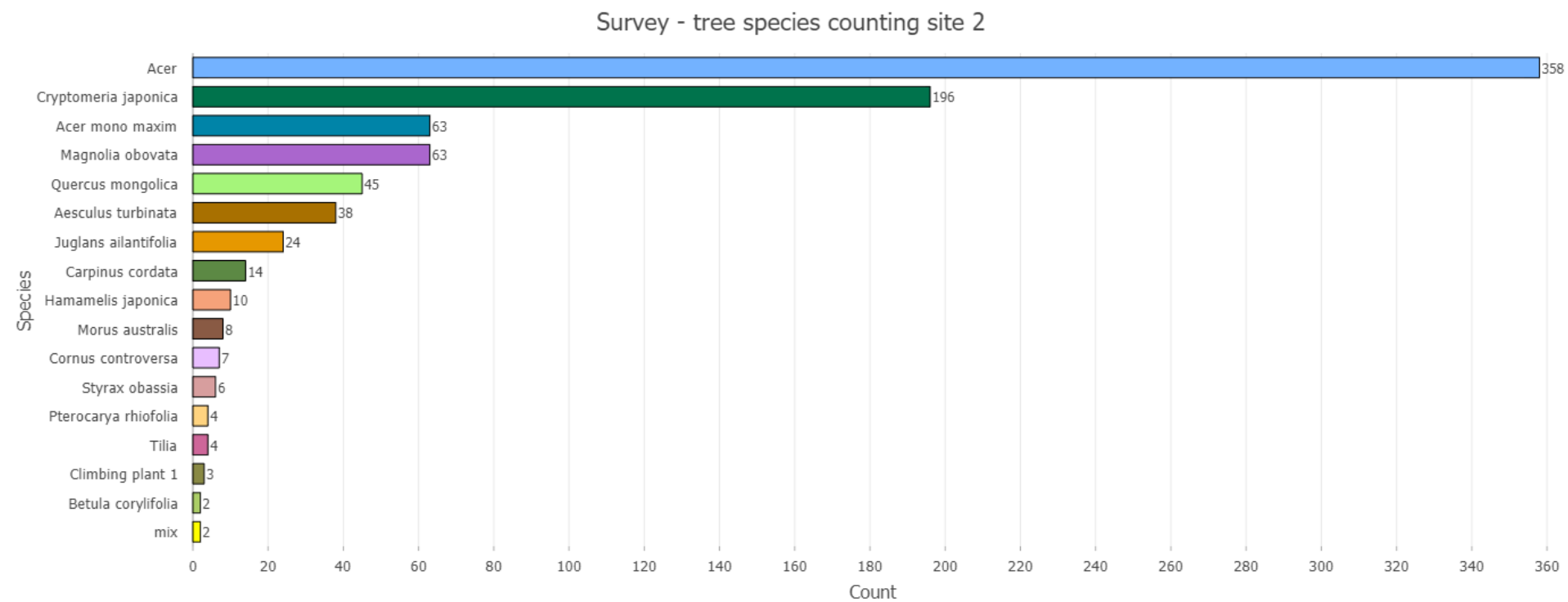


Field survey data site 13

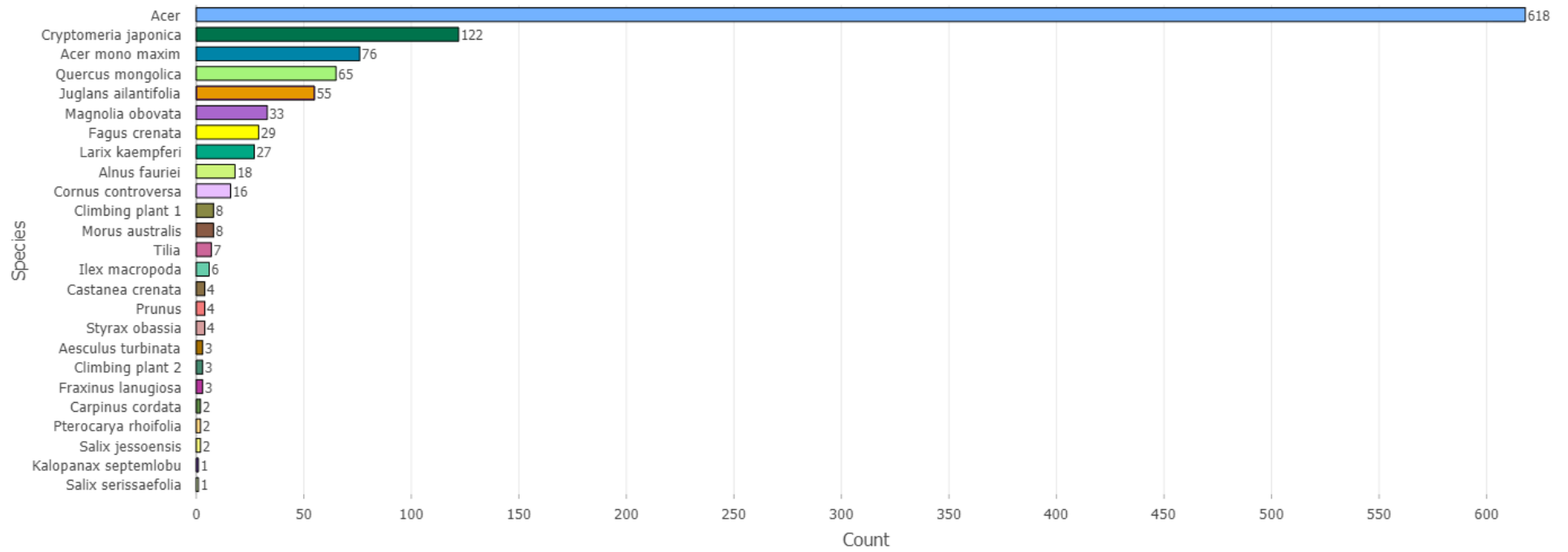


Part 2:

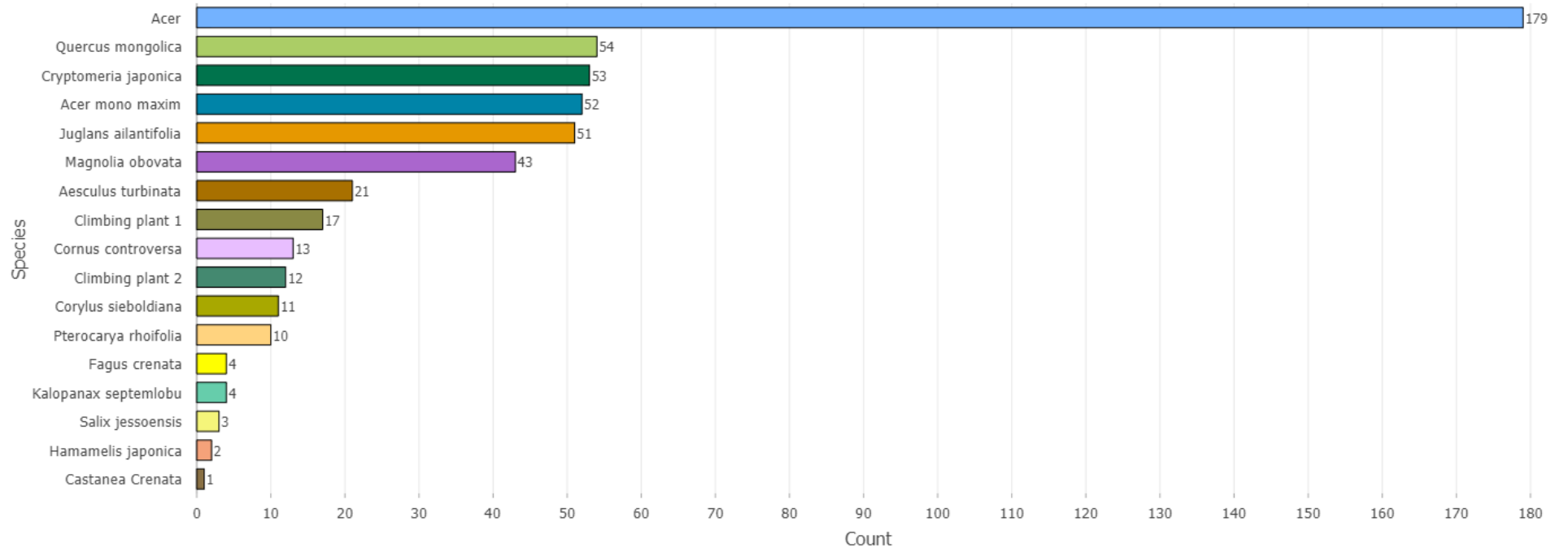
As for the slope sites no field work was performed in ArcGIS, image counts were used for the survey and are presented in this part.



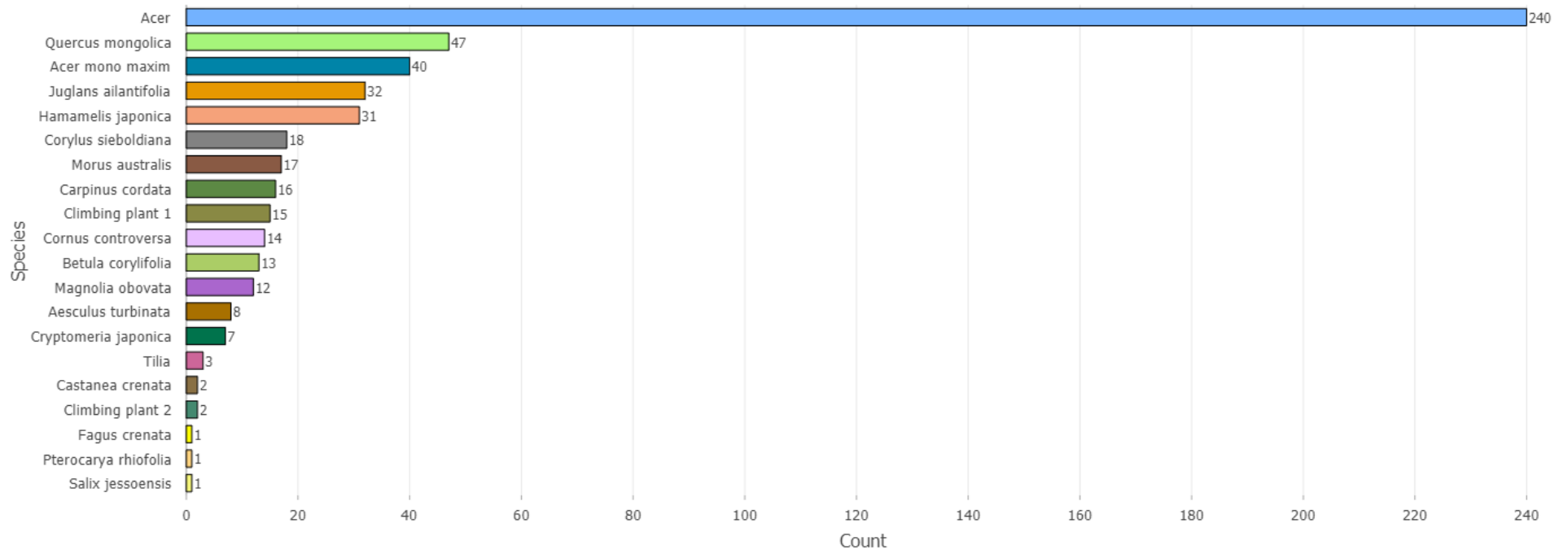
Survey - tree species counting site 3



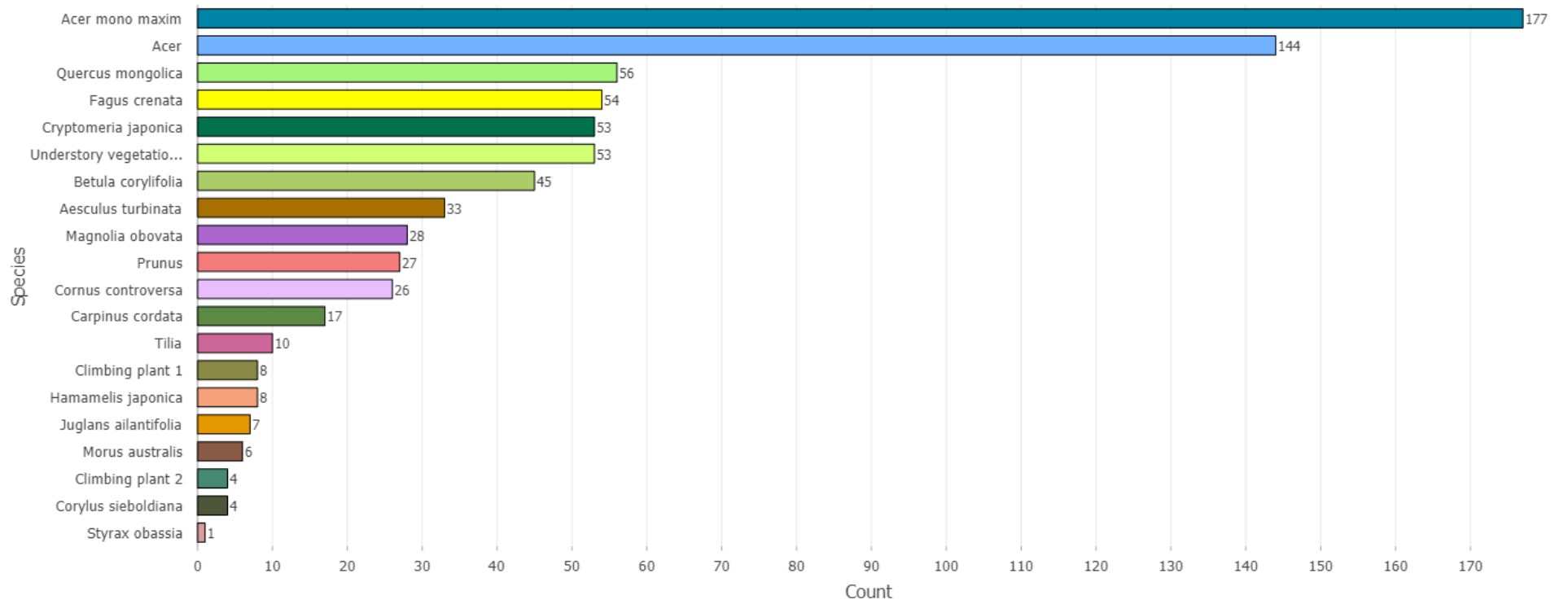
Survey - tree species countings site 5



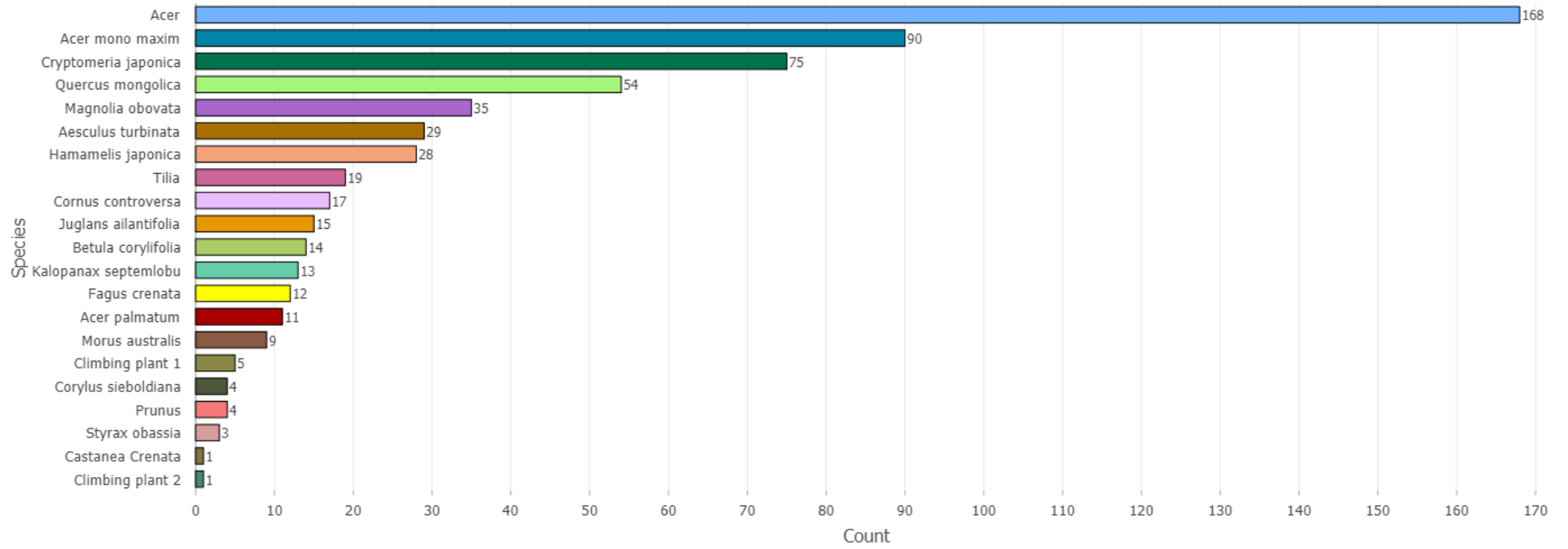
Survey - tree species counting site 8



Survey – tree species counting site 9

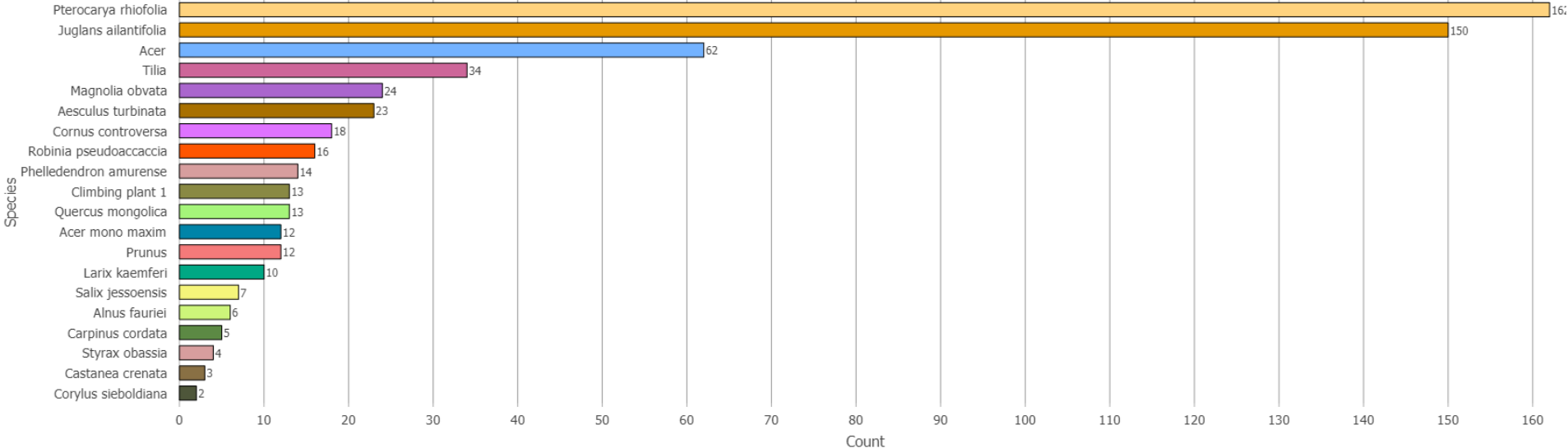


Survey - Tree species counting site 10

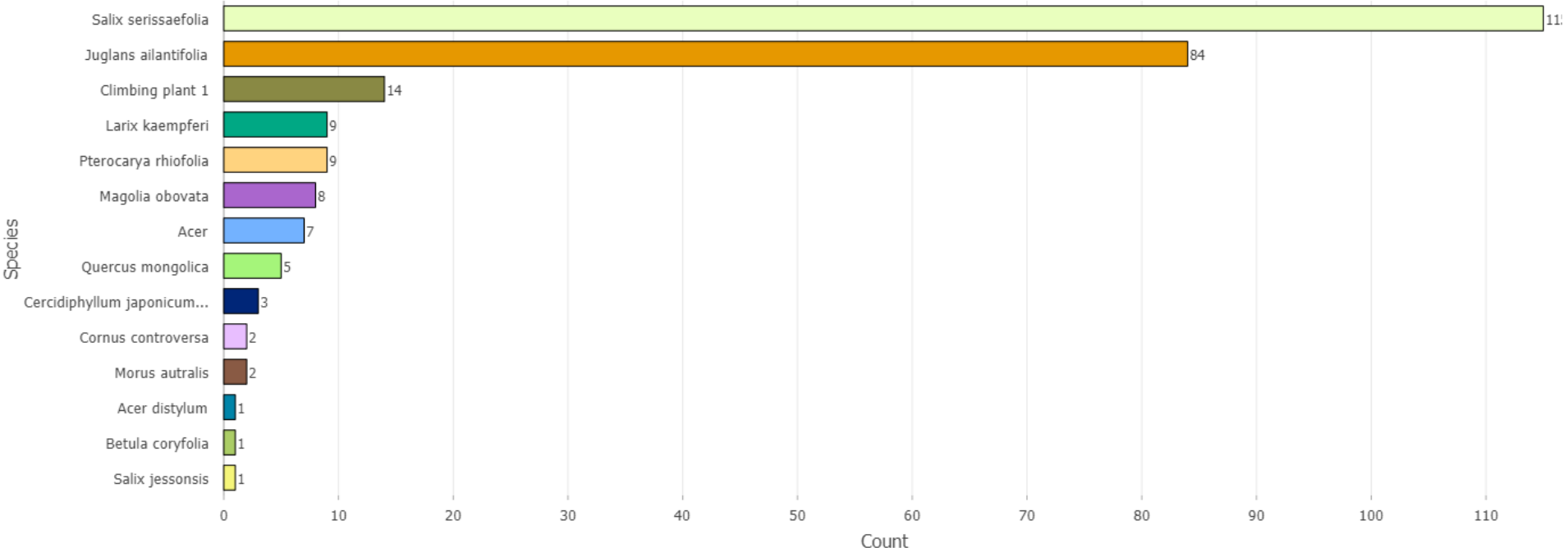


Part 3: Counting performed based on summer and winter images.

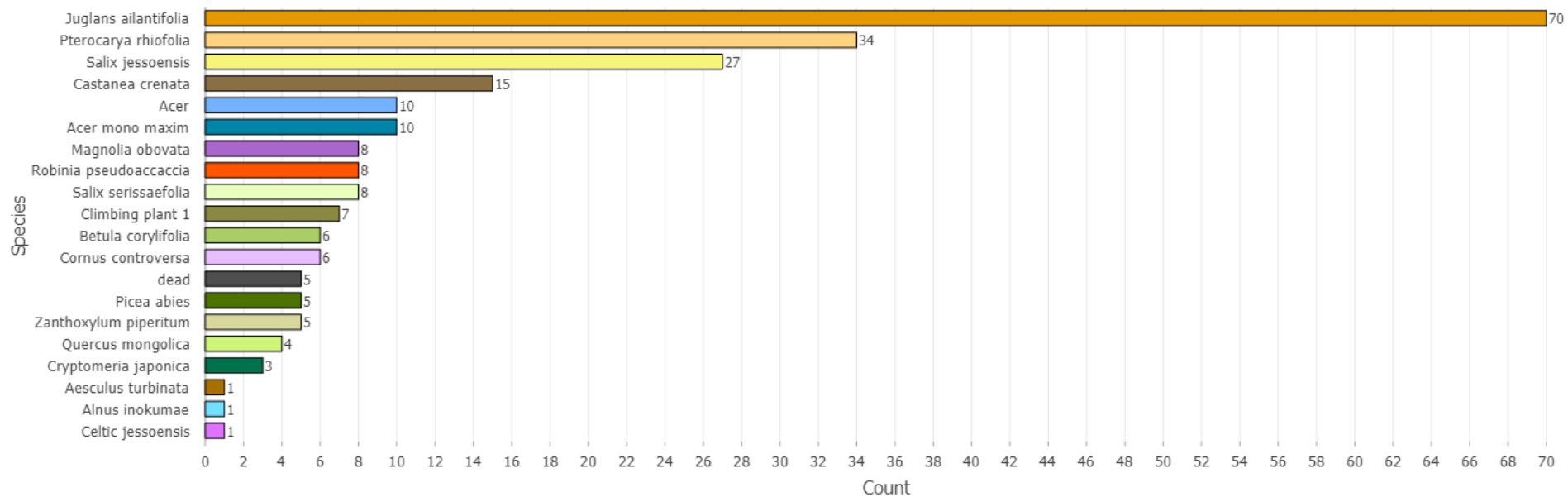
Winter survey – tree species counts site 1



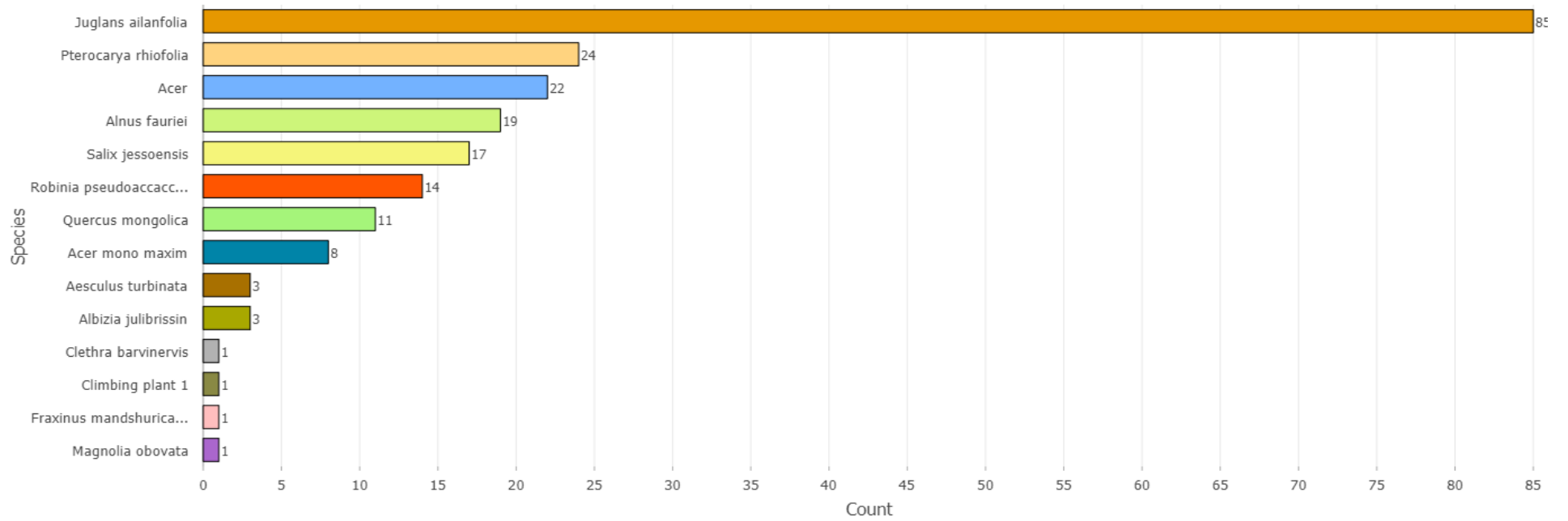
Winter survey – tree species counts site 4



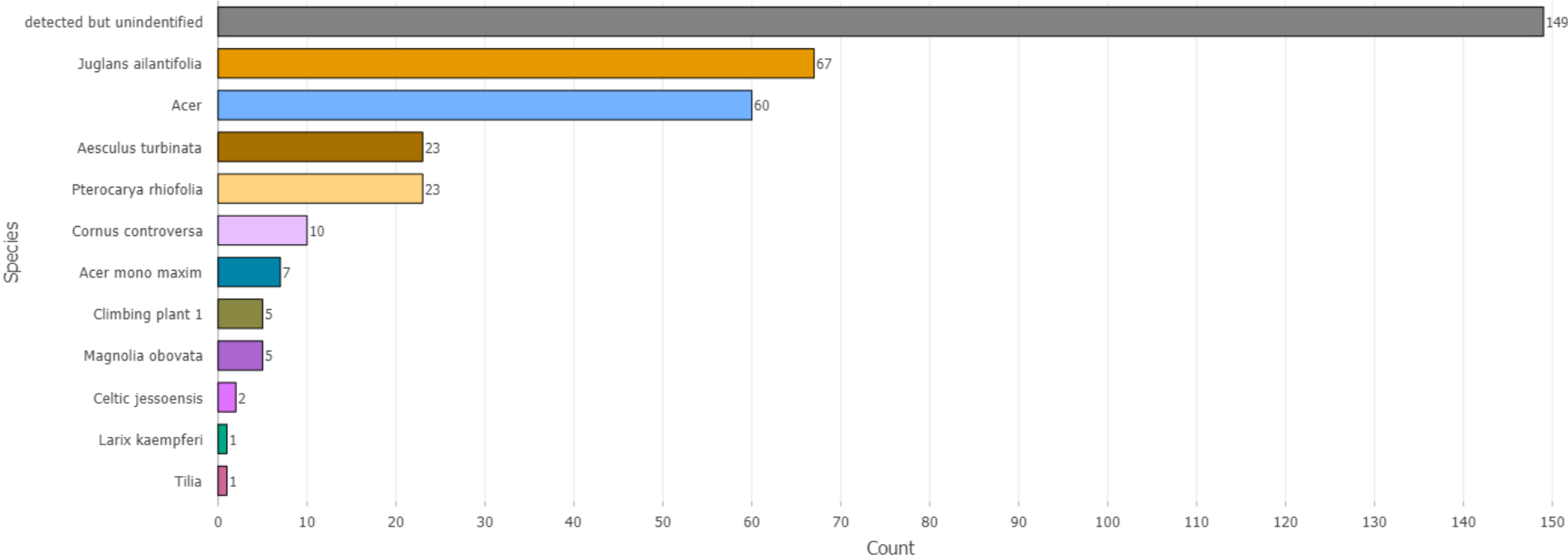
Winter survey - tree species countings site 6



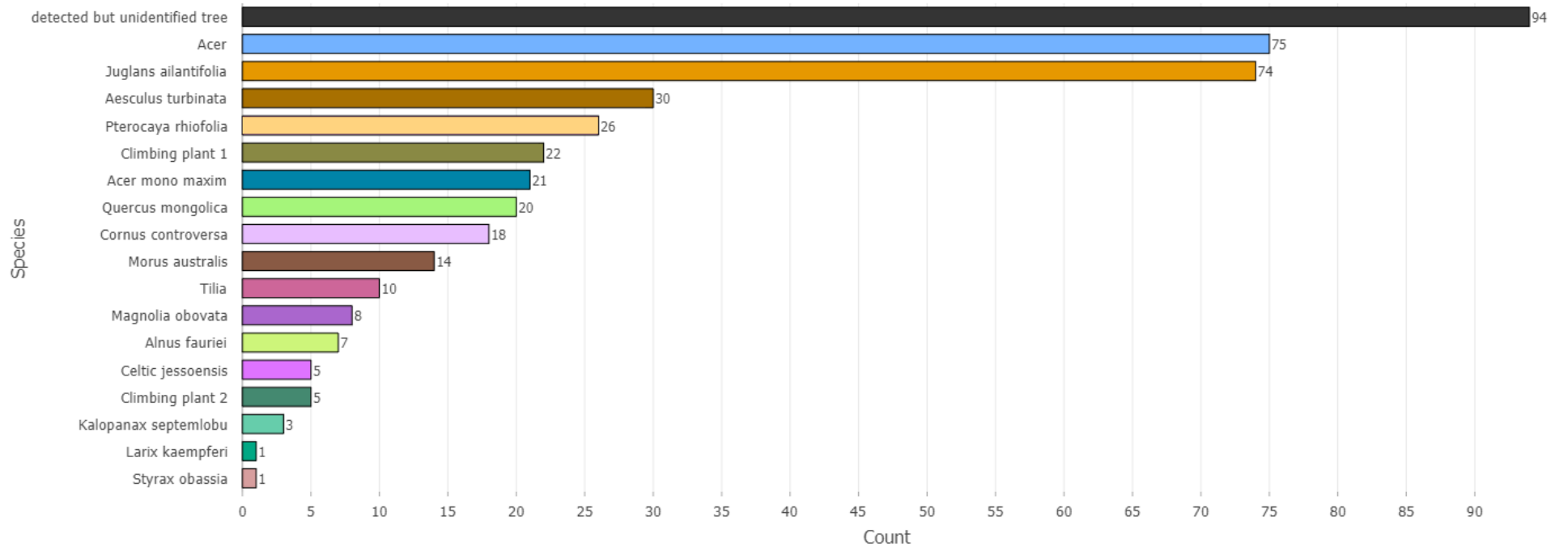
Winter survey – tree species counts site 7



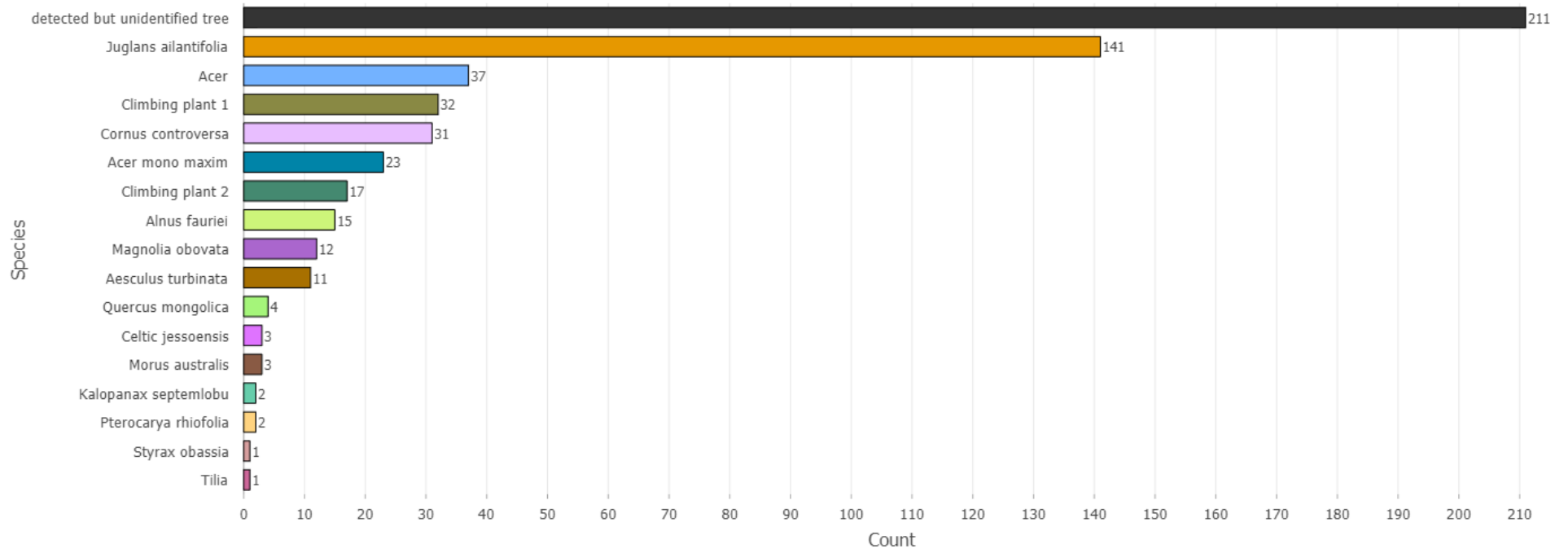
Winter survey - tree species counts site 11



Winter survey - tree species counts site 12



Winter survey - tree species counts site 13



Appendix L – Relative densities

Relative densities calculated for site 1, 3, 4, 6, 7, 8/9, 10, 11, 12 and 13 for tree species, which were identified during the field work.

Tree species	Site 1	Site 4	Site 6	Site 7	Site 3	Site 8/9	Site 10	Site 11	Site 12	Site 13
Salix jessoensis	1.23	0.00	7.56	2.77	0.47	0.63	0.34	0.00	0.00	0.00
Salix serissaefolia	0.00	29.98	3.11	0.00	0.47	0.00	0.00	0.00	0.00	0.00
Juglans ailantifolia	19.75	23.89	14.67	24.04	10.39	2.35	1.01	15.46	22.49	32.35
Pterocarya rhoifolia	23.73	11.71	12.22	10.43	0.79	0.00	1.01	9.59	12.88	2.14
Aesculus turbinata	5.08	4.92	4.44	2.98	1.26	0.00	14.43	8.61	12.45	6.15
Magnolia obovata	3.70	0.00	2.00	0.00	5.51	3.29	1.01	0.78	1.53	5.61
Phelledendron amurense	2.61	0.00	0.44	0.21	0.00	0.00	0.00	0.39	0.00	0.00
Robinia Pseudoacacia	2.88	2.58	6.22	4.26	0.00	0.16	0.67	0.39	0.22	0.00
Quercus mongolica	3.98	3.51	2.44	3.40	10.55	16.43	25.50	0.20	5.02	1.34
Fagus Crenata	0.00	0.00	1.56	0.43	7.40	10.33	13.76	0.00	0.00	0.00
Cornus Controversa	3.98	0.94	4.22	1.70	2.83	0.63	0.00	3.72	6.11	10.16
Weigela hortensis	0.41	0.23	0.67	8.51	0.00	0.00	0.00	1.17	0.44	0.00
Alnus fauriei	4.39	0.23	2.89	15.53	5.98	0.63	0.00	0.20	0.00	8.02
Ilex geniculata	0.00	0.00	0.00	0.00	4.57	0.00	0.00	0.00	0.00	0.00
Carpinus cordata	0.96	0.23	0.00	0.21	0.16	2.03	0.00	0.20	2.84	1.07
Sorbus sambucifolia	0.00	3.75	0.00	0.00	0.00	0.00	0.00	0.00	0.00	0.00
Sorbus alnifolia	0.00	0.70	4.44	0.00	0.00	0.00	0.00	4.89	1.09	0.00
Styrax obassia	3.02	5.39	2.00	0.85	3.78	5.63	0.00	0.00	2.40	2.14
Lindera umbellata	0.55	0.00	0.89	4.47	4.41	0.00	0.00	0.00	4.15	0.00
Hamamelis japonica	0.00	0.00	0.00	0.00	0.63	1.25	1.34	0.00	0.00	0.00
Cercidiphyllum magnificum	0.00	0.70	0.00	0.00	0.00	0.00	0.00	0.00	0.00	0.00
Tilia maximowiczina	7.00	0.00	0.89	0.64	1.57	0.00	0.34	0.00	1.31	0.00
Morus australis	0.00	0.94	1.33	0.21	0.00	0.00	0.00	4.11	6.11	0.80
Alnus inokumae	0.00	0.00	0.22	0.00	0.00	0.00	0.00	0.00	0.00	0.00
Castanea crenata	0.41	0.00	3.56	0.00	0.00	0.00	2.35	0.00	0.00	0.00
Corylus sieboldiana	0.27	0.00	0.00	0.00	0.47	9.70	4.03	0.20	0.22	0.00
Prunus speciosa	0.00	0.00	0.00	0.00	0.00	0.00	0.00	0.00	0.00	0.80

Prunus serrulata/grayana	1.65	0.00	0.00	0.21	1.10	4.69	3.02	0.00	0.00	0.00
Prunus salicina Lindley	0.00	0.23	0.00	0.00	0.00	0.00	0.00	0.39	0.00	0.00
Aralia elata Seemann	0.14	0.00	0.00	0.00	0.00	0.00	0.00	0.00	0.00	0.00
Acer palmatum	3.57	6.09	15.11	0.00	0.63	26.13	15.10	10.37	8.73	0.00
Acer sieboldianum	7.82	0.23	2.22	7.02	21.89	2.50	0.00	1.57	0.00	6.68
Acer japonicum	0.41	0.00	0.00	5.53	1.10	0.16	0.00	3.33	1.97	0.00
Acer mono Maxim.	0.27	1.64	2.00	1.70	1.73	0.00	12.08	0.78	2.62	6.68
Alangium planifolium	0.00	0.00	0.00	0.00	0.00	0.00	0.00	0.00	0.00	0.00
Acer pictum subsp. mono	0.00	0.00	0.00	0.00	0.00	6.10	0.00	0.00	0.00	0.00
Acer rufinerve Sieb. et Zucc.	0.41	0.00	0.00	0.00	0.00	0.00	0.00	0.00	0.00	0.00
Acer buergerianum	0.14	0.00	0.00	0.00	0.00	0.00	0.00	0.00	0.00	0.00
Larix kampferi	1.37	1.87	0.00	0.00	6.30	0.00	0.00	0.20	0.00	0.00
Ginkgo biloba	0.14	0.00	0.00	0.00	0.00	0.00	0.00	0.00	0.00	0.00
Fraxinus lanuginosa	0.00	0.00	0.00	0.00	0.63	0.00	0.00	0.00	0.00	0.00
Fraxinus platyoda	0.00	0.00	0.00	0.00	0.16	0.00	0.00	0.00	0.00	0.00
Celtis jessoensis	0.00	0.00	0.44	0.00	3.31	0.31	0.00	0.39	1.09	0.80
Betula schmidtii	0.00	0.00	0.00	0.00	0.00	0.47	0.00	0.00	0.00	0.00
Cryptomeria japonica	0.00	0.00	0.00	0.00	0.00	0.47	0.34	0.00	0.00	0.00
Betula maximowicziana	0.00	0.00	0.00	0.00	0.00	0.00	0.67	0.00	0.00	0.00
Betula corylifolia	0.00	0.00	1.33	0.00	0.00	0.00	0.00	0.00	0.00	0.00
Sorbus japonica	0.00	0.00	0.00	0.00	0.00	0.00	0.00	0.00	0.00	0.53
Camellia japonica	0.00	0.00	0.00	0.00	0.00	0.00	0.00	16.63	0.00	13.37
Acer disyllum	0.00	0.00	0.00	0.00	0.00	0.00	0.00	0.00	0.00	0.27
Tilia japonica	0.00	0.00	0.00	0.00	0.00	0.31	1.01	0.20	0.00	0.53
Alnus wirsata	0.00	0.00	0.00	0.21	0.00	0.00	0.00	0.00	0.00	0.00
Quercus detala	0.00	0.00	0.00	0.21	0.00	0.00	0.00	0.00	0.00	0.00
Wisteria floribunda	0.00	0.00	0.00	0.43	0.00	1.25	0.00	0.39	0.00	0.00
Fagus Japonica	0.00	0.00	0.00	0.21	0.00	0.00	0.00	0.00	0.00	0.00
Aleurites fordii/ Vernicia fordii	0.00	0.00	0.00	0.21	0.00	0.00	0.00	0.00	0.00	0.00
Platycarya strobilacea	0.00	0.00	0.00	0.85	0.00	0.00	0.00	0.00	0.00	0.00
Abizia Julibrissin	0.00	0.00	0.00	0.64	0.00	0.00	0.00	0.00	0.00	0.00
Alnus pendula	0.00	0.00	0.00	0.00	0.00	0.00	0.00	0.39	0.00	0.00

Symplocos chinesis	0.00	0.00	0.00	0.00	0.00	0.00	0.00	0.98	0.44	0.00
Acer amonesum	0.00	0.00	0.00	0.00	0.00	0.00	0.00	9.20	0.00	0.00
Pterostyrax corymbosa	0.00	0.00	0.00	0.00	0.00	0.00	1.01	0.00	0.00	0.00
Acer nippon	0.00	0.00	0.22	0.00	0.00	0.00	0.00	0.00	0.00	0.00
Alnus japonica	0.00	0.00	0.00	0.21	0.00	0.00	0.00	0.00	0.00	0.00
Vaccinium oldhamii	0.00	0.00	0.00	0.00	0.00	0.00	0.00	1.37	0.00	0.00
Picea abies	0.00	0.00	1.11	0.00	0.00	0.00	0.00	0.00	0.00	0.00
Euonymus sieboldianus	0.00	0.00	0.00	0.00	0.00	4.54	0.00	0.00	0.00	0.00
Clethra barvinervis	0.00	0.00	0.00	0.21	0.00	0.00	0.00	2.74	0.00	0.27
Kalopanax Septemlobus	0.00	0.00	0.00	0.00	0.00	0.00	0.00	0.00	0.00	0.27
Unknown	0.14	0.23	1.78	1.70	1.89	0.00	1.01	1.17	5.90	0.00
Sum	100. 0	100.0	100.0	100.0	100.0	100.0	100.0	100.0	100.0	100.0

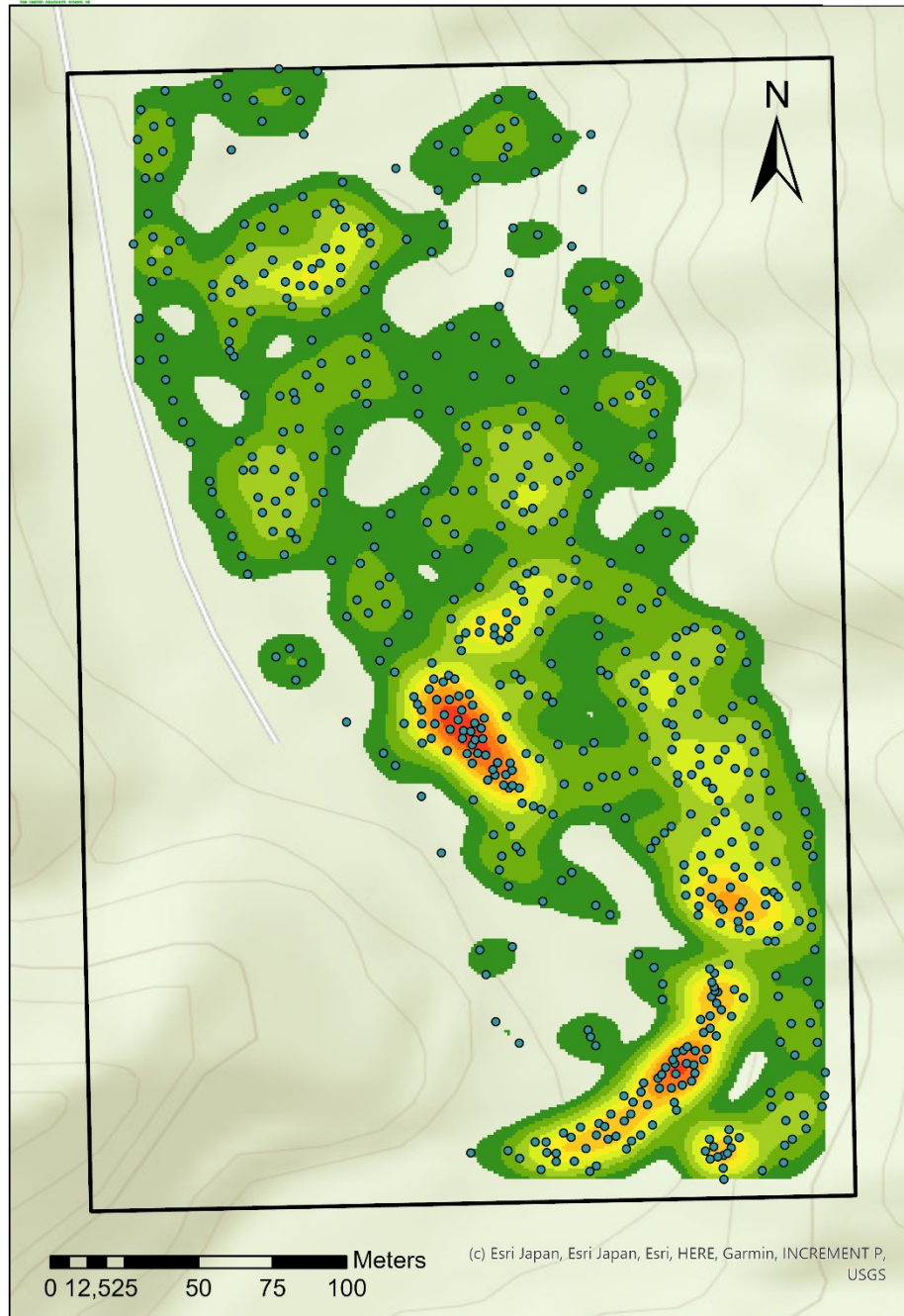
Appendix M – Results image analysis

There are maps contained from density, count and hot spot analysis. Analyses were performed with ArcGIS pro.

Part 1: Density maps

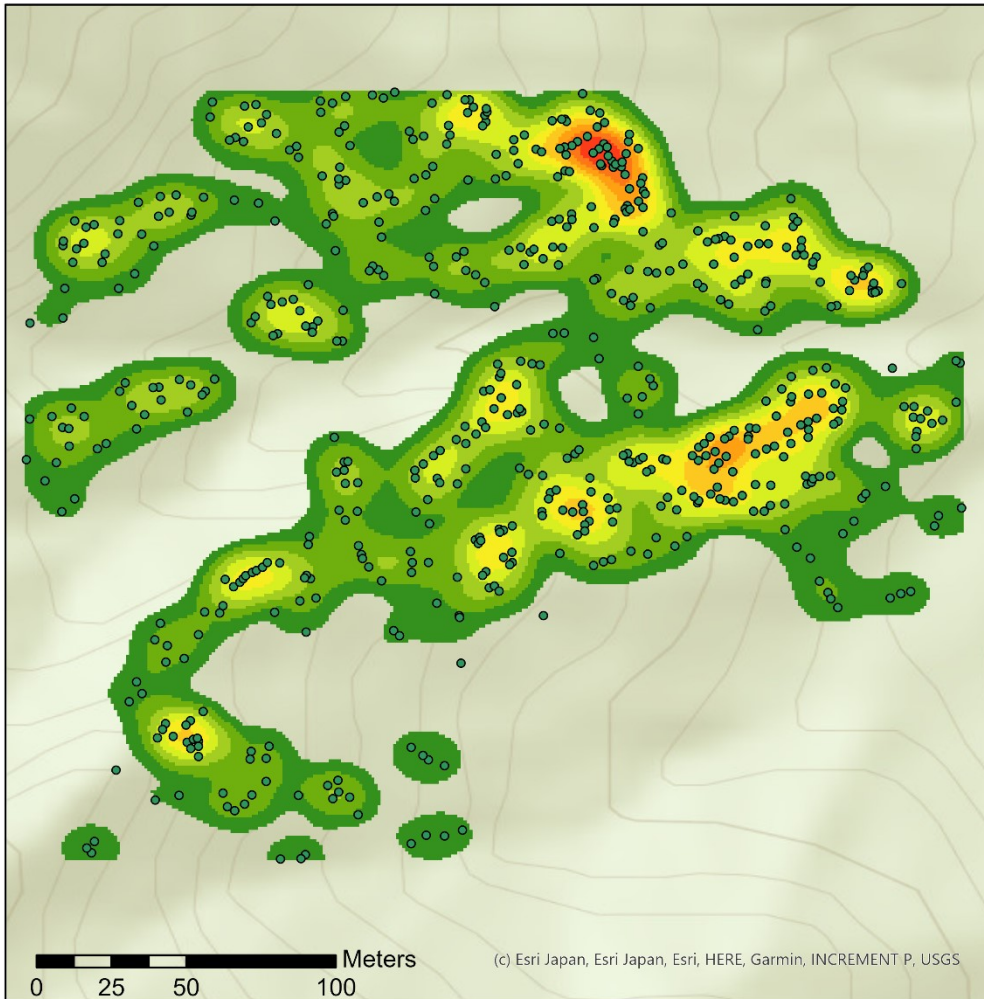


Density map site 1
by Sarah Kentsch



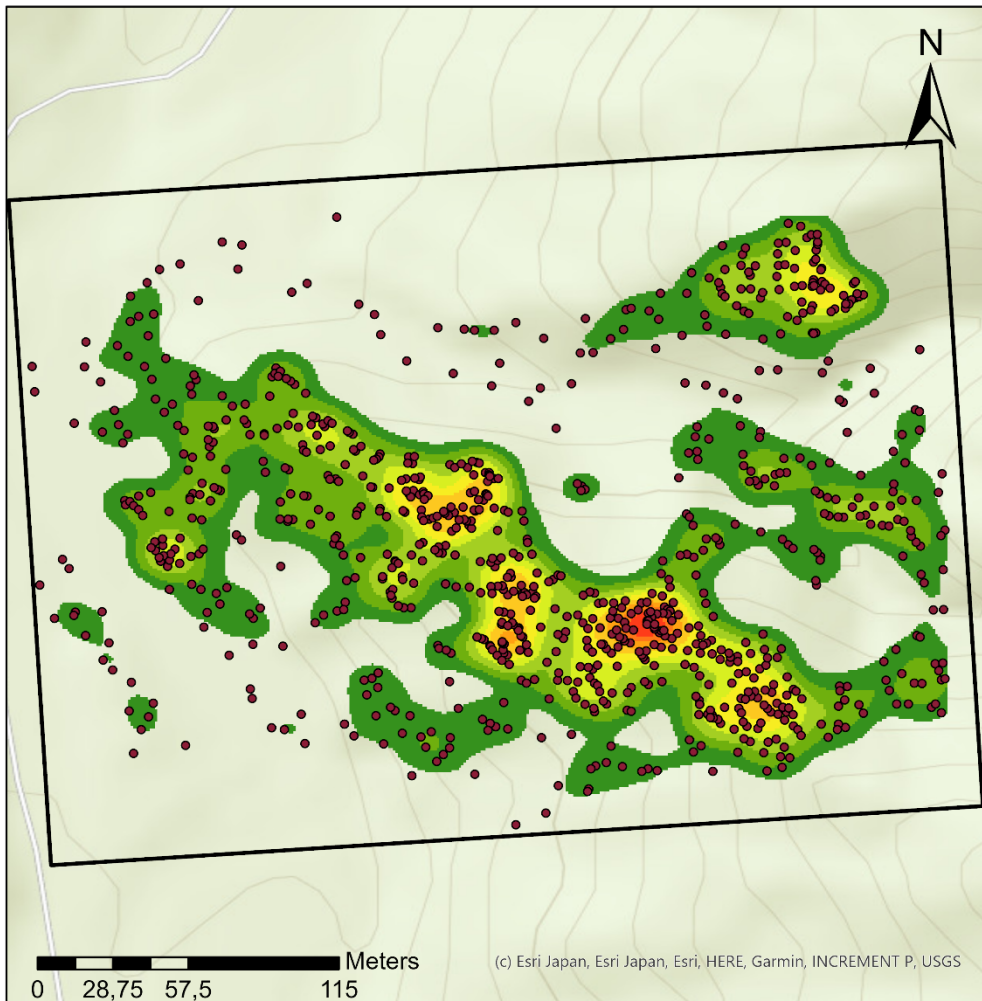


Density map site 2 by Sarah Kentsch





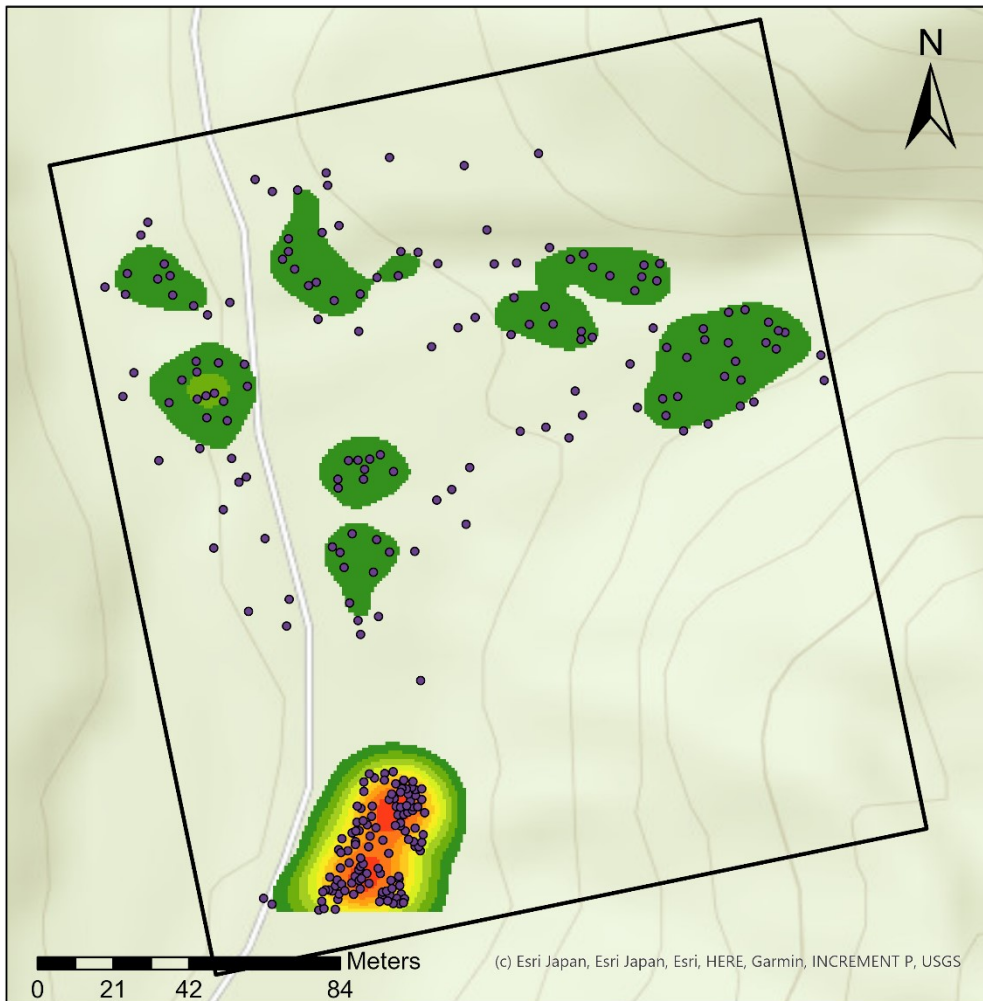
Density map site 3 by Sarah Kentsch



- WinterPointsS3
- Site3



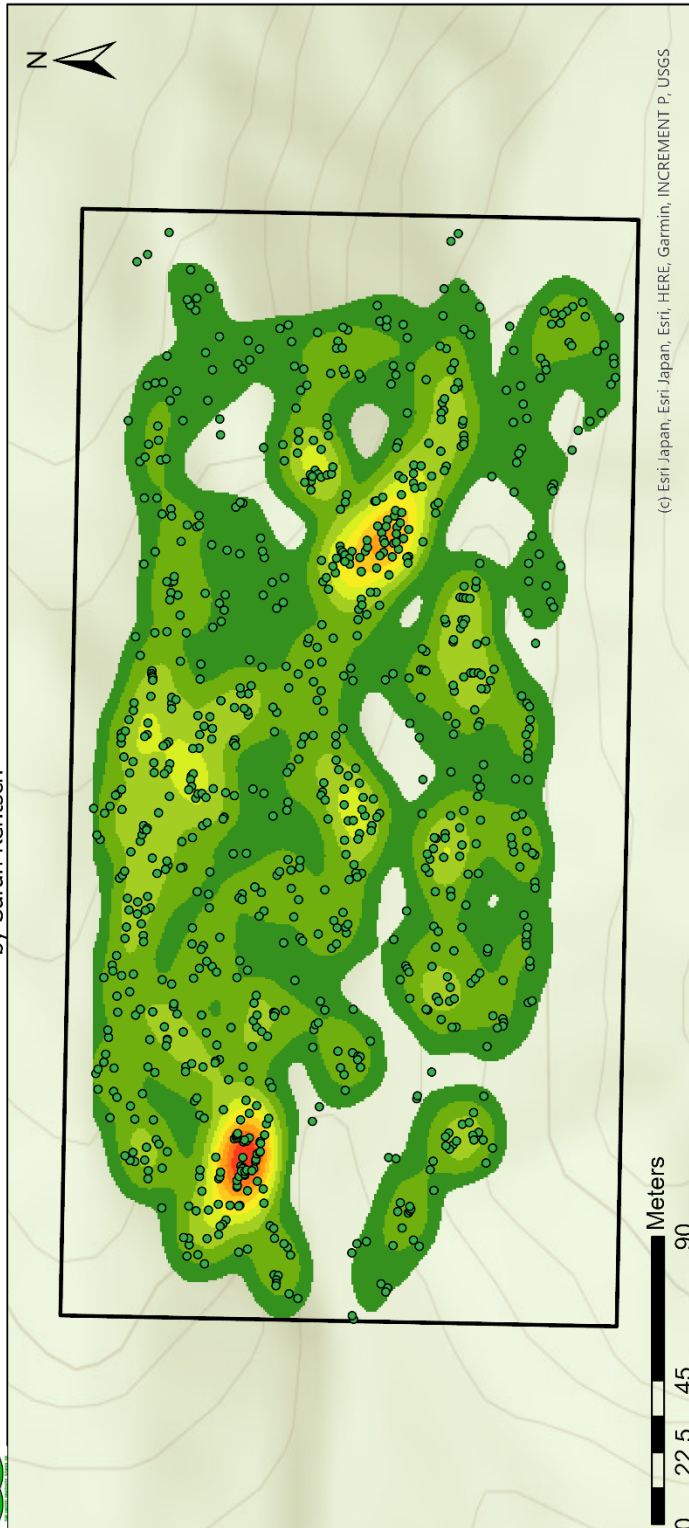
Density map site 4 by Sarah Kentsch



- WinterPointsS4
- Site4



Density map site 5 by Sarah Kentsch

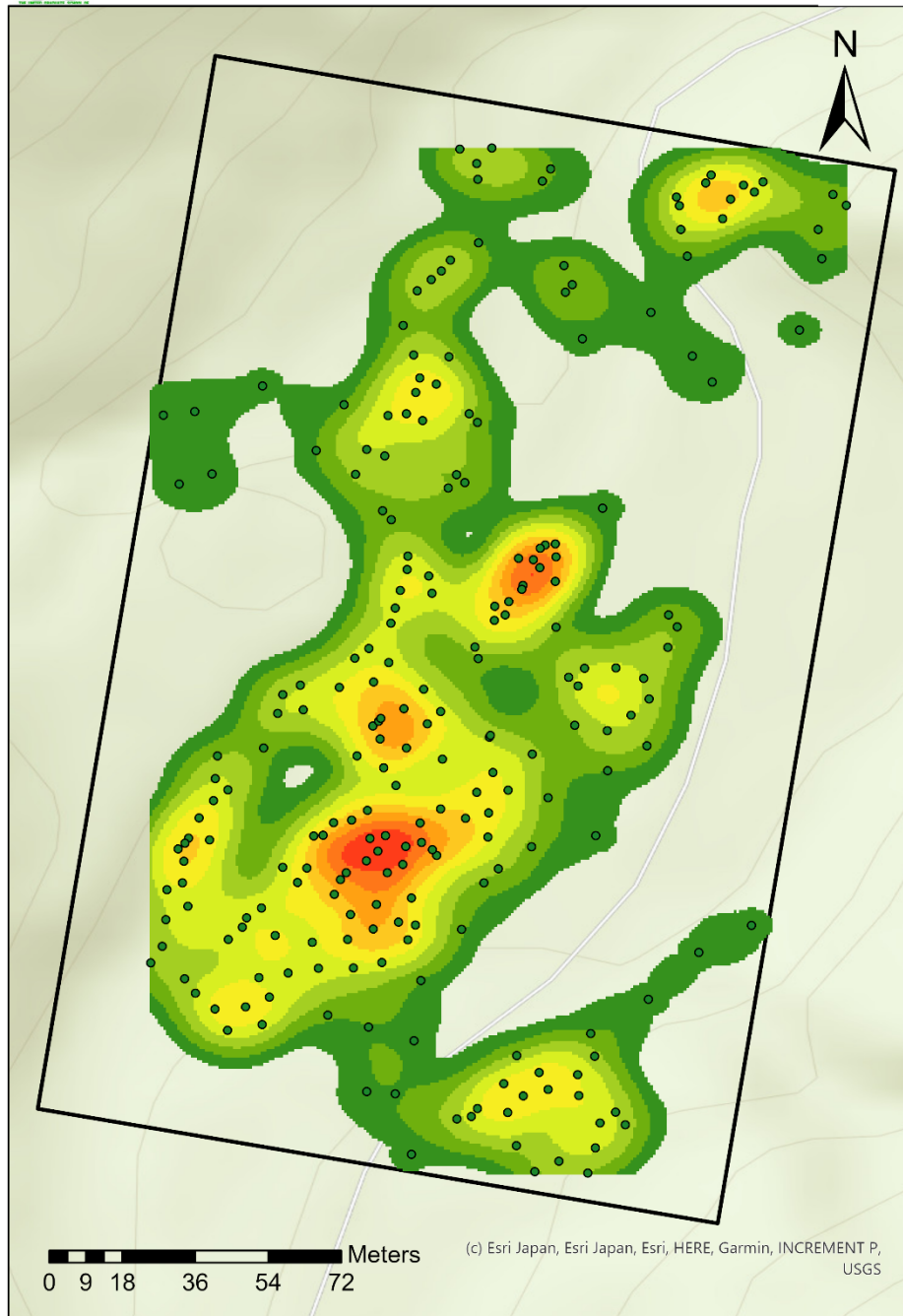


(c) Esri Japan, Esri Japan, Esri, HERE, Garmin, INCREMENT P, USGS

- WinterPointsS5
- KernelS5_16
- VALUE
- 0,000001 - 0,012546
- 0,012547 - 0,025092
- 0,025093 - 0,037638
- 0,037639 - 0,050183
- 0,050184 - 0,062729
- 0,06273 - 0,075275
- 0,075276 - 0,087821
- 0,087822 - 0,100367
- 0,100368 - 0,112913
- 0,112914 - 0,125458
- Site



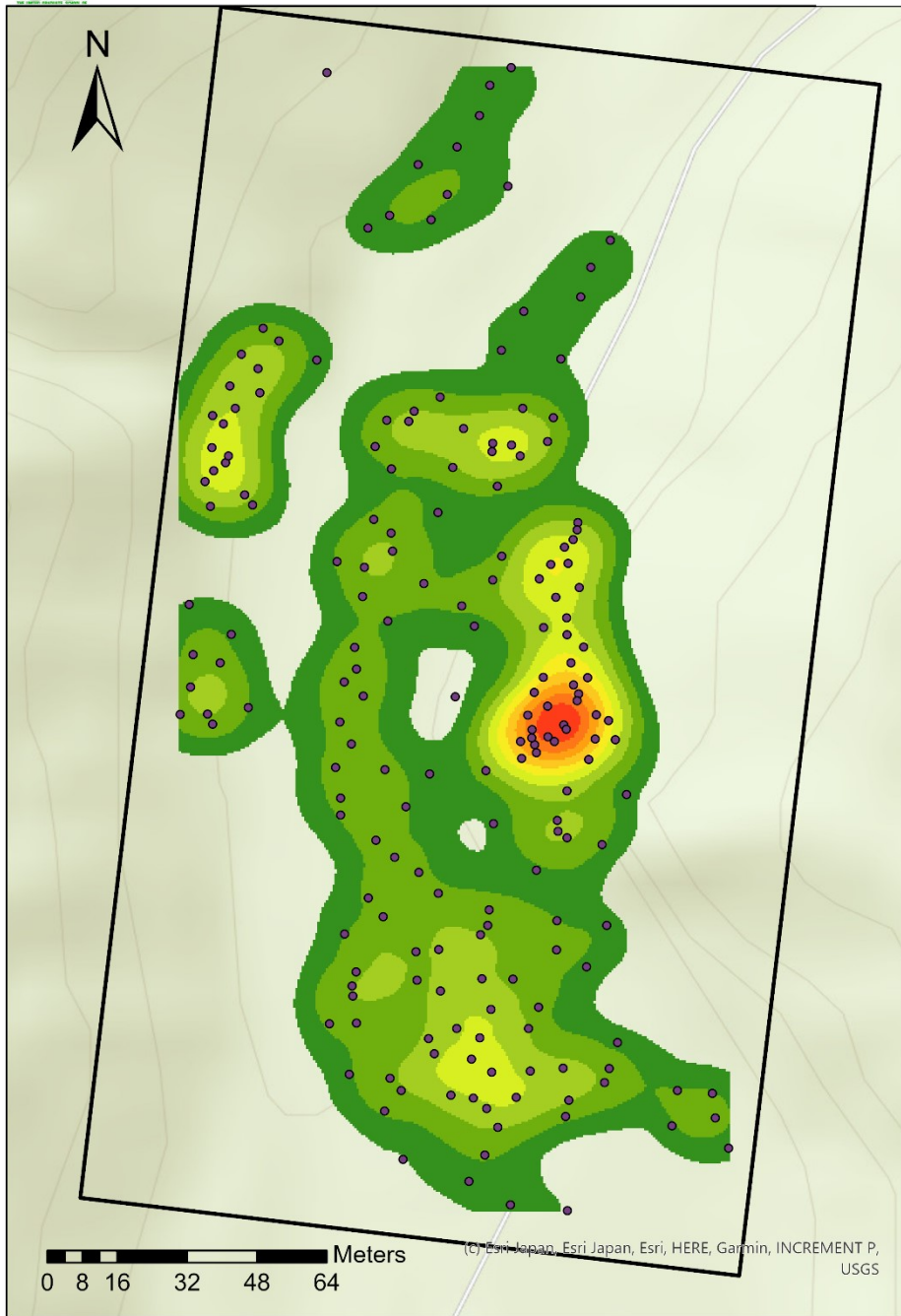
Density map site 6 by Sarah Kentsch



- WinterTreesS6
- Site6



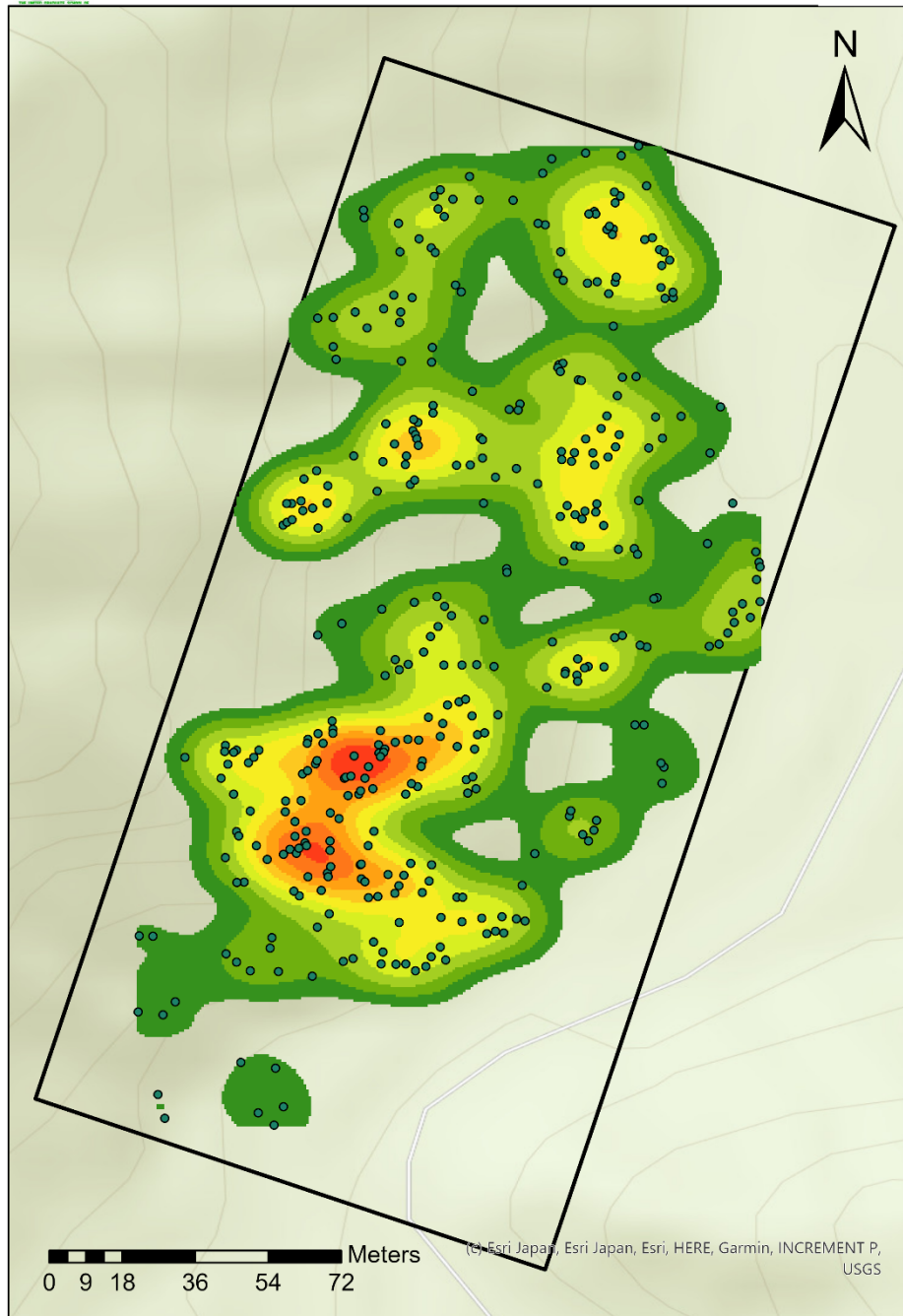
Density map site 7 by Sarah Kentsch



- WinterPointsS7
- ▭ Site7



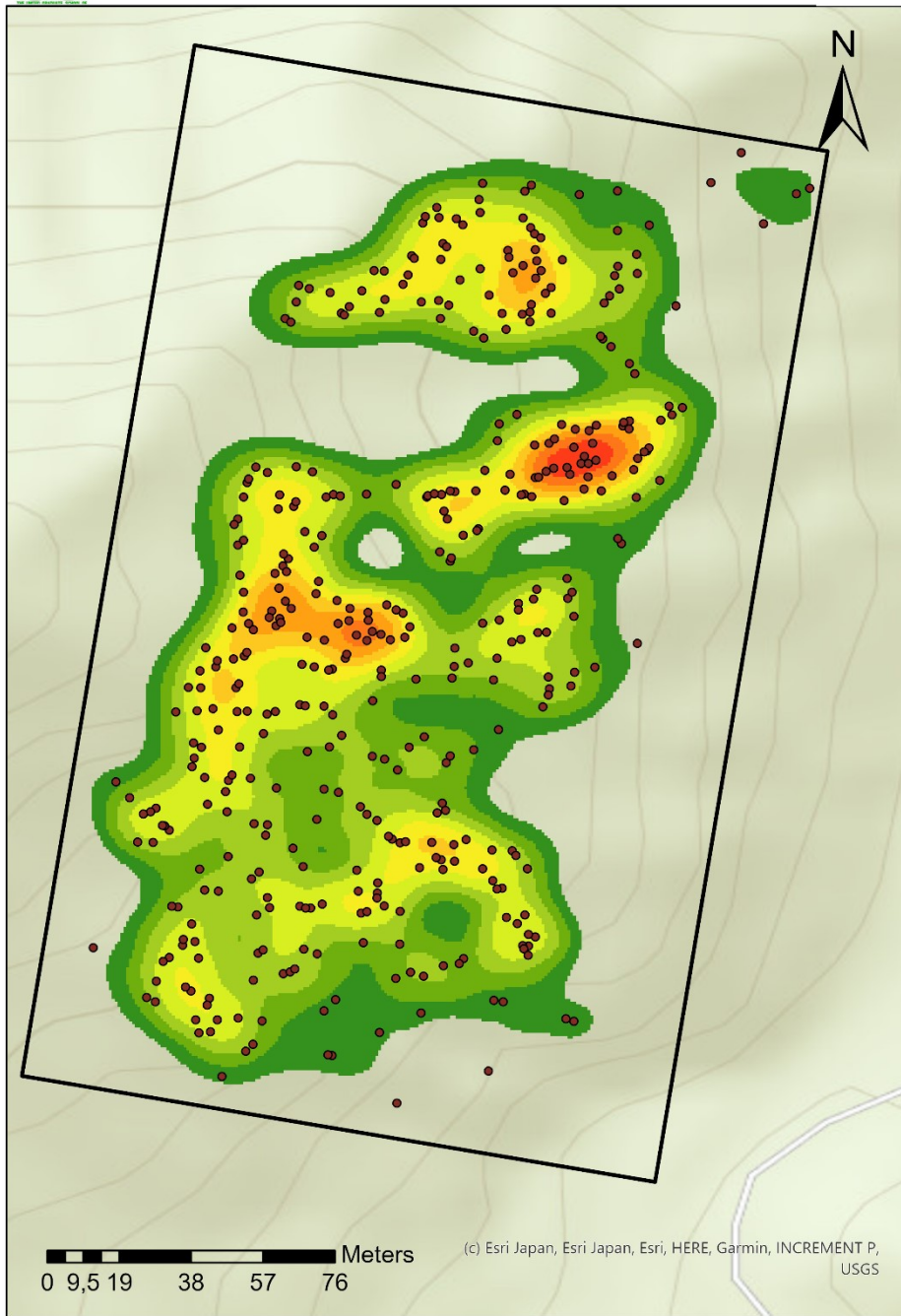
Density map site 8 by Sarah Kentsch



- WinterPointsS8
- ▭ Site8



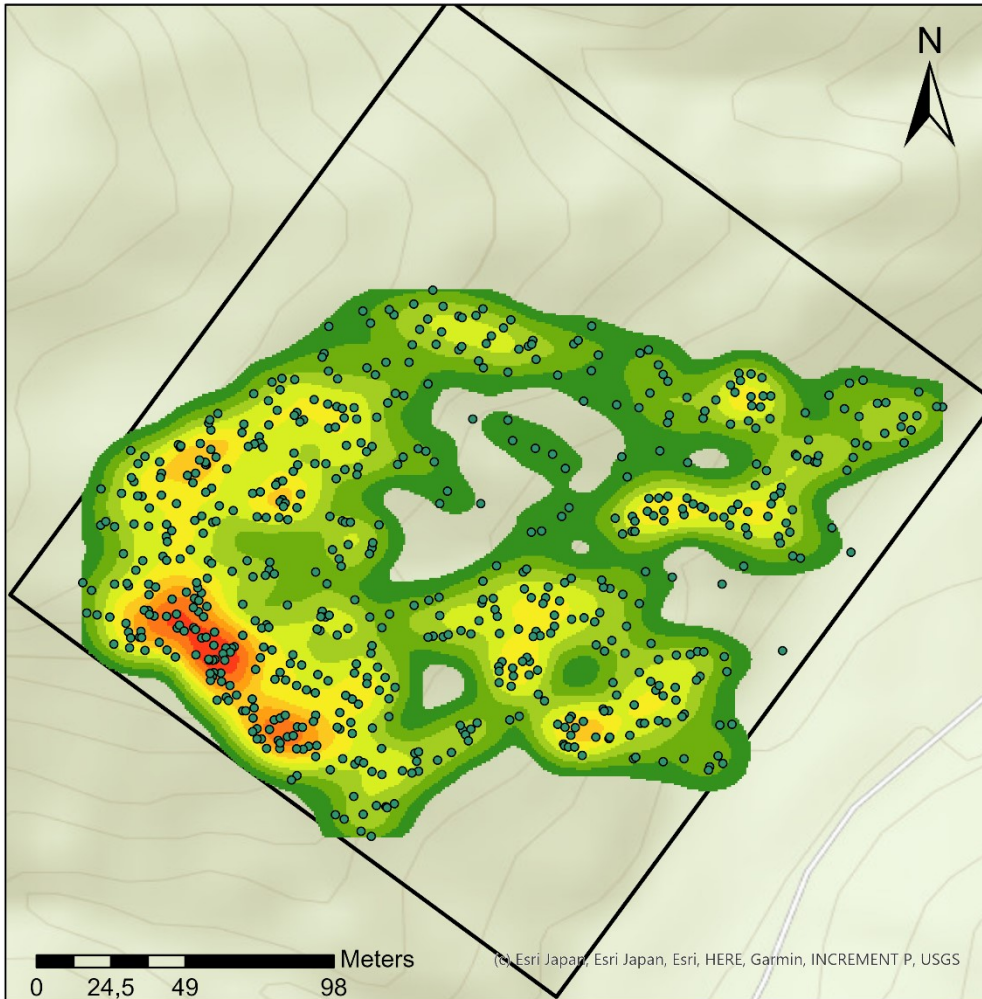
Density map site 9 by Sarah Kentsch



- WinterPointsS9
- ▭ Site9



Density map site 10 by Sarah Kentsch

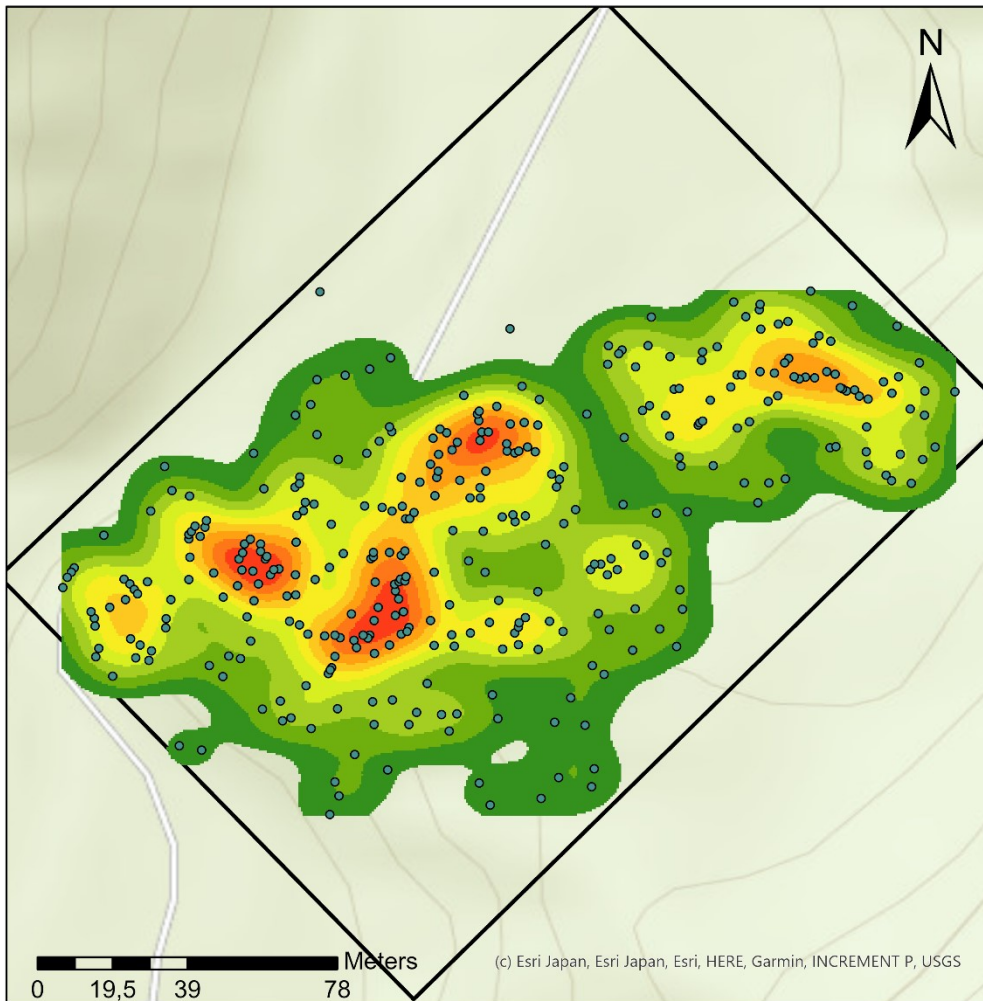


- WinterPointsS10
- Site10



Density map site 11

by Sarah Kentsch

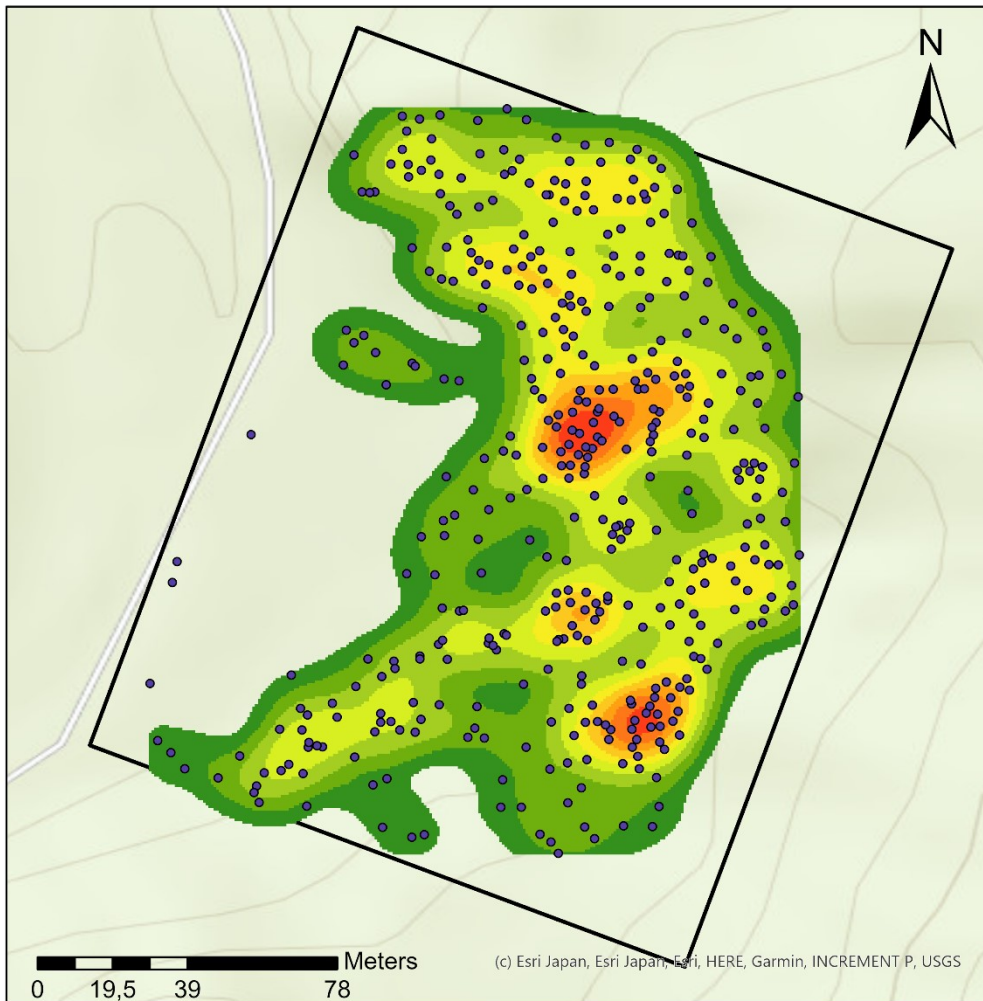


- WinterPointsS11
- Site11



Density map site 12

by Sarah Kentsch

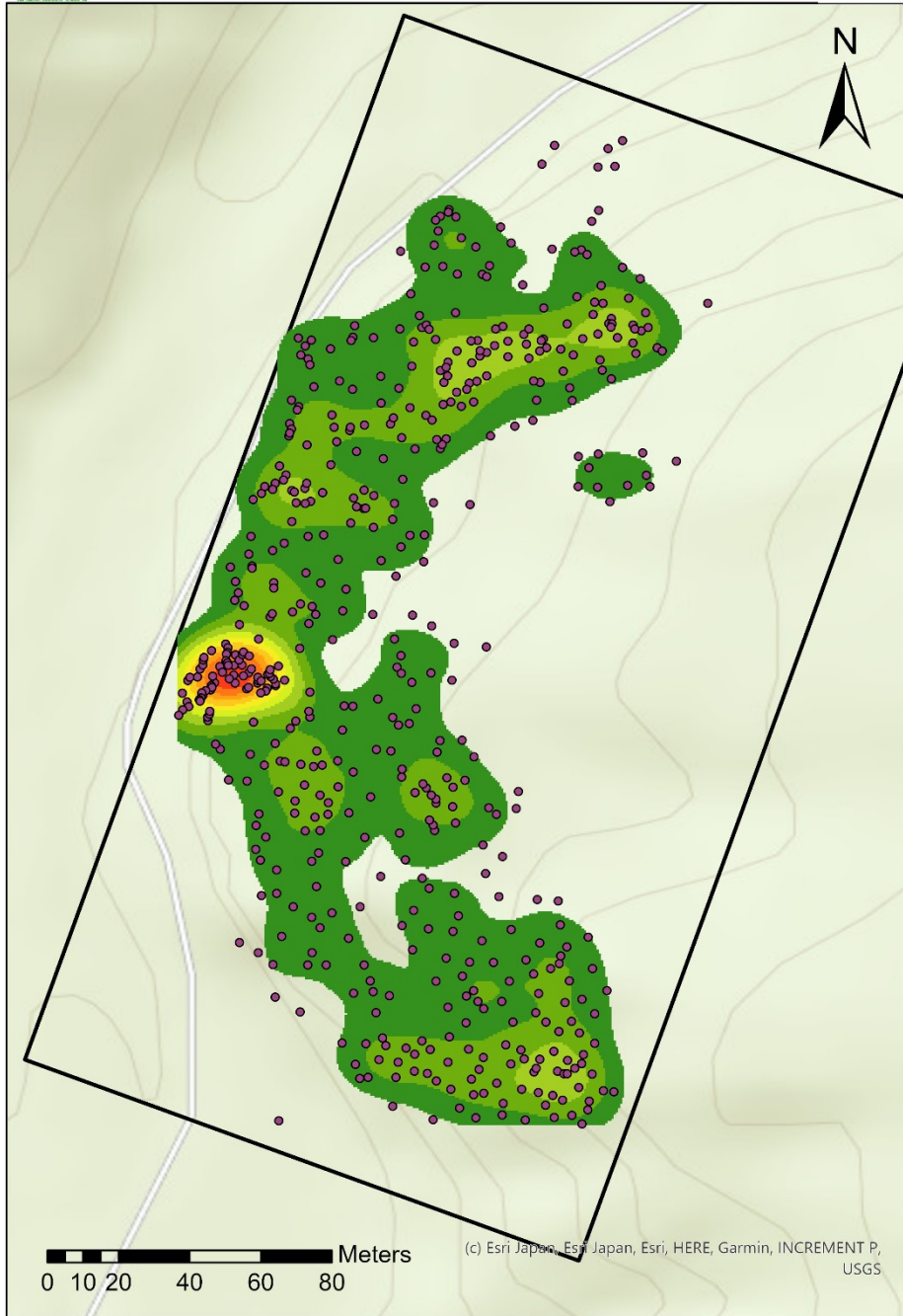


- WinterTreesS12
- Site12



Density map site 13

by Sarah Kentsch

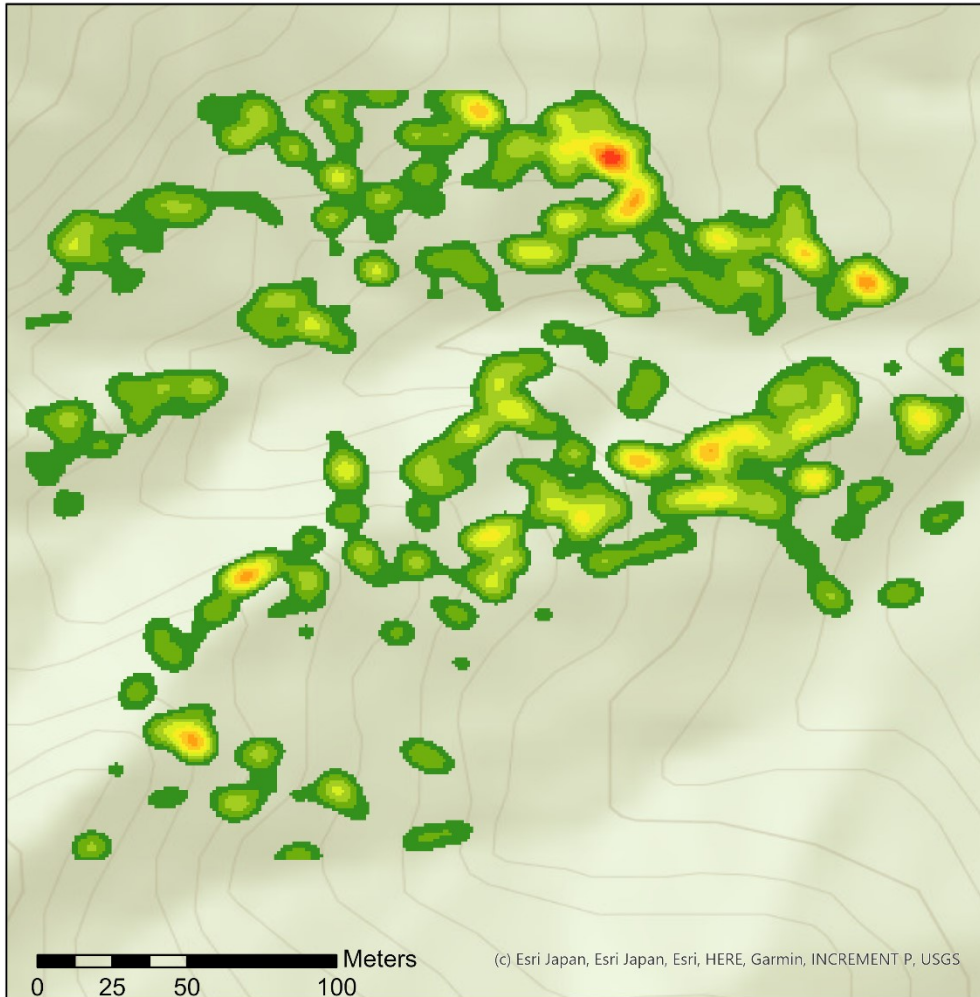


- WinterPointsS13
- ▭ Site13

Part 2: Density lower radius (6m)



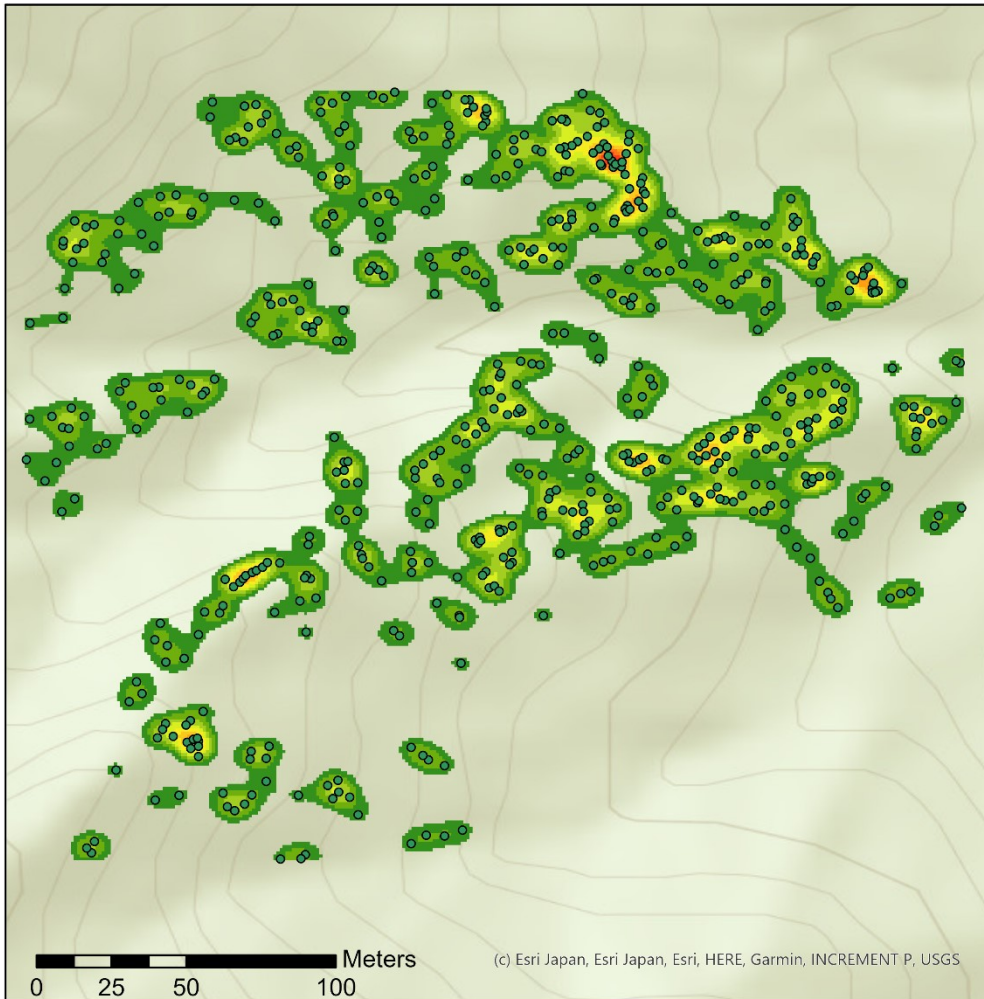
Density map site 2
by Sarah Kentsch





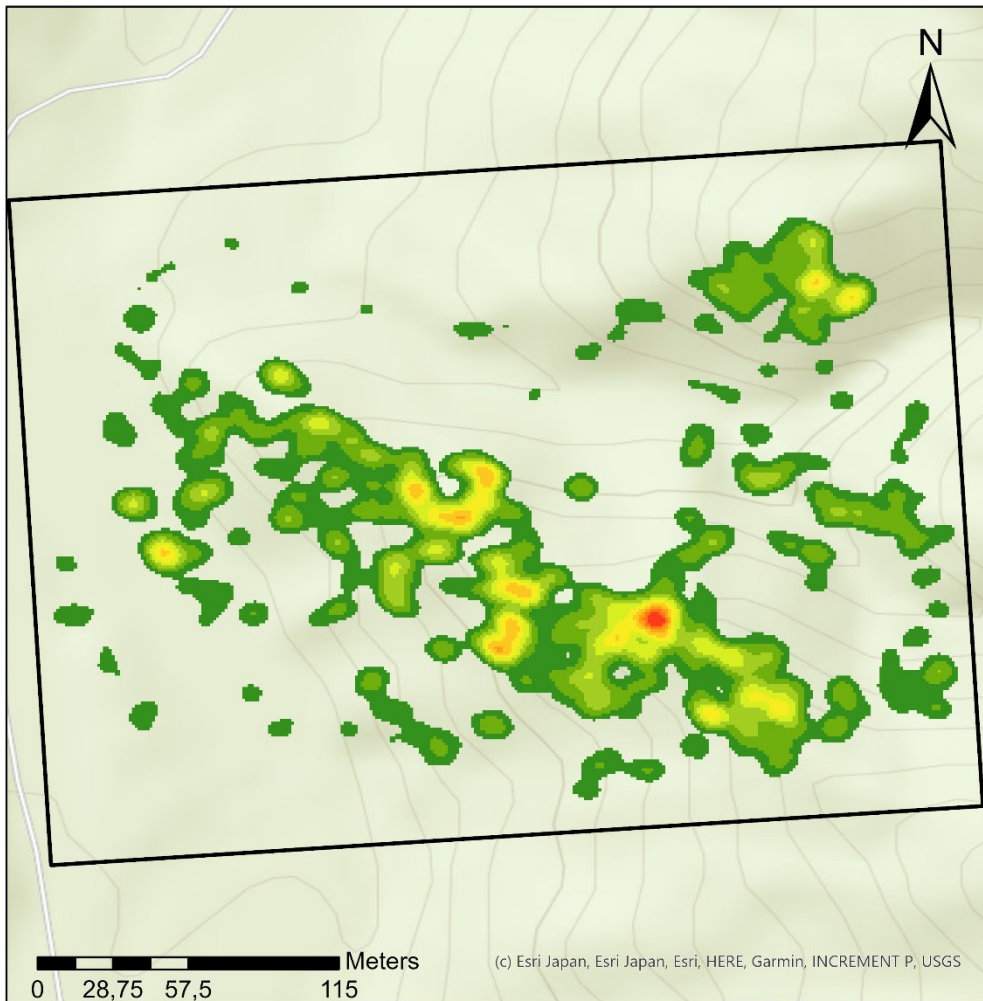
Density map site 2

by Sarah Kentsch





Density map site 3 by Sarah Kentsch

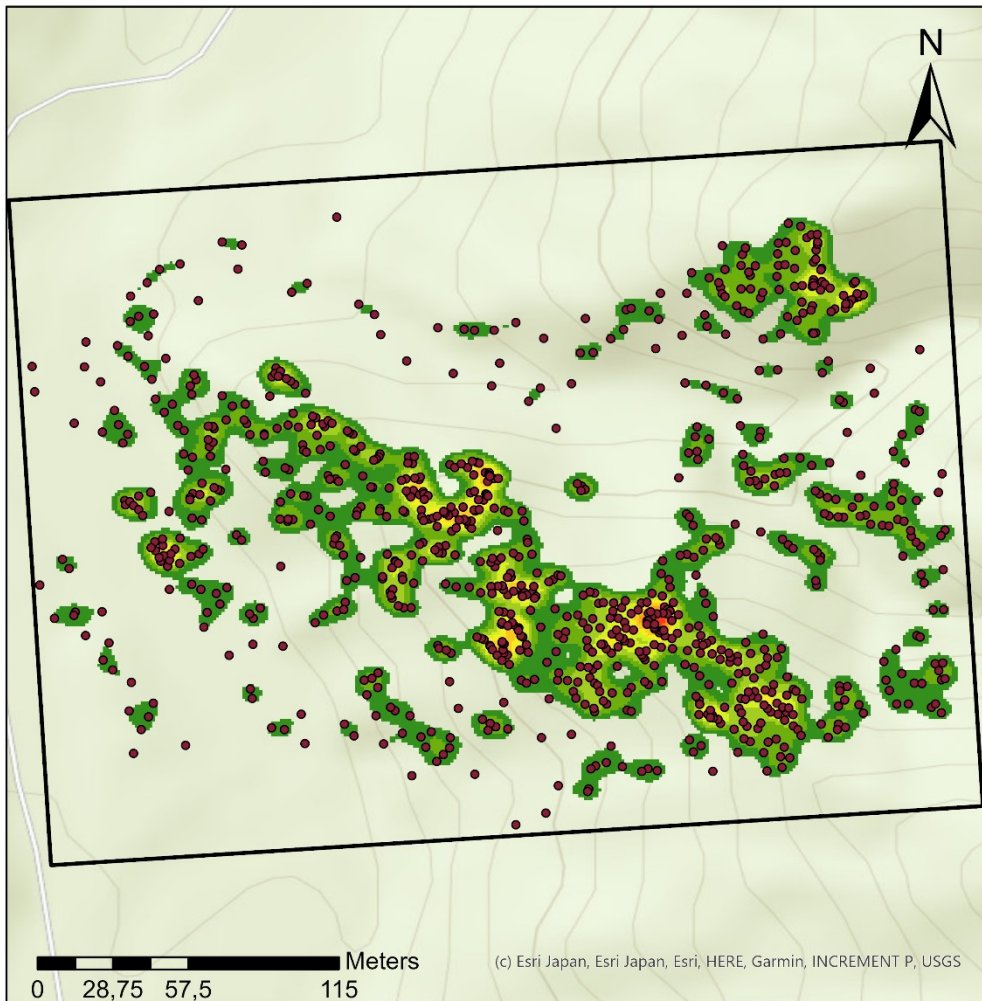


(c) Esri Japan, Esri Japan, Esri, HERE, Garmin, INCREMENT P, USGS

Site3



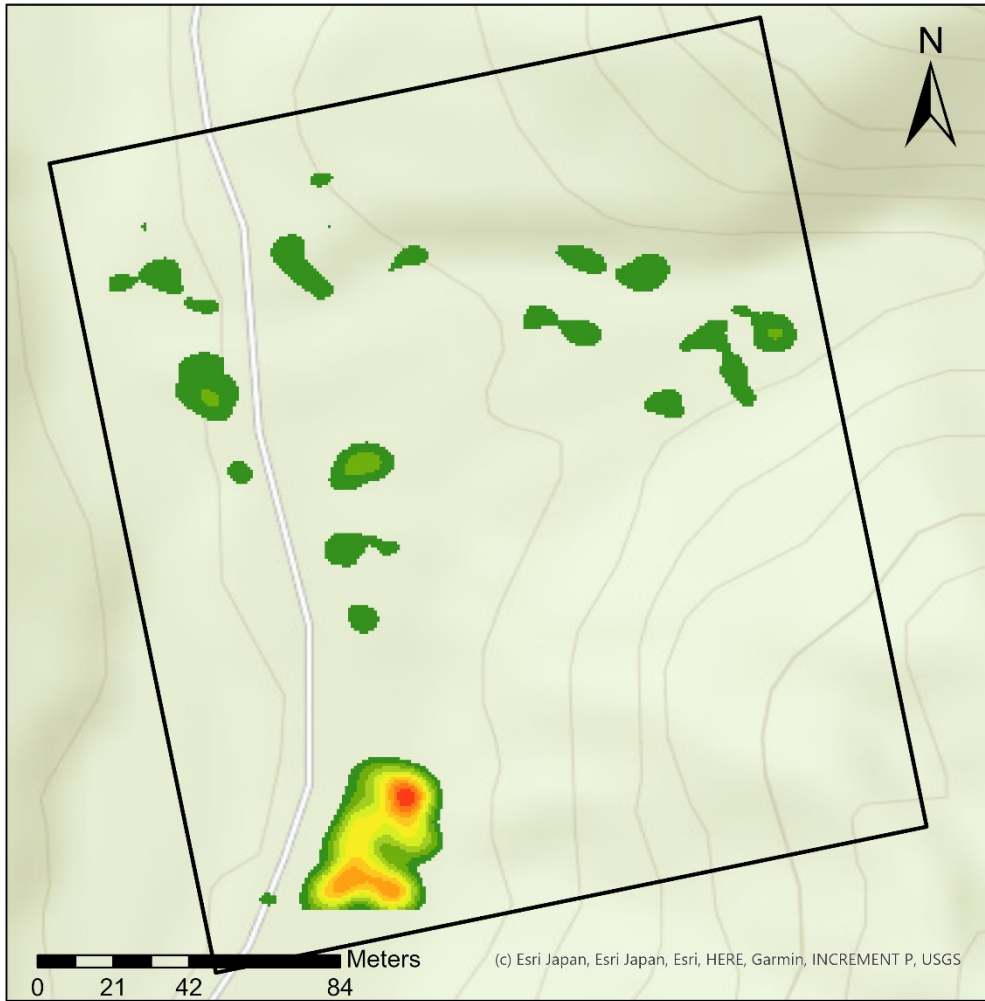
Density map site 3 by Sarah Kentsch



- WinterPointsS3
- Site3



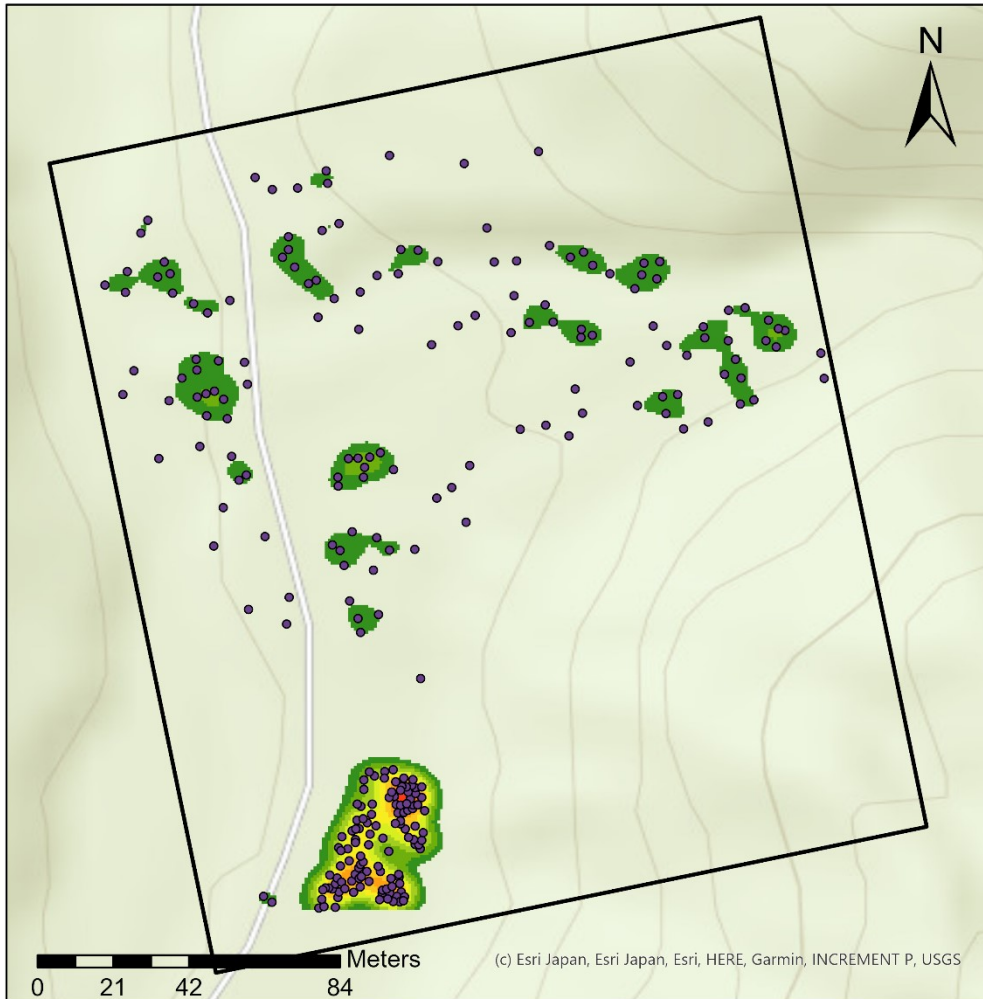
Density map site 4 by Sarah Kentsch



Site4



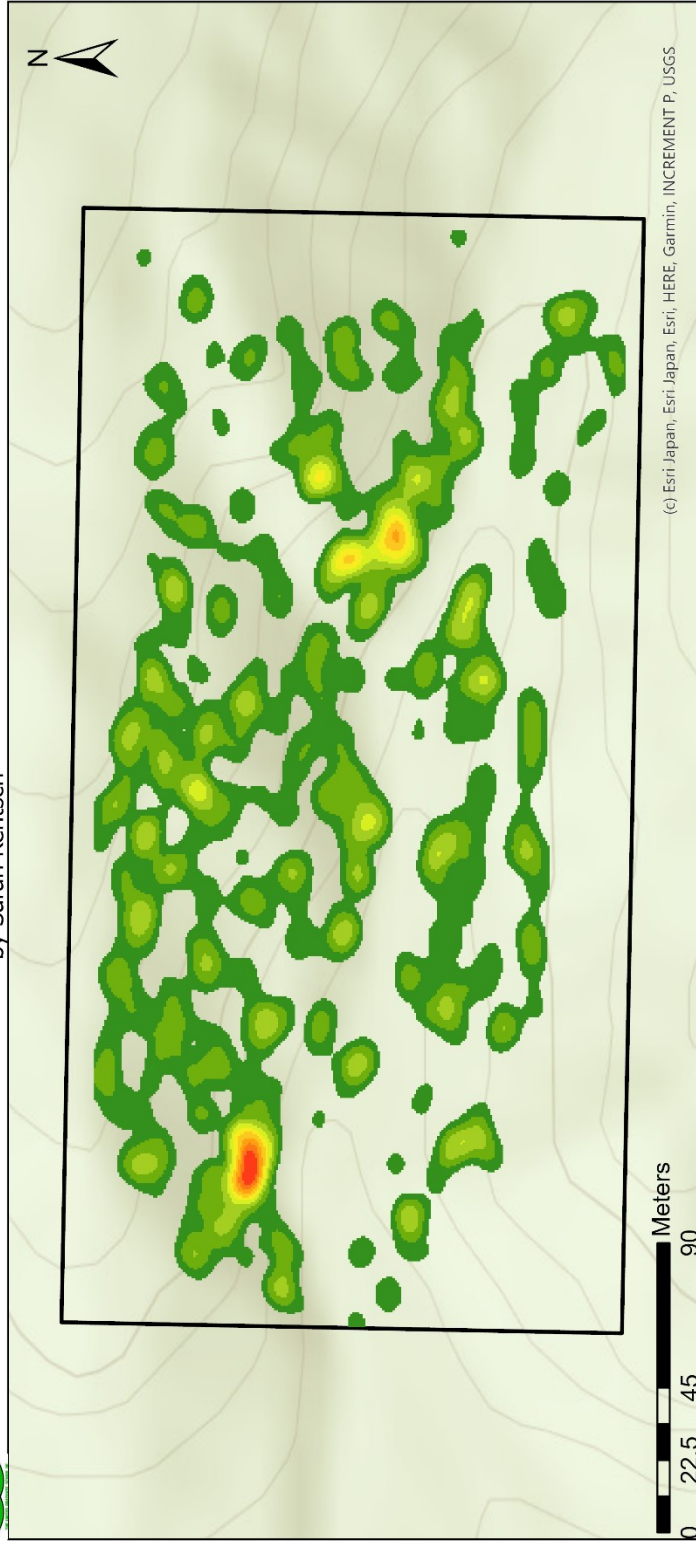
Density map site 4 by Sarah Kentsch



- WinterPointsS4
- Site4



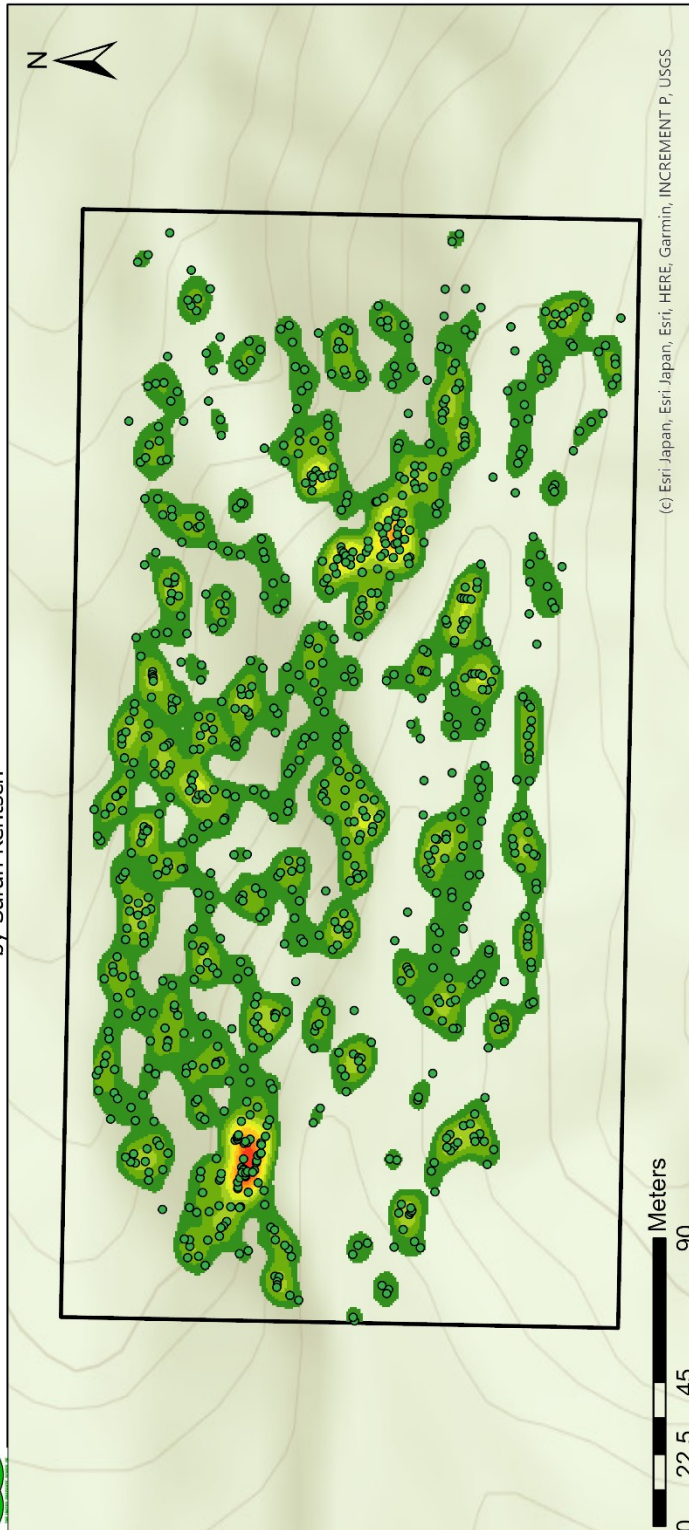
Density map site 5 by Sarah Kentsch



KernelS5	VALUE
0,045644 - 0,068464	0,000001 - 0,022821
0,068465 - 0,091286	0,022822 - 0,045643
0,091287 - 0,114107	0,045644 - 0,068464
0,114108 - 0,136929	0,068465 - 0,091286
0,13693 - 0,15975	0,091287 - 0,114107
0,159751 - 0,182572	0,114108 - 0,136929
0,182573 - 0,205393	0,13693 - 0,15975
0,205394 - 0,228215	0,159751 - 0,182572
Site5	0,182573 - 0,205393
	0,205394 - 0,228215



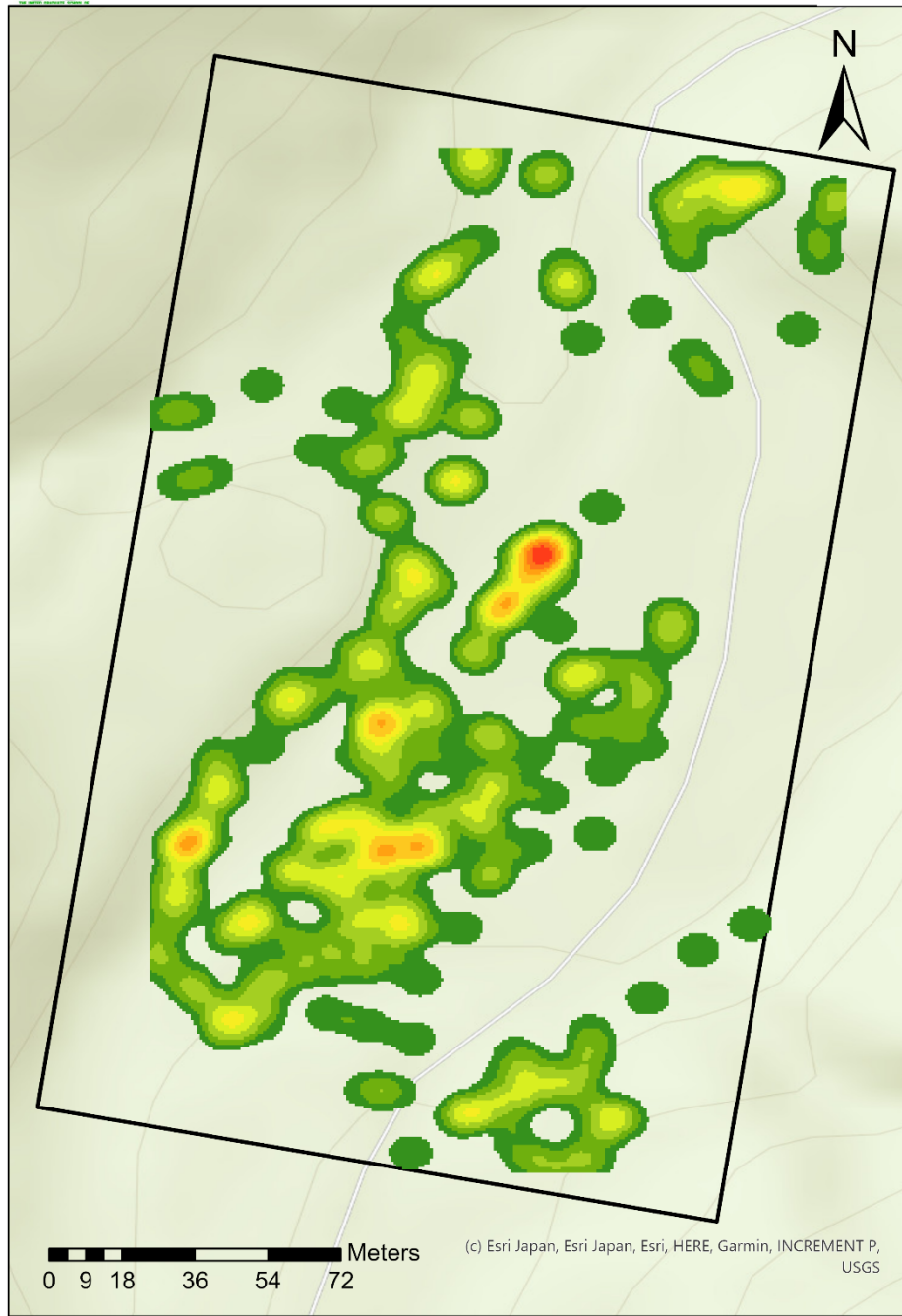
Density map site 5
by Sarah Kentsch



- WinterPointsS5
- KernelS5
- VALUE
- 0,000001 - 0,022821
- 0,022822 - 0,045643
- 0,045644 - 0,068464
- 0,068465 - 0,091286
- 0,091287 - 0,114107
- 0,114108 - 0,136929
- 0,13693 - 0,15975
- 0,159751 - 0,182572
- 0,182573 - 0,205393
- 0,205394 - 0,228215
- Site

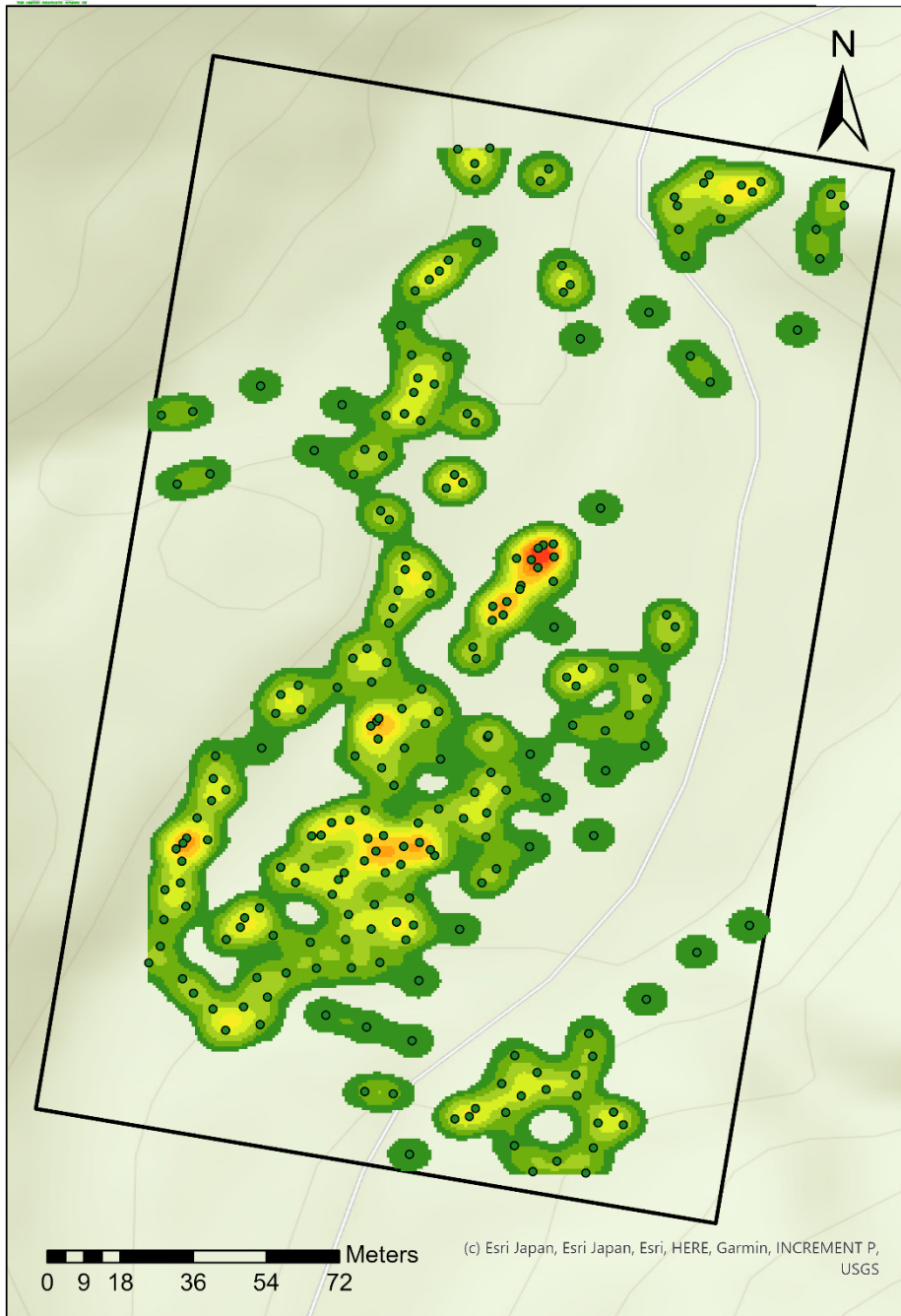


Density map site 6 by Sarah Kentsch





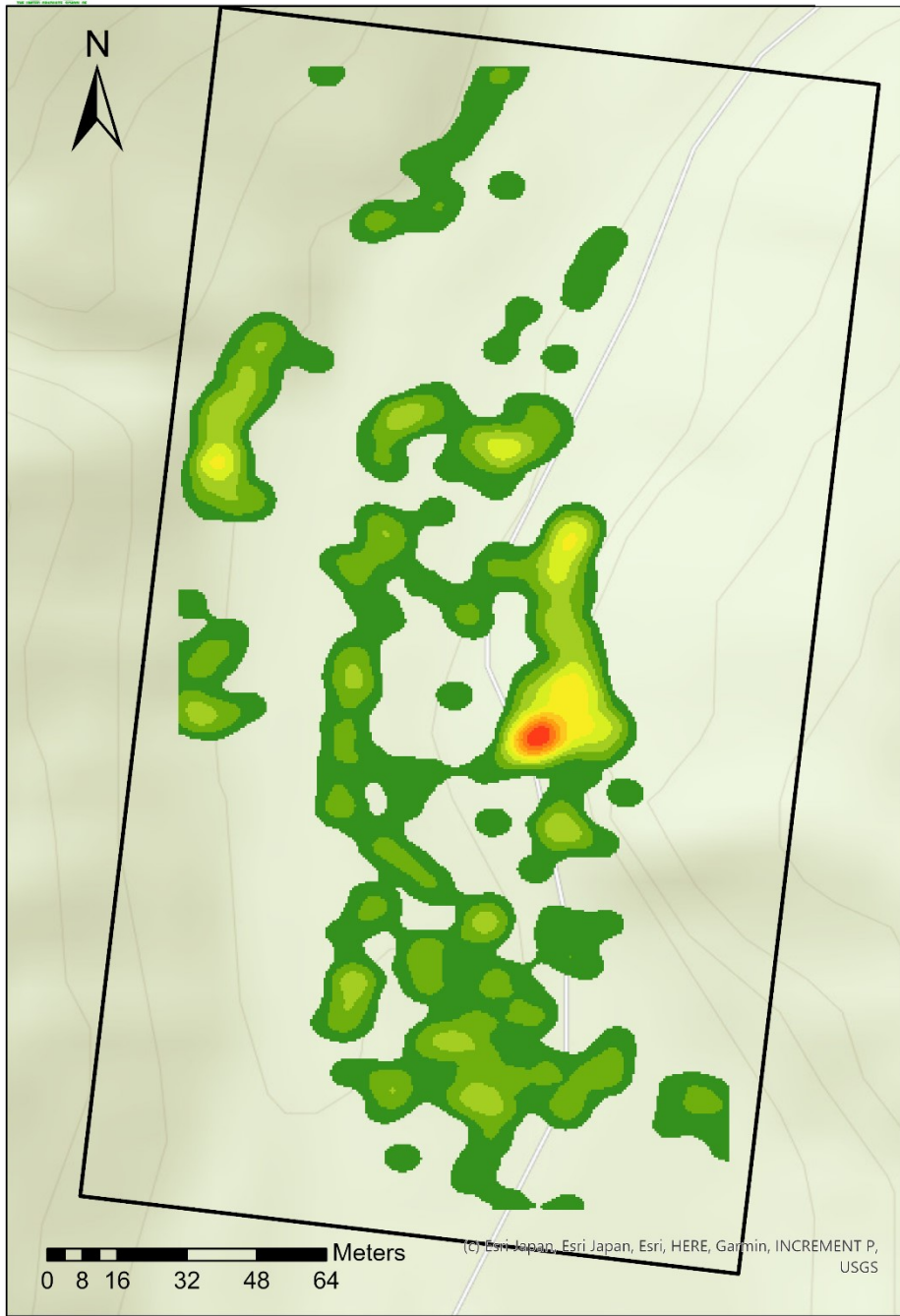
Density map site 6 by Sarah Kentsch



- WinterTreesS6
- ▭ Site6

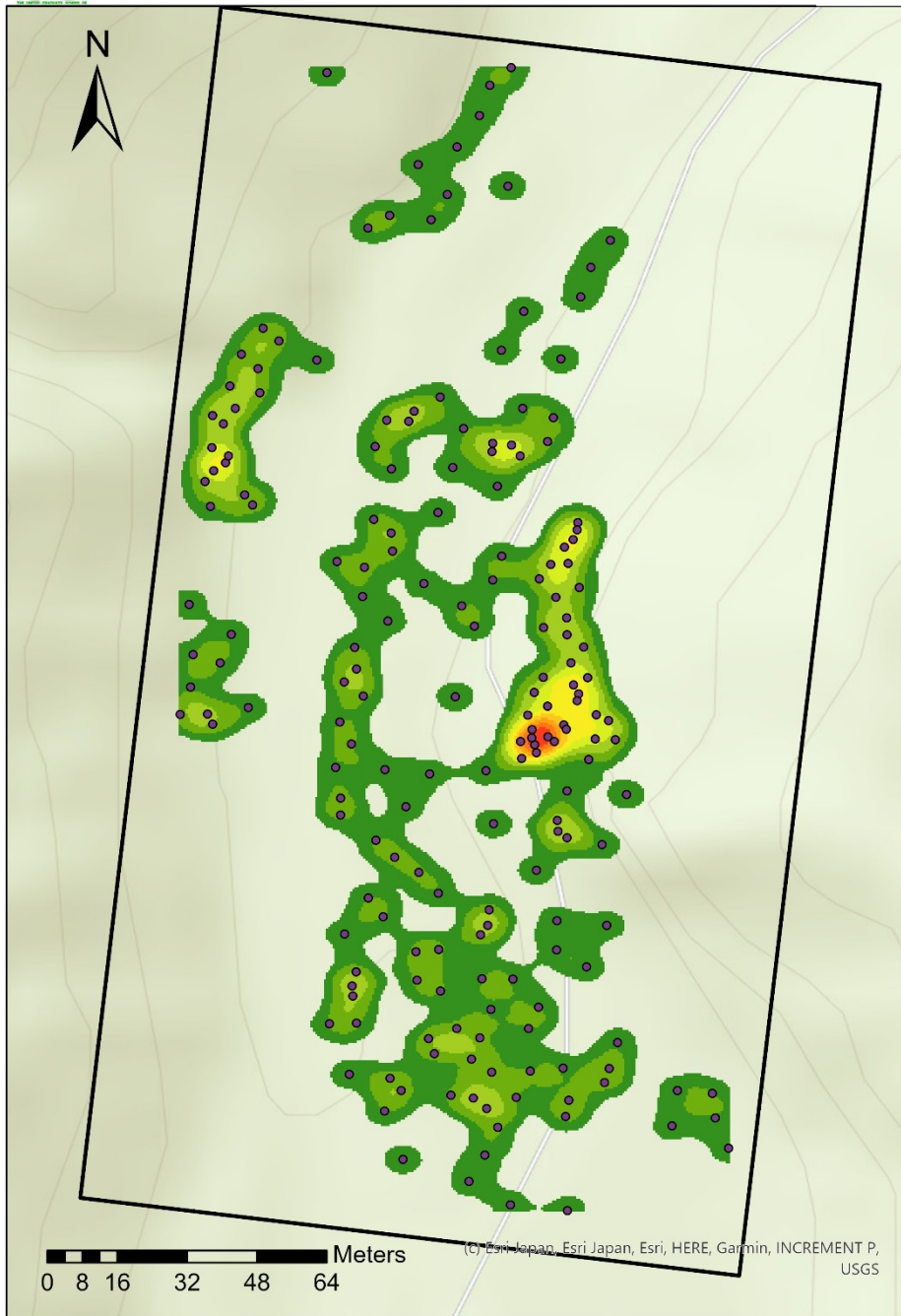


Density map site 7 by Sarah Kentsch





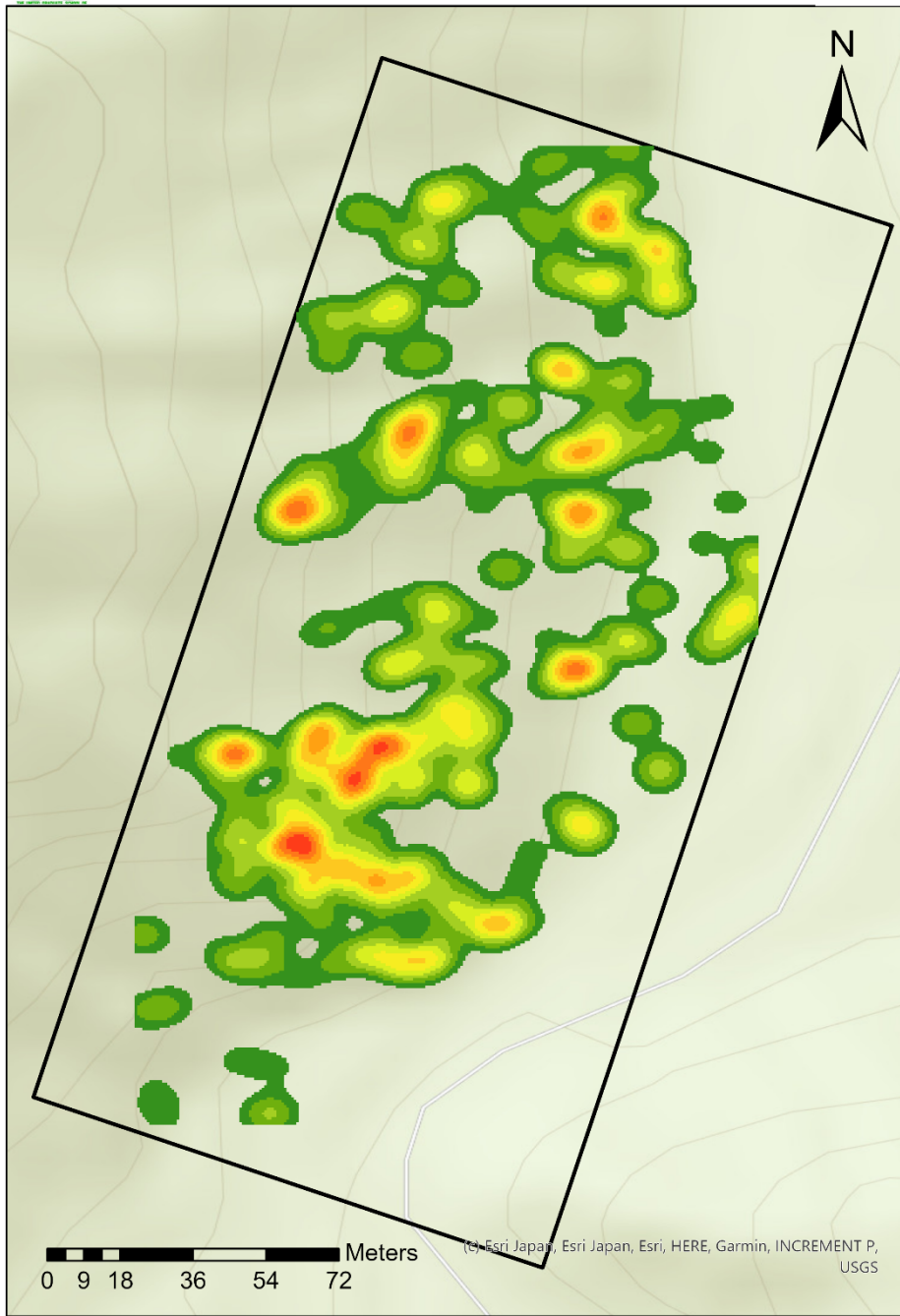
Density map site 7 by Sarah Kentsch



- WinterPointsS7
- ▭ Site7

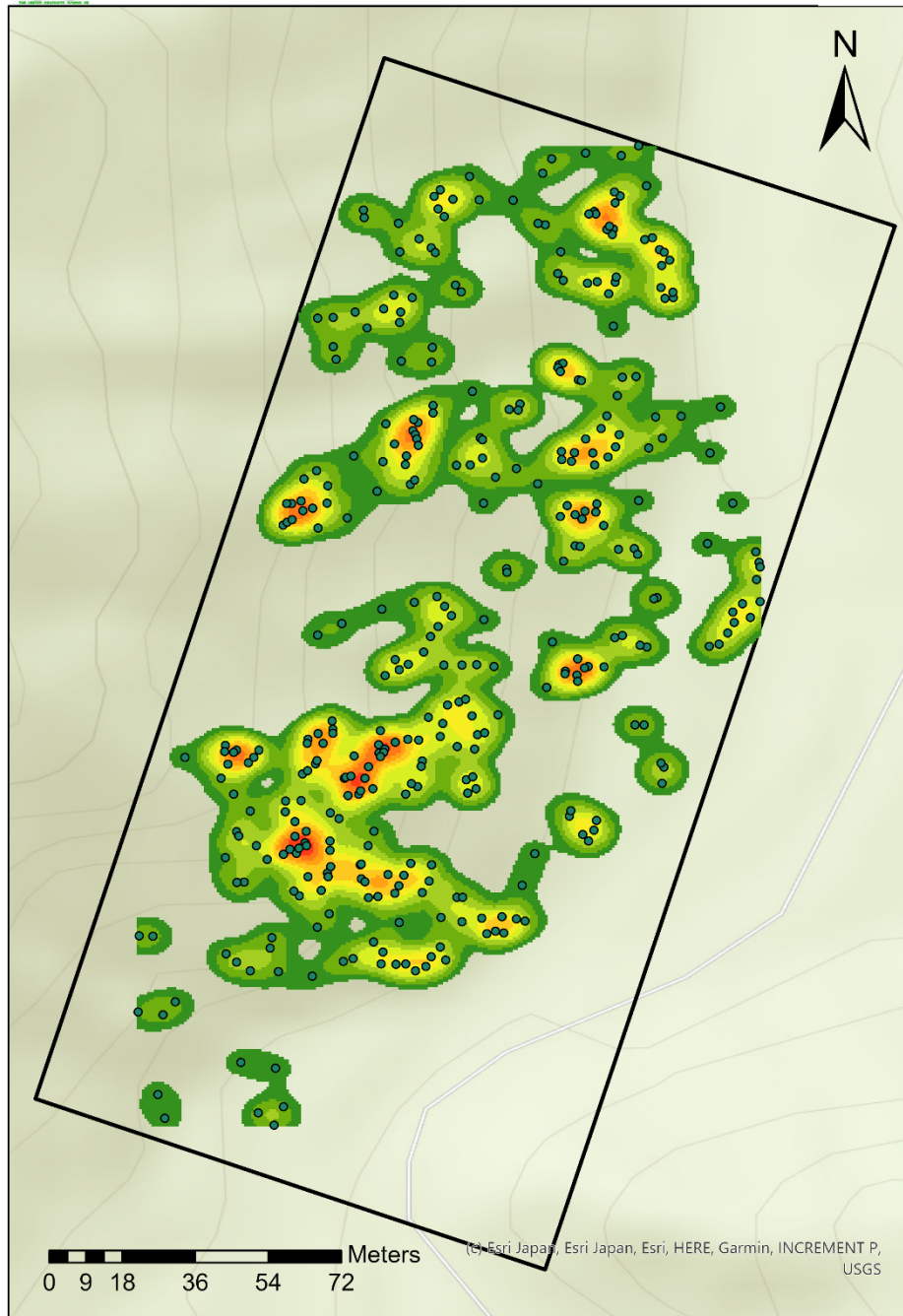


Density map site 8 by Sarah Kentsch





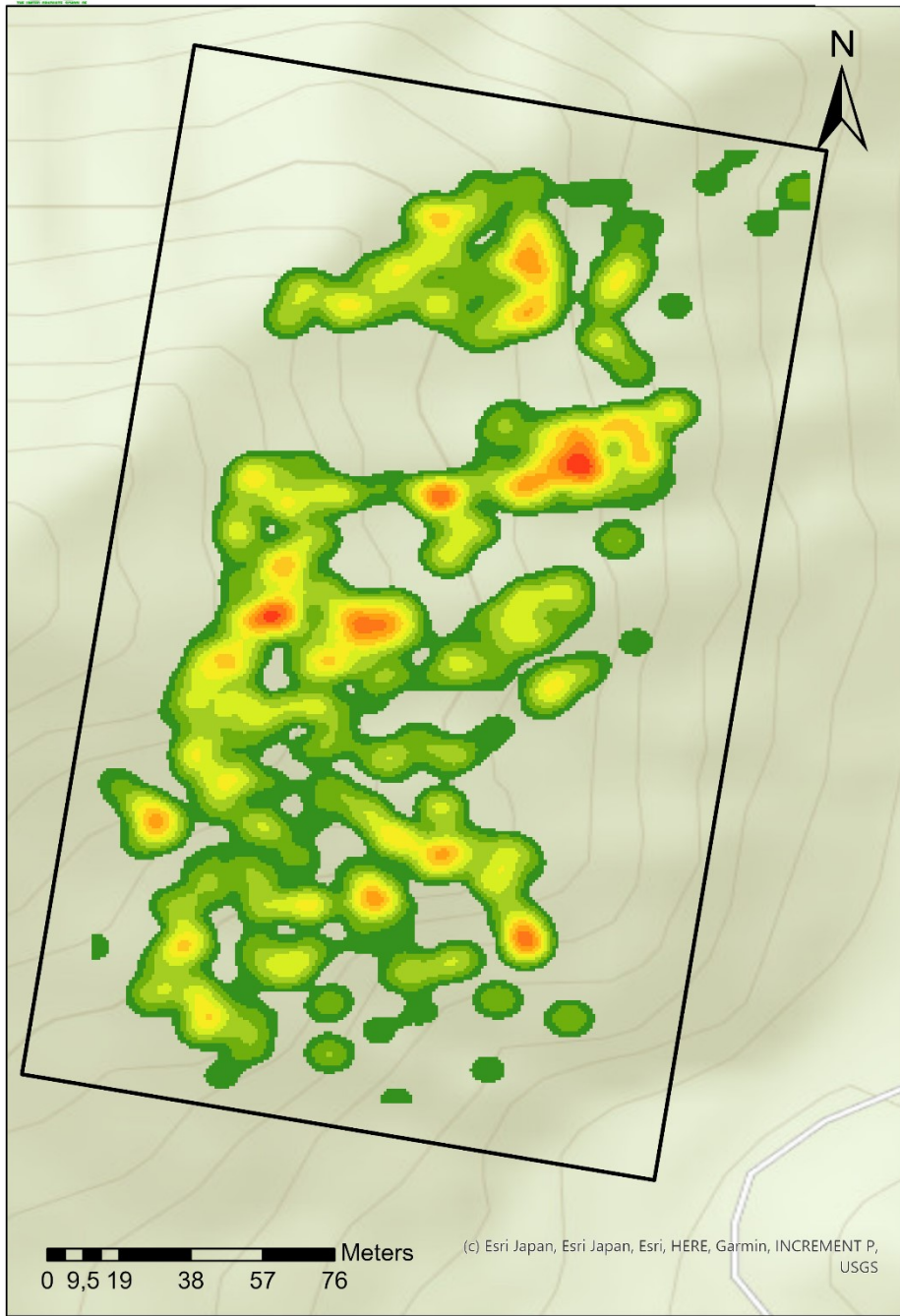
Density map site 8 by Sarah Kentsch



- WinterPointsS8
- ▭ Site8

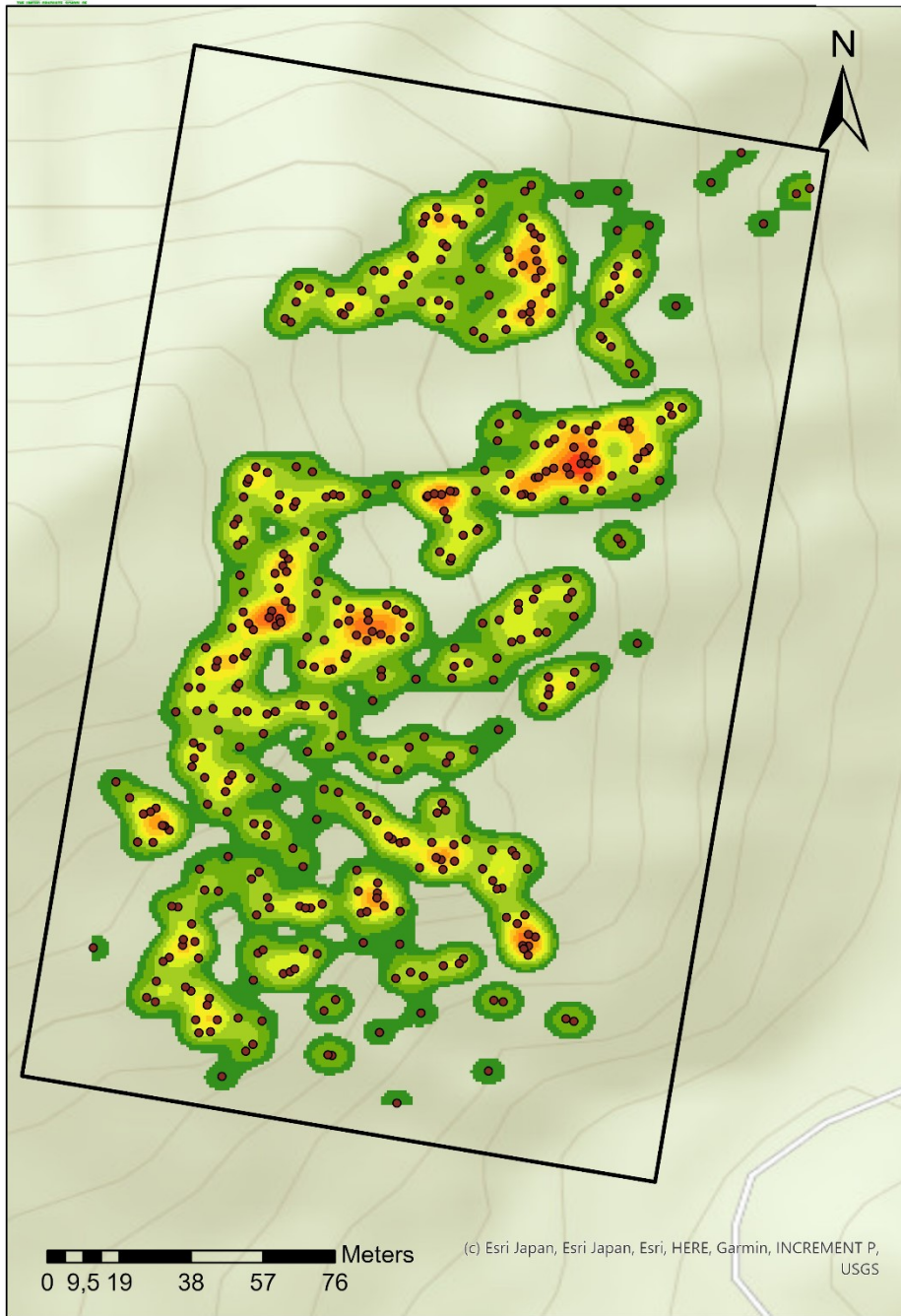


Density map site 9 by Sarah Kentsch





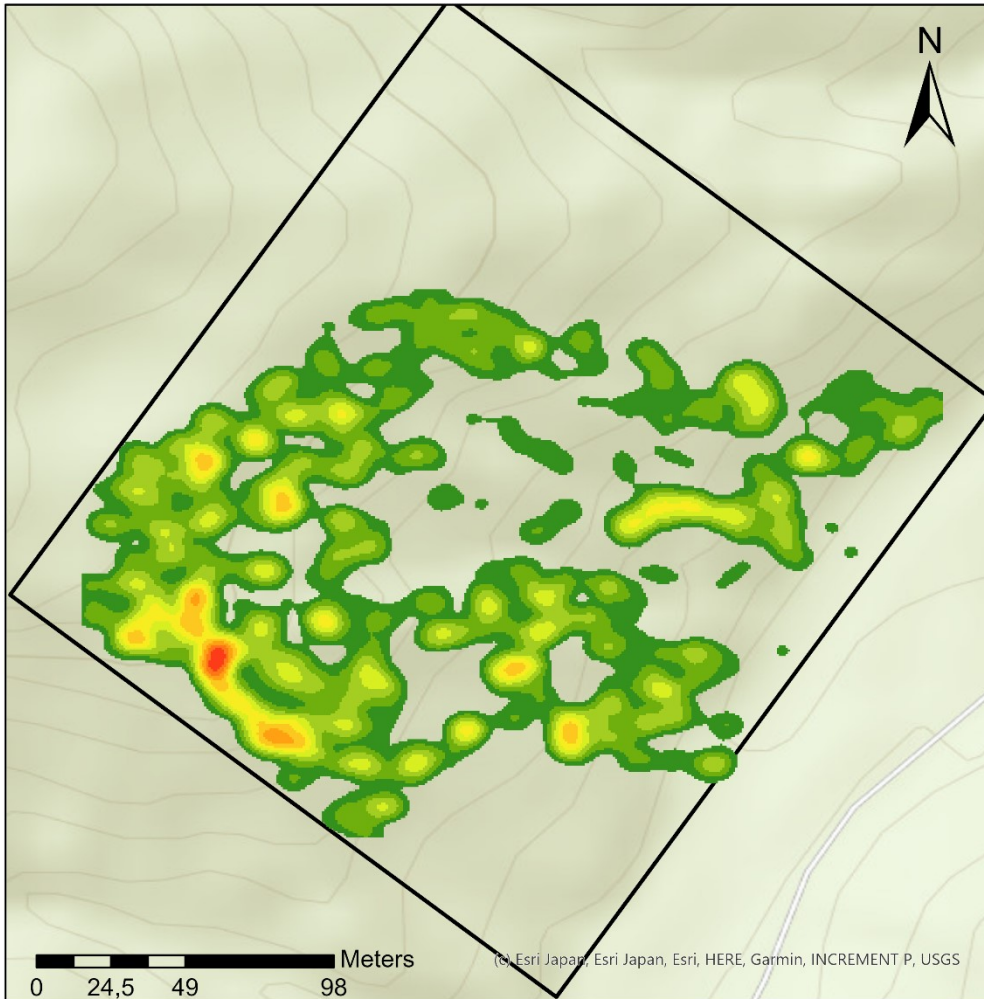
Density map site 9 by Sarah Kentsch



- WinterPointsS9
- ▭ Site9



Density map site 10 by Sarah Kentsch

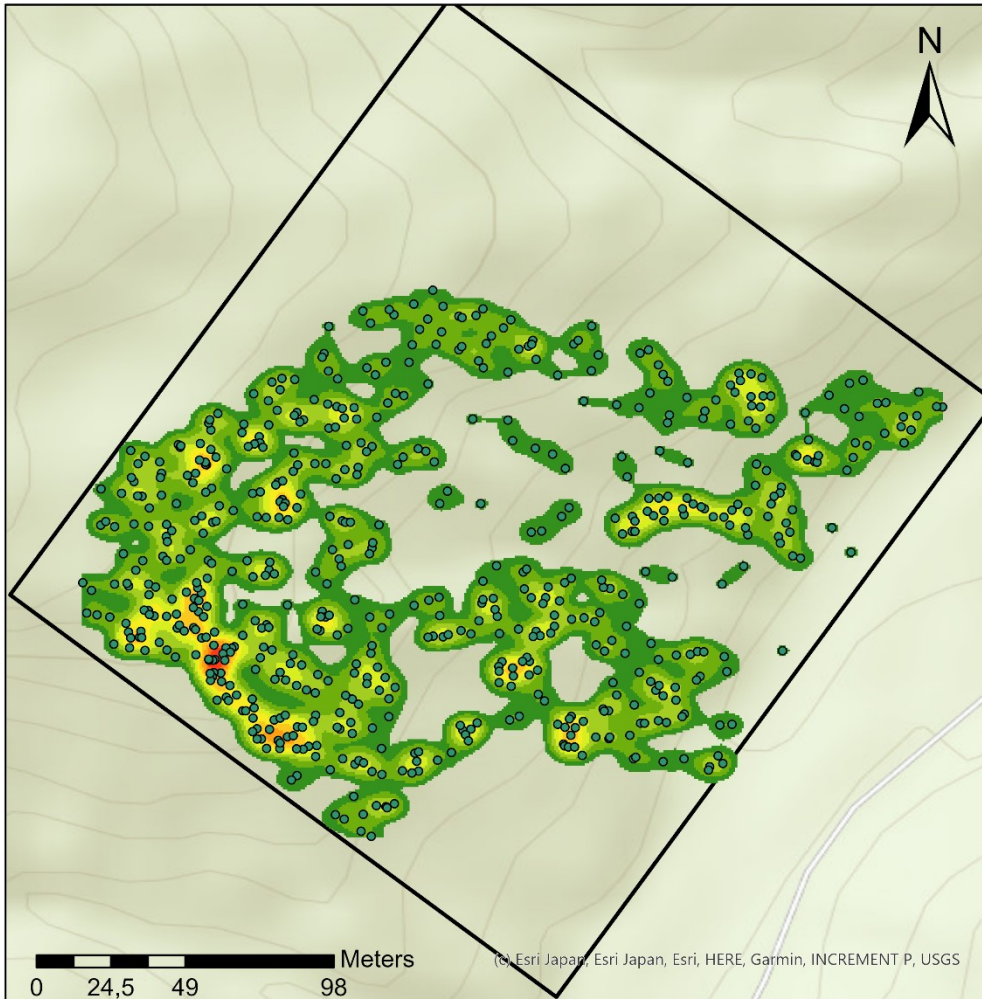


Site10



Density map site 10

by Sarah Kentsch

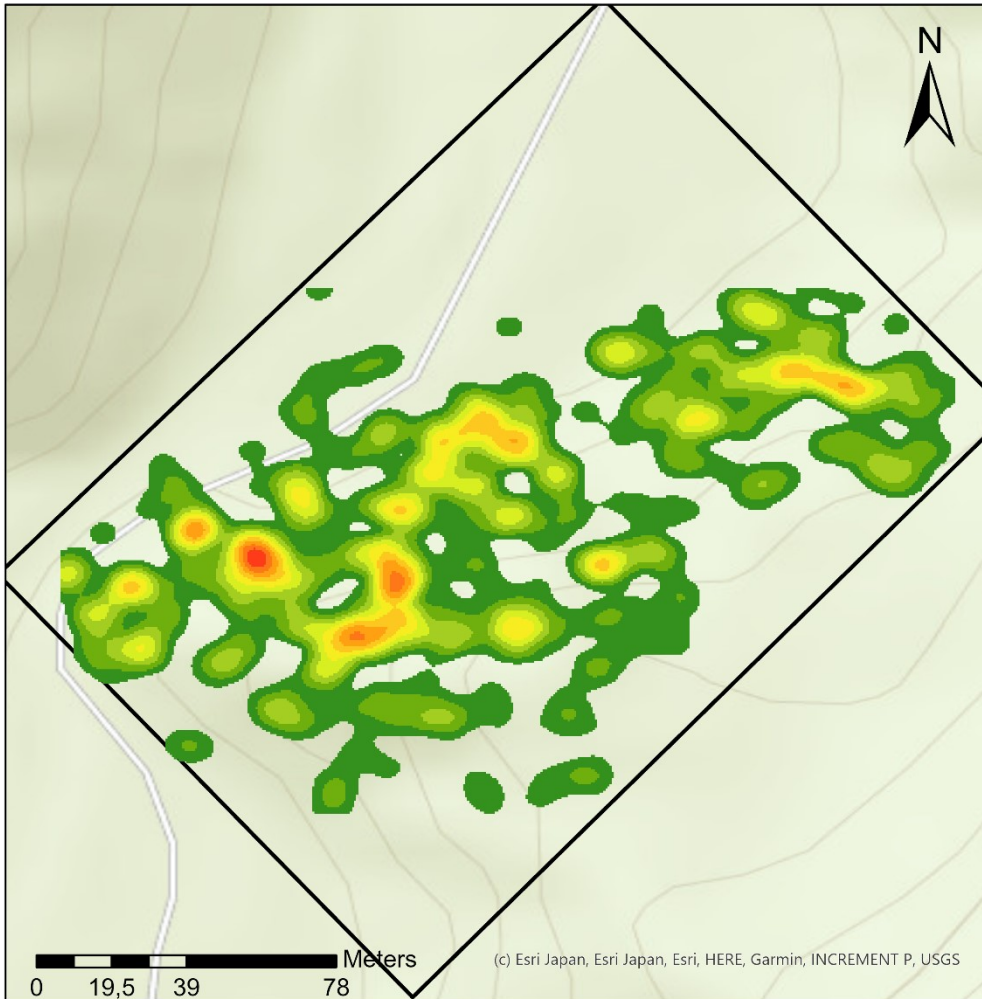


(c) Esri Japan, Esri Japan, Esri, HERE, Garmin, INCREMENT P, USGS

- WinterPointsS10
- Site10



Density map site 11 by Sarah Kentsch

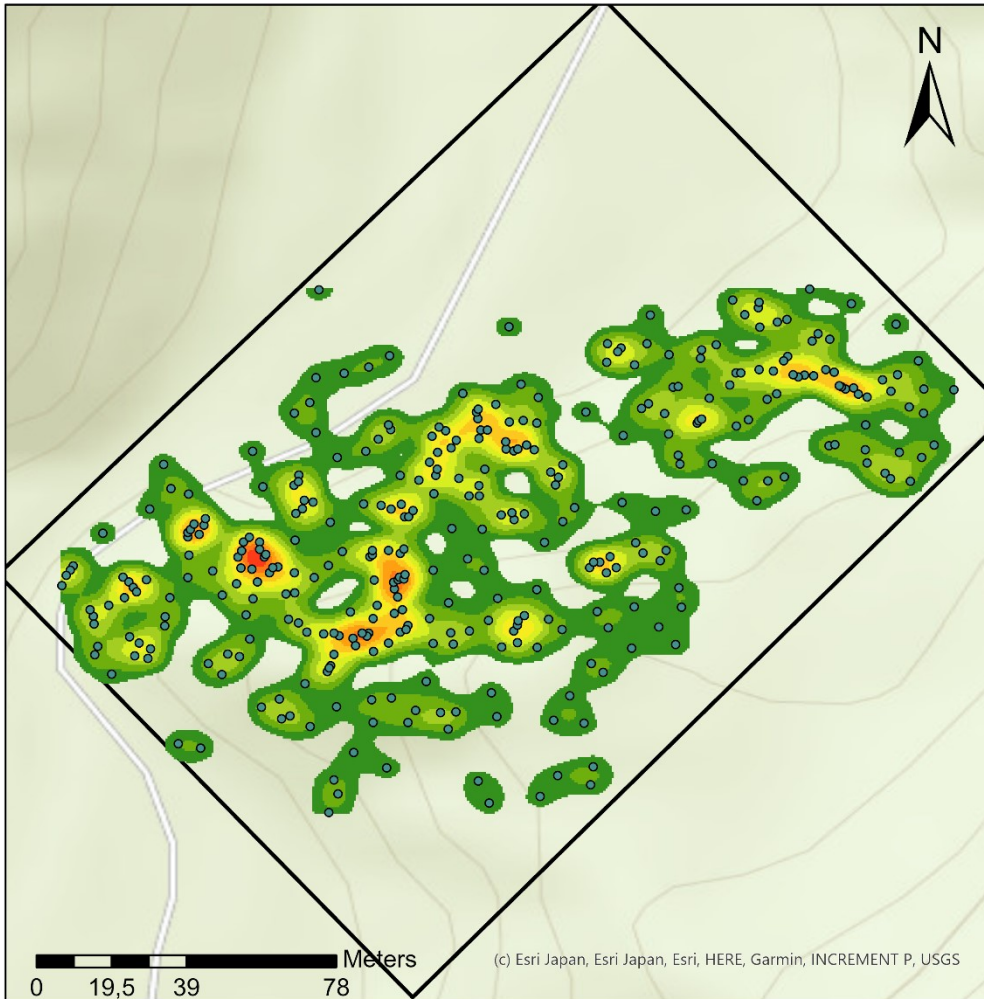


(c) Esri Japan, Esri Japan, Esri, HERE, Garmin, INCREMENT P, USGS

Site11



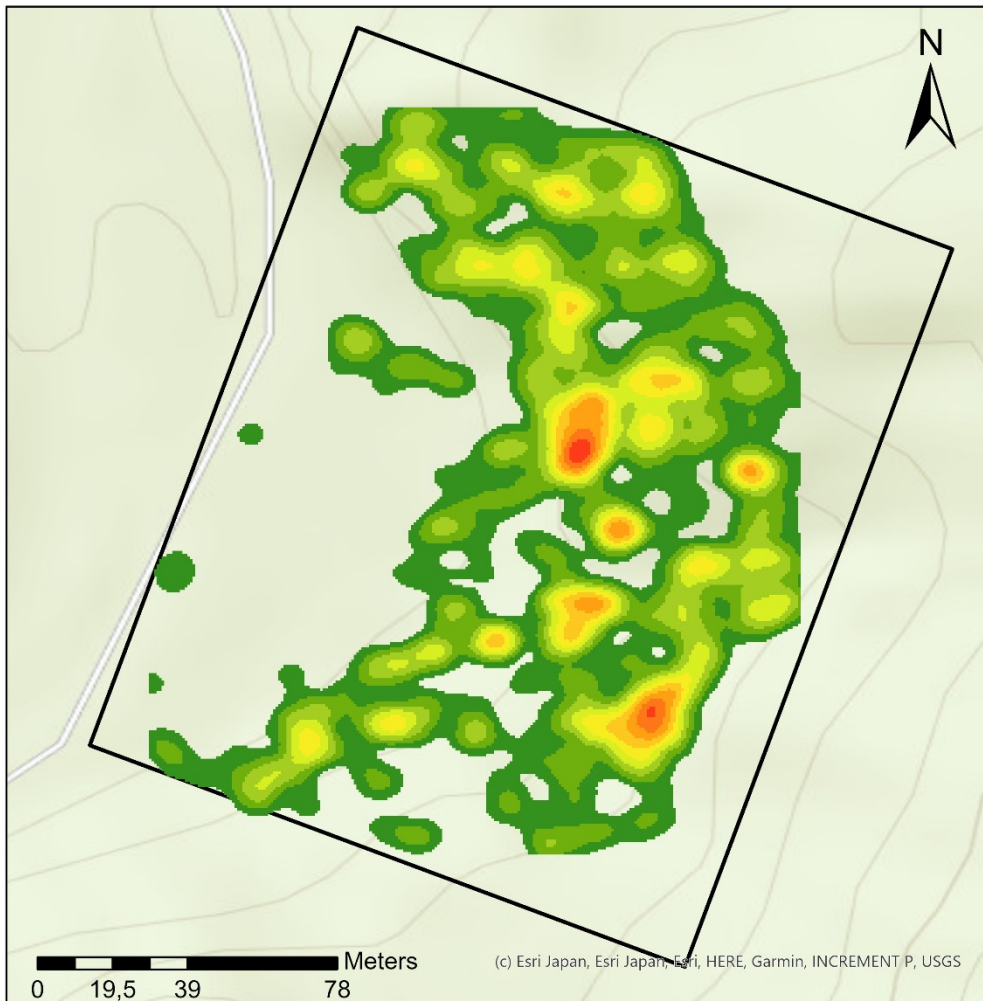
Density map site 11 by Sarah Kentsch



- WinterPointsS11
- Site11



Density map site 12 by Sarah Kentsch

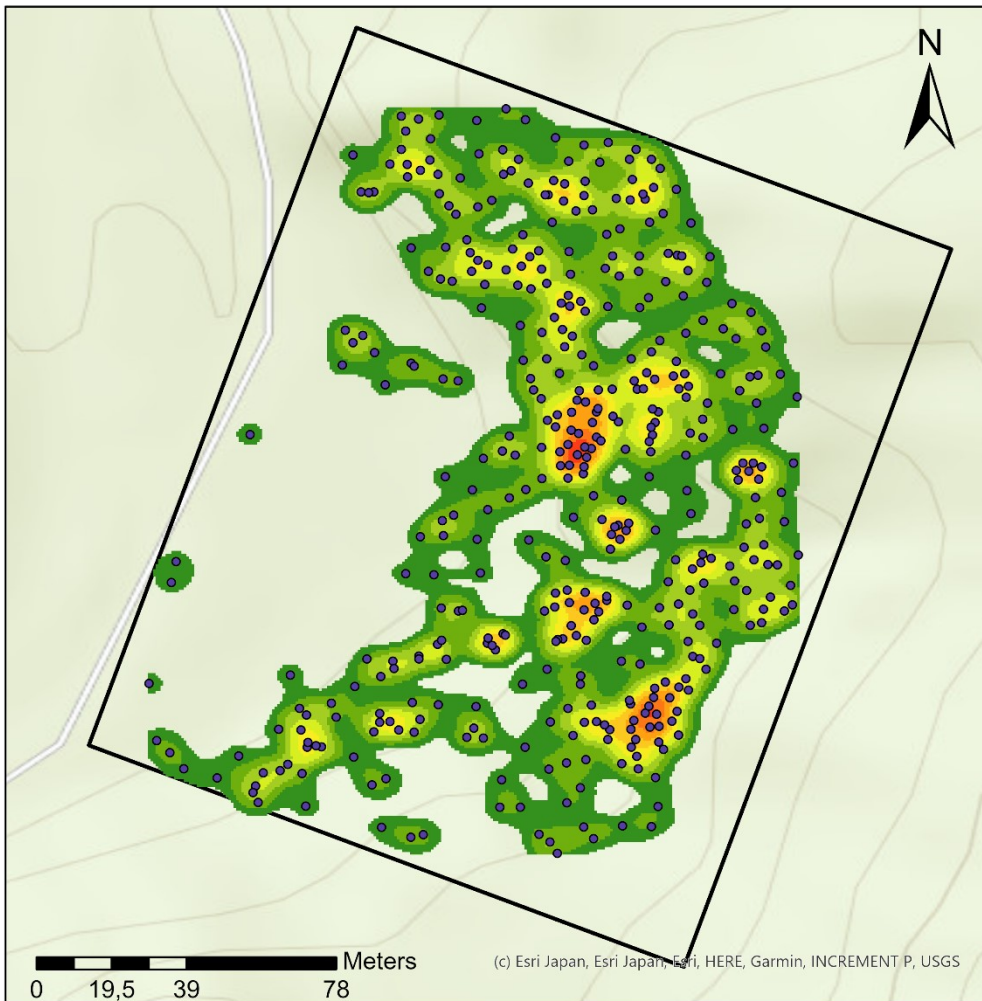


Site12



Density map site 12

by Sarah Kentsch

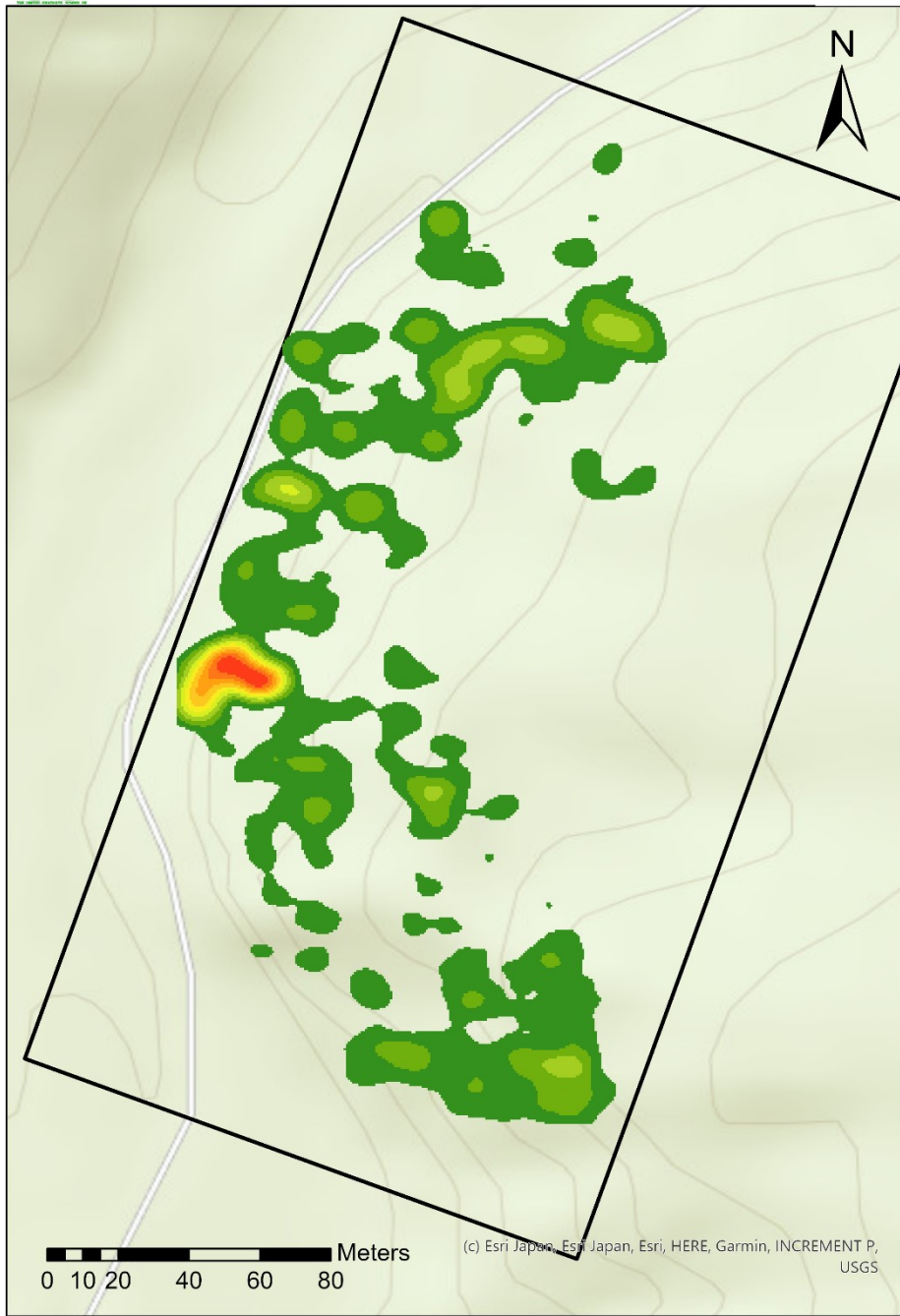


(c) Esri Japan, Esri Japan, Esri, HERE, Garmin, INCREMENT P, USGS

- WinterTreesS12
- Site12

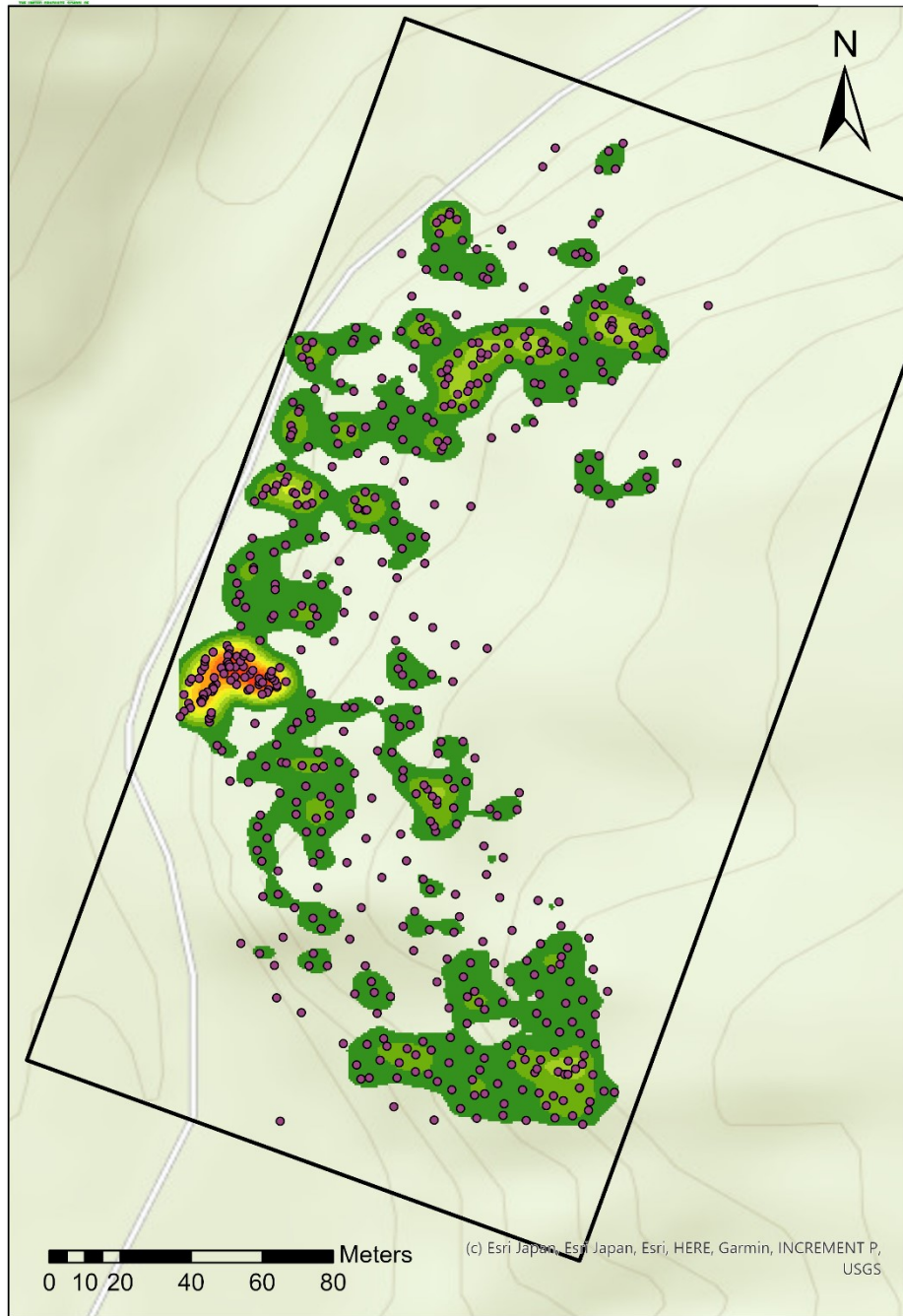


Density map site 13 by Sarah Kentsch





Density map site 13 by Sarah Kentsch

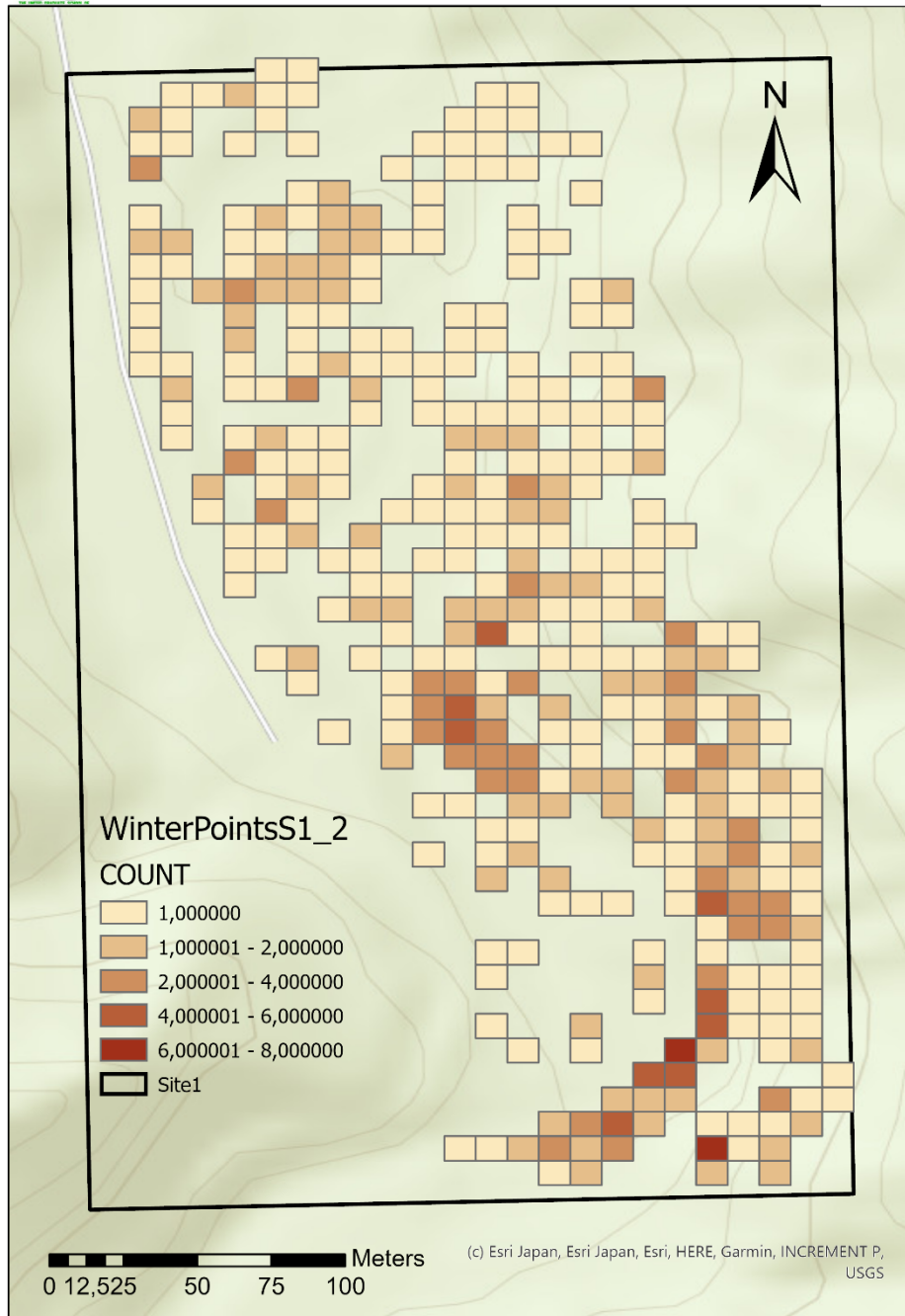


- WinterPointsS13
- Site13

Part 2: Count maps for each site.



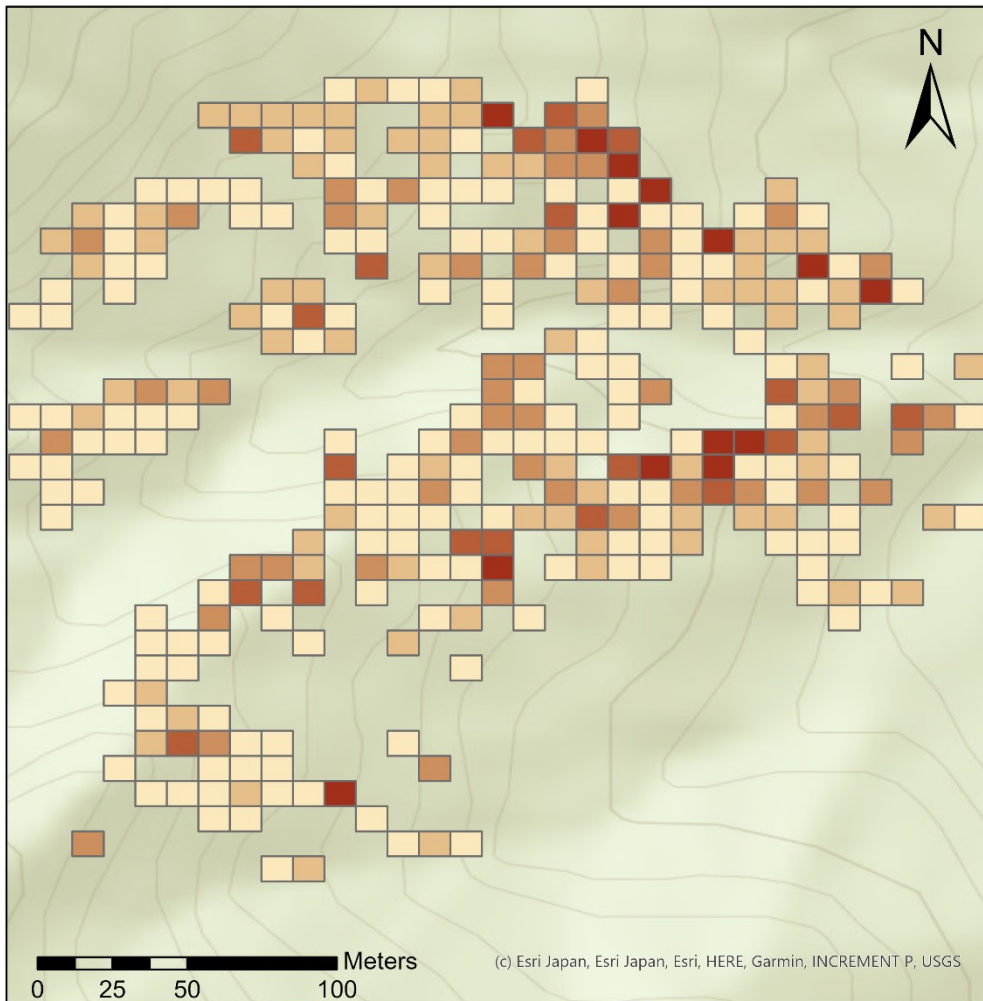
Count map site 1
by Sarah Kentsch



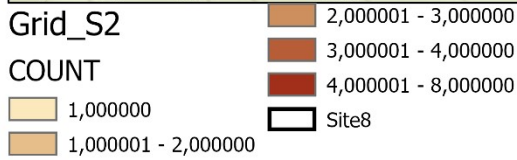


Count map site 2

by Sarah Kentsch

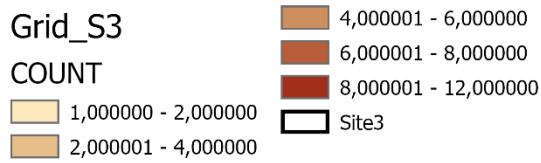
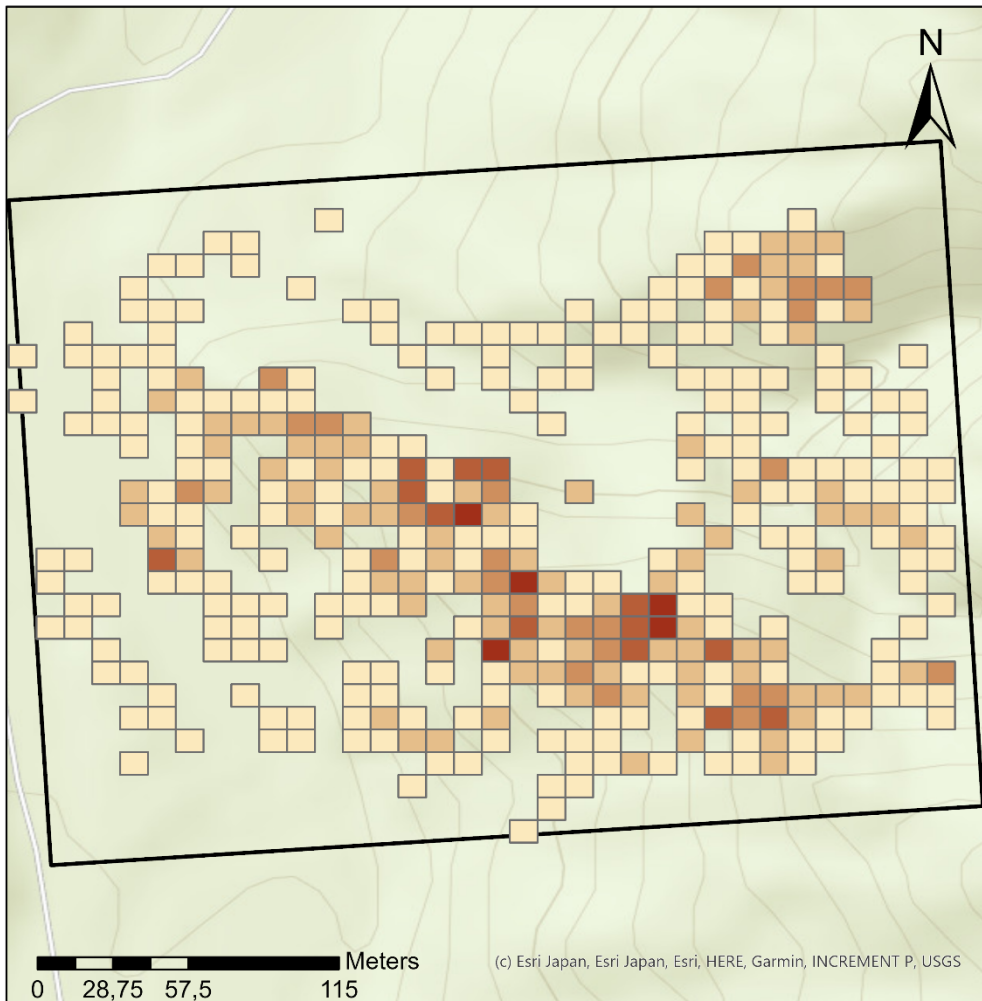


(c) Esri Japan, Esri Japan, Esri, HERE, Garmin, INCREMENT P, USGS



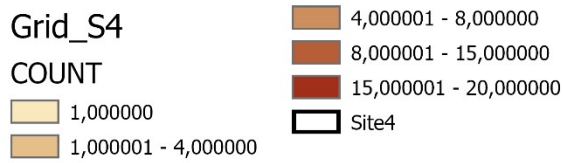
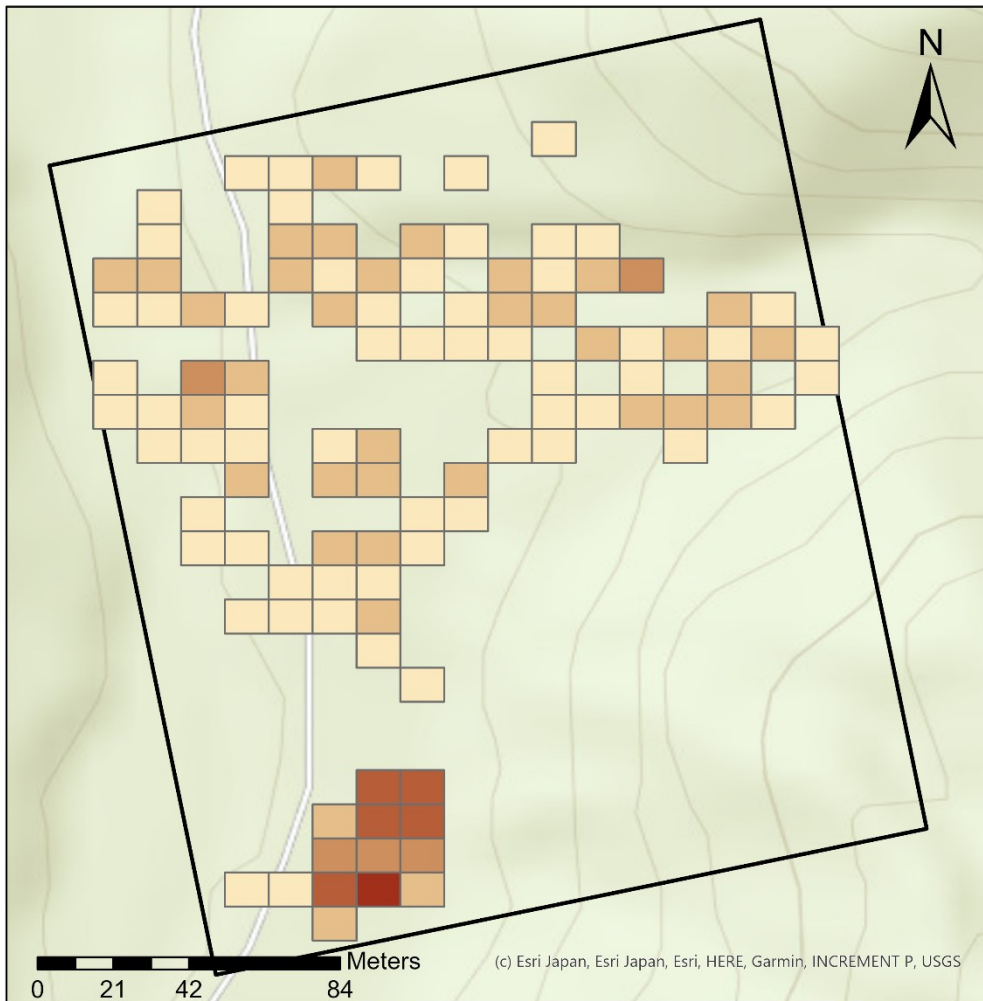


Count map site 3 by Sarah Kentsch



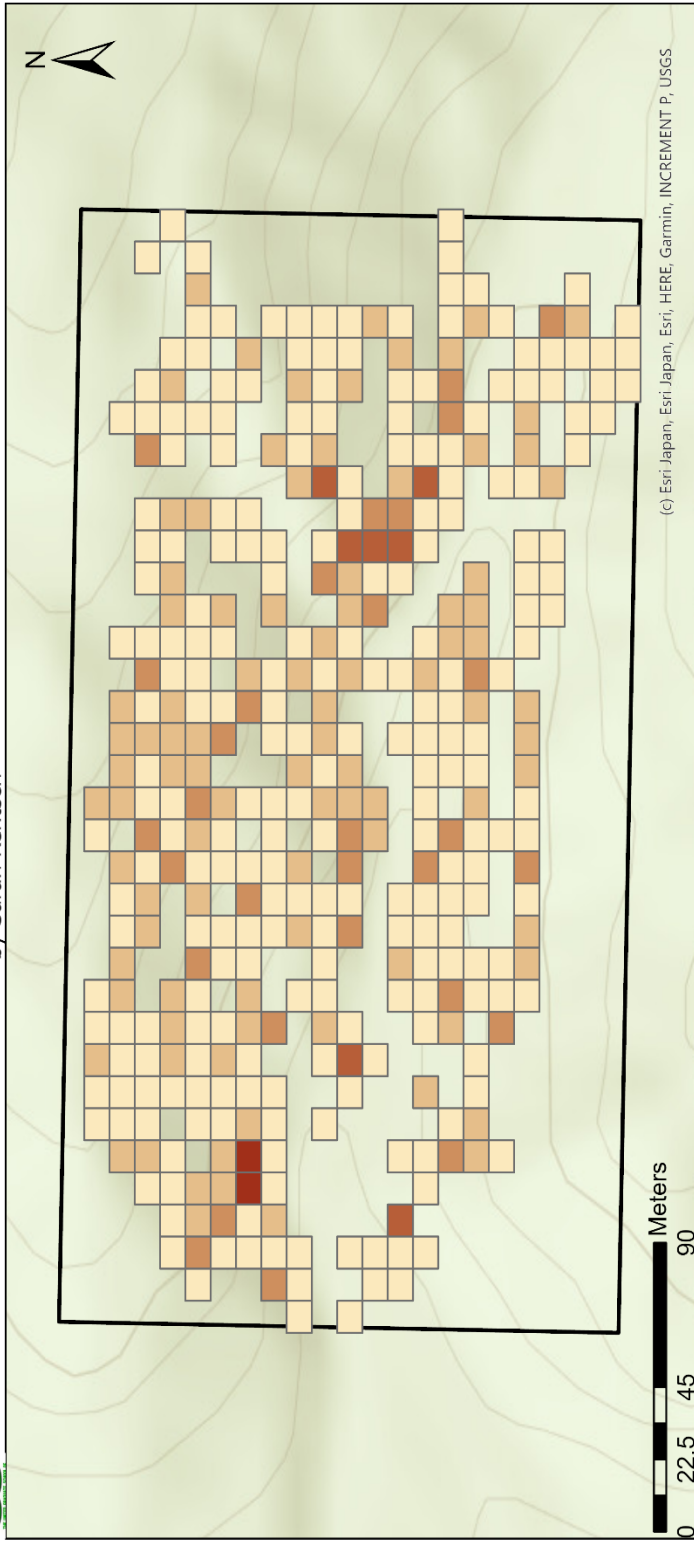


Count map site 4 by Sarah Kentsch





Count map site 5 by Sarah Kentsch



(c) Esri, Japan, Esri, HERE, Garmin, INCREMENT P, USGS

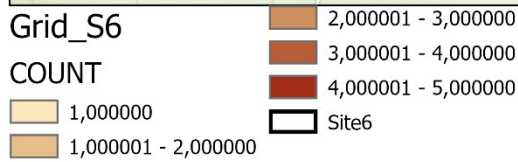
Grid_S5

4,000001 - 6,000000	6,000001 - 9,000000	9,000001 - 17,000000	Site5
1,000000 - 2,000000	2,000001 - 4,000000		

COUNT

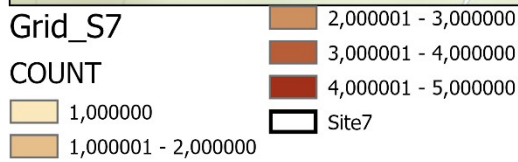
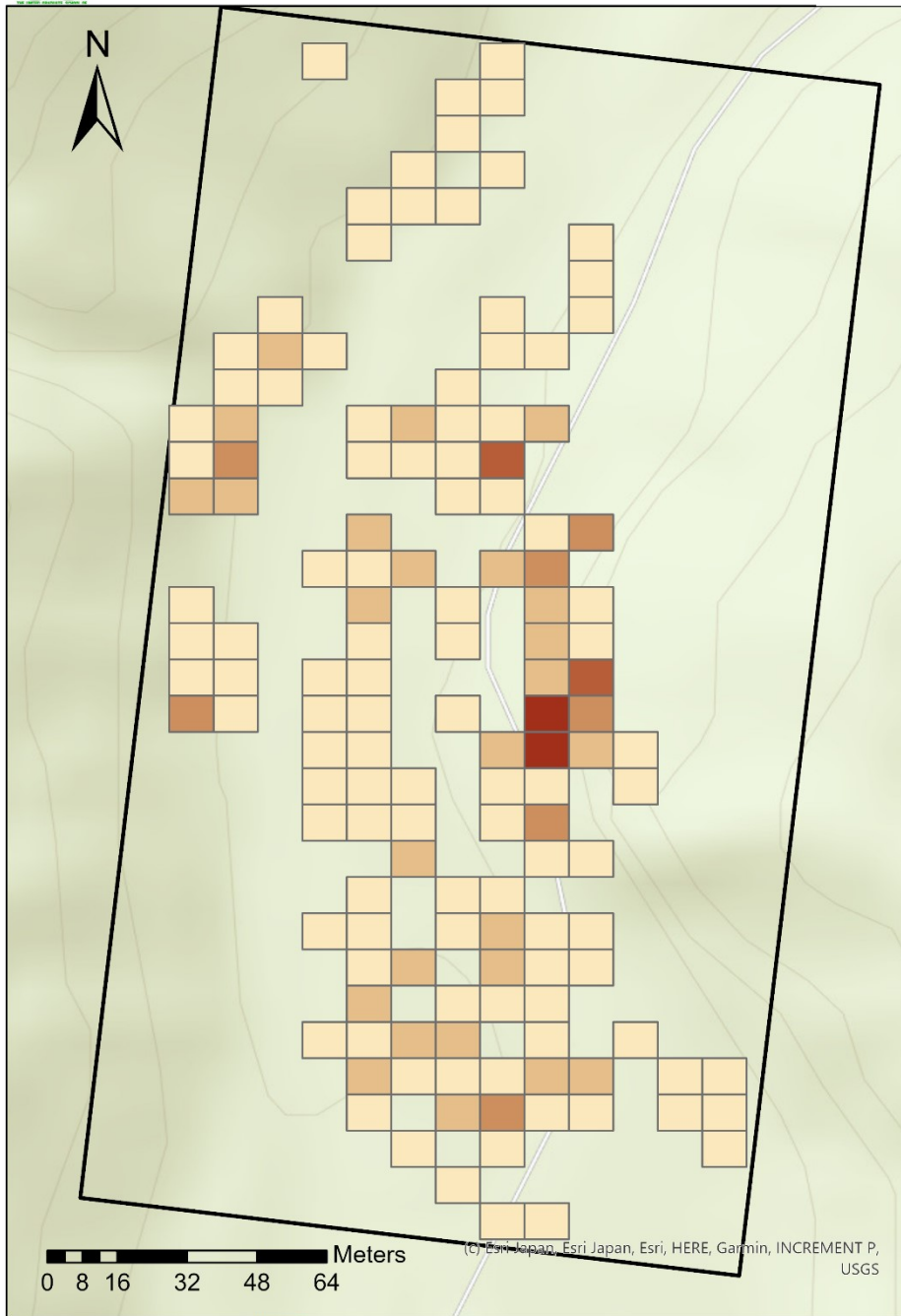


Count map site 6 by Sarah Kentsch



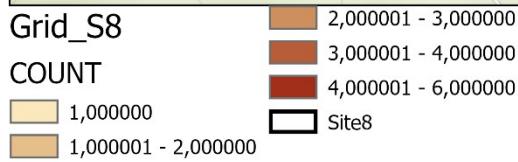
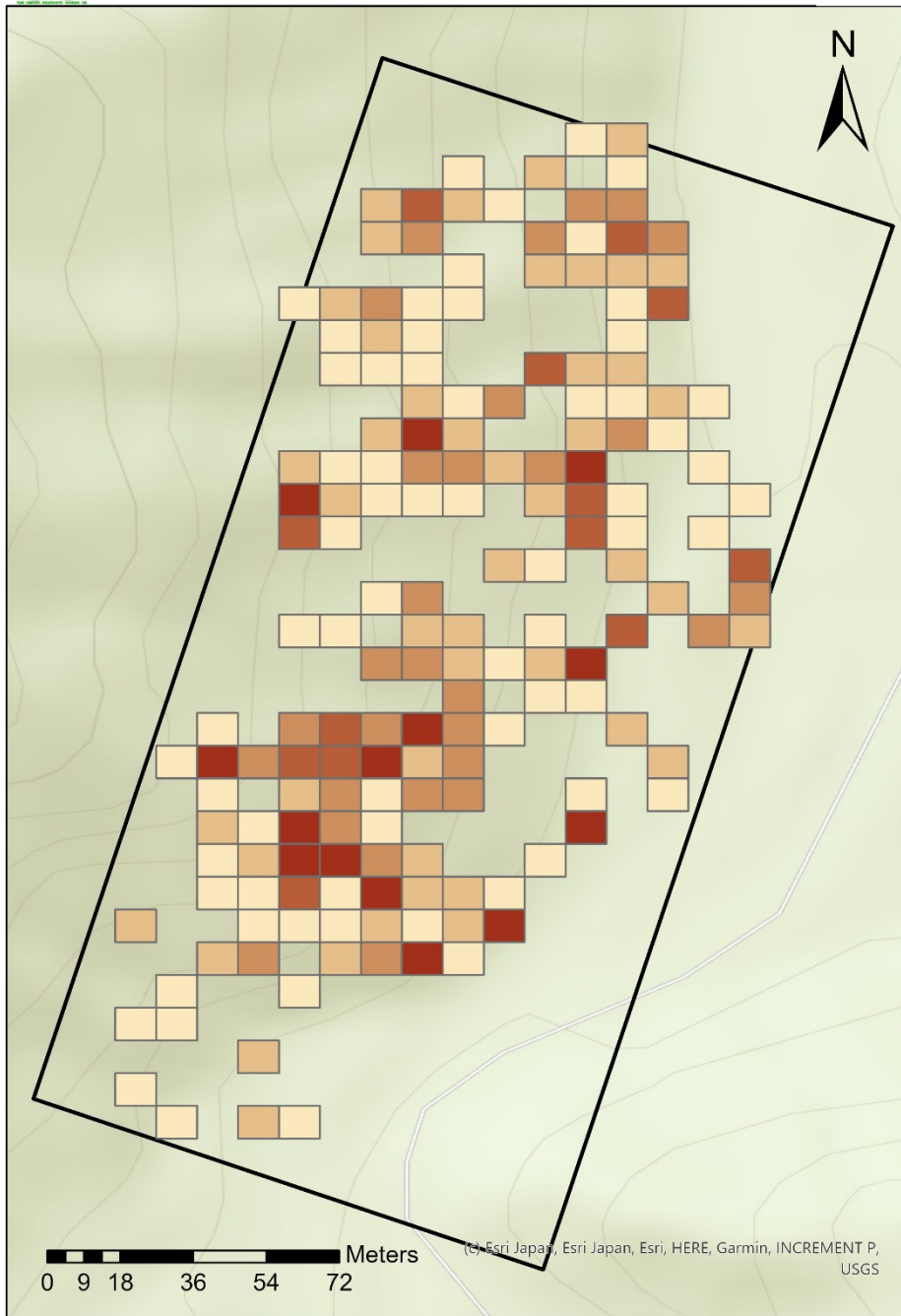


Count map site 7 by Sarah Kentsch



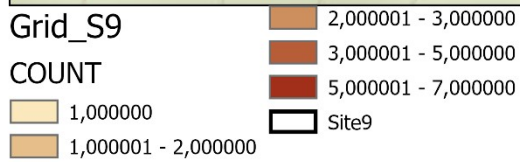
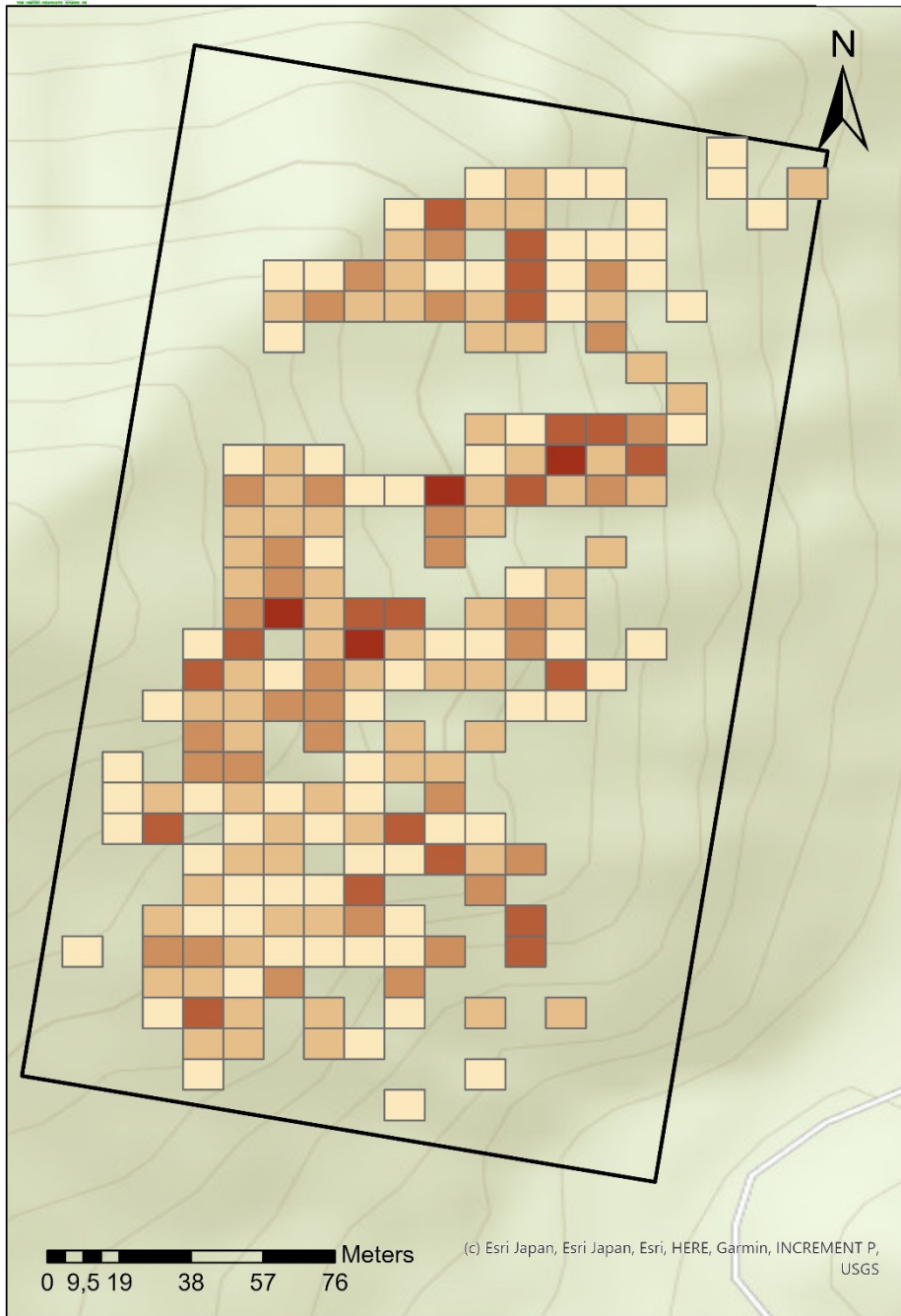


Count map site 8 by Sarah Kentsch



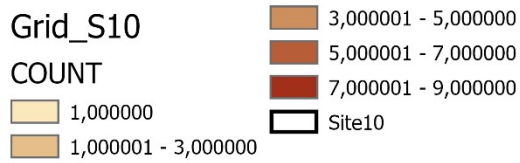
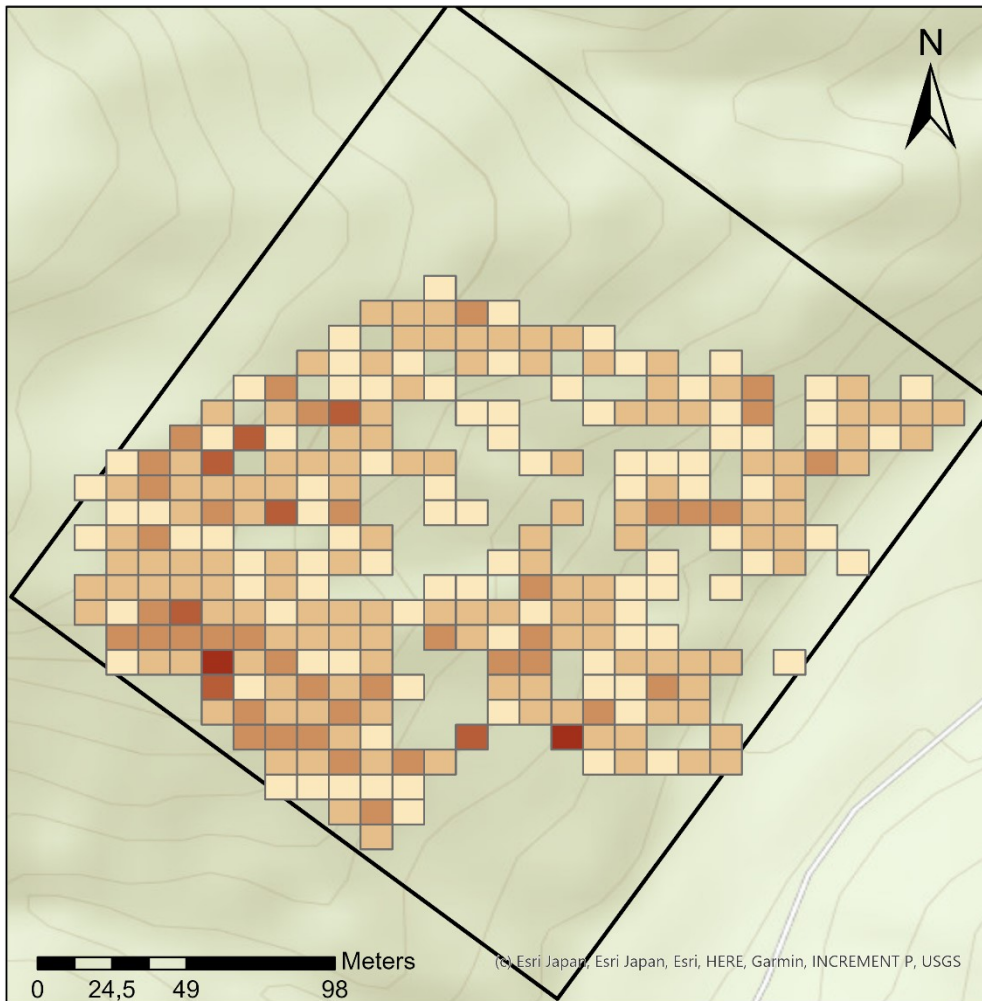


Count map site 9 by Sarah Kentsch





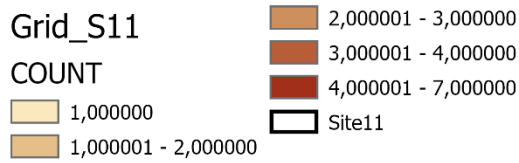
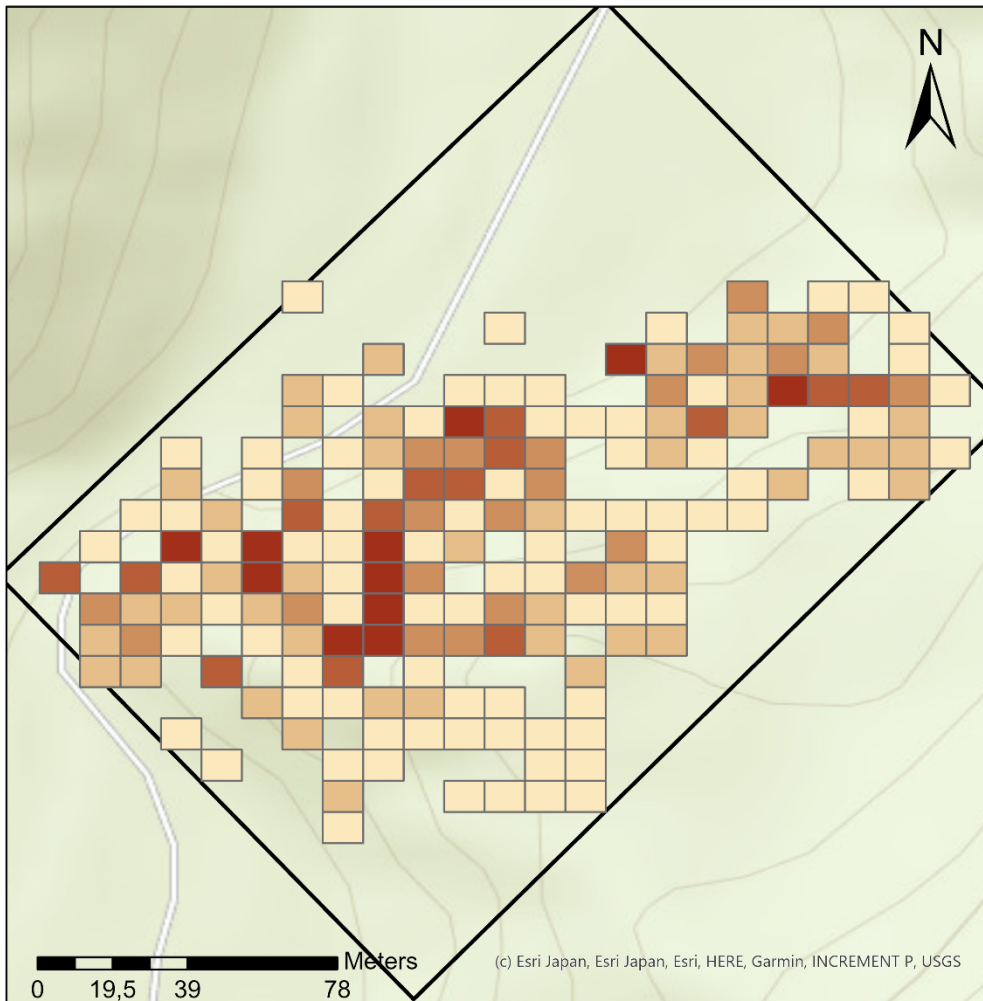
Count map site 10 by Sarah Kentsch





Count map site 11

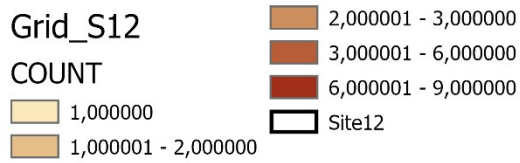
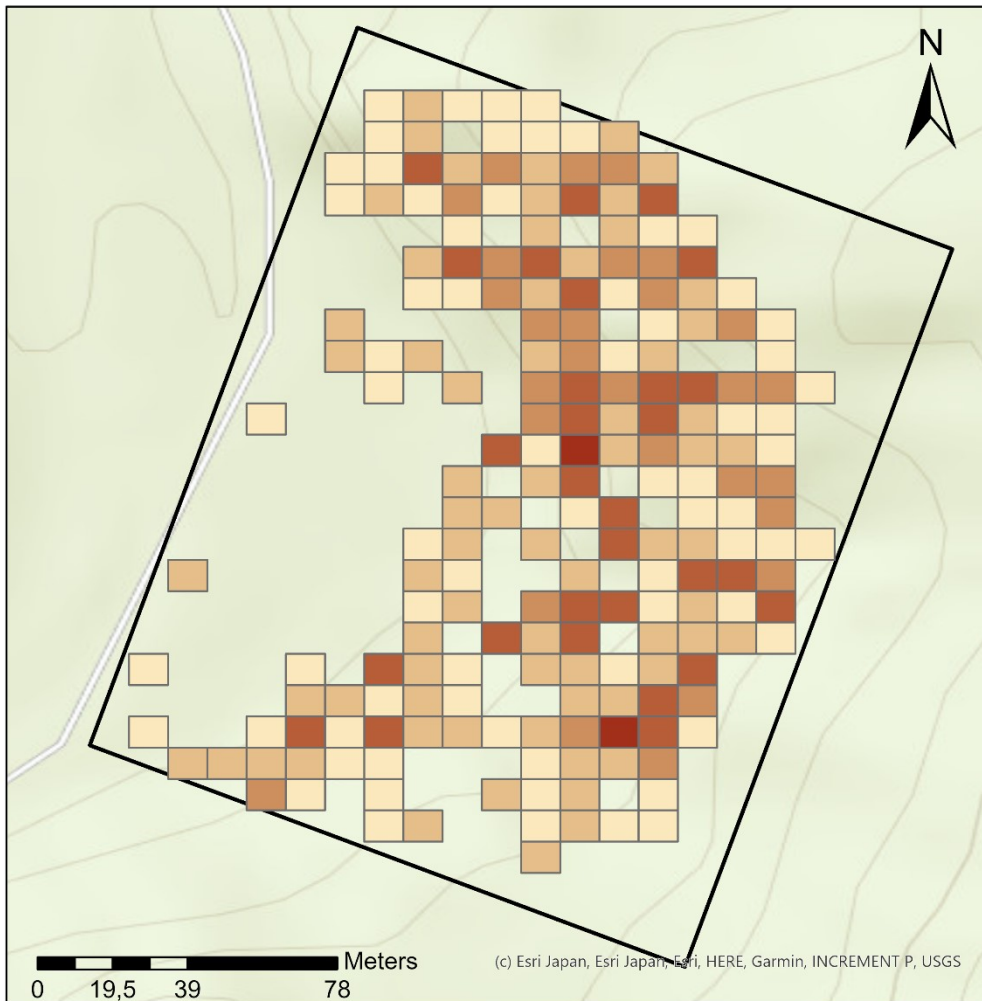
by Sarah Kentsch





Count map site 12

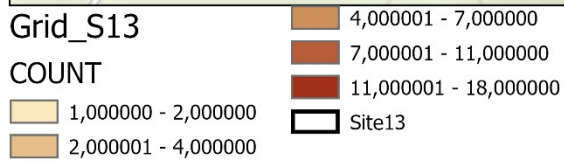
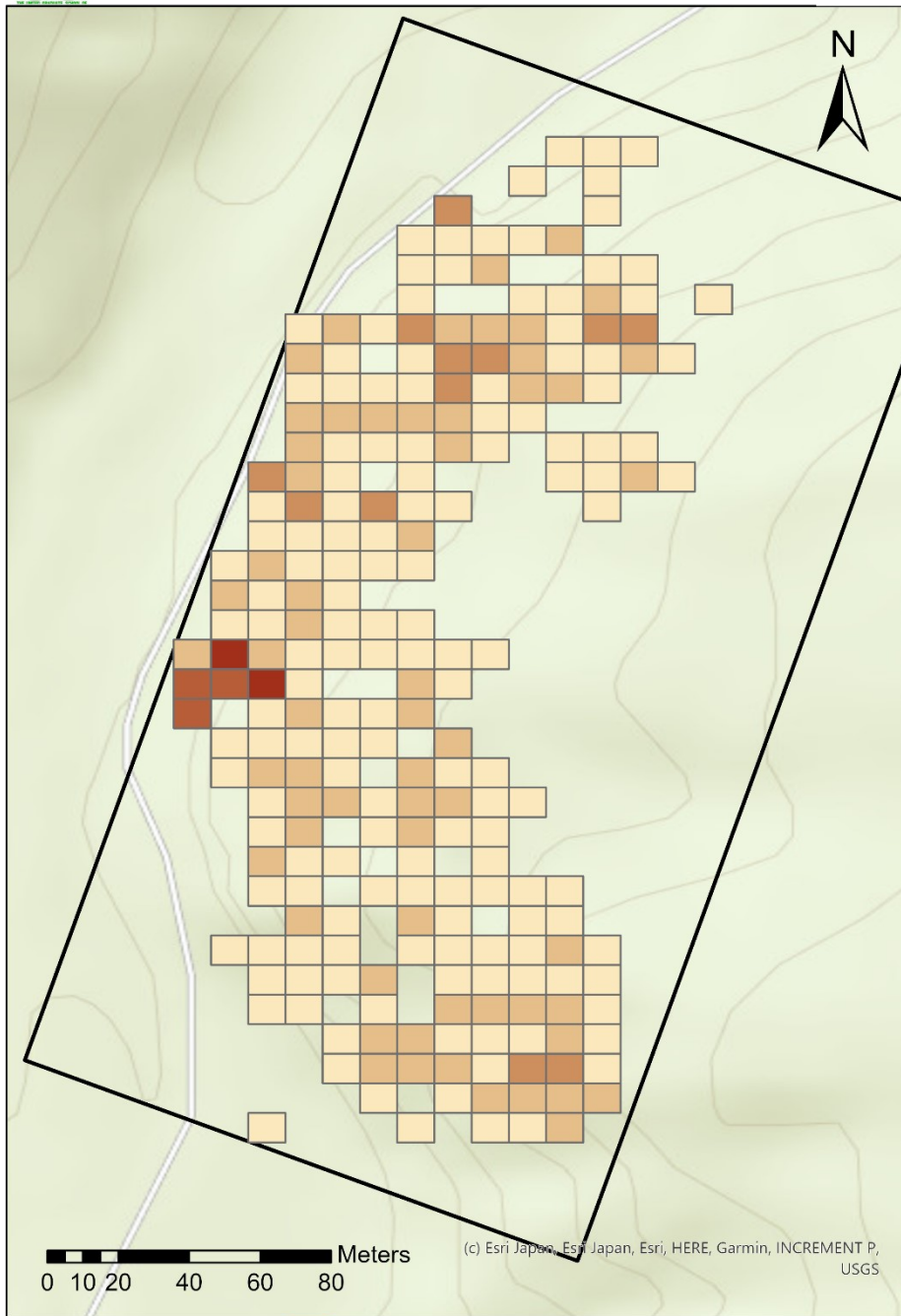
by Sarah Kentsch





Count map site 6

by Sarah Kentsch

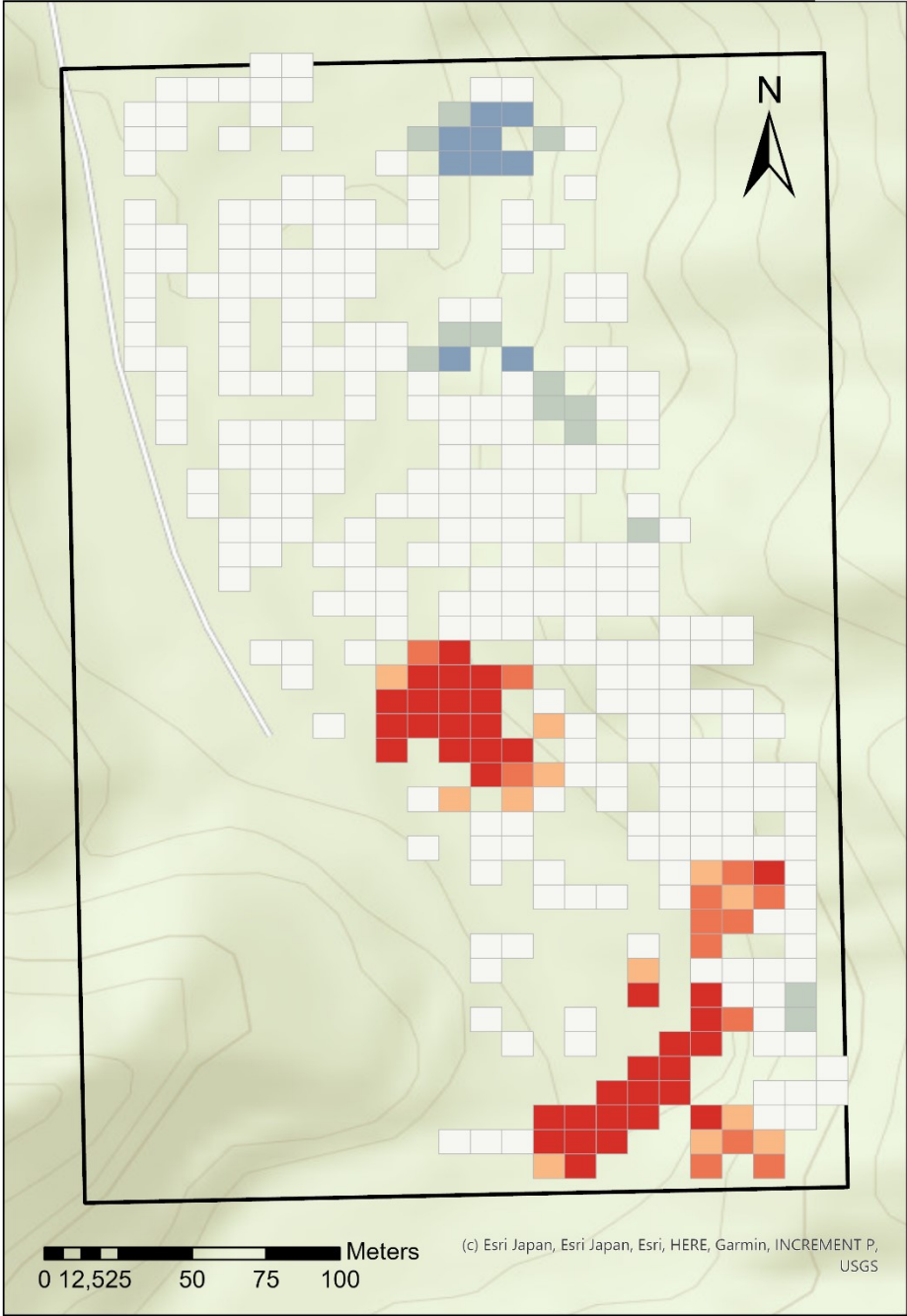


Part 3: Hot spot maps for each site



Hot spot analysis site 1

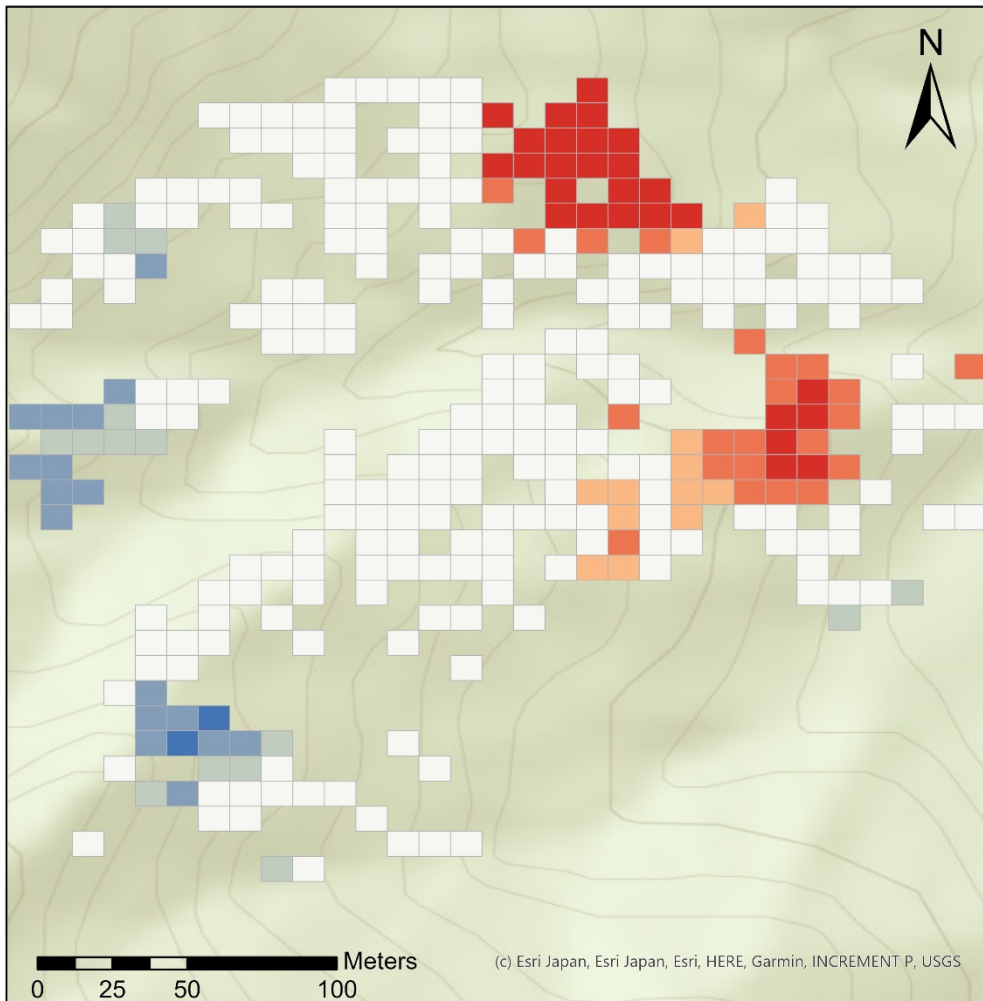
by Sarah Kentsch



(c) Esri Japan, Esri Japan, Esri, HERE, Garmin, INCREMENT P, USGS



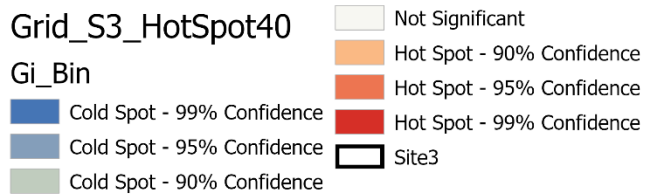
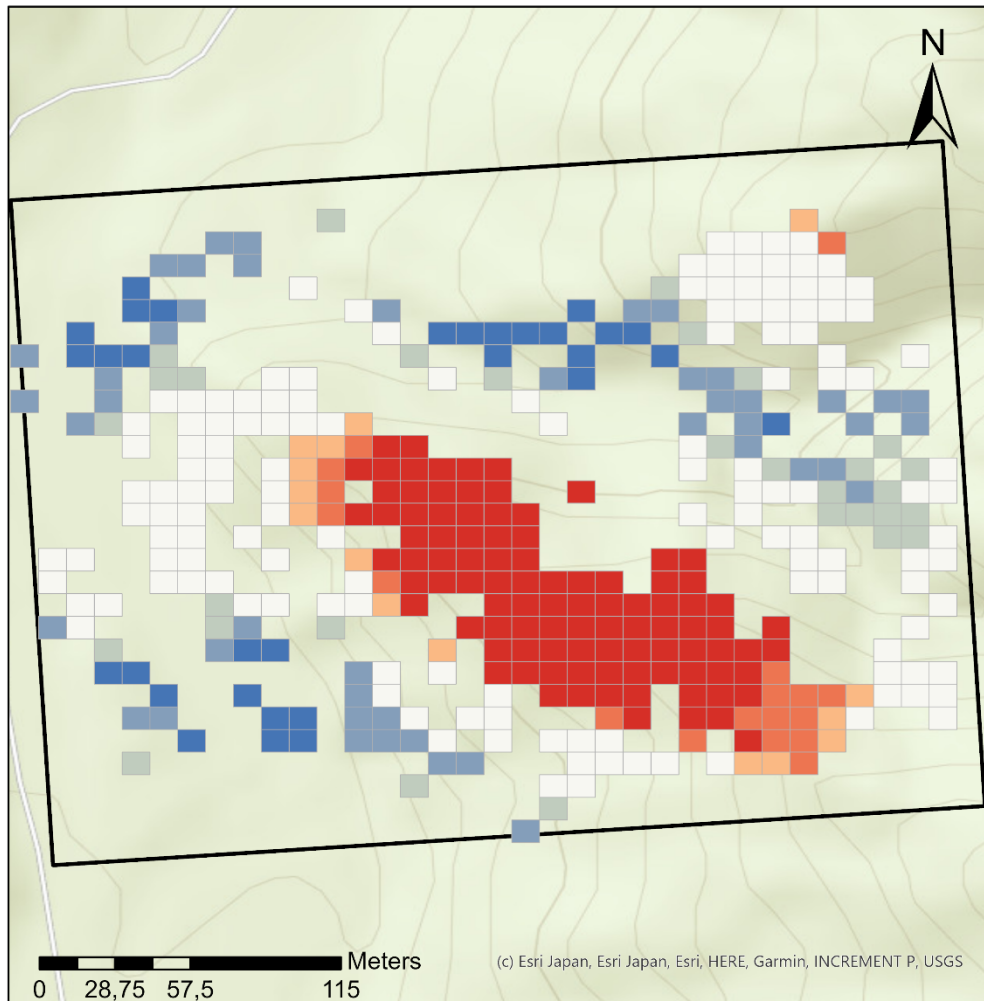
Hot spot analysis site 2 by Sarah Kentsch



- Grid_S2_HotSpot40**
- Not Significant
 - Hot Spot - 90% Confidence
 - Hot Spot - 95% Confidence
 - Hot Spot - 99% Confidence
- Gi_Bin**
- Cold Spot - 99% Confidence
 - Cold Spot - 95% Confidence
 - Cold Spot - 90% Confidence
 - Site8

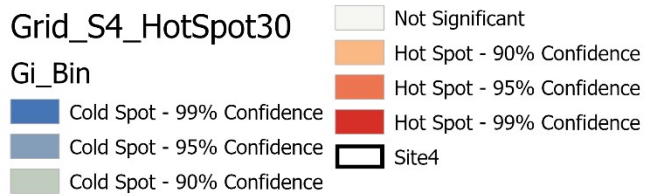
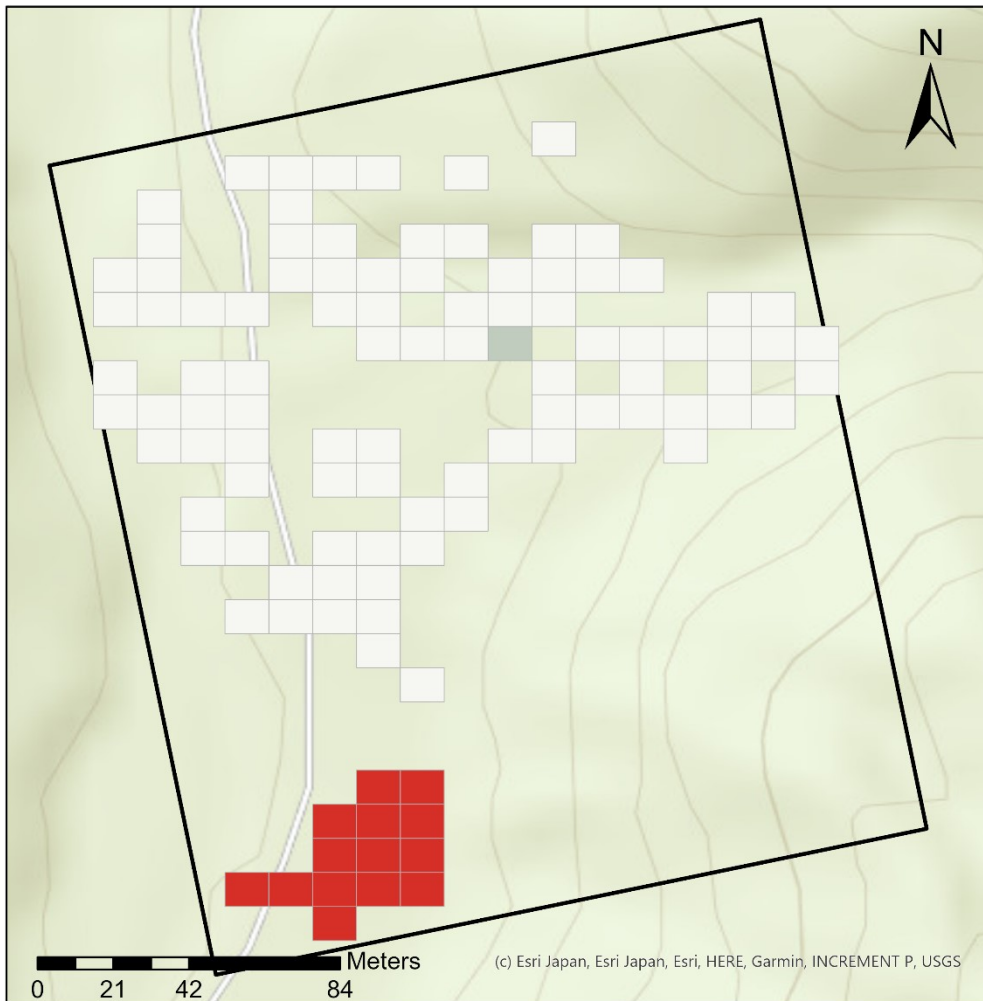


Hot spot analysis site 3 by Sarah Kentsch





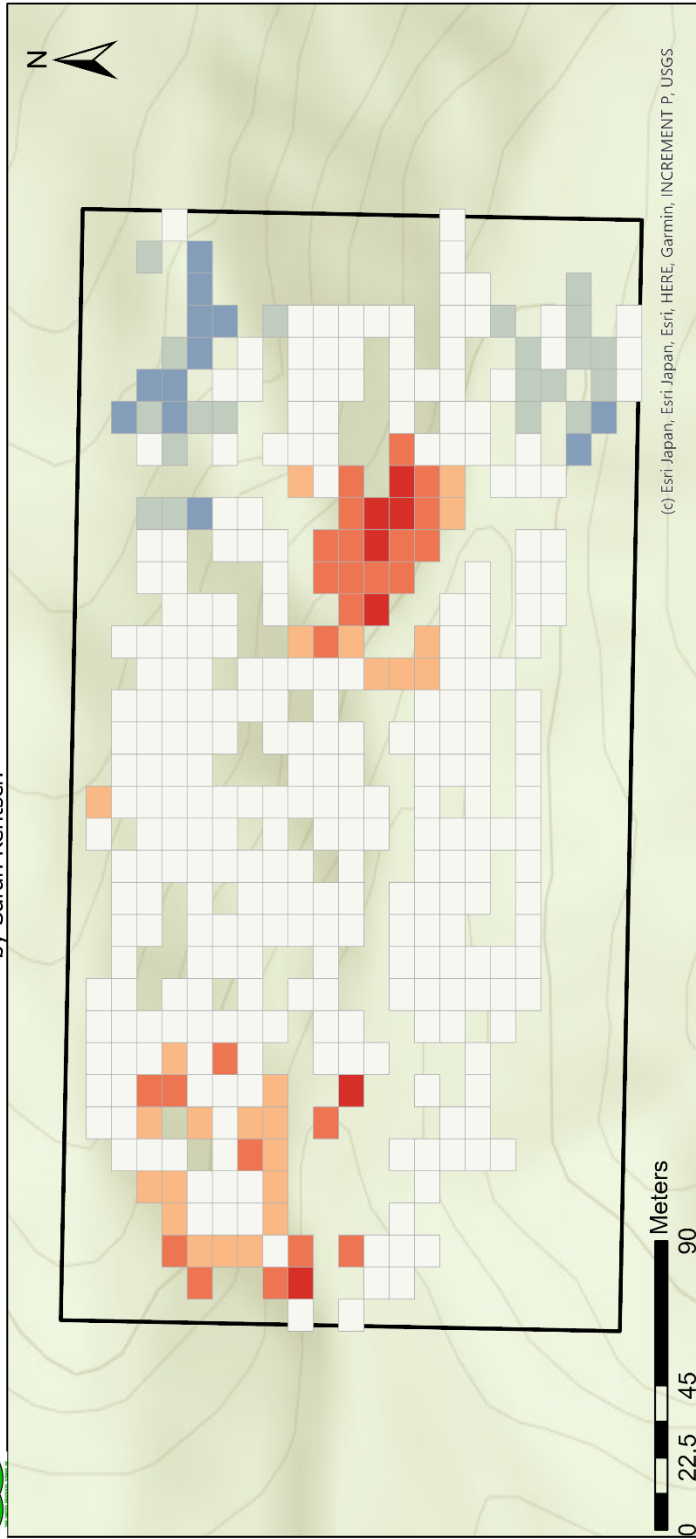
Hot spot analysis site 4 by Sarah Kentsch





Hot spot analysis site 5

by Sarah Kentsch



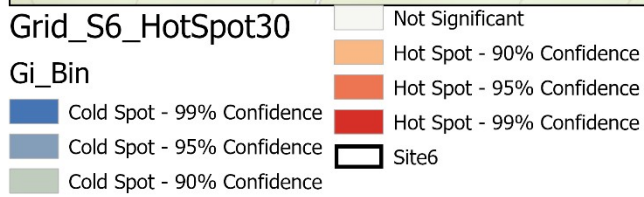
(c) Esri, Japan, Esri, HERE, Garmin, INCREMENT P, USGS.

Grid_S5_HotSpot40

- | | |
|---------------|----------------------------|
| White | Not Significant |
| Orange | Hot Spot - 90% Confidence |
| Red-Orange | Hot Spot - 95% Confidence |
| Red | Hot Spot - 99% Confidence |
| Blue | Cold Spot - 99% Confidence |
| Light Blue | Cold Spot - 95% Confidence |
| Grey | Cold Spot - 90% Confidence |
| Black outline | Site5 |

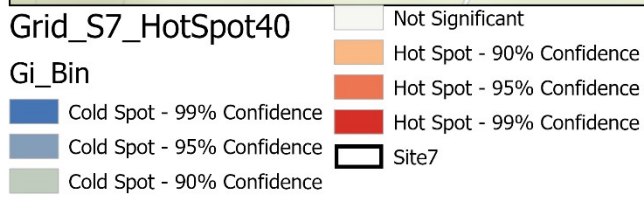
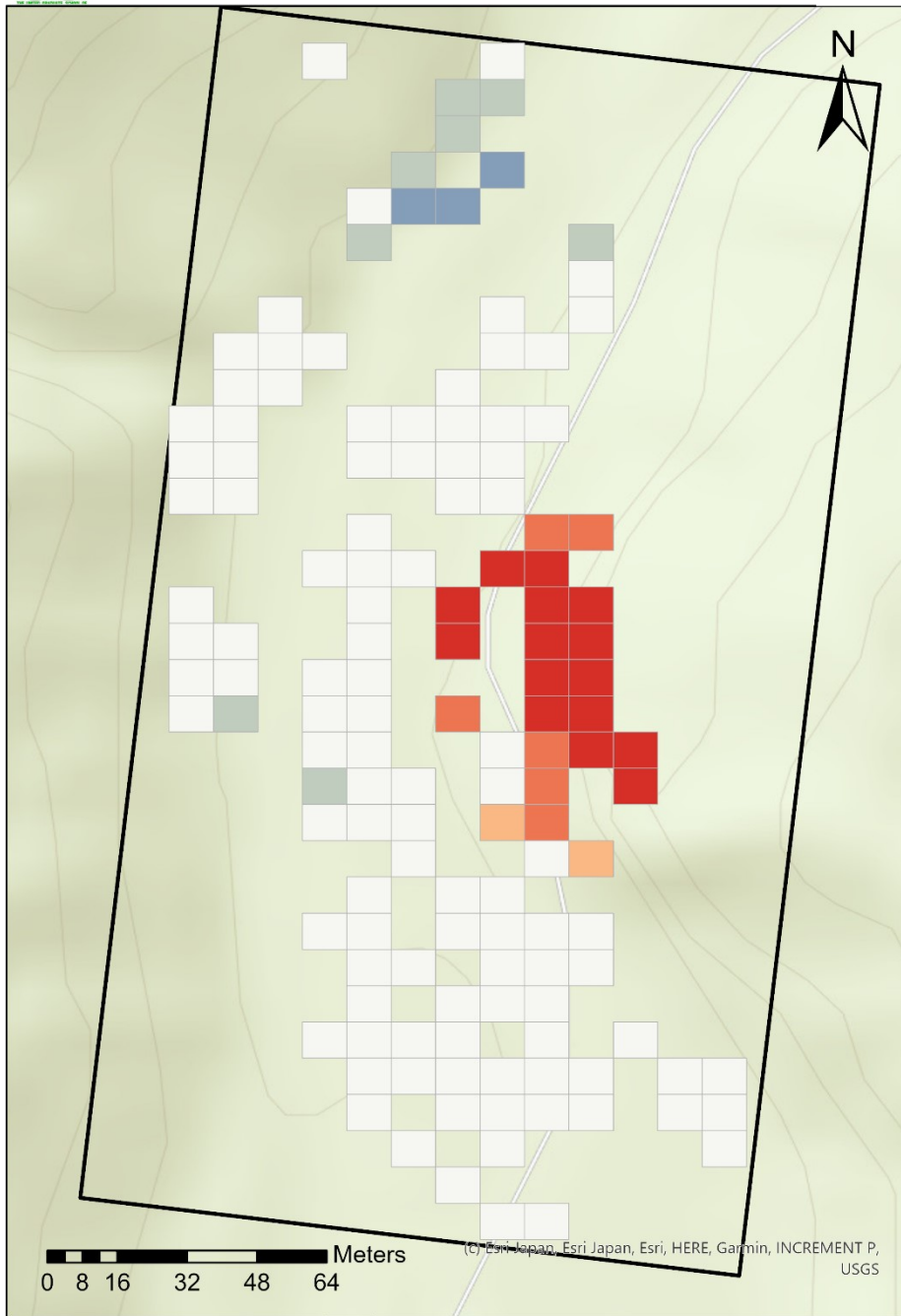


Hot spot analysis site 6 by Sarah Kentsch



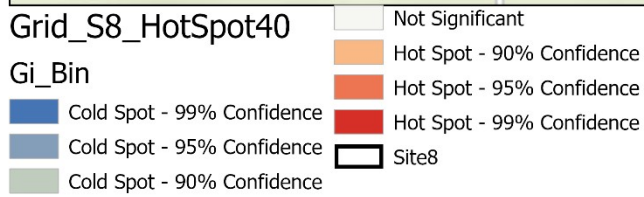
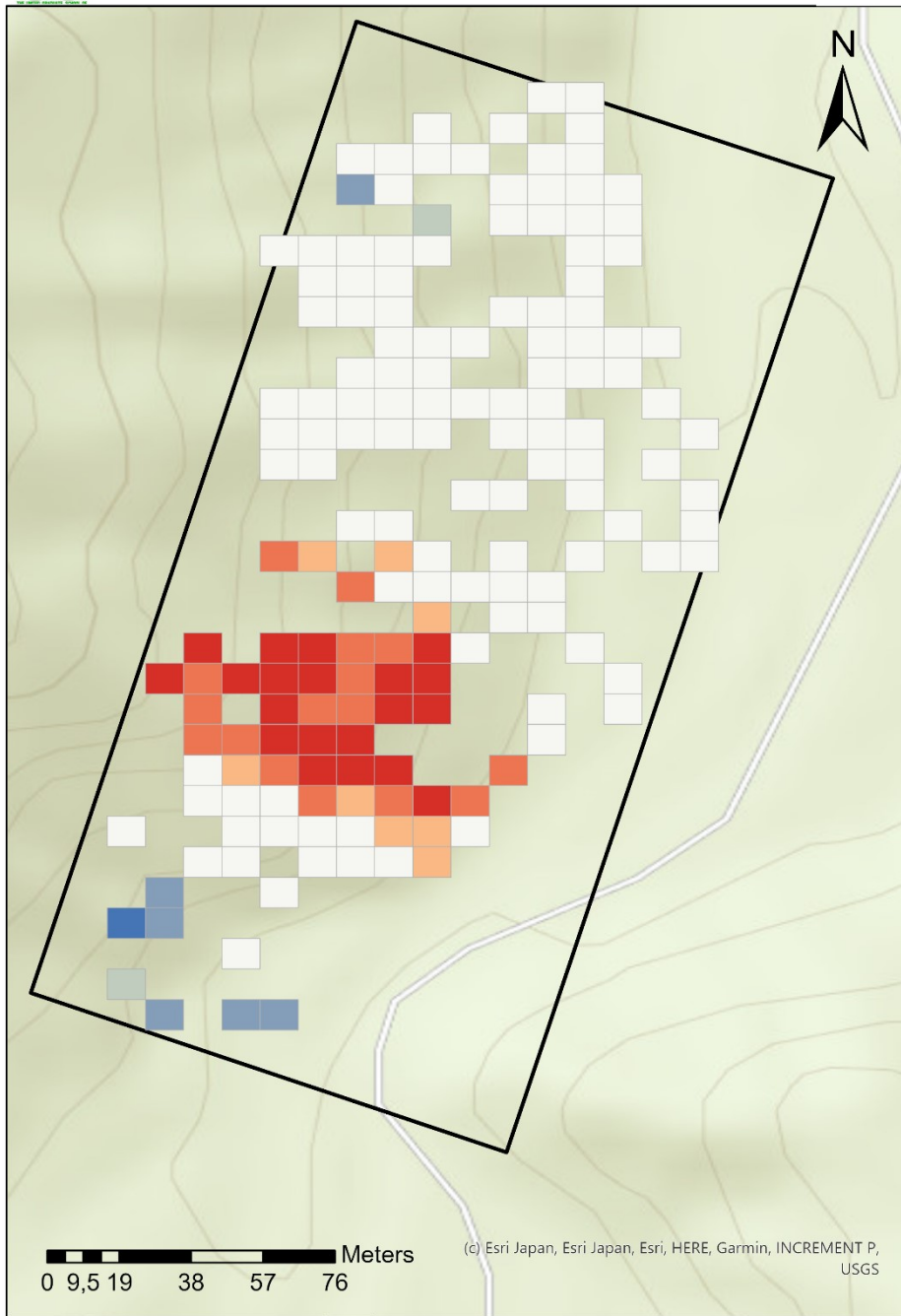


Hot spot analysis site 7 by Sarah Kentsch



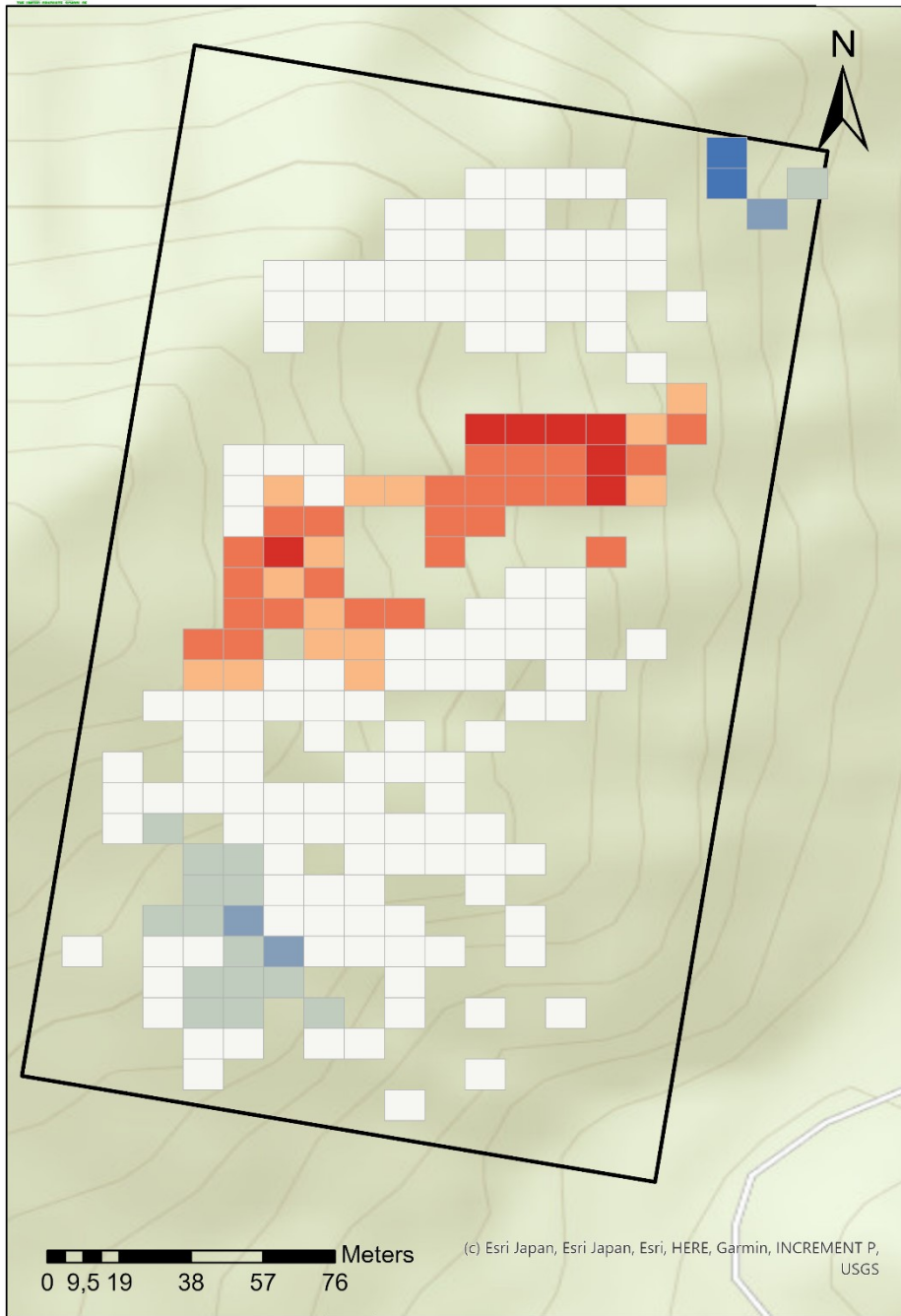


Hot spot analysis site 8 by Sarah Kentsch





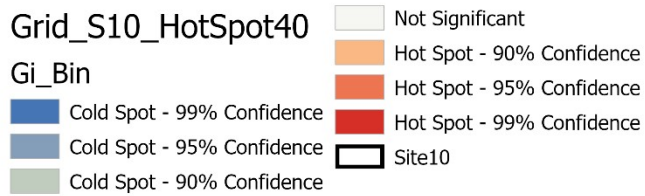
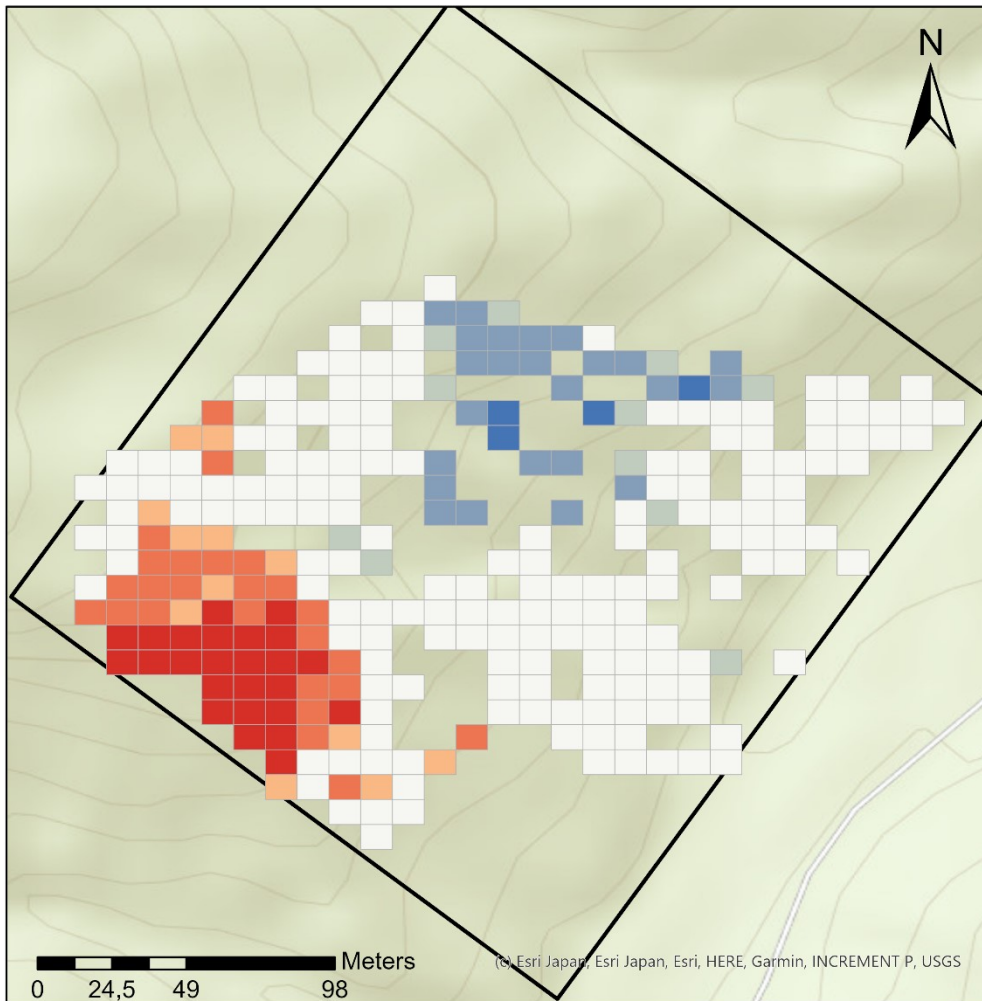
Hot spot analysis site 9 by Sarah Kentsch



- | | |
|----------------------------|---------------------------|
| Grid_S9_HotSpot40 | Not Significant |
| | Hot Spot - 90% Confidence |
| | Hot Spot - 95% Confidence |
| | Hot Spot - 99% Confidence |
| Gi_Bin | |
| Cold Spot - 99% Confidence | |
| Cold Spot - 95% Confidence | |
| Cold Spot - 90% Confidence | |
| | Site9 |



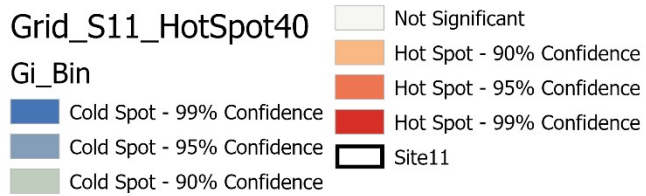
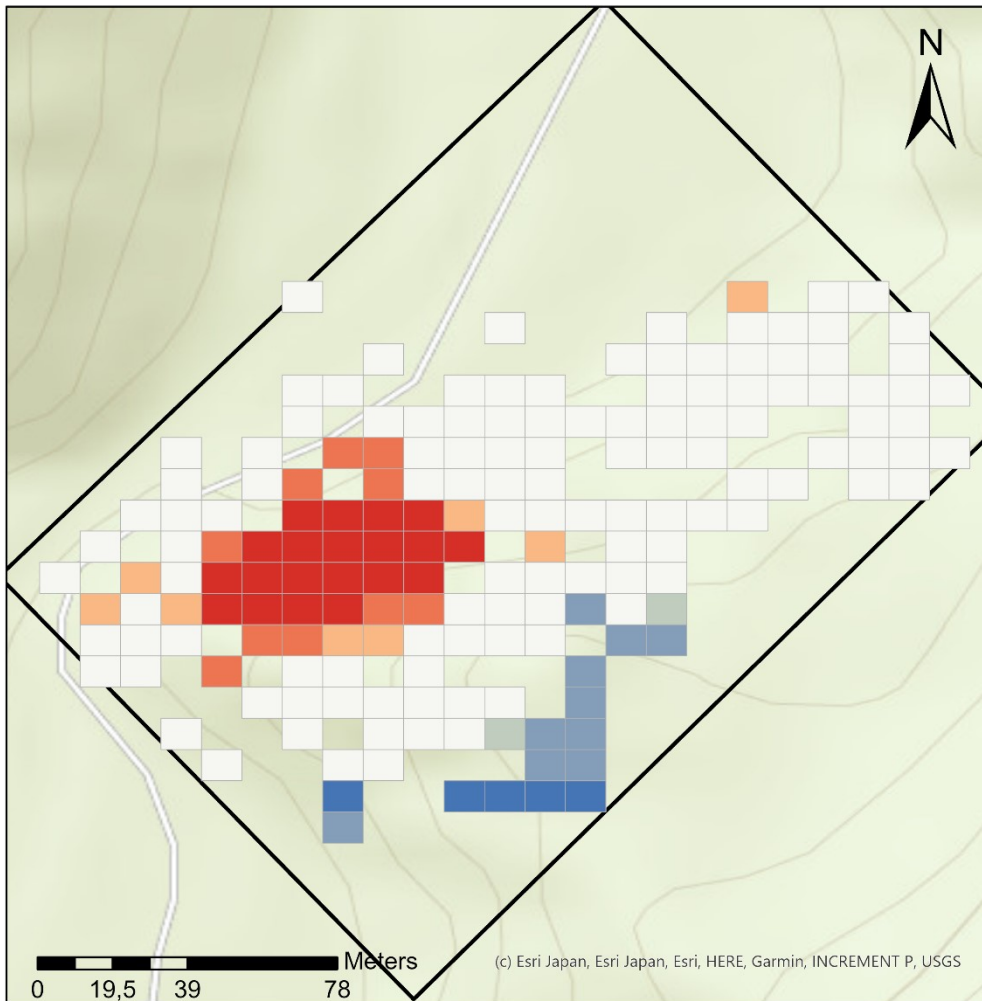
Hot spot analysis site 10 by Sarah Kentsch





Hot spot analysis site 11

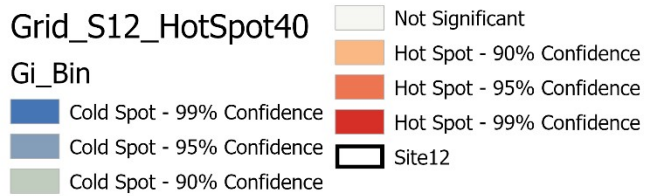
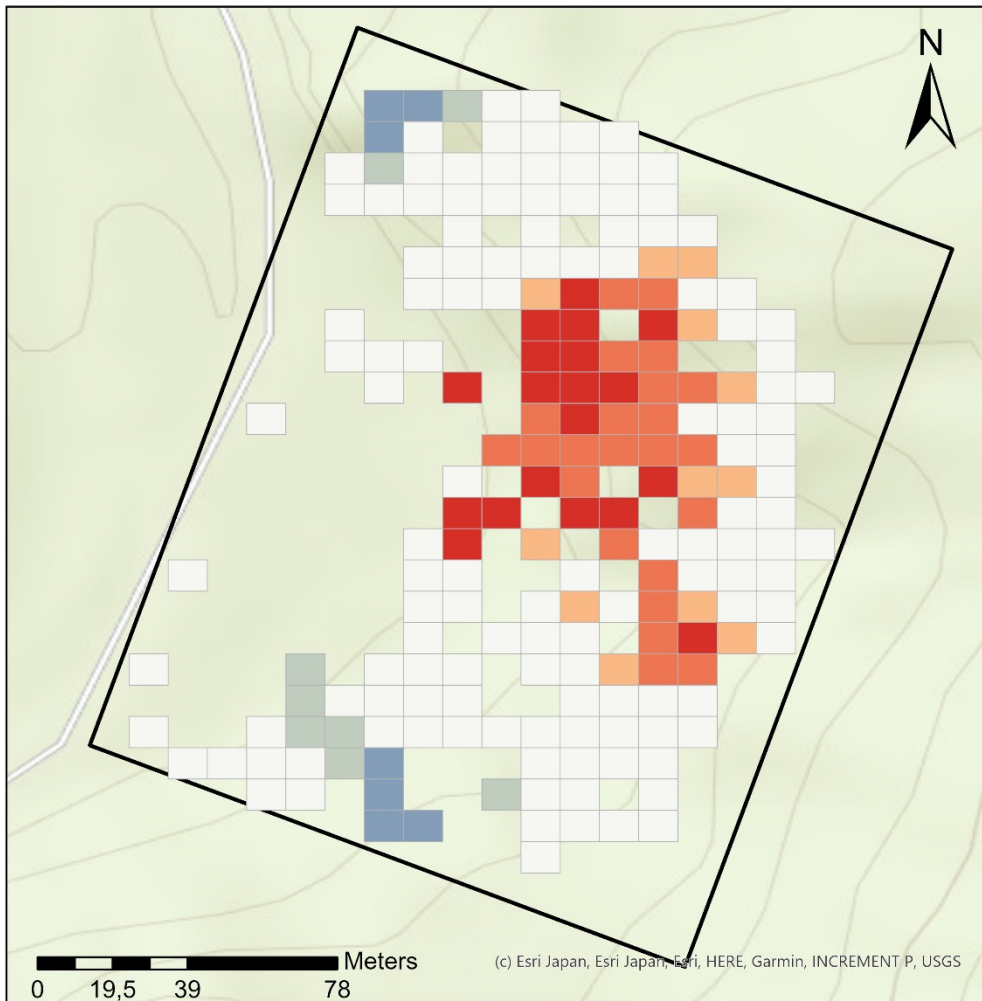
by Sarah Kentsch





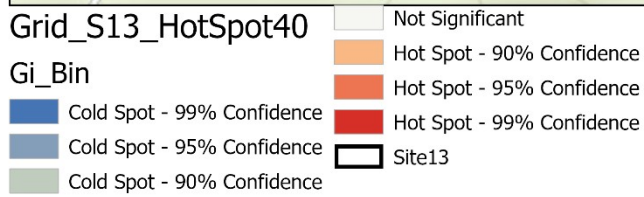
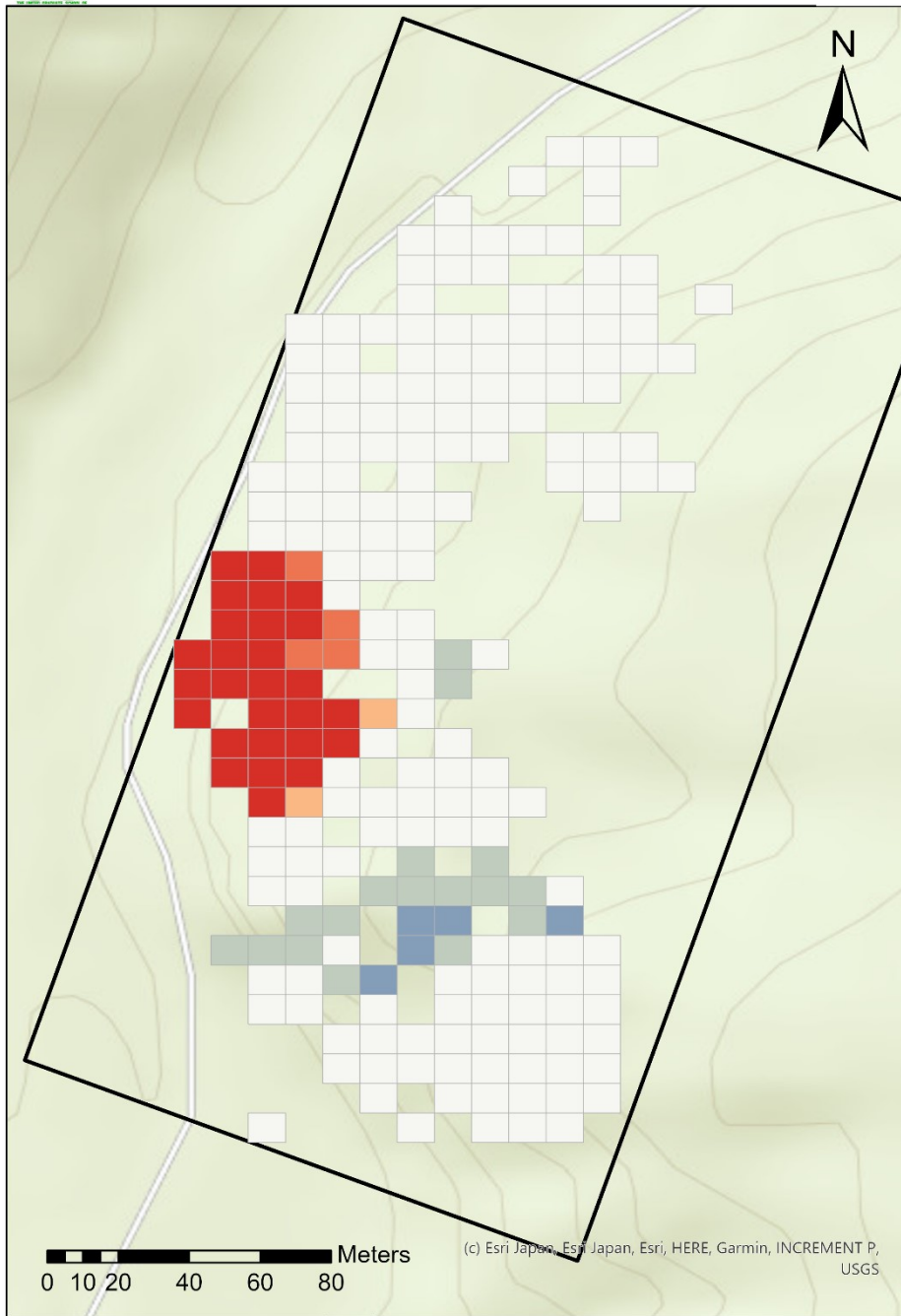
Hot spot analysis site 12

by Sarah Kentsch





Hot spot analysis site 13 by Sarah Kentsch



Appendix N – GIS analyses maps

Contained are distribution maps based on image analysis performed in ArcGIS pro. The analyses were performed for small-leaved Acer species, *Acer mono maxim*, *Aesculus turbinata*, *Cornus controversa*, *Fagus crenata*, *Juglans ailantifolia*, *Magnolia obovata*, *Pterocarya rhoifolia*, *Quercus mongolica*, *Robinia pseudoacacia*, *Salix* species and *Tilia* species.

Part 1: Contained the maps for the different species for the sites located in the south (6, 7, 8, 9, 10, 11, 12, 13)

Part 2: Contained the maps for the different species for the sites located in the south (1, 2, 3, 4, 5).

Part 3: Hot spot analysis for the northern sites for the different tree species

Part 4: Hot spot analysis for the southern sites for the different tree species.

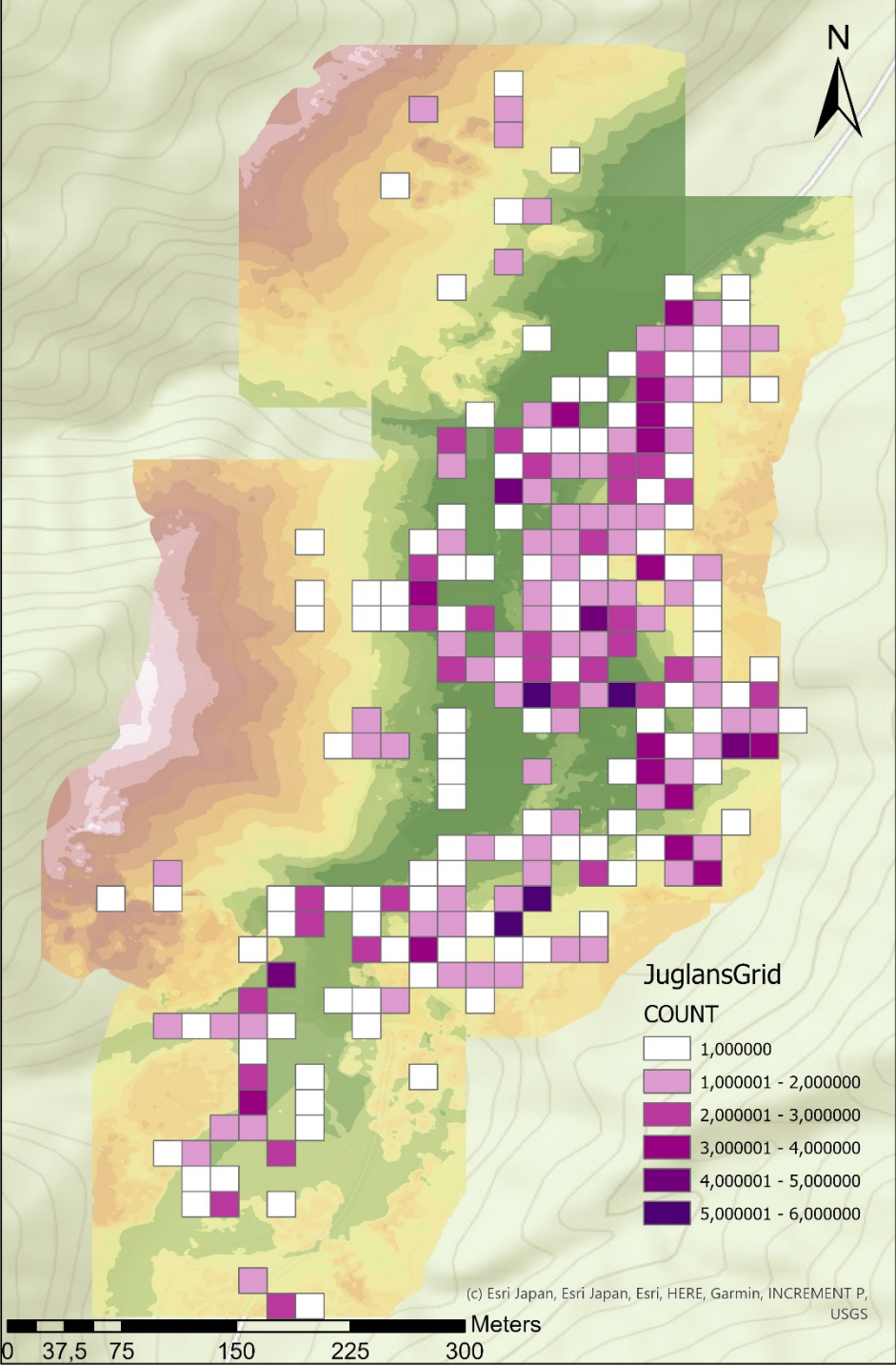
Part 5: Hot spot analysis to differentiate between riparian and terrace/slope sites.

Part 1: Contained the maps for the different species for the sites located in the south (6, 7, 8, 9, 10, 11, 12, 13)



Juglans ailantifolia distribution

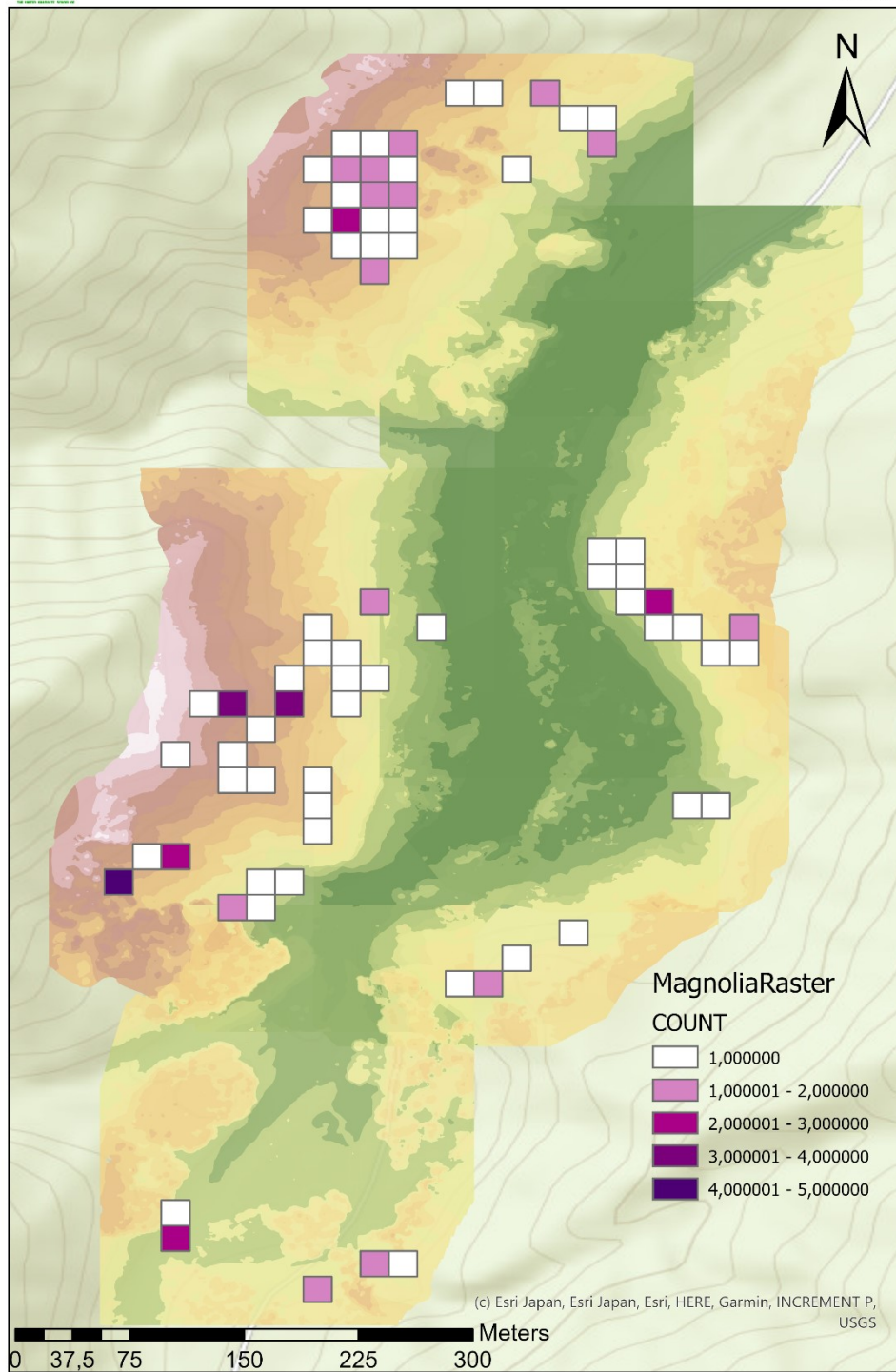
by Sarah Kentsch





Magnolia obovata distribution

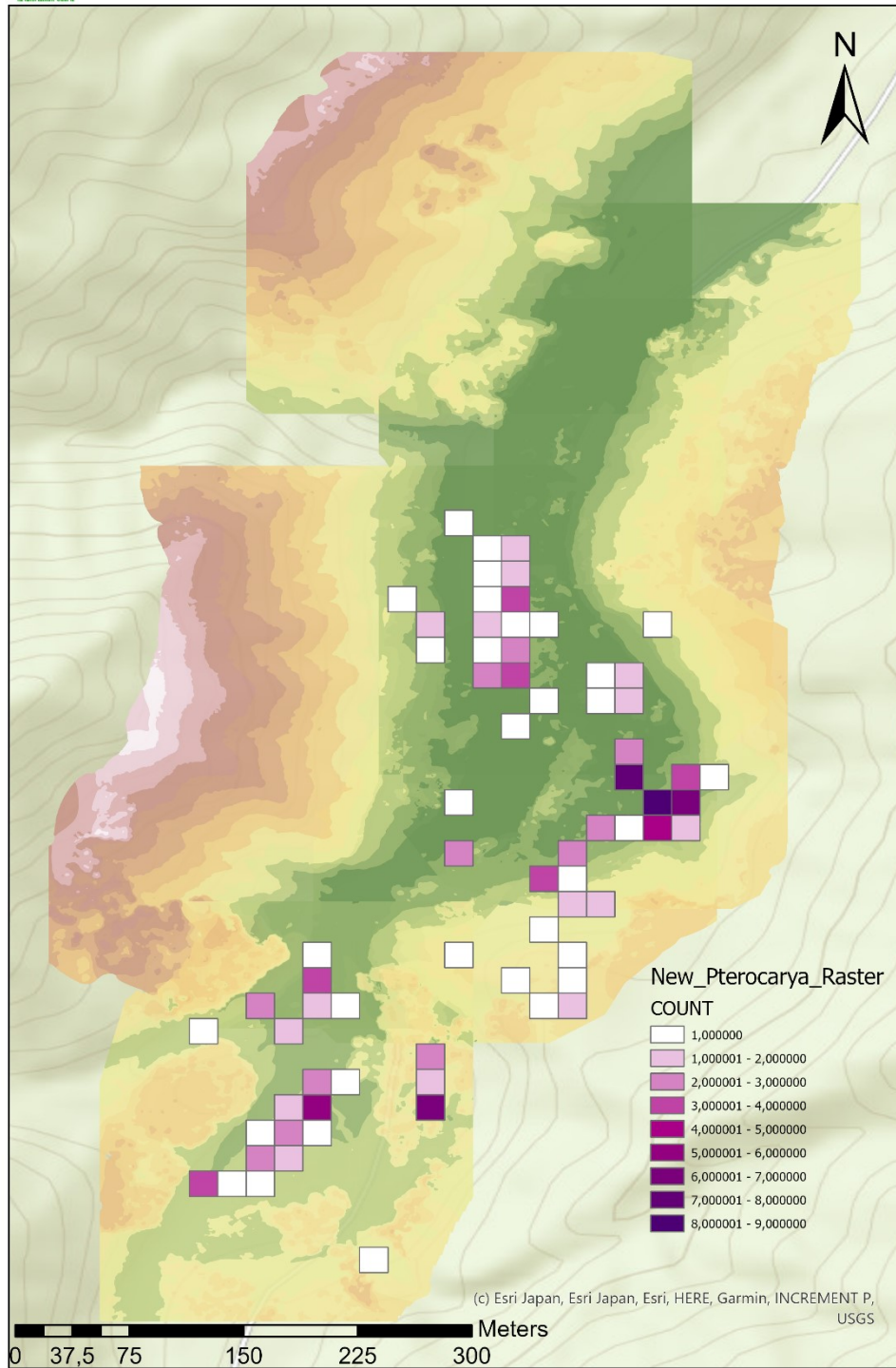
by Sarah Kentsch





Pterocarya rhoifolia distribution

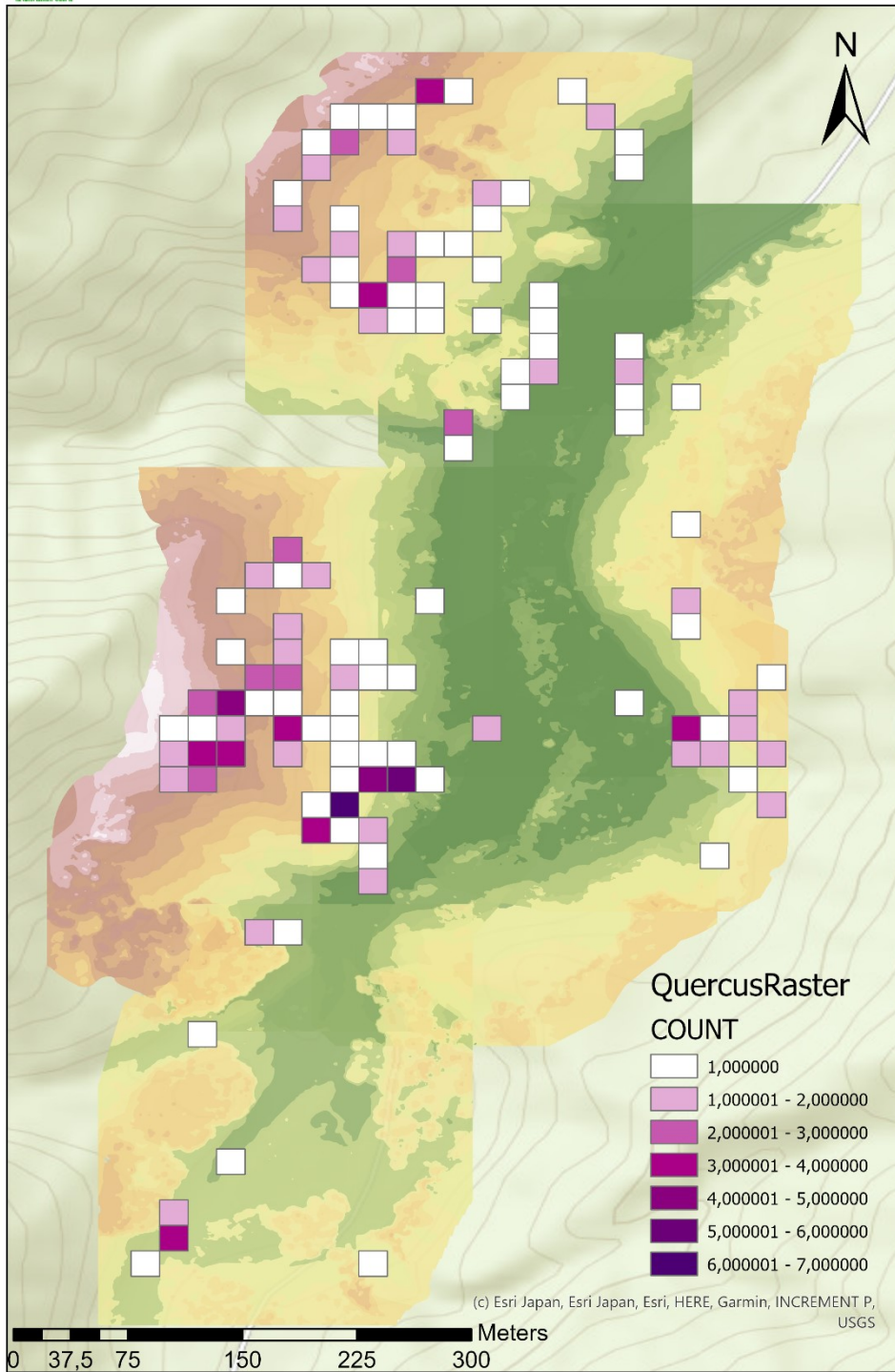
by Sarah Kentsch





Quercus mongolica distribution

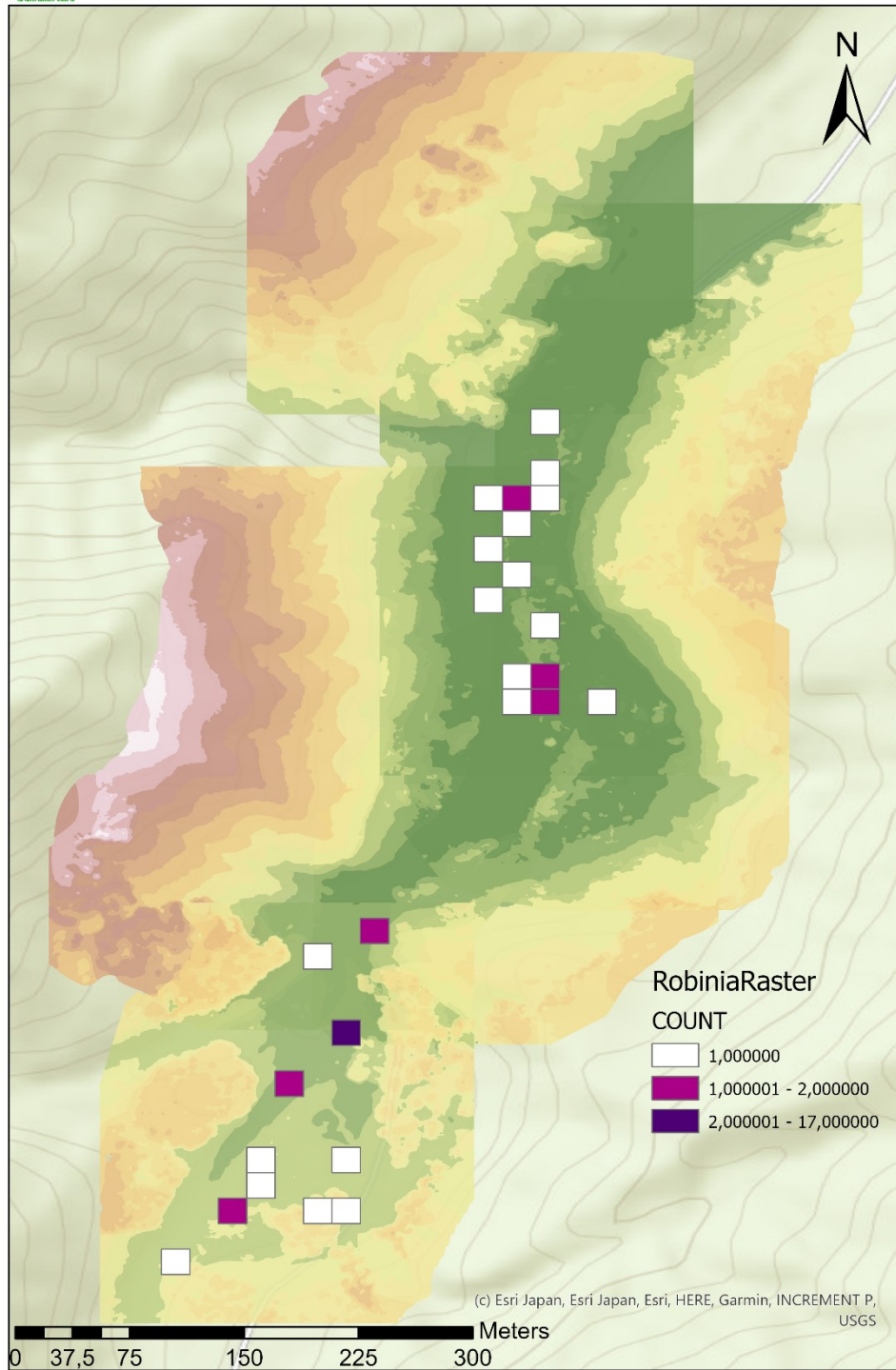
by Sarah Kentsch





Robinia pseudoacacia distribution

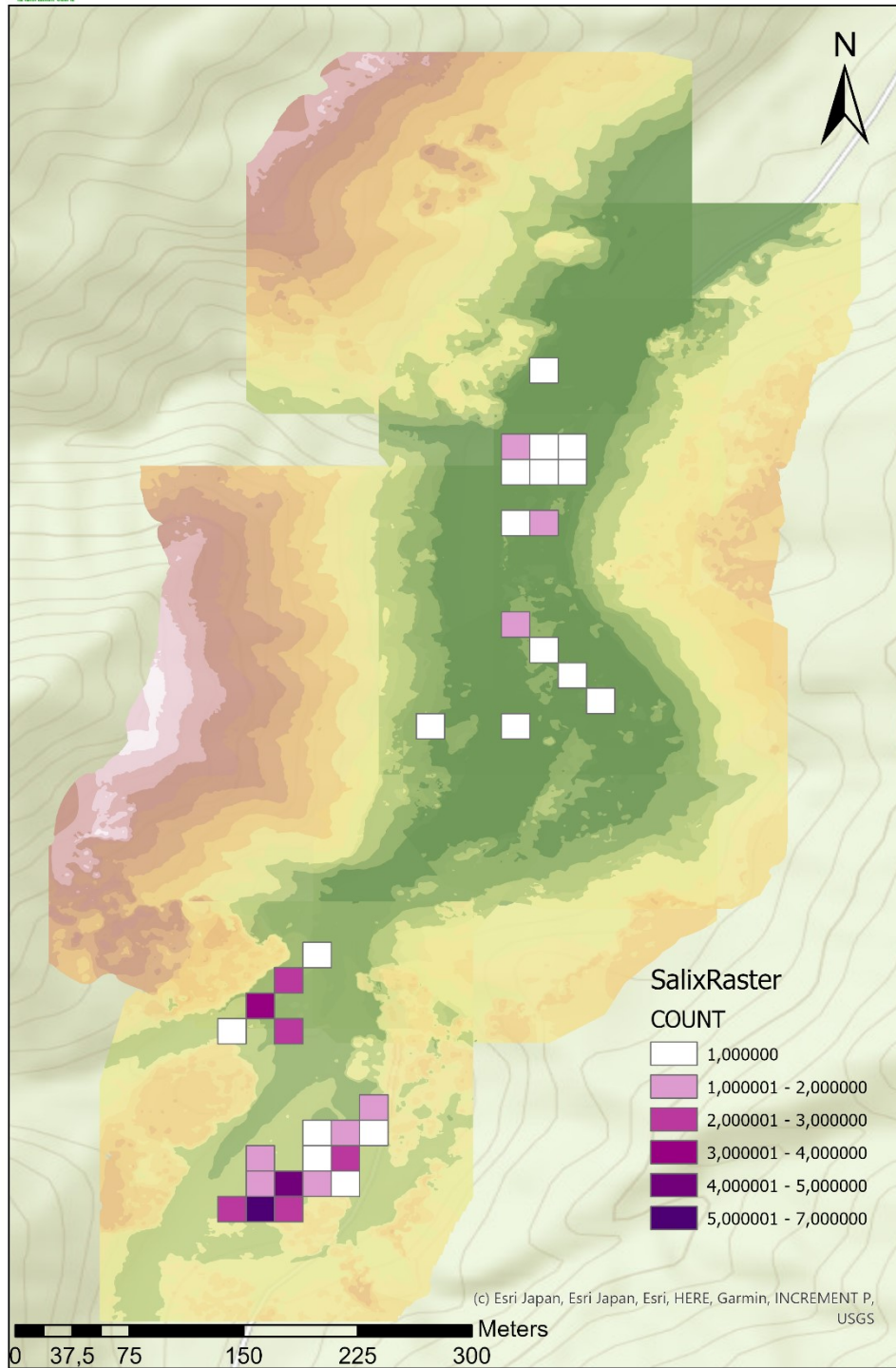
by Sarah Kentsch





Salix distribution

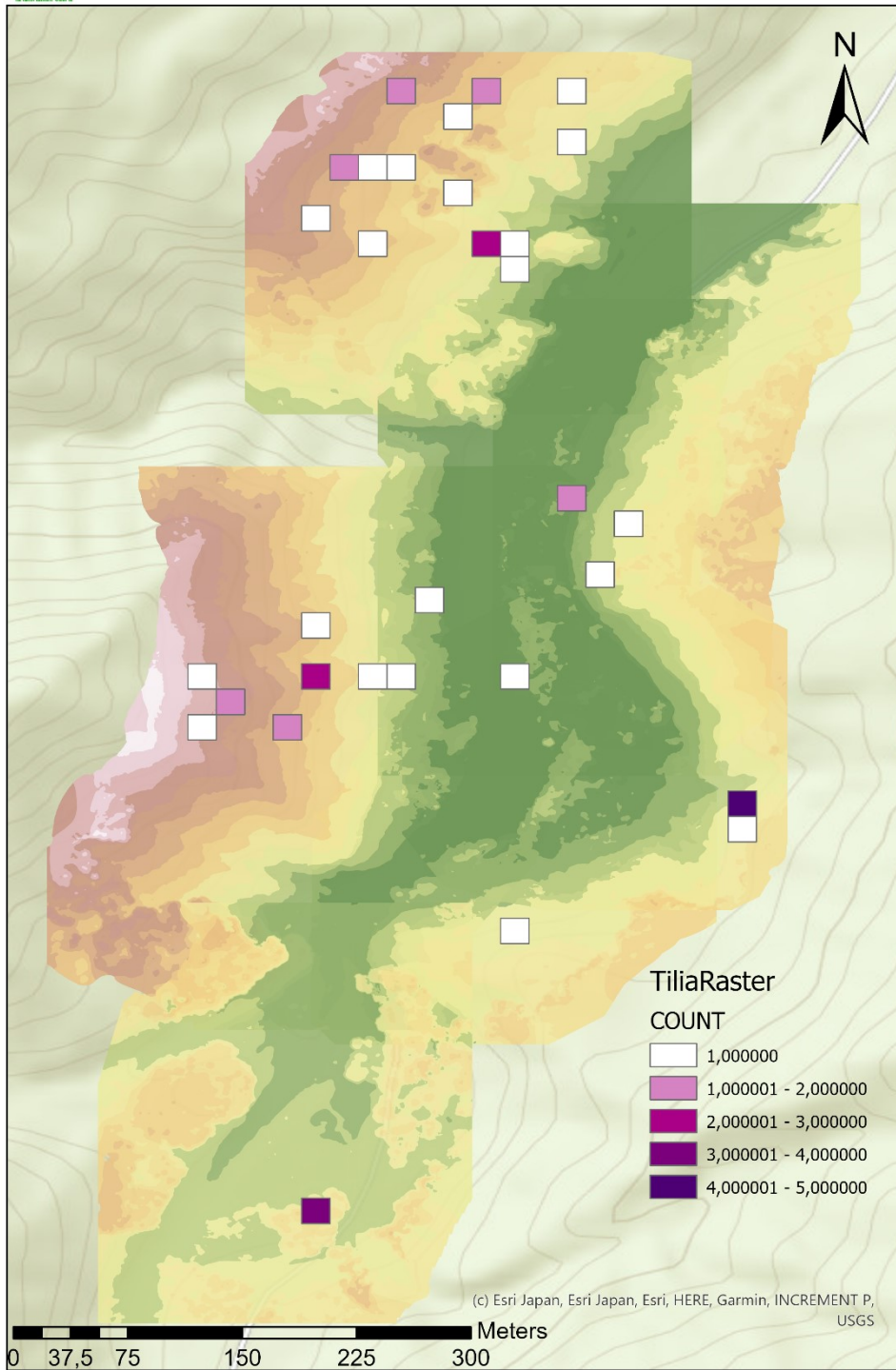
by Sarah Kentsch





Tilia distribution

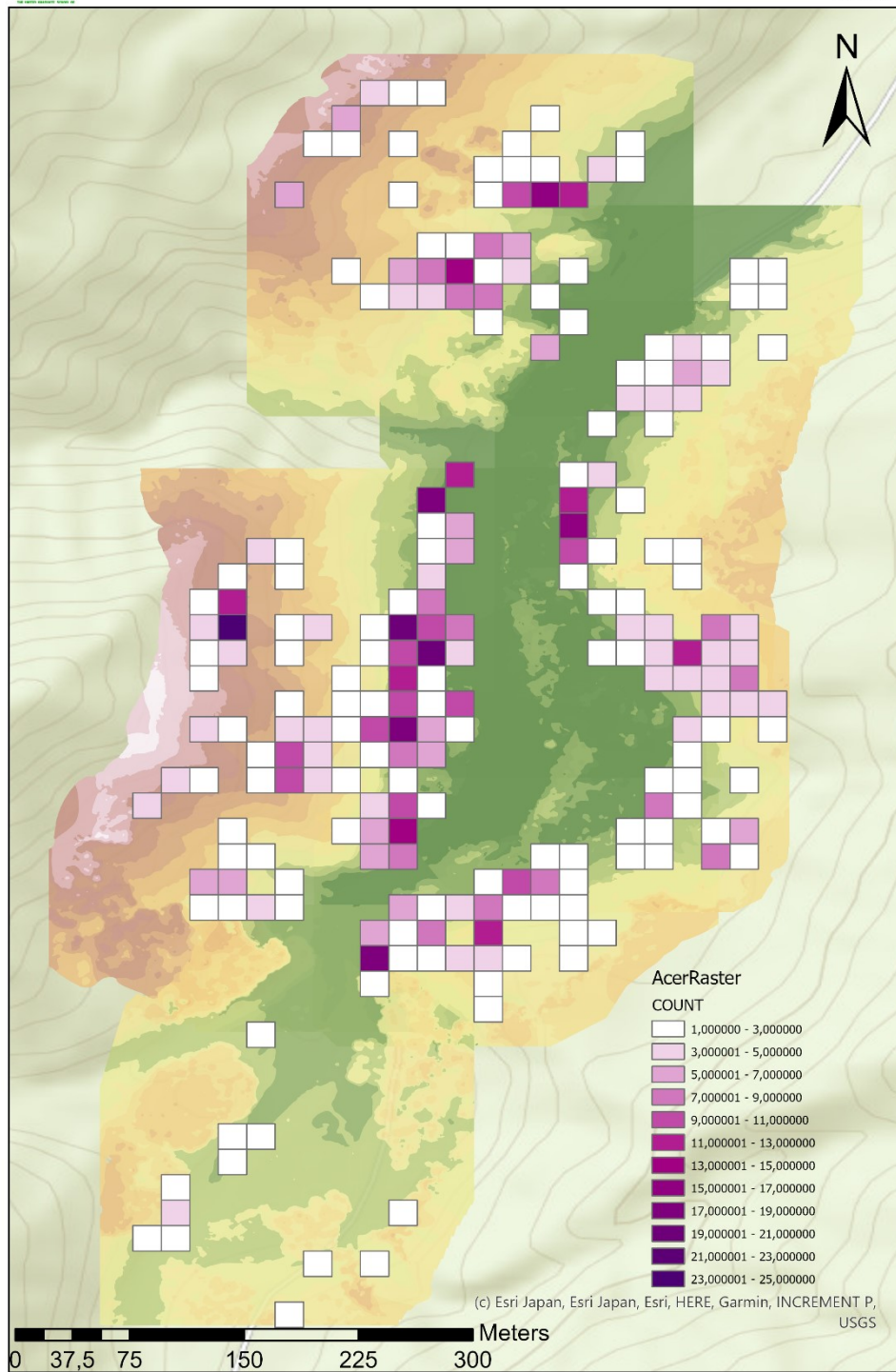
by Sarah Kentsch





Acer distribution

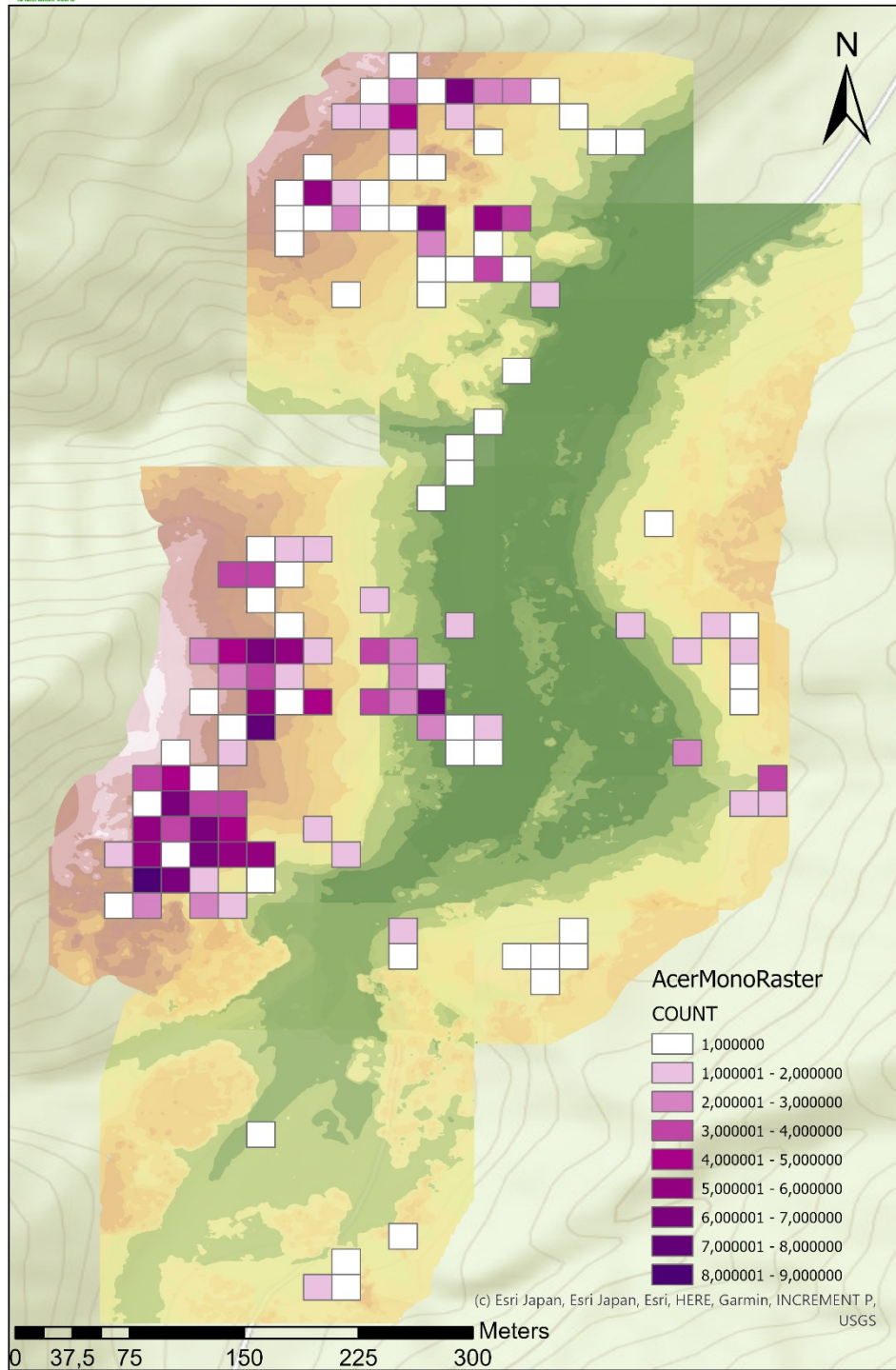
by Sarah Kentsch





Acer mono maxim distribution

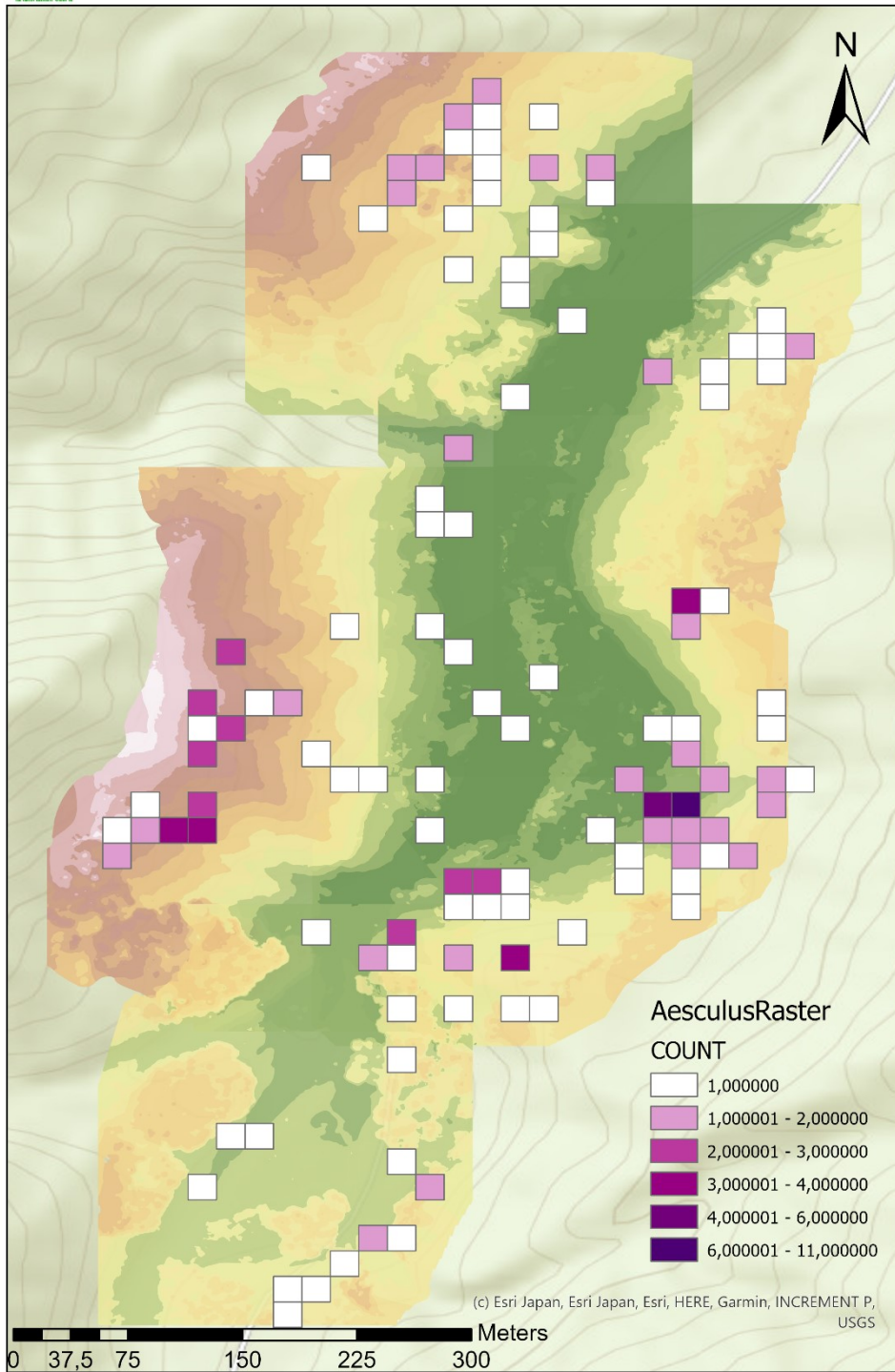
by Sarah Kentsch





Aesculus turbinata distribution

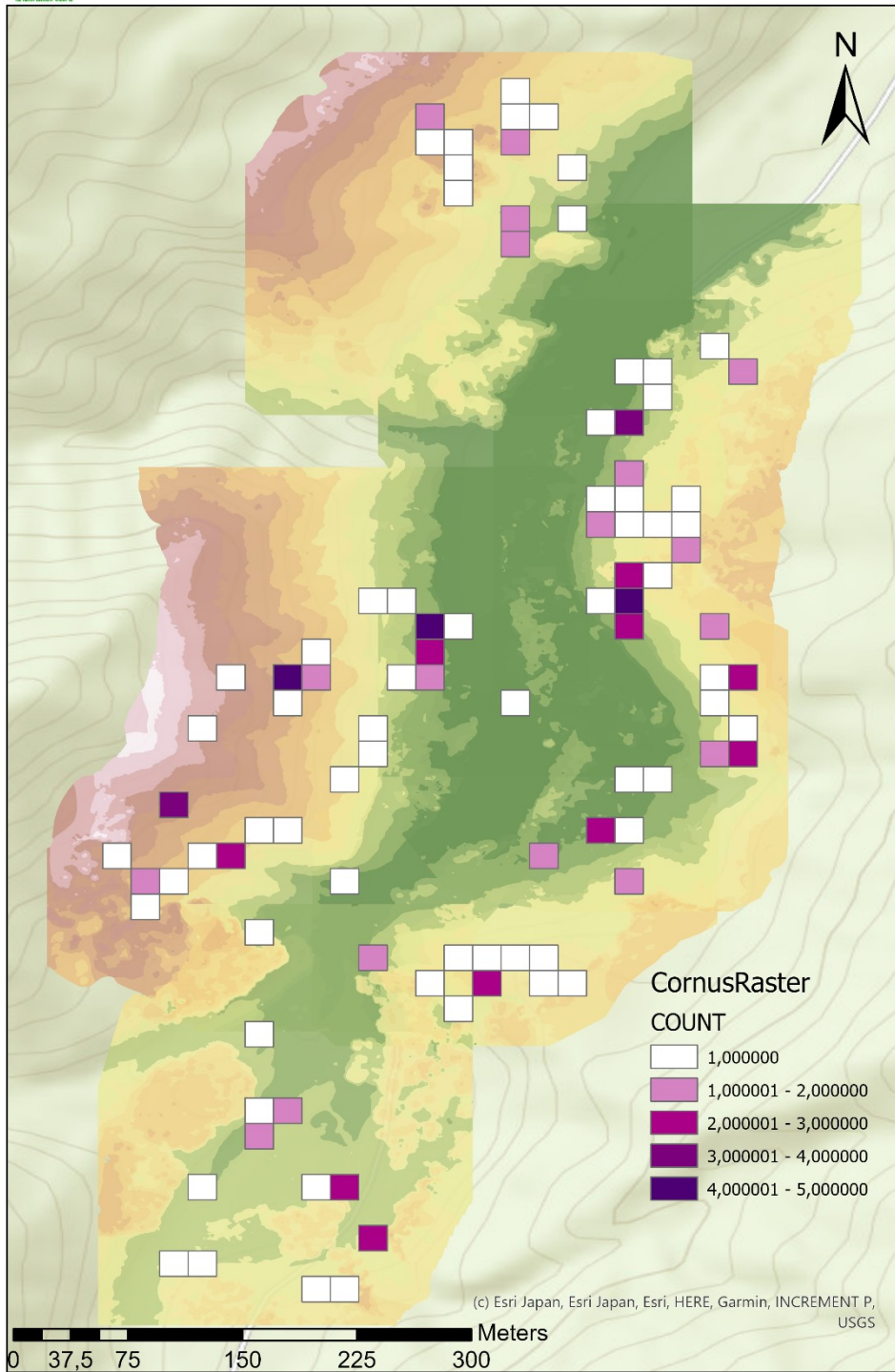
by Sarah Kentsch





Cornus controversa distribution

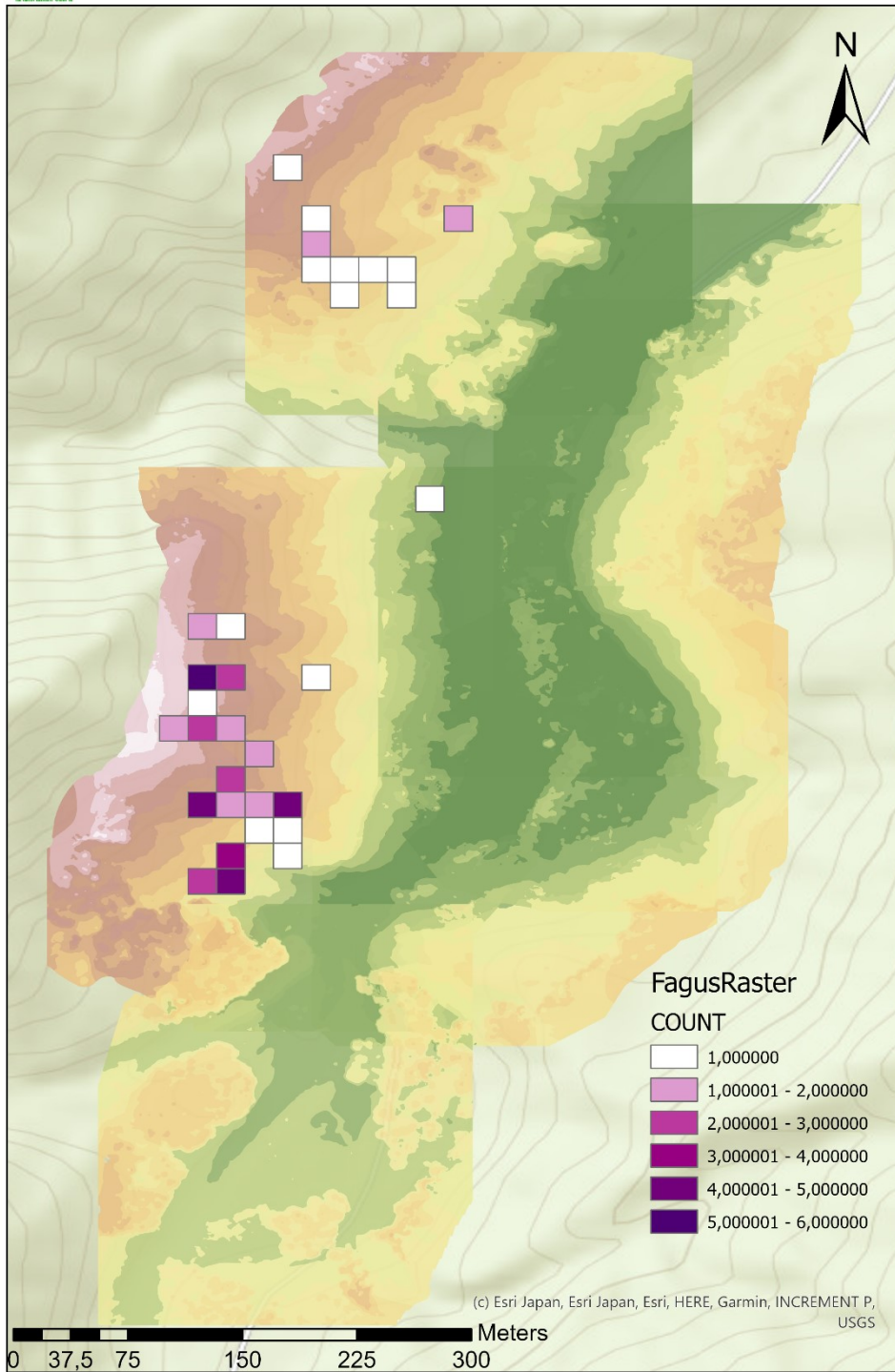
by Sarah Kentsch





Fagus crenata distribution

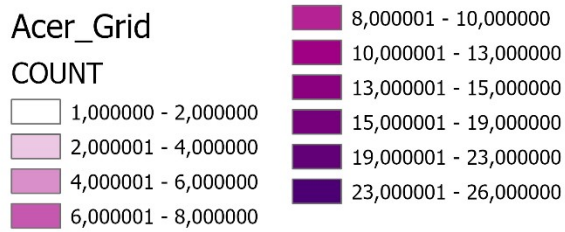
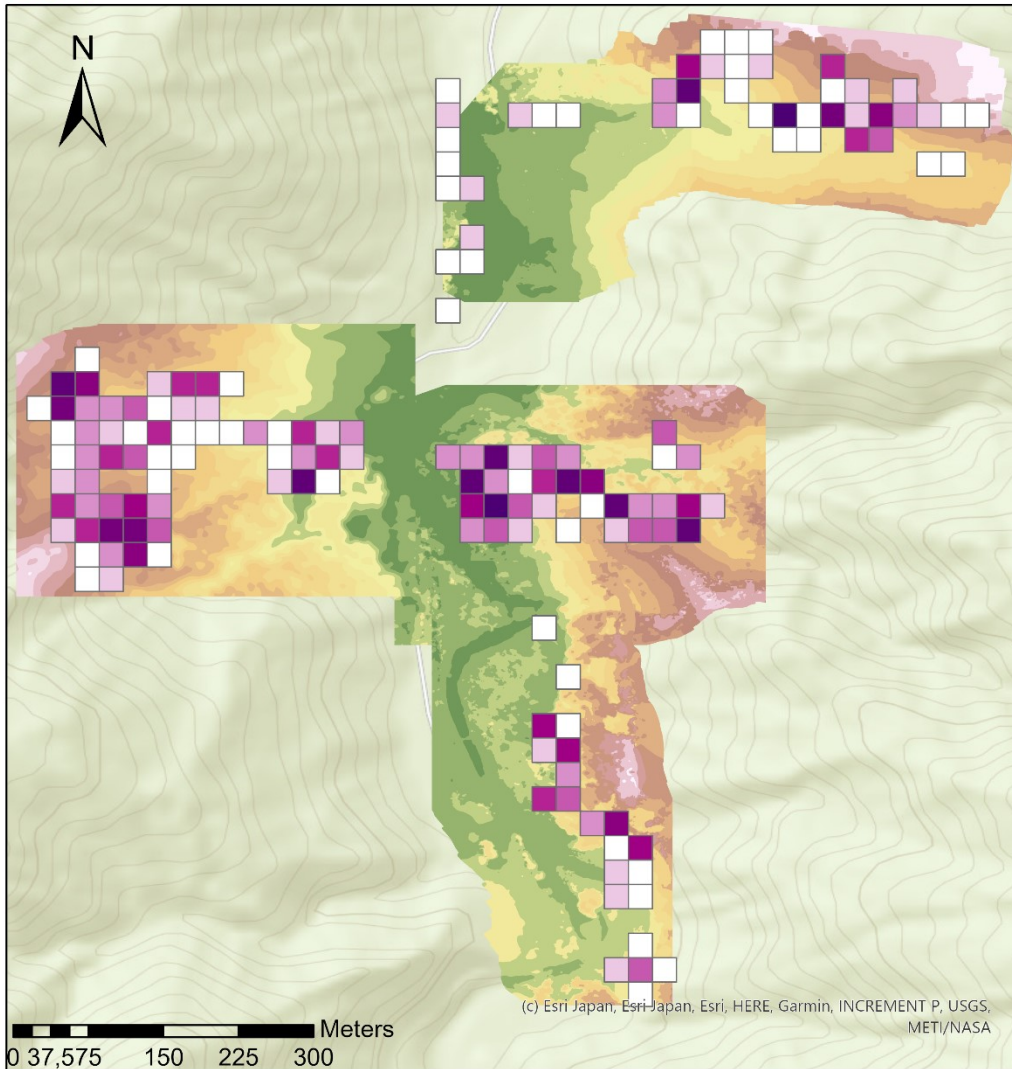
by Sarah Kentsch



Part 2: Contained the maps for the different species for the sites located in the south (1, 2, 3, 4, 5).

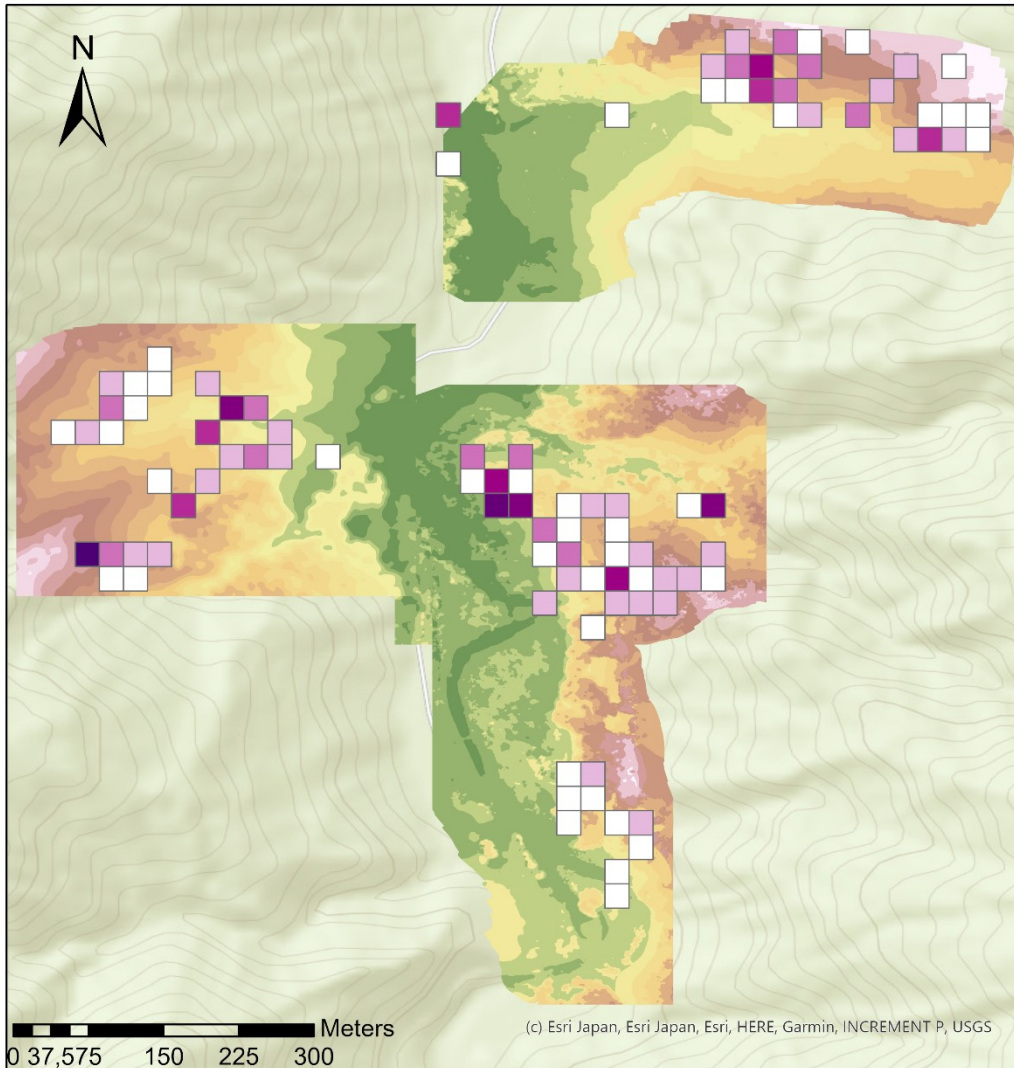


Acer distribution by Sarah Kentsch





Acer mono maxim distribution by Sarah Kentsch



Acermono_Grid

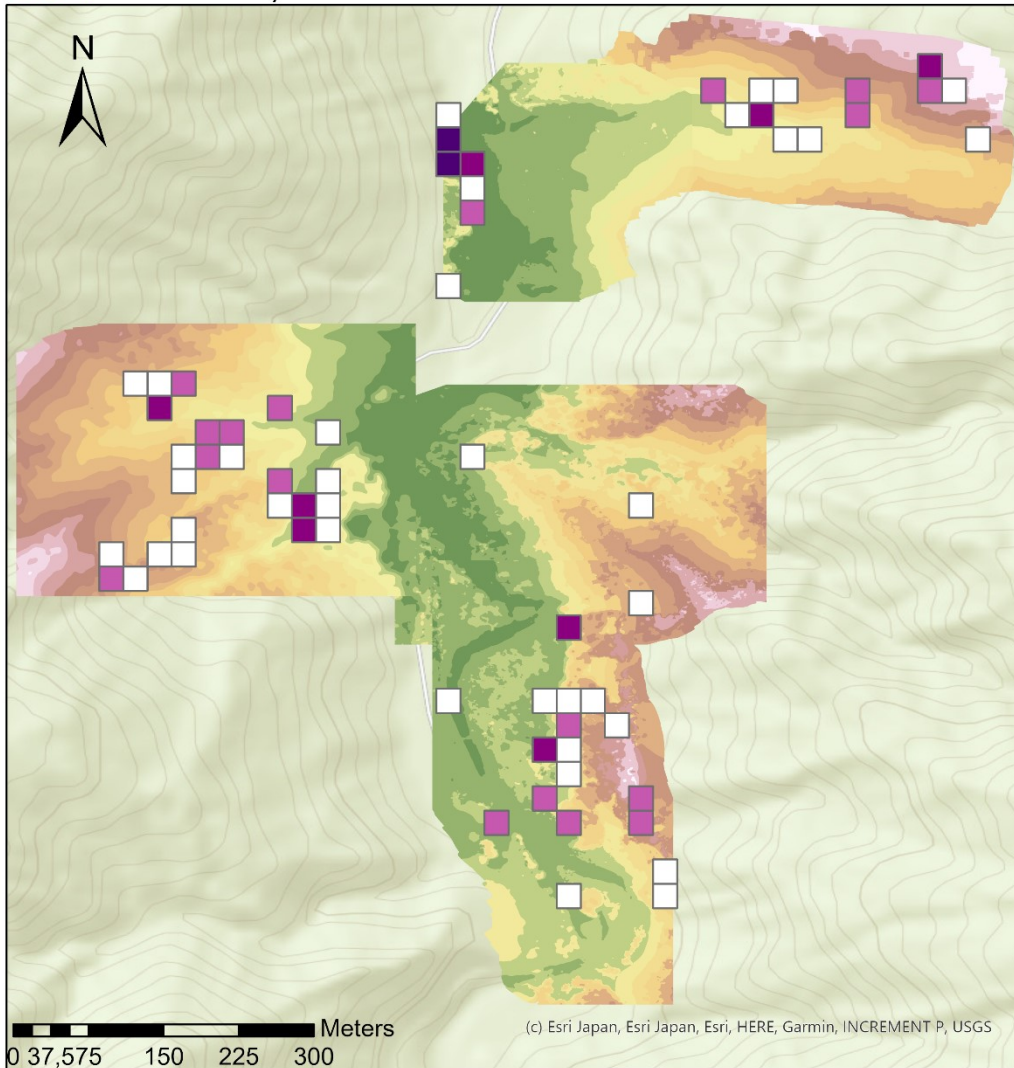
COUNT

	1,000000
	1,000001 - 2,000000
	2,000001 - 3,000000
	3,000001 - 4,000000
	4,000001 - 5,000000
	5,000001 - 6,000000
	6,000001 - 8,000000
	8,000001 - 9,000000



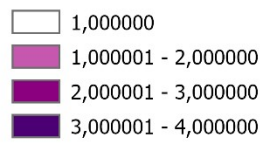
Aesculus turbinata distribution

by Sarah Kentsch



Aesculus_Grid

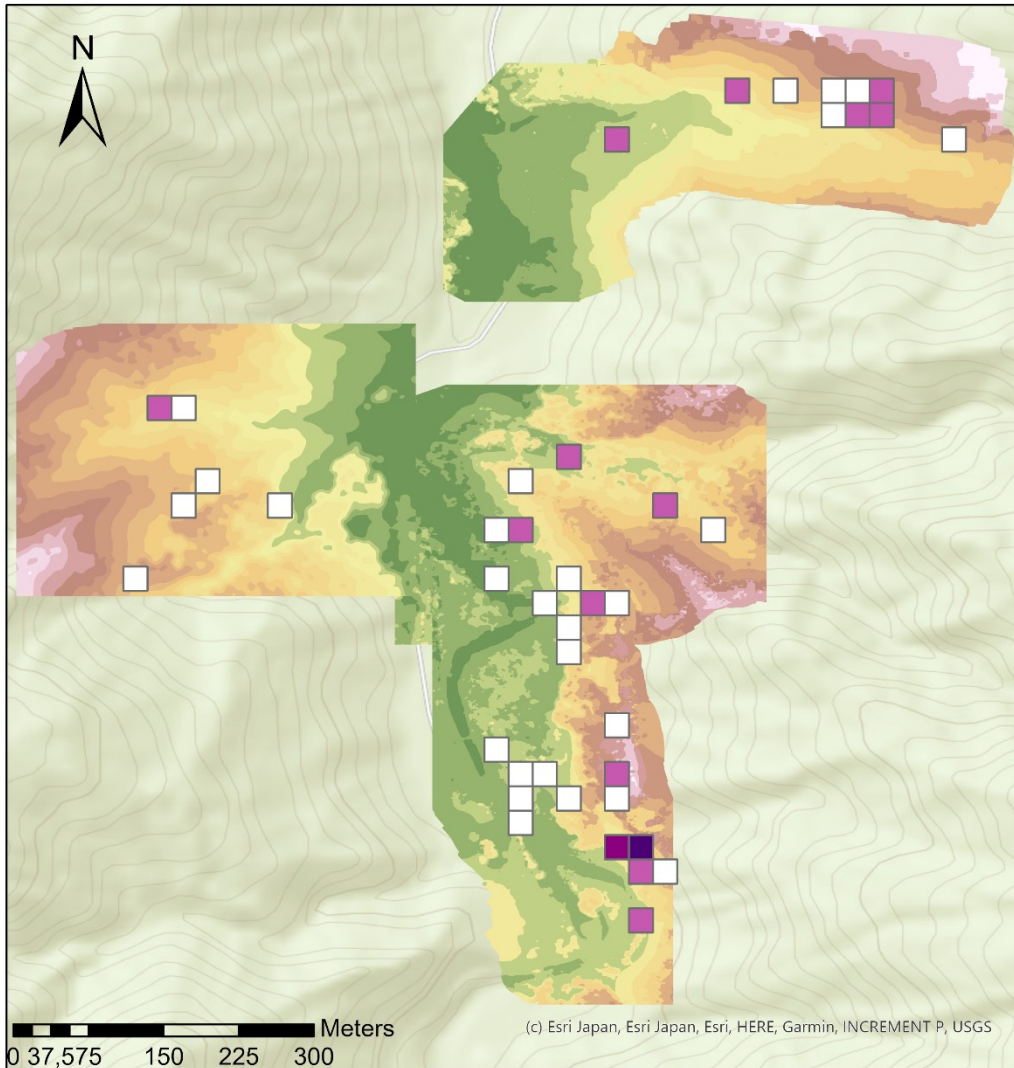
COUNT









Cornus controversa distribution

by Sarah Kentsch



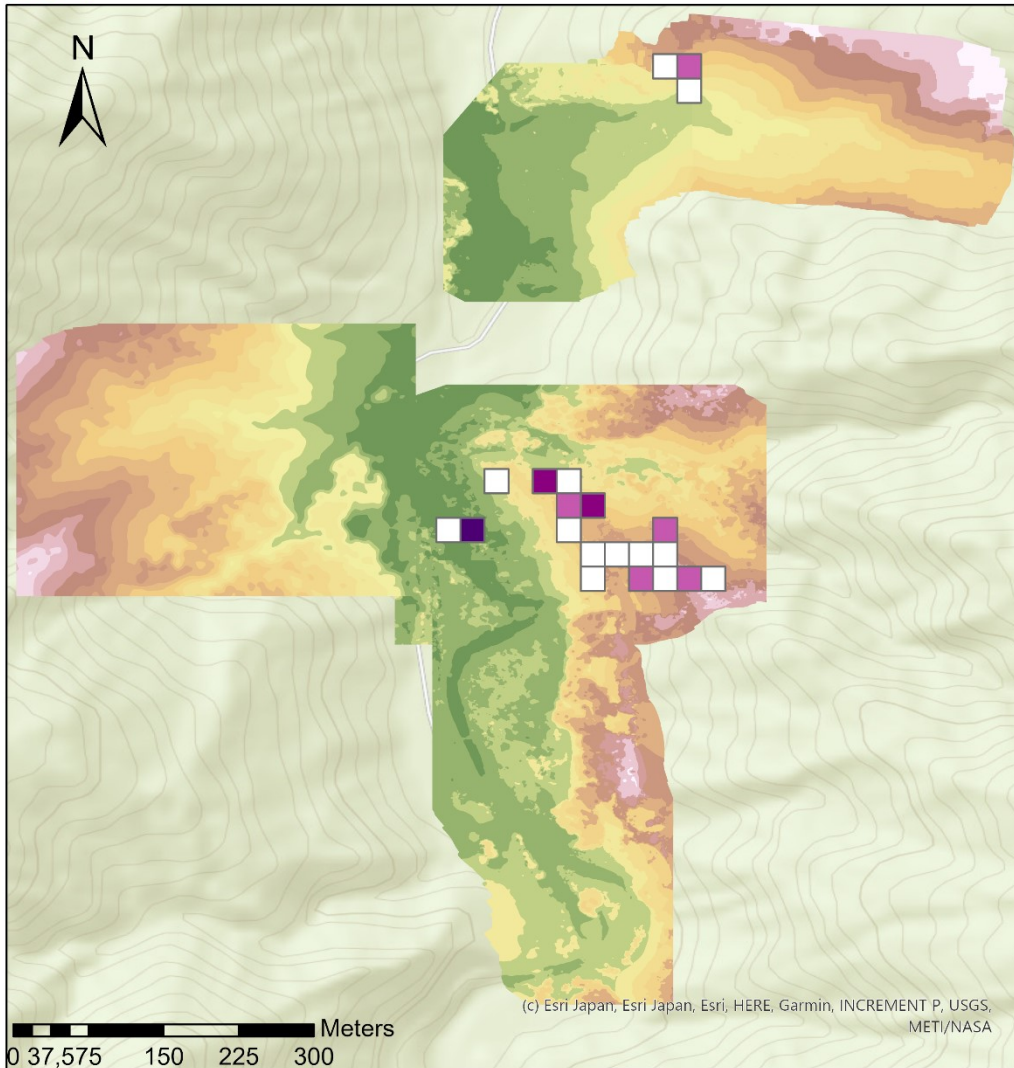
Cornus_Grid

COUNT

-  1,000000
-  1,000001 - 2,000000
-  2,000001 - 3,000000
-  3,000001 - 10,000000







Fagus crenata distribution by Sarah Kentsch



Fagus_Grid

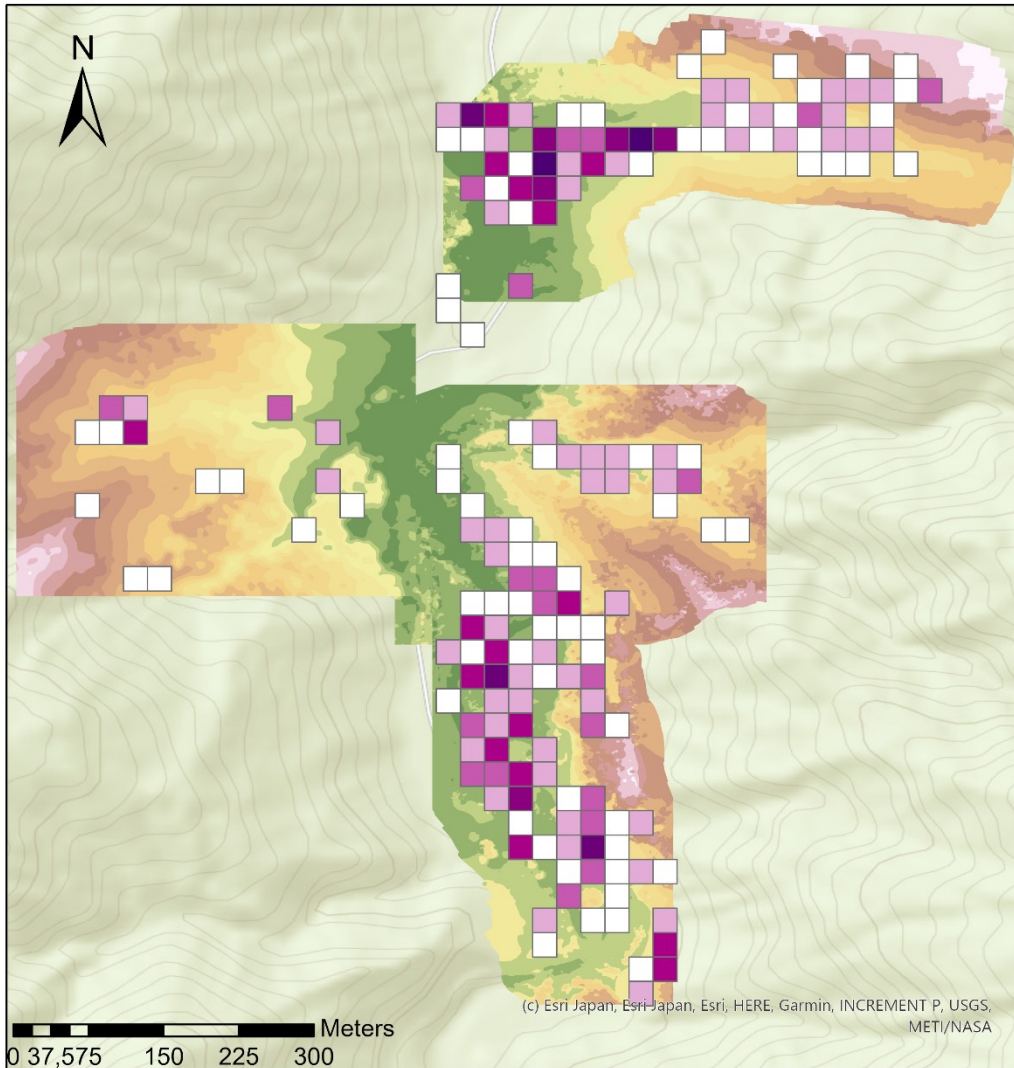
COUNT

-  1,000000
-  1,000001 - 2,000000
-  2,000001 - 3,000000
-  3,000001 - 4,000000



Juglans ailantifolia distribution

by Sarah Kentsch



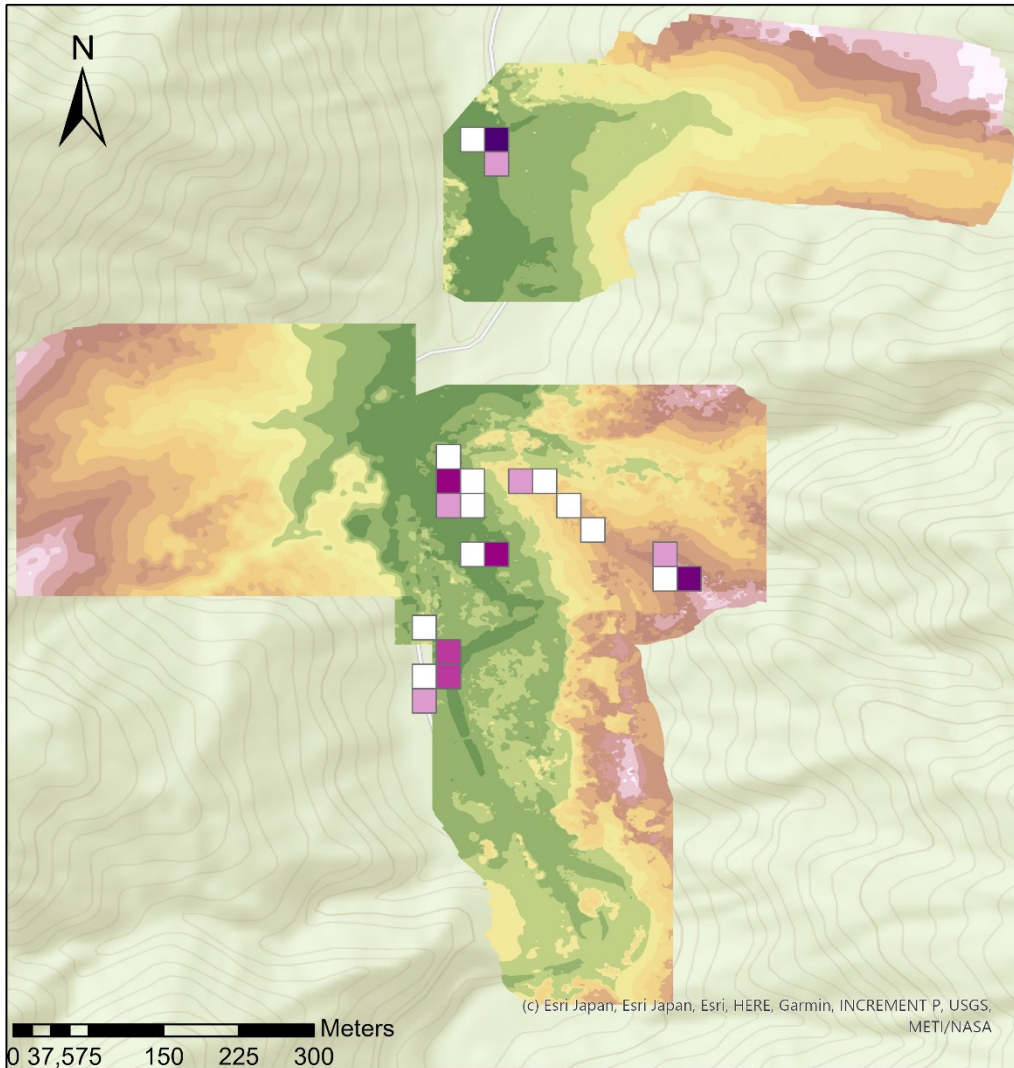
Juglans_Grid

COUNT

	1,000000
	1,000001 - 2,000000
	2,000001 - 3,000000
	3,000001 - 4,000000
	4,000001 - 5,000000
	5,000001 - 6,000000
	6,000001 - 10,000000

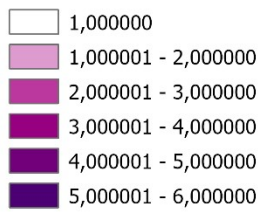


Larix kaempferi distribution by Sarah Kentsch



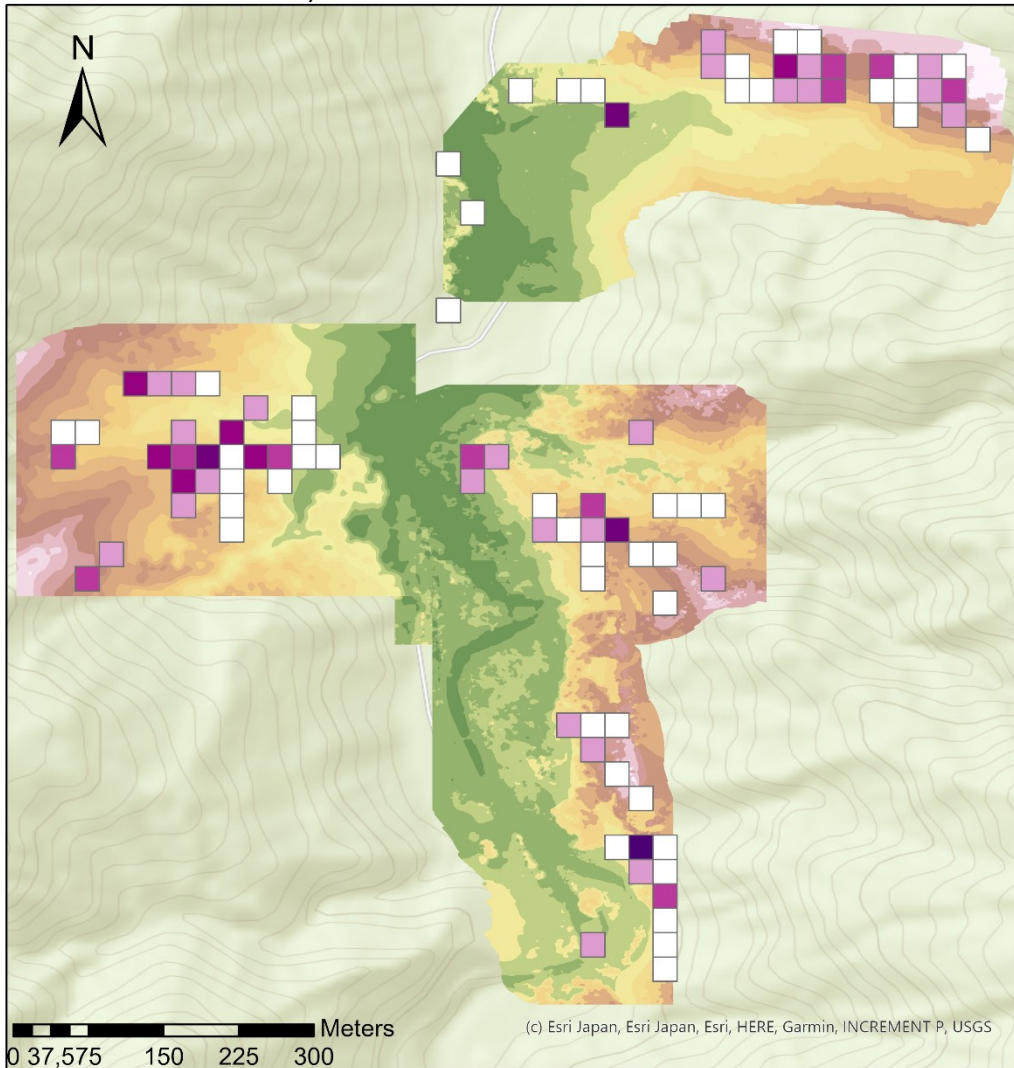
Larix_Grid

COUNT



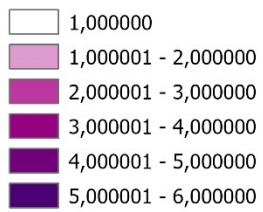


Magnolia obovata distribution by Sarah Kentsch



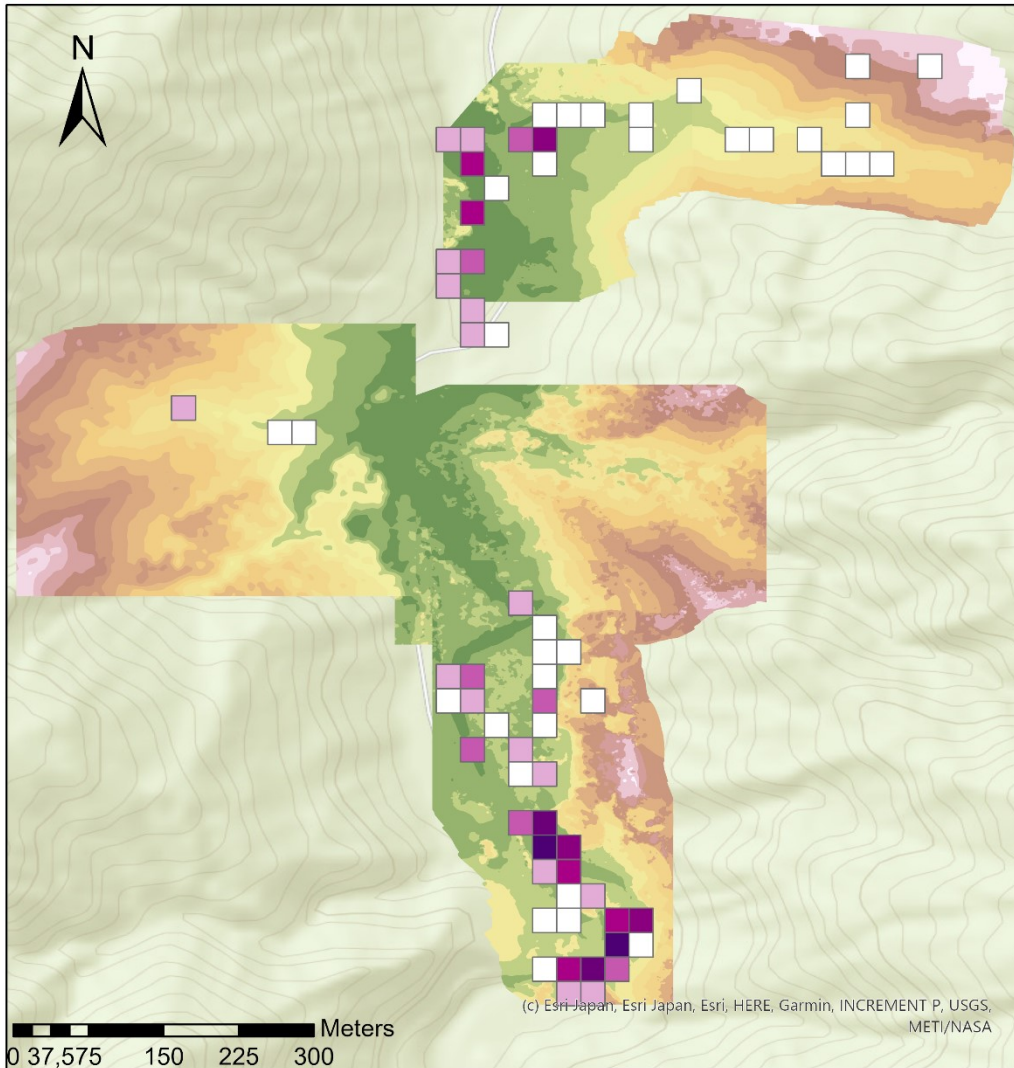
Magnolia_Grid

COUNT





Pterocarya rhoifolia distribution by Sarah Kentsch



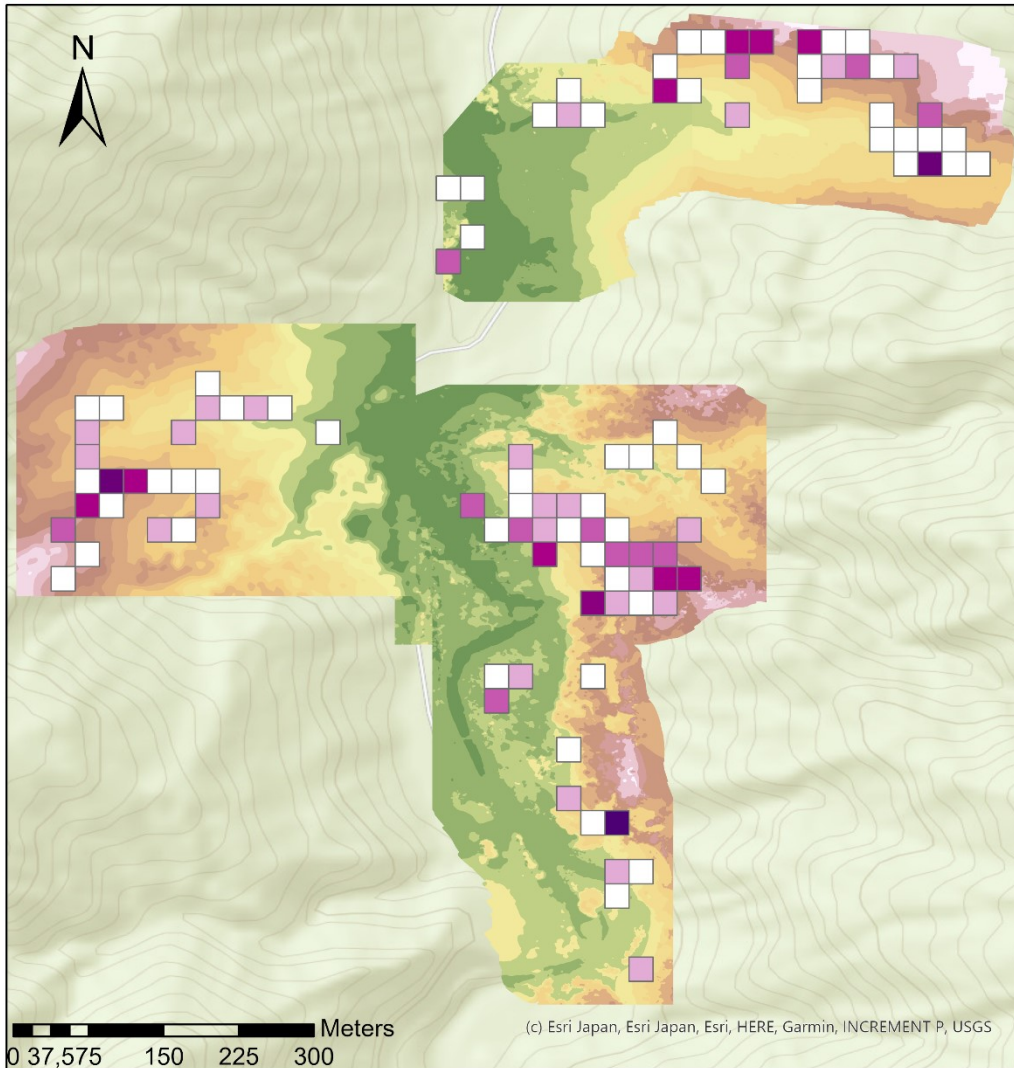
Pterocarya_Grid

COUNT

	1,000000
	1,000001 - 3,000000
	3,000001 - 5,000000
	5,000001 - 8,000000
	8,000001 - 10,000000
	10,000001 - 17,000000
	17,000001 - 23,000000



Quercus mongolica distribution by Sarah Kentsch



Quercus_Grid

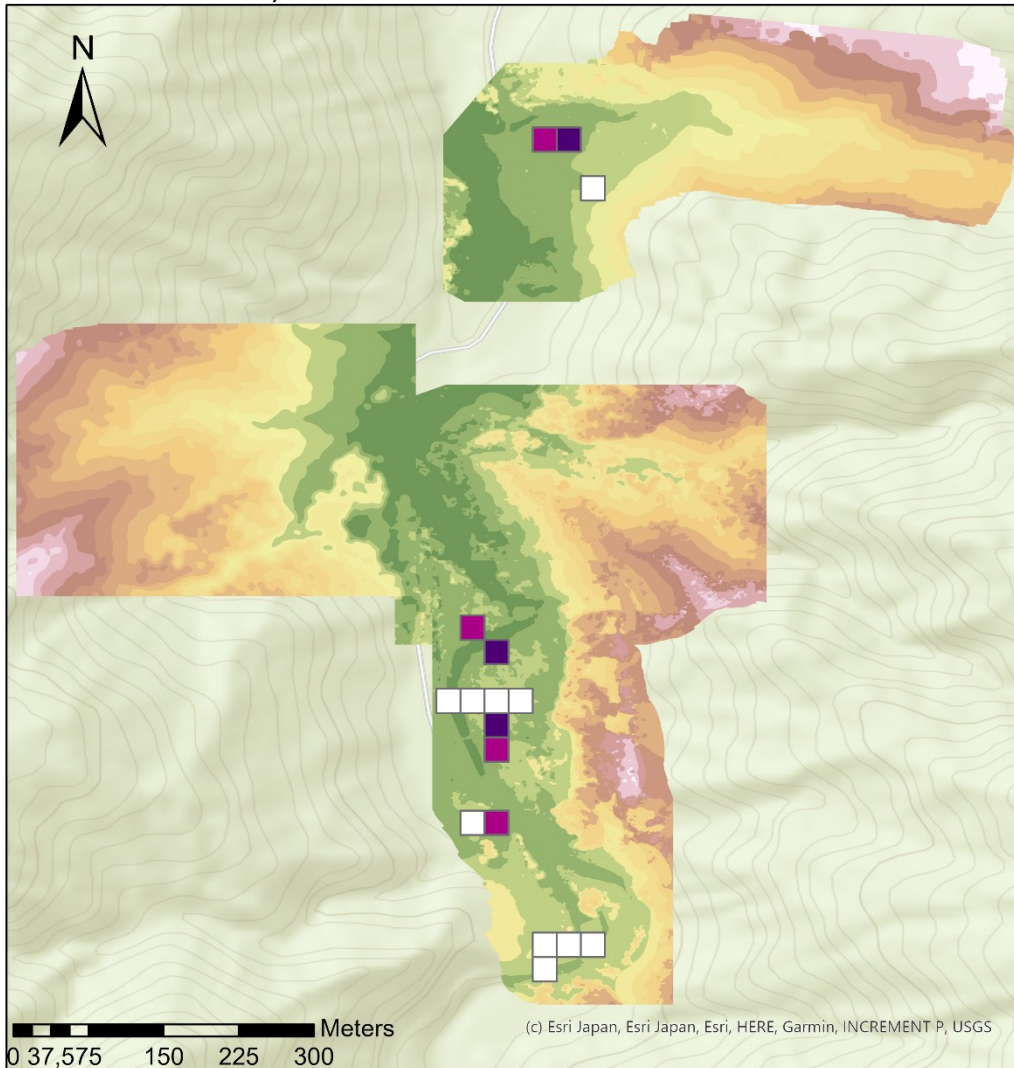
COUNT

White	1,000000
Light Pink	1,000001 - 2,000000
Medium Pink	2,000001 - 3,000000
Dark Pink	3,000001 - 4,000000
Red	4,000001 - 5,000000
Dark Red	5,000001 - 6,000000
Dark Purple	6,000001 - 12,000000



Robinia pseudoacacia distribution

by Sarah Kentsch



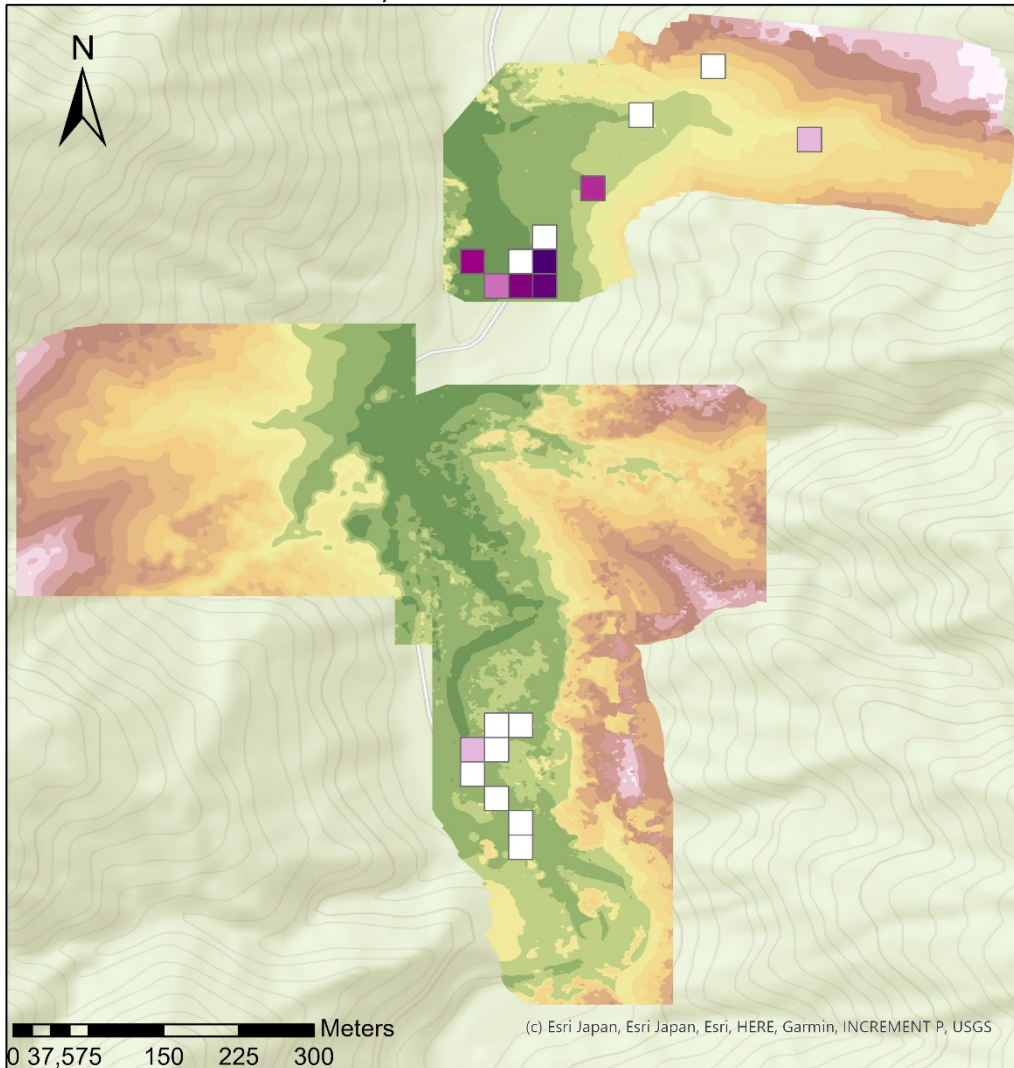
Robinia_Grid

COUNT

- 1,000000
- 1,000001 - 2,000000
- 2,000001 - 3,000000



Salix distribution by Sarah Kentsch



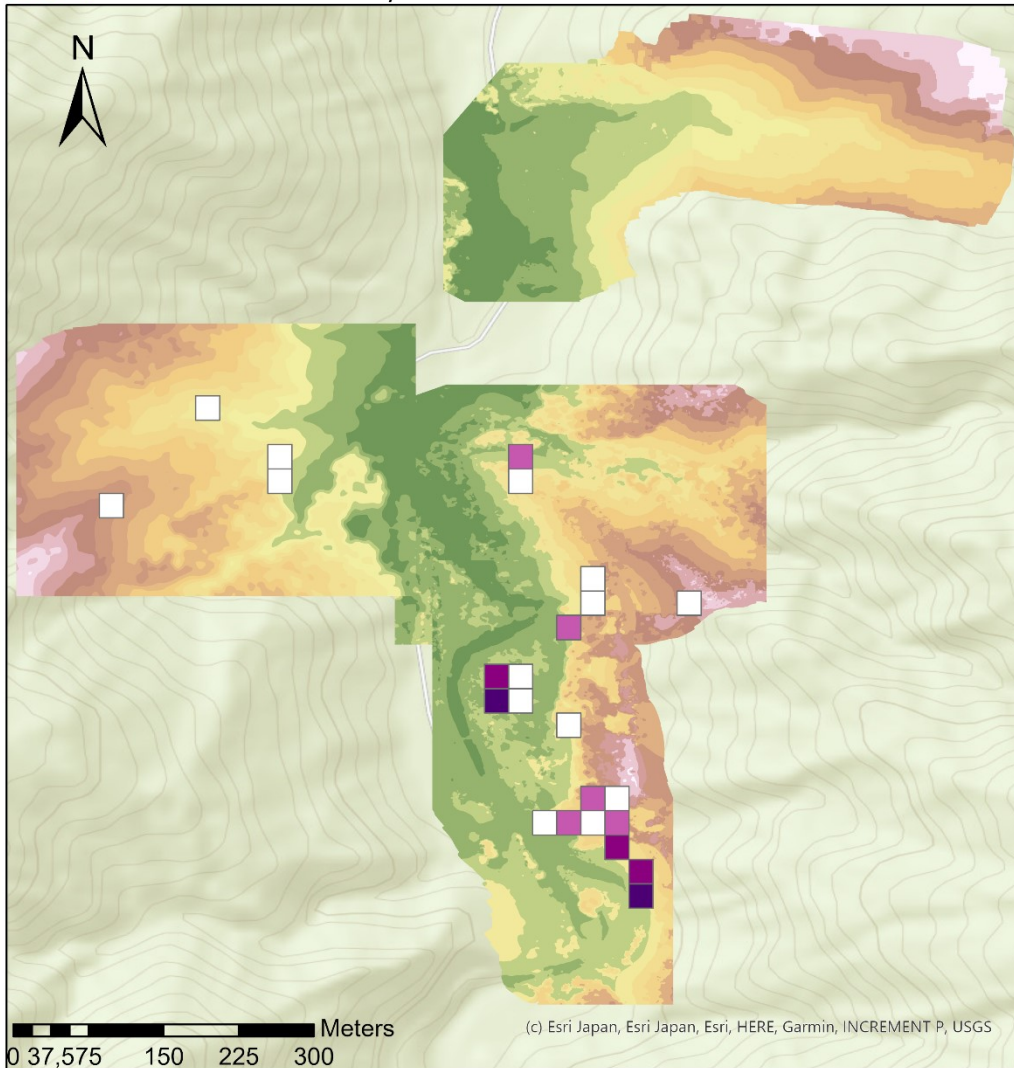
Salix_Grid

COUNT

	1,000000
	1,000001 - 2,000000
	2,000001 - 3,000000
	3,000001 - 5,000000
	5,000001 - 8,000000
	8,000001 - 17,000000
	17,000001 - 36,000000
	36,000001 - 60,000000







Tilia distribution by Sarah Kentsch



Tilia_Grid

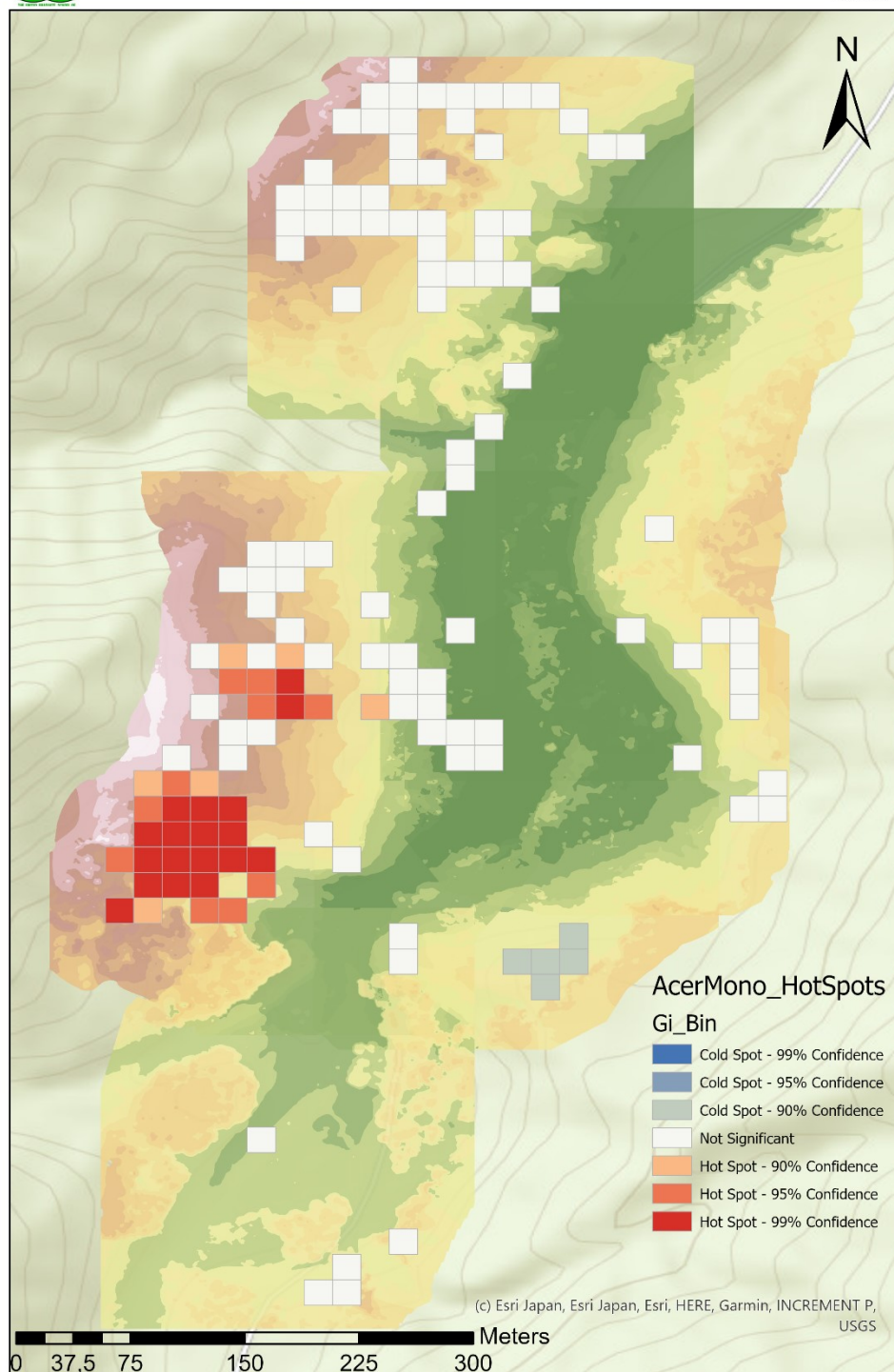
COUNT

-  1,000000
-  1,000001 - 2,000000
-  2,000001 - 4,000000
-  4,000001 - 13,000000

Part 3: Hot spot analysis for the northern sites for the different tree species.

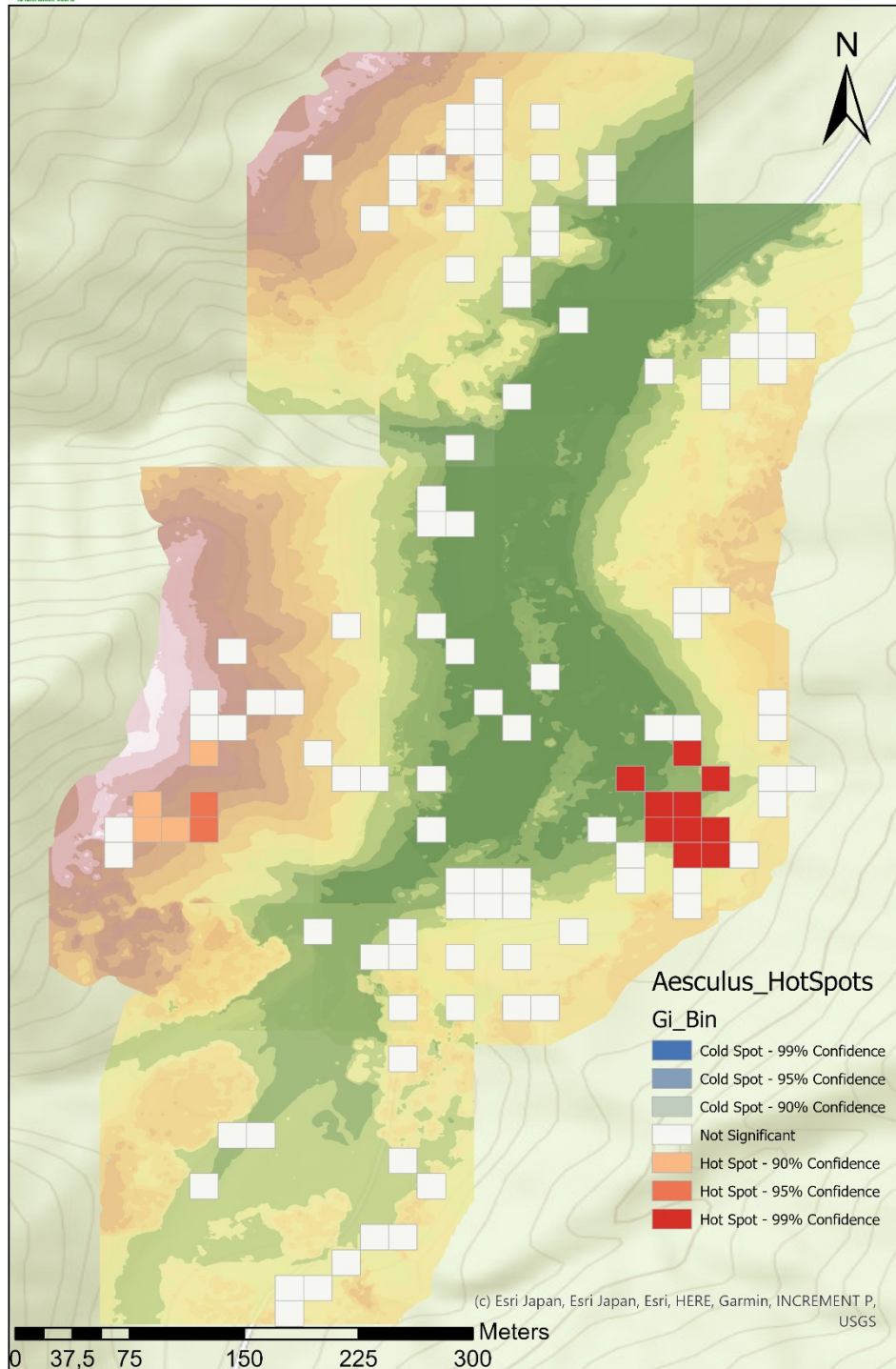


Hot spot analysis Acer mono maxim
by Sarah Kentsch



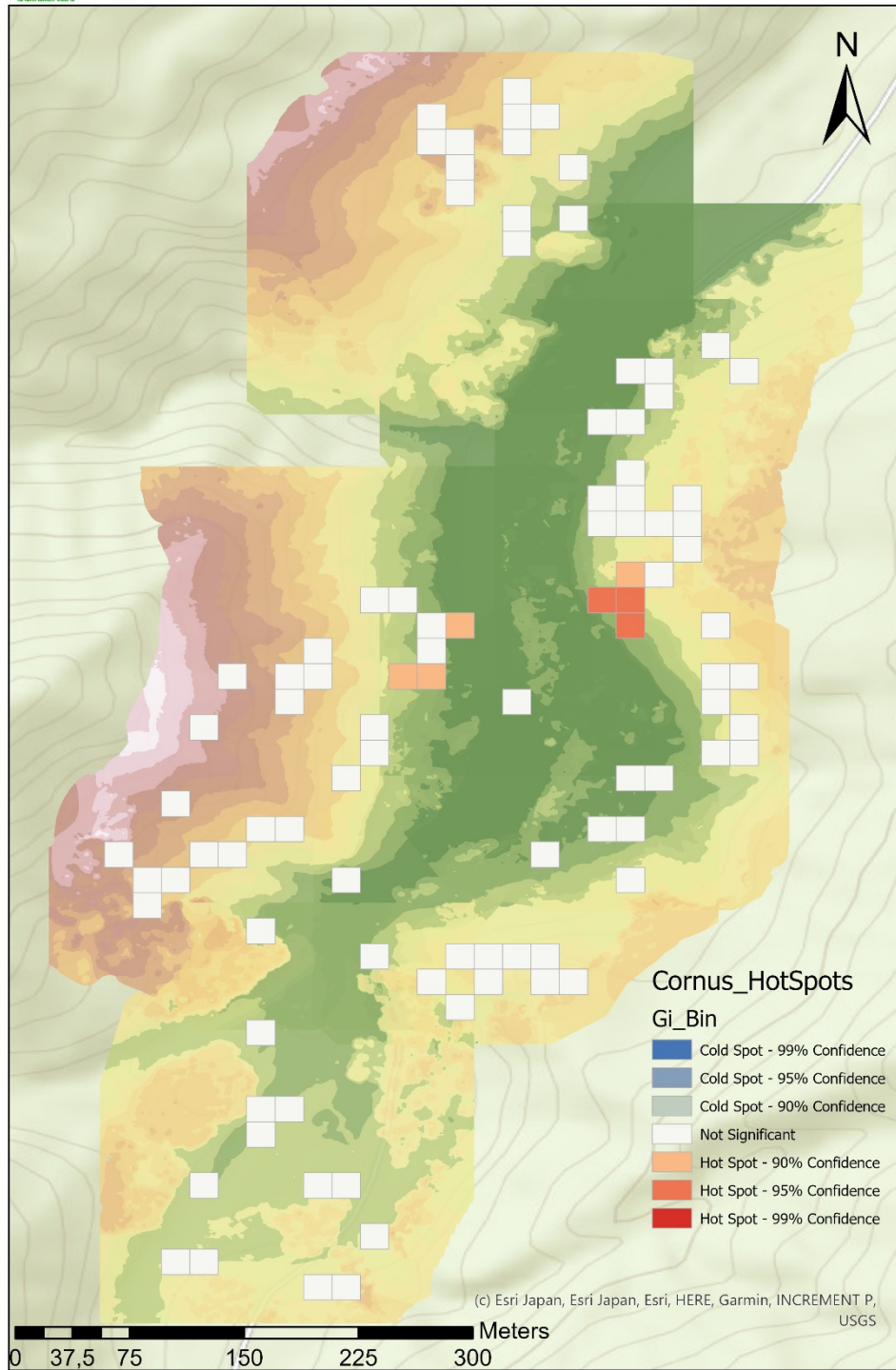


Hot spot analysis *Aesculus turbinata* by Sarah Kentsch



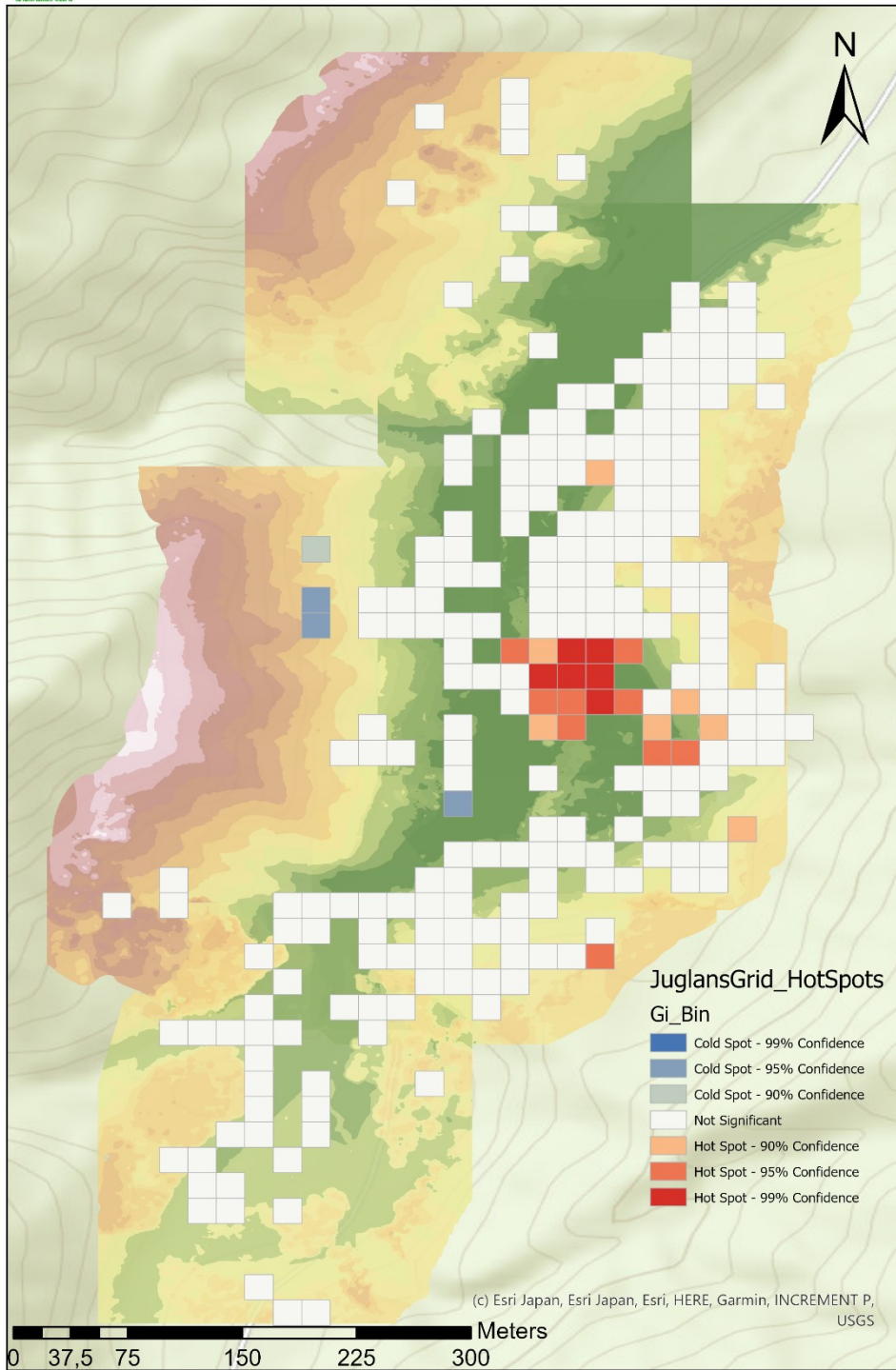


Hot spot analysis *Cornus controversa* by Sarah Kentsch





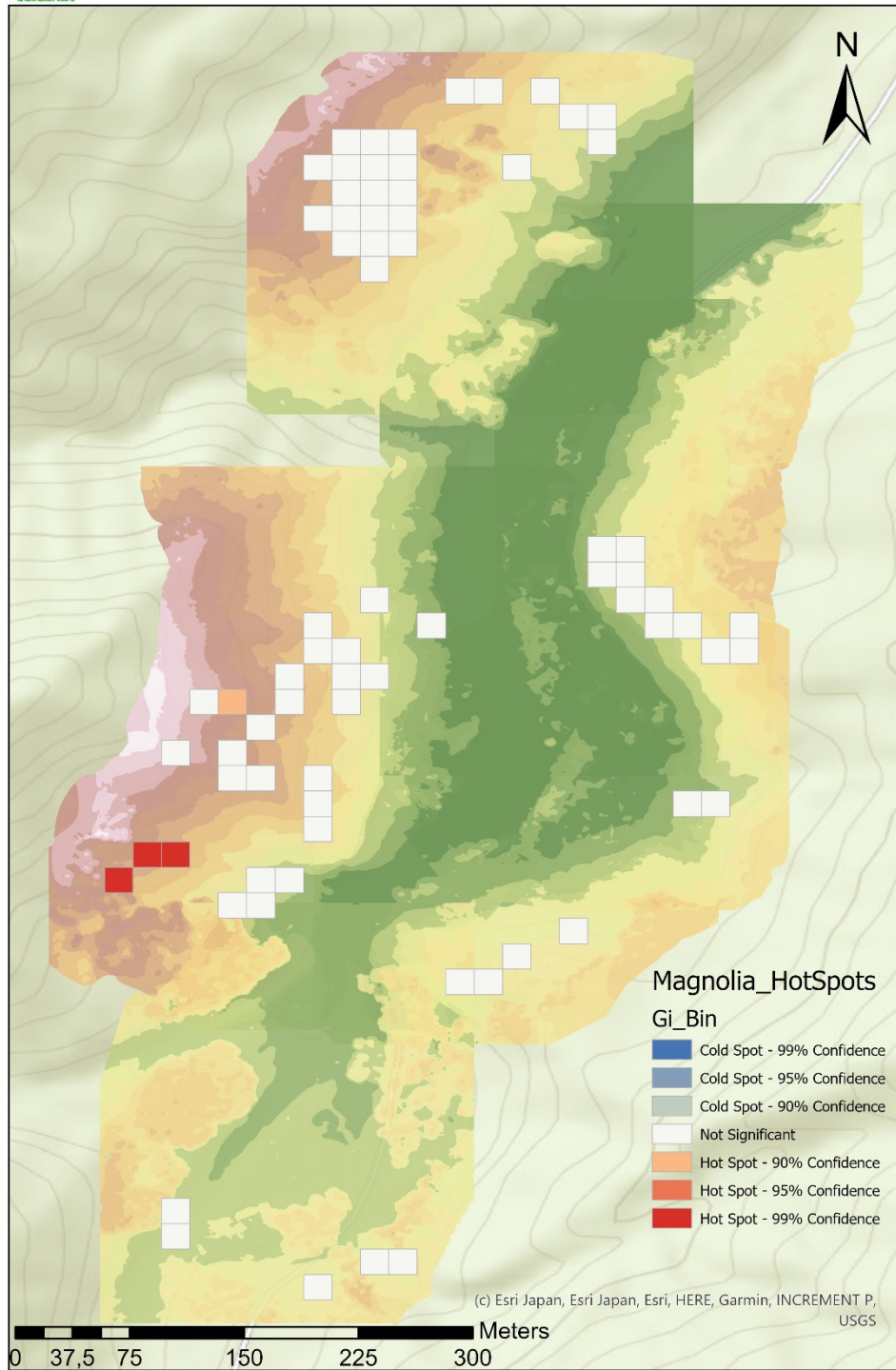
Hot spot analysis *Juglans ailantifolia* by Sarah Kentsch





Hot spot analysis *Magnolia obovata*

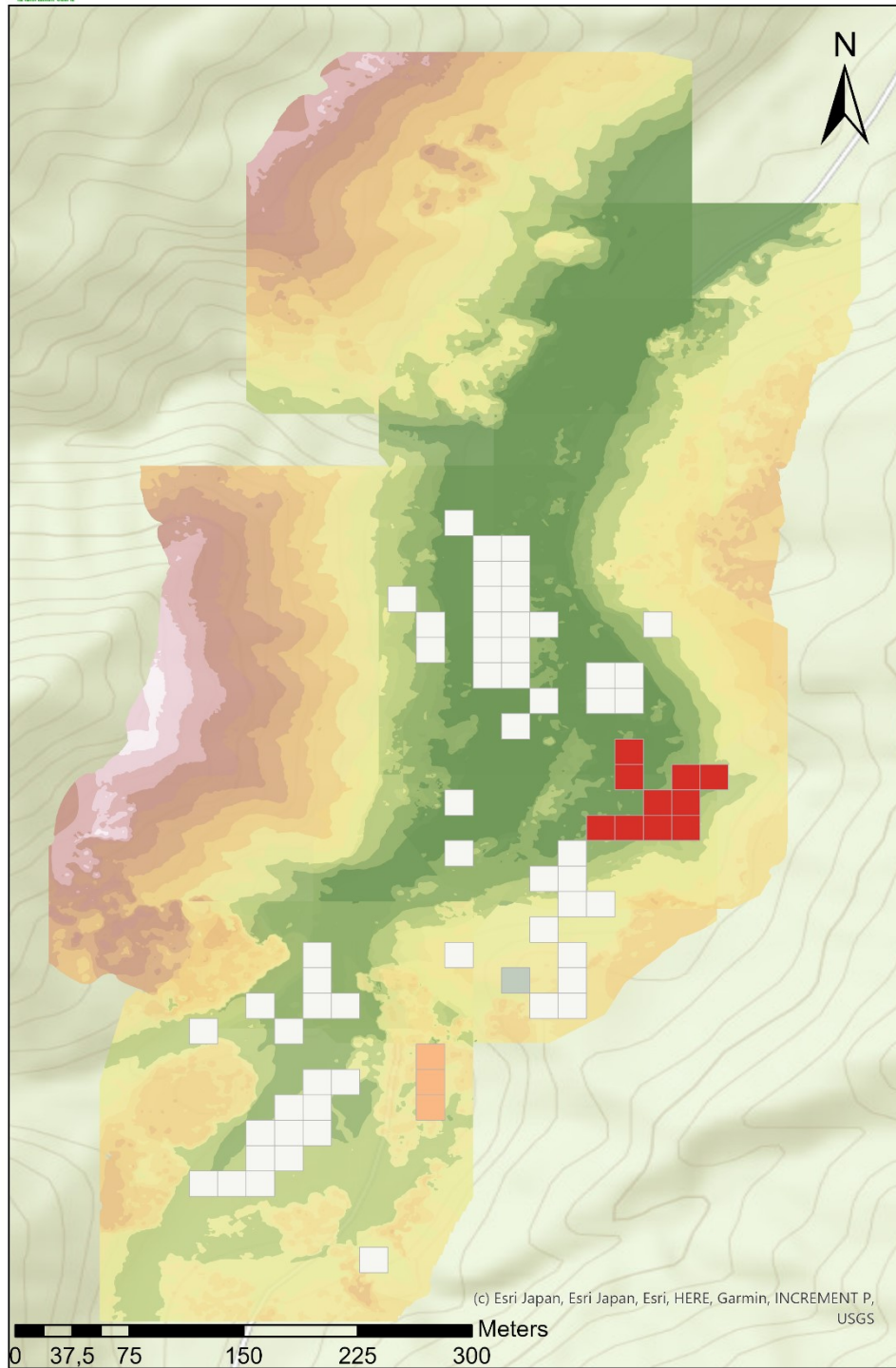
by Sarah Kentsch





Hot spot analysis *Pterocarya rhoifolia*

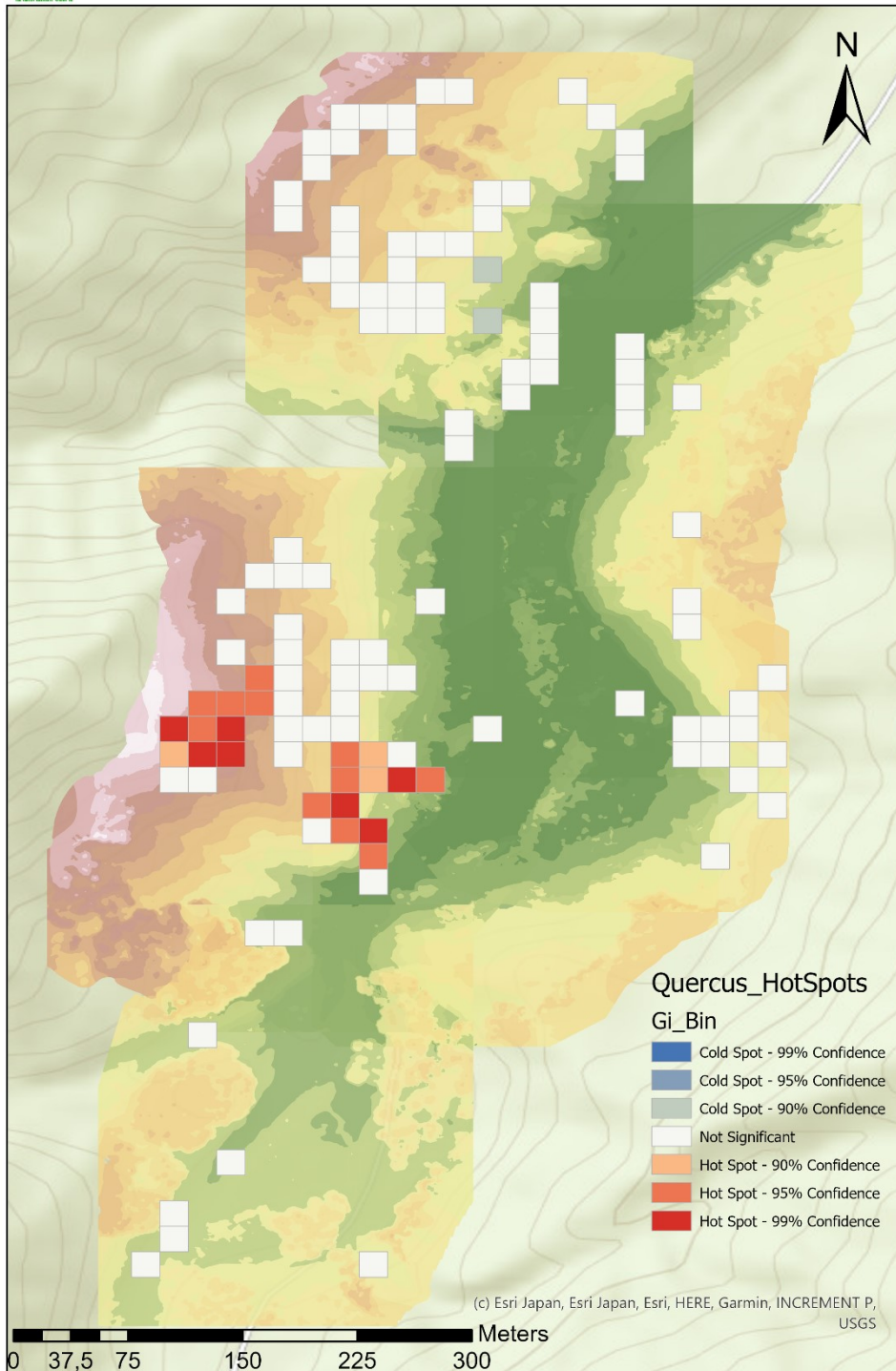
by Sarah Kentsch





Hot spot analysis *Quercus crenata*

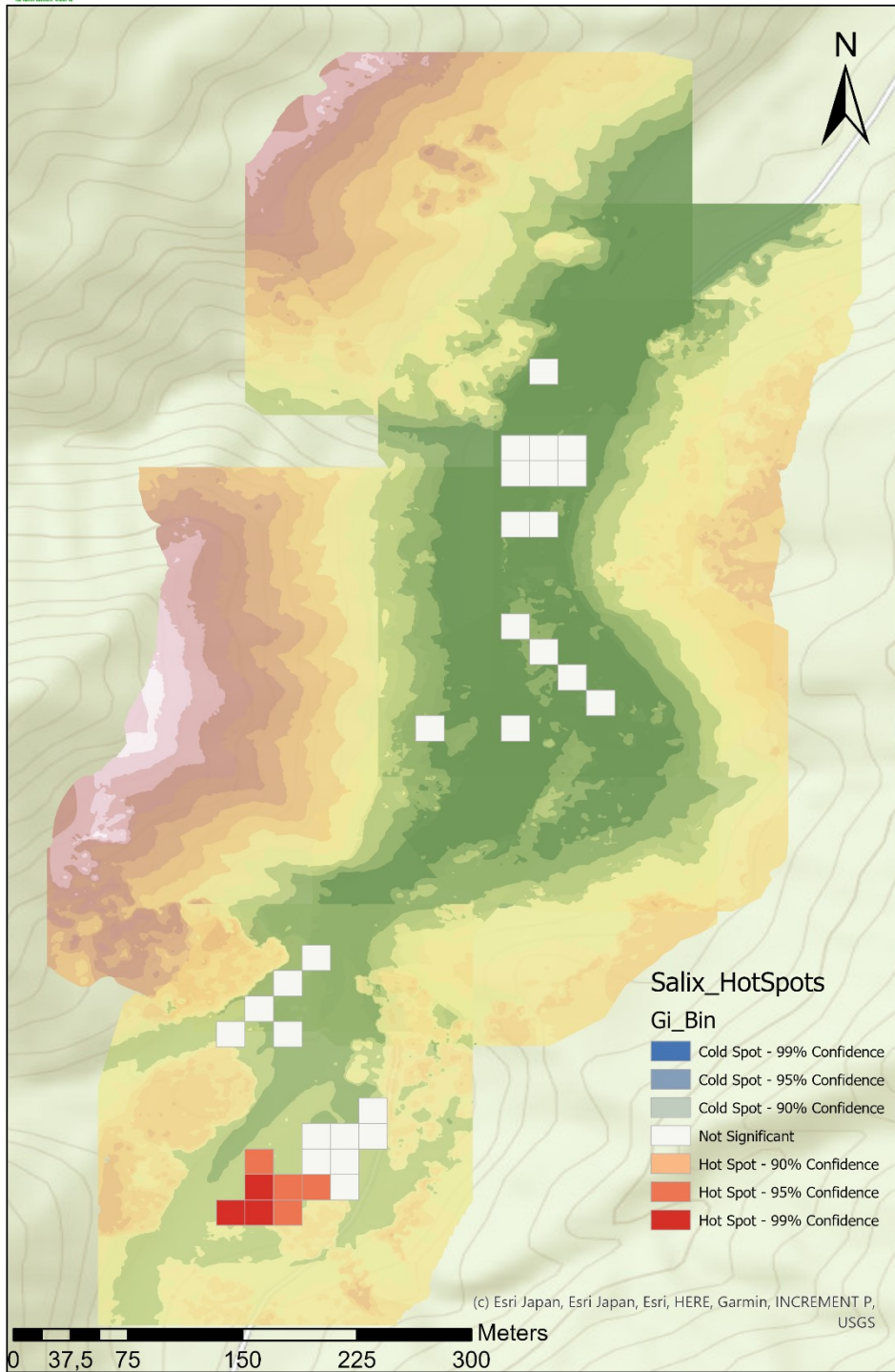
by Sarah Kentsch





Hot spot analysis Salix species

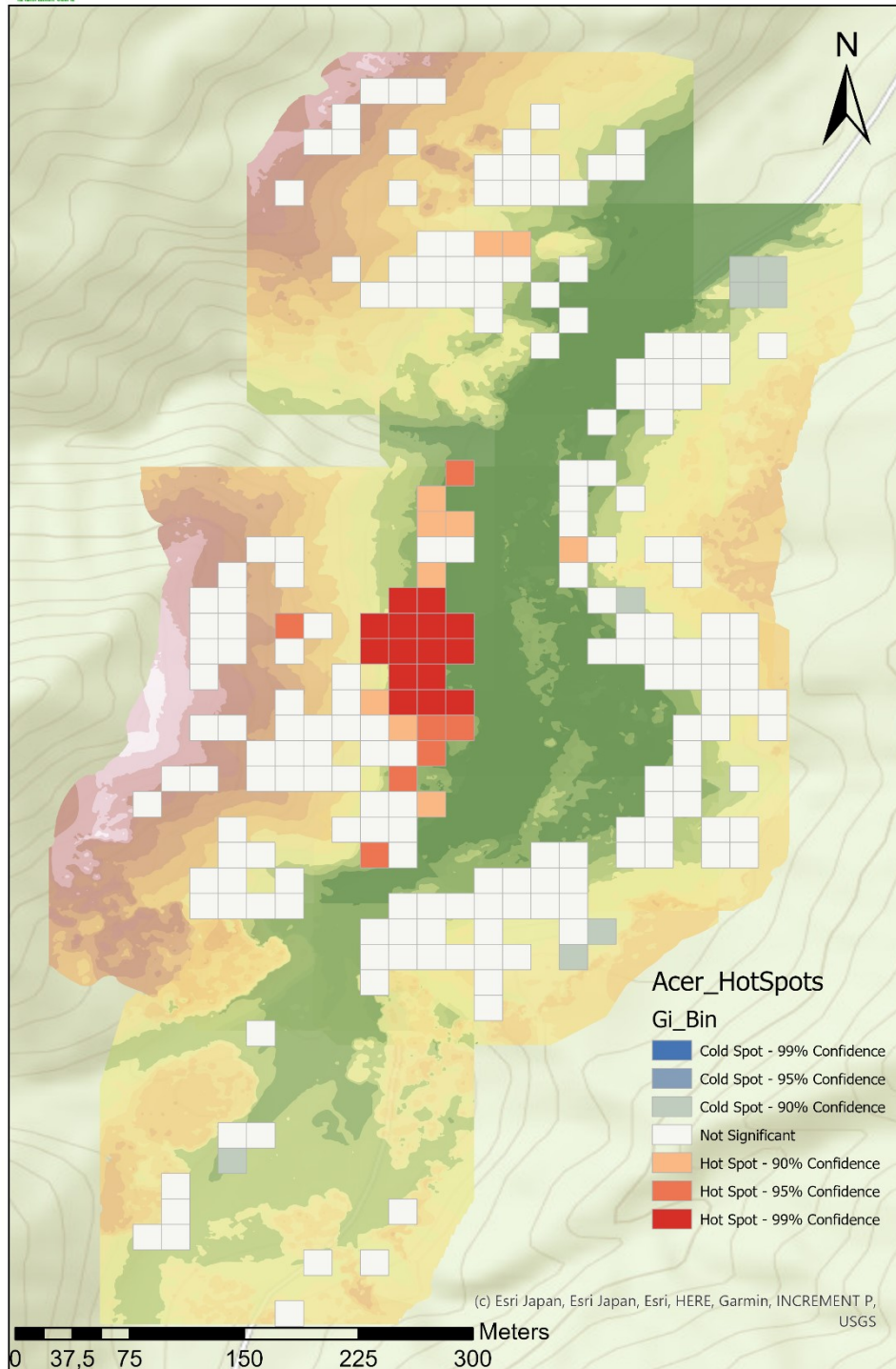
by Sarah Kentsch





Hot spot analysis Acer species

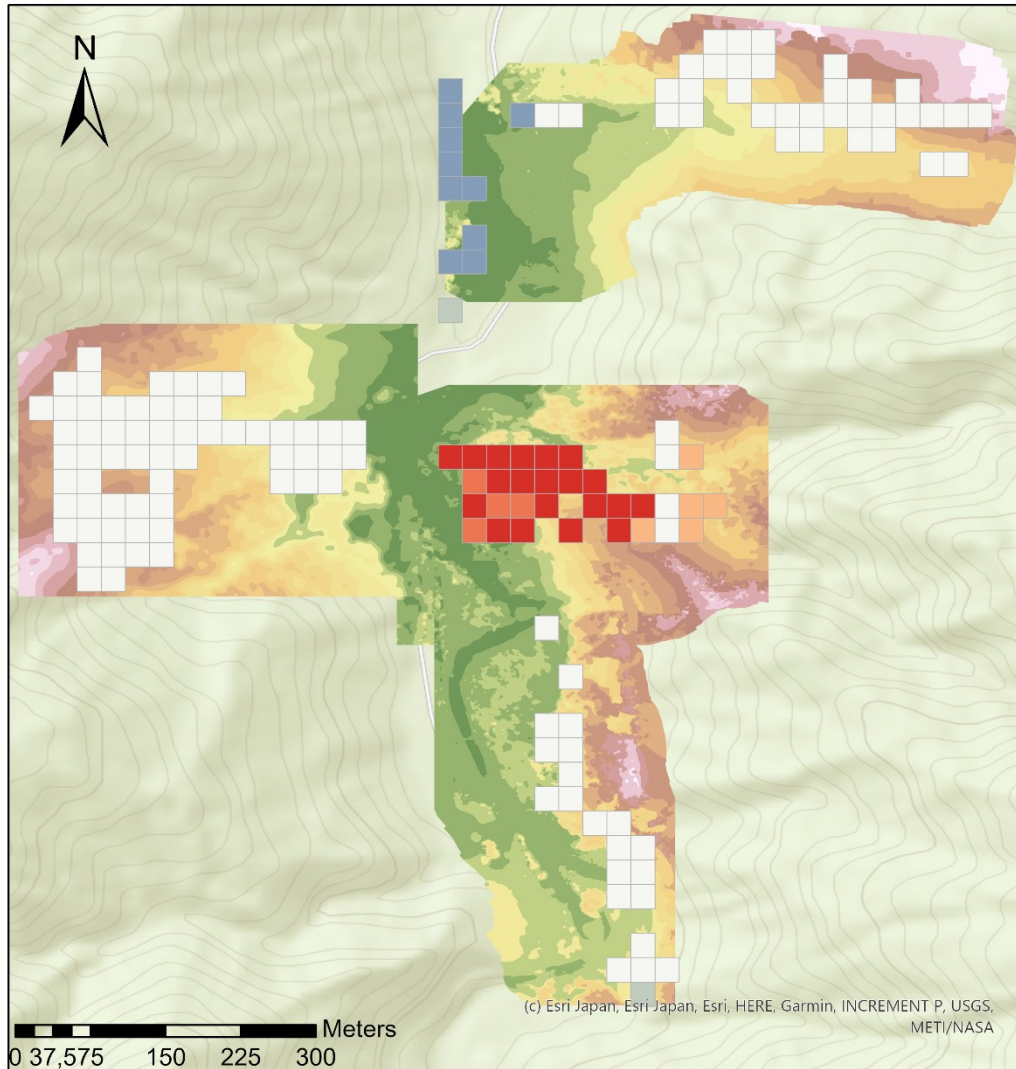
by Sarah Kentsch



Part 4: Hot spot analysis for the southern sites for the different tree species.



Acer Hot spot analysis
by Sarah Kentsch



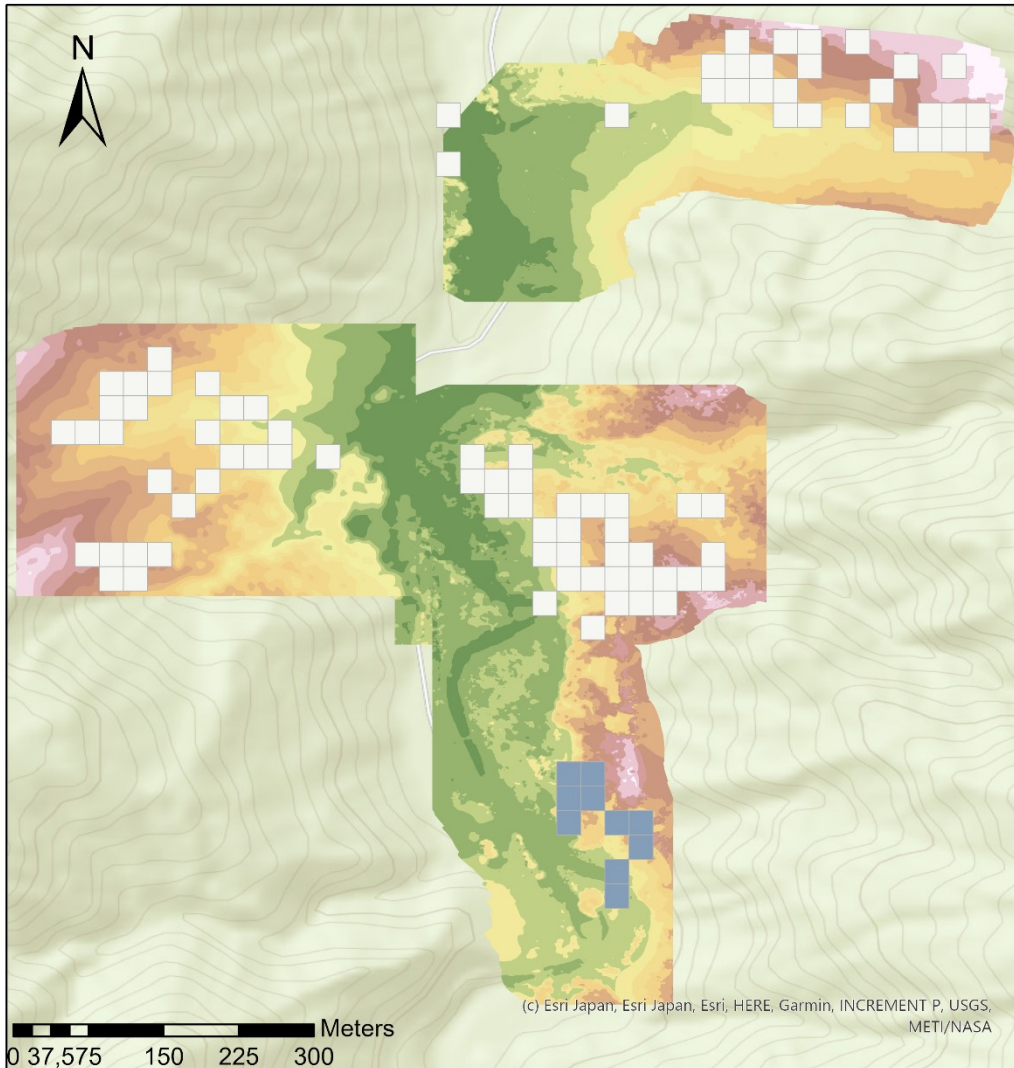
Acer_HotSpots

Gi_Bin

- Cold Spot - 99% Confidence
- Cold Spot - 95% Confidence
- Cold Spot - 90% Confidence
- Not Significant
- Hot Spot - 90% Confidence
- Hot Spot - 95% Confidence
- Hot Spot - 99% Confidence










Acer mono maxim Hot spot analysis by Sarah Kentsch



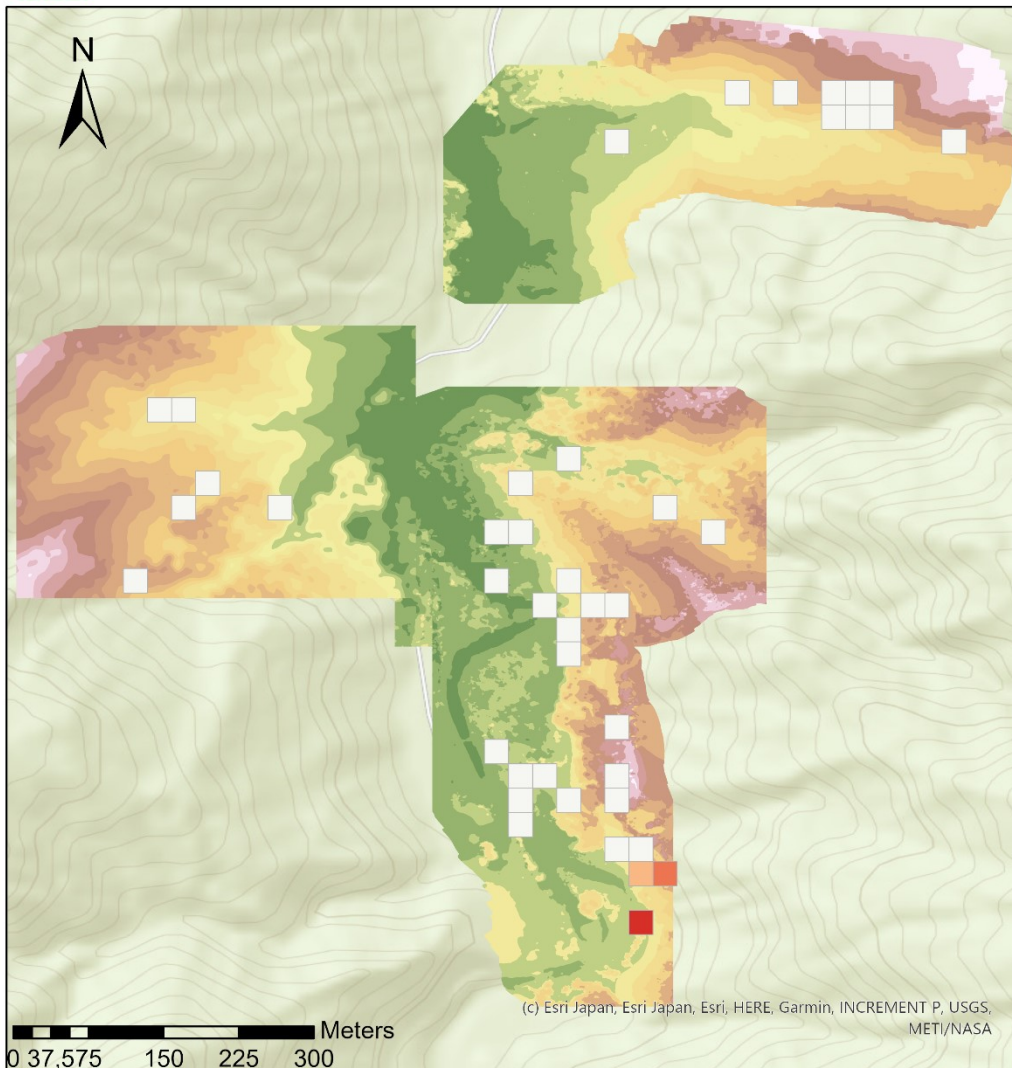
Acermono_HotSpots

Gi_Bin

-  Cold Spot - 99% Confidence
-  Cold Spot - 95% Confidence
-  Cold Spot - 90% Confidence
-  Not Significant
-  Hot Spot - 90% Confidence
-  Hot Spot - 95% Confidence
-  Hot Spot - 99% Confidence










Cornus controversa Hot spot analysis by Sarah Kentsch



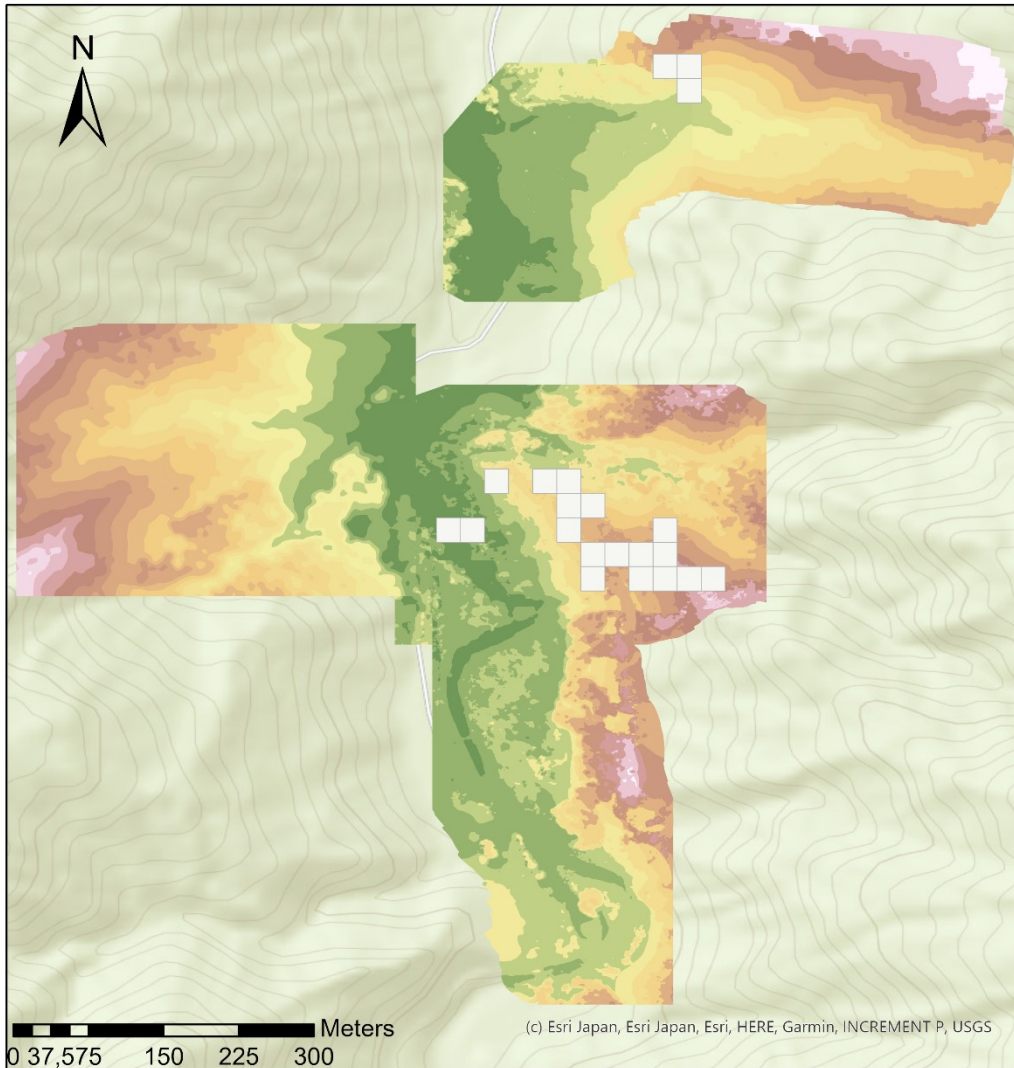
Cornus_HotSpots

Gi_Bin

-  Cold Spot - 99% Confidence
-  Cold Spot - 95% Confidence
-  Cold Spot - 90% Confidence
-  Not Significant
-  Hot Spot - 90% Confidence
-  Hot Spot - 95% Confidence
-  Hot Spot - 99% Confidence



Fagus crenata Hot spot analysis by Sarah Kentsch



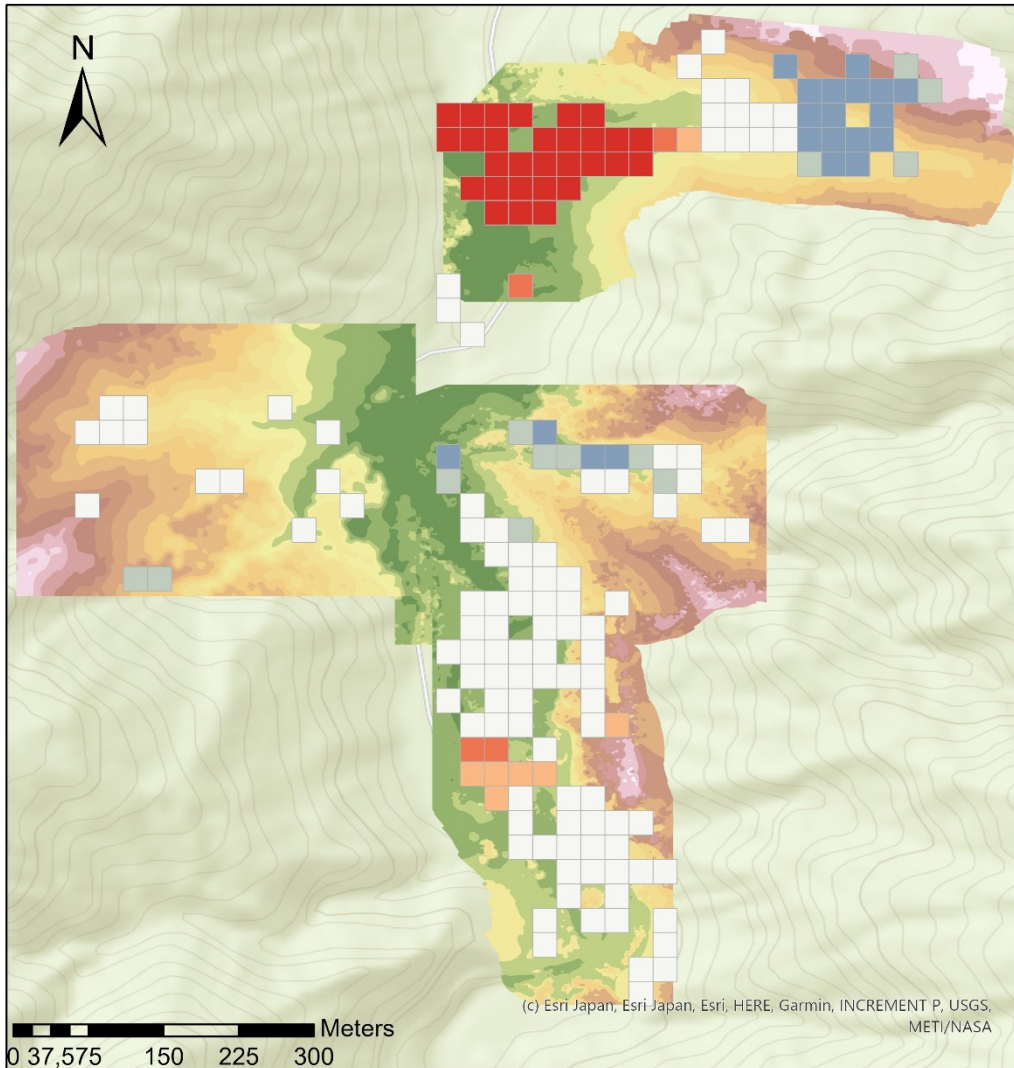
Fagus_HotSpots

Gi_Bin

- Cold Spot - 99% Confidence
- Cold Spot - 95% Confidence
- Cold Spot - 90% Confidence
- Not Significant
- Hot Spot - 90% Confidence
- Hot Spot - 95% Confidence
- Hot Spot - 99% Confidence










Juglans ailantifolia Hot spot analysis by Sarah Kentsch



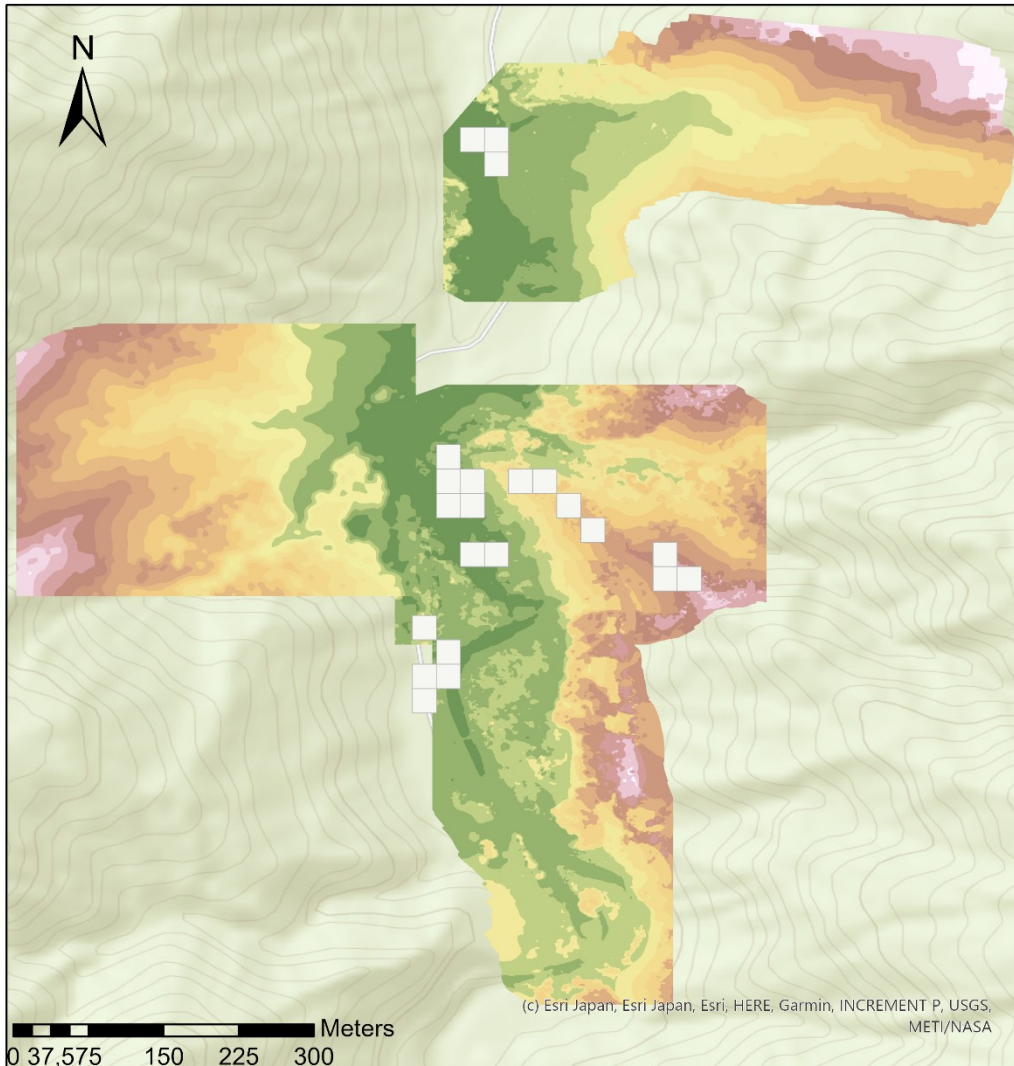
Juglans_HotSpots

Gi_Bin

-  Cold Spot - 99% Confidence
-  Cold Spot - 95% Confidence
-  Cold Spot - 90% Confidence
-  Not Significant
-  Hot Spot - 90% Confidence
-  Hot Spot - 95% Confidence
-  Hot Spot - 99% Confidence










Larix kaempferi Hot spot analysis by Sarah Kentsch



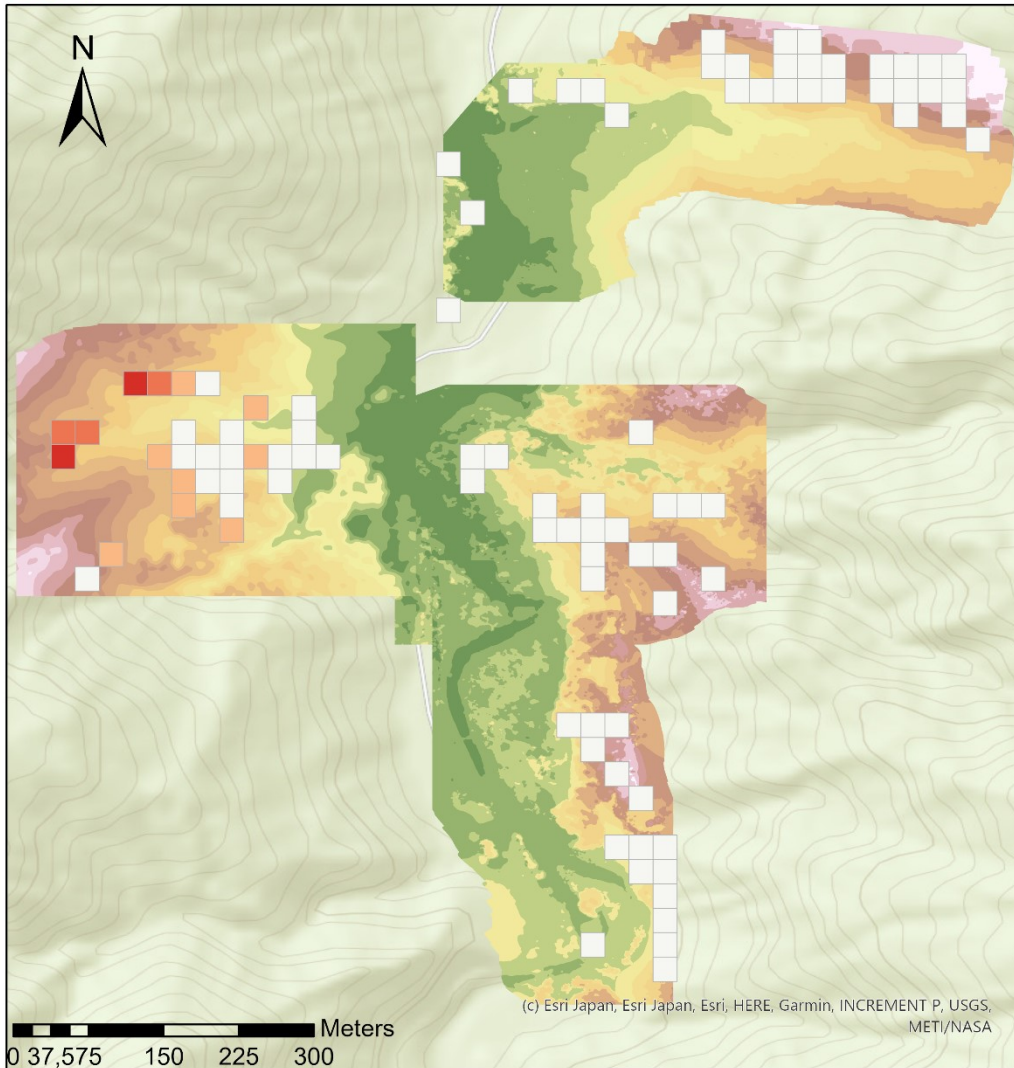
Larix_HotSpots

Gi_Bin

-  Cold Spot - 99% Confidence
-  Cold Spot - 95% Confidence
-  Cold Spot - 90% Confidence
-  Not Significant
-  Hot Spot - 90% Confidence
-  Hot Spot - 95% Confidence
-  Hot Spot - 99% Confidence



Magnolia obovata Hot spot analysis by Sarah Kentsch



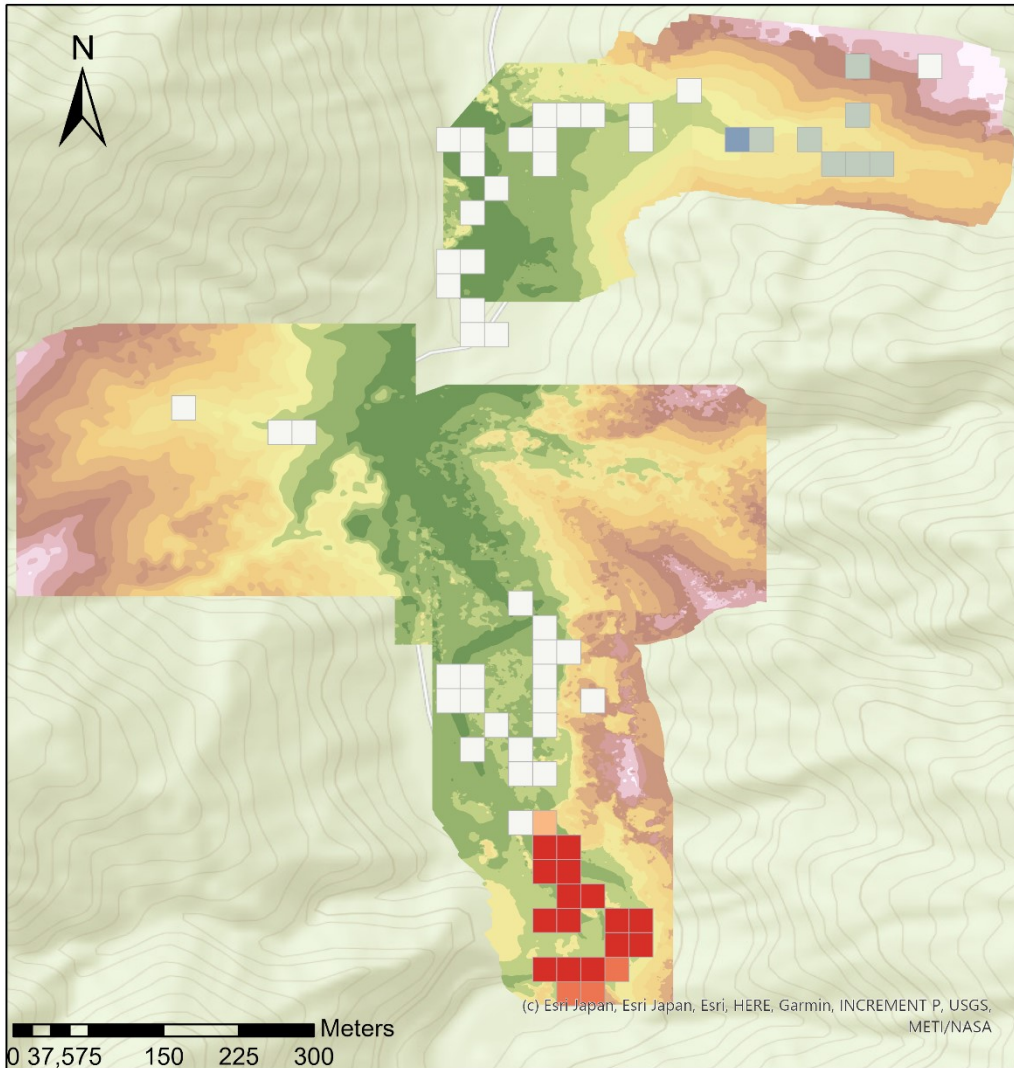
Magnolia_HotSpots

Gi_Bin

- Cold Spot - 99% Confidence
- Cold Spot - 95% Confidence
- Cold Spot - 90% Confidence
- Not Significant
- Hot Spot - 90% Confidence
- Hot Spot - 95% Confidence
- Hot Spot - 99% Confidence










Pterocarya rhoifolia Hot spot analysis by Sarah Kentsch



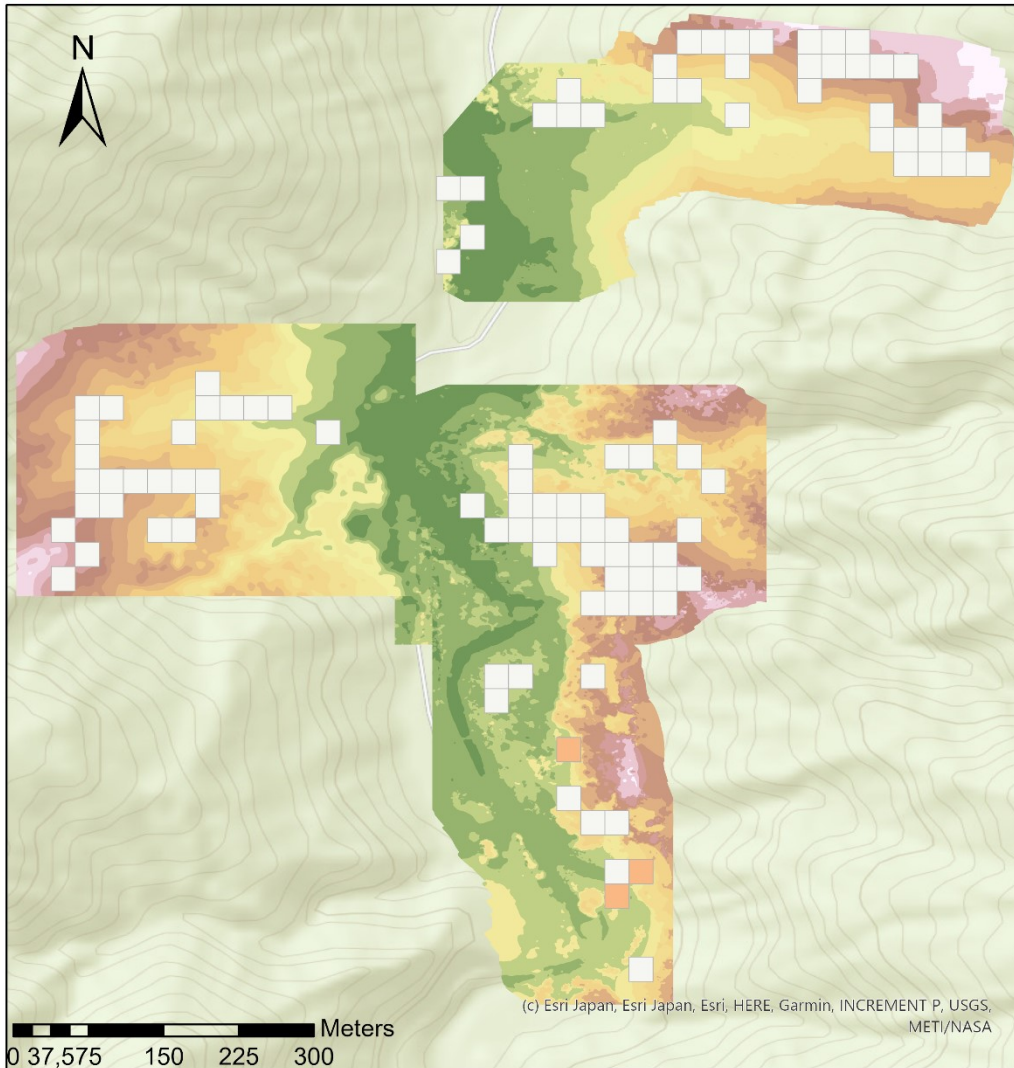
Pterocarya_HotSpots

Gi_Bin

-  Cold Spot - 99% Confidence
-  Cold Spot - 95% Confidence
-  Cold Spot - 90% Confidence
-  Not Significant
-  Hot Spot - 90% Confidence
-  Hot Spot - 95% Confidence
-  Hot Spot - 99% Confidence










Quercus mongolica Hot spot analysis by Sarah Kentsch



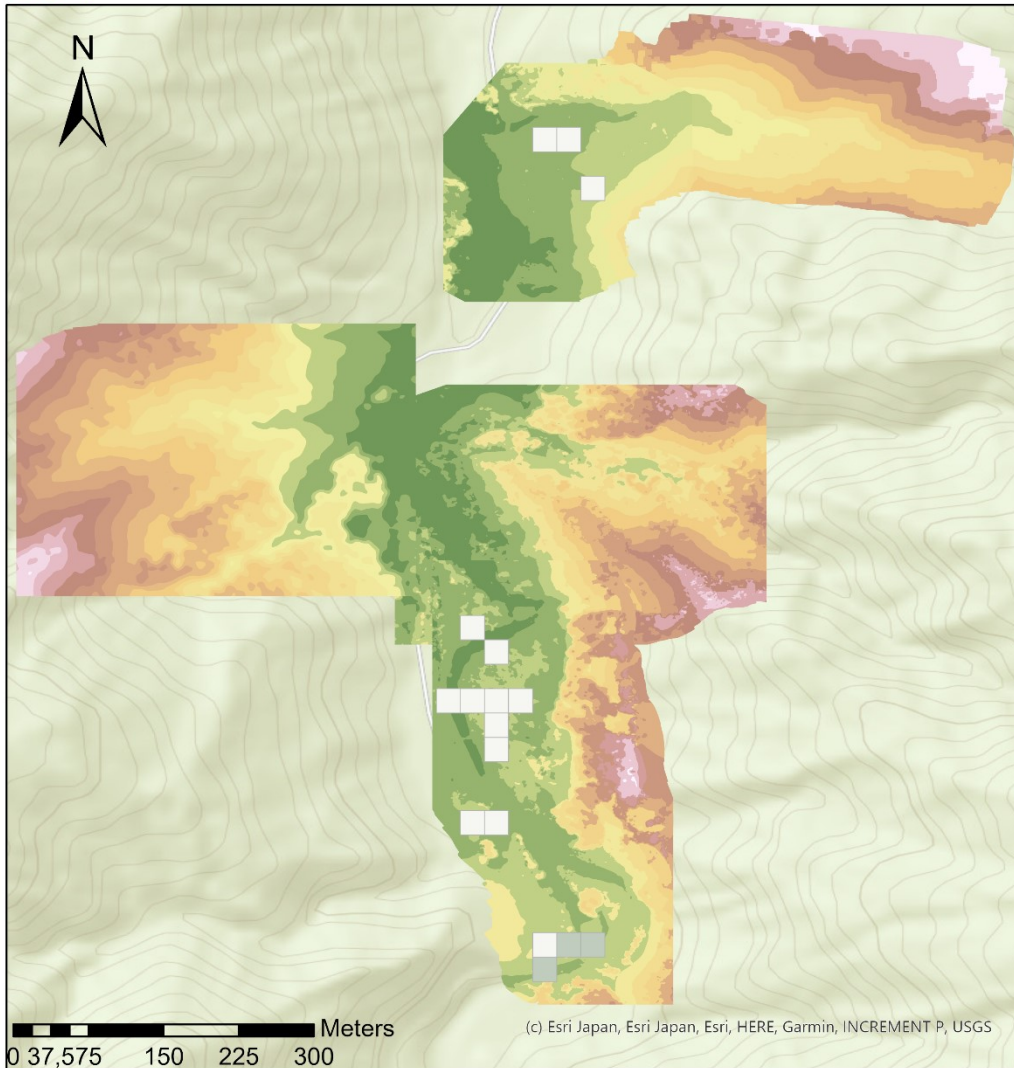
Quercus_HotSpots

Gi_Bin

-  Cold Spot - 99% Confidence
-  Cold Spot - 95% Confidence
-  Cold Spot - 90% Confidence
-  Not Significant
-  Hot Spot - 90% Confidence
-  Hot Spot - 95% Confidence
-  Hot Spot - 99% Confidence










Robinia pseudoacacia Hot spot analysis by Sarah Kentsch



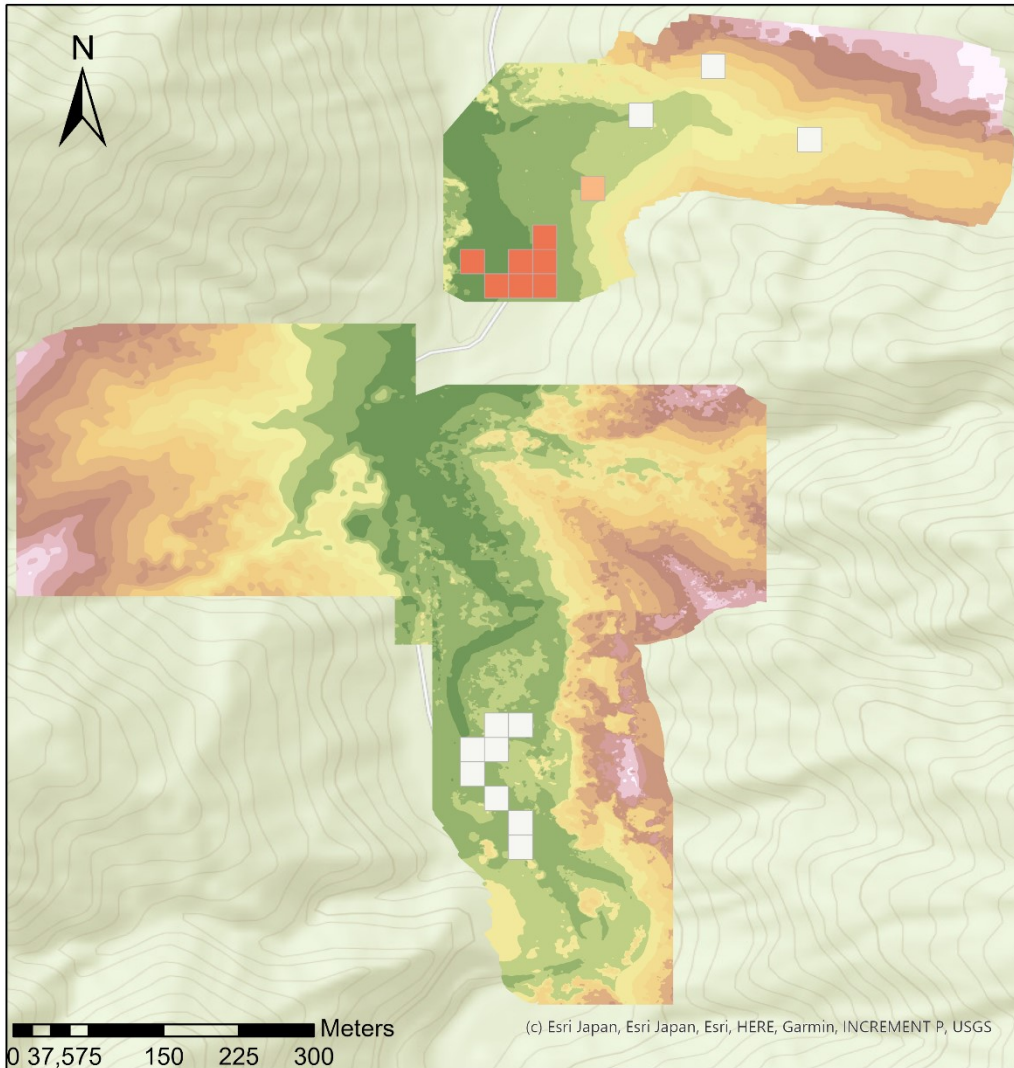
Robinia_HotSpots

Gi_Bin

-  Cold Spot - 99% Confidence
-  Cold Spot - 95% Confidence
-  Cold Spot - 90% Confidence
-  Not Significant
-  Hot Spot - 90% Confidence
-  Hot Spot - 95% Confidence
-  Hot Spot - 99% Confidence










Salix Hot spot analysis by Sarah Kentsch



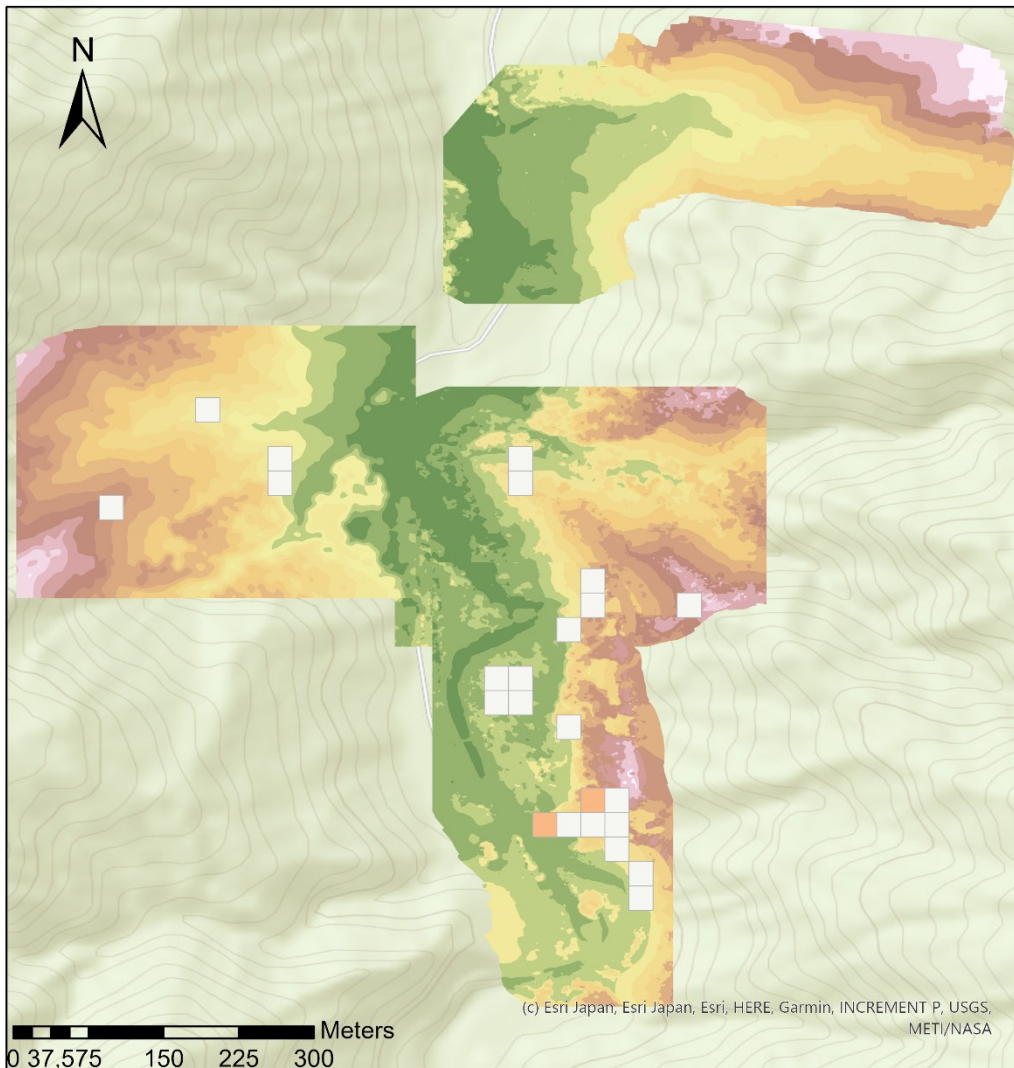
Salix_HotSpots

Gi_Bin

-  Cold Spot - 99% Confidence
-  Cold Spot - 95% Confidence
-  Cold Spot - 90% Confidence
-  Not Significant
-  Hot Spot - 90% Confidence
-  Hot Spot - 95% Confidence
-  Hot Spot - 99% Confidence










Tilia Hot spot analysis by Sarah Kentsch



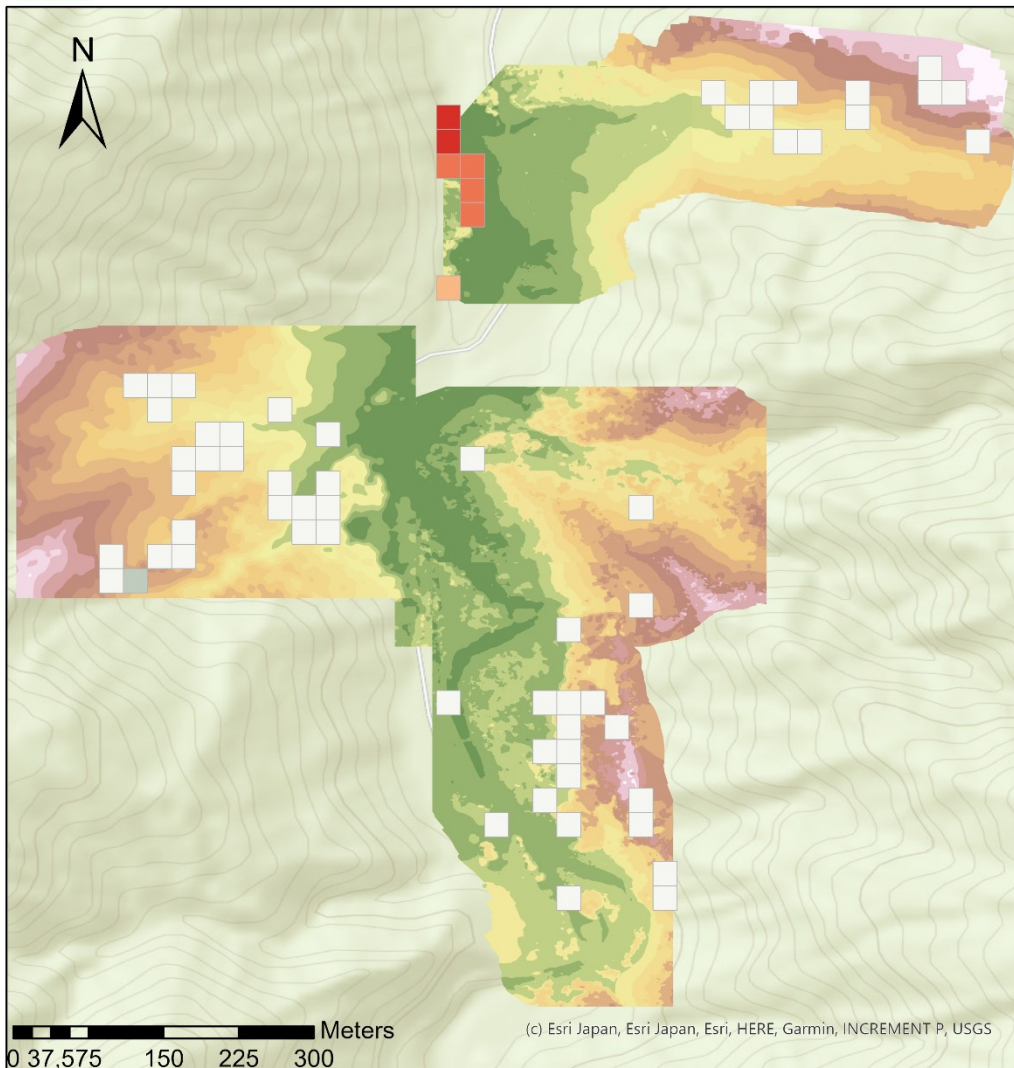
Tilia_HotSpots

Gi_Bin

-  Cold Spot - 99% Confidence
-  Cold Spot - 95% Confidence
-  Cold Spot - 90% Confidence
-  Not Significant
-  Hot Spot - 90% Confidence
-  Hot Spot - 95% Confidence
-  Hot Spot - 99% Confidence










Aesculus turbinata Hot spot analysis by Sarah Kentsch



Aesculus_HotSpots

Gi_Bin

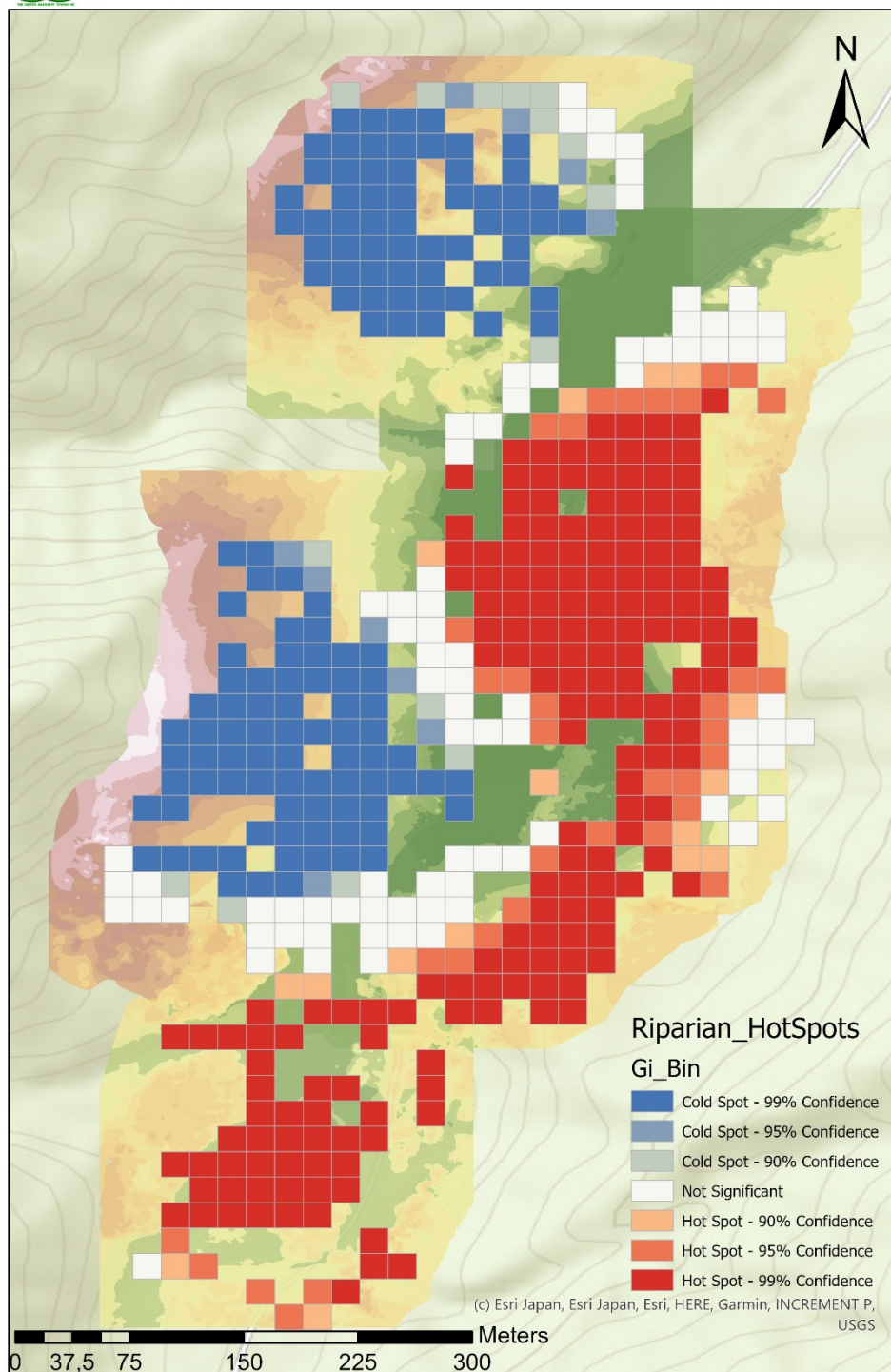
-  Cold Spot - 99% Confidence
-  Cold Spot - 95% Confidence
-  Cold Spot - 90% Confidence
-  Not Significant
-  Hot Spot - 90% Confidence
-  Hot Spot - 95% Confidence
-  Hot Spot - 99% Confidence

Part 5: Hot spot analysis to differentiate between riparian and terrace/slope sites.



Hot spot analysis Riparian - Terrasse

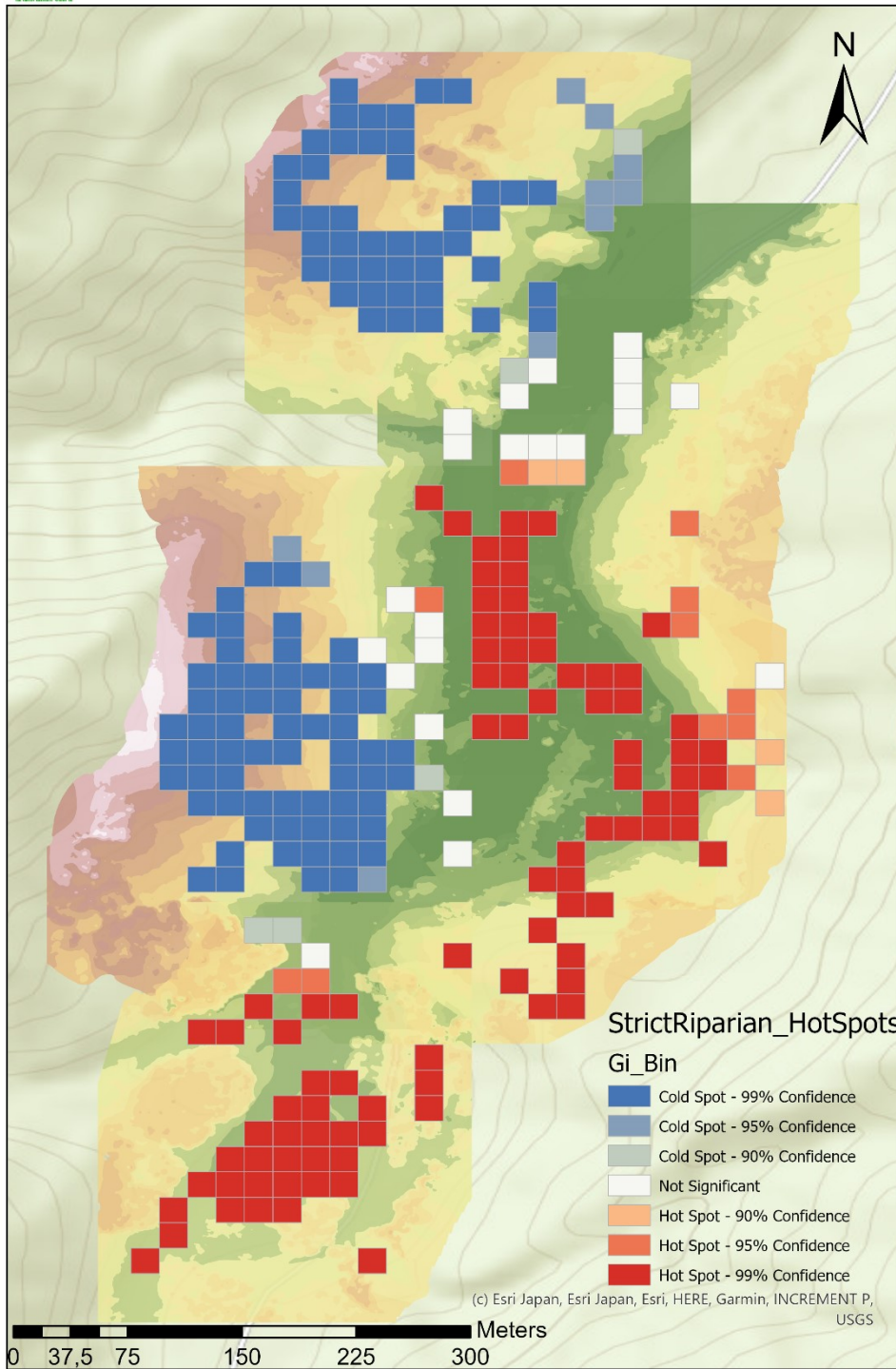
by Sarah Kentsch





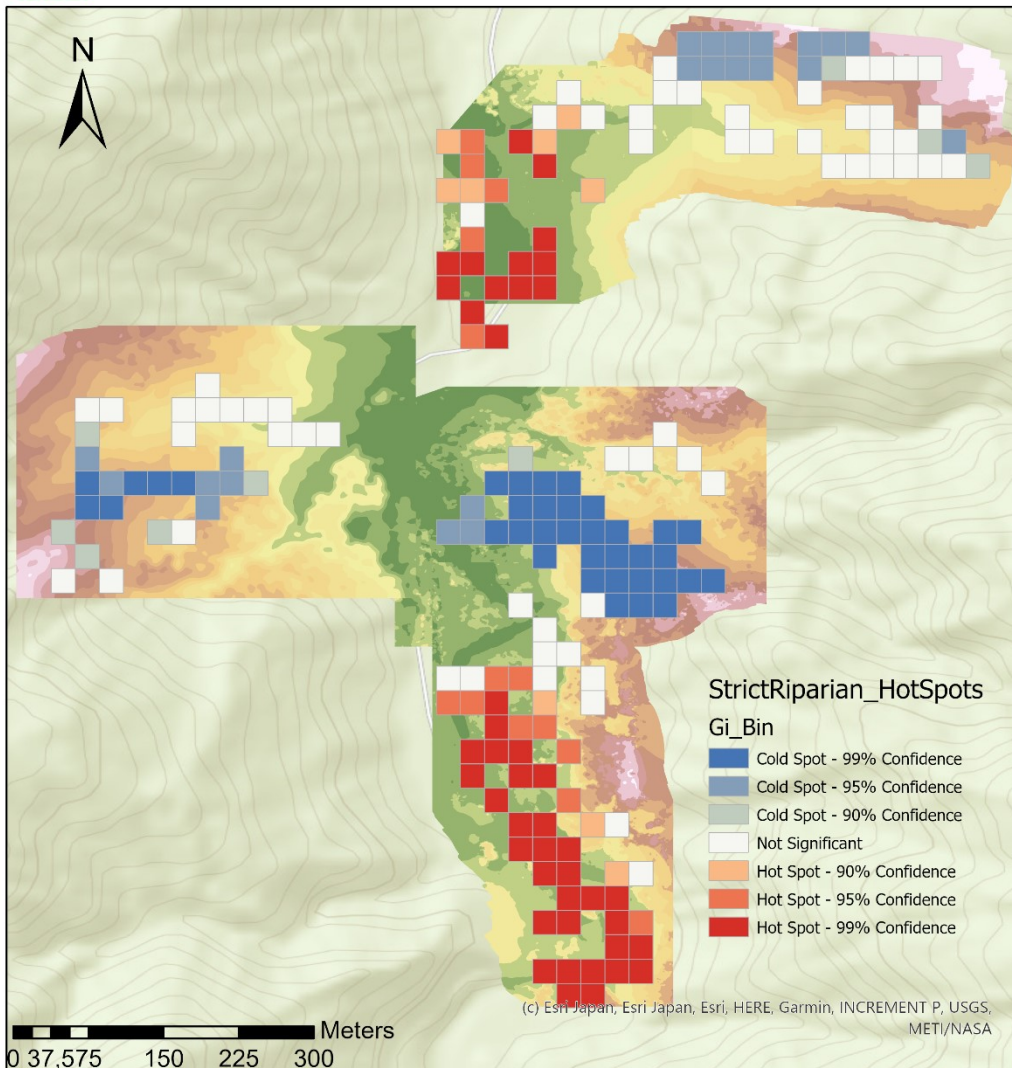
Hot spot analysis Riparian - Terrasse II

by Sarah Kentsch



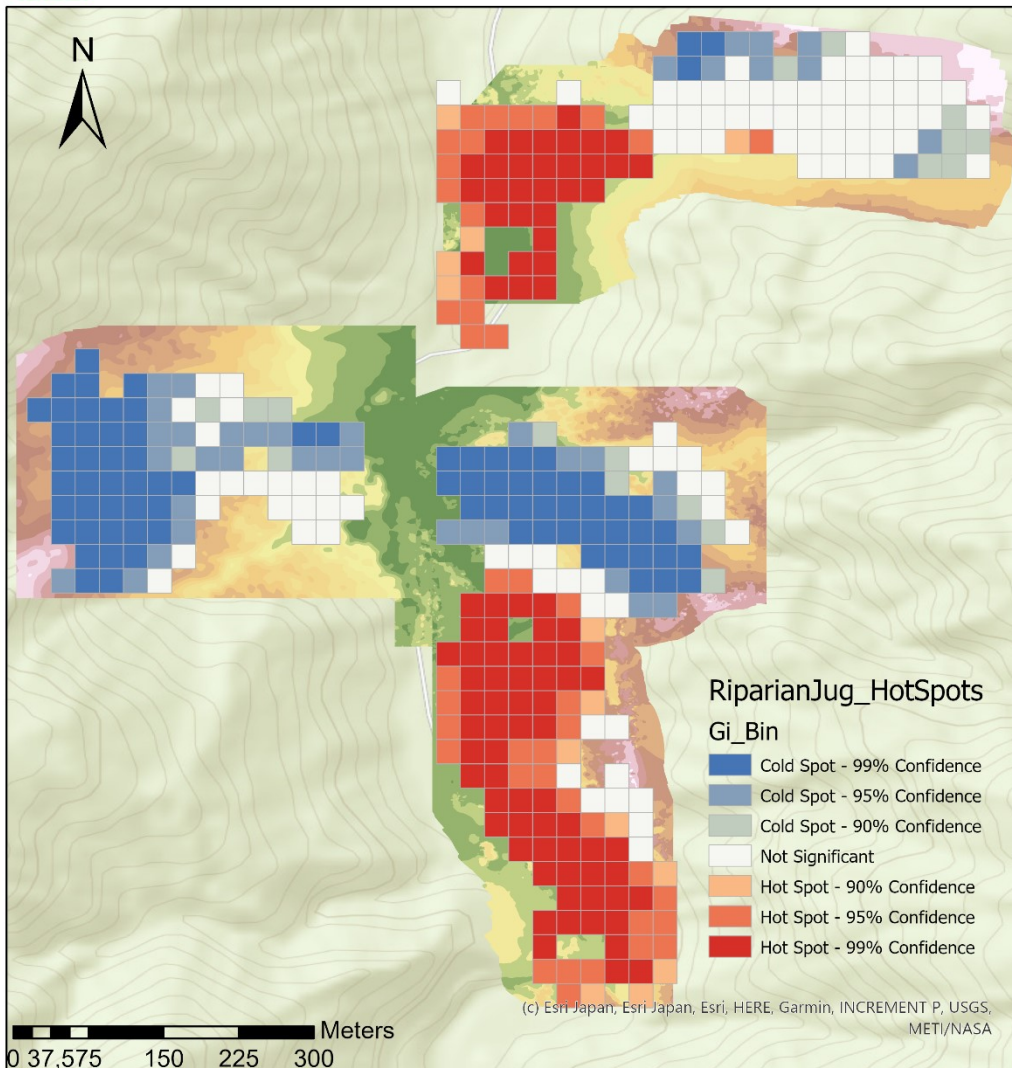


Hot spot analysis Riparian - Terrasse II by Sarah Kentsch





Hot spot analysis Riparian - Terrasse III by Sarah Kentsch



Appendix O – Height/Distance diagrams

Contains the diagrams of the distribution along the river and with increasing height for several tree species characteristic for YURF.

